Functionalized peptides targeting the neurotensin receptor 1: Dually labeled ligands as special molecular tools and subnanomolar binding proteolytically stable fluorescent probes and PET tracers

Dissertation

zur Erlangung des Doktorgrades der Naturwissenschaften (Dr. rer. nat.)

an der Fakultät für Chemie und Pharmazie

der Universität Regensburg



vorgelegt von

Fabian Ertl

aus Neustadt an der Waldnaab

2025

Die vorliegende Arbeit entstand in der Zeit von Dezember 2020 bis August 2025 unter der Anleitung von Herrn Prof. Dr. Max Keller an der Fakultät für Chemie und Pharmazie der Universität Regensburg

Das Promotionsgesuch wurde eingereicht im:	August 2025
Tag der mündlichen Prüfung:	08.10.2025
Vorsitzender des Prüfungsausschusses:	Prof. Dr. Steffen Pockes
Erstgutachter:	Prof. Dr. Max Keller
Zweitgutachter:	Prof. Dr. Pierre Koch
Drittprüfer:	Prof. Dr. Joachim Wegener

Acknowledgements

An dieser Stelle möchte ich mich ganz herzlich bei allen bedanken, die mich auf diesem Weg begleitet haben und zum Gelingen dieser Arbeit beigetragen haben.

Zuallererst möchte ich Herrn Prof. Dr. Max Keller besonders danken. Dieses äußerst interessante Thema hat mich immer mit Freude erfüllt und ich habe wirklich sehr gerne daran gearbeitet (und bleibe gerne noch etwas länger dabei)! Deine Unterstützung durch regelmäßiges Erkundigen, durch zahlreiche und hilfreiche Tipps und Ideen und durch deine aktive Mithilfe bei Experimenten hat maßgeblich zum Erfolg dieser Arbeit beigetragen. Deine Positivität, welche auch durch missglückte Synthesen oder Experimente nicht geschmälert wurde, hat sich auch auf mich übertragen und mich weiterhin motiviert. Zudem habe ich von Dir lernen dürfen, wie man richtig wissenschaftlich arbeitet und auch publiziert. Außerdem möchte ich mich für die Möglichkeit bedanken, Forschungsaufenthalte im Ausland absolvieren zu dürfen! Das waren ganz besondere Highlights.

Mein nächster großer Dank gilt Herrn Prof. Dr. Pierre Koch. Von Anfang an hast Du Interesse an meinem Themengebiet gezeigt und mich auch dementsprechend unterstützt. Vielen Dank auch für etwaige Ratschläge und Deinen unermüdlichen Einsatz für den Lehrstuhl. Ich danke Dir auch vielmals für die Übernahme des Zweitgutachtens.

Ich danke Herrn Prof. Dr. Joachim Wegener für die Übernahme des Drittprüfers und das damit verbundene Interesse an meiner Arbeit.

Zudem danke ich Herrn Prof. Dr. Steffen Pockes für die Übernahme des Prüfungsvorsitzes und die zahlreichen Gespräche, was Beruf, Fußball und sonstiges anging.

Special thanks go to Prof. Dr. Nicholas Holliday for giving me the great opportunity to work in your lab at the University of Nottingham. The warm welcome and the high level of expertise in your lab helped me settle in quickly and to learn a new technique (high-content imaging) which was crucial for the publication of Chapter 3. I am particularly grateful to Nicola Dijon, who not only introduced me to the lab and supported me in all my experiments, but especially ensured that I settled in personally and got to know new people and the city of Nottingham.

Another special thanks go to Prof. Dr. Ago Rinken for giving me the great opportunity of a research stay in your lab at the University of Tartu. Your expertise greatly contributed to expanding my knowledge in the field of BBVs, FA, and GPCRs. You made sure that everything ran smoothly throughout my stay. The FA assays performed in your lab were of great importance for the publication of Chapter 3. I would also like to thank Dr. Sergei Kopanchuk, Dr. Santa Veikšina, Dr. Maris-Johanna Tahk und Tõnis Laasfeld for their tremendous support during the entire stay, from preparaing BBVs to conducting and analyzing experiments.

Ich danke der deutschen Forschungsgemeinschaft (DFG, Projekt KE 1857/1-3) für die Förderung dieser Arbeit und dem Graduiertenkolleg 1910 „Medicinal chemistry of selective GPCR ligands“, gefördert durch die DFG, für die Finanzierung der Auslandsaufenthalte sowie der Möglichkeit an tollen Workshops, Tagungen und Retreats teilzunehmen.

Ein ganz besonderer Dank gilt auch Herrn Dr. Jakob Gleixner und Frau Dr. Lisa Schindler (mit dem Anschreiben auf LinkedIn hat alles begonnen!). Ihr beide habt mich auf diese Stelle gebracht und sofort mein Interesse geweckt. Dir, Jakob, möchte ich vor allem für die tolle Zeit in Estland danken (wann sind schon mal zwei Oberpfälzer in einem estnischem Labor? :D).

Dir, Lisa, danke ich vor allem für die große Ehre, dass ich dein Laborpartner sein durfte. Die persönlichen und fachlichen Gespräche, vor allem am Anfang, haben mir sehr viel geholfen.

I would like to thank Dr. Laura Humphrys, especially for the wonderful time I spent at your house during my stay in Nottingham.

Zudem danke ich Herrn Dr. Albert Gattor, Frau Dr. Carina Höring, Frau Dr. Lisa Forster, Frau Dr. Denise Mönnich, Herrn Dr. Christoph Müller und Frau Dr. Nicole Plank für die tolle Aufnahme am Lehrstuhl, vor allem zu Beginn in der Corona-Zeit, sowie für die fachliche Unterstützung.

Ich danke Herrn Thomas Brunner, mit dem ich zuletzt die Ehre hatte, das Labor zu teilen.

Ich bedanke mich bei Frau Franziska Schettler, Herrn Simon Groß, Frau Beate Hoffelner, Herrn Andreas Gerull, Frau Elena Schmid und allen Mitgliedern des Lehrstuhls für die tolle Arbeitsatmosphäre und alle Aktivitäten außerhalb der Arbeit.

Mein besonderer Dank gilt auch Frau Maria Beer-Krön, Frau Susanne Bollwein und Frau Brigitte Wenzl für die Zellkultur und das Durchführen von Experimenten. Insbesondere danke ich Frau Maria Beer-Krön, die größtenteils „meine" Zellen kultiviert und vorbereitet hat sowie Frau Susanne Bollwein, die mir am Schluss mit jeglichen Experimenten geholfen hat.

Ich danke Frau Lydia Schneider und Frau Annalena Wein für das reibungslose Durchführen des Fura-Assays.

Ich danke Herrn Peter Richthammer für die Unterstützung bei allen technischen und handwerklichen Angelegenheiten sowie Frau Silvia Heinrich für die Hilfe und Übernahme bei allen bürokratischen und organisatorischen Angelegenheiten.

Außerdem möchte ich mich bei allen Praktikant:innen (Ramona Paulus, Johannes Pröbstle, Catrin Gehle, Nina Stumm, Sylvia Karl, Ola Shalha, Darline Meier) für das Interesse und den wichtigen praktischen Beitrag danken.

Ich danke allen beteiligten Coautor:innen für die Bereitstellung von Materialien (Zellen, Chemikalien), die reibungslose Durchführung von Experimenten und die wertvollen Beiträge zu Manuskripten und dieser Dissertation.

Herrn Fritz Kastner, Herrn Tuan Anh Nguyen, Herrn Sebastian Bock, Herrn Josef Kiermaier und Herrn Wolfgang Söllner für die zügige und einwandfreie Bearbeitung der Messaufträge bei NMR- und Massenspektren.

Ein ganz besonderer, riesiger Dank gilt meiner Freundin Clara Frey. Deine Liebe, Geduld und Unterstützung hat mir in jedem Moment weitergeholfen. Ich freue mich riesig auf alles Zukünftige mit Dir!

Ein großer Dank geht auch an meinen gesamten Freundes- und Familienkreis!

Zu guter Letzt möchte ich mich aber besonders bei meiner Familie, Petra, Michael und Marie Ertl, für den bedingungslosen Rückhalt bedanken. Insbesondere meinen Eltern Petra und Michael habe ich zu verdanken, dass ich diesen Weg gehen konnte, auf welchem ich ständig auf Euch zählen konnte. Ohne Euch wäre ich niemals, wo ich jetzt bin!

Publications

Peer-reviewed articles published prior to the submission of the thesis

Ertl, F. J., Friedel, A., Schmid, E. J., Höring, C., Archipowa, N., Koch, P., Maschauer, S., Kutta, R. J., Prante, O., and Keller, M. (2025) High-affinity and proteolytically stable peptidic fluorescent NTS1R ligands. *J. Med. Chem. 68*, 19482-19502.

Ertl, F. J., Kopanchuk, S., Dijon, N. C., Veikšina, S., Tahk, M.-J., Laasfeld, T., Schettler, F., Gattor, A. O., Hübner, H., Archipowa, N., Köckenberger, J., Heinrich, M. R., Gmeiner P., Kutta, R. J., Holliday, N. D., Rinken, A., Keller, M. (2024) Dually labeled neurotensin NTS_1R ligands for probing radiochemical and fluorescence-based binding assays *J. Med. Chem. 67*, 16664-16691.

Scheuerer, S., Motlova, L., Schäker-Hübner, L., Sellmer, A., Feller, F., Ertl, F. J., Koch, P., Hansen, F. K., Barinka, C., Mahboobi, S. (2024) Biological and structural investigations of tetrahydro-b-carboline-based selective HDAC6 inhibitors with improved stability, *Eur. J. Med. Chem. 276*, 116676.

Archipowa, N., Wittmann, L., Köckenberger, J., Ertl, F. J., Gleixner, J., Keller, M., Heinrich, M. R., Kutta, R. J., (2023) Characterization of fluorescent dyes frequently used for bioimaging: Photophysics and photocatalytical reactions with proteins, *J. Phys. Chem. B 127*, 9532-9542.

Konieczny, A., Conrad, M., Ertl, F. J., Gleixner, J., Gattor, A. O., Grätz, L., Schmidt, M. F., Neu, E., Horn, A. H. C., Wifling, D., Gmeiner, P., Clark, T., Sticht, H., and Keller, M. (2021) N-terminus to arginine side-chain cyclization of linear peptidic neuropeptide Y Y_4 receptor ligands result in picomolar binding constants, *J. Med. Chem. 64*, 16746-16769.

Poster presentations

Ertl, F. J., Keller, M.
Fluorescent neurotensin NTS_1R ligands with subnanomolar binding affinity. *Frontiers in Medicinal Chemistry*, 2025, Erlangen, Germany.

Ertl, F. J., Kopanchuk, S., Dijon, N. C., Veikšina, S., Tahk, M.-J., Laasfeld, T., Schettler, F., Gattor, A. O., Hübner, H., Archipowa, N., Köckenberger, J., Heinrich, M. R., Gmeiner P., Kutta, R. J., Holliday, N. D., Rinken, A., Keller, M.
Synthesis and characterization of dually labeled NTS_1R ligands. *Frontiers in Medicinal Chemistry*, 2024, Munich, Germany

Ertl, F. J., Dijon, N. C., Köckenberger, J., Heinrich, M. R., R. J., Holliday, N. D., Keller, M.
Synthesis and characterization of fluorescently labeled NT(8-13) derivatives. *11th Austrian Peptide Symposium*, 2022, Vienna, Austria

Professional training

From December 2020 until March 2023 member of the research training group (Graduiertenkolleg 1910) “Medicinal chemistry of selective GPCR ligands”

Table of contents

1 General introduction 1

1.1 Neurotensin receptors and their endogenous and synthetic ligands 3

1.1.1 Neurotensin receptors 3

1.1.2 Endogenous NTSR ligands 3

1.1.3 The lead compound NT(8-13) and non-peptidic NTSR ligands 3

1.1.4 Expression and physiological role of NTS_1R, NTS_2R, and NTS_3R 4

1.2 Radio- and fluorescently labeled ligands as tools for binding assays 6

1.2.1 History of radioligands 6

1.2.2 Radioligands for neurotensin receptors 6

1.2.3 Isotopes in radiochemical binding assays 7

1.2.4 History of fluorescent ligands 8

1.2.5 Fluorescent ligands for neurotensin receptors 8

1.2.6 Fluorophores 9

1.3 Radioligands for tumor imaging and cancer therapy 10

1.3.1 Theranostics 10

1.3.2 Development of NTS_1R radioligands/theranostics 12

1.4 Scope of the thesis 15

1.5 References 17

2 Peptidic NTS_1R ligands containing cyclic basic amino acids 31

2.1 Introduction 33

2.2 Results and discussion 35

2.2.1 Synthesis of cyclic amino acid derivatives 35

2.2.2 Synthesis of peptidic NTS_1R ligands 38

2.2.3 NTS_1R and NTS_2R binding 41

2.2.4 NTS_1R agonism of **2.25** and **2.26** 43

2.2.5 Proteolytic stability of **2.25** and **2.26** 44

2.3 Conclusion 45

2.4 Experimental section 46

2.4.1 General experimental conditions 46

2.4.2 Experimental protocols and analytical data 48

2.4.3 Cell culture 55

2.4.4 NTS_1R binding assay 55

2.4.5 Fura-2 Ca^{2+} assay 55

2.4.6 Stability in human plasma 55

2.5 References 56

A2 Appendix Chapter 2 60

A2.1 Table A2.1 60

A2.2 RP-HPLC chromatograms of compounds **2.5a**, **2.5b**, **2.8**, **2.11a**, **2.11b**, **2.15**, **2.18**, **2.20**-**2.22**, and **2.25**-**2.32** (purity controls) 61

A2.3 ^{1}H-NMR spectra of compounds **2.8**, **2.15**, **2.18**, and **2.20**-**2.22** and ^{13}C-spectra of compounds **2.8**, **2.15**, **2.18**, and **2.22** 68

3 Dually labeled neurotensin NTS_1R ligands for probing radiochemical and fluorescence-based binding assays 75

3.1 Introduction 77

3.2 Results and discussion 80

3.2.1 Ligand design 80

3.2.2 Synthesis 81

3.2.3 Chemical and proteolytic stability of **3.13** and **3.18** 86

3.2.4 Neurotensin receptor binding and agonism 87

3.2.5 Fluorescence characterization 89

3.2.6 Investigation of NTS_1R binding of **3.13**, [^{3}H]**3.13**, **3.18**, and [^{3}H]**3.18** in fluorescence-based and radiochemical assays 89

3.2.6.1 Equilibrium saturation binding with **3.13**, [^{3}H]**3.13**, **3.18**, and [^{3}H]**3.1** 90

3.2.6.2 Investigation of the association and dissociation kinetics of **3.13**, [^{3}H]**3.13**, **3.18**, and [^{3}H]**3.18** 92

3.2.6.3 Competition binding experiments using **3.13**, [^{3}H]**3.13**, **3.18**, and [^{3}H]**3.18** as labeled probes 98

3.2.6.4 Binding of [^{3}H]**3.13** to membranes of CHO-hNTS_1R cells 101

3.3 Conclusion 104

3.4 Experimental section 106

3.4.1 General experimental conditions 106

3.4.2 Experimental protocols and analytical data 108

3.4.3 Synthesis of [^{3}H]**3.13** and [^{3}H]**3.18** 117

3.4.4 Chemical stability 118

3.4.5 Stability in human plasma 119

3.4.6 Excitation spectra, emission spectra, and fluorescence quantum yields 119

3.4.7 Cell culture 120

3.4.8 Molecular cloning and baculovirus generation 120

3.4.9 CHO-hNTS$_1$R cell membrane preparations 120

3.4.10 Buffers used for binding and functional assays 121

3.4.11 Radiochemical competition binding assay with [^{3}H]**1.7** 121

3.4.12 Fura-2 Ca^{2+} assay 122

3.4.13 High-content imaging binding experiments 123

3.4.14 Flow cytometric binding experiments 125

3.4.15 Fluorescence anisotropy binding experiments 128

3.4.16 Radiochemical NTS$_1$R binding assays with [^{3}H]**3.13** and [^{3}H]**3.18** 130

3.4.17 Saturation binding, association, and dissociation experiments with [^{3}H]**3.13** at membranes of CHO-hNTS$_1$R cells 134

3.4.18 Confocal microscopy 135

3.4.19 Calculation of Propagated Errors 135

3.5 References 136

A3 Appendix Chapter 3 143

A3.1 Figures A3.1-A3.17 143

A3.2 Scheme A3.1 157

A3.3 Tables A3.1 and A3.2 157

A3.4 RP-HPLC chromatograms of **3.6**-**3.9**, **3.10a**, **3.10b** and **3.13**-**3.20** (purity controls) 158

A3.5 ^{1}H-NMR spectra of compounds **3.6**-**3.9**, **3.10a**, **3.13** and **3.18**, and ^{13}C-NMR spectra of compounds **3.6**-**3.9** and **3.10a** in DMSO-d_6 and DMSO-d_6/D_2O 4:1 163

A3.6 References 173

4 High-affinity and proteolytically stable peptidic fluorescent NTS$_1$R ligands 175

4.1 Introduction 177

4.2 Results and discussion 180

4.2.1 Synthesis 180

4.2.2 Chemical and proteolytic stability 183

4.2.3 Neurotensin receptor binding studied in radiochemical competition binding assays 184

4.2.4 NTS$_1$R agonism 185

4.2.5 Photophysical characterization 186

4.2.6 Investigation of NTS$_1$R binding of **4.19** and **4.21** by flow cytometry 187

4.2.7 Cooperativity between **4.21** and the allosteric NTS$_1$R modulator SBI-553 ... 193

4.2.8 Confocal Microscopy 195

4.2.9 Biomolecular imaging of NTS$_1$R expression in cells and tumor tissue 197

4.3 Conclusion 200

4.4 Experimental section 201

4.4.1 General experimental conditions 201

4.4.2 Experimental protocols and analytical data 204

4.4.3 Capillary electrophoresis 210

4.4.4 Chemical stability 210

4.4.5 Stability in human plasma 210

4.4.6 Excitation spectra, emission spectra, and fluorescence quantum yields 210

4.4.7 Cell culture 211

4.4.8 Buffers used for binding and functional assays 211

4.4.9 Radiochemical competition binding assays with [^{3}H]**1.7** 212

4.4.10 Fura-2 Ca^{2+} assay 212

4.4.11 Flow cytometric binding experiments 213

4.4.12 Confocal microscopy 216

4.4.13 Biomolecular imaging 217

4.4.14 Calculation of Propagated Errors 218

4.5 References 219

A4 Appendix Chapter 4 225

A4.1 Synthesis of Fmoc-L-(trimethylsilyl)alanine ((*R*)-**4.10**) 225

A4.2 Figures A4.1-A4.13 227

A4.3 Table A4.1 235

A4.4 Electropherograms of the CE analysis of (*R*,*S*)-**4.10** and (*R*)-**4.10** 236

A4.5 RP-HPLC chromatograms of **4.6**, **4.10**, **4.14**-**4.17b**, **4.19**, and **4.21** (purity controls) 237

A4.6 ^{1}H-NMR spectrum and ^{13}C-NMR spectrum of compound **4.10** in $CDCl_3$ 241

A4.7 ^{1}H-NMR spectra of compounds **4.14-4.17b**, **4.19**, and **4.21** and ^{13}C-NMR spectra of compounds **4.14-4.17b** in DMSO-d_6 and DMSO-d_6/D_2O 4:1 v/v 242

A4.8 References 253

5 Development of proteolytically stable peptidic NTS_1R PET ligands with subnanomolar binding affinity 255

5.1 Introduction 257

5.2 Results and discussion 259

5.2.1 Synthesis 259

5.2.2 Chemical stability of **5.6**-**5.11** 261

5.2.3 Proteolytic stability of **5.9**-**5.11** 263

5.2.4 Determination of NTS_1R binding 263

5.2.5 NTS_1R agonism 265

5.2.6 Synthesis of [^{68}Ga]**5.9** 265

5.2.7 Distribution coefficient $logD_{7.4}$ and proteolytic stability of [^{68}Ga]**5.9** 266

5.3 Conclusion 267

5.4 Experimental section 268

5.4.1 General experimental conditions 268

5.4.2 Experimental protocols and analytical data 269

5.4.3 Cell culture 273

5.4.4 NTS_1R binding assay 273

5.4.5 Fura-2 Ca^{2+} assay 274

5.4.6 Chemical stability 274

5.4.7 Stability in human plasma 274

5.4.8 Radiosynthesis of [^{68}Ga]**5.9** 274

5.4.9 Determination of the distribution coefficient log$D_{7.4}$ 275

5.4.10 Stability of [^{68}Ga]**5.9** in human plasma 275

5.5 References 276

A5 Appendix Chapter 5 279

A5.1 Figures A5.1-A5.8 279

A5.2 Table A5.1 284

A5.3 RP-HPLC chromatograms of compounds **5.6**-**5.11** (purity controls) 285

A5.4 RP-HPLC chromatograms of compounds **5.6**-**5.11** using methanol and 0.05% aqueous formic acid as eluents (control of the Ga^{3+} insertion) 287

A5.5 ^{1}H-NMR spectra of compounds **5.6**-**5.11** 290

6 Design and synthesis of macrocyclic peptidic NTS_1R ligands 297

6.1 Introduction 299

6.2 Results and discussion 302

6.2.1 Cyclization approach 302

6.2.2 Synthesis 303

6.2.3 Determination of NTS_1R binding affinities 305

6.3 Conclusion 307

6.4 Experimental section 308

6.4.1 General 308

6.4.2 Experimental protocols and analytical data 310

6.4.3 Cell culture 311

6.4.4 NTS_1R binding assay 311

6.5 References 312

Summary 319

Abbreviations 323

Overview of bold compound numbers and corresponding laboratory codes 328

Chapter 1

General introduction

1.1 Neurotensin receptors and their endogenous and synthetic ligands

1.1.1 Neurotensin receptors

The neurotensin receptor (NTSR) family consists of three receptor subtypes: NTS_1R, NTS_2R, and NTS_3R.[1-5] The NTS_1R and NTS_2R belong to class A of G-protein coupled receptors (GPCRs),[1-5] whereas the NTS_3R is a sortilin receptor and contains a yeast-related Vps10p-domain.[1,3-12] The NTS_1R couples preferably to $G_{q/11}$ G-proteins, which activates the phospholipase C followed by the production of inositol trisphosphate and an increase of the intracellular Ca^{2+}-concentration.[1,2,4] NTS_2R, sharing about 64% homology with the NTS_1R,[1,3] shows controversial signaling pathways depending on the type of tissue, cell type, and species. For example, it was demonstrated that the human NTS_2R can be constitutively active and binds to G_q or $G_{i/o}$.[1,2,4,13-15] The single-domain transmembrane protein NTS_3R plays a role in internalization of receptor ligands ("scavenger"), such as neurotensin and lipoprotein lipase, and in intracellular transport and secretion of NTS_1R.[3,4,8,11,16]

1.1.2 Endogenous NTSR ligands

Two endogenous ligands addressing the neurotensin receptors exist in the human body: neuromedin N (**1.1**) and neurotensin (**1.2**) (amino acid sequences shown in Figure 1.1A). The hexapeptide **1.1** shows a clear preference for the NTS_1R over both NTS_2R and NTS_3R.[6,17,18] The 13-amino acid long peptide **1.2** acts as agonist at the NTS_1R[1-5] and, depending on the species and cell type, as agonist, antagonist, or inverse agonist at the NTS_2R, which is still highly debated.[2-4,14,19,20] Neurotensin exhibits a slightly lower binding affinity to the NTS_2R compared to the NTS_1R (Figure 1.1A).[21,22] Additionally, the tridecapeptide **1.2** is internalized by the NTS_3R[3,4,8,11,16] and shows a nanomolar IC_{50} value for the NTS_3R (determined in a radiochemical competition binding assay) at human microglial cells (Figure 1.1A).[9]

1.1.3 The lead compound NT(8-13) and non-peptidic NTSR ligands

Truncation studies revealed that the C-terminal part of **1.2** is crucial for receptor binding. According, the N-terminal part NT(1-7) exhibits no activity at neurotensin receptors.[23,24] It was demonstrated that the hexapeptide NT(8-13) (**1.3**) shows retained and even higher binding affinity than **1.2** (Figure 1.1A), making it the lead structure of choice for the development of peptidic NTSR ligands.[3,4,23,25] N-terminal shortening of **1.3** by one more amino acid, i.e., Arg^8, resulted in a markable decrease in NTS_1R binding affinity.[23,24,26-28] Amidation or removal of the C-terminal amino acid, Leu^{13}, led to a total loss of NTS_1R binding affinity.[23,24,26-28] **1.3**, like

1.2, shows a slight preference for NTS_1R over NTS_2R and a high NTS_1R selectivity over NTS_3R (Figure 1.1A).

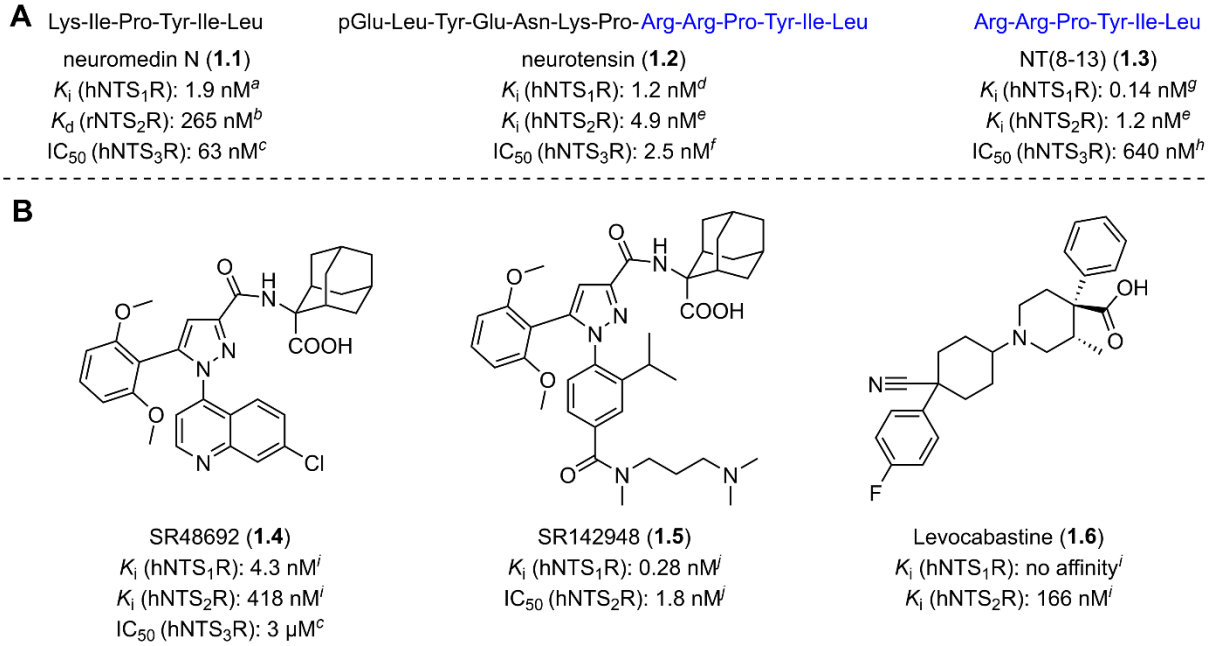


Figure 1.1. (A) Amino acid sequences and NTSR binding affinities of the endogenous ligands neuromedin N (**1.1**) and neurotensin (**1.2**) and NT(8-13) (**1.3**). (B) Structures and binding affinities of the non-peptidic compounds SR48692 (**1.4**), SR142948 (**1.5**), and levocabastine (**1.6**). [a]Skrzydelski *et al.*[17] [b]Tóth *et al.*[18] [c]Mazella *et al.*[6] [d]Granier *et al.*[27] [e]Einsiedel *et al.*[21] [f]Martin *et al.*[9] [g]Keller *et al.*[29] [h]Kokko *et al.*[30] [i]Richard *et al.*[14] [j]Gully *et al.*[31]

In the 1990s, two important non-peptidic NTS_1R antagonists were described: SR48692 (**1.4**)[32] and SR142948 (**1.5**)[31] (Figure 1.1B). Both exhibit NTS_1R binding affinities with K_i values in the nanomolar range, with **1.5** showing NTS_1R affinity comparable to that of **1.3**. Whereas **1.4** can discriminate between NTS_1R and NTS_2R, compound **1.5** binds both receptors with similar affinities.[31] Interestingly, both NTS_1R antagonists were reported to act as agonists at the NTS_2R.[14,19] The antihistaminic levocabastine (**1.6**) was discovered to bind the NTS_2R while showing no binding affinity at the NTS_1R.[14,33-37]

1.1.4 Expression and physiological role of NTS_1R, NTS_2R, and NTS_3R

Table 1.1 shows where the different neurotensin receptors are expressed and what physiological effects are mediated by each receptor. An interesting aspect is the (over)expression of NTS_1R and/or NTS_2R in various tumor types suggesting that these receptors can potentially serve as targets for tumor visualization and therapy using radioactively labeled NTS_1R or NTS_2R ligands. Moreover, the treatment of psychotic disorders, pain and Parkinsons´s disease via activation of neurotensin receptors (especially NTS_1R and NTS_2R) were and are considered.

Table 1.1. Expression (including tumor tissues) and physiological role of NTS_1R, NTS_2R, and NTS_3R.

receptor	location of expression (rat, mouse, or human)	physiological relevance
NTS_1R	• CNS: cerebral cortex, hypothalamus, basal ganglia, limbic system, substantia nigra, brainstem, spinal cord[1,4,38-45] • neurons[4] • peripheral nervous system: peripheral ganglia[46] • pancreas[47,48] • gastrointestinal tract: stomach, ileum, jejunum, colon[4,49,50] • tumor tissue: prostate and colon carcinoma, breast cancer, pancreatic adenocarcinoma, lung cancer, Ewing's sarcoma[51-58]	• modulation of dopaminergic neurotransmission[4] • circadian rhythm[4] • antipsychotic effects[5] • stimulation of cell growth[1,2,4] • hypothermia[3,5] • food intake↓[5] • analgesia[4,5] • cardiovascular effects such as a decrease in blood pressure[5] • effects on the gastrointestinal tract (motility↓, gastric acid↓, pancreatic secretion↑)[3] • potential target for tumor diagnosis and treatment[5]
NTS_2R	• CNS: olfactory system, cerebral and cerebellar cortices, substantia nigra, brainstem, hypothalamus, hippocampus, spinal cord[1,3,4,34,59-65] • neurons (predominantly in dendrites)[4] • pancreas[47,48,66] • gastrointestinal tract: parietal cells[67] • tumor tissue: chronic B-cell leukemia, prostate cancer[68-70]	• analgesia[4,5,65] • inflammatory responses[4] • neuronal regeneration[4] • potential target for tumor diagnosis and treatment[68-70]
NTS_3R	• CNS: amygdala, substantia nigra, thalamus, brainstem, cerebral and cerebellar cortices[4,62,71,72] • neurons (including dendrites)[4] • pancreas[47,48] • adipocytes[73,74] • thyroid[71,72] • heart[71,72,75] • skeletal muscle[71,72] • placenta[71,72] • testis[71,72,76] • granulosa cells[76] • tumor tissue: breast and prostate cancer, ovarian carcinoma, thyroid cancer, pancreatic adenocarcinoma[65,77-80]	• migration of and release of cytokines and chemokines from microglial cells[5] • sorting of the Glut4-transporter[5] • sorting and internalization of neurotensin ("scavenger")[3,4,8,11,16,65] • food intake↓[5]

Note: the receptor expression reported in references 40, 43, 50, 59, and 60 is based on the determination of the respective mRNA. In the case of all other references, expression was studied on the protein level.

1.2 Radio- and fluorescently labeled ligands as tools for binding assays

1.2.1 History of radioligands

The general start of radioligands can be dated back to the year 1941: even if radioactive iodine is not a "real" ligand, it is the first known application of a radioactive substance to humans in medicine. It was used for the visualization of the thyroid and for the treatment of hyperthyroidism.[81,82] In 1953, insulin was labeled with ^{131}I (presumably at the sidechain of tyrosine residues) to study the biodistribution and metabolism of insulin in rats and humans.[83] [^{3}H]Noradrenaline was the first described tritium-labeled radioligand in 1959, which was utilized to explore the influence of drugs on the uptake and metabolism of noradrenaline in cats.[84,85] This was directly followed by the report of a tritiated angiotensin II derivative[86] and a ^{14}C-labeled estrogene.[87] The development of [^{3}H]naloxone in 1973 marked the first major milestone in the use of a radioligand in binding assays. Pert and Snyder performed saturation and competition binding experiments at brain (rat) and small intestine (guinea pig) homogenates. This is also the first description of binding constants determined in a radiochemical assay.[88] Using [^{3}H]dopamine, [^{3}H]haloperidol, [^{3}H]serotonin, and [^{3}H]spiperone, tritium labeling was further exploited to determine binding affinities of labeled and non-labeled compounds (K_d and IC_{50} values) and to map the distribution of dopamine and serotonin receptors in the rat brain via autoradiography.[89-93]

1.2.2 Radioligands for neurotensin receptors

Neurotensin, which was discovered and isolated in 1973 by Carraway and Leeman,[94] was iodinated and tritiated in 1977. The resulting [^{3}H]neurotensin and [^{125}I]neurotensin derivatives represent the first radioligands targeting neurotensin receptors and were characterized in terms of binding kinetics and in saturation and competition binding assays (Figure 1.2).[95-98] More than a decade later, the equipotent hexapeptide NT(8-13) was also tritiated to yield [^{3}H]NT(8-13) ([^{3}H]**1.3**), a radioligand with an NTS_1R binding affinity below 1 nM (see Figure 1.2).[99] In the late 90s, the antagonists **1.4** and **1.5** were labeled with tritium to obtain the first antagonistic and non-peptidic radioligands for the NTS_1R and NTS_2R ([^{3}H]**1.4** and [^{3}H]**1.5**, Figure 1.2).[100-102]

During the past 20-30 years, many studies used the aforementioned radioligands, but recent advances in this field led to the tritiated NT(8-13)-derivative [^{3}H]UR-MK300 ([^{3}H]**1.7**) (see Figure 1.2) representing an advanced labeled probe with improved binding properties and an easier synthetical access.[29]

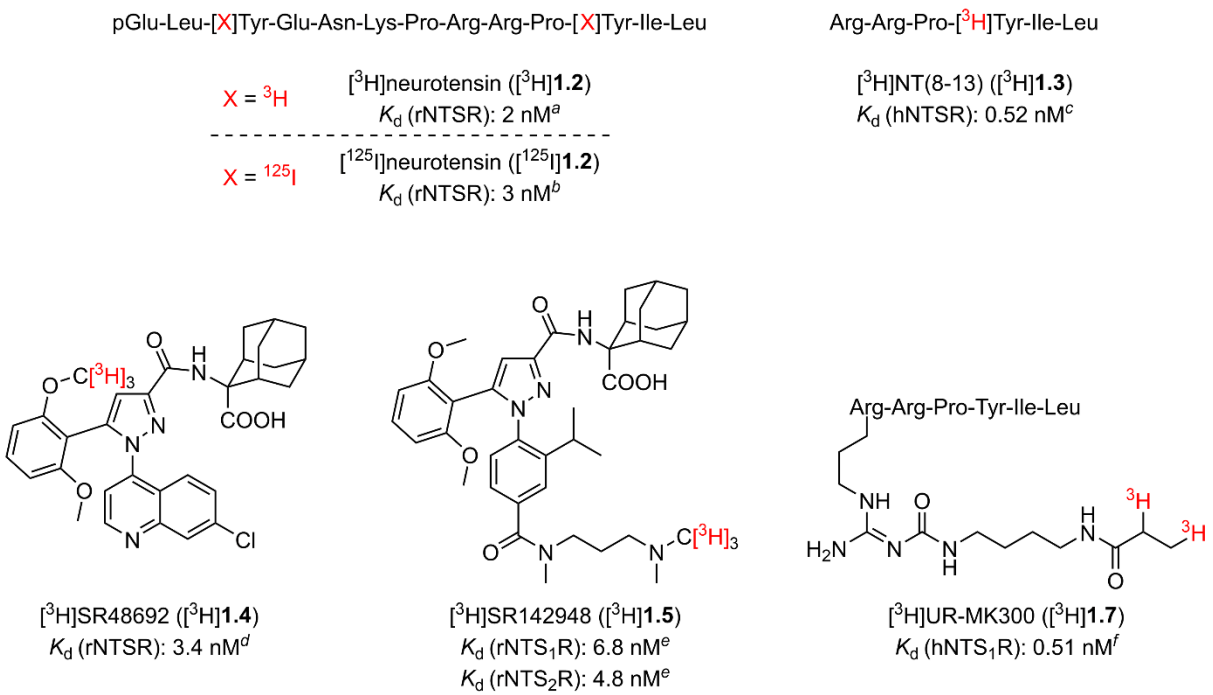


Figure 1.2. Amino acid sequences or structures of reported radioligands targeting neurotensin receptors. Note: the tritium atoms do not represent the quantity of tritium isotopes. They only indicate that tritium is present in the respective positions. Structures were drawn based on the cited literature. The first report of [^{3}H]**1.4** did not differentiate between neurotensin receptor subtypes. [a]Kitabgi *et al.*[95] [b]Uhl *et al.*[96] [c]Kanba *et al.*[99] [d]Labbé-Jullié *et al.*[100] [e]Betancur *et al.*[101] [f]Keller *et al.*[29]

1.2.3 Isotopes in radiochemical binding assays

The most common and recently used isotopes in radiochemical binding assays, ^{3}H and ^{125}I, are specified in Table 1.2. ^{14}C, ^{32}P, and ^{35}S might also serve as appropriate isotopes, but not to the same extent as tritium and radioactive iodine.

Table 1.2. Characteristics of radioisotopes commonly incorporated in radioligands and used in radiochemical binding assays.[103,104]

isotope	emitting type	$t_{1/2}$	specific activity [Ci/mmol]	introduction to radioligand
^{3}H	β^-	12.4 years	30-100	"substitution" of hydrogen atoms by ^{3}H
^{125}I	γ	60 days	~ 2000	iodination of aromatic residues

The β^--emitting tritium has several advantages over ^{125}I: it has a longer half-life enabling longer use of the probes and tritium-labeled ligands are chemically almost equivalent to their non-radioactive analog (exchange of a hydrogen atom by a tritium atom), which is beneficial in terms of preserving the ligand structure. The low radiation energy of tritium is advantageous with respect to safety precautions (in water, the range is within a few micrometers) and stability

(in general low radiolysis). Radioactive iodine shows very high specific activity which allows the reliable detection of low amounts of radioligand, for example in the case of low receptor expression.[103,104]

1.2.4 History of fluorescent ligands

The first use of a fluorescent probe was described in the year 1941 where Coons and coworkers were able to detect a pneumococcal antigen with fluorescein-labeled antibodies.[105] Over three decades later, the first fluorescently labeled receptor ligand was reported: fluorescent α-bungarotoxin was used to label nicotinic acetylcholine receptors in skeletal muscle.[106,107] This approach was also successfully pursued for other receptors such as histamine, opioid, and adrenoreceptors.[107-112] The fluorescent ligands were used to visualize and localize receptors in tissues. Furthermore, the labeled probes were used in competition binding assays to determine receptor-ligand binding constants of non-labeled compounds.

1.2.5 Fluorescent ligands for neurotensin receptors

Faure and coworkers developed the fluorescein-labeled neurotensin derivative **1.8** in 1974, representing the first fluorescent ligand in the field of neurotensin receptors (Figure 1.3).[113] Since that many different NT(8-13)-derived ligands with a fluorescence label have been synthesized. The most promising candidates to date will be described in detail in Chapter 4. Notably, a recent study described an allosteric fluorescent NTS_1R ligand which can serve as molecular tool to identify allosteric modulators of the NTS_1R (compound **1.9**, Figure 1.3).[114]

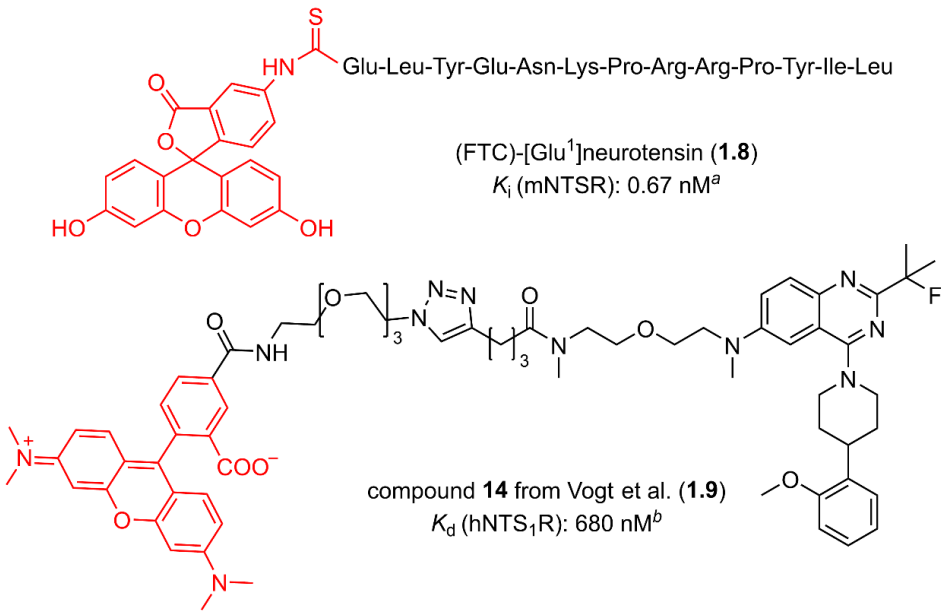


Figure 1.3. Structure of the first described fluorescent ligand **1.8**, targeting the neurotensin receptors, and the 5-TAMRA-labeled allosteric NTS_1R ligand **1.9**. [a]Faure *et al.*[113] [b]Vogt *et al.*[114]

In contrast to radioligands, an antagonistic fluorescent ligand for neurotensin receptors has not been reported to date.

1.2.6 Fluorophores

While the number of radioisotopes useful for receptor-ligand binding assay is low, there is an broad variety of fluorophores available. Since the synthesis of fluorescein in 1871 by Adolf von Baeyer,[115] the portfolio of fluorophores has grown immensely. Commercially available dyes cover excitation wavelengths across the UV, the entire visible spectrum, and the near-infrared range, and are available with various functional groups, enabling a straightforward conjugation to the molecule of choice. Table 1.3 shows only a small selection of commonly used fluorophores, together with their characteristics. In general, there is no ideal fluorophore – thus, the choice rather depends on the intended use. For example, live cell imaging might require dyes with higher excitation wavelengths to decrease autofluorescence, whereas fluorescence polarization assays require a labeled probe with an appropriate fluorescence lifetime (τ_{fl}).[116-120] Additionally, every dye comes with its up- and downsides. Fluorescein shows a high quantum yield and fluorescence lifetime but it exhibits low photostability which was improved with the development of BDP FL and AF 488 (see Table 1.3). Besides the "classical" rhodamine- and cyanine-type dyes, companies have synthesized a variety of fluorophore series such as BODIPY and AlexaFluor (AF®) across the entire visible spectrum. Due to this wide range, individually "tailored" fluorescent ligands are easily accessible.

Table 1.3. Excitation and emission maxima, quantum yield, photostability, and fluorescence lifetime of a selection of fluorophores.

fluorophore	type	excitation / emission maxima [nm][a]	Φ (%)[a]	photostability[b]	τ_{fl} [ns]
fluorescein	xanthene	492 / 517	0.93	low	≈ 4[121] (PBS)
5-TAMRA	rhodamine	541 / 567	0.10	high	2.6[122] (PBS)
Cy3	indolinium-type cyanine	555 / 570	0.31	high	0.2[123] (TRIS buffer)
Cy5		646 / 662	0.20	moderate	0.9[124] (PBS)
sulfoCy7		750 / 773	0.30	moderate	1.4[125] (DMSO)
BDP® FL	BODIPY	503 / 511	0.95	high	6[126] (H_2O)
BDP® 630/650		628 / 642	0.91	high	3.89[127] (H_2O)
AF® 488	rhodamine	490 / 525	0.92 (PBS)	moderate	4.1[d] (H_2O)
AF® 555	cyanine dyes	553 / 568	0.10 (PBS)	high	0.3[d] (H_2O)
AF® 647		650 / 671	0.33 (PBS)	high	1[d] (H_2O)
AF® 750	-[c]	752 / 776	0.12 (PBS)	low	0.7[d] (H_2O)

[a]Data were obtained from suppliers (Lumiprobe and ThermoFisher). Solvent information is not provided unless otherwise stated. [b]The information is based on photostability tests performed by ThermoFisher or on statements (in blue) from other suppliers. [c]Structure of AF® 750 is not published. [d]Fluorescence lifetimes of AlexaFluor dyes were obtained from ThermoFisher. AF® = AlexaFluor

It should be noted that Table 1.3 shows the properties of the free dyes. These can change upon conjugation to a receptor ligand or in the presence of proteins such as BSA as recently demonstrated, e.g., for the fluorescent dyes 5-TAMRA and Cy3B.[122]

1.3 Radioligands for tumor imaging and cancer therapy

1.3.1 Theranostics

With the clinical approval of the somatostatin analogs [^{68}Ga]Ga-DOTA-TATE and [^{177}Lu]Lu-DOTA-TATE for the imaging and treatment, respectively, of neuroendocrine tumors, the era of theranostics has begun. The term “theranostics” is derived from the words “diagnostics” and

"therapeutics" and means that the same precursor is used for both imaging and therapy.[128-130] This can be achieved by incorporating different metal ion isotopes such as the positron-emitting $^{68}Ga^{3+}$ (PET imaging) and the β^--emitting $^{177}Lu^{3+}$ (therapy) (in the case of DOTA-TATE).[128-130] Generating such theranostic pairs requires precursors which can be labelled with different radioisotopes. Since many tracer nuclides are metal ions and tend to form stable complexes with chelators containing several electron-pair donors, labelling precursors are typically obtained by conjugation of a chelator such as DOTA to a receptor ligand. Figure 1.4 shows a variety of chelators which are commercially available and in clinical use (except for NOPO).[130] The stability of the formed complexes depends on both the metal ion and chelator type and must therefore be evaluated experimentally or based on literature data for each individual combination.

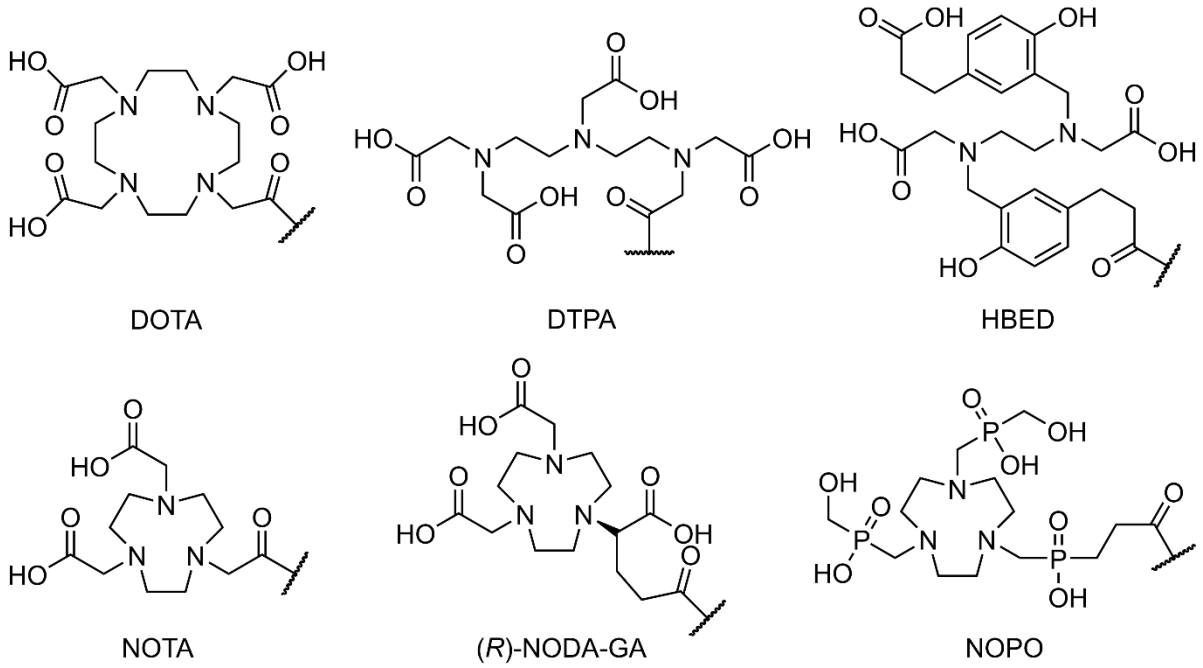


Figure 1.4. Structures of different chelators useful for the complexation of radiometal ions. Wavy lines indicate the position of attachment to the bioactive compound of choice.

As becomes obvious from the selection of radioisotopes shown in Table 1.4, a huge variety of radionuclides is currently considered clinically relevant, and the number is still growing. The decay mode of a radioisotope determines its possible use: Positron- or γ-emitting metal ions are suitable for imaging via PET and SPECT, respectively. Besides the diagnostic modality, these emitters, especially $^{99m}Tc^{4+}$, can also be utilized for radioguided surgery (removal of tumor tissue).[131,132] Isotopes with sufficiently long half-lives such as $^{99m}Tc^{4+}$ or $^{111}In^{3+}$ offer the combination of both aspects (imaging and radioguided surgery) with a single injection.[133] As α- and β^--emitters produce radiation that penetrates tissue in the low micro- and millimeter range (depending on their energy), cancer tissue can be radiated specifically and healthy tissue

will not be damaged, provided that the tracer accumulates specifically in the tumor tissue.[128] $^{67}Ga^{3+}$ and $^{111}In^{3+}$ emit, besides γ-radiation, Auger electrons which have low energies and extremely short travel distances in tissues (nanometer range). Conjugated to a receptor ligand which is internalized upon binding, these isotopes enable a highly specific targeting of cancer cells (the range and penetration is confined within a single cell).[128,130] For certain elements such as copper and gallium, radioisotopes, which can be used for diagnosis and/or therapy, can be generated. Other radiometals such as $^{111}In^{3+}$ or $^{166}Ho^{3+}$ allow both applications based on one isotope.

According to the World Nuclear Association, 90% of the applications of radiopharmaceuticals are for diagnosis and 80% of these use the isotope $^{99m}Tc^{4+}$ (last updated on January 10, 2025).

Table 1.4. Selection of clinically used radioisotopes, their physical properties, source and application.[128-130,134]

radionuclide	half-time	decay[a]	source	application
^{18}F[b]	110 min	β^+	cyclotron	PET
^{64}Cu	12.7 h	β^+ / β^-	cyclotron	PET, therapy
^{67}Cu	62 h	β^-	accelerator	therapy
^{67}Ga	3.3 d	γ	cyclotron	SPECT, Auger therapy
^{68}Ga	68 min	β^+	$^{68}Ge/^{68}Ga$ generator	PET
^{90}Y	64 h	β^-	$^{90}Sr/^{90}Y$ generator	therapy
^{99m}Tc	6 h	γ	$^{99}Mo/^{99m}Tc$ generator	SPECT
^{111}In	2.8 d	γ	cyclotron	SPECT, Auger therapy
^{161}Tb	7 d	β^-	reactor	(Auger) therapy
^{166}Ho	27 h	γ / β^-	reactor	SPECT, therapy
^{177}Lu	6.6 d	β^-	reactor	therapy
^{225}Ac	9.9 d	α	cyclotron	therapy
^{227}Th	18.7 d	α	reactor	therapy

[a]Only the decay modes important for the application are shown. [b]Incorporated in chelators in combination with aluminium ($[^{18}F]AlF^{2+}$).

1.3.2 Development of NTS_1R radioligands/theranostics

To date, a wide range of radiolabeled compounds designed to target tumors with NTS_1R (over)expression have been reported.[58,135] Although many tracers have been investigated in vivo in rodents, no NTS_1R radioligand has yet been established for clinical use. Regarding peptidic ligands, so far, only a ^{99m}Tc-containing peptide (**1.10**, see Figure 1.5A) was evaluated in ductal pancreatic adenocarcinoma patients,[136,137] representing the first application of NTS_1R radioligands in humans. Since that, no further NT(8-13)-derived compound was transferred to

the clinic which is mainly due to the low metabolic stability and fast clearance by the kidneys of the hydrophilic peptides.[135] This issue has been overcome using non-peptidic antagonists as they are not prone to enzymatic degradation. In 2018, the DOTA-conjugated antagonist ^{177}Lu-3BP-227 (**1.11**, see Figure 1.5A), synthesized by 3B Pharmaceuticals, was tested in clinical trials. **1.11** was evaluated in a phase I dose escalation study in pancreatic adenocarcinoma patients (see results at clinicaltrials.gov, ID: NCT03525392). The study was stopped during this phase although promising results such as high tumor uptake and low toxicity were observed.[138] The reasons for this termination are not openly discussed in the literature, but it should be emphasized that it was not due to safety concerns (according to the website of clinicaltrials.gov).

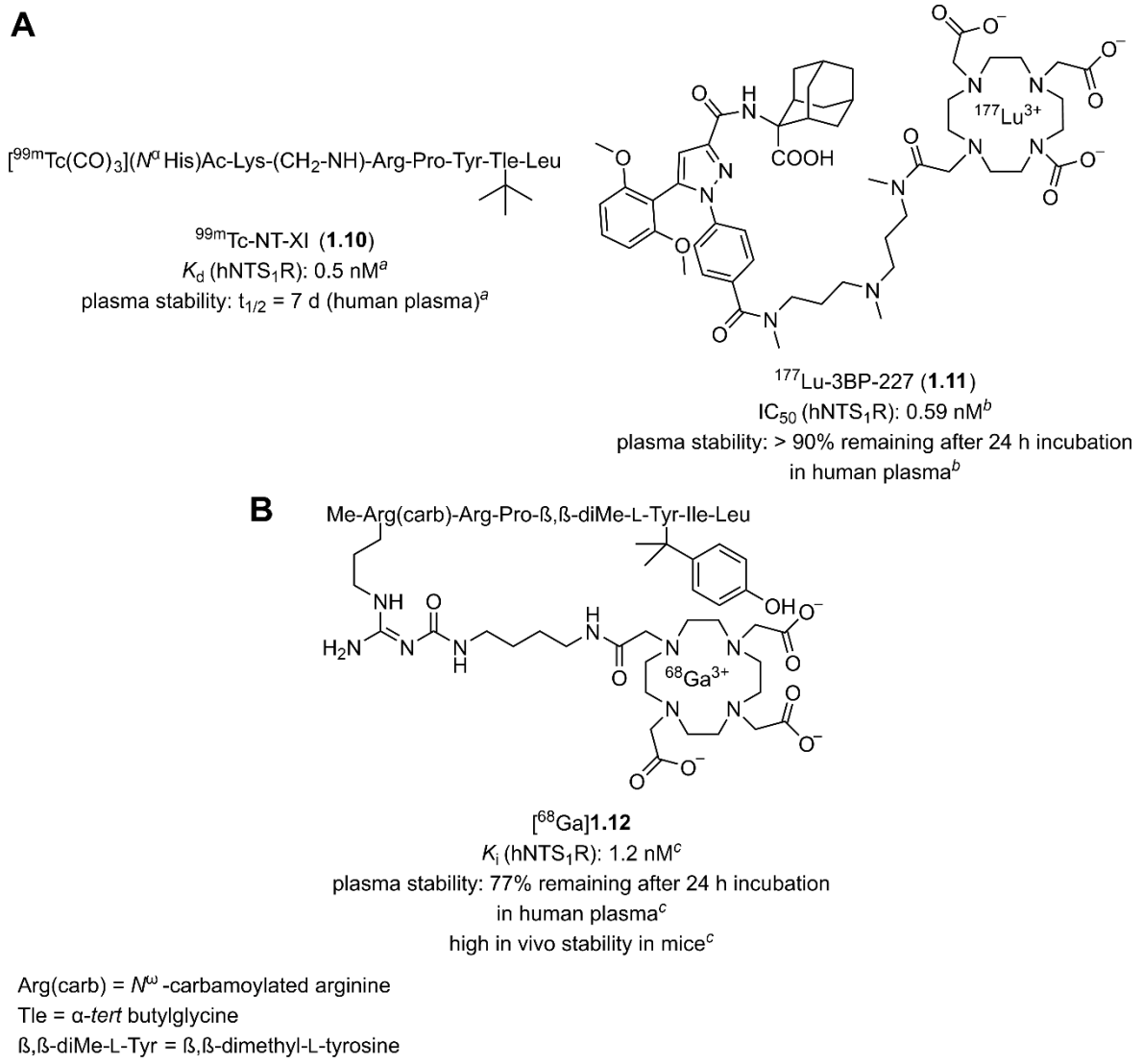


Figure 1.5. (A) Structures of compounds **1.10** and **1.11** which were subjected to humans in clinical studies. (B) Structure of the promising NTS$_1$R PET ligand **1.12**. [a]Bruehlmeier *et al.*[136] [b]Osterkamp *et al.*[139] [c]Schindler *et al.*[140]

Recent developments of potential NTS_1R radioligands have not only been focused on antagonists, but also on peptidic ligands with the focus on the improvement of the metabolic stability while retaining high NTS_1R binding affinity. Schindler and coworkers[140] demonstrated that the incorporation of a dimethylated tyrosine derivative in position 11 markedly enhanced the in vivo stability while retaining high NTS_1R binding affinity (compound **1.12**, Figure 1.5B). The ^{68}Ga-labeled PET ligand **1.12** was investigated in tumor-bearing mice. These studies gave promising results in terms of accumulation and retention of the tracer in the tumor.[140]

1.4 Scope of the thesis

An essential step in the development of therapeutics targeting GPCRs is the determination of in vitro binding affinities of newly synthesized compounds in competition binding assays. Such experiments require a labeled ligand that can be detected. For many decades, radiolabeled receptor ligands were used for receptor-ligand binding studies, but the recent development of fluorescent ligands and fluorescence-based techniques, allowing a fast and sensitive detection of fluorescence, generated new possibilities for target-drug binding studies. Since both kinds of labels have several advantages and disadvantages, a systematic comparison of radiochemical and fluorescence-based binding assays was one of the main goals of this thesis. As a proof of concept, the NTS_1R, a peptidic GPCR representing a potential target for cancer and pain treatment, was chosen as the receptor under study, for which labeled ligands were developed.

Deng and coworkers[141] prepared a dually labeled (radio- and fluorescence label) peptidic NTS_1R ligand which exhibited, despite the attachment of a bulky chelator and fluorophore, nanomolar NTS_1R binding affinity. A cyclic arginine derivative seemed to be a structural key element for the high binding affinity. Inspired by this, the cyclic arginine derivative had to be (re)synthesized and incorporated in peptidic NTS_1R ligands. Additionally, due to a collaboration with Prof. O. Reiser (Institute of Organic Chemistry, University of Regensburg), an unnatural pyrrolidine-type β-amino acid had to be embedded in neurotensin(8-13)-derived peptides. The prepared peptides had to be characterized with regard to their NTS_1R binding affinities, agonistic potencies, and proteolytic stabilities (Chapter 2).

A direct comparison of radiochemical and fluorescence-based binding assays is difficult since both types of assays use differently labeled probes, which are in general structurally different even if derived from the same receptor ligand. Moreover, different techniques for ligand detection must be used. Therefore, a dually labeled NTS_1R ligand (tritium and fluorescence) and its cold analog, representing, apart from the hydrogen-tritium exchange, chemically identical structures, had to be synthesized using orthogonal functionalities (alkyne and amino group) for label attachment. Two tritiated ligands, bearing different fluorophores, had to be characterized in radiochemical binding assays, whereas their cold analogs had to be investigated in three types of fluorescence-based assays (high-content imaging, flow cytometry, fluorescence anisotropy). The results had to be systematically compared (Chapter 3).

Furthermore, three recently reported structural modifications applied to the hexapeptide NT(8-13), conveying very high NTS_1R binding affinity,[142] the feasibility of peptide conjugation via

an arginine side chain,[29] and enhanced metabolic stability,[140] had to combined in one molecule. The resulting labeling precursor had to be conjugated to different fluorophores (Chapter 4) and chelators (Chapter 5), and their NTS_1R binding affinities had to be determined. The fluorescent probes had to be characterized in flow cytometric assays and used for the imaging of receptor expression in tumor cells and tumor tissue (Chapter 4). Natural Ga^{3+} had to be incorporated in the chelator-conjugated peptides, followed by the characterization of the potential PET ligands in terms of NTS_1R binding affinity and proteolytic stability. For one selected ligand, the respective $^{68}Ga^{3+}$-containing compound had to be prepared and studied with respect to its in vitro plasma stability and hydrophilicity (Chapter 5).

Inspired by the high-affinity cyclic peptidic neuropeptide Y Y_4 receptor ligands reported by Konieczny and coworkers,[143] this thesis also aimed for the synthesis and characterization of cyclic NT(8-13) derivatives (Chapter 6).

1.5 References

1. Vincent, J. P.; Mazella, J.; Kitabgi, P. Neurotensin and neurotensin receptors. *Trends Pharmacol. Sci.* **1999**, *20*, 302-309.
2. Pelaprat, D. Interactions between neurotensin receptors and G proteins. *Peptides* **2006**, *27*, 2476-2487.
3. Kleczkowska, P.; Lipkowski, A. W. Neurotensin and neurotensin receptors: Characteristic, structure-activity relationship and pain modulation--a review. *Eur. J. Pharmacol.* **2013**, *716*, 54-60.
4. Sarret, P.; Cavelier, F. Neurotensin and its receptors q. *Neurosci. Biobehav. Psych.* **2018**.
5. Iyer, M. R.; Kunos, G. Therapeutic approaches targeting the neurotensin receptors. *Expert Opin. Ther. Pat.* **2021**, *31*, 361-386.
6. Mazella, J.; Zsurger, N.; Navarro, V.; Chabry, J.; Kaghad, M.; Caput, D.; Ferrara, P.; Vita, N.; Gully, D.; Maffrand, J. P.; Vincent, J. P. The 100-kDa neurotensin receptor is gp95/sortilin, a non-G-protein-coupled receptor. *J. Biol. Chem.* **1998**, *273*, 26273-26276.
7. Jacobsen, L.; Madsen, P.; Jacobsen, C.; Nielsen, M. S.; Gliemann, J.; Petersen, C. M. Activation and functional characterization of the mosaic receptor SorLA/LR11. *J. Biol. Chem.* **2001**, *276*, 22788-22796.
8. Mazella, J. Sortilin/neurotensin receptor-3: A new tool to investigate neurotensin signaling and cellular trafficking? *Cell. Signalling* **2001**, *13*, 1-6.
9. Martin, S.; Vincent, J. P.; Mazella, J. Involvement of the neurotensin receptor-3 in the neurotensin-induced migration of human microglia. *J. Neurosci.* **2003**, *23*, 1198-1205.
10. Martin, S.; Dicou, E.; Vincent, J. P.; Mazella, J. Neurotensin and the neurotensin receptor-3 in microglial cells. *J. Neurosci. Res.* **2005**, *81*, 322-326.
11. Christou, N.; Blondy, S.; David, V.; Verdier, M.; Lalloue, F.; Jauberteau, M. O.; Mathonnet, M.; Perraud, A. Neurotensin pathway in digestive cancers and clinical applications: an overview. *Cell Death Dis.* **2020**, *11*, 1027.
12. Kyriatzis, G.; Khrestchatisky, M.; Ferhat, L.; Chatzaki, E. A. Neurotensin and Neurotensin Receptors in Stress-related Disorders: Pathophysiology & Novel Drug Targets. *Curr Neuropharmacol* **2024**, *22*, 916-934.
13. Gendron, L.; Perron, A.; Payet, M. D.; Gallo-Payet, N.; Sarret, P.; Beaudet, A. Low-affinity neurotensin receptor (NTS2) signaling: Internalization-dependent activation of extracellular signal-regulated kinases 1/2. *Mol. Pharmacol.* **2004**, *66*, 1421-1430.

14. Richard, F.; Barroso, S.; Martinez, J.; Labbe-Jullie, C.; Kitabgi, P. Agonism, inverse agonism, and neutral antagonism at the constitutively active human neurotensin receptor 2. *Mol. Pharmacol.* **2001**, *60*, 1392-1398.
15. Mazella, J.; Vincent, J. P. Internalization and recycling properties of neurotensin receptors. *Peptides* **2006**, *27*, 2488-2492.
16. Morinville, A.; Martin, S.; Lavallee, M.; Vincent, J. P.; Beaudet, A.; Mazella, J. Internalization and trafficking of neurotensin via NTS3 receptors in HT29 cells. *Int. J. Biochem. Cell Biol.* **2004**, *36*, 2153-2168.
17. Skrzydelski, D.; Lhiaubet, A. M.; Lebeau, A.; Forgez, P.; Yamada, M.; Hermans, E.; Rostene, W.; Pelaprat, D. Differential involvement of intracellular domains of the rat NTS1 neurotensin receptor in coupling to G proteins: A molecular basis for agonist-directed trafficking of receptor stimulus. *Mol. Pharmacol.* **2003**, *64*, 421-429.
18. Toth, F.; Mallareddy, J. R.; Tourwe, D.; Lipkowski, A. W.; Bujalska-Zadrozny, M.; Benyhe, S.; Ballet, S.; Toth, G.; Kleczkowska, P. Synthesis and binding characteristics of [(3)H]neuromedin N, a NTS2 receptor ligand. *Neuropeptides* **2016**, *57*, 15-20.
19. Vita, N.; Oury-Donat, F.; Chalon, P.; Guillemot, M.; Kaghad, M.; Bachy, A.; Thurneyssen, O.; Garcia, S.; Poinot-Chazel, C.; Casellas, P.; Keane, P.; Le Fur, G.; Maffrand, J. P.; Soubrie, P.; Caput, D.; Ferrara, P. Neurotensin is an antagonist of the human neurotensin NT receptor expressed in chinese hamster ovary cells. *Eur. J. Pharmacol.* **1998**, *360*, 265-272.
20. Dobner, P. R. Multitasking with neurotensin in the central nervous system. *Cell Mol. Life Sci.* **2005**, *62*, 1946-1963.
21. Einsiedel, J.; Held, C.; Hervet, M.; Plomer, M.; Tschammer, N.; Hubner, H.; Gmeiner, P. Discovery of highly potent and neurotensin receptor 2 selective neurotensin mimetics. *J. Med. Chem.* **2011**, *54*, 2915-2923.
22. Fanelli, R.; Floquet, N.; Besserer-Offroy, E.; Delort, B.; Vivancos, M.; Longpre, J. M.; Renault, P.; Martinez, J.; Sarret, P.; Cavelier, F. Use of molecular modeling to design selective NTS2 neurotensin analogues. *J. Med. Chem.* **2017**, *60*, 3303-3313.
23. Tanaka, K.; Masu, M.; Nakanishi, S. Structure and functional expression of the cloned rat neurotensin receptor. *Neuron* **1990**, *4*, 847-854.
24. Stpierre, S.; Lalonde, J. M.; Gendreau, M.; Quirion, R.; Regoli, D.; Rioux, F. Synthesis of peptides by the solid-phase method. 6. Neurotensin, fragments, and analogs. *J. Med. Chem.* **1981**, *24*, 370-376.

25. Tyler-McMahon, B. M.; Boules, M.; Richelson, E. Neurotensin: Peptide for the next millennium. *Regul. Pept.* **2000**, *93*, 125-136.
26. Kitabgi, P.; Poustis, C.; Granier, C.; Vanrietschoten, J.; Rivier, J.; Morgat, J. L.; Freychet, P. Neurotensin binding to extraneural and neural receptors - Comparison with biological-activity and structure-activity-relationships. *Mol. Pharmacol.* **1980**, *18*, 11-19.
27. Granier, C.; Vanrietschoten, J.; Kitabgi, P.; Poustis, C.; Freychet, P. Synthesis and characterization of neurotensin analogs for structure activity relationship studies - Acetyl-neurotensin-(8-13) is the shortest analog with full binding and pharmacological activities. *Eur. J. Biochem.* **1982**, *124*, 117-124.
28. Henry, J. A.; Horwell, D. C.; Meecham, K. G.; Rees, D. C. A structure-affinity study of the amino-acid side-chains in neurotensin - N and C-Terminal deletions and Ala-scan. *Bioorg. Med. Chem. Lett.* **1993**, *3*, 949-952.
29. Keller, M.; Kuhn, K. K.; Einsiedel, J.; Hubner, H.; Biselli, S.; Mollereau, C.; Wifling, D.; Svobodova, J.; Bernhardt, G.; Cabrele, C.; Vanderheyden, P. M.; Gmeiner, P.; Buschauer, A. Mimicking of arginine by functionalized N(omega)-carbamoylated arginine as a new broadly applicable approach to labeled bioactive peptides: High affinity angiotensin, neuropeptide Y, neuropeptide FF, and neurotensin neceptor ligands as examples. *J. Med. Chem.* **2016**, *59*, 1925-1945.
30. Kokko, K. P.; Hadden, M. K.; Orwig, K. S.; Mazella, J.; Dix, T. A. In vitro analysis of stable, receptor-selective neurotensin[8-13] analogues. *J. Med. Chem.* **2003**, *46*, 4141-4148.
31. Gully, D.; Labeeuw, B.; Boigegrain, R.; Oury-Donat, F.; Bachy, A.; Poncelet, M.; Steinberg, R.; Suaud-Chagny, M. F.; Santucci, V.; Vita, N.; Pecceu, F.; Labbe-Jullie, C.; Kitabgi, P.; Soubrie, P.; Le Fur, G.; Maffrand, J. P. Biochemical and pharmacological activities of SR 142948A, a new potent neurotensin receptor antagonist. *J. Pharmacol. Exp. Ther.* **1997**, *280*, 802-812.
32. Gully, D.; Canton, M.; Boigegrain, R.; Jeanjean, F.; Molimard, J. C.; Poncelet, M.; Gueudet, C.; Heaulme, M.; Leyris, R.; Brouard, A.; et al. Biochemical and pharmacological profile of a potent and selective nonpeptide antagonist of the neurotensin receptor. *Proc. Natl. Acad. Sci. U. S. A.* **1993**, *90*, 65-69.
33. Schotte, A.; Leysen, J. E.; Laduron, P. M. Evidence for a displaceable non-specific [3H]neurotensin binding site in rat brain. *Naunyn Schmiedebergs Arch. Pharmacol.* **1986**, *333*, 400-405.

34. Kitabgi, P.; Rostene, W.; Dussaillant, M.; Schotte, A.; Laduron, P. M.; Vincent, J. P. Two populations of neurotensin binding sites in murine brain: Discrimination by the antihistamine levocabastine reveals markedly different radioautographic distribution. *Eur. J. Pharmacol.* **1987**, *140*, 285-293.
35. Chalon, P.; Vita, N.; Kaghad, M.; Guillemot, M.; Bonnin, J.; Delpech, B.; Le Fur, G.; Ferrara, P.; Caput, D. Molecular cloning of a levocabastine-sensitive neurotensin binding site. *FEBS Lett.* **1996**, *386*, 91-94.
36. Mazella, J.; Botto, J. M.; Guillemare, E.; Coppola, T.; Sarret, P.; Vincent, J. P. Structure, functional expression, and cerebral localization of the levocabastine-sensitive neurotensin/neuromedin N receptor from mouse brain. *J. Neurosci.* **1996**, *16*, 5613-5620.
37. Bredeloux, P.; Costentin, J.; Dubuc, I. Interactions between NTS2 neurotensin and opioid receptors on two nociceptive responses assessed on the hot. *Behav. Brain. Res.* **2006**, *175*, 399-407.
38. Sarrieau, A.; Javoy-Agid, F.; Kitabgi, P.; Dussaillant, M.; Vial, M.; Vincent, J. P.; Agid, Y.; Rostene, W. H. Characterization and autoradiographic distribution of neurotensin binding sites in the human brain. *Brain Res.* **1985**, *348*, 375-380.
39. Moyse, E.; Rostene, W.; Vial, M.; Leonard, K.; Mazella, J.; Kitabgi, P.; Vincent, J. P.; Beaudet, A. Distribution of neurotensin binding sites in rat brain: A light microscopic radioautographic study using monoiodo [125I]Tyr3-neurotensin. *Neuroscience* **1987**, *22*, 525-536.
40. Elde, R.; Schalling, M.; Ceccatelli, S.; Nakanishi, S.; Hokfelt, T. Localization of neuropeptide receptor mRNA in rat brain: Initial observations using probes for neurotensin and substance P receptors. *Neurosci. Lett.* **1990**, *120*, 134-138.
41. Boudin, H.; Pelaprat, D.; Rostene, W.; Beaudet, A. Cellular distribution of neurotensin receptors in rat brain: Immunohistochemical study using an antipeptide antibody against the cloned high affinity receptor. *J. Comp. Neurol.* **1996**, *373*, 76-89.
42. Boudin, H.; Pelaprat, D.; Rostene, W.; Pickel, V. M.; Beaudet, A. Correlative ultrastructural distribution of neurotensin receptor proteins and binding sites in the rat substantia nigra. *J. Neurosci.* **1998**, *18*, 8473-8484.
43. Alexander, M. J.; Leeman, S. E. Widespread expression in adult rat forebrain of mRNA encoding high-affinity neurotensin receptor. *J. Comp. Neurol.* **1998**, *402*, 475-500.
44. Fassio, A.; Evans, G.; Grisshammer, R.; Bolam, J. P.; Mimmack, M.; Emson, P. C. Distribution of the neurotensin receptor NTS1 in the rat CNS studied using an amino-terminal directed antibody. *Neuropharmacology* **2000**, *39*, 1430-1442.

45. Roussy, G.; Dansereau, M. A.; Dore-Savard, L.; Belleville, K.; Beaudet, N.; Richelson, E.; Sarret, P. Spinal NTS1 receptors regulate nociceptive signaling in a rat formalin tonic pain model. *J. Neurochem.* **2008**, *105*, 1100-1114.
46. Porzionato, A.; Macchi, V.; Amagliani, A.; Castagliuolo, I.; Parenti, A.; De Caro, R. Neurotensin receptor 1 immunoreactivity in the peripheral ganglia and carotid body. *Eur. J. Histochem.* **2009**, *53*, e16.
47. Coppola, T.; Beraud-Dufour, S.; Antoine, A.; Vincent, J. P.; Mazella, J. Neurotensin protects pancreatic beta cells from apoptosis. *Int. J. Biochem. Cell Biol.* **2008**, *40*, 2296-2302.
48. Beraud-Dufour, S.; Coppola, T.; Massa, F.; Mazella, J. Neurotensin receptor-2 and -3 are crucial for the anti-apoptotic effect of neurotensin on pancreatic beta-TC3 cells. *Int. J. Biochem. Cell Biol.* **2009**, *41*, 2398-2402.
49. Azriel, Y.; Burcher, E. Characterization and autoradiographic localization of neurotensin binding sites in human sigmoid colon. *J. Pharmacol. Exp. Ther.* **2001**, *297*, 1074-1081.
50. Gilliam-Vigh, H.; Jorsal, T.; Nielsen, S. W.; Forman, J. L.; Pedersen, J.; Poulsen, S. S.; Vilsboll, T.; Knop, F. K. Expression of neurotensin and its receptors along the intestinal tract in type 2 diabetes patients and healthy controls. *J. Clin. Endocrinol. Metab.* **2023**, *108*, 2211-2216.
51. Reubi, J. C.; Waser, B.; Friess, H.; Buchler, M.; Laissue, J. Neurotensin receptors: A new marker for human ductal pancreatic adenocarcinoma. *Gut* **1998**, *42*, 546-550.
52. Reubi, J. C.; Waser, B.; Schaer, J. C.; Laissue, J. A. Neurotensin receptors in human neoplasms: High incidence in Ewing's sarcomas. *Int. J. Cancer* **1999**, *82*, 213-218.
53. Wu, Z.; Martinez-Fong, D.; Tredaniel, J.; Forgez, P. Neurotensin and its high affinity receptor 1 as a potential pharmacological target in cancer therapy. *Front. Endocrinol.* **2012**, *3*, 184.
54. Yin, X.; Wang, M.; Wang, H.; Deng, H.; He, T.; Tan, Y.; Zhu, Z.; Wu, Z.; Hu, S.; Li, Z. Evaluation of neurotensin receptor 1 as a potential imaging target in pancreatic ductal adenocarcinoma. *Amino Acids* **2017**, *49*, 1325-1335.
55. He, T.; Wang, M.; Wang, H.; Tan, H.; Tang, Y.; Smith, E.; Wu, Z.; Liao, W.; Hu, S.; Li, Z. Evaluation of neurotensin receptor 1 as potential biomarker for prostate cancer theranostic use. *Eur. J. Nucl. Med. Mol. Imaging* **2019**, *46*, 2199-2207.
56. Morgat, C.; Brouste, V.; Chastel, A.; Velasco, V.; Macgrogan, G.; Hindie, E. Expression of neurotensin receptor-1 (NTS(1)) in primary breast tumors, cellular distribution, and

association with clinical and biological factors. *Breast Cancer Res. Treat.* **2021**, *190*, 403-413.

57. Szarynska, M.; Olejniczak-Keder, A.; Podplonska, K.; Prahl, A.; Ilowska, E. Bradykinin and neurotensin analogues as potential compounds in colon cancer therapy. *Int. J. Mol. Sci.* **2023**, *24*.
58. Pan, M.; Chen, Q.; Yao, S. Recent advances in small molecular PET tracers for pancreatic cancer diagnosis: Preclinical stage. *Mini-Rev. Med. Chem.* **2025**, *25*, 745-759.
59. Sarret, P.; Beaudet, A.; Vincent, J. P.; Mazella, J. Regional and cellular distribution of low affinity neurotensin receptor mRNA in adult and developing mouse brain. *J. Comp. Neurol.* **1998**, *394*, 344-356.
60. Nouel, D.; Sarret, P.; Vincent, J. P.; Mazella, J.; Beaudet, A. Pharmacological, molecular and functional characterization of glial neurotensin receptors. *Neuroscience* **1999**, *94*, 1189-1197.
61. Asselin, M. L.; Dubuc, I.; Coquerel, A.; Costentin, J. Localization of neurotensin NTS2 receptors in rat brain, using [3H]levocabastine. *NeuroReport* **2001**, *12*, 1087-1091.
62. Sarret, P.; Krzywkowski, P.; Segal, L.; Nielsen, M. S.; Petersen, C. M.; Mazella, J.; Stroh, T.; Beaudet, A. Distribution of NTS3 receptor/sortilin mRNA and protein in the rat central nervous system. *J. Comp. Neurol.* **2003**, *461*, 483-505.
63. Sarret, P.; Perron, A.; Stroh, T.; Beaudet, A. Immunohistochemical distribution of NTS2 neurotensin receptors in the rat central nervous system. *J. Comp. Neurol.* **2003**, *461*, 520-538.
64. Sarret, P.; Esdaile, M. J.; Perron, A.; Martinez, J.; Stroh, T.; Beaudet, A. Potent spinal analgesia elicited through stimulation of NTS2 neurotensin receptors. *J. Neurosci.* **2005**, *25*, 8188-8196.
65. Mazella, J.; Vincent, J. P. Functional roles of the NTS2 and NTS3 receptors. *Peptides* **2006**, *27*, 2469-2475.
66. Béraud-Dufour, S.; Abderrahmani, A.; Noel, J.; Brau, F.; Waeber, G.; Mazella, J.; Coppola, T. Neurotensin is a regulator of insulin secretion in pancreatic beta-cells. *Int. J. Biochem. Cell Biol.* **2010**, *42*, 1681-1688.
67. Schulz, S.; Rocken, C.; Ebert, M. P.; Schulz, S. Immunocytochemical identification of low-affinity NTS2 neurotensin receptors in parietal cells of human gastric mucosa. *J. Endocrinol.* **2006**, *191*, 121-128.

68. Swift, S. L.; Burns, J. E.; Maitland, N. J. Altered expression of neurotensin receptors is associated with the differentiation state of prostate cancer. *Cancer Res.* **2010**, *70*, 347-356.
69. Saada, S.; Marget, P.; Fauchais, A. L.; Lise, M. C.; Chemin, G.; Sindou, P.; Martel, C.; Delpy, L.; Vidal, E.; Jaccard, A.; Troutaud, D.; Lalloué, F.; Jauberteau, M. O. Differential expression of neurotensin and specific receptors, NTSR1 and NTSR2, in normal and malignant human B lymphocytes. *J. Immunol.* **2012**, *189*, 5293-5303.
70. Abbaci, A.; Talbot, H.; Saada, S.; Gachard, N.; Abraham, J.; Jaccard, A.; Bordessoule, D.; Fauchais, A. L.; Naves, T.; Jauberteau, M. O. Neurotensin receptor type 2 protects B-cell chronic lymphocytic leukemia cells from apoptosis. *Oncogene* **2018**, *37*, 756-767.
71. Petersen, C. M.; Nielsen, M. S.; Nykjaer, A.; Jacobsen, L.; Tommerup, N.; Rasmussen, H. H.; Roigaard, H.; Gliemann, J.; Madsen, P.; Moestrup, S. K. Molecular identification of a novel candidate sorting receptor purified from human brain by receptor-associated protein affinity chromatography. *J. Biol. Chem.* **1997**, *272*, 3599-3605.
72. Kyriatzis, G.; Khrestchatisky, M.; Ferhat, L.; Chatzaki, E. A. Neurotensin and neurotensin receptors in stress-related disorders: Pathophysiology & novel drug targets. *Curr. Neuropharmacol.* **2024**, *22*, 916-934.
73. Morris, N. J.; Ross, S. A.; Lane, W. S.; Moestrup, S. K.; Petersen, C. M.; Keller, S. R.; Lienhard, G. E. Sortilin is the major 110-kDa protein in GLUT4 vesicles from adipocytes. *J. Biol. Chem.* **1998**, *273*, 3582-3587.
74. Nielsen, M. S.; Jacobsen, C.; Olivecrona, G.; Gliemann, J.; Petersen, C. M. Sortilin/neurotensin receptor-3 binds and mediates degradation of lipoprotein lipase. *J. Biol. Chem.* **1999**, *274*, 8832-8836.
75. Osadchii, O. E. Emerging role of neurotensin in regulation of the cardiovascular system. *Eur. J. Pharmacol.* **2015**, *762*, 184-192.
76. Arbogast, P.; Gauchotte, G.; Mougel, R.; Morel, O.; Ziyyat, A.; Agopiantz, M. Neurotensin and its involvement in reproductive functions: An exhaustive review of the literature. *Int. J. Mol. Sci.* **2023**, *24*.
77. Hemmati, S.; Zarnani, A. H.; Mahmoudi, A. R.; Sadeghi, M. R.; Soltanghoraee, H.; Akhondi, M. M.; Tarahomi, M.; Jeddi-Tehrani, M.; Rabbani, H. Ectopic expression of sortilin 1 (NTR-3) in patients with ovarian carcinoma. *Avicenna J. Med. Biotechnol.* **2009**, *1*, 125-131.
78. Roselli, S.; Pundavela, J.; Demont, Y.; Faulkner, S.; Keene, S.; Attia, J.; Jiang, C. C.; Zhang, X. D.; Walker, M. M.; Hondermarck, H. Sortilin is associated with breast cancer

aggressiveness and contributes to tumor cell adhesion and invasion. *OncoTargets Ther.* **2015**, *6*, 10473-10486.

79. Kim, J. T.; Napier, D. L.; Weiss, H. L.; Lee, E. Y.; Townsend, C. M., Jr.; Evers, B. M. Neurotensin receptor 3/sortilin contributes to tumorigenesis of neuroendocrine tumors through augmentation of cell adhesion and migration. *Neoplasia* **2018**, *20*, 175-181.
80. Nikolaou, S.; Qiu, S.; Fiorentino, F.; Simillis, C.; Rasheed, S.; Tekkis, P.; Kontovounisios, C. The role of neurotensin and its receptors in non-gastrointestinal cancers: A review. *Cell Commun. Signaling* **2020**, *18*, 68.
81. Hertz, S.; Roberts, A. Radioactive iodine in the study of thyroid physiology; The use of radioactive iodine therapy in hyperthyroidism. *JAMA, J. Am. Med. Assoc.* **1946**, *131*, 81-86.
82. Ehrhardt, J. D., Jr.; Gulec, S. A review of the history of radioactive iodine theranostics: The origin of nuclear ontology. *Mol. Imaging Radionucl. Ther.* **2020**, *29*, 88-97.
83. Elgee, N. J.; Williams, R. H.; Lee, N. D.; Wong, T.; Hogness, J. R. Studies of radioactive insulin. *Diabetes* **1953**, *2*, 370-371.
84. Axelrod, J.; Tomchick, R. Activation and inhibition of adrenaline metabolism. *Nature* **1959**, *184(Suppl 26)*, 2027.
85. Hertting, G.; Axelrod, J.; Whitby, L. G. Effect of drugs on the uptake and metabolism of H3-norepinephrine. *J. Pharmacol. Exp. Ther.* **1961**, *134*, 146-153.
86. Khairallah, P. A.; Page, I. H.; Bumpus, F. M.; Smeby, R. R. Angiotensin II: Its metabolic fate. *Science* **1962**, *138*, 523-525.
87. Demetriou, J. A.; Crowley, L. G.; Kushinsky, S.; Donovan, A. J.; Kotin, P.; Macdonald, I. Radioactive estrogens in tissues of postmenopausal women with breast neoplasms. *Cancer Res.* **1964**, *24*, 926-934.
88. Pert, C. B.; Snyder, S. H. Opiate receptor: Demonstration in nervous tissue. *Science* **1973**, *179*, 1011-1014.
89. Seeman, P.; Chau-Wong, M.; Tedesco, J.; Wong, K. Brain receptors for antipsychotic drugs and dopamine: Direct binding assays. *Proc. Natl. Acad. Sci. U. S. A.* **1975**, *72*, 4376-4380.
90. List, S. J.; Seeman, P. Resolution of dopamine and serotonin receptor components of [3H]spiperone binding to rat brain regions. *Proc. Natl. Acad. Sci. U. S. A.* **1981**, *78*, 2620-2624.
91. Pazos, A.; Palacios, J. M. Quantitative autoradiographic mapping of serotonin receptors in the rat brain. I. Serotonin-1 receptors. *Brain Res.* **1985**, *346*, 205-230.

92. Pazos, A.; Cortes, R.; Palacios, J. M. Quantitative autoradiographic mapping of serotonin receptors in the rat brain. II. Serotonin-2 receptors. *Brain Res.* **1985**, *346*, 231-249.
93. Seeman, M. V. Philip Seeman's contributions to the story of schizophrenia. *Psychol. Med.* **2022**, *52*, 2401-2403.
94. Carraway, R.; Leeman, S. E. The isolation of a new hypotensive peptide, neurotensin, from bovine hypothalami. *J. Biol. Chem.* **1973**, *248*, 6854-6861.
95. Kitabgi, P.; Carraway, R.; Van Rietschoten, J.; Granier, C.; Morgat, J. L.; Menez, A.; Leeman, S.; Freychet, P. Neurotensin: Specific binding to synaptic membranes from rat brain. *Proc. Natl. Acad. Sci. U. S. A.* **1977**, *74*, 1846-1850.
96. Uhl, G. R.; Bennett, J. P., Jr.; Snyder, S. H. Neurotensin, a central nervous system peptide: Apparent receptor binding in brain membranes. *Brain Res.* **1977**, *130*, 299-313.
97. Lazarus, L. H.; Brown, M. R.; Perrin, M. H. Distribution, localization and characteristics of neurotensin binding sites in the rat brain. *Neuropharmacology* **1977**, *16*, 625-629.
98. Sadoul, J. L.; Mazella, J.; Amar, S.; Kitabgi, P.; Vincent, J. P. Preparation of neurotensin selectively iodinated on the tyrosine 3 residue. Biological activity and binding properties on mammalian neurotensin receptors. *Biochem. Biophys. Res. Commun.* **1984**, *120*, 812-819.
99. Kanba, K. S.; Kanba, S.; Nelson, A.; Okazaki, H.; Richelson, E. [3H]Neurotensin(8-13) binds in human brain to the same sites as does [3H]neurotensin but with higher affinity. *J. Neurochem.* **1988**, *50*, 131-137.
100. Labbe-Jullie, C.; Botto, J. M.; Mas, M. V.; Chabry, J.; Mazella, J.; Vincent, J. P.; Gully, D.; Maffrand, J. P.; Kitabgi, P. [3H]SR 48692, the first nonpeptide neurotensin antagonist radioligand: characterization of binding properties and evidence for distinct agonist and antagonist binding domains on the rat neurotensin receptor. *Mol. Pharmacol.* **1995**, *47*, 1050-1056.
101. Betancur, C.; Canton, M.; Burgos, A.; Labeeuw, B.; Gully, D.; Rostene, W.; Pelaprat, D. Characterization of binding sites of a new neurotensin receptor antagonist, [3H]SR 142948A, in the rat brain. *Eur. J. Pharmacol.* **1998**, *343*, 67-77.
102. Betancur, C.; Canton, M.; Gully, D.; Vela, G.; Pelaprat, D.; Rostene, W. Characterization and distribution of binding sites for a new neurotensin receptor antagonist ligand, [3H]SR 48692, in the guinea pig brain. *J. Pharmacol. Exp. Ther.* **1995**, *273*, 1450-1458.
103. Flanagan, C. A. GPCR-radioligand binding assays. *Methods Cell Biol.* **2016**, *132*, 191-215.

104. Maguire, J. J.; Kuc, R. E.; Davenport, A. P. Radioligand binding assays and their analysis. *Methods Mol. Biol.* **2012**, *897*, 31-77.
105. Coons, A. H.; Creech, H. J.; Jones, R. N.; Berliner, E. The demonstration of pneumococcal antigen in tissues by the use of fluorescent antibody. *J. Immunol.* **1942**, *45*, 159-170.
106. Anderson, M. J.; Cohen, M. W. Fluorescent staining of acetylcholine receptors in vertebrate skeletal muscle. *J. Physiol.* **1974**, *237*, 385-400.
107. McGrath, J. C.; Arribas, S.; Daly, C. J. Fluorescent ligands for the study of receptors. *Trends Pharmacol. Sci.* **1996**, *17*, 393-399.
108. Melamed, E.; Lahav, M.; Atlas, D. Direct localisation of beta-adrenoceptor sites in rat cerebellum by a new fluorescent analogue of propranolol. *Nature* **1976**, *261*, 420-422.
109. Atlas, D.; Melamed, E. Direct mapping of beta-adrenergic receptors in the rat central nervous system by a novel fluorescent beta-blocker. *Brain Res.* **1978**, *150*, 377-385.
110. Hazum, E.; Chang, K. J.; Cuatrecasas, P. Role of disulphide and sulphydryl groups in clustering of enkephalin receptors in neuroblastoma cells. *Nature* **1979**, *282*, 626-628.
111. Hazum, E.; Chang, K. J.; Cuatrecasas, P. Cluster formation of opiate (enkephalin) receptors in neuroblastoma cells: Differences between agonists and antagonists and possible relationships to biological functions. *Proc. Natl. Acad. Sci. U. S. A.* **1980**, *77*, 3038-3041.
112. Petty, H. R.; Francis, J. W. Polymorphonuclear leukocyte histamine receptors: Occurrence in cell surface clusters and their redistribution during locomotion. *Proc. Natl. Acad. Sci. U. S. A.* **1986**, *83*, 4332-4335.
113. Faure, M. P.; Gaudreau, P.; Shaw, I.; Cashman, N. R.; Beaudet, A. Synthesis of a biologically active fluorescent probe for labeling neurotensin receptors. *J. Histochem. Cytochem.* **1994**, *42*, 755-763.
114. Vogt, H.; Shinkwin, P.; Huber, M. E.; Staffen, N.; Hubner, H.; Gmeiner, P.; Schiedel, M.; Weikert, D. Development of a fluorescent ligand for the intracellular allosteric binding site of the neurotensin receptor 1. *ACS Pharmacol. Transl. Sci.* **2024**, *7*, 1533-1545.
115. Baeyer, A. Ueber eine neue Klasse von Farbstoffen. *Berichte der deutschen chemischen Gesellschaft zu Berlin* **1871**, *4*, 555-558.
116. Benson, R. C.; Meyer, R. A.; Zaruba, M. E.; McKhann, G. M. Cellular autofluorescence--is it due to flavins? *J. Histochem. Cytochem.* **1979**, *27*, 44-48.

117. Monici, M. Cell and tissue autofluorescence research and diagnostic applications. *Biotechnol. Annu. Rev.* **2005**, *11*, 227-256.
118. Jameson, D. M.; Ross, J. A. Fluorescence polarization/anisotropy in diagnostics and imaging. *Chem. Rev.* **2010**, *110*, 2685-2708.
119. Zhang, H.; Wu, Q.; Berezin, M. Y. Fluorescence anisotropy (polarization): From drug screening to precision medicine. *Expert Opin. Drug Discovery* **2015**, *10*, 1145-1161.
120. Rinken, A.; Lavogina, D.; Kopanchuk, S. Assays with detection of fluorescence anisotropy: Challenges and possibilities for characterizing ligand binding to GPCRs. *Trends Pharmacol. Sci.* **2018**, *39*, 187-199.
121. Hammer, M.; Schweitzer, D.; Richter, S.; Königsdörffer, E. Sodium fluorescein as a retinal pH indicator? *Physiol. Meas.* **2005**, *26*, N9-N12.
122. Archipowa, N.; Wittmann, L.; Kockenberger, J.; Ertl, F. J.; Gleixner, J.; Keller, M.; Heinrich, M. R.; Kutta, R. J. Characterization of fluorescent dyes frequently used for bioimaging: Photophysics and photocatalytical reactions with proteins. *J. Phys. Chem. B* **2023**, *127*, 9532-9542.
123. Sanborn, M. E.; Connolly, B. K.; Gurunathan, K.; Levitus, M. Fluorescence properties and photophysics of the sulfoindocyanine Cy3 linked covalently to DNA. *J. Phys. Chem. B* **2007**, *111*, 11064-11074.
124. Helmerich, D. A.; Beliu, G.; Matikonda, S. S.; Schnermann, M. J.; Sauer, M. Photoblueing of organic dyes can cause artifacts in super-resolution microscopy. *Nat. Methods* **2021**, *18*, 253-257.
125. Sandberg, E.; Piguet, J.; Kostiv, U.; Baryshnikov, G.; Liu, H.; Widengren, J. Photoisomerization of heptamethine cyanine dyes results in red-emissive species: Implications for near-IR, single-molecule, and super-resolution fluorescence spectroscopy and imaging. *J. Phys. Chem. B* **2023**, *127*, 3208-3222.
126. Hinkeldey, B.; Schmitt, A.; Jung, G. Comparative photostability studies of BODIPY and fluorescein dyes by using fluorescence correlation spectroscopy. *ChemPhysChem* **2008**, *9*, 2019-2027.
127. Buschmann, V.; Weston, K. D.; Sauer, M. Spectroscopic study and evaluation of red-absorbing fluorescent dyes. *Bioconjugate Chem.* **2003**, *14*, 195-204.
128. Orsini, F.; Guidoccio, F.; Mariani, G. Radiopharmaceuticals for therapy. In *Nuclear medicine textbook*, Volterrani, D., Ed. Springer Nature: Switzerland, 2019; pp 99-116.
129. Lepareur, N.; Ramee, B.; Mougin-Degraef, M.; Bourgeois, M. Clinical advances and perspectives in targeted radionuclide therapy. *Pharmaceutics* **2023**, *15*.

130. Zhang, S. Q.; Wang, X. K.; Gao, X.; Chen, X. Y.; Li, L. E.; Li, G. Q.; Liu, C.; Miao, Y.; Wang, R.; Hu, K. Radiopharmaceuticals and their applications in medicine. *Signal Transduct. Tar.* **2025**, *10*.
131. Povoski, S. P.; Neff, R. L.; Mojzisik, C. M.; O'Malley, D. M.; Hinkle, G. H.; Hall, N. C.; Murrey, D. A., Jr.; Knopp, M. V.; Martin, E. W., Jr. A comprehensive overview of radioguided surgery using gamma detection probe technology. *World J. Surg. Oncol.* **2009**, *7*, 11.
132. Fragoso Costa, P.; Shi, K.; Holm, S.; Vidal-Sicart, S.; Kracmerova, T.; Tosi, G.; Grimm, J.; Visvikis, D.; Knapp, W. H.; Gnanasegaran, G.; van Leeuwen, F. W. B. Surgical radioguidance with beta-emitting radionuclides; challenges and possibilities: A position paper by the EANM. *Eur. J. Nucl. Med. Mol. Imaging* **2024**, *51*, 2903-2921.
133. Van Oosterom, M. N.; Rietbergen, D. D. D.; Welling, M. M.; Van Der Poel, H. G.; Maurer, T.; Van Leeuwen, F. W. B. Recent advances in nuclear and hybrid detection modalities for image-guided surgery. *Expert Rev. Med. Devices* **2019**, *16*, 711-734.
134. Van Laere, C.; Koole, M.; Deroose, C. M.; de Voorde, M. V.; Baete, K.; Cocolios, T. E.; Duchemin, C.; Ooms, M.; Cleeren, F. Terbium radionuclides for theranostic applications in nuclear medicine: from atom to bedside. *Theranostics* **2024**, *14*, 1720-1743.
135. Maschauer, S.; Prante, O. Radiopharmaceuticals for imaging and endoradiotherapy of neurotensin receptor-positive tumors. *J. Labelled Compd. Radiopharm.* **2018**, *61*, 309-325.
136. Bruehlmeier, M.; Garayoa, E. G.; Blanc, A.; Holzer, B.; Gergely, S.; Tourwe, D.; Schubiger, P. A.; Blauenstein, P. Stabilization of neurotensin analogues: Effect on peptide catabolism, biodistribution and tumor binding. *Nucl. Med. Biol.* **2002**, *29*, 321-327.
137. Buchegger, F.; Bonvin, F.; Kosinski, M.; Schaffland, A. O.; Prior, J.; Reubi, J. C.; Blauenstein, P.; Tourwe, D.; Garcia Garayoa, E.; Bischof Delaloye, A. Radiolabeled neurotensin analog, 99mTc-NT-XI, evaluated in ductal pancreatic adenocarcinoma patients. *J. Nucl. Med.* **2003**, *44*, 1649-1654.
138. Baum, R. P.; Singh, A.; Schuchardt, C.; Kulkarni, H. R.; Klette, I.; Wiessalla, S.; Osterkamp, F.; Reineke, U.; Smerling, C. (177)Lu-3BP-227 for neurotensin receptor 1-targeted therapy of metastatic pancreatic adenocarcinoma: First clinical results. *J. Nucl. Med.* **2018**, *59*, 809-814.
139. Osterkamp, F.; Smerling, C.; Reineke, U.; Haase, C.; Ungewiss, J. Neurotensin receptor ligands. WO2014/086499, 2012; 3B Pharmaceuticals GmbH.

140. Schindler, L.; Moosbauer, J.; Schmidt, D.; Spruss, T.; Gratz, L.; Ludeke, S.; Hofheinz, F.; Meister, S.; Echtenacher, B.; Bernhardt, G.; Pietzsch, J.; Hellwig, D.; Keller, M. Development of a neurotensin-derived (68)Ga-labeled PET ligand with high in vivo stability for imaging of NTS(1) receptor-expressing tumors. *Cancers (Basel)* **2022**, *14*.
141. Deng, H.; Wang, H.; Wang, M.; Li, Z.; Wu, Z. Synthesis and evaluation of 64Cu-DOTA-NT-Cy5.5 as a dual-modality PET/fluorescence probe to image neurotensin receptor-positive tumor. *Mol. Pharmacol.* **2015**, *12*, 3054-3061.
142. Fanelli, R.; Besserer-Offroy, E.; Rene, A.; Cote, J.; Tetreault, P.; Collerette-Tremblay, J.; Longpre, J. M.; Leduc, R.; Martinez, J.; Sarret, P.; Cavelier, F. Synthesis and characterization in vitro and in vivo of (l)-(trimethylsilyl)alanine containing neurotensin analogues. *J. Med. Chem.* **2015**, *58*, 7785-7795.
143. Konieczny, A.; Conrad, M.; Ertl, F. J.; Gleixner, J.; Gattor, A. O.; Gratz, L.; Schmidt, M. F.; Neu, E.; Horn, A. H. C.; Wifling, D.; Gmeiner, P.; Clark, T.; Sticht, H.; Keller, M. N-Terminus to arginine side-chain cyclization of linear peptidic neuropeptide Y Y(4) receptor ligands results in picomolar binding constants. *J. Med. Chem.* **2021**, *64*, 16746-16769.

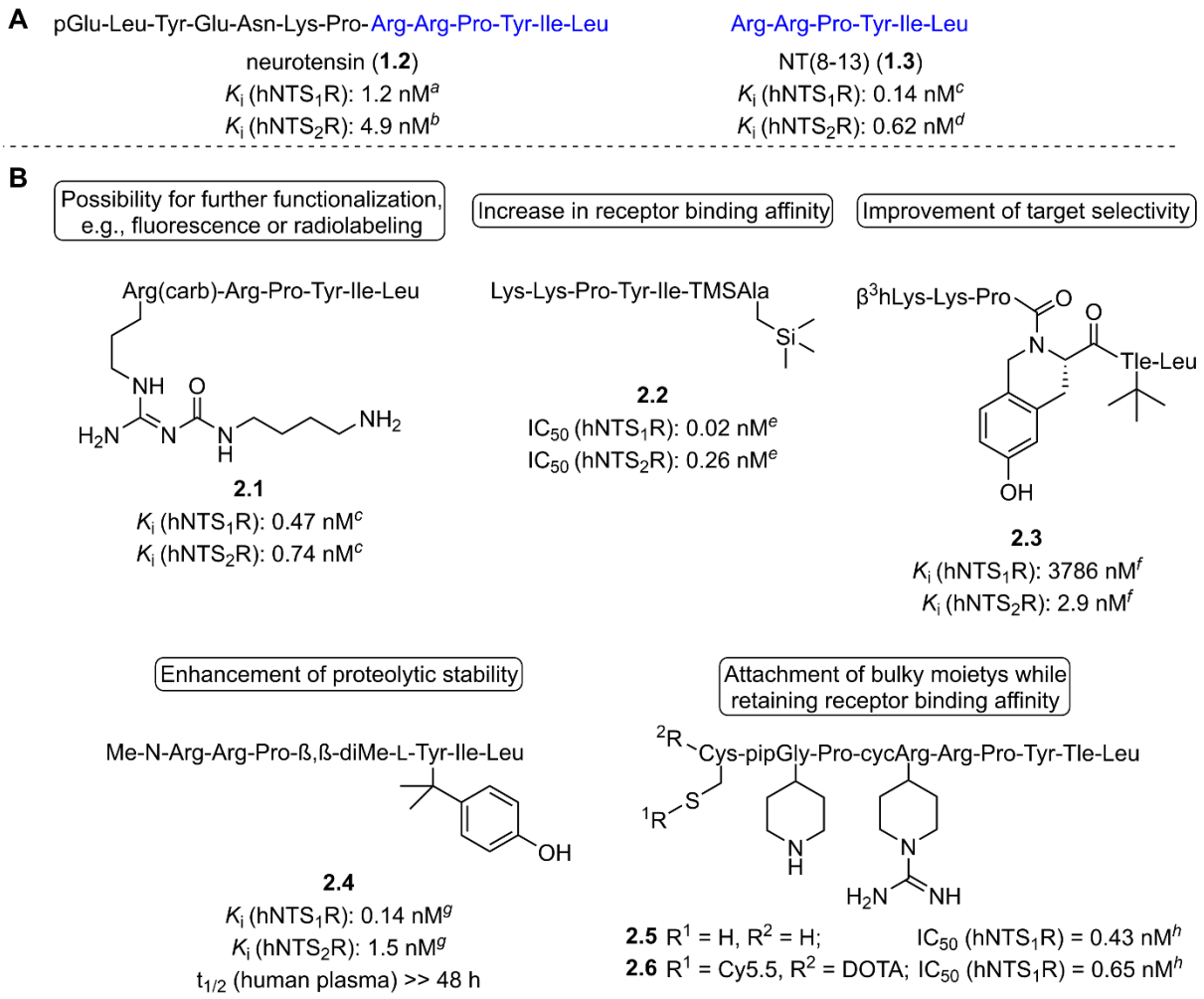
Chapter 2

Peptidic NTS_1R ligands containing cyclic basic amino acids

2.1 Introduction

Over the past few decades, therapeutics based on proteins and peptides have gained increasing importance. However, utilizing these molecules in their natural sequences is limited as they are often prone to enzymatic degradation, resulting in short half-lives. A key strategy to overcome this challenge is the replacement of natural amino acids by unnatural surrogates. Besides an improvement of proteolytic stability, these structural modifications may also result in increased target affinity and selectivity, improved cellular uptake, may even enable a penetration across the blood-brain barrier, and can provide the possibility of functionalization.[1-15] In most cases, unnatural amino acids must act as a bioisosteric replacement, since otherwise important interactions with the target are weakened or even get lost, leading to decreased affinities or activities. For example, alkaline amino acids such as arginine or lysine often form salt bridges between their positively charged side chains and negatively charged residues of the target. Accordingly, a bioisostere of the arginine or lysine side chain should enable the formation of a salt bridge in the same position.

The neurotensin receptors type 1 (NTS_1R) and type 2 (NTS_2R), which belong to class A of G-protein coupled receptors (GPCRs) and represent potential therapeutic targets, are endogenously activated by the 13 amino acid peptide neurotensin (**1.2**). The truncated C-terminal hexapeptide NT(8-13) (**1.3**) still exhibits high binding affinity and activity (Figure 2.1A). To date, various efforts have been made to modify or improve certain properties of peptidic NTS_1R ligands through the incorporation of unnatural amino acids in NT(8-13)-derived analogs (examples shown in Figure 2.1B). This led to compounds with a functionality for peptide conjugation (e.g., to obtain radio- or fluorescent ligands) (**2.1**), markedly higher receptor binding affinity (**2.2**), improved NTS_2R selectivity (**2.3**), and enhanced proteolytic stability (**2.4**).



Arg(carb) = N^{ω}-carbamoylated arginine
TMSAla = (trimethylsilyl)alanine
β^3hLys = β^3-homolysine
Tle = α-*tert*-butylglycine
pipGly = piperidinylglycine
cycArg = (1-amidinopyridinyl)glycine
ß,ß-diMe-L-Tyr = ß,ß-dimethyl-L-tyrosine
DOTA = 1,4,7,10-tetraazacyclododecane-1,4,7,10-tetraacetic acid

Figure 2.1. (A) Peptide sequences and NTS_1R and NTS_2R binding affinities of the endogenous ligand neurotensin (**1.2**) and the hexapeptide NT(8-13) (**1.3**). (B) Reported peptidic NTS_1R and/or NTS_2R ligands containing unnatural amino acids to alter certain properties. [a]Granier *et al.*[16] [b]Einsiedel *et al.*[17] [c]Keller *et al.*[6] [d]Ertl *et al.*[18] [e]Fanelli *et al.*[4] [f]Eiselt *et al.*[19] [g]Schindler *et al.*[20] [h]Deng *et al.*[5]

Since one of the main perspectives of this work was the development of dually labelled (tritium and fluorescence) NTS_1R ligands, which can be studied in both radiochemical and fluorescence-based assays, the bifunctional peptide **2.6** developed by Deng and coworkers was of particular interest. Peptide **2.6**, bearing a fluorescent dye (Cy5.5) and a chelator (DOTA), both representing bulky moieties that often impair receptor binding, shows almost the same NTS_1R binding affinity as its non-conjugated precursor **2.5** (Figure 2.1B).[5] To what extent this phenomenon can be attributed to the presence of a cyclic arginine derivative (in Figure 2.1

referred to as "cycArg") in position 8 is not discussed by Deng and coauthors.[5] Amino acid variations in positions < 8 most likely have little impact on NTS_1R binding because the receptor binding pocket is occupied by the NT(8-13)-sequence in neurotensin.[21-23]

Therefore, aiming for precursors for the synthesis of dually labeled NT(8-13) derivatives, which are structurally similar to **2.6**, the cyclic arginine derivative 'cycArg' was synthesized and incorporated in place of Arg^8 or Arg^9 into NT(8-13)-derived peptides. The NTS_1R binding affinities of these peptides were determined in a radioligand competition binding assay.

Moreover, a pyrrolidine-type β-amino acid (Gp-βAPCA) with a basic side chain (guanidinopropyl) (synthesized in the group of Prof. Dr. Oliver Reiser, Institute of Organic Chemistry, University of Regensburg) was incorporated instead of Arg^8 or Arg^9 in **1.3** and the resulting derivatives were investigated with respect to NTS_1R and NTS_2R binding, NTS_1R agonism, and proteolytic stability. Note that the NT(8-13) analogs obtained by incorporation of Gp-βAPCA (two peptides) are discussed first in the following.

2.2 Results and discussion

2.2.1 Synthesis of cyclic amino acid derivatives

The unnatural cyclic amino acid (*S*,*S*)-**2.7** represents a pyrrolidine-type β-amino acid, whereas compound (*S*)-**2.8** features a piperidine-type α-amino acid (Figure 2.2). Both derivatives possess a basic guanidinium group and can therefore serve as bioisosteric replacements for natural arginine. (*S*,*S*)-**2.7** and (*S*)-**2.8** represent the protected forms useful for solid-phase peptide synthesis (SPPS) (Fmoc strategy). The enantioselective synthesis of (*S*,*S*)-**2.7** was performed by Dr. Eva Plut.[24]

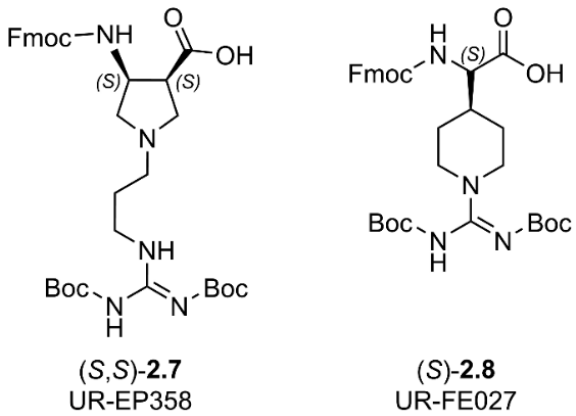


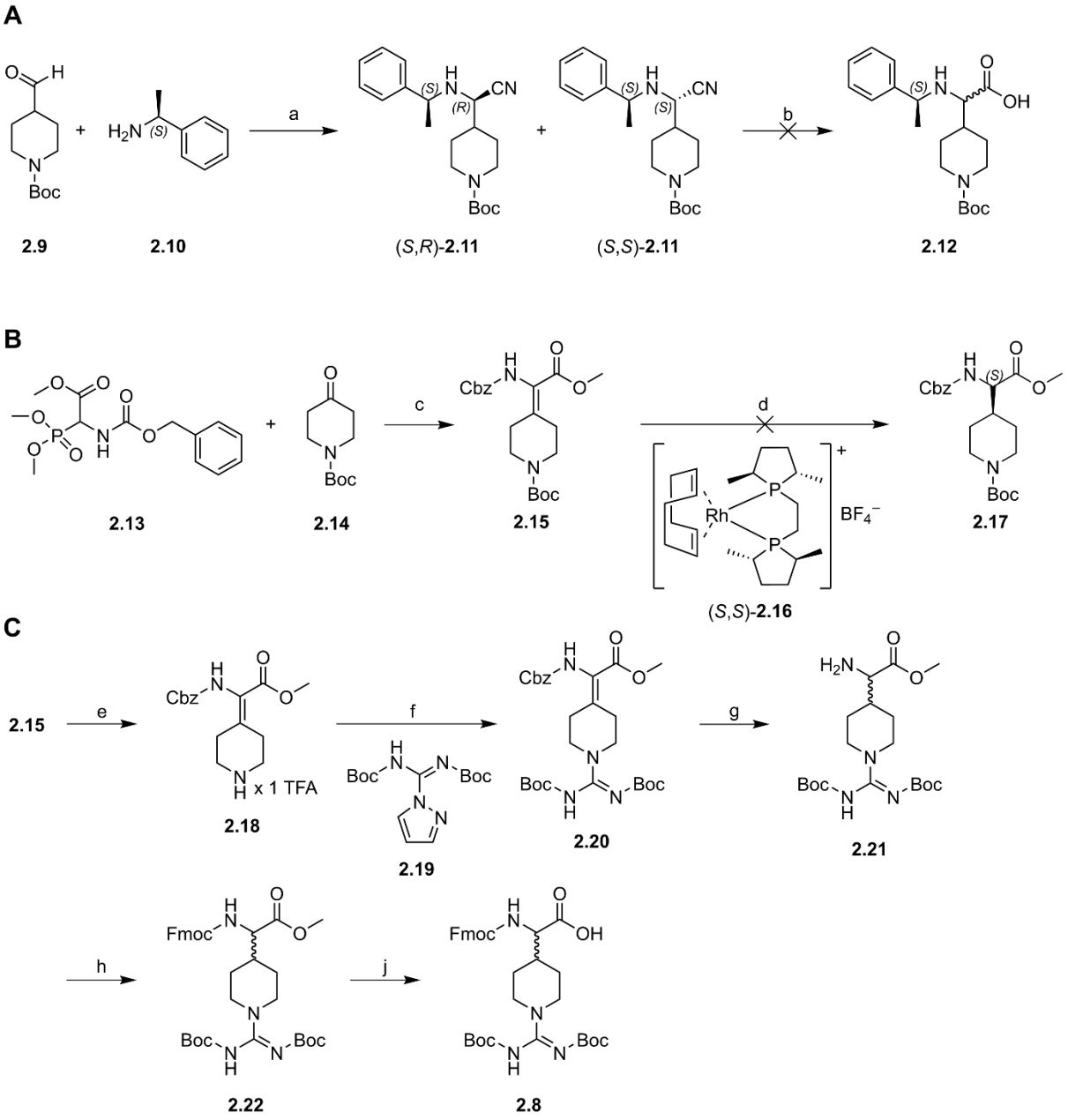
Figure 2.2. Structures of the unnatural cyclic amino acids (*S*,*S*)-**2.7** (UR-EP358) and (*S*)-**2.8** (UR-FE027).

Since the incorporation of D-amino acids in **1.3** results in a decrease in binding affinity,[25] enantiopure L-configured **2.8** ((*S*)-**2.8**) was favored for the synthesis of NT(8-13) derivatives containing the cyclic unnatural amino acid derived from **2.8**. To obtain enantiopure (*S*)-**2.8**, two reported approaches for an asymmetric syntheses of (*S*)-**2.8** were followed. The first approach was based on a Strecker synthesis exploiting the use of enantiopure (*S*)-1-phenylethylamine (**2.10**), which yielded two diastereomeric nitriles, (*S*,*R*)-**2.11** and (*S*,*S*)-**2.11** (Scheme 2.1A).[26] Analytical RP-HPLC revealed a marked difference in retention times and a diastereomeric ratio of approximately 30:70 (Figure 2.3), hence, a separation of (*S*,*R*)-**2.11** and (*S*,*S*)-**2.11** was conveniently feasible by automated reversed-phase flash chromatography (120 g C18 silica cartridge) using the pumps and detector of a preparative HPLC system (note: the cartridge could be loaded with up to 300 mg per run). Since an assignment of the absolute configuration was not carried out, the isolated diastereomers are referred to as **2.11a** and **2.11b**, where **2.11a** represents the diastereomer with the lower retention time when analyzed by RP-HPLC.

To preserve the acid-labile Boc-protecting group at the piperidine nitrogen, an alkaline hydrolysis of the nitrile to the carboxylic acid (**2.12**) was chosen. According to reported procedures, conversion of similar nitriles was accomplished using highly concentrated sodium hydroxide solutions und elevated temperature or reflux conditions in a mixture of H_2O and protic or aprotic solvents (MeOH, EtOH, 2-propanol, THF, or dioxane).[27-29] Several attempts using the aforementioned conditions and solvents failed as no product formation was observed (in some cases, the hydrolysis stopped at the amide stage). As this approach was not further pursued, efforts to determine the absolute configuration of **2.11a** and **2.11b** were not undertaken. Acidic hydrolysis of the nitrile using strong acids in high concentrations was not considered as this would result in a cleavage of the Boc-group and potentially also the 1-phenylethyl group of the molecule.[26]

In a second strategy, a reported Horner-Wadsworth-Emmons reaction using methyl 2-(((benzyloxy)carbonyl)amino)-2-(dimethoxyphosphoryl)acetate (**2.13**) and the ketone *tert*-butyl 4-oxopiperidine-1-carboxylate (**2.14**) was applied (Scheme 2.1B).[30] The product **2.15**, an α,β-unsaturated methyl carboxylate, was selectively precipitated by treatment with light petroleum/ethyl acetate 5:1 v/v resulting in pure **2.15**. The next step was an asymmetric hydrogenation using a chiral catalyst. Since Monovich and coworkers obtained the (*R*)-configured compound (*R*)-**2.17** when using (*R*,*R*)-Me-BPE-Rh ((*R*,*R*)-**2.16**) as a catalyst, it was assumed that a reduction in the presence of (*S*,*S*)-Me-BPE-Rh ((*S*,*S*)-**2.16**) would yield (*S*)-**2.17**.

Scheme 2.1. Different approaches for the synthesis of the cyclic arginine derivative (*S*)-**2.8**.



(A) Approach 1: asymmetric Strecker synthesis followed by separating the diastereomers and hydrolysis of the nitrile. (B) Approach 2: Horner-Wadsworth-Emmons reaction followed by asymmetric reduction using a chiral rhodium catalyst. (C) Approach 3: Horner-Wadsworth-Emmons reaction followed by guanidinylation, non-asymmetric reduction, Fmoc protection and hydrolysis of the methyl ester. Reagents and conditions: (a) potassium cyanide, H_2O/MeOH 1:1 v/v, rt, overnight, 32% (mixture of diastereomers), diastereomers were separated by RP-flash chromatography; (b) 0.5 N, 9 N, 33%, or 50% sodium hydroxide in H_2O or MeOH/THF, dioxane, MeOH, EtOH, or 2-propanol, rt, 100 °C, or reflux, 12-24 h; (c) 1,1,3,3-tetramethylguanidine, THF, rt, 21 h, 69%; (d) H_2 (1 atm or 6 atm), degassed MeOH, rt, 3-24 h; (e) TFA/CH_2Cl_2 1:5 v/v, rt, 30 min, 99%; (f) DIPEA, DMF, rt, overnight, 53%; (g) H_2 (1 atm), Pd/C, 2-propanol, rt, 30 min, 81%; (h) FmocOSu, Et_3N, CH_2Cl_2, rt, 16 h, 88%; (j) 0.5 M sodium hydroxide, $CaCl_2$, 2-propanol/H_2O 5:2 v/v, rt, 5 h, 86%.

However, no conversion of **2.15** was observed. The exact reproduction of the reported reduction of **2.15** using (*R*,*R*)-**2.16** as catalyst, performed as a control reaction, was also not successful. It should be noted that in this case the chiral catalysts were obtained from the same supplier (Strem Chemicals, Bischheim, France) as reported by Monovich *et al.*[30] All precautions, mentioned by the authors, such as the use of degassed MeOH or working under nitrogen purge were considered as well.

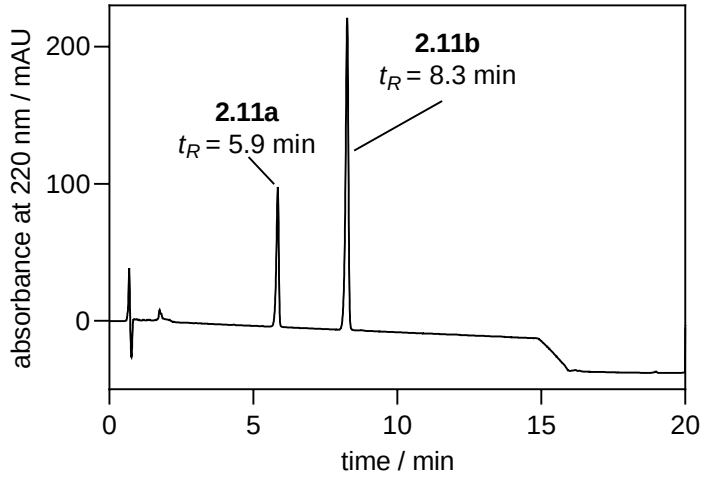


Figure 2.3. RP-HPLC chromatogram of the diastereomeric mixture of **2.11a** and **2.11b**.

Finally, as the third approach, racemic **2.8** was prepared from compound **2.15** (Scheme 2.1C). First, the Boc-protecting group in **2.15** was removed with TFA affording **2.18** which was subjected to a guanidinylation with *N*,*N*′-di-Boc-1*H*-pyrazole-1-carboxamidine (**2.19**) to yield **2.20**. The alkene and Cbz-protecting group in **2.20** were simultaneously reduced and cleaved, respectively, by the use of hydrogen gas and palladium on activated charcoal, affording the racemic amine **2.21**. Fmoc protection of the α-amino group in **2.21** gave **2.22**, and subsequent alkaline hydrolysis of the methyl ester in **2.22** gave the racemic cyclic arginine derivative **2.8**, ready to be incorporated into peptidic NTS_1R ligands via SPPS using the Fmoc-strategy.

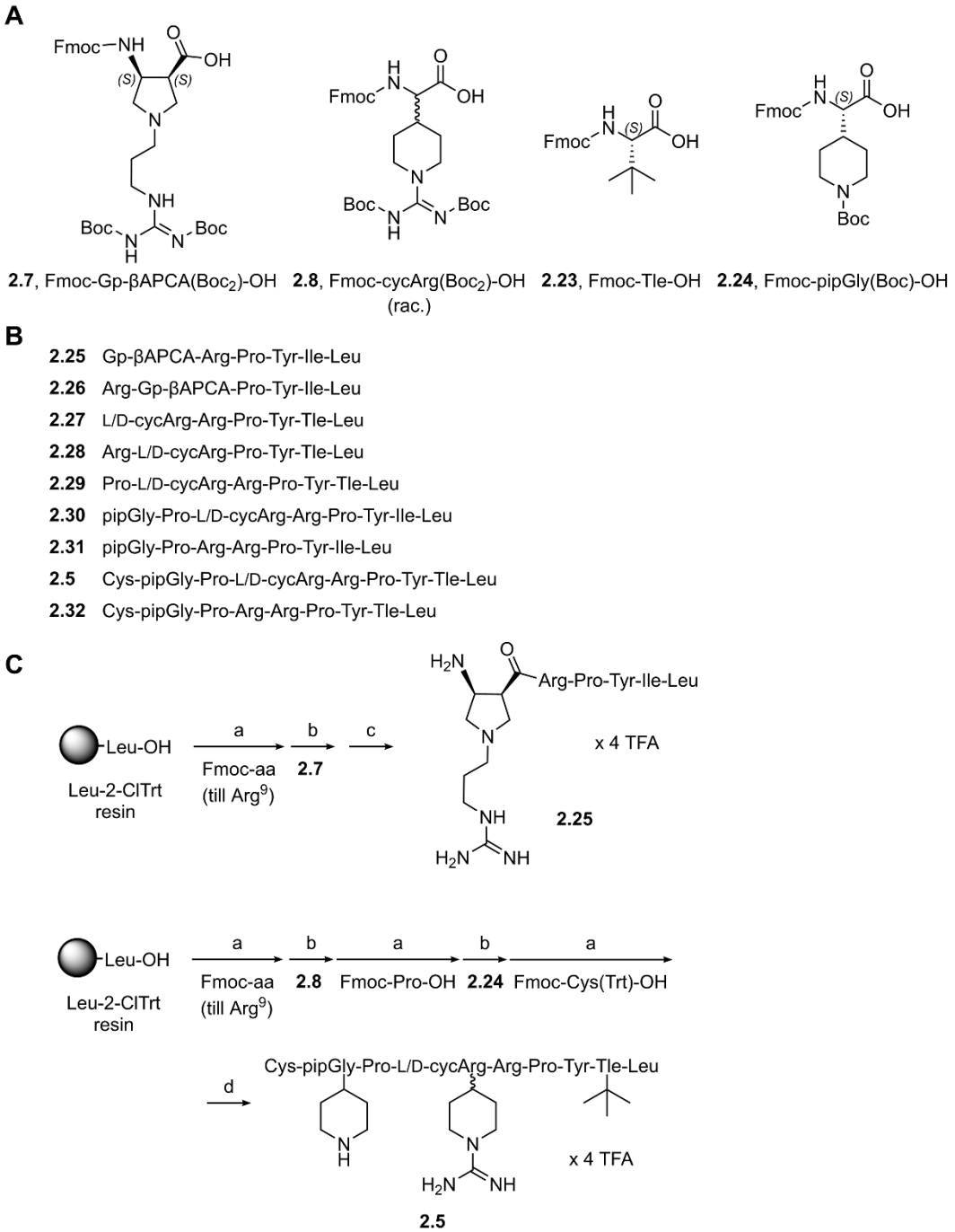
2.2.2 Synthesis of peptidic NTS_1R ligands

Fmoc-protected natural amino acids (Leu, Ile, Tyr, Pro, Arg, Cys) and unnatural amino acids (**2.7**, **2.8**, **2.23**, and **2.24**, Scheme 2.2A) were used to synthesize the peptides **2.5** and **2.25**-**2.33** (amino acid sequences shown in Scheme 2.2B) via SPPS following the standard Fmoc strategy. To exemplify this procedure, the synthesis of peptides **2.5** and **2.25** is illustrated in Scheme 2.2C.

The peptides **2.25** and **2.26** were obtained by replacement of Arg^8 and Arg^9, respectively, in **1.3** by the unnatural β-amino acid derived from enantiomerically pure (*S*,*S*)-**2.7**. Similarly, the

exchange of Arg^8 or Arg^9 using the cyclic arginine derivative **2.8** yielded the peptides **2.27** and **2.28**, both representing diastereomeric mixtures since the racemate of **2.8** was used (Scheme 2.2B). Moreover, Ile^{12} was replaced by Tle in these two peptides. N-terminal elongation of **2.27** by one proline, which corresponds to Pro^7 in neurotensin, led to compound **2.29**, also obtained as a mixture of two diastereomers. N-terminal elongation of the sequence of **2.29** by pipGly, which serves as bioisosteric replacement of Lys^6 in neurotensin, and replacement of Tle^{12} to Ile^{12} gave **2.30**, again as diastereomeric mixture (note: pipGly was commercially available as pure (*S*)-enantiomer). Finally, the reported peptide **2.5**,[5] representing the N-terminally cysteinylated congener of **2.30**, was synthesized and obtained as a mixture with its epimer containing D-cycArg instead of L-cycArg in position 8. Furthermore, the reference peptides **2.31** and **2.32**, containing natural arginine in position 8, were synthesized as congeners of **2.30** and **2.5**, respectively. Using achiral preparative HPLC, a separation of the obtained diastereomers was feasible in the case of **2.27**, **2.30**, and **2.5**. This is in the following indicated with the letters **a** and **b**, where **a** represents the diastereomer that eluted first when separated by RP-HPLC (note: compound numbers without letter represent diastereomeric mixtures). **2.28a** was also obtained as pure diastereomer, whereas **2.28b** could not be separated from an impurity (corresponding to peptide devoid of **2.8** as confirmed by HRMS). RP-HPLC analysis of crude **2.29** showed a split peak, representing the two diastereomers **2.29a** and **2.29b** (confirmed by HRMS). As these could not be separated, **2.29** was studied as diastereomeric mixture in competition binding assays.

Scheme 2.2. Synthesis of the peptides **2.5** and **2.25**-**2.32**.



(A) Structures of used unnatural amino acids. (B) Amino acid sequences of peptides **2.5** and **2.25**-**2.32**. Overall yields of SPPS: 3-67%. (C) SPPS exemplarily shown for peptides **2.25** and **2.5**. Reagents and conditions: (a) amino acid coupling: Fmoc-amino acid or **2.23**/HOBt/HBTU/DIPEA (5/5/4.9/10 equiv.), DMF/NMP 4:1 v/v, 35 °C, 2 × 45 min ("double" coupling), Fmoc deprotection: 20% piperidine in DMF/NMP 4:1 v/v, rt, 2 × 10 min; (b) **2.7**, **2.8**, or **2.24**/HOBt/HBTU/DIPEA (3/3/2.95/6 equiv.), DMF/NMP 4:1 v/v, 35 °C, 16 h ("single" coupling), Fmoc deprotection: as under (a); (c) (1) TFA/CH_2Cl_2 1:3 v/v, rt, 2 × 20 min; (2) TFA/H_2O 95:5 v/v, rt, 3 h; (d) (1) TFA/CH_2Cl_2 1:3 v/v, rt, 2 × 20 min; (2) TFA/H_2O/EDT/TIA/TIS 90:1:3:3:3 v/v, rt, 5 h.

2.2.3 NTS$_1$R and NTS$_2$R binding

NTS$_1$R binding affinities of peptides **2.5** and **2.25-2.32** were studied in a reported radiochemical competition binding assays using intact HT-29 cells and [^{3}H]**1.7** ([^{3}H]UR-MK300, structure shown in Figure 1.2, Chapter 1) as radioligand. Displacement curves are shown in Figure 2.4 and pK_i and K_i values are presented in Table 2.1. Replacing Arg^8 in **1.3** by the pyrrolidine-type β-amino acid **2.7** (peptide **2.25**) was well tolerated while the exchange of Arg^9 (peptide **2.26**) led to a marked decrease in NTS$_1$R binding affinity by more than two log units. Incorporation of the cyclized arginine derivative **2.8** instead of Arg^8 and Tle instead of Ile^{12} in **1.3** (**2.27a** and **2.27b**) resulted in slightly lower NTS$_1$R affinities compared to **1.3**. The K_i value of **2.27b** was 5-fold higher than the K_i of **2.27a**. With regard to a reported D-amino acid scan in **1.3**, showing that the D-configuration leads to reduced NTS$_1$R binding in any amino acid position in **1.3**,[25] this result indicates that **2.27b** represents the peptide containing the D-configured cyclic arginine in position 8. Noteworthy, as the exchange of Ile^{12} by Tle^{12} is known to result in decreased NTS$_1$R binding (typically 2-20fold based on the K_i values),[9,20,31-34] the observed reduction in binding affinity can be largely attributed to the presence of Tle in position 12. The regioisomer of **2.27a** (peptide **2.28a**), containing the cyclic arginine in position 9, exhibited a slightly lower binding affinity compared to **2.27a** (Table 2.1). **2.28b** was not investigated since it was contaminated with an impurity. Peptide **2.29**, representing **2.27** N-terminally elongated with proline, was studied as diastereomeric mixture and gave a 12-fold higher K_i value than **1.3** and a ca. 3-fold higher K_i than **2.27a**.

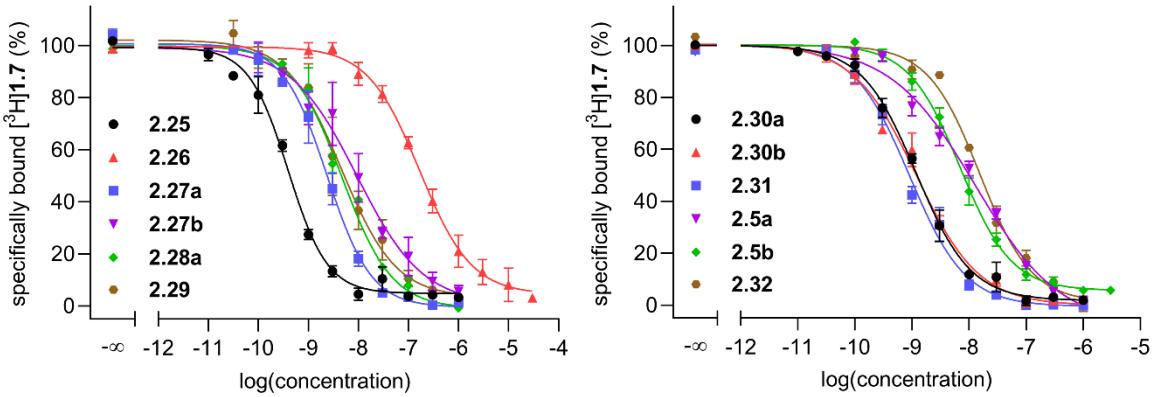


Figure 2.4. Radioligand displacement curves from competition binding experiments with [^{3}H]**1.7** (K_d = 0.41 nM,[20] c = 1 nM) and **2.5a**, **2.5b**, or **2.25-2.32** at intact HT-29 cells. Data represent mean values ± SEM from at least three independent experiments performed in triplicate. For pK_i and K_i values, see Table 2.1.

The octapeptides **2.30a** and **2.30b**, containing the cyclic arginine derived from **2.8** in position 8 and pipGly in position 6, showed equal NTS$_1$R binding affinities with K_i values of 0.39 and 0.40 nM, respectively. The high affinity can most likely be attributed to the presence of

isoleucine in position 12 (instead of Tle[12] as in **2.5**, **2.27**, **2.28**, **2.29**, and **2.32**), representing the 'original' amino acid in this position as present in **1.2** or **1.3**. Compounds **2.5a** and **2.5b**, one of them corresponding to the reported peptide **2.5** (cf. Figure 2.1B), showed binding affinities in the low nanomolar range with K_i values of 3.9 and 2.1 nM, respectively. To evaluate the possible benefit of the incorporation of the cyclic arginine derived from **2.8**, the reference peptides **2.31** and **2.32**, both containing natural arginine instead of the cyclic arginine present in **2.30** and **2.5**, were additionally studied. The NTS_1R binding affinities of **2.30a**, **2.30b**, and **2.31** as well as those of **2.5a**, **2.5b**, and **2.32** laid within a narrow range (Table 2.1), indicating that the replacement of Arg[8] by the cyclic arginine derived from **2.8** has no beneficial effect on NTS_1R binding affinity.

Table 2.1. NTS_1R binding affinities of **1.3**, **2.5a**, **2.5b**, and **2.25**-**2.32**, NTS_2R binding affinities of **1.3**, **2.25**, and **2.26**, and agonistic potencies of **1.3**, **2.25**, and **2.26**.

compd.	NTS_1R		NTS_2R
	$pK_i \pm SEM^a$ / K_i [nM][a]	$pEC_{50} \pm SEM^b$ / EC_{50} [nM][b]	$pK_i \pm SEM^c$ / K_i [nM][c]
1.3	9.85[d] / 0.14[d]	11.03 ± 0.10 / 0.0093	9.23[e] / 0.62[e]
2.25	9.94 ± 0.05 / 0.12	10.35 ± 0.19 / 0.047	9.60 ± 0.04 / 0.26
2.26	7.22 ± 0.03 / 60	9.46 ± 0.10 / 0.35	7.69 ± 0.13 / 23
2.27a	9.21 ± 0.03 / 0.61	n.d.	n.d.
2.27b	8.58 ± 0.14 / 2.9	n.d.	n.d.
2.28a	8.86 ± 0.06 / 1.4	n.d.	n.d.
2.28b	n.d.	n.d.	n.d.
2.29	8.92 ± 0.26 / 1.7	n.d.	n.d.
2.30a	9.43 ± 0.10 / 0.39	n.d.	n.d.
2.30b	9.41 ± 0.05 / 0.40	n.d.	n.d.
2.31	9.42 ± 0.15 / 0.48	n.d.	n.d.
2.5a	8.43 ± 0.06 / 3.9	n.d.	n.d.
2.5b	8.69 ± 0.07 / 2.1	n.d.	n.d.
2.32	8.34 ± 0.09 / 4.8	n.d.	n.d.

[a]Determined by radioligand competition binding with [^{3}H]**1.7**[6] at HT-29 colon carcinoma cells. [b]Determined in a Fura-2 Ca^{2+} assay at CHO-hNTS_1R cells. [c]Determined by competition binding with [^{3}H]**1.7**[6] at homogenates of HEK293T-hNTS_2R cells. [d]Keller *et al.* (reported K_i value of 0.14 nM was converted to pK_i).[6] [e]see Chapter 3. Data represent mean values ± SEM (pK_i, pEC_{50}) or mean values (K_i, EC_{50}) from at least three independent experiments performed in triplicate. n.d. = not determined.

Moreover, the NTS_2R binding affinities of peptides **2.25** and **2.26** were determined at homogenates of HEK293T-hNTS_2R cells. Both compounds exhibited similar pK_i values as found for the NTS_1R (Table 2.1).

2.2.4 NTS_1R agonism of 2.25 and 2.26

The NTS_1R agonism of **2.25** and its isomer **2.26** was investigated in a Fura-2 Ca^{2+} assay using CHO-hNTS_1R cells (concentration-response curves shown in Figure 2.5). Compounds **2.25** and **2.26** proved to be full agonists with lower potencies compared to **1.3**. All pEC_{50} values were higher compared to the respective pK_i values obtained from radiochemical competition binding experiments (see Table 2.1), which can be explained by the overexpression of NTS_1R in CHO-hNTS_1R cells resulting in a receptor reserve (for a detailed explanation see chapter 3).[18] **2.26** showed a lower potency than **2.25** which is consistent with the observed difference in their determined binding affinities (cf. Table 2.1).

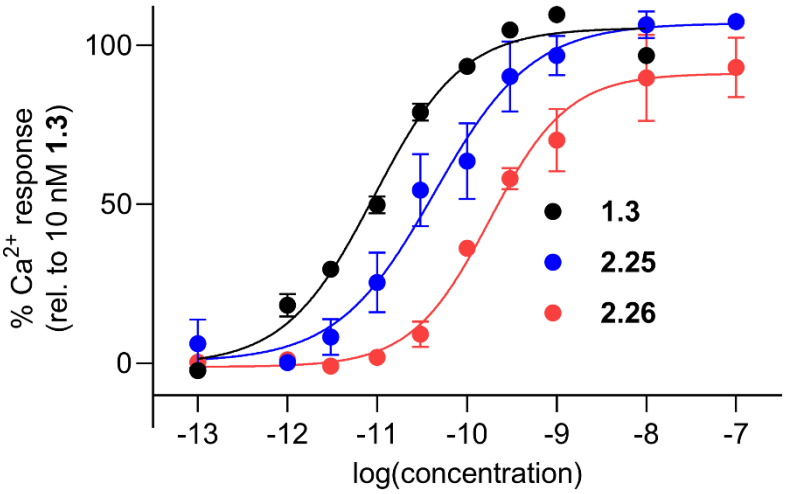


Figure 2.5. Concentration-response curves of **1.3**, **2.25**, and **2.26**, obtained from a Fura-2 Ca^{2+} assay performed with CHO-hNTS_1R cells. Data represent mean values ± SEM from at least three independent experiments (performed in triplicate).

2.2.5 Proteolytic stability of 2.25 and 2.26

The stability of peptides **2.25** and **2.26** was investigated in human plasma at 37 °C over 24 h. Both compounds were prone to rapid enzymatic degradation: after 2 h, less than 10% of the initial amount of intact peptide was found (Table 2.2). **1.3**, which is even less stable in human plasma ($t_{1/2}$ < 5 min),[9] was reported to be attacked N-terminally and C-terminally by proteases.[9,35,36] Provided that the incorporation of the cyclic β-amino acid derived from (*S,S*)-**2.7** in position 8 (**2.26**) or 9 (**2.26**) in **1.3** prevents an N-terminal degradation by proteases, the observed instability must be due to a C-terminal proteolytic cleavage of **2.25** and **2.26**. This is in agreement with recent studies showing that the C-terminal sequence -Tyr-Ile-Leu, as also present in **2.25** and **2.26**, is highly prone to proteolytic degradation.

Table 2.2. Stabilities of **2.25** and **2.26** in human plasma/PBS 1:2 v/v (37 °C).

compd.	% intact compound in plasma after the specified incubation times[a]			
	0.5 h	2 h	6 h	24 h
2.25	74 ± 2	3 ± 0.2	< 1	< 1
2.26	15 ± 1	6 ± 1	< 1	< 1

[a]The initial concentration of the peptide in human plasma/PBS (1:2 v/v) was 80 µM. Data represent mean values ± SEM from two or three independent experiments (SEM not given when no degradation was observed).

2.3 Conclusion

Replacing Arg^8 in **1.3** (NT(8-13)) by a pyrrolidine-type β-amino acid derived from the protected form **2.7** was well tolerated with respect to NTS_1R and NTS_2R binding, whereas the same modification in position 9 resulted in decreased binding affinity. Both NT(8-13)-derivatives (**2.25** and **2.26**) showed low plasma stability. A potential protective effect of the cyclic β-amino acid against N-terminal degradation of the peptide needs to be elucidated in future studies.

Since the asymmetric synthesis of the guanidino-piperidine-type α-amino acid (*S*)-**2.8** failed, racemic **2.8** was prepared and used for the synthesis of several NT(8-13) analogs (**2.5** and **2.27**-**2.32**), which were obtained as diastereomeric mixtures. Separation of the diastereomers by achiral preparative HPLC was successful in the case of **2.27**, **2.30**, and **2.5**. In general, the peptides exhibited slightly decreased NTS_1R binding affinities compared to **1.3**. Compounds **2.31** and **2.32**, containing natural arginine instead of the unnatural cyclic arginine derived from **2.8**, revealed that the incorporation of **2.8** had no additional benefit regarding the NTS_1R binding affinity. The peptides **2.5a** and **2.5b**, one of them corresponds to the published peptide **2.5** (cf. Figure 2.1B) that served as main inspiration for this study, showed similar NTS_1R binding affinities with K_i values of 3.9 nM and 2.1 nM, respectively. With these K_i values, the reported NTS_1R binding affinity of **2.5** (IC_{50} = 0.43 nM) could not be confirmed. In summary, the findings from the present study led to the conclusion that it is not worthwhile to invest laborious efforts in the synthesis of enantiomerically pure (*S*)-**2.8** and NT(8-13) analogs containing the cyclic arginine derived from (*S*)-**2.8**.

2.4 Experimental section

2.4.1 General experimental conditions

Materials. The protected amino acids Fmoc-Tyr(tBu)-OH, Fmoc-Arg(Pbf)-OH, Fmoc-Cys(Trt)-OH, and *N*,*N*′-di-Boc-1*H*-pyrazole-1-carboxamidine (**2.19**) were purchased from Carbolution Chemicals (St. Ingbert, Germany). Fmoc-Pro-OH, Fmoc-Ile-OH, Fmoc-α-*tert*-butylglycine-OH (Tle) (**2.23**), H-Leu-2-ClTrt resin, (*S*)-1-phenylethylamine (**2.10**), and HBTU were from Merck (Darmstadt, Germany). FmocOSu and piperidine were obtained from Iris Biotech (Marktredwitz, Germany). HOBt was from Sigma-Aldrich (Taufkirchen, Germany). NMP and DMF for peptide synthesis, anhydrous DMF and NMP, dichloromethane, and TFA were purchased from Fisher Scientific (Schwerte, Germany). *Tert*-butyl 4-formylpiperidine-1-carboxylate (**2.9**), methyl 2-(((benzyloxy)carbonyl)amino)-2-(dimethoxyphosphoryl)acetate (**2.13**), 1,1,3,3-tetramethylguanidine, *tert*-butyl 4-oxopiperidine-1-carboxylate (**2.14**), and DIPEA were obtained from ABCR (Karslruhe, Germany). (*R*,*R*)-Me-BPE-Rh ((*R*,*R*)-**2.16**) and (*S*,*S*)-Me-BPE-Rh ((*S*,*S*)-**2.16**) were purchased from Strem Chemicals (Bischheim, France). Fmoc-pipGly(Boc)-OH (**2.24**) was from GL Biochem (Shanghai, China). 1,4-Dithiothreitol was obtained from Carl Roth (Karlsruhe, Germany). Acetonitrile (HPLC gradient grade) was from VWR (Ismaning, Germany). NT(8-13) (**1.3**) was synthesized via SPPS in-house. Bacitracin, HEPES, and bovine serum albumin (BSA) were obtained from Serva (Heidelberg, Germany). Fetal bovine serum (FBS) was purchased from Pan-Biotech (Aidenbach, Germany). The radioligand [^{3}H]**1.7** (molar activity: 2.41 TBq/mmol) was prepared according to a described procedure.[6] Compound **2.7**[24] was synthesized by Dr. Eva Plut in the group of Prof. Dr. O. Reiser (Institute of Organic Chemistry, Faculty of Chemistry and Pharmacy, University of Regensburg). Millipore water was consistently used for the preparation of stock solutions, buffers, and aqueous eluents for HPLC. Polypropylene reaction vessels with screw cap (1.5 and 2 mL) from Sarstedt (Nümbrecht, Germany) were used for small-scale reactions (e.g., activation of Fmoc-protected amino acids) and to keep stock solutions.

NMR spectroscopy. NMR spectra of compounds **2.8**, **2.15**, **2.18**, and **2.20**-**2.22** were recorded on a Bruker AVANCE 400 (^{1}H, 400 MHz; ^{13}C, 100 MHz) or on a Bruker AVANCE 600 instrument with cryogenic probe (^{1}H: 600 MHz; ^{13}C: 150 MHz) (Bruker, Karlsruhe, Germany). NMR spectra were calibrated based on the solvent residual peaks (^{1}H-NMR: $CDCl_3$: δ = 7.26 ppm, CD_3OD-d_4: δ = 3.31 ppm, DMSO-d_6: δ = 2.50 ppm; ^{13}C-NMR: $CDCl_3$: δ = 77.16 ppm, DMSO-d_6: δ = 39.50 ppm). NMR data are reported as described in Chapter 3.

Mass spectroscopy. High-resolution mass spectrometry (HRMS) was performed as described in Chapter 3.

Flash chromatography. A Puriflash XS520Plus System (Interchim, Montlucon Cedex, France) was used to purify compounds via automated flash column chromatography. Purifications were carried out using technical grade solvents. Geduran Si 60 silica gel (pore size 60 Å, particle size 40-63 µm, Merck) was used for the preparation of precolumns. Prepacked silica columns were used for the purification (40-120 g silica, particle size 30-50 µM, Interchim).

Preparative HPLC. Preparative HPLC and lyophilization were performed using the same systems as described in Chapter 3.

Analytical HPLC. Analytical HPLC analysis was performed using the same system, column, flow rate, detection wavelength, eluents and column temperature as described in Chapter 3. The following linear gradients were applied: compounds **2.11a** and **2.11b**: 0-14 min: acetonitrile (A)/0.04% aqueous TFA (B) 42:58-60:40, 14-15 min: 30:70-95:5, 15-20 min: 95:5 (isocratic); compounds **2.8**, **2.15**, **2.18**, and **2.20**-**2.22**: 0-20 min: A/B 10:90-90:10, 20-21 min: 90:10-95:5, 21-24 min: 95:5 (isocratic); compounds **2.5a** and **2.5b**: 0-14 min: A/B 10:90-30:70, 14-15 min: 30:70-95:5, 15-18 min: 95:5 (isocratic); compounds **2.25**-**2.32**: 0-14 min: A/B 10:90-30:70, 14-15 min: 30:70-95:5, 15-20 min: 95:5 (isocratic). Retention (capacity) factors *k* were calculated as described in Chapter 3.

General procedure for solid phase peptide synthesis. Peptides were synthesized manually by SPPS according to the Fmoc strategy. A H-Leu-2-ClTrt resin was used as solid phase and DMF/NMP 4:1 v/v was used as solvent. 5-mL NORM-JECT syringes (B. Braun-Melsungen, Melsungen, Germany), equipped with a 35-µm polypropylene frit (Roland Vetter Laborbedarf, Ammerbuch, Germany), were used as reaction vessels. The resin was allowed to swell in solvent for 30 min at rt. Fmoc-amino acids (except for **2.7**, **2.8**, and **2.24**), used in 5-fold excess, were preactivated with HOBt/HBTU/DIPEA (5/4.9/10 equiv.) in solvent (about 2.2 mL/mmol amino acid) for at least 5 min before addition to the resin. The Fmoc-protected unnatural amino acids **2.7**, **2.8**, and **2.24** were used in 3-fold (**2.7** and **2.24**) or 2.5-fold excess (**2.8**) and were preactivated with HOBt/HBTU/DIPEA (3/2.95/6 or 2.5/2.45/5 equiv.) in anhydrous solvent (about 1.6 mL/mmol amino acid) for 5-10 min prior to addition to the resin. Amino acid coupling was carried out on a shaker (Heidolph Multi Reax; Heidolph Instruments, Schwabach, Germany) covered with a thermostat controlled (35 °C) box. In the case of standard amino acids and **2.23**, "double" coupling (2 × 45 min) was performed. **2.7**, **2.8**, and **2.24** were attached by a

single coupling procedure (35 °C, 16 h). After coupling of an Fmoc-amino acid, the resin was washed with solvent (4 ×) followed by Fmoc deprotection using 20% piperidine in solvent (2 × 10 min at rt) and subsequent washing of the resin with solvent (6 × ca. 1 mL). After coupling of the last amino acid and final Fmoc deprotection, the resin was washed with solvent (6 ×) and CH_2Cl_2 (3 ×) (treated with potassium carbonate). Peptides were cleaved off the resin using CH_2Cl_2/TFA 3:1 v/v (2 × 20 min at rt). The liquids (2 × ca. 2 mL) were collected in a 100-mL round bottom flask and the resin was washed once with CH_2Cl_2/TFA 3:1 v/v (2 mL). The volatiles of the combined liquids were removed by evaporation and, in the case of **2.25-2.31**, TFA/H_2O 95:5 v/v (2 mL per 100 mg resin) was added to the residue and the mixture was stirred at rt for 5 h. The volatiles were removed by evaporation followed by the addition of H_2O (ca. 50 mL) and lyophilization to obtain the crude peptide, which was subjected to purification by preparative HPLC. Resins, containing the peptides **2.5** or **2.32**, were treated differently: after evaporation of the volatiles of the combined liquids, TFA/H_2O/EDT/TIA/TIS 90:1:3:3:3 v/v (2 mL per 100 mg resin) was added and the mixture was stirred at rt for 3 h. Crude peptides were precipitated using cold diethyl ether (-20 °C) followed by centrifugation and separation of the precipitate. The precipitate was dissolved in acetonitrile/0.1% aqueous TFA 15:85 v/v and 1,4-dithiothreitol (final concentration = 10 mM) was added to reduce potential disulfide bridges. To ensure a complete reduction, the mixture was shaken at 50 °C for 30 min before the subsequent purification by preparative HPLC.

Compound characterization. Compounds **2.8**, **2.15**, **2.18**, and **2.22** were characterized by HRMS, ^{1}H-, ^{13}C-, and 2D-NMR spectroscopy (2D: ^{1}H-COSY, HSQC, HMBC), and RP-HPLC. Compounds **2.20** and **2.21** were characterized by HRMS, ^{1}H-NMR spectroscopy, and RP-HPLC. (*S*,*R*)-**2.11** and (*S*,*S*)-**2.11** and peptides **2.5** and **2.25-2.32** were characterized by HRMS and RP-HPLC. HPLC purities of all target compounds were ≥ 97% (UV detection, 220 nm).

2.4.2 Experimental protocols and analytical data

Cys-β,β-(3-aza)pent-1,5-diyl-Ala-Pro-β,β-(3-amidino-3-aza)pent-1,5-diyl-L-Ala-Arg-Pro-Tyr-β-methyl-Val-Leu tetrakis(hydrotrifluoroacetate) and Cys-β,β-(3-aza)pent-1,5-diyl -Ala-Pro-β,β-(3-amidino-3-aza)pent-1,5-diyl-D-Ala-Arg-Pro-Tyr-β-methyl-Val-Leu tetrakis(hydrotrifluoroacetate) (2.5a and 2.5b).[a] Peptides **2.5a** and **2.5b**, representing diastereomers, were synthesized on a H-Leu-2-ClTrt resin (60 mg, 0.79 mmol/g) according to the general procedure. Since **2.8** was used as racemic mixture (cf. Scheme 2.1C) for the peptide synthesis, two diastereomeric peptides were obtained, which were separated by preparative HPLC (gradient: 0-40 min: acetonitrile/0.1% aqueous TFA 15:85-45:55, t_R (**2.5a**) = 12 min, t_R

(**2.5b**) = 13 min) resulting in white fluffy solids (**2.5a**: 7.4 mg, 10%; **2.5b**: 12.3 mg, 16%). HRMS (ESI): *m/z* $[M+4H]^{4+}$ calcd. for $[C_{55}H_{94}N_{16}O_{11}S]^{4+}$ 296.6747, found: 296.6748 (**2.5a**), 296.6747 (**2.5b**). RP-HPLC (220 nm): **2.5a**: > 99% (t_R = 6.4 min, k = 7.4), **2.5b**: > 99% (t_R = 6.9 min, k = 8.1). $C_{55}H_{90}N_{16}O_{11}S \cdot C_8H_4F_{12}O_8$ (1183.49 + 456.09). [a]Stereochemistry not assigned.

2-((((9*H*-Fluoren-9-yl)methoxy)carbonyl)amino)-2-(1-(*N*,*N*'-bis(*tert*-butoxycarbonyl)-carbamimidoyl)piperidin-4-yl)acetic acid (2.8). Compound **2.22** (463 mg, 0.73 mmol) and $CaCl_2$ (6.22 g, 56 mmol, final concentration = 0.8 M) were dissolved in 2-propanol/H_2O 5:2 v/v (70 mL). After the addition of a 0.5 M NaOH solution (1.75 mL, 0.87 mmol), the mixture was stirred at rt for 5 h followed by evaporation of the volatiles. The residue was diluted with H_2O and lyophilized. Purification by column chromatography (CH_2Cl_2/MeOH 99:1 to 90:10 v/v) yielded racemic **2.8** as a white solid (392 mg, 86%). ^{1}H-NMR (600 MHz, DMSO-d_6): δ (ppm) 1.20-1.57 (m, 22H), 1.60-1.81 (m, 2H), 1.97-2.15 (m, 1H), 2.91-3.22 (m, 2H), 3.95-3.99 (m, 1H), 4.00-4.06 (m, 1H), 4.19-4.25 (t, 1H, *J* 7.0 Hz), 4.25-4.33 (d, 2H, *J* 7.4 Hz), 7.30-7.35 (m, 2H), 7.40-7.44 (m, 2H), 7.59-7.81 (m, 3H), 7.86-7.93 (m, 2H), 12.36-13.31 (br s, 1H). ^{13}C-NMR (150 MHz, DMSO-d_6): δ (ppm) 27.28, 27.75 (7 carbon atoms), 28.04, 36.48, 40.06 (interfering with the solvent signal, identified via HSQC), 46.66, 57.77, 65.75, 81.74 (2 carbon atoms, identified via HMBC), 120.12, 120.14, 125.32, 125.34, 127.08 (2 carbon atoms), 127.65, 127.67, 140.72 (2 carbon atoms), 143.77, 143.81, 150.49 (2 carbon atoms), 154.88, 156.32, 172.55. HRMS (ESI): *m/z* $[M+1H]^{1+}$ calcd. for $[C_{33}H_{43}N_4O_8]^{1+}$ 623.3076, found: 623.3083. RP-HPLC (220 nm): 96% (t_R = 11.0 min, k = 13.5). $C_{33}H_{42}N_4O_8$ (622.72).

***Tert*-butyl 4-((*R*)-cyano(((*S*)-1-phenylethyl)amino)methyl)piperidine-1-carboxylate (*S*,*R*-2.11) and *tert*-butyl 4-((*S*)-cyano(((*S*)-1-phenylethyl)amino)methyl)piperidine-1-carboxylate (*S*,*S*-2.11).** A solution of potassium cyanide (1.60 g, 24.6 mmol) in H_2O (32 mL) was added to a stirred solution of (*S*)-1-phenylethylamine (**2.10**) (3.0 mL, 23.4 mmol) in MeOH (32 mL), followed by the addition of *tert*-butyl 4-formylpiperidine-1-carboxylate (**2.9**) (5.0 g, 23.4 mmol). The mixture was stirred at rt overnight. Subsequently, it was diluted with H_2O (80 mL) and filtered. The product was extracted from the filtrate with CH_2Cl_2 (3 × 80 mL), the organic phases were combined and dried over Na_2SO_4 followed by evaporation of the volatiles. Purification by column chromatography (CH_2Cl_2 to CH_2Cl_2/ethyl acetate 1:1 v/v) yielded a colorless oil (2.8 g, 32%). The diastereomers were separated by flash chromatography using

the preparative HPLC system and conditions as described under *Preparative HPLC* with the following modifications: the column was replaced by a Puriflash RP-C18HQ cartridge (15 µm, 120 g) (Interchim, Montlucon Cedex, France) and the flow was increased to 40 mL/min. The following gradient was applied: 0-25 min: acetonitrile/0.1% aqueous TFA 45:55-70/30. The diastereomers were separable with retention times of 14 min (**2.11a**) and 18 min (**2.11b**). HRMS (ESI): *m/z* $[M+Na]^{1+}$ calcd. for $[C_{20}H_{29}N_3NaO_2]^{1+}$ 366.2152, found: 366.2158 (**2.11a**), 366.2160 (**2.11b**). RP-HPLC (220 nm): **2.11a**: 90% (t_R = 5.7 min, k = 6.5), **2.11b**: 95% (t_R = 8.1 min, k = 9.7). $C_{20}H_{29}N_3O_2 \cdot C_2HF_3O_2$ (343.47 + 114.03).

***Tert*-butyl 4-(1-(((benzyloxy)carbonyl)amino)-2-methoxy-2-oxoethylidene)piperidine-1-carboxylate (2.15).**[30] Compound **2.15** was synthesized according to a reported procedure[30] using 2.3 g of 1,1,3,3-tetramethylguanidine (19.6 mmol), 5.0 g of methyl 2-(((benzyloxy)carbonyl)amino)-2-(dimethoxyphosphoryl)acetate (**2.13**) (15.1 mmol), and 4.5 g of *tert*-butyl 4-oxopiperidine-1-carboxylate (**2.14**) (22.6 mmol). **2.15** was obtained as colorless crystalline solid (4.20 g, 69%). ^{1}H-NMR (400 MHz, $CDCl_3$): δ (ppm) 1.44 (s, 9H), 2.34-2.43 (m, 2H), 1.68-2.93 (m, 2H), 3.27-3.85 (m, 7H), 5.11 (s, 2H), 6.27 (s, 1H), 7.23-7.43 (m, 5H, interfering with solvent signal). ^{13}C-NMR (100 MHz, $CDCl_3$): δ (ppm) 28.48 (3 carbon atoms), 29.79, 30.42, 41.19, 43.12, 52.05, 67.39, 79.96, 120.38, 128.22 (2 carbon atoms), 128.34, 128.60 (2 carbon atoms), 136.11, 147.03, 154.74, 165.13, 207.94. HRMS (ESI): *m/z* $[M+1H]^{1+}$ calcd. for $[C_{21}H_{29}N_2O_6]^{1+}$ 405.2021, found: 405.2021. RP-HPLC (220 nm): > 99% (t_R = 12.1 min, k = 14.8). $C_{21}H_{28}N_2O_6$ (404.46).

Methyl 2-(((benzyloxy)carbonyl)amino)-2-(piperidin-4-ylidene)acetate hydrotrifluoroacetate (2.18). Compound **2.15** (1.06 g, 2.62 mmol) was dissolved in CH_2Cl_2 (50 mL) and TFA (10 mL) was added. After stirring at rt for 30 min, the volatiles were evaporated, CH_2Cl_2 (ca. 50 mL) was added and the volatiles were evaporated. This process was repeated once. This procedure gave **2.18** as yellow oil (0.80 g, 73%), which was used in the next step without further purification. ^{1}H-NMR (400 MHz, $CDCl_3$): δ (ppm) 2.52-2.71 (m, 2H), 3.07-3.40 (m, 5H), 3.47-3.60 (m, 1H), 3.64-3.89 (m, 3H), 5.13 (s, 2H), 6.56 (s, 1H), 7.27-7.44 (m, 5H), 8.43 (s, 2H), 11.53 (proton signal of TFA). ^{13}C-NMR (100 MHz, $CDCl_3$): δ (ppm) 26.34, 27.48, 44.45, 44.81, 52.65, 68.13, 111.14 (TFA), 114.00 (TFA), 116.85 (TFA), 119.71 (TFA), 122.19, 128.23, 128.80 (4 carbon atoms), 135.55, 140.28, 155.50, 161.19 (q, J 39.6 Hz) (TFA), 164.71. HRMS (ESI): *m/z* $[M+1H]^{1+}$ calcd. for $[C_{16}H_{21}N_2O_4]^{1+}$ 305.1496, found:

305.1498. RP-HPLC (220 nm): 98% (t_R = 4.5 min, k = 4.9). $C_{16}H_{20}N_2O_4 \cdot C_2HF_3O_2$ (304.35+ 114.03).

Methyl 2-(((benzyloxy)carbonyl)amino)-2-(1-(*N*,*N*'-bis(*tert*-butoxycarbonyl)-carbamimidoyl)piperidin-4-ylidene)acetate (2.20). DIPEA (4.70 mL, 27.0 mmol) and *N*,*N*'-di-Boc-1*H*-pyrazole-1-carboxamidine (**2.19**) (767 mg, 2.47 mmol) were added to a solution of **2.18** (684 mg, 2.25 mmol) in DMF (14 mL) and the mixture was stirred at rt overnight. After dilution with ethyl acetate (25 mL), the solution was washed with a saturated sodium bicarbonate solution and brine. Evaporation of the solvent of the organic phase gave the crude product which was subjected to flash column chromatography (light petroleum/ethyl acetate 3:1 to 1:1 v/v). **2.20** was obtained as a white solid (653 mg, 53%). ^{1}H-NMR (400 MHz, $CDCl_3$): δ (ppm) 1.46-1.51 (m, 18H), 2.48-2.62 (m, 2H), 2.91-3.10 (m, 2H), 3.40-3.67 (m, 4H), 3.75 (s, 3H), 5.13 (s, 2H), 6.08 (s, 1H), 7.27-7.47 (m, 5H), 10.19 (s, 1H). HRMS (ESI): *m/z* $[M+1H]^{1+}$ calcd. for $[C_{27}H_{39}N_4O_8]^{1+}$ 547.2763, found: 547.2769. RP-HPLC (220 nm): 96% (t_R = 10.0 min, k = 12.2). $C_{27}H_{38}N_4O_8$ (546.62).

Methyl 2-amino-2-(1-(*N*,*N*'-bis(*tert*-butoxycarbonyl)carbamimidoyl)piperidin-4-yl)-acetate (2.21). Under a nitrogen atmosphere, a 10% Pd/C catalyst (100 mg) was added to a solution of **2.20** (653 mg, 1.20 mmol) in 2-propanol (60 mL) followed by closing the single-neck round-bottom flask with a septum. With a needle, connected to a balloon filled with H_2, the septum was pierced and the needle was immersed in the vigorously stirred suspension. After approximately 30 min (the major amount of H_2 has been consumed), the reaction was stopped, the catalyst was removed via centrifugation and filtration using a 25 mm syringe filter (nylon, 0.2 µm, PP housing, Phenomenex), and the solvent of the filtrate was evaporated. **2.21** was obtained as yellow oil (403 mg, 81%), which was used for the next step without purification. ^{1}H-NMR (400 MHz, CD_3OD): δ (ppm) 1.43 (s, 18H), 1.57-1.72 (m, 2H), 1.79-1.91 (m, 1H), 2.77-2.94 (m, 2H), 3.25-3.30 (m, 4H), 3.69 (s, 3H), 3.95-4.23 (m, 2H). Two exchangeable protons (NH) were not apparent. HRMS (ESI): *m/z* $[M+1H]^{1+}$ calcd. for $[C_{19}H_{35}N_4O_6]^{1+}$ 415.2552, found: 415.2555. RP-HPLC (220 nm): > 99% (t_R = 4.9 min, k = 5.4). $C_{19}H_{34}N_4O_6$ (414.50).

Methyl 2-((((9*H*-fluoren-9-yl)methoxy)carbonyl)amino)-2-(1-(*N*,*N*'-bis(*tert*-butoxy-carbonyl)carbamimidoyl)piperidin-4-yl)acetate (2.22). Triethylamine (141 µL, 0.97 mmol) and FmocOSu (394 mg, 1.17 mmol) were added to a solution of **2.21** (403 mg, 0.97 mmol) in CH_2Cl_2 (60 mL). After stirring at rt for 16 h, the solvent was evaporated and the crude product was subjected to flash column chromatography (CH_2Cl_2/MeOH 99:1 to 97:3 v/v) affording **2.22** as a white solid (542 mg, 88%). ^{1}H-NMR (400 MHz, $CDCl_3$): δ (ppm) 1.36-1.61 (m, 22H), 1.61-1.90 (m, 2H), 1.93-2.11 (m, 1H), 2.70-3.03 (m, 2H), 3.75 (s, 3H), 4.19-4.24 (m, 1H), 4.32-4.42 (m, 2H), 4.42-4.51 (m, 1H), 5.34 (d, 1H, *J* 8.8 Hz), 7.27-7.36 (m, 2H), 7.36-7.44 (m, 2H), 7.49-7.63 (m, 2H), 7.71-7.79 (m, 2H), 10.15 (s, 1H). ^{13}C-NMR (100 MHz, $CDCl_3$): δ (ppm) 27.17, 28.25 (5 carbon atoms), 39.46, 46.95, 47.32, 52.57, 57.67, 67.10, 79.64, 82.05, 120.08, 120.11, 125.10, 125.21, 127.18, 127.20, 127.83 (2 carbon atoms), 141.43 (2 carbon atoms), 143.77 (2 carbon atoms), 143.90, 150.85, 155.04 (2 carbon atoms), 156.17, 162.98 (2 carbon atoms), 171.90 HRMS (ESI): *m/z* $[M+1H]^{1+}$ calcd. for $[C_{34}H_{45}N_4O_8]^{1+}$ 637.3232, found: 637.3235. RP-HPLC (220 nm): > 99% (t_R = 11.9 min, *k* = 14.7). $C_{34}H_{44}N_4O_8$ (636.75).

***N*$^{\alpha}$-((3*S*,4*S*)-4-Amino-1-(3-guanidinopropyl)pyrrolidin-3-yl)carbonyl-Arg-Pro-Tyr-Ile-Leu tetrakis(hydrotrifluoroacetate) (2.25).** Peptide **2.25** was synthesized on a H-Leu-2-ClTrt resin (60 mg, 0.79 mmol/g) according to the general procedure. Purification by preparative HPLC (gradient: 0-20 min: acetonitrile/0.1% aqueous TFA 10:90-50:50, t_R = 10 min) yielded **2.25** as a white fluffy solid (38.8 mg, 67%). HRMS (ESI): *m/z* $[M+3H]^{3+}$ calcd. for $[C_{41}H_{72}N_{13}O_8]^{3+}$ 291.5204, found: 291.5213. RP-HPLC (220 nm): > 99% (t_R = 6.5 min, *k* = 7.6). $C_{41}H_{69}N_{13}O_8 \cdot C_8H_4F_{12}O_8$ (872.09 + 456.09).

***N*$^{\alpha}$-(((3*S*,4*S*)-4-(Arginylamino)-1-(3-guanidinopropyl)pyrrolidin-3-yl)carbonyl)-Pro-Tyr-Ile-Leu tetrakis(hydrotrifluoroacetate) (2.26).** Peptide **2.26** was synthesized on a H-Leu-2-ClTrt resin (40 mg, 0.79 mmol/g) according to the general procedure. Purification by preparative HPLC (gradient: 0-30 min: acetonitrile/0.1% aqueous TFA 10:90-40:60, t_R = 12 min) yielded **2.26** as a white fluffy solid (24.2 mg, 63%). HRMS (ESI): *m/z* $[M+3H]^{3+}$ calcd. for $[C_{41}H_{72}N_{13}O_8]^{3+}$ 291.5204, found: 291.5209. RP-HPLC (220 nm): > 99% (t_R = 6.5 min, *k* = 7.6). $C_{41}H_{69}N_{13}O_8 \cdot C_8H_4F_{12}O_8$ (872.09 + 456.09).

β,β-(3-Amidino-3-aza)pent-1,5-diyl-L-Ala-Arg-Pro-Tyr-β-methyl-Val-Leu tris(hydrotrifluoroacetate) and β,β-(3-Amidino-3-aza)pent-1,5-diyl-D-Ala-Arg-Pro-Tyr-β-methyl-Val-Leu tris(hydrotrifluoroacetate) (2.27a and 2.27b).[a] Peptides **2.27a** and **2.27b**, representing diastereomers, were synthesized on a H-Leu-2-ClTrt resin (30 mg, 0.79 mmol/g) according to the general procedure. Since **2.8** was used as racemic mixture (cf. Scheme 2.1C) for the peptide synthesis, two diastereomers were obtained, which were separated by preparative HPLC (gradient: 0-30 min: acetonitrile/0.1% aqueous TFA 10:90-30:70, t_R (**2.27a**) = 20 min, t_R (**2.27b**) = 21 min) resulting in white fluffy solids (**2.27a**: 2.3 mg, 11%; **2.27b**: 2.5 mg, 11%). HRMS (ESI): *m/z* $[M+3H]^{3+}$ calcd. for $[C_{40}H_{69}N_{12}O_8]^{3+}$ 281.8448, found: 281.8458 (**2.27a**); 281.8458 (**2.27b**). RP-HPLC (220 nm): **2.27a**: 98% (t_R = 6.9 min, k = 8.1), **2.27b**: 98% (t_R = 7.2 min, k = 8.5). $C_{40}H_{66}N_{12}O_8 \cdot C_6H_3F_9O_6$ (843.04 + 342.07). [a]Stereochemistry not assigned.

Arg-β,β-(3-amidino-3-aza)pent-1,5-diyl-L-Ala-Pro-Tyr-β-methyl-Val-Leu tris(hydrotrifluoroacetate) and Arg-β,β-(3-amidino-3-aza)pent-1,5-diyl-D-Ala-Pro-Tyr-β-methyl-Val-Leu tris(hydrotrifluoroacetate) (2.28a and 2.28b).[a] Peptides **2.28a** and **2.28b**, representing diastereomers, were synthesized on a H-Leu-2-ClTrt resin (30 mg, 0.79 mmol/g) according to the general procedure. Since **2.8** was used as racemic mixture (cf. Scheme 2.1C) for the peptide synthesis, two diastereomers were obtained, which were purified by preparative HPLC (gradient: 0-30 min: acetonitrile/0.1% aqueous TFA 18:82-38:62, t_R (**2.28a**) = 9 min, t_R (**2.28b**) = 10 min). Whereas **2.28a** could be isolated with high purity, **2.28b** could not be separated from an impurity. **2.28a** was obtained as a white fluffy solid (3.3 mg, 12%). HRMS (ESI): *m/z* $[M+3H]^{3+}$ calcd. for $[C_{40}H_{69}N_{12}O_8]^{3+}$ 281.8448, found: 281.8451 (**2.28a**). RP-HPLC (220 nm): **2.28a**: > 99% (t_R = 7.1 min, k = 8.3). $C_{40}H_{66}N_{12}O_8 \cdot C_6H_3F_9O_6$ (843.04 + 342.07). [a]Stereochemistry not assigned.

Pro-β,β-(3-amidino-3-aza)pent-1,5-diyl-L-Ala-Arg-Pro-Tyr-β-methyl-Val-Leu tris(hydrotrifluoroacetate) and Pro-β,β-(3-amidino-3-aza)pent-1,5-diyl-D-Ala-Arg-Pro-Tyr-β-methyl-Val-Leu tris(hydrotrifluoroacetate) (2.29a and 2.29b).[a] Peptides **2.29a** and **2.29b**, representing diastereomers, were synthesized on a H-Leu-2-ClTrt resin (30 mg, 0.79 mmol/g) according to the general procedure. Since **2.8** was used as racemic mixture (cf. Scheme 2.1C) for the peptide synthesis, two diastereomers were obtained, which were purified by preparative HPLC, but could not be separated (gradient: 0-30 min: acetonitrile/0.1% aqueous

TFA 20:80-40:60, t_R (**2.29a** and **2.29b**) = 9 min). Lyophilisation of the eluate gave a white fluffy solid containing **2.29a** and **2.29b** (6.8 mg, 22%). HRMS (ESI): *m/z* $[M+3H]^{3+}$ calcd. for $[C_{45}H_{76}N_{13}O_9]^{3+}$ 314.5302, found: 314.5311 (**2.29a** and **2.29b**). RP-HPLC (220 nm): **2.29a** and **2.29b**: 97% (t_R = 7.7 min, *k* = 9.1). $C_{45}H_{73}N_{13}O_9 \cdot C_6H_3F_9O_6$ (940.16 + 342.07). [a]Stereochemistry not assigned.

β,β-(3-Aza)pent-1,5-diyl-Ala-Pro-β,β-(3-amidino-3-aza)pent-1,5-diyl-L-Ala-Arg-Pro-Tyr-Ile-Leu tetrakis(hydrotrifluoroacetate) and β,β-(3-Aza)pent-1,5-diyl-Ala-Pro-β,β-(3-amidino-3-aza)pent-1,5-diyl-D-Ala-Arg-Pro-Tyr-Ile-Leu tetrakis(hydrotrifluoroacetate) (2.30a and 2.30b).[a] Peptides **2.30a** and **2.30b**, representing diastereomers, were synthesized on a H-Leu-2-ClTrt resin (30 mg, 0.79 mmol/g) according to the general procedure. Since **2.8** was used as racemic mixture (cf. Scheme 2.1C) for the peptide synthesis, two diastereomers were obtained, which were separated by preparative HPLC (gradient: 0-40 min: acetonitrile/0.1% aqueous TFA 10:90-40:60, t_R (**2.30a**) = 18 min, t_R (**2.30b**) = 19 min) resulting in white fluffy solids (**2.30a**: 1.2 mg, 3%; **2.30b**: 1.3 mg, 4%). HRMS (ESI): *m/z* $[M+4H]^{4+}$ calcd. for $[C_{52}H_{89}N_{15}O_{10}]^{4+}$ 270.9224, found: 270.9235 (**2.30a**); 270.9232 (**2.30b**). RP-HPLC (220 nm): **2.30a**: 98% (t_R = 6.9 min, *k* = 8.1), **2.30b**: 97% (t_R = 7.2 min, *k* = 8.5). $C_{52}H_{85}N_{15}O_{10} \cdot C_8H_4F_{12}O_8$ (1080.35 + 456.09). [a]Stereochemistry not assigned.

β,β-(3-Aza)pent-1,5-diyl-Ala-Pro-Arg-Arg-Pro-Tyr-Ile-Leu tetrakis(hydrotrifluoroacetate) (2.31). Peptide **2.31** was synthesized on a H-Leu-2-ClTrt resin (30 mg, 0.79 mmol/g) according to the general procedure. Purification by preparative HPLC (gradient: 0-40 min: acetonitrile/0.1% aqueous TFA 15:85-45:55, t_R = 12 min) yielded **2.31** as a white fluffy solid (3.5 mg, 10%). HRMS (ESI): *m/z* $[M+4H]^{4+}$ calcd. for $[C_{50}H_{87}N_{15}O_{10}]^{4+}$ 264.4185, found: 264.4195. RP-HPLC (220 nm): 96% (t_R = 6.9 min, *k* = 8.1). $C_{50}H_{83}N_{15}O_{10} \cdot C_8H_4F_{12}O_8$ (1054.31 + 456.09).

Cys-β,β-(3-aza)pent-1,5-diyl-Ala-Pro-Arg-Arg-Pro-Tyr-β-methyl-Val-Leu tetrakis(hydrotrifluoroacetate) (2.32). Peptide **2.32** was synthesized on a H-Leu-2-ClTrt resin (30 mg, 0.79 mmol/g) according to the general procedure. Purification by preparative HPLC (gradient: 0-40 min: acetonitrile/0.1% aqueous TFA 15:85-45:55, t_R = 10 min) yielded **2.32** as a white fluffy solid (4.0 mg, 10%). HRMS (ESI): *m/z* $[M+4H]^{4+}$ calcd. for

$[C_{53}H_{92}N_{16}O_{11}S]^{4+}$ 290.1708, found: 290.1719. RP-HPLC (220 nm): 96% (t_R = 7.1 min, k = 8.3). $C_{53}H_{88}N_{16}O_{11}S \cdot C_8H_4F_{12}O_8$ (1157.45 + 456.09).

2.4.3 Cell culture

Cells were cultured in T75 or T175 culture flasks (Sarstedt) in a humidified atmosphere (95% air and 5% CO_2) at 37 °C. HT-29 colon carcinoma cells (DSMZ-no. ACC 299) were grown in antibiotic-free RPMI-1640 medium (Sigma) supplemented with 7.5% FBS (Sigma) and CHO-$hNTS_1R$ cells (kindly provided by Harald Hübner and Peter Gmeiner, Department of Chemie und Pharmazie, Naturwissenschaftliche Fakultät, Friedrich-Alexander-Universität) were cultured in DMEM/HAM's F12 (Sigma, Taufkirchen, Germany) medium (1:1) supplemented with 7.5% FBS, L-glutamine (Sigma) (630 µg/mL) and hygromycin B (Carl Roth, Karlsruhe, Germany) (250 µg/mL).

2.4.4 NTS_1R binding assay

NTS_1R radioligand competition binding experiments with [^{3}H]**1.7** (molar activity: 2.41 TBq/mmol) and the peptides **2.5a**, **2.5b**, and **2.25**-**2.32** were performed with intact $hNTS_1R$-expressing HT-29 colon carcinoma cells as described in Chapter 3. Data were analyzed as reported in Chapter 3.

NTS_2R binding assays with [^{3}H]**1.7** and the peptides **2.25** and **2.26** were performed with homogenates from HEK293T cells as described in Chapter 3.

2.4.5 Fura-2 Ca^{2+} assay

NTS_1R agonistic potencies of **2.25** and **2.26** was determined as described under *Fura-2 Ca^{2+} assay* in Chapter 3.

2.4.6 Stability in human plasma

The proteolytic stability of **2.25** and **2.26** was investigated as described under *Stability in human plasma* in Chapter 3. Obtained recoveries and calculated recovery ratios are shown in Table A2.1 (Appendix).

2.5 References

1. Schafmeister, C. E.; Po, J.; Verdine, G. L. An all-hydrocarbon cross-linking system for enhancing the helicity and metabolic stability of peptides. *J. Am. Chem. Soc.* **2000**, *122*, 5891-5892.
2. Gentilucci, L.; De Marco, R.; Cerisoli, L. Chemical modifications designed to improve peptide stability: incorporation of non-natural amino acids, pseudo-peptide bonds, and cyclization. *Curr. Pharm. Des.* **2010**, *16*, 3185-3203.
3. Lang, K.; Chin, J. W. Cellular incorporation of unnatural amino acids and bioorthogonal labeling of proteins. *Chem. Rev.* **2014**, *114*, 4764-4806.
4. Fanelli, R.; Besserer-Offroy, E.; Rene, A.; Cote, J.; Tetreault, P.; Collerette-Tremblay, J.; Longpre, J. M.; Leduc, R.; Martinez, J.; Sarret, P.; Cavelier, F. Synthesis and characterization in vitro and in vivo of (l)-(trimethylsilyl)alanine containing neurotensin analogues. *J. Med. Chem.* **2015**, *58*, 7785-7795.
5. Deng, H.; Wang, H.; Wang, M.; Li, Z.; Wu, Z. Synthesis and evaluation of 64Cu-DOTA-NT-Cy5.5 as a dual-modality PET/fluorescence probe to image neurotensin receptor-positive tumor. *Mol. Pharmacol.* **2015**, *12*, 3054-3061.
6. Keller, M.; Kuhn, K. K.; Einsiedel, J.; Hubner, H.; Biselli, S.; Mollereau, C.; Wifling, D.; Svobodova, J.; Bernhardt, G.; Cabrele, C.; Vanderheyden, P. M.; Gmeiner, P.; Buschauer, A. Mimicking of arginine by functionalized N(omega)-carbamoylated arginine as a new broadly applicable approach to labeled bioactive peptides: High affinity angiotensin, neuropeptide Y, neuropeptide FF, and neurotensin receptor ligands as examples. *J. Med. Chem.* **2016**, *59*, 1925-1945.
7. Oliva, R.; Chino, M.; Pane, K.; Pistorio, V.; De Santis, A.; Pizzo, E.; D'Errico, G.; Pavone, V.; Lombardi, A.; Del Vecchio, P.; Notomista, E.; Nastri, F.; Petraccone, L. Exploring the role of unnatural amino acids in antimicrobial peptides. *Sci. Rep.* **2018**, *8*, 8888.
8. Basith, S.; Cui, M. H.; Macalino, S. J. Y.; Park, J.; Clavio, N. A. B.; Kang, S.; Choi, S. Exploring G protein-coupled receptors (GPCRs) ligand space via cheminformatics approaches: Impact on rational drug design. *Front. Pharmacol.* **2018**, *9*.
9. Schindler, L.; Bernhardt, G.; Keller, M. Modifications at Arg and Ile give neurotensin(8-13) derivatives with high stability and retained NTS(1) receptor affinity. *ACS Med. Chem. Lett.* **2019**, *10*, 960-965.
10. Oeller, M.; Kang, R. J. D.; Bolt, H. L.; Gomes Dos Santos, A. L.; Weinmann, A. L.; Nikitidis, A.; Zlatoidsky, P.; Su, W.; Czechtizky, W.; De Maria, L.; Sormanni, P.;

Vendruscolo, M. Sequence-based prediction of the intrinsic solubility of peptides containing non-natural amino acids. *Nat. Commun.* **2023**, *14*, 7475.

11. Wang, X.; Yang, X.; Wang, Q.; Meng, D. Unnatural amino acids: promising implications for the development of new antimicrobial peptides. *Crit. Rev. Microbiol.* **2023**, *49*, 231-255.
12. Sharma, K. K.; Sharma, K.; Rao, K.; Sharma, A.; Rathod, G. K.; Aaghaz, S.; Sehra, N.; Parmar, R.; VanVeller, B.; Jain, R. Unnatural amino acids: Strategies, designs, and applications in medicinal chemistry and drug discovery. *J. Med. Chem.* **2024**, *67*, 19932-19965.
13. Enninful, G. N.; Kuppusamy, R.; Tiburu, E. K.; Kumar, N.; Willcox, M. D. P. Non-canonical amino acid bioincorporation into antimicrobial peptides and its challenges. *J. Pept. Sci.* **2024**, *30*, e3560.
14. Yi, M.; Ashton-Rickardt, G.; Tan, W.; Liu, Z.; He, H.; Hsieh, J. T.; Xu, B. Accelerating cellular uptake with unnatural amino acid for inhibiting immunosuppressive cancer cells. *Chemistry* **2024**, *30*, e202400691.
15. Day, G. J.; Zaytsev, A. V.; Brewster, R. C.; Kozhevnikov, V. N.; Jarvis, A. G. A dual-purpose non-canonical amino acid for the expanded genetic code: Combining metal-binding and click chemistry. *Angew. Chem. Int. Ed.* **2024**, *63*, e202413073.
16. Granier, C.; van Rietschoten, J.; Kitabgi, P.; Poustis, C.; Freychet, P. Synthesis and characterization of neurotensin analogues for structure/activity relationship studies. Acetyl-neurotensin-(8--13) is the shortest analogue with full binding and pharmacological activities. *Eur. J. Biochem.* **1982**, *124*, 117-124.
17. Einsiedel, J.; Held, C.; Hervet, M.; Plomer, M.; Tschammer, N.; Hubner, H.; Gmeiner, P. Discovery of highly potent and neurotensin receptor 2 selective neurotensin mimetics. *J. Med. Chem.* **2011**, *54*, 2915-2923.
18. Ertl, F. J.; Kopanchuk, S.; Dijon, N. C.; Veiksina, S.; Tahk, M. J.; Laasfeld, T.; Schettler, F.; Gattor, A. O.; Hubner, H.; Archipowa, N.; Kockenberger, J.; Heinrich, M. R.; Gmeiner, P.; Kutta, R. J.; Holliday, N. D.; Rinken, A.; Keller, M. Dually labeled neurotensin NTS(1)R ligands for probing radiochemical and fluorescence-based binding assays. *J. Med. Chem.* **2024**, *67*, 16664-16691.
19. Eiselt, E.; Gonzalez, S.; Martin, C.; Chartier, M.; Betti, C.; Longpre, J. M.; Cavelier, F.; Tourwe, D.; Gendron, L.; Ballet, S.; Sarret, P. Neurotensin analogues containing cyclic surrogates of tyrosine at position 11 improve NTS2 selectivity leading to analgesia without hypotension and hypothermia. *ACS Chem. Neurosci.* **2019**, *10*, 4535-4544.

20. Schindler, L.; Moosbauer, J.; Schmidt, D.; Spruss, T.; Gratz, L.; Ludeke, S.; Hofheinz, F.; Meister, S.; Echtenacher, B.; Bernhardt, G.; Pietzsch, J.; Hellwig, D.; Keller, M. Development of a neurotensin-derived (68)Ga-labeled PET ligand with high in vivo stability for imaging of NTS(1) receptor-expressing tumors. *Cancers (Basel)* **2022**, *14*.
21. White, J. F.; Noinaj, N.; Shibata, Y.; Love, J.; Kloss, B.; Xu, F.; Gvozdenovic-Jeremic, J.; Shah, P.; Shiloach, J.; Tate, C. G.; Grisshammer, R. Structure of the agonist-bound neurotensin receptor. *Nature* **2012**, *490*, 508-513.
22. Egloff, P.; Hillenbrand, M.; Klenk, C.; Batyuk, A.; Heine, P.; Balada, S.; Schlinkmann, K. M.; Scott, D. J.; Schutz, M.; Pluckthun, A. Structure of signaling-competent neurotensin receptor 1 obtained by directed evolution in Escherichia coli. *Proc. Natl. Acad. Sci. U. S. A.* **2014**, *111*, E655-662.
23. Krumm, B. E.; Lee, S.; Bhattacharya, S.; Botos, I.; White, C. F.; Du, H.; Vaidehi, N.; Grisshammer, R. Structure and dynamics of a constitutively active neurotensin receptor. *Sci. Rep.* **2016**, *6*, 38564.
24. Plut, E. Synthesis of unnatural cyclic amino acids and their application in biologically active peptides. Doctoral Thesis, University of Regensburg, Regensburg, Germany, 2024.
25. Einsiedel, J.; Hubner, H.; Hervet, M.; Harterich, S.; Koschatzky, S.; Gmeiner, P. Peptide backbone modifications on the C-terminal hexapeptide of neurotensin. *Bioorg. Med. Chem. Lett.* **2008**, *18*, 2013-2018.
26. Perez-Fuertes, Y.; Taylor, J. E.; Tickell, D. A.; Mahon, M. F.; Bull, S. D.; James, T. D. Asymmetric Strecker synthesis of alpha-arylglycines. *J. Org. Chem.* **2011**, *76*, 6038-6047.
27. Hesk, D.; Cesarz, D.; Magatti, C.; Voronin, K.; Lavey, C.; McNamara, P.; Koharski, D.; Saluja, S.; Hendershot, S.; Pham, H.; Truong, V. Synthesis of [3H], [$13C_2$15N] and [14C]Sch 66336(Sarasar ™). *J. Labelled Compd. Radiopharm.* **2005**, *48*, 11-23.
28. Theodorou, V.; Paraskevopoulos, G.; Skobridis, K. A mild alkaline hydrolysis of N- and N,N-substituted amides and nitriles. *Arkivoc* **2015**, *7*, 101-112.
29. Lee, J.; Chen, D. Y. A local-desymmetrization-based divergent synthesis of quinine and quinidine. *Angew. Chem. Int. Ed.* **2019**, *58*, 488-493.
30. Monovich, L. G.; Tommasi, R. A.; Fujimoto, R. A.; Blancuzzi, V.; Clark, K.; Cornell, W. D.; Doti, R.; Doughty, J.; Fang, J.; Farley, D.; Fitt, J.; Ganu, V.; Goldberg, R.; Goldstein, R.; Lavoie, S.; Kulathila, R.; Macchia, W.; Parker, D. T.; Melton, R.; O'Byrne, E.; Pastor, G.; Pellas, T.; Quadros, E.; Reel, N.; Roland, D. M.; Sakane, Y.; Singh, H.; Skiles, J.; Somers, J.; Toscano, K.; Wigg, A.; Zhou, S.; Zhu, L.; Shieh, W. C.; Xue, S.; McQuire,

L. W. Discovery of potent, selective, and orally active carboxylic acid based inhibitors of matrix metalloproteinase-13. *J. Med. Chem.* **2009**, *52*, 3523-3538.

31. Bergmann, R.; Scheunemann, M.; Heichert, C.; Mading, P.; Wittrisch, H.; Kretzschmar, M.; Rodig, H.; Tourwe, D.; Iterbeke, K.; Chavatte, K.; Zips, D.; Reubi, J. C.; Johannsen, B. Biodistribution and catabolism of (18)F-labeled neurotensin(8-13) analogs. *Nucl. Med. Biol.* **2002**, *29*, 61-72.
32. Kokko, K. P.; Hadden, M. K.; Orwig, K. S.; Mazella, J.; Dix, T. A. In vitro analysis of stable, receptor-selective neurotensin[8-13] analogues. *J. Med. Chem.* **2003**, *46*, 4141-4148.
33. Nock, B. A.; Nikolopoulou, A.; Reubi, J. C.; Maes, V.; Conrath, P.; Tourwe, D.; Maina, T. Toward stable N4-modified neurotensins for NTS1-receptor-targeted tumor imaging with 99mTc. *J. Med. Chem.* **2006**, *49*, 4767-4776.
34. Alshoukr, P.; Rosant, C.; Maes, V.; Abdelhak, J.; Raguin, O.; Burg, S.; Sarda, L.; Barbet, J.; Tourwé, D.; Pelaprat, D.; Gruaz-Guyon, A. Novel neurotensin analogues for radioisotope targeting to neurotensin receptor-positive tumors. *Bioconjugate Chem.* **2009**, *20*, 1602-1610.
35. Garcia-Garayoa, E.; Allemann-Tannahill, L.; Blauenstein, P.; Willmann, M.; Carrel-Remy, N.; Tourwe, D.; Iterbeke, K.; Conrath, P.; Schubiger, P. A. In vitro and in vivo evaluation of new radiolabeled neurotensin(8-13) analogues with high affinity for NT1 receptors. *Nucl. Med. Biol.* **2001**, *28*, 75-84.
36. Kitabgi, P.; De Nadai, F.; Rovere, C.; Bidard, J. N. Biosynthesis, maturation, release, and degradation of neurotensin and neuromedin N. *Ann. N.Y. Acad. Sci.* **1992**, *668*, 30-42.

Appendix Chapter 2

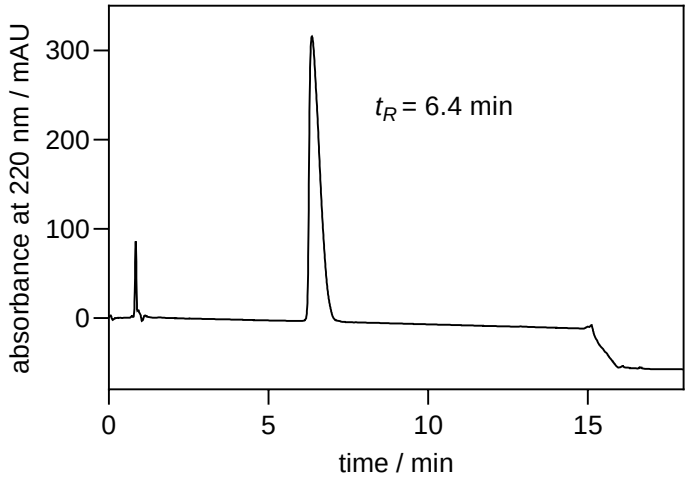
A2.1 Table A2.1

Table A2.1. Recoveries of **2.25** and **2.26** from human plasma/PBS 1:2 v/v and ratios of compound-recovery over recovery of internal standard (1-methyl-D-tryptophan).

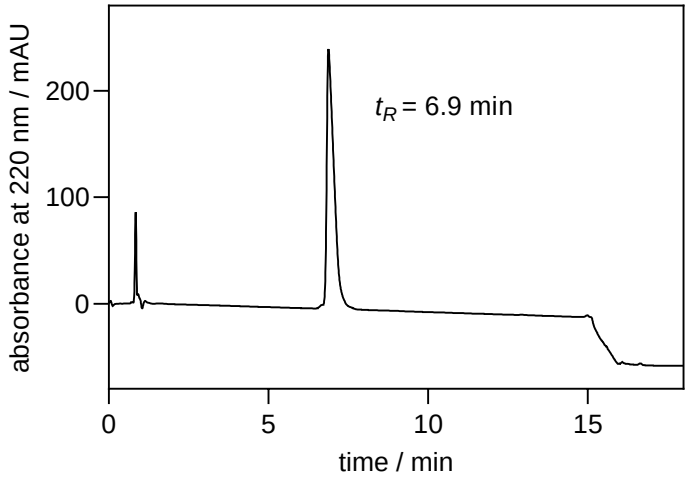
compd.	recovery compd. (%)[a]	recovery 1-methyl-D-tryptophan (%)[a]	ratio[b]
2.25	63	76	0.83
	67	96	0.69
	51	53	0.96
	69	92	0.75
			(0.81 ± 0.06)
2.26	109	101	1.08
	105	99	1.05
	101	102	0.99
	84	84	1.00
			(1.03 ± 0.02)

[a]Recoveries of the peptides and of the internal standard from human plasma/PBS 1:2 v/v using a peptide concentration of 40 µM and an internal standard concentration of 10 µM (four independent experiments). [b]Ratios of peptide recovery over recovery of internal standard calculated for individual experiments, as well as mean recovery ratios ± SEM (given in parenthesis).

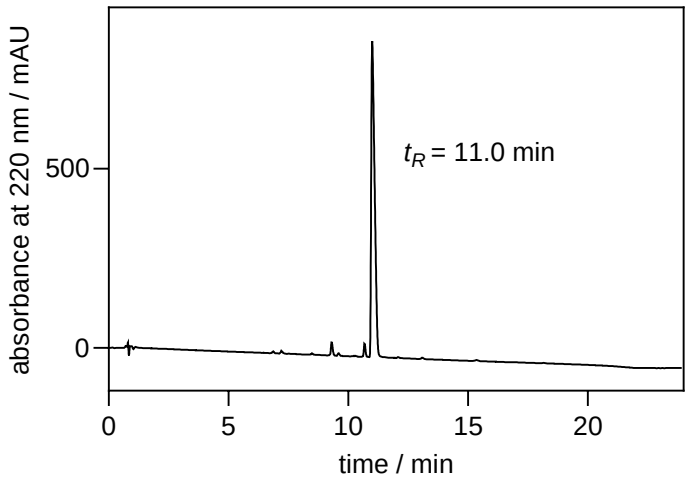
A2.2 RP-HPLC chromatograms of compounds 2.5a, 2.5b, 2.8, 2.11a, 2.11b, 2.15, 2.18, 2.20-2.22, and 2.25-2.32 (purity controls)



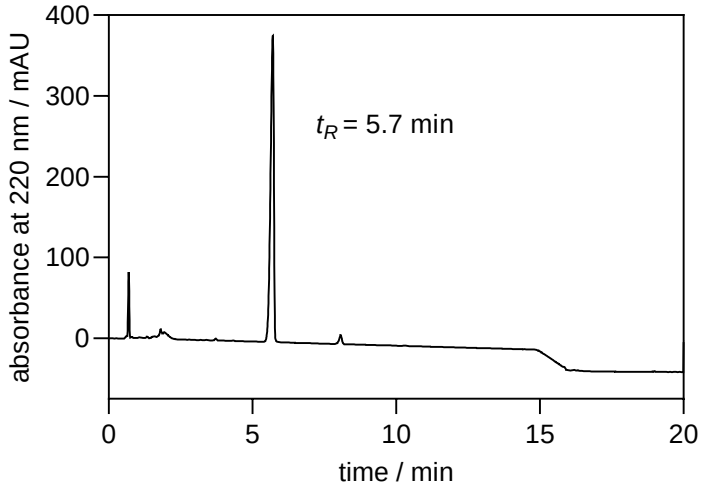
RP-HPLC analysis of compound **2.5a**



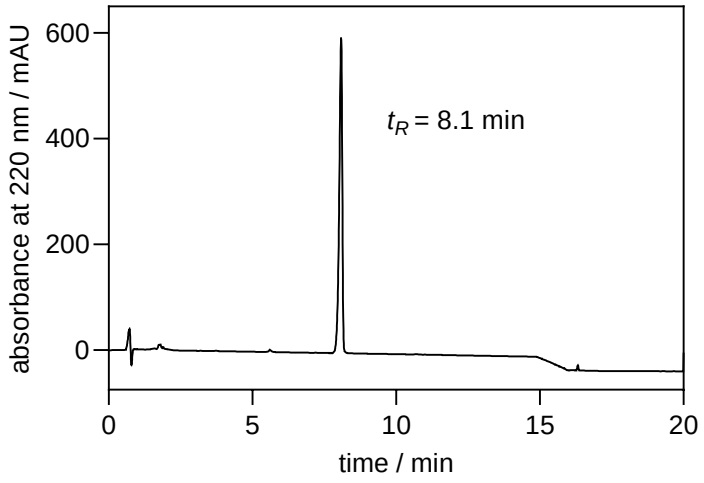
RP-HPLC analysis of compound **2.5b**



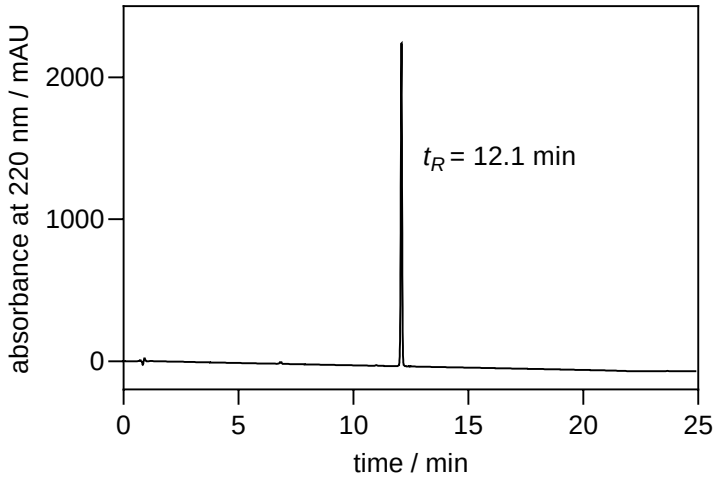
RP-HPLC analysis of compound **2.8**



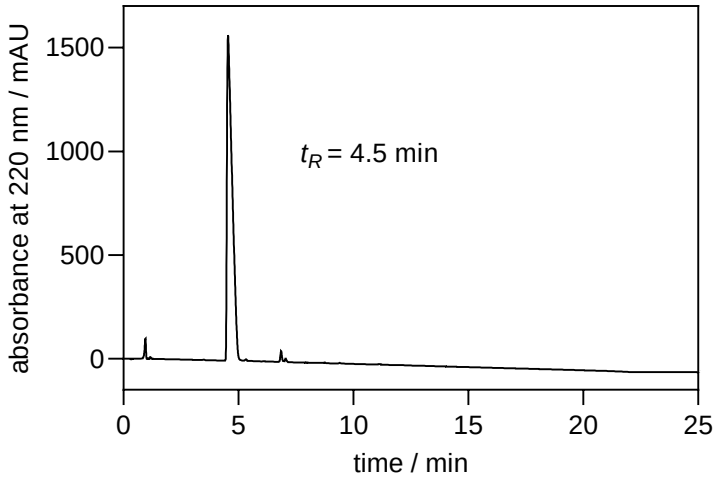
RP-HPLC analysis of compound **2.11a**



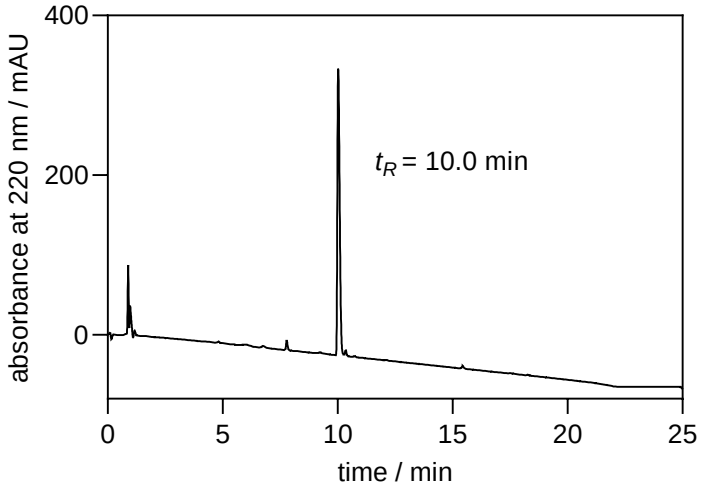
RP-HPLC analysis of compound **2.11b**



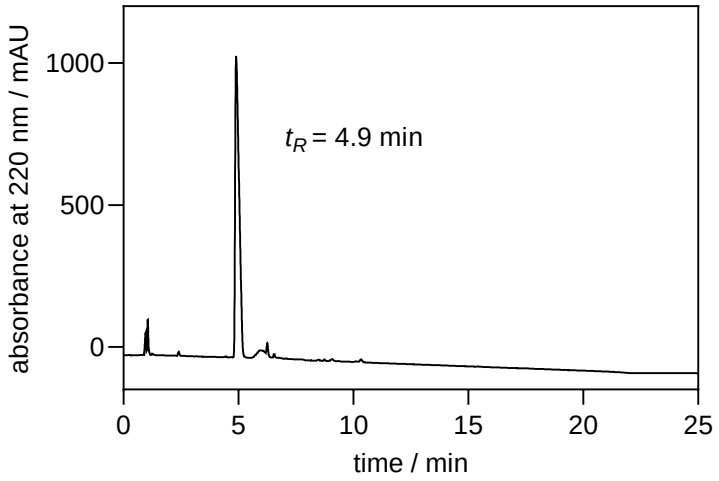
RP-HPLC analysis of compound **2.15**



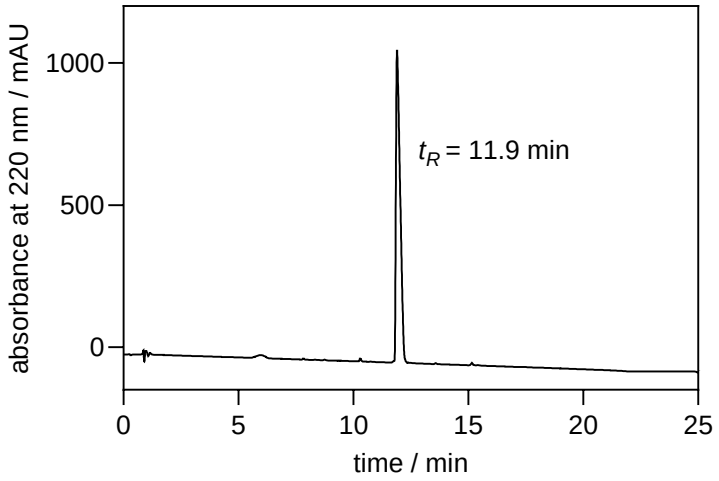
RP-HPLC analysis of compound **2.18**



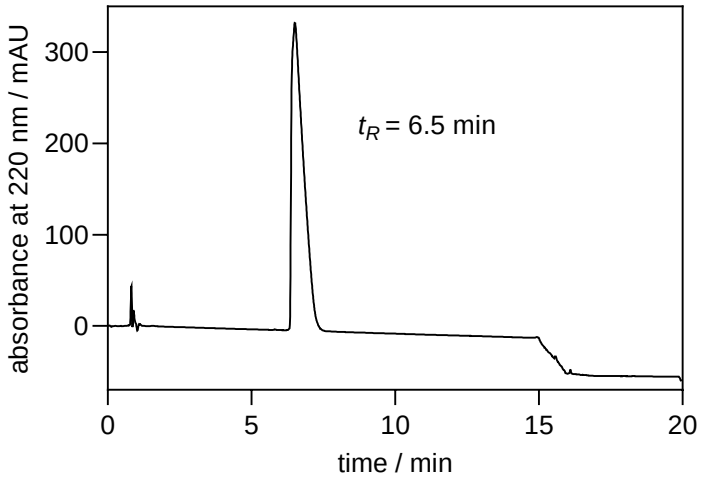
RP-HPLC analysis of compound **2.20**



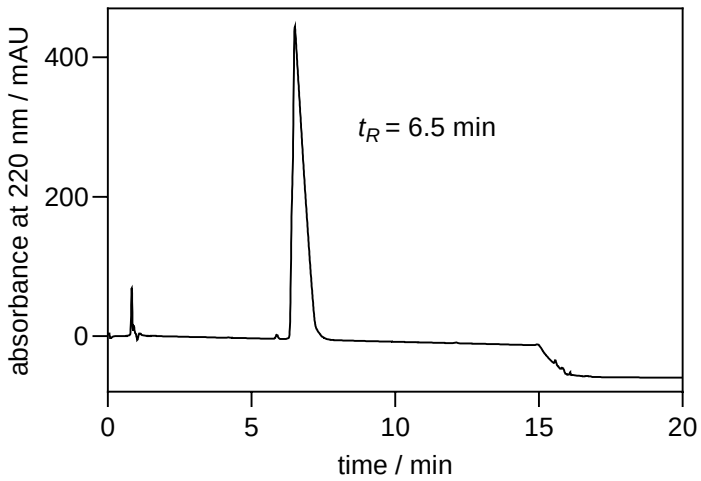
RP-HPLC analysis of compound **2.21**



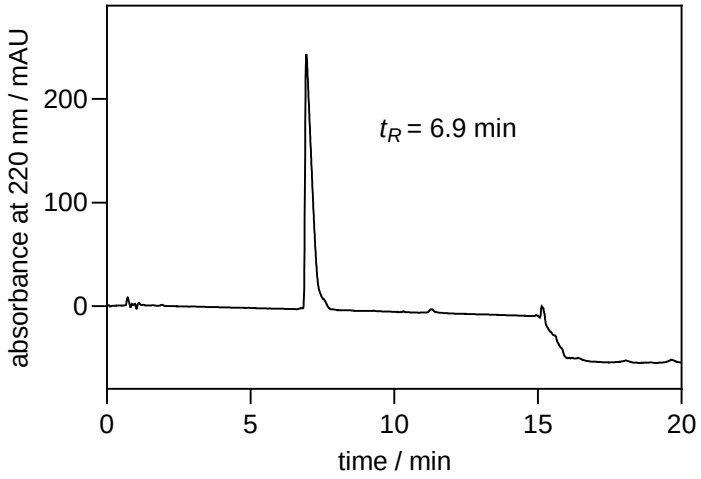
RP-HPLC analysis of compound **2.22**



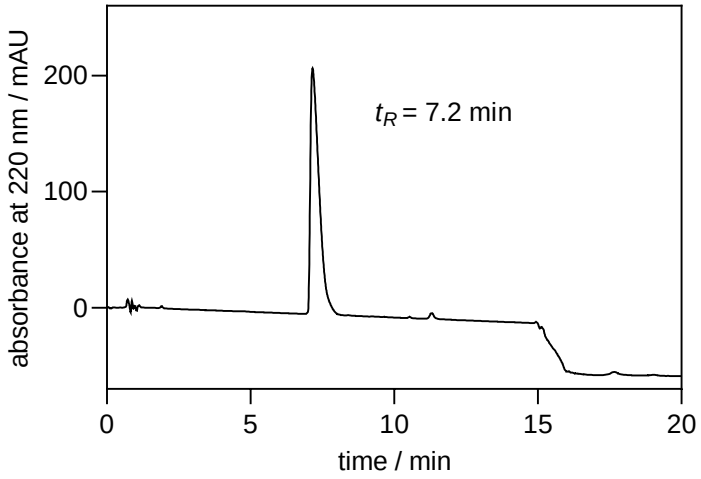
RP-HPLC analysis of compound **2.25**



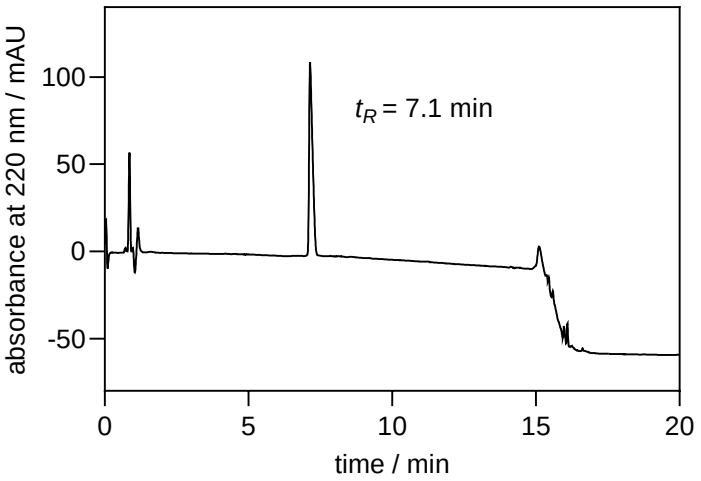
RP-HPLC analysis of compound **2.26**



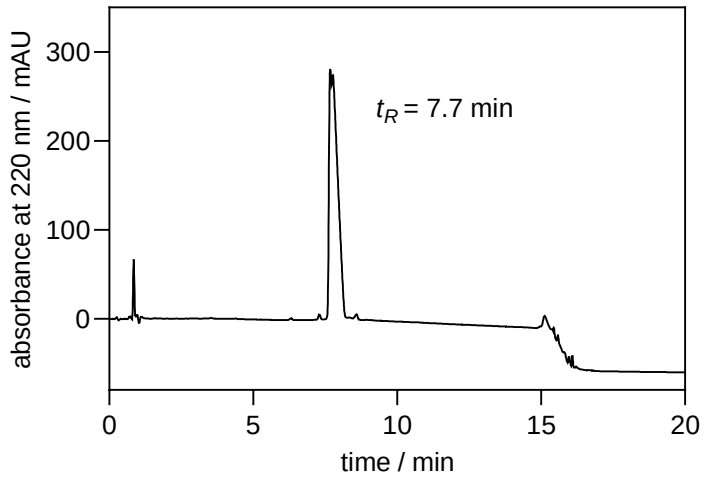
RP-HPLC analysis of compound **2.27a**



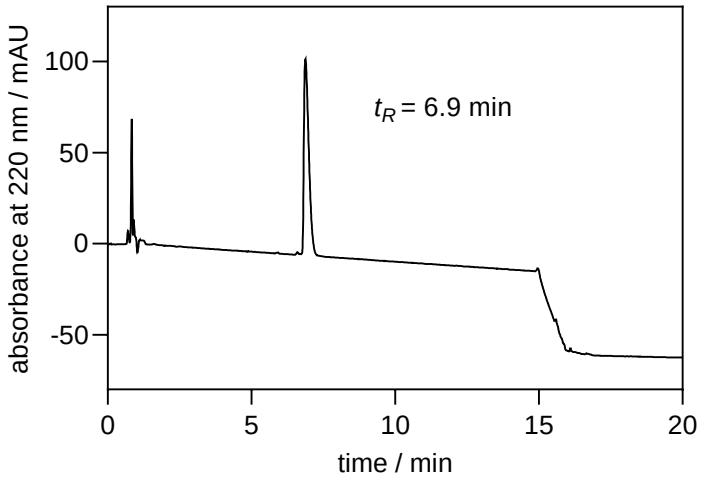
RP-HPLC analysis of compound **2.27b**



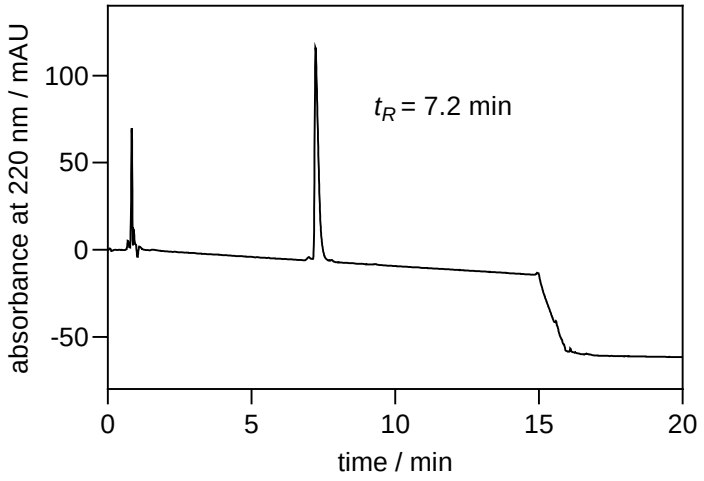
RP-HPLC analysis of compound **2.28a**



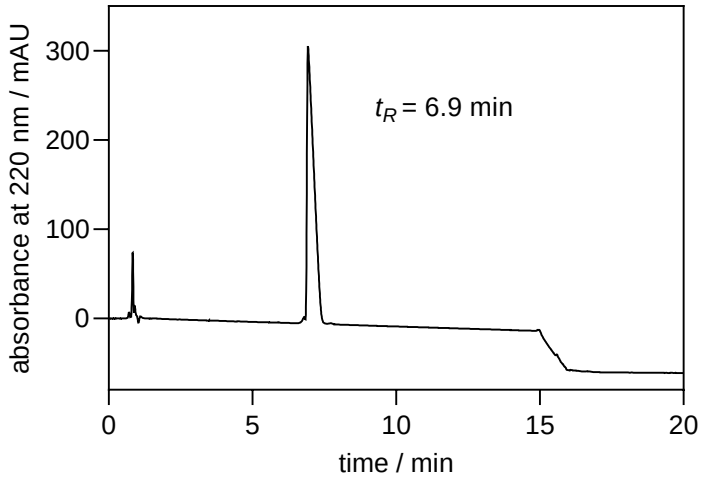
RP-HPLC analysis of compound **2.29**
(mixture of two diastereomers)



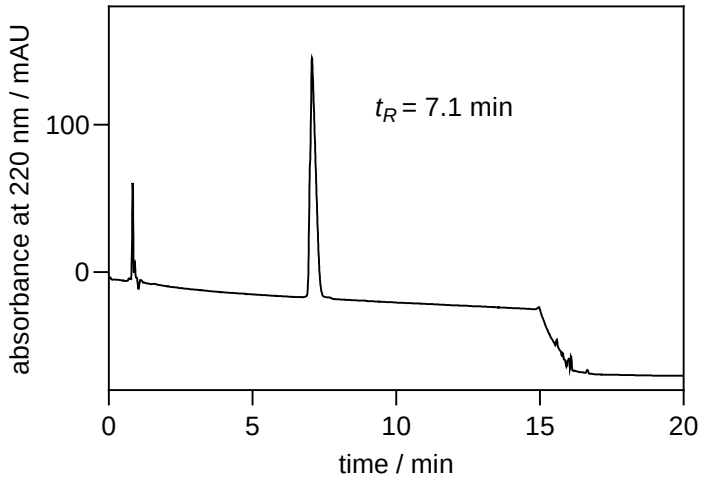
RP-HPLC analysis of compound **2.30a**



RP-HPLC analysis of compound **2.30b**

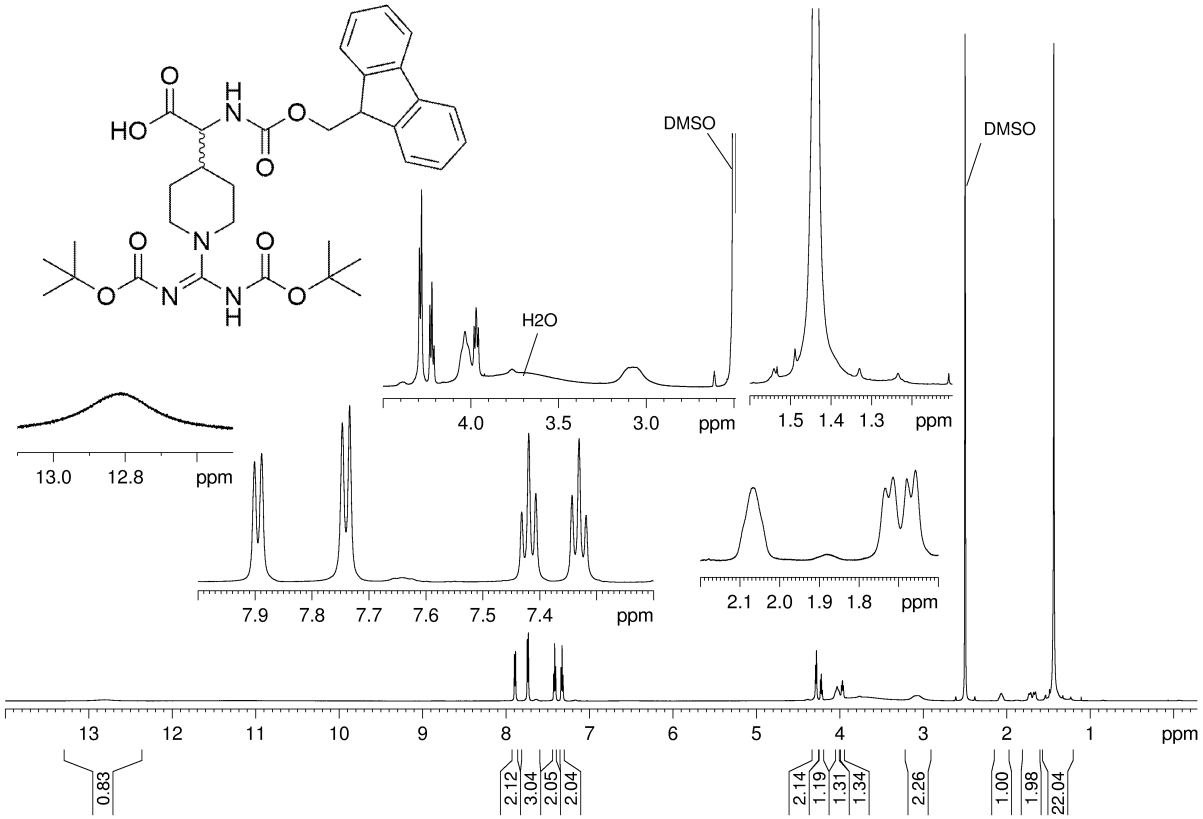


RP-HPLC analysis of compound **2.31**

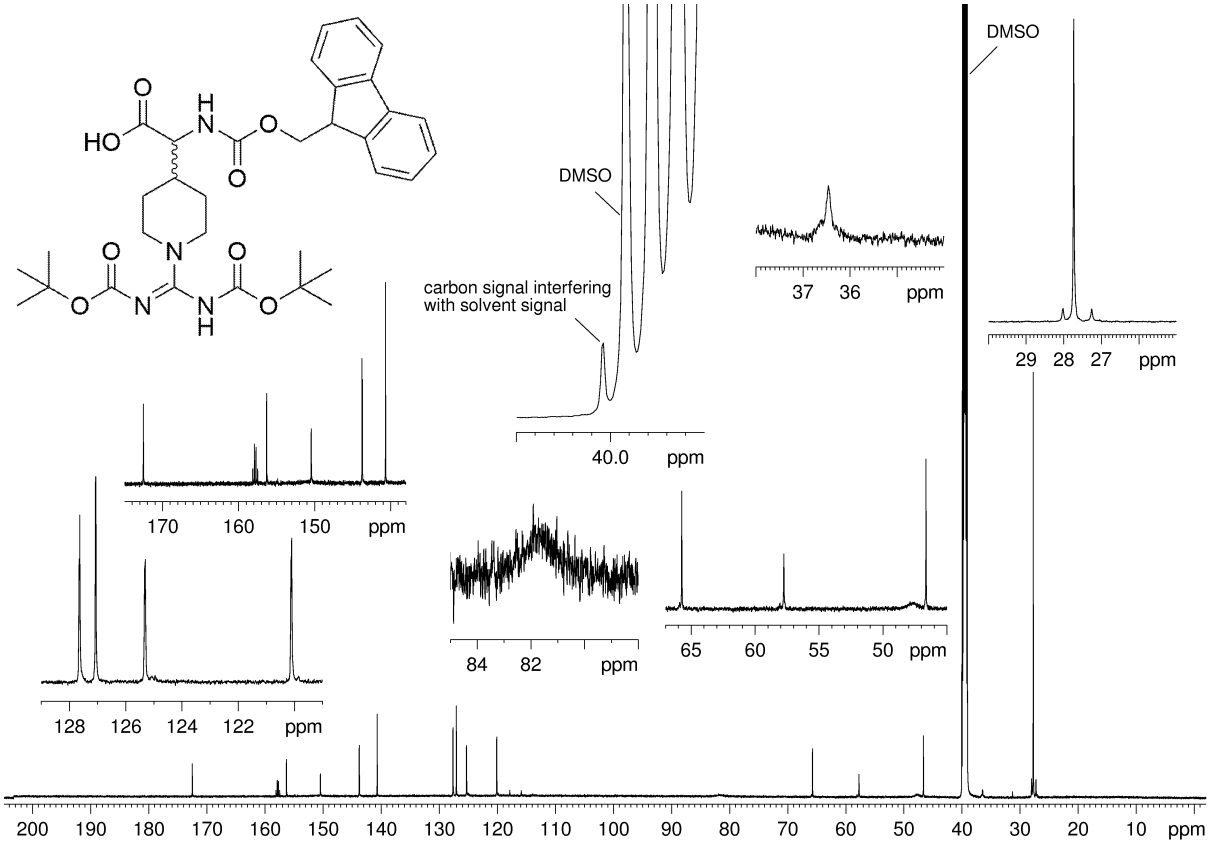


RP-HPLC analysis of compound **2.32**

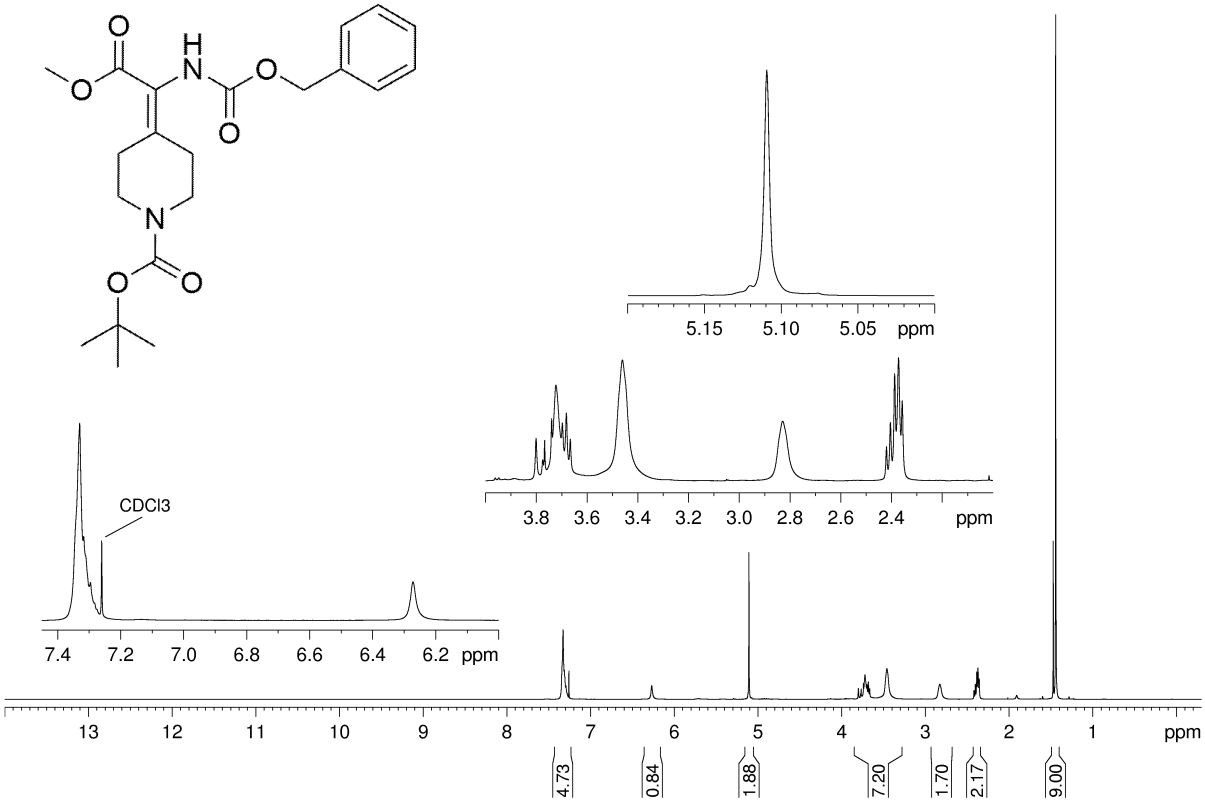
A2.3 ^{1}H-NMR spectra of compounds 2.8, 2.15, 2.18, and 2.20-2.22 and ^{13}C-spectra of compounds 2.8, 2.15, 2.18, and 2.22



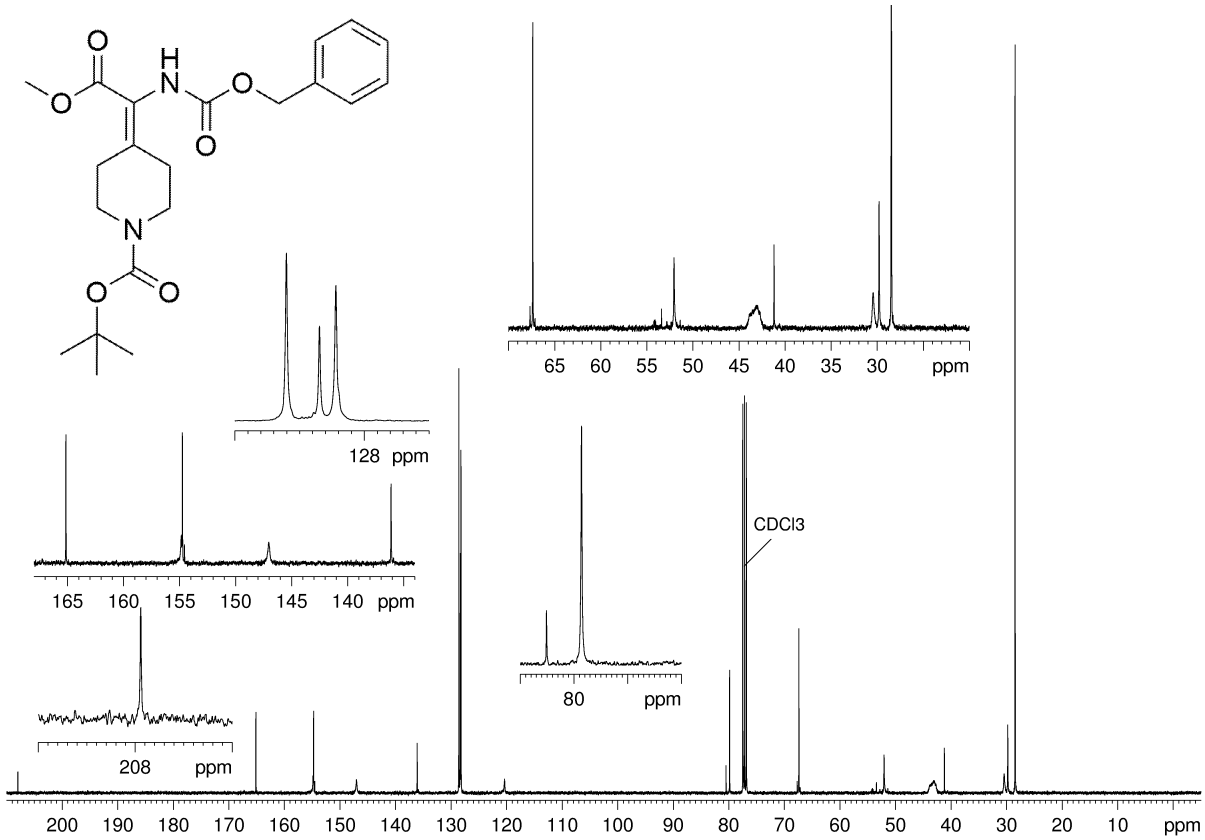
^{1}H-NMR spectrum (600 MHz, DMSO-d_6) of compound **2.8**



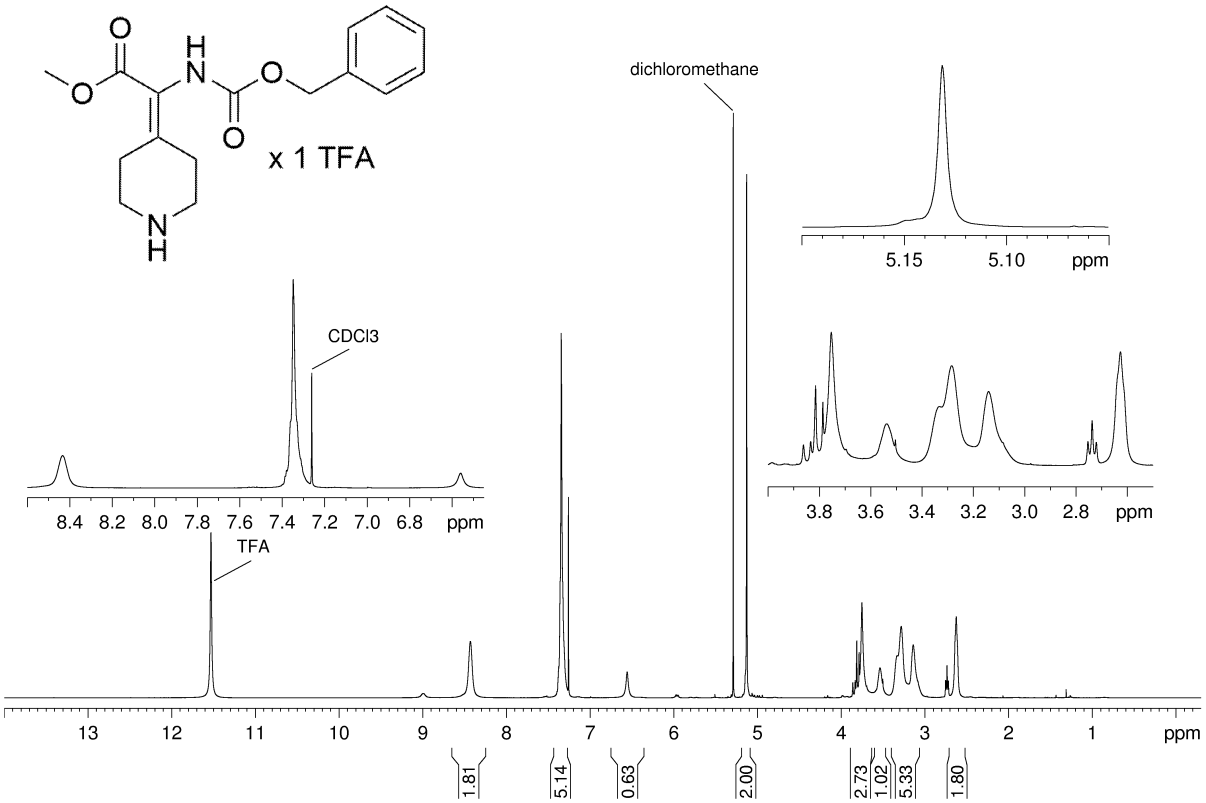
^{13}C-NMR spectrum (150 MHz, DMSO-d_6) of compound **2.8**



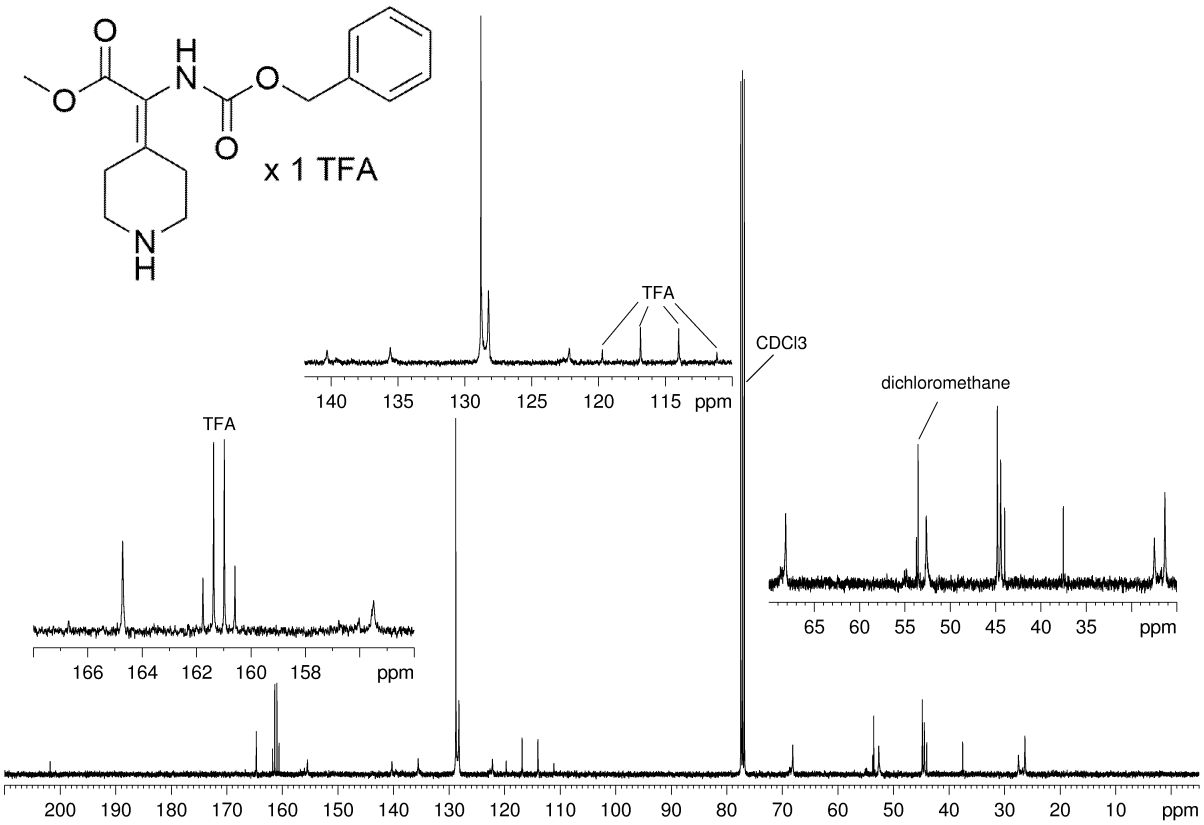
^{1}H-NMR spectrum (400 MHz, $CDCl_3$) of compound **2.15**



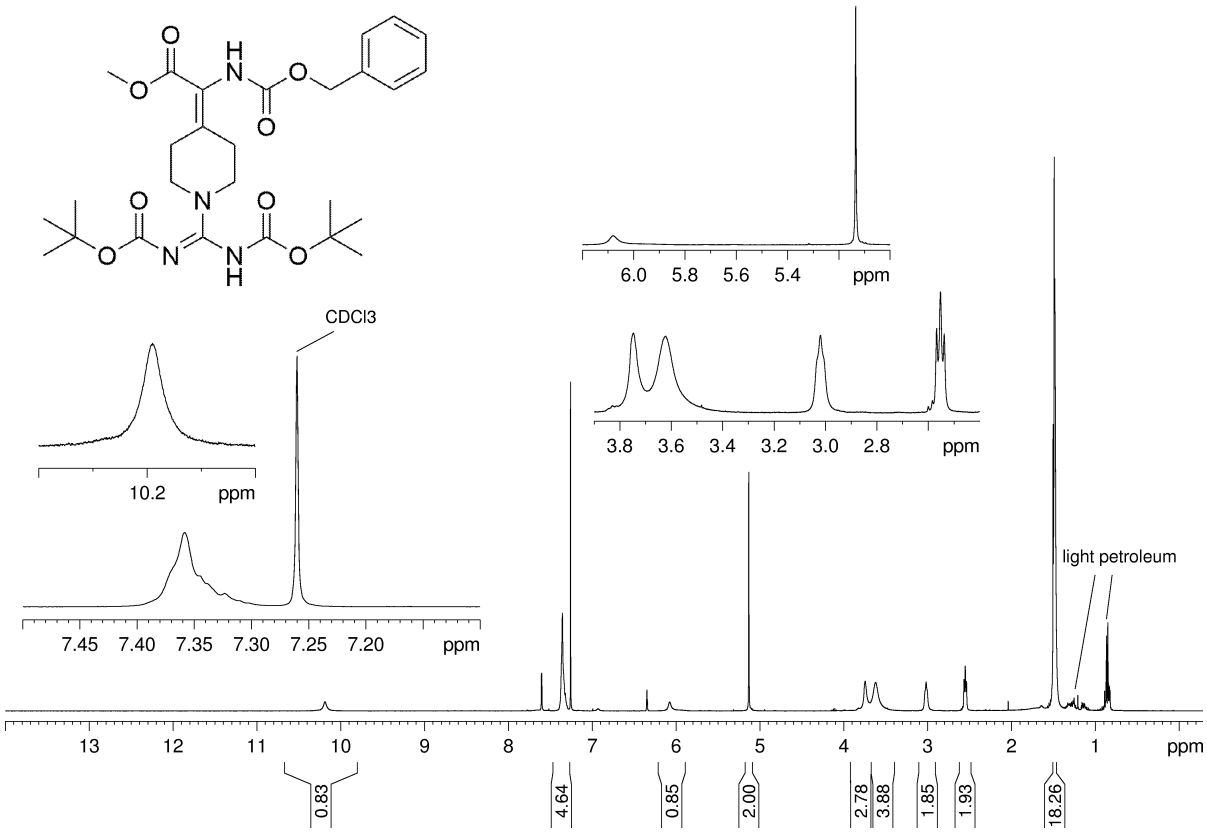
^{13}C-NMR spectrum (100 MHz, $CDCl_3$) of compound **2.15**



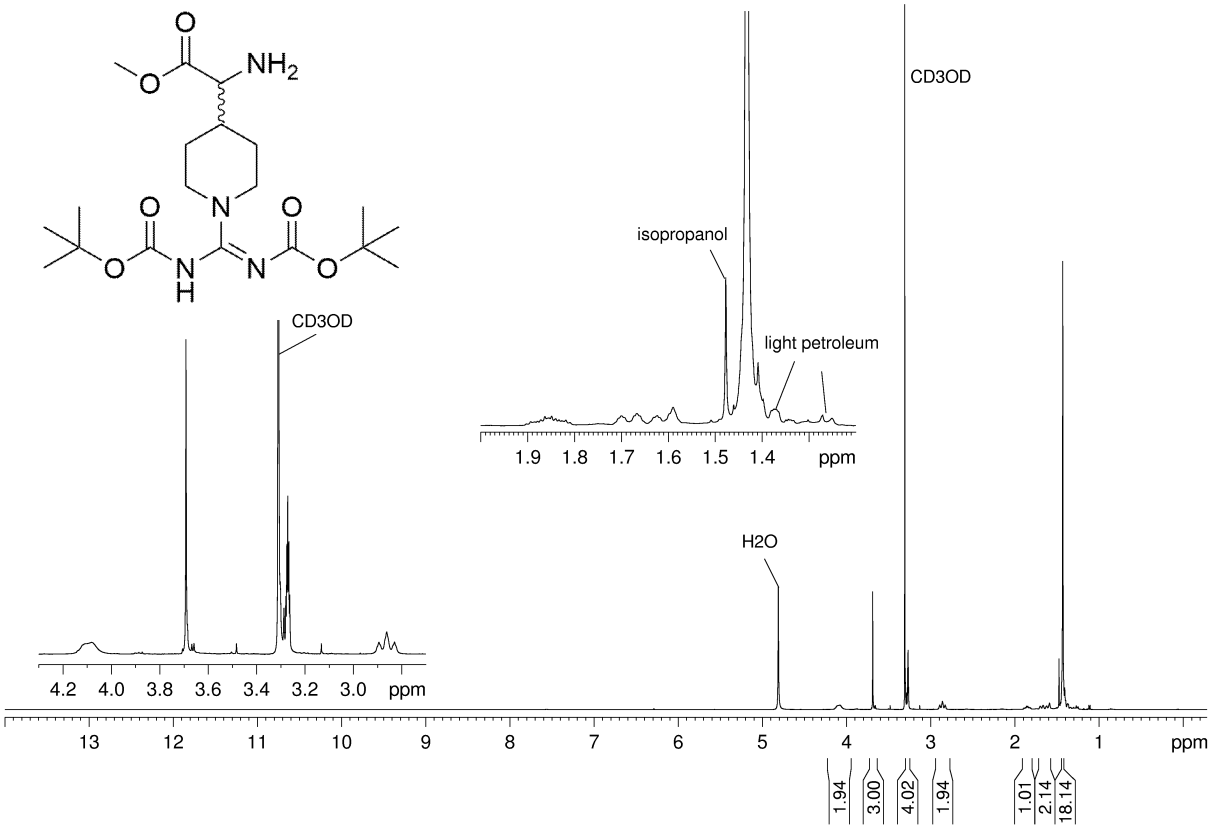
^{1}H-NMR spectrum (400 MHz, $CDCl_3$) of compound **2.18**



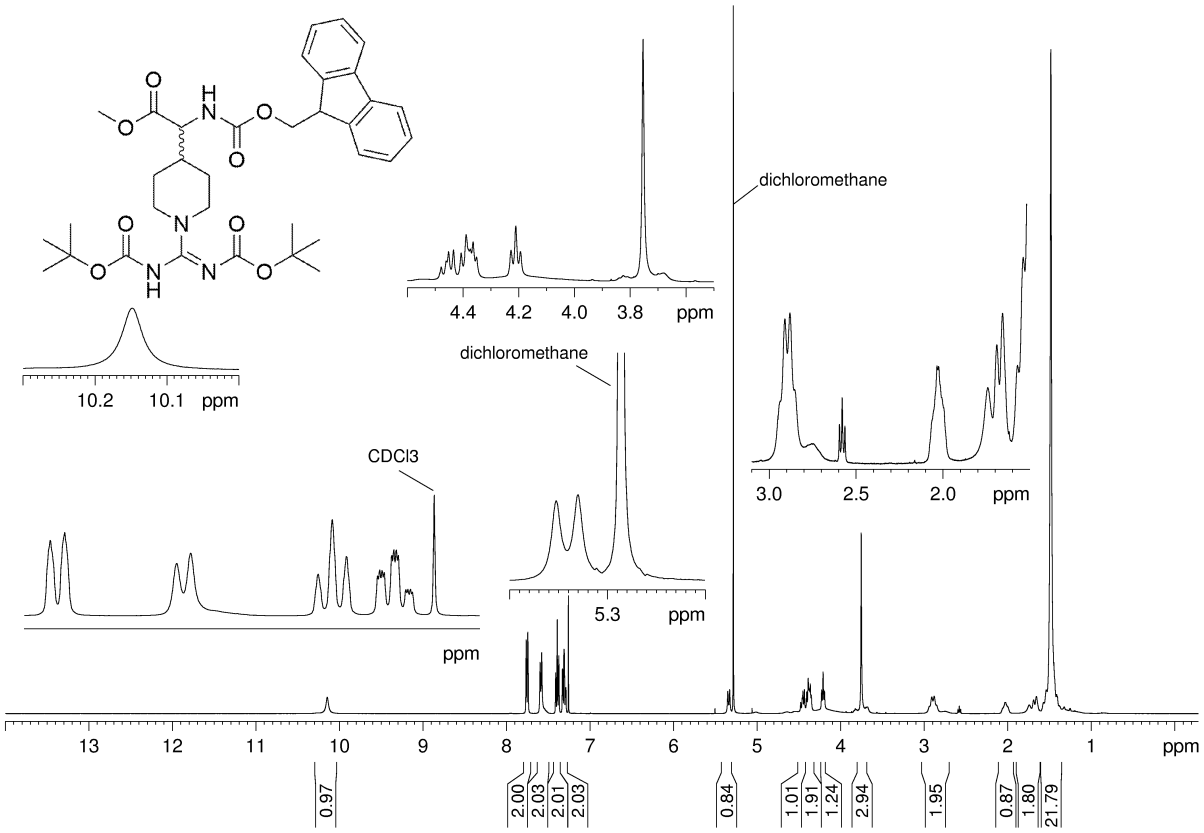
^{13}C-NMR spectrum (100 MHz, $CDCl_3$) of compound **2.18**



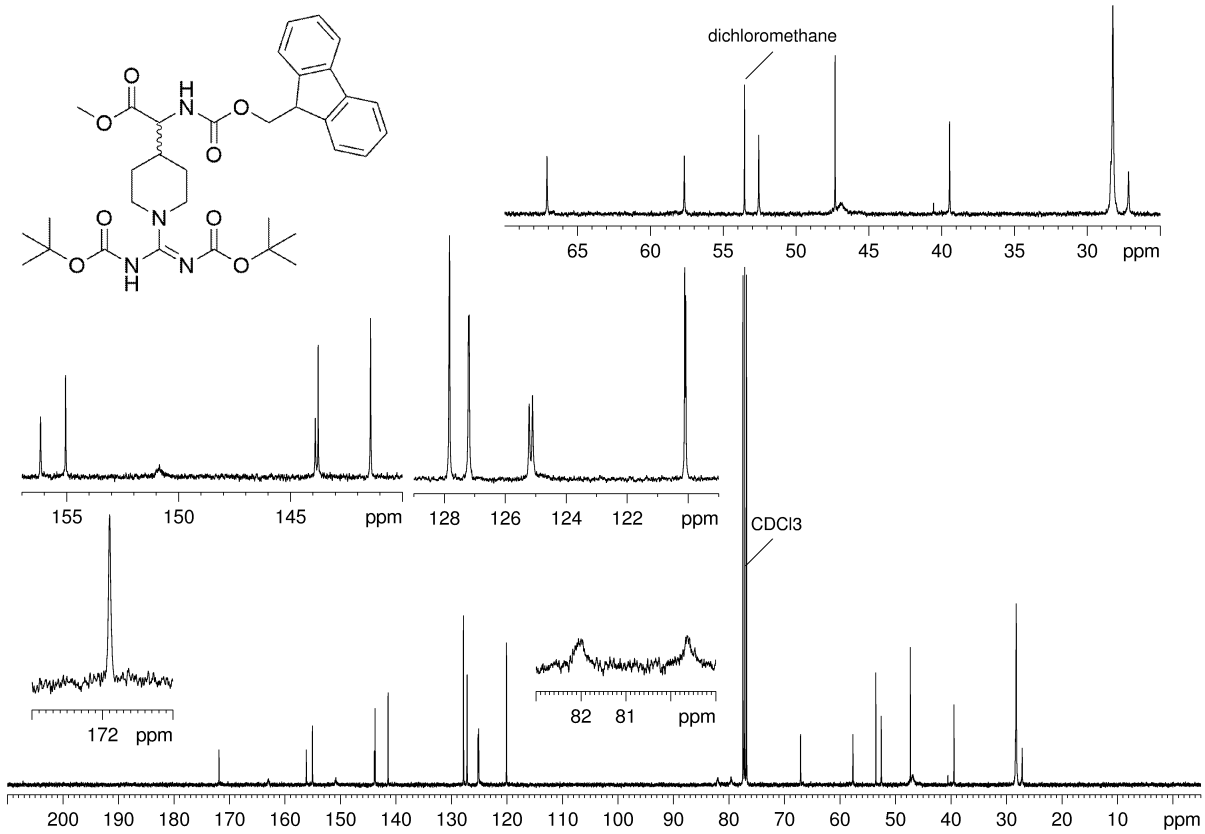
^{1}H-NMR spectrum (400 MHz, $CDCl_3$) of compound **2.20**



^{1}H-NMR spectrum (400 MHz, CD_3OD) of compound **2.21**



^{1}H-NMR spectrum (400 MHz, $CDCl_3$) of compound **2.22**



^{13}C-NMR spectrum (100 MHz, $CDCl_3$) of compound **2.22**

Chapter 3

Dually labeled neurotensin NTS_1R ligands for probing radiochemical and fluorescence-based binding assays

---

This chapter was published in *Journal of Medicinal Chemistry* in collaboration with cooperation partners prior to the submission of the thesis (reused with permissions from ACS, Copyright 2024):

Ertl, F. J.; Kopanchuk, S.; Dijon, N. C.; Veiksina, S.; Tahk, M. J.; Laasfeld, T.; Schettler, F.; Gattor, A. O.; Hubner, H.; Archipowa, N.; Kockenberger, J.; Heinrich, M. R.; Gmeiner, P.; Kutta, R. J.; Holliday, N. D.; Rinken, A. and Keller, M. (2024) Dually labeled neurotensin NTS(1)R ligands for probing radiochemical and fluorescence-based binding assays, *J. Med. Chem.*, 67, 16664-16691. https://doi.org/10.1021/acs.jmedchem.4c01470

Contributions of the co-authors to the work presented in this chapter: Johannes Köckenberger performed the synthesis of the fluorescent dye **3.21**. Nataliya Archipowa and Roger-Jan Kutta determined fluorescence quantum yields. Harald Hübner performed radiochemical NTS_2R binding studies. Franziska Schettler and Albert O. Gattor supported radiochemical binding studies at the NTS_1R. Nicola C. Dijon supported HCI binding assays and performed confocal microscopy imaging experiments. Santa Veiksina performed molecular cloning and prepared the BBVs. Maris-Johanna Tahk, Sergei Kopanchuk, and Tõnis Laasfeld supported fluorescence anisotropy assays. Max Keller initiated and planned the project. Max Keller, Ago Rinken, Nicholas D. Holliday, Markus R. Heinrich, Peter Gmeiner and Roger-Jan Kutta supervised the research.

Note: The compound assigned with **2.24** in Chapter 2 is also part of Chapter 3. To avoid an assignment of several numbers to the same compound, the number **2.24** is also used in this chapter, which had been published as scientific article prior to submission of this thesis. Instead of reorganizing the compound numbers, the number designating the same compound as **2.24** in the published article was omitted in Chapter 3 resulting in a gap in compound numbering, i.e., **3.3** is missing.

3.1 Introduction

The development of pharmacological tools and therapeutics acting at biological receptors involves the determination of ligand-receptor binding affinities. The standard method for studying ligand-receptor binding is the competition binding assay requiring a well characterized labeled receptor ligand. Half a century ago, binding affinities were nearly exclusively determined in radioligand competition binding assays, using a radiolabeled probe that is displaced from the receptor by the studied compound. Today, various luminescence-based methods, such as high-content imaging (HCI), flow cytometry (FC), fluorescence anisotropy (FA) measurements, and bioluminescence resonance energy transfer (BRET)-based binding assays are available to study ligand-receptor binding. The different techniques have advantages and disadvantages. The radiochemical binding assay is highly sensitive and advantageous with respect to the quantification of bound and free labeled ligand. Moreover, the labeling procedure (introduction of a radionuclide such as iodine-125 or tritium) has usually little impact on the ligand structure and consequently also on the bioactivity of the labeled probe. On the downside, radiochemical assays are associated with special safety precautions, the need for specialized laboratory permits, high costs (purchase of radioligands, radioactive waste disposal in the case of long-lived isotopes such as tritium) and the emergence of undefined ligand species in the radioligand stock due to radionuclide disintegration. Furthermore, the radiochemical binding assay requires a separation of unbound and bound radioligand after sample incubation precluding a measurement under equilibrium conditions. Most disadvantages associated with radiochemical assays turn into advantages when ligand-receptor binding is studied by fluorescence-based methods: several techniques (e.g., FC, FA- and BRET-based assays) enable a measurement of bound ligand under homogenous conditions, the potential health risk is very low, and waste disposal is inexpensive. Moreover, several luminescence-based methods allow a fast and automated sample measurement by multimode plate readers (e.g., HCI, FA, BRET). However, there are also drawbacks connected with fluorescence-based binding assays. The attachment of a bulky fluorescent dye to a ligand likely affects receptor binding affinity, and the hydrophobic nature of the fluorescent dye usually results in unfavorable physicochemical properties of the fluorescent ligand potentially causing poor solubility and higher unspecific binding. Fluorescence properties such as quantum yield and spectral characteristics depend on many factors, such as the chemical or biological environment (solvent polarity, buffer supplements, cellular proteins and lipids), the concentration of fluorescence quenchers (e.g., molecular oxygen), pH and temperature, impeding a quantification of the concentration of

bound and unbound fluorescent ligand.[1] Moreover, fluorophores can be prone to photobleaching and might catalyze photoreactions.[2-5]

Due to the different kind of labels, radioligands and fluorescent ligands are, even if derived from the same pharmacophore or ligand, structurally different, and their receptor binding characteristics cannot be studied in the same type of binding assay. This means that radiochemical and fluorescence-based binding assays usually cannot be directly compared based on the labeled ligands. They can merely be compared indirectly by the determination of ligand-receptor binding affinities of unlabeled ligands in competition binding assays. To enable a direct comparison of radiochemical and fluorescence-based binding assays, we synthesized tritium labeled fluorescent ligands and their structurally identical "cold"/non-radioactive analogs, which were investigated in both radiochemical and fluorescence-based binding assays, respectively. The neurotensin (NT) receptor type 1 (NTS_1R),[6] for which peptidic fluorescent and tritiated ligands were already reported (examples shown in Figure 3.1A),[7-17] was chosen as model system.

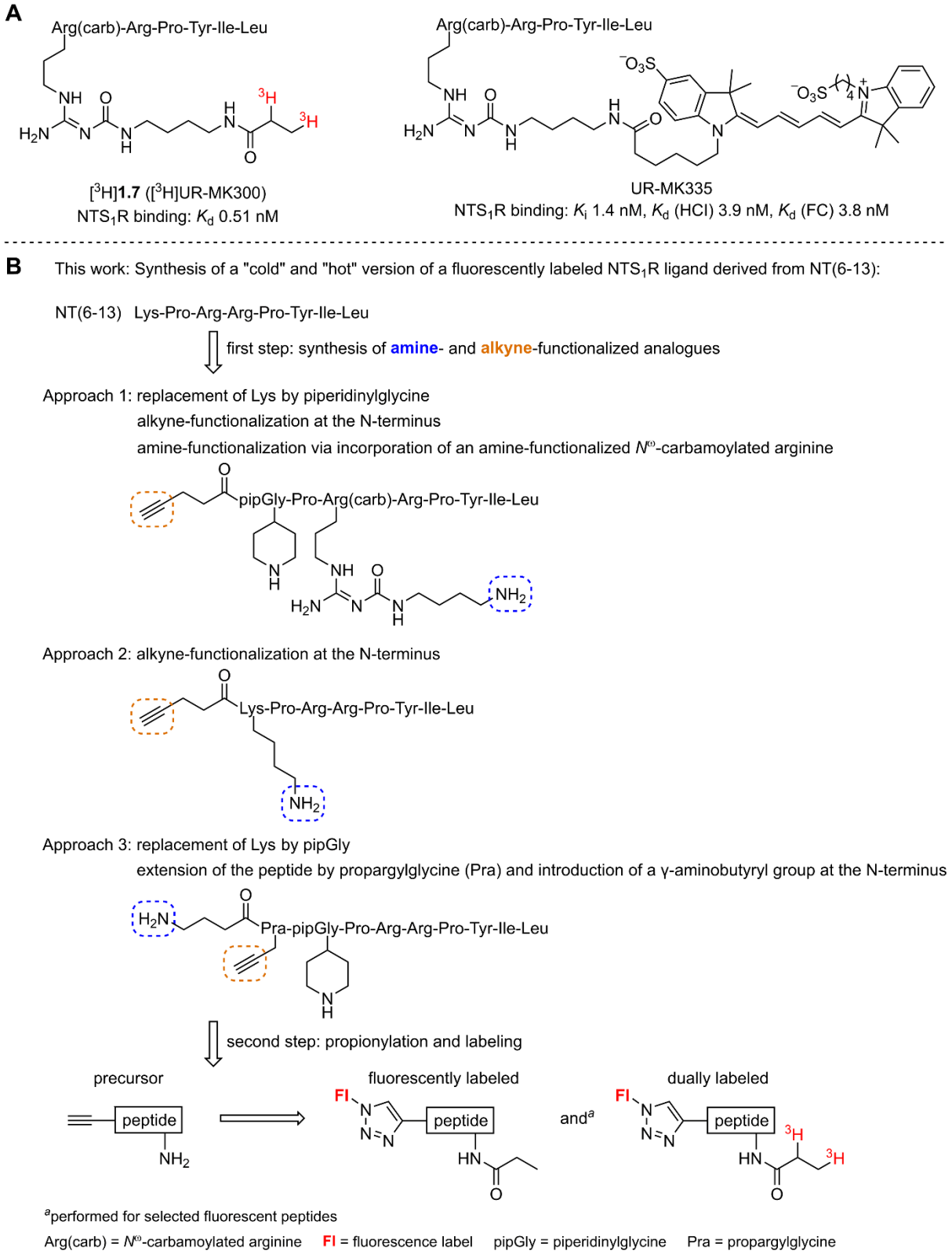


Figure 3.1. (A) Structures and NTS_1R binding affinities of the reported tritium-labeled NT(8-13) derivative [^{3}H]**1.7** ([^{3}H]UR-MK300)[13] and the sulfo-Cy5 labeled ligand UR-MK335[16] both bearing the label at an N^{ω}-carbamoylated arginine. (B) Concept of the present study: design and synthesis of fluorescently labeled NT(6-13) derivatives and their structurally identical tritium-labeled analogs as molecular tools to be studied in fluorescence-based and radiochemical binding assays. Three different approaches were pursued. Note that the tritium atoms in the [^{3}H]propionyl residues do not represent a quantity of tritium isotopes; they only indicate that tritium is present in the respective position.

Aiming for dually labeled ligands, a series of NT(6-13) derivatives, carrying two orthogonal functionalities (alkyne, amine), were synthesized followed by propionylation at the amino group and fluorescence labeling via the alkyne functionality to obtain the "cold" fluorescent ligands (Figure 3.1B) (note: the propionyl moiety was chosen since succinimidyl [^{3}H]propionate is a commercially available labeling reagent allowing for an introduction of [^{3}H]propionyl groups). For two selected fluorescent ligands, the tritiated analogs were prepared by introducing a [^{3}H]propionyl moiety instead of the propionyl group (Figure 3.1). While the "cold" fluorescent ligands were characterized by saturation, kinetic, and competition binding studies in three different fluorescence-based assays (high-content imaging (HCI), flow cytometry (FC), fluorescence anisotropy (FA); comprehensive reviews about these methods have been published[18-22]), the dually labeled peptides were investigated in radiochemical saturation, kinetic, and competition binding assays. To note, for the benefit of a better comparison, all binding studies were performed using wild-type hNTS$_1$R, i.e., genetically modified proteins such as hNTS$_1$R fused to nanoluciferase (useful for BRET binding assays)[23] were not involved. Likewise, the same type of buffer was used for all binding studies.

3.2 Results and discussion

3.2.1 Ligand design

As lead compound, NT(6-13) (cf. Figure 3.1B) was chosen since crystal structures of the NTS$_1$R in complex with NT analogs revealed that the NTS$_1$R binding site is occupied by the C-terminal hexapeptide sequence NT(8-13) (**1.3**; for amino acid sequence see Figure 1.1, Chapter 1).[24-26] An N-terminal extension of the NT(8-13) peptide sequence does not substantially effect NTS$_1$R binding as exemplified by a reported study demonstrating almost equal NTS$_1$R affinities for full length neurotensin, NT(6-13), and **1.3**.[27] Therefore, Lys^6 and Pro^7 in NT(6-13) can serve as a spacer between the N-terminus of **1.3** and a bulky, N-terminally introduced substituent as confirmed by NT(6-13)-derived PET ligands showing high NTS$_1$R affinity.[12,28] It should be noted that structural modifications at the C-terminus were not considered because this would have high impact on NTS$_1$R binding affinity due to the localization of the C-terminus of **1.3** in the deep part of the binding pocket.[24]

For the majority of the fluorescently labeled peptides, the bulky fluorescent dye and the propionyl group were attached N-terminally and at an amino acid side chain, respectively. Thus, the introduction of a propionyl or tritiated propionyl moiety required an amino-functionalized side chain, and conjugation to the fluorescent dye via click chemistry required an alkyne-

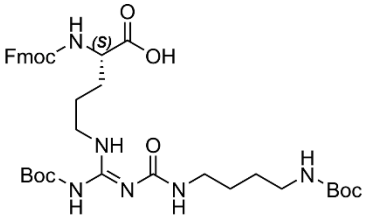
functionalized N-terminus. According to approach 1 (cf. Figure 3.1B), the primary amino group was introduced by incorporation of an amino-functionalized N^{ω}-carbamoylated arginine derived from **3.1**.[13] To avoid the presence of two side chains with a primary amino group in these peptides, Lys^6 was replaced by piperidinylglycine (pipGly) as a lysine mimic, reported to act as a bioisoster of lysine.[12,28,29] To note, for steric reasons, the primary amino group of the amino-functionalized N^{ω}-carbamoylated arginine is preferred over the secondary amino group in pipGly by acylating reagents, allowing a selective propionylation of the former. In the case of NT(6-13) derivatives containing lysine or D-lysine, the amino-functionalized side chain for propionylation is provided by lysine (approach 2, Figure 3.1B). For approaches 1 and 2, the alkyne moiety was introduced by N-terminal acylation of the peptides with 4-pentynoic acid.
Regarding approach 3 (cf. Figure 3.1B), Lys^6 is replaced by pipGly and the peptide is N-terminally extended by propargylglycine (Pra), which carries an γ-aminobutyryl residue at the N^{α}-nitrogen atom, meaning that the fluorescent dye is attached to the side chain of Pra and the propionyl group is introduced N-terminally.
The rhodamine-type dye 5-TAMRA and the indolinium-type cyanine dye Cy3B (cf. Scheme 3.2), both exhibiting a high extinction coefficient, high fluorescence quantum yield, and a fluorescence lifetime well compatible with fluorescence polarization-based binding assays,[5,21,30] were used as fluorescence label.

3.2.2 Synthesis

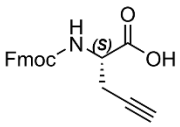
Using Fmoc-protected derivatives of proteinogenic amino acids (Arg, Ile, Leu, Lys, Pro) and unnatural amino acids (**3.1**, **3.2**, **2.24**, and **3.4**, see Scheme 3.1A), the amine- and alkyne-functionalized precursor peptides **3.6**-**3.9**, **3.10a** and **3.10b** (sequences shown in Scheme 3.1B) were synthesized by solid-phase peptide synthesis (SPPS). To exemplify the peptide synthesis, the preparation of **3.6**, containing an amino-functionalized N^{ω}-carbamoylated arginine derived from **3.1**, is shown in Scheme 3.1C. In **3.6**-**3.8**, **3.10a**, and **3.10b**, the alkyne group was introduced N-terminally by final treatment of the resin-bound, Fmoc-deprotected peptide with succinimidyl ester **3.5**.

Scheme 3.1. Synthesis of amine- and alkyne-functionalized precursor peptides.

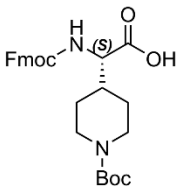
A



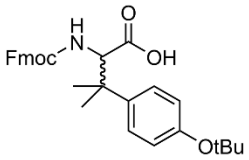
3.1, Fmoc-Arg(carb)(Boc)-OH



3.2, Fmoc-Pra-OH



2.24, Fmoc-pipGly(Boc)-OH



3.4, Fmoc-ß,ß-diMe-DL-Tyr(tBu)-OH (rac.)

B

3.6 pentynyl-pipGly-Pro-Arg(carb)-Arg-Pro-Tyr-Ile-Leu

3.7 pentynyl-Lys-Pro-Arg-Arg-Pro-Tyr-Ile-Leu

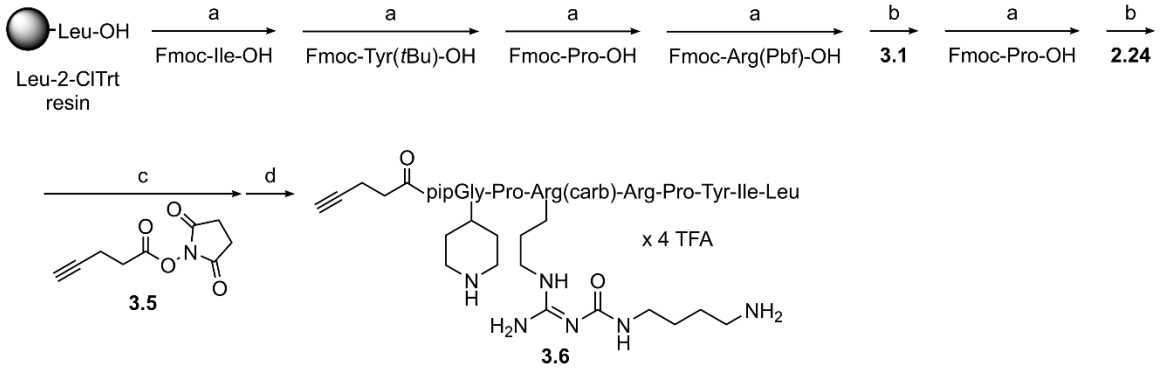
3.8 pentynyl-D-Lys-Pro-Arg-Arg-Pro-Tyr-Ile-Leu

3.9 H_2N-GAB-Pra-pipGly-Pro-Arg-Arg-Pro-Tyr-Ile-Leu

3.10a pentynyl-pipGly-Pro-Arg(carb)-Arg-Pro-ß,ß-diMe-L-Tyr-Ile-Leu

3.10b pentynyl-pipGly-Pro-Arg(carb)-Arg-Pro-ß,ß-diMe-D-Tyr-Ile-Leu

C



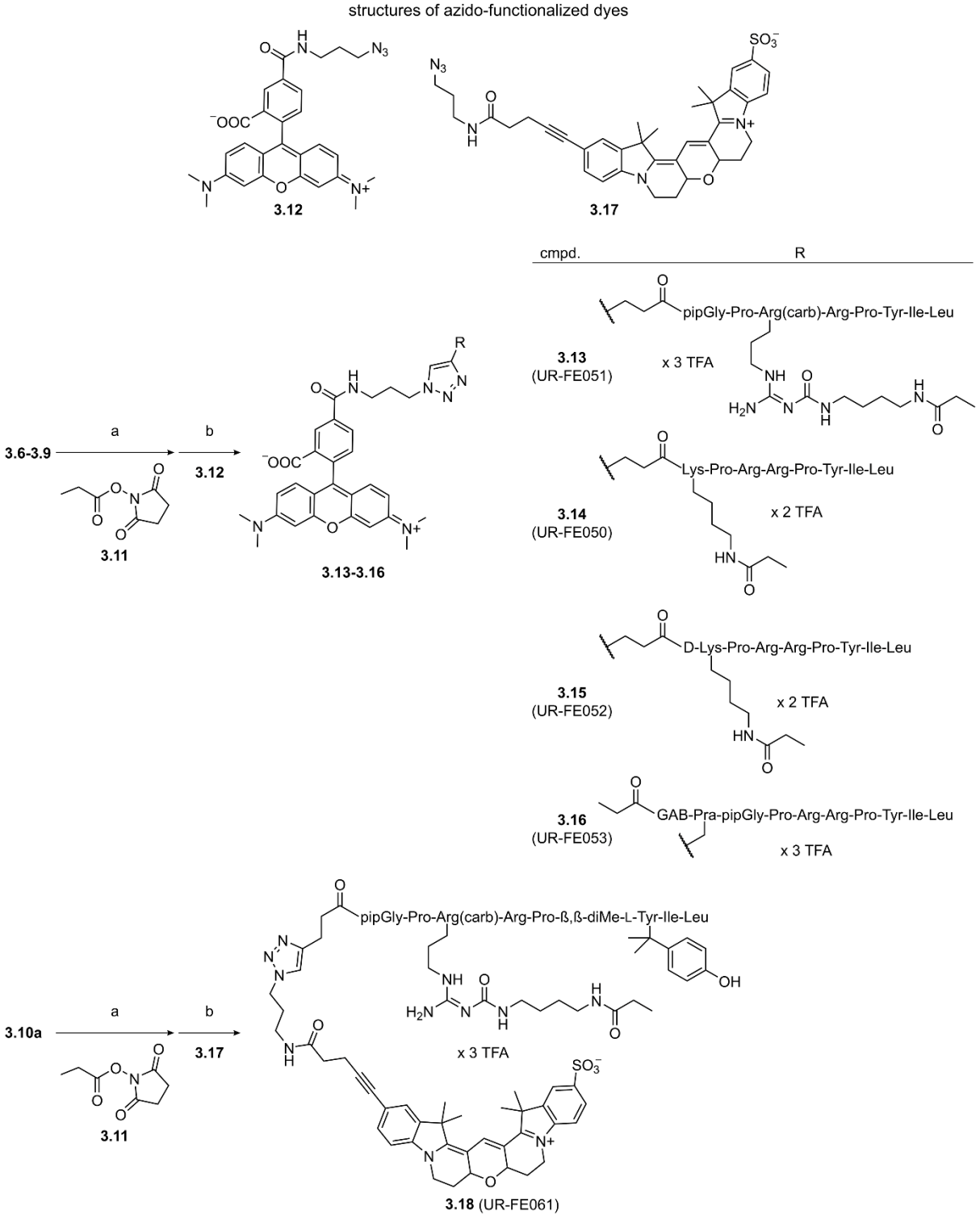
(A) Structures of used unnatural amino acids. (B) Amino acid sequences of the amine- and alkyne-functionalized precursor peptides **3.6**-**3.9**, **3.10a** and **3.10b**. GAB = γ-aminobutyryl. Overall yields for SPPS: 10-38%. (C) SPPS exemplarily shown for peptide **3.6**. Reagents and conditions: (a) amino acid coupling: Fmoc-amino acid/HOBt/HBTU/DIPEA (5/5/4.9/10 equiv.), DMF/NMP 4:1 v/v, 35 °C, 2 × 45 min ("double" coupling), Fmoc deprotection: 20% piperidine in DMF/NMP 4:1 v/v, rt, 2 x 10 min; (b) **3.1** or **2.24**/HOBt/HBTU/DIPEA (3/3/2.95/6 equiv.), DMF/NMP 4:1 v/v, 35 °C, 16 h ("single" coupling), Fmoc deprotection: as under (a); (c) **3.5**/DIPEA (10/10 equiv.), DMF/NMP 4:1 v/v, 35 °C, 30 min; (d) (1) TFA/CH_2Cl_2 1:3 v/v. rt, 2 x 20 min; (2) TFA/H_2O 95:5 v/v, rt, 5 h.

In peptide **3.9**, the alkyne moiety was introduced by incorporation of Pra in the N-terminal position. To introduce an amino-functionalized spacer, this peptide was N-terminally acylated with γ-aminobutyric acid. Worth mentioning, SPPS of **3.9** (exact mass: 1233.7346 Da) yielded a side product (mass identified by HRMS: 1310.9922 Da) in approximately equal amount to **3.9**, supposedly caused by the non-protected alkyne group in Fmoc-Pra-OH (**3.2**). Separation of the side product from **3.9** by preparative RP-HPLC was laborious due to similar retention times. Peptides **3.10a** and **3.10b** represent congeners of **3.6**, containing, compared to **3.6**, β,β-dimethyl-L-tyrosine (**3.10a**) or β,β-dimethyl-D-tyrosine (**3.10b**) instead of L-tyrosine. This modification was taken into consideration due to a recent study on NT(8-13)-derived PET

ligands where the replacement of tyrosine by β,β-dimethyl-L-tyrosine resulted in analogs with high in vitro (blood plasma) and high in vivo stability, and increased NTS_1R affinity.[31] As Fmoc-β,β-dimethyl-DL-Tyr(tBu)-OH (**3.4**) was commercially available only as racemic mixture and used as such for peptide synthesis, two diastereomers (**3.10a** and **3.10b**) were obtained, which could be separated by preparative RP-HPLC. The assignment of the absolute configuration to β,β-dimethyl-tyrosine in **3.10a** and **3.10b** was based on reported, structurally closely related NT(8-13) derivatives, also containing β,β-dimethyl-L-tyrosine or β,β-dimethyl-D-tyrosine in position 11 (structures shown in Figure A3.1A, Appendix).[31] The absolute configuration at the α-carbon of the β,β-dimethylated tyrosine in these peptides was determined based on CD spectroscopy involving an all-L-configured reference peptide.[31] The assignment of the configuration to the β,β-dimethylated tyrosine in **3.10a** and **3.10b** was guided by, first, the elution order in RP-HPLC, and second, the NTS_1R binding affinity. In the reported study, the peptide containing β,β-dimethyl-L-tyrosine eluted first and showed considerably higher NTS_1R binding affinity compared to the diastereomer containing β,β-dimethyl-D-tyrosine (K_i: 0.14 vs. 56 nM).[31] Since **3.10a** eluted before **3.10b** in RP-HPLC (same stationary phase and eluent as used in the reported study) and exhibits markedly higher NTS_1R affinity than **3.10b** (Table 3.1), it represents the diastereomer with β,β-dimethyl-L-tyrosine and, consequently, **3.10b** contains β,β-dimethyl-D-tyrosine. The lower NTS_1R affinity of the diastereomer containing the D-configured dimethylated tyrosine is also in agreement with a reported D-amino acid scan in **1.3**, showing that inversion of the stereochemistry in positions 10-13 of **1.3** results in a marked decrease in NTS_1R binding.[32]

To obtain the non-tritiated 5-TAMRA-labeled ligands **3.13-3.16**, the precursor peptides **3.6-3.9** were first treated with succinimidyl propionate (**3.11**) followed by a copper(I)-catalyzed azide-alkyne 1,3-dipolar cycloaddition using the azido-functionalized 5-TAMRA derivative of **3.12** (Scheme 3.2). Propionylation of **3.10a** and subsequent click reaction with the azido-functionalized Cy3B derivative **3.17** (synthesis shown in Scheme A3.1, Appendix) gave fluorescent ligand **3.18**.

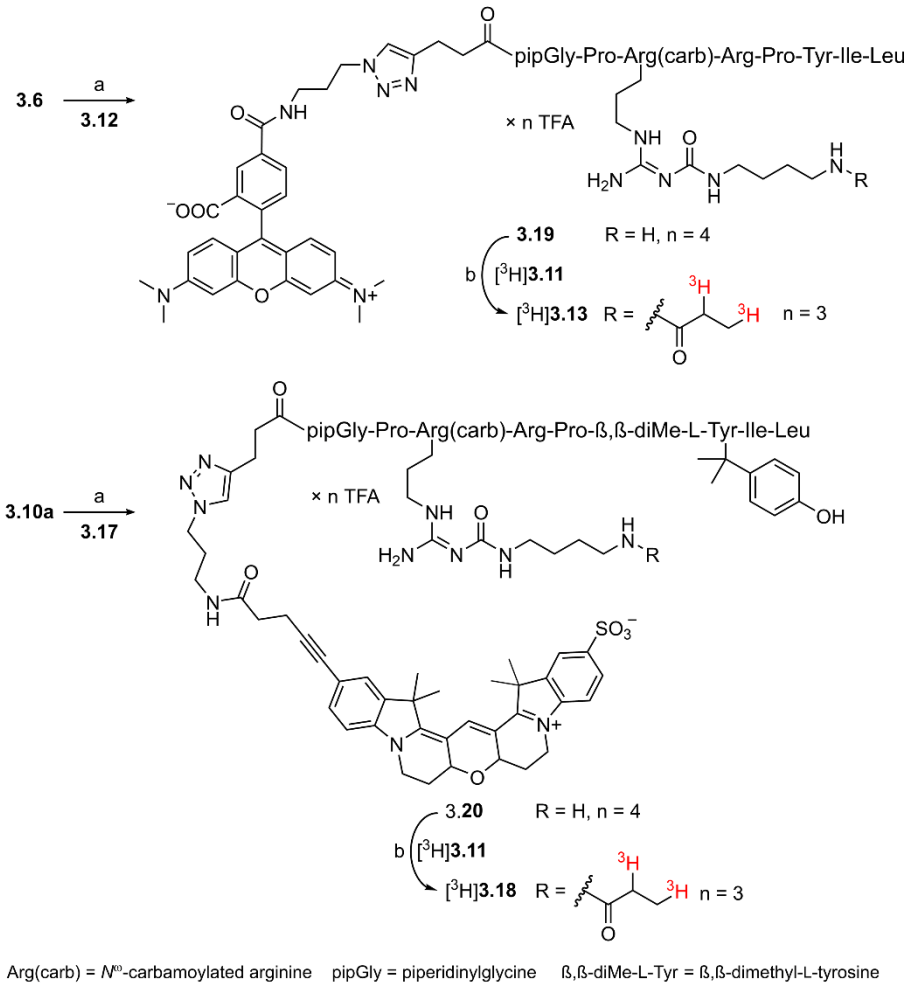
Scheme 3.2. Synthesis of the fluorescently labeled peptides **3.13**-**3.16** and **3.18**.



Reagents and conditions: (a) DIPEA, DMF, rt, 1-2 h; (b) $CuSO_4$, sodium ascorbate, NMP/PBS 1:1 v/v, rt, 2 h; overall yields: 35% (**3.13**), 48% (**3.14**), 43% (**3.15**), 12% (**3.16**), 15% (**3.18**).

From the series of fluorescent peptides (**3.13**-**3.16**, **3.18**), the tritiated analogs were prepared for the 5-TAMRA-labeled peptide **3.13** (UR-FE051) and the Cy3B-conjugated peptide **3.18** (UR-FE061). The selection of **3.13** from the 5-TAMRA-labeled compound series (**3.13**-**3.16**) was guided by the NTS$_1$R binding affinity and the synthetic accessibility of the respective precursor peptide: **3.13** and **3.16** showed the highest NTS$_1$R binding affinity with comparable K_i values of 1.1 nM and 0.77 nM, respectively (Table 3.1). Looking at the synthesis of their precursor peptides **3.6** and **3.9**, the purification of **3.9**, containing the unnatural amino acid Pra, was considerably less convenient compared to **3.6** (discussed afore). Therefore, **3.13** was selected from the series of 5-TAMRA-labeled peptides.

Scheme 3.3. Synthesis of the dually labeled NTS$_1$R ligands [^{3}H]**3.13** and [^{3}H]**3.18**.



Reagents and conditions: (a) $CuSO_4$, sodium ascorbate, NMP/PBS 1:1 v/v, rt, 2 h, 61% (**3.19**), 34% (**3.20**); (b) DIPEA, DMF/NMP 75:25 v/v, rt, 3 h, radiochemical yields: 35% ([^{3}H]**3.13**), 45% ([^{3}H]**3.18**). Note that the tritium atoms in the [^{3}H]propionyl residues do not represent a quantity of tritium isotopes; they only indicate that tritium is present in the respective position.

For the synthesis of the tritiated ligands [^{3}H]**3.13** and [^{3}H]**3.18**, the precursor peptides **3.6** and **3.10a** were conjugated to the fluorescent dyes 5-TAMRA and Cy3B, respectively, to afford **3.19** and **3.20** (Scheme 3.3). Treatment of an excess of **3.19** and **3.20** with [^{3}H]**3.11** gave the

tritiated fluorescent ligands [^{3}H]**3.13** and [^{3}H]**3.18**, respectively, which were obtained in high radiochemical purity after purification by RP-HPLC using an analytical HPLC system (Figure 3.2A).

Over a period of eleven months, degradation of both dually labeled ligands by radiolysis was low (Figure 3.2B).

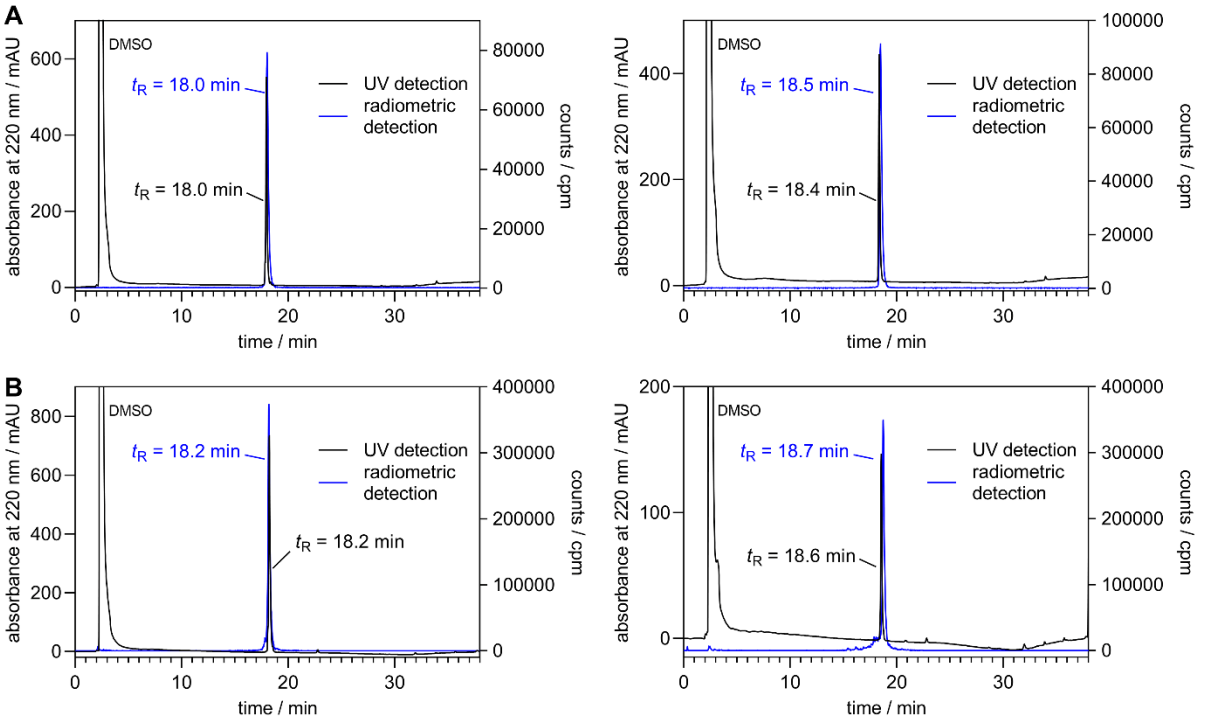


Figure 3.2. (A) Radiochemical purities (> 99%) of [^{3}H]**3.13** and [^{3}H]**3.18** directly after synthesis determined by RP-HPLC analysis. (B) Radiochemical purities of [^{3}H]**3.13** and [^{3}H]**3.18** determined 11 months after synthesis. The purities amounted to 92% ([^{3}H]**3.13**) and 80% ([^{3}H]**3.18**).

3.2.3 Chemical and proteolytic stability of 3.13 and 3.18

The stability of the fluorescently labeled peptides **3.13** and **3.18** was studied in phosphate-buffered saline (PBS, pH = 7.4) at room temperature over 48 h and in human plasma at 37 °C over 48 h. In PBS, **3.13** showed a very slow degradation observable after 24 h of incubation (Figure A3.2, Appendix). Peptide **3.18** proved to be highly stable over 48 h (Figure A3.3, Appendix). Interestingly, both **3.13** and **3.18** exhibited high stability in human plasma (> 50% intact peptide after 24 h) (see also Table A3.1, Appendix). An N-terminal degradation of **3.13** and **3.18** by proteases is considered unlikely due to the N-terminal modification of the peptides (attachment of a fluorescent dye via the 4-pentynoyl moiety). In the case of **3.13**, containing an unmodified, i.e., the same C-terminal sequence (···Pro-Tyr-Ile-Leu) as **1.2** or **1.3**, a rapid C-terminal degradation by proteases was expected (e.g., cleavage of the C-terminal dipeptide Ile-Leu[33]) because for NT(8-13) analogs, containing this C-terminal sequence, a low proteolytic

stability was reported.[27,31,34-38] Presumably, the presence of the bulky fluorescent dye at the N-terminus combined with the N^{ω}-carbamoylated arginine in position 11 of **3.13** impedes C-terminal degradation of the peptide by proteases. Unlike **3.13**, a high stability of **3.18** in blood plasma was indeed expected due to the presence of β,β-dimethyl-tyrosine in position 11, reported to stabilize NT(8-13) analogs against C-terminal proteolytic degradation.[31]

3.2.4 Neurotensin receptor binding and agonism

NTS_1R binding affinities were determined in a reported competition binding assay[13] using intact $hNTS_1R$-expressing HT-29 colon carcinoma cells and [^{3}H]**1.7** (structure see Figure 3.1A) as radioligand (competition binding curves shown in Figure A3.4, Appendix). The amino- and alkyne-functionalized precursor peptides **3.6-3.9** and **3.10a** displayed high NTS_1R affinity with K_i values ≤ 1.1 nM (Table 3.1). Compound **3.10b**, containing β,β-dimethyl-D-tyrosine in position 11, showed considerably lower affinity (K_i = 140 nM). Propionylation and conjugation of the precursor peptides **3.6-3.9** and **3.10a** to the fluorescent dyes 5-TAMRA or Cy3B did only marginally affect NTS_1R binding as becomes obvious from the high binding affinities of the fluorescent peptides **3.13-3.16** and **3.18** (K_i values: 0.77-4.2 nM).

Table 3.1. NTS_1R and NTS_2R binding affinities and NTS_1R agonistic potencies.

compd.	NTS_1R		NTS_2R
	pK_i ± SEM[a] / K_i [nM][a]	pEC_{50} ± SEM[b] / EC_{50} [nM][b]	pK_i ± SEM[c] / K_i [nM][c]
1.3	9.85[d] / 0.14[d]	11.04 ± 0.1 / 0.0091	9.23 ± 0.06 / 0.62
3.6	9.22 ± 0.3 / 0.64	11.19 ± 0.07 / 0.0065	n.d.
3.7	9.27 ± 0.04 / 0.54	n.d.	n.d.
3.8	9.08 ± 0.05 / 0.85	n.d.	n.d.
3.9	9.52 ± 0.2 / 0.33	n.d.	n.d.
3.10a	8.97 ± 0.01 / 1.1	9.50 ± 0.10 / 0.32	n.d.
3.10b	6.87 ± 0.05 / 140	n.d.	n.d.
3.13	9.05 ± 0.2 / 1.1	10.30 ± 0.2 / 0.050	8.62 ± 0.2 / 2.4
3.14	8.86 ± 0.09 / 1.5	n.d.	n.d.
3.15	8.53 ± 0.06 / 3.0	n.d.	n.d.
3.16	9.14 ± 0.08 / 0.77	n.d.	n.d.
3.18	8.39 ± 0.07 / 4.2	9.41 ± 0.2 / 0.39	8.71 ± 0.1 / 1.9

[a]Determined by radioligand competition binding with [^{3}H]**1.7**[13] at HT-29 colon carcinoma cells. [b]Determined in a Fura-2 Ca^{2+} assay at CHO-NTS_1R cells. [c]Determined by competition binding with [^{3}H]**1.7**[13] at homogenates of HEK293T-$hNTS_2R$ cells. [d]Keller *et al.* (reported K_i value of 0.14 nM was converted to pK_i).[13] Data represent mean values ± SEM (pK_i, pEC_{50}) or mean values (K_i, EC_{50}) from at least three independent experiments performed in triplicate.
n.d. = not determined.

For peptides **3.13** and **3.18**, NTS_2R binding affinities were determined at homogenates of HEK293T-hNTS_2R cells also using [^{3}H]**1.7** as radiolabeled probe. These studies revealed that **3.13** and **3.18** bind to the NTS_2R with almost equal affinity as to NTS_1R (Table 3.1). For the present study, NTS_1R selectivity was not needed since all cellular systems (CHO cells, HT-29 cells, Sf9 insect cells for BBV production) used for binding experiments expressed NTS_1R, but not NTS_2R. CHO cells and Sf9 cells were transfected with a vector encoding for the NTS_1R, and in the case of HT-29 cells, endogenously expressing NTS_1R, the absence of NTS_2R was proven previously.[13]

NTS_1R agonism was investigated for **1.3**, the precursor peptides **3.6** and **3.10a**, and the fluorescently labeled peptides **3.13** and **3.18** in a Fura-2 Ca^{2+} assay using CHO-hNTS_1R cells (concentration-response curves shown in Figure A3.5, Appendix). In general, all studied compounds proved to be full agonists and showed higher pEC_{50} values (0.5-2 orders of magnitude) compared to the respective pK_i values (Table 3.1). The high pEC_{50} values can be explained by the overexpression of NTS_1R in stably transfected CHO-hNTS_1R cells (ca. 300,000 receptors/cell[13]) resulting in an excess of receptors over intracellular G_q-proteins (receptor reserve). In this case, a low receptor occupancy is sufficient to induce the maximal cellular response leading to apparently higher potencies.

3.2.5 Fluorescence characterization

For the fluorescently labeled peptides **3.13** and **3.18**, which were studied in various fluorescence-based binding assays (see below), excitation and emission spectra were recorded in PBS and PBS supplemented with 1% BSA (spectra shown in Figure A3.6, Appendix; excitation and emission maxima summarized in Table 3.2). Fluorescence quantum yields of **3.13** and **3.18** were determined in the same solvents. While the emission quantum yield of the 5-TAMRA-labeled ligand **3.13** was equal in neat PBS and PBS with 1% BSA, the quantum yield of the Cy3B-labeled ligand **3.18** was markedly reduced in the presence of BSA (Table 3.2) indicating either an impact of a potential unspecific interaction of the dye with the protein on its photophysical relaxation pathways or a (diffusion-controlled or within the aforementioned unspecific complex) reaction between the excited dye and a solvent exposed amino acid. Interestingly, a recently reported Cy3B-labeled peptidic neuropeptide Y Y_4 receptor ligand showed almost equal quantum yields in PBS and PBS supplemented with 1% BSA (69% vs. 67%),[39] indicating that this ligand exhibits less interactions with BSA or a different binding motif for attaching to BSA.

Table 3.2. Excitation and emission maxima and fluorescence quantum yields of **3.13** and **3.18**.

compd.	λ_{ex} [nm] / λ_{em} [nm] | Δ[eV]		Φ (%)	
	PBS	PBS + 1% BSA	PBS	PBS + 1% BSA
3.13	558 / 584 | 0.10	559 / 583 | 0.091	45	44
3.18	571 / 584 | 0.048	571 / 585 | 0.052	77	62

3.2.6 Investigation of NTS_1R binding of 3.13, [^{3}H]3.13, 3.18, and [^{3}H]3.18 in fluorescence-based and radiochemical assays

Equilibrium saturation binding, association and dissociation kinetics, and competition binding of **3.13** and **3.18** were studied by three different fluorescence-based methods (HCI, FC, and FA). HCI and FC experiments were performed with intact CHO-hNTS_1R cells. It should be noted that HCI necessitates the use of adherent cells, whereas FC requires the use of cell suspensions. Unlike HCI and FC, FA binding experiments were performed with hNTS_1R-displaying BBVs. In analogy to the characterization of **3.13** and **3.18** in fluorescence-based assays, NTS_1R binding of the dually labeled ligands [^{3}H]**3.13** and [^{3}H]**3.18** was studied in radiochemical assays. To enable a close comparison with HCI and FC, these experiments were carried out with adherent and suspended CHO-hNTS_1R cells. For all binding studies, DPBS was used as binding buffer slightly varying with respect to the supplements (for details see

Experimental Section). The assay temperature was 23 °C except for FA-based assays, which were performed at 27 °C. Concerning the fluorescence-based methods, measurements under homogeneous conditions were feasible with FC and FA. In the case of HCI, measurements were performed under non-homogenous conditions since a washing step was performed immediately before plate reading for the purpose of fluorescence background reduction.

As the obtained binding data of **3.13** and **3.18**, as well as [^{3}H]**3.13** and [^{3}H]**3.18** were similar and for the purpose of better comprehension, here we present and discuss the data of **3.13** and [^{3}H]**3.13** in the first place. Graphs showing saturation binding, association and dissociation kinetics and displacement curves (competition binding) of **3.18** and [^{3}H]**3.18** are shown in Figures A3.7-A3.9 (Appendix).

3.2.6.1 Equilibrium saturation binding with 3.13, [^{3}H]3.13, 3.18, and [^{3}H]3.18

HCI, FC and radiochemical equilibrium binding experiments, using increasing concentrations of the title compounds, yielded saturable NTS_1R binding throughout (Figure 3.3; Figure A3.7, Appendix). Unlike the HCI, FC, and radiochemical binding assays, requiring a large excess of the labeled ligand relative to the receptor concentration, FA measurements require approximately equal concentrations of the labeled ligand and receptor. Therefore, ligand depletion needs to be taken into account in the case of FA binding assays. For a detailed introduction to FA binding assays, see, e.g., Rinken *et al.*[21] All saturation binding experiments were performed in 96-well plates. In the case of FC, this was feasible since the used flow cytometer (FACSCanto II, Becton Dickinson) was equipped with an autosampler (HTS unit) allowing an automated injection from microtiter plates.

The dissociation constants (K_d values) obtained from the different binding assays performed with intact CHO-hNTS_1R cells (HCI, FC, radiochemical assay) or BBVs (FA) were in excellent agreement (Table 3.3, row 1). The K_d values were also in good agreement with the K_i values of **3.13** and **3.18** determined by competition binding with [^{3}H]**1.7** at HT-29 colon carcinoma cells (see Table 3.1). To challenge the HCI, FC, and radiochemical assay, saturation binding of **3.13**, [^{3}H]**3.13**, **3.18** and [^{3}H]**3.18** was also studied at HT-29 cells showing a considerably lower NTS_1R expression compared to CHO-hNTS_1R cells.[13] Although specific binding was lower in absolute values and consequently also relative to unspecific binding due to the lower receptor expression, well reproducible saturation isotherms could be obtained (Figure 3.3A, 3.3B, and 3.3D; Figure A3.7A, A3.7B, and A3.7D, Appendix). However, the K_d values were slightly less consistent compared to the K_d values obtained from experiments with CHO-hNTS_1R cells (Table 3.3).

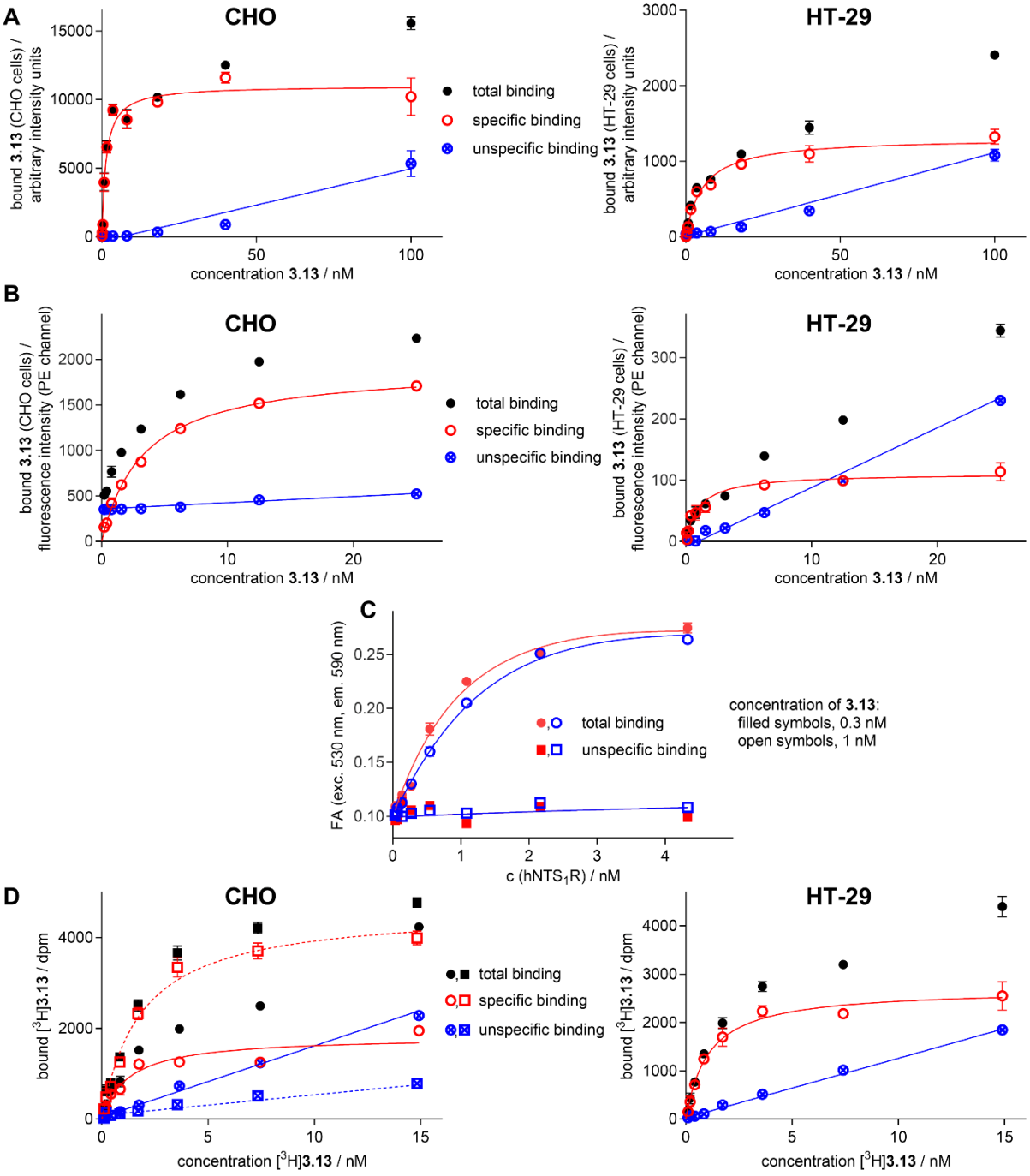


Figure 3.3. NTS$_1$R equilibrium binding of **3.13** and [^{3}H]**3.13** studied by different methods. (A) Binding isotherms (specific binding, open symbols) of **3.13** obtained from high-content imaging (HCI) binding experiments performed at intact CHO-hNTS$_1$R and HT-29 cells (incubation: 90 min at 23 °C). (B) Binding isotherms (specific binding, open symbols) of **3.13** obtained from flow cytometric (FC) saturation binding experiments performed at intact CHO-hNTS$_1$R and HT-29 cells (incubation: 90 min at 23 °C). (C) Binding isotherms (total binding, circles) of **3.13** obtained from FA-based binding experiments using fixed concentrations of **3.13** (0.3 or 1 nM) and increasing amounts of NTS$_1$R-displaying BBVs (depicted data represent snapshots at 10 min incubation at 27 °C). (D) Binding isotherms of [^{3}H]**3.13** from radiochemical saturation binding experiments performed at intact CHO-hNTS$_1$R cells (adherent and in suspension) and at adherent HT-29 cells (incubation: 90 min at 23 °C). Circles represent adherent cells, squares represent suspended cells. Unspecific binding was determined in the presence of 1 µM **1.3** (A, B, and D) or 1 µM **1.5** (C). K_d values are presented in Table 3.3. Data represent mean values ± SEM (total and unspecific binding) or calculated values ± propagated error from representative experiments performed in triplicate (A, B and D) or duplicate (C).

3.2.6.2 Investigation of the association and dissociation kinetics of 3.13, [^{3}H]3.13, 3.18, and [^{3}H]3.18

The association of the title compounds to NTS_1R, studied at live CHO-hNTS_1R cells (HCI, FC, radiochemical assay) or BBVs (FA), was nearly monophasic in the case of HCI, FC, and FA (Figure 3.4A and 3.4B; Figure A3.8A and A3.8B, Appendix). In the case of **3.13**, for both HCI and FC association experiments, a second, delayed (> 90 min) phase was observed after the initial, clearly plateauing association phase (Figure 3.4A). Due to the late appearance and the slow rise of specific binding within the second phase relative to the initial association phase, data of the second slow phase were not included in the data analysis.

The radiochemical association experiments with [^{3}H]**3.13** and [^{3}H]**3.18** yielded a clear biphasic association (Figure 3.4C; Figure A3.8C, Appendix). It should be mentioned that the reproducibility of these experiments was lower compared to the fluorescence-based methods resulting in higher error bars. The variations of the values within a triplicate were also increased. This phenomenon was even more pronounced in the case of radiochemical dissociation experiments as discussed below. As fitting of the data using the two phase association fit (GraphPad Prism 5) failed for several individual experiments (ambiguous results), the following procedure was applied as an approximation: data describing the initial fast association phase, plateauing after ca. 10 min, were analyzed by a one phase association fit (GraphPad Prism 5) followed by a two phase association fit for which $k_{obs(fast)}$ was constrained to the k_{obs} value obtained from the initial monophasic fit. Applying this approach, biphasic fitting of the data was feasible and $k_{obs(slow)}$ values could be obtained (Figure 3.4C; Figure A3.8C, Appendix; Table 3.3).

Notably, a biphasic association was not observed for the radioligand [^{3}H]**1.7** (adherent cells, same procedure as used for [^{3}H]**3.13** and [^{3}H]**3.18**), being devoid of a fluorescence label.[13] Consequently, the fluorescent dye present in [^{3}H]**3.13** and [^{3}H]**3.18** seems to have an impact on the results of radiochemical association experiments. To further test the radiochemical association assay, [^{3}H]**3.13** was also studied at membrane preparations of CHO-hNTS_1R cells allowing a decoupling of G-protein from the receptor by the addition of GppNHp[40-47] and precluding receptor internalization (discussed below). Comparing the radiochemical association experiments (cell suspension) with the FC assay, these two methods differ by non-homogenous vs. homogenous conditions and by the sample setup (96-well plates vs. 5-mL tubes). To note, in contrast to FC saturation binding experiments, performed in 96 well plates, samples for association and dissociation experiments were prepared in 5-mL polypropylene tubes, i.e., data for the different time points originated from the same sample. These two main

differences could also account for the observed differences in the association curves and the robustness of the data obtained from the radiochemical and the FC assay. As the radiochemical and the FC assay both use intact suspended CHO-hNTS_1R cells, an internalization of the ligand-receptor complex would occur in either case, suggesting that the pronounced biphasic association curve observed for the radiochemical assay cannot be explained by endocytosis of ligand-bound NTS_1R (NTS_1R-mediated uptake of **3.13** and **3.18** in adherent CHO-hNTS_1R cells was proven by confocal microscopy, see Figures A3.10-A3.15, Appendix). Likewise, the difference between the association curve radiochemically determined at adherent CHO-hNTS_1R cells and the association curve obtained from HCI experiments (cf. Figure 3.4A and 3.4C, and Figure A3.8A and A3.8C, Appendix) can most likely not be attributed to an internalization of ligand-receptor complex since the cellular uptake can take place in both cases. As discussed below, radiochemical association experiments with [^{3}H]**3.13** using membranes of CHO-hNTS_1R cells (receptor uncoupled from G-protein) indicated that the biphasic association can be attributed to the presence of two subpopulations of NTS_1R (coupled to and uncoupled from G-protein) in intact cells. Thus, it remains a matter of speculation why the fluorescence-based methods cannot reproduce the biphasic association curves obtained from radiochemical association experiments. This method-dependent bias needs to be explored in future studies. Altered fluorescence properties (upon ligand binding and/or cellular uptake) and different sensitivities for the detection of bound ligand could be potential reasons.

The hydrogen-tritium exchange in the propionyl group is considered to have no effect since the propionyl residue in **1.7**, located at the same position as in **3.13** (Arg^8), does not contribute to receptor binding.[13] Comparing HCI with FC, the association of **3.13** to NTS_1R determined by FC was considerably faster than observed by HCI (Figure 3.4A, k_{on} values presented in Table 3.3), which could also be attributed to non-homogenous vs. homogenous conditions and the different sample setup (adherent cells in 96-well plates vs. suspended cells in 5-mL tubes).

Table 3.3. Parameters characterizing NTS_1R binding of **3.13**, [^{3}H]**3.13**, **3.18**, and [^{3}H]**3.18** determined in different types of binding assays.

parameter	ligand	receptor source	HCI (adherent)	FC (suspension)	FA	radiochemical	
						adherent	suspension
K_d [nM]	**3.13**, [^{3}H]**3.13**	CHO-hNTS_1R cells	1.1 ± 0.2	2.6 ± 0.5	-	1.3 ± 0.1	1.8 ± 0.2
		HT-29 cells	4.7 ± 1.1	0.25 ± 0.1	-	1.2 ± 0.1	n.d.
		NTS_1R-BBV	-	-	1.3 ± 0.1	-	-
	3.18, [^{3}H]**3.18**	CHO-hNTS_1R cells	1.3 ± 0.3	3.1 ± 0.3		1.1 ± 0.2	1.2 ± 0.1
		HT-29 cells	2.3 ± 0.3	0.65 ± 0.09		1.9 ± 0.3	n.d.
		NTS_1R-BBV	-	-	1.5 ± 0.1	-	-
k_{obs} [min^{-1}]	**3.13**, [^{3}H]**3.13**	CHO-hNTS_1R cells	0.084 ± 0.003	0.50 ± 0.08	-	0.57 ± 0.08[a] 0.011 ± 0.001[b]	1.5 ± 0.3[a] 0.051 ± 0.001[b]
		NTS_1R-BBV	-	-	n.a.	-	-
	3.18, [^{3}H]**3.18**	CHO-hNTS_1R cells	0.072 ± 0.006	0.18 ± 0.07	-	0.14 ± 0.03[a] 0.013 ± 0.002[b]	0.15 ± 0.03[a] 0.006 ± 0.002[b]
		NTS_1R-BBV	-	-	n.a.	-	-
k_{off} [min^{-1}]	**3.13**, [^{3}H]**3.13**	CHO-hNTS_1R cells	0.044 ± 0.002	0.020 ± 0.002	-	0.014 ± 0.04	0.036 ± 0.006
		NTS_1R-BBV	-	-	0.61 ± 0.03	-	-
	3.18, [^{3}H]**3.18**	CHO-hNTS_1R cells	0.051 ± 0.002	0.024 ± 0.002	-	0.026 ± 0.007	0.030 ± 0.004
		NTS_1R-BBV	-	-	0.56 ± 0.04	-	-
k_{on} [min^{-1} nM^{-1}]	**3.13**, [^{3}H]**3.13**	CHO-hNTS_1R cells	0.016 ± 0.002	0.48 ± 0.09	-	0.33 ± 0.1[c]	0.81 ± 0.2[c]
		NTS_1R-BBV	-	-	1.0 ± 0.2	-	-
	3.18, [^{3}H]**3.18**	CHO-hNTS_1R cells	0.0081 ± 0.003	0.16 ± 0.07	-	0.10 ± 0.04[c]	0.097 ± 0.13[c]
		NTS_1R-BBV	-	-	1.4 ± 0.3	-	-
K_d(kin) [nM]	**3.13**, [^{3}H]**3.13**	CHO-hNTS_1R cells	2.8 ± 0.5	0.041 ± 0.01		0.41 ± 0.2	0.044 ± 0.02
		NTS_1R-BBV	-	-	1.0 ± 0.3	-	-
	3.18, [^{3}H]**3.18**	CHO-hNTS_1R cells	6.4 ± 2.7	0.15 ± 0.08	-	0.26 ± 0.2	0.31 ± 0.44
		NTS_1R-BBV	-	-	1.4 ± 0.3	-	-

[a] $k_{obs(fast)}$ of the monophasic exponential fit (data describing the initial dissociation phase). [b] $k_{obs(slow)}$ of the biphasic exponential fit. [c] $k_{on(fast)}$ calculated from k_{off}, $k_{obs(fast)}$ and the ligand concentration used for the association experiments (note: $k_{on(slow)}$ is not given as the values calculated from k_{off}, $k_{obs(slow)}$ and the ligand concentration were negative.). K_d, k_{obs}, and k_{off} values represent mean values ± SEM from at least three independent experiments; k_{on} and K_d(kin) values represent calculated values ± propagated error (HCI, FC, radiochemical assay) or mean values ± SEM from at least three individual experiments (FA).

Dissociation curves obtained from HCI, FC, FA, and radiochemical assays were all nearly monophasic (Figure 3.4; Figure A3.8, Appendix) giving similar k_{off} values except FA, which gave higher k_{off} values (Table 3.3). However, the dissociation curves differed considerably in terms of the plateaus representing long-lasting binding or irreversibly bound ligand. The highest plateaus were observed for HCI (**3.13**: 40%, **3.18**: 70%) and FC (**3.13**: 53%, **3.18**: 64%). An incomplete dissociation from NTS_1R can be explained by internalization of the ligand-receptor complex and intracellular dissociation of fluorescent ligand from the receptor. Indeed, an NTS_1R-mediated cellular uptake of **3.13** and **3.18** was confirmed by confocal microscopy (Figures A3.10-A3.15, Appendix) and the images from HCI dissociation experiments showed that the decrease in intracellular fluorescence stopped at a certain level during the dissociation process (Figure A3.16, Appendix). In the case of radiochemical dissociation experiments performed with adherent cells, the reproducibility was considerably lower compared to HCI resulting in high error bars (Figure 3.4C; Figure A3.8C, Appendix). When using cell suspensions, the radiochemical dissociation experiments performed in 96-well plates resulted in no reproducible data at all (Figure A3.17A, Appendix) (to note, these experiments were performed by three different operators experienced in studying ligand binding kinetics in radiochemical assays). Interestingly, the use of a sample setup similar to that used for FC (sample preparation in falcon tubes instead of 96-well plates), allowing data acquisition for the various time points from the same sample, had a dramatic effect on the results: these experiments resulted in highly reproducible monophasic dissociation curves with a low plateau of 12% (**3.13**) and 18% (**3.18**) (blue curves in Figure 3.4C and Figure A3.8C, Appendix). These results suggest that the high variability of the data obtained from radiochemical dissociation experiments performed in 96-well plates is indeed caused by the respective experimental setup (use of 96 well plates meaning separate sample preparations for each time point) and cannot be attributed to the cellular uptake of the radiolabeled fluorescent ligand by internalization of ligand-receptor complex. The observed differences with respect to the plateaus obtained from the different radiochemical dissociation experiments (cell suspensions (falcon tubes) vs. intact adherent cells: 12% vs. 39% (**3.13**, cf. Figure 3.4C), and 18% vs. 39% (**3.18**, cf. Figure A3.8C, Appendix)) indicate that the underlying mechanisms (internalization and potentially externalization) are different in adherent cells compared to suspended cells. However, both HCI dissociation experiments (adherent cells) and FC dissociation studies (suspended cells) yielded pronounced plateaus comparable to that obtained for radiochemical dissociation experiments performed at adherent cells (Figure 3.4A and 3.4C; Figure A3.8A and A3.8C, Appendix). If the plateau is only caused by the cellular uptake of the ligand-receptor complex by internalization

resulting in intracellularly “trapped” ligand, one would expect similar results for the fluorescence-based and the radiochemical assays. This inconsistency indicates that also unsteady photophysical properties of the fluorescent ligands might play a role as discussed below in more detail.

To further test the 96-well sample setup, dissociation experiments were also performed with the non-fluorescent radioligand [^{3}H]**1.7** in 96-well plates at suspended CHO-hNTS$_1$R cells. As these experiments gave reproducible monophasic dissociation curves indicating a complete dissociation (Figure A3.17B, Appendix), the irreproducibility of the radiochemical dissociation experiments with [^{3}H]**3.13** and [^{3}H]**3.18** (cell suspensions) can also be attributed to the fluorescent dye in these dually labeled ligands besides - or in conjunction with - the technical setup of the assay.

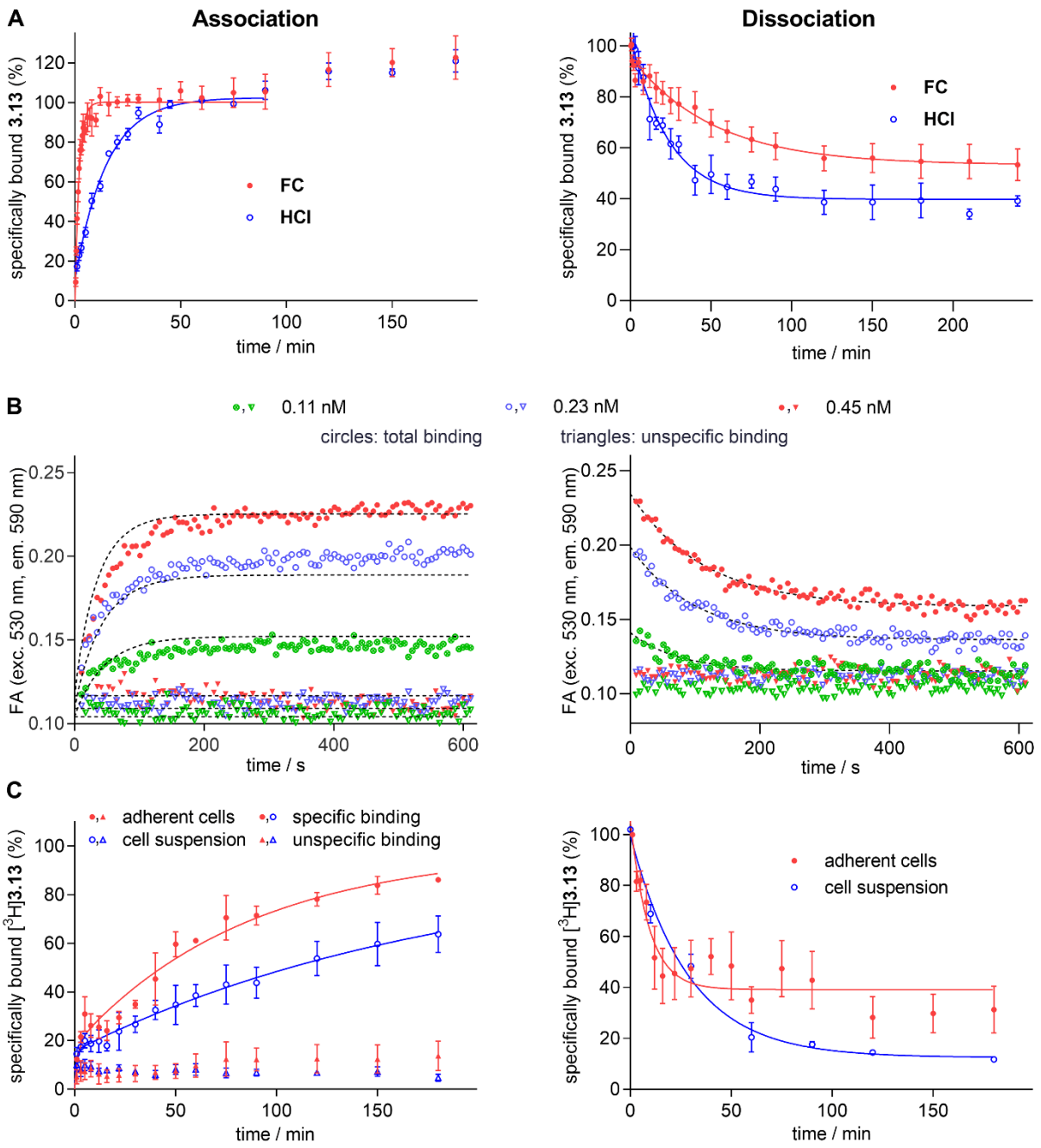


Figure 3.4. Binding kinetics of **3.13** and [^{3}H]**3.13** at NTS$_1$R studied by different methods. (A) Association and dissociation of **3.13** studied by HCI and FC at live adherent CHO-hNTS$_1$R cells (HCI) or suspended CHO-hNTS$_1$R cells (FC) at 23 °C. Concentrations of **3.13** used for the association: 2.5 nM (HCI) and 1 nM (FC); concentrations of **3.13** used during the preincubation period (90 min) of dissociation experiments: 2.5 nM (HCI) and 10 nM (FC). The last three data points were excluded from the fit. (B) Association and dissociation of **3.13** (0.3 nM) determined in an FA-based assay for three different NTS$_1$R concentrations (green, blue, and red symbols) at 27 °C using NTS$_1$R-displaying BBVs. Total binding is represented by circles and unspecific binding is represented by triangles. Following the association for up to 180 min did not reveal a second association phase (data not shown). (C) Association and dissociation of [^{3}H]**3.13** studied at live adherent CHO-hNTS$_1$R cells and suspended CHO-hNTS$_1$R cells at 23 °C. Concentrations of **3.13** used for the association: 1.3 nM (adherent cells) and 1.8 nM (cell suspension); concentrations of **3.13** used during the preincubation period (90 min) of dissociation experiments: 6.5 nM (adherent cells) and 5 nM (cell suspension). For the biphasic association, unspecific binding, remaining at a constant level, is shown to demonstrate that both association phases account for binding to NTS$_1$R. Proportion of fast/slow kinetic components (association): 19%/81% (adherent cells), 21%/79% (suspended cells). In the case of dissociation experiments performed with suspended cells, less times were studied because these experiments were laborious due to the use of falcon tubes instead of 96-well plates (in this case, a separate work-up process with the cell harvester had to be carried out for each timepoint).
Dissociation and association rate constants are presented in Table 3.3. Data represent mean values ± SEM from at least three independent experiments performed in triplicate (A (HCI), C (association, dissociation at adherent cells)), or duplicate (A (FC), B, C (dissociation with cell suspensions)).

Regarding HCI, FA, and the radiochemical assay using adherent cells, the kinetically derived dissociation constants K_d(kin), calculated from k_{off} and k_{on}, deviated less than a factor of 5 from the K_d values determined in equilibrium saturation binding experiments (Table 3.3). For FC, the K_d(kin) values of **3.13** and **3.18** were markedly lower than the K_d from saturation binding studies. This could be due to overestimated k_{obs} and/or underestimated k_{off} values by the FC method.

While the K_d(kin) value of [^{3}H]**3.18** determined at cell suspensions was only slightly lower than the K_d from saturation binding experiments, the K_d(kin) value of [^{3}H]**3.13** was markedly lower (factor 41) than the K_d (Table 3.3) suggesting that the results of kinetic experiments also depend on the type of fluorescent dye.

It should be emphasized that shifts of the excitation and emission spectra and changes in fluorescence quantum yield, potentially occurring upon receptor binding and cellular uptake of the fluorescent ligand by internalization of the ligand-receptor complex (*cf.* Figures A3.10-A3.15, Appendix), can impact the fluorescence signals detected by HCI and FC. In contrast, altered fluorescence properties usually do not substantially influence FA measurements since the parallel and perpendicular fluorescence detected by FA would be equally affected, thus accounting for a compensation of the effect. Presumably, besides the different sources of NTS_1R (intact adherent cells, intact suspended cells, BBVs), these methodological differences account for the observed differences in association and dissociation kinetics between HCI and FA as well as FC and FA. The hypothesis of changes in fluorescence properties upon receptor binding or cellular uptake is supported by the results of the radiochemical dissociation experiments performed with suspended CHO-hNTS_1R cells: these experiments, performed under the same conditions as FC dissociation studies, yielded an almost complete dissociation of [^{3}H]**3.13** from the receptor (Figure 3.4C), whereas in the FC assay, a plateau at approximately 50% specifically bound ligand was found (Figure 3.4A) (to note, the radiochemical assay is unaffected by changes in the photophysics of the fluorescent dye).

3.2.6.3 Competition binding experiments using 3.13, [^{3}H]3.13, 3.18, and [^{3}H]3.18 as labeled probes

Like saturation binding assays, all competition binding experiments were performed in 96-well plates. For all kinds of studied NTS_1R binding assays, the K_i values of the agonist **1.3** and the antagonist **1.5** (SR142948; for structure see Figure 1.1, Chapter 1) were determined by displacing **3.13**, [^{3}H]**3.13**, **3.18**, or [^{3}H]**3.18** from NTS_1R (displacement curves and pK_i values presented in Figure 3.5 and Figure A3.9, Appendix). Additionally, the pK_i values of **3.13** and **3.18** were determined in the radiochemical competition binding assays. For HCI and FC, the

obtained NTS_1R affinities of **1.3** and **1.5** were in good agreement with reported binding data (**1.3**: K_i 0.14 nM,[13,48] 0.24 nM,[49] 0.29 nM,[50] 1.0 nM;[51] **1.5**: K_i 1.0 nM,[52] 1.1 nM[13]). The NTS_1R binding affinities of **1.3** obtained from the FA and the radiochemical assay using adherent cells were slightly lower compared to reported data.[13,48-51] NTS_1R affinities of **1.5** determined with **3.13** and **3.18** in the FA assay (pK_i = 8.97 and 9.19, respectively) were perfectly in line with reported data.[13,52] The NTS_1R binding affinity of **1.3** obtained from the radiochemical competition binding assays using cell suspensions were in good agreement with the aforementioned literature data. In contrast, NTS_1R affinities of **1.5** determined by competition binding with [^{3}H]**3.13** and [^{3}H]**3.18** (adherent and suspended cells) were slightly lower than the aforementioned literature data. Noteworthy, the NTS_1R binding affinities of **3.13** and **3.18** obtained by competition binding with their tritiated analogs were in good agreement with the K_d values of [^{3}H]**3.13** and [^{3}H]**3.18** determined by saturation binding (see Table 3.3, Figure 3.5C, and Figure A3.9C, Appendix).

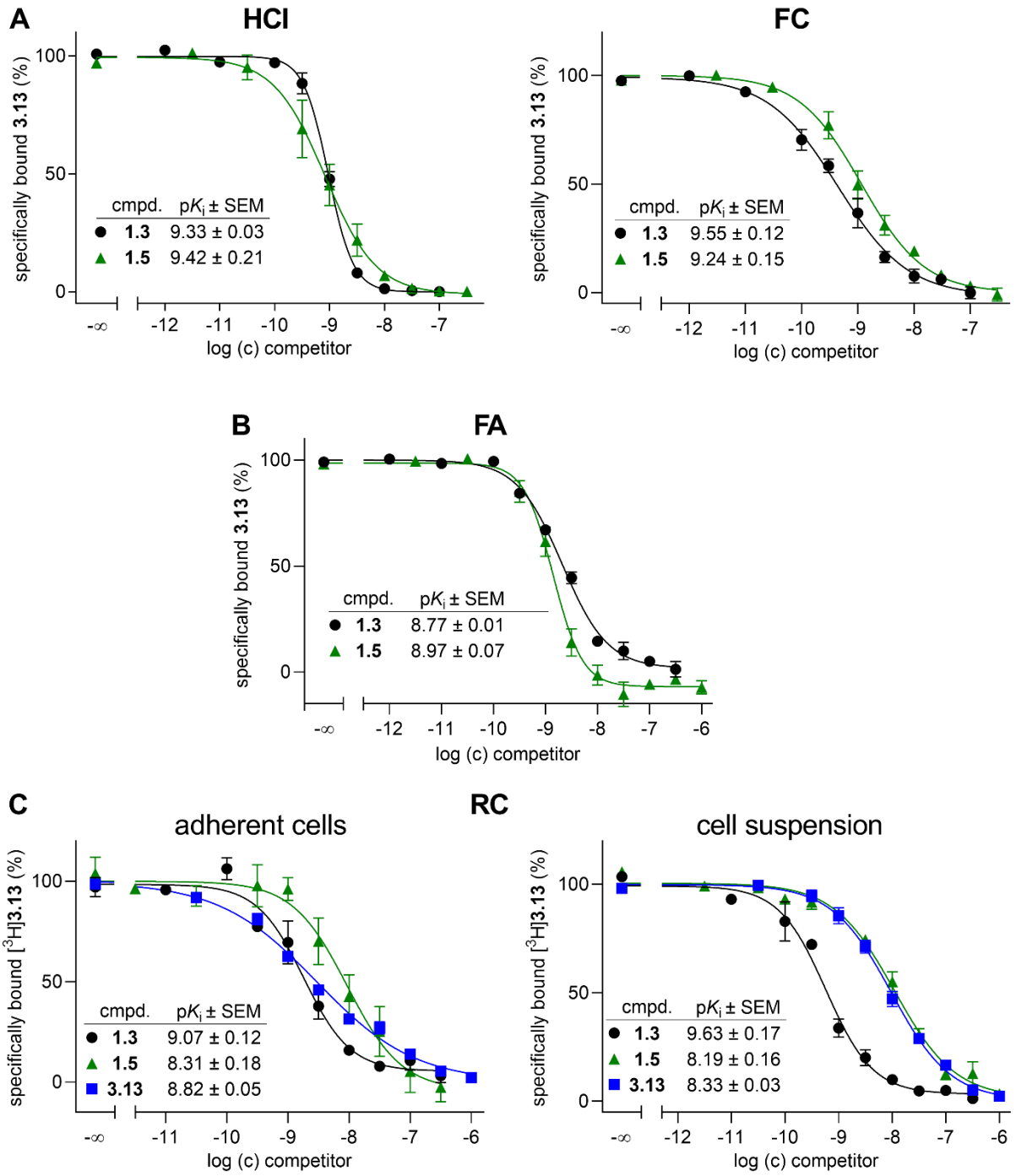


Figure 3.5. Displacement curves and corresponding pK_i values from competition binding studies performed with **3.13** or [^{3}H]**3.13** and **1.3** and **1.5** using different types of binding assays (A: high-content imaging and flow cytometry; B: fluorescence anisotropy; C: radiochemical binding assay). Used concentrations of **3.13**: 1.1 nM (A (HCI)), 2.6 nM (A (FC)), 0.3 nM (B). Used concentrations of [^{3}H]**3.13** (C): 1.3 nM (adherent cells), 1.8 nM (cell suspension). Incubation times: 90 min (A, B, C). Incubation temperatures: 23 °C (A, C), 27 °C (B). Data represent mean value ± SEM from at least three individual experiments performed in triplicate.

3.2.6.4 Binding of [^{3}H]3.13 to membranes of CHO-hNTS_1R cells

As [^{3}H]**3.13** showed a pronounced biphasic association when studied at intact CHO-hNTS_1R cells (Figure 3.4C), NTS_1R binding of this dually labeled peptide was additionally investigated using membrane preparations enabling the uncoupling of G-protein from the receptor, e.g., by adding the G-protein inhibitor GppNHp.[40-47] These experiments were performed in 96-well plates using the same procedure as for radiochemical binding experiments with intact suspended cells, but using cell membranes instead of whole cells. Binding of [^{3}H]**3.13** to the NTS_1R was saturable (Figure 3.6A). As expected, the K_d value of [^{3}H]**3.13** obtained from equilibrium saturation binding experiments at cell membranes in the presence of 50 µM GppNHp (K_d = 6.2 ± 1.3 nM, mean values ± SEM from three independent experiments performed in triplicate) was higher than the K_d determined at intact cells (K_d = 1.8 nM, cf. Table 3.3). To note, in addition to GppNHp, saponin (100 µg/mL) was added to the samples to improve ligand permeabilization into vesicles that are likely to occur in membrane preparations. The association curve of [^{3}H]**3.13** obtained from experiments with cell membranes (Figure 3.6B) was considerably different compared to the association curve observed for intact suspended cells (cf. Figure 3.4C). The biphasic character almost disappeared and with a k_{on} value of 0.13 ± 0.05 $nM^{-1}min^{-1}$ (calculated value ± propagated error) the association was slower compared to the initial phase found for experiments with intact cells (k_{on} = 0.81 $nM^{-1}min^{-1}$, cf. Table 3.3). This indicated the existence of two subpopulations of NTS_1R in intact cells, one population coupled to G-protein and the other not bound to G-protein as a consequence of the overexpression of NTS_1R in CHO-hNTS_1R cells. However, this conclusion is not in line with the data obtained from fluorescence-based (HCI, FC) association experiments at intact CHO-hNTS_1R cells (Figure 3.4A), showing a course comparable to that found for the radiochemical association experiments performed with cell membranes (Figure 3.6B). As mentioned before, the exploration of this phenomenon requires additional studies.

Dissociation experiments with [^{3}H]**3.13** at cell membranes were, unlike dissociation studies at intact suspended cells (sample preparation in 96-well plates), highly reproducible yielding a clearly monophasic curve and a complete dissociation (Figure 3.6C) with a k_{off} value of 0.37 ± 0.08 min^{-1} (mean values ± SEM from three independent experiments performed in triplicate). This revealed that the technical setup of the assay causes an irreproducibility of the radiochemical dissociation assay (suspended cells, sample preparation in 96-welll plates; cf. Figure A3.17A, Appendix) (see also discussion above) only in conjunction with the use of intact cells, allowing a cellular uptake of ligand/agonist-receptor complex. The K_d(kin) value, calculated from k_{off} and k_{on}, amounted to 2.7 ± 1.6 nM (calculated value ± propagated error),

deviating less than a factor of 2.5 from the K_d value obtained from saturation binding studies (K_d = 6.2 nM). When comparing the data of the dissociation kinetics obtained from the radiochemical assay performed at cell membranes with the results from the fluorescence-based methods, the highest agreement in k_{off} values is found for the FA assay (k_{off} ([^{3}H]**3.13**) = 0.37 min^{-1}, k_{off} (**3.13**, FA) = 0.61 min^{-1}). Likewise, the K_d(kin) values obtained from the radiochemical (cell membranes) and the FA assay showed the highest agreement with the K_d from saturation binding studies ([^{3}H]**3.13**: K_d(kin) = 2.7 nM, K_d = 6.2 nM; **3.13**: K_d(kin) = 1.0 nM, K_d = 1.3 nM). This is consistent with the fact that internalization of agonist-receptor complex cannot occur when membrane preparations or BBVs[53] are used as receptor source, supporting an action according to the law of mass action.

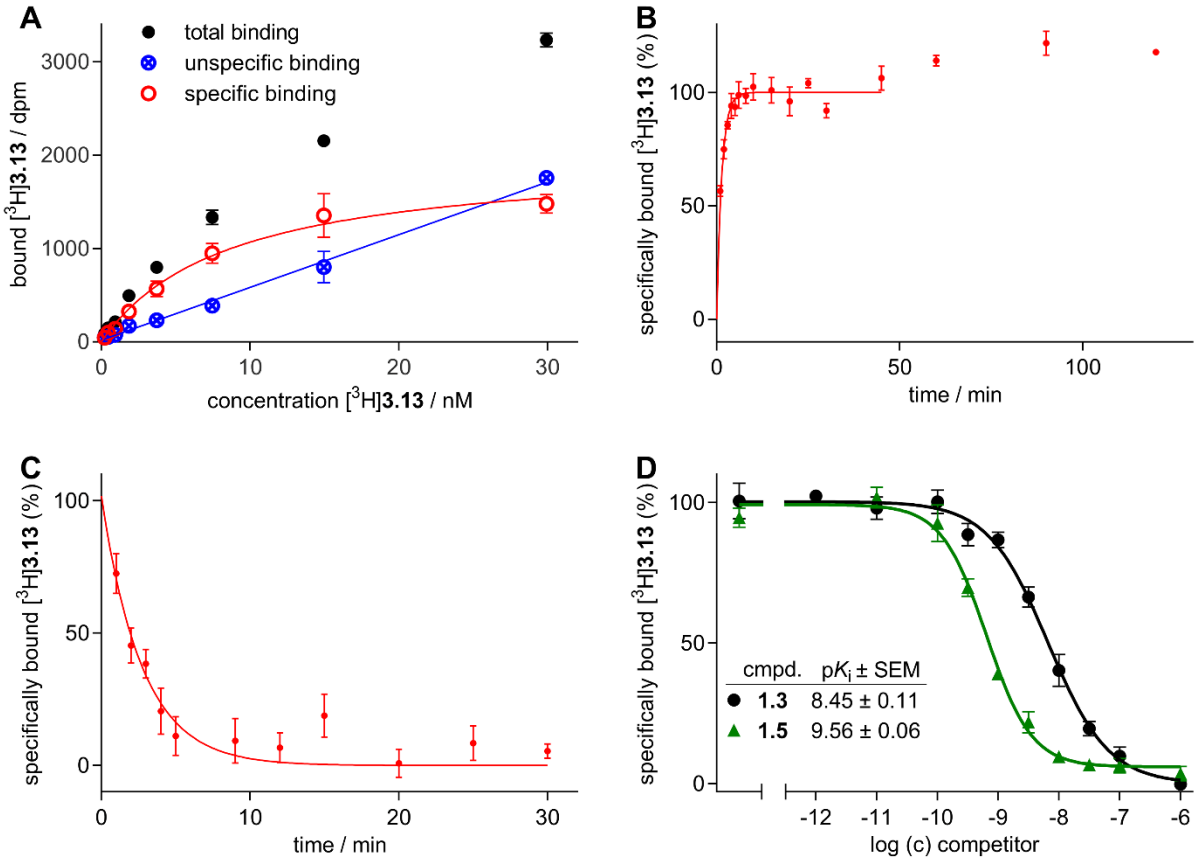


Figure 3.6. NTS$_1$R binding characteristics of [^{3}H]**3.13** studied at membranes of CHO-hNTS$_1$R cells at 23 °C. (A) Representative binding isotherm (specific binding, open symbols) of [^{3}H]**3.13** obtained from a radiochemical saturation binding experiment. Data represent mean values ± SEM (total and unspecific binding) or calculated values ± propagated error from a representative experiment performed in triplicate. (B) Association of [^{3}H]**3.13** (c = 2.5 nM) to NTS$_1$R. The last three data points were excluded from the fit. Data represent mean values ± SEM obtained from five independent experiments performed in triplicate. (C) Dissociation of [^{3}H]**3.13**. Concentration of [^{3}H]**3.13** used for the preincubation (30 min): 12 nM. Data were normalized based on Y_0 (100%) obtained from a one phase decay fit (GraphPad Prism). The fit (plateau value constrained to zero, for details see Experimental Section) was extrapolated to t = 0 min. Data represent mean values ± SEM obtained from three independent experiments performed in triplicate. (D) Displacement curves and corresponding pK_i values from competition binding studies performed with [^{3}H]**3.13** (c = 6.2 nM) and **1.3** and **1.5**. Data represent mean values ± SEM obtained from three independent experiments performed in triplicate.

The NTS_1R binding affinities of **1.3** and **1.5**, determined by competition binding with [^{3}H]**3.13** at cell membranes (Figure 3.6D), were lower and higher, respectively, compared to the aforementioned reported binding data. This is in agreement with the uncoupling of the receptor from G-protein resulting in a destabilization of the active receptor conformation,[47] and, in turn, in decreased agonist affinity and potentially in increased antagonist affinity (reported, e.g., for the β2 adrenergic receptor[47] and the muscarinic acetylcholine M_2 receptor).[42,54]

3.3 Conclusion

The determination of ligand-receptor binding affinities usually requires labeled ligands that are used as probes in radiochemical or luminescence-based competition binding assays. A comparison of the different types of binding assays is limited due to the fact that radioligands, being structurally different from fluorescent ligands, cannot be used in fluorescence-based assays and vice versa. To enable a close comparison of radiochemical and fluorescence-based ligand-receptor binding assays, a proof-of-concept study was performed with two tritium-labeled fluorescent neurotensin receptor ligands ([^{3}H]**3.13**, [^{3}H]**3.18**) and their non-tritiated analogs (**3.13**, **3.18**), which were characterized in radiochemical and fluorescence-based (high-content imaging, flow cytometry, and fluorescence anisotropy) NTS_1R binding assays. While equilibrium binding experiments (saturation and competition binding) gave well comparable dissociation constants (K_d, K_i), the results from kinetic studies (association and dissociation experiments) were less consistent, not only when comparing radiochemical with fluorescence-based, but also among the fluorescence-based methods. Obviously, this is caused by the different kinds of signal detection in conjunction with effects mediated by the fluorescent dye. Indeed, the study revealed that the presence of a fluorescence label in a radioligand can cause a radiochemical assay to fail that works with a structurally closely related non-fluorescently labeled radioligand. Notably, the labeled ligands used in the present study represent NTS_1R agonists inducing receptor internalization in intact cells, which likely affects the ligand binding kinetics. Therefore, the same study conducted with appropriately labeled antagonists might give a different picture. In summary, the presented results demonstrate that, despite marked differences in kinetic parameters, there is a solid agreement of K_d values (labeled ligands) and K_i values (unlabeled ligands) derived from the different methods. This suggests that, for binding assays using non-modified (wild-type) receptors, the method-dependent bias is low with respect to the determination of ligand-receptor affinities. A main question raised by the present study is to what extent do the changing fluorescence properties (receptor-bound vs. free fluorescent ligand) influence the results of fluorescence-based binding assays. This needs to be addressed in future studies by a systematic exploration of changes in the photophysics of fluorescent ligands upon receptor binding.

Beyond the purpose of the present study, i.e., the comparison of different kinds of binding assays, the introduced fluorescently labeled NTS_1R ligands represent tool compounds useful to characterize non-labeled NTS_1R ligands. Besides the determination of binding affinities of orthosteric NTS_1R ligands, they could also serve to characterize allosteric NTS_1R modulators,

which effect the binding affinity of orthosteric ligands. This includes novel chemotypes such as SBI-553[55] addressing an intracellular allosteric binding site of NTS_1R.

3.4 Experimental section

3.4.1 General experimental conditions

Materials. The protected amino acids Fmoc-Tyr(tBu)-OH, Fmoc-Leu-OH, Fmoc-Arg(Pbf)-OH, Fmoc-D-Lys(Boc)-OH and Fmoc-Pra-OH (**3.2**) were purchased from Carbolution Chemicals (St. Ingbert, Germany). Fmoc-Lys(Boc)-OH, Fmoc-Pro-OH, Fmoc-Ile-OH, HBTU and H-Leu-2-ClTrt resin were from Merck (Darmstadt, Germany). Fmoc-pipGly(Boc)-OH (**2.24**) was from GL Biochem (Shanghai, China). Fmoc-β,β-dimethyl-Tyr(*t*Bu)-OH (racemic) (**3.4**) was obtained from Iris Biotech (Marktredwitz, Germany). HOBt and Triton X-100 were from Sigma-Aldrich (Taufkirchen, Germany). NMP and DMF for peptide synthesis, anhydrous DMF and NMP, dichloromethane, piperidine, saponin and TFA were purchased from Fisher Scientific (Schwerte, Germany). DIPEA was obtained from ABCR (Karslruhe, Germany). Acetonitrile (HPLC gradient grade) was from VWR (Ismaning, Germany). **1.3** was synthesized via SPPS in-house. **1.5** was purchased from Tocris Bioscience (Bristol, UK). Bacitracin, HEPES, and bovine serum albumin (BSA) were obtained from Serva (Heidelberg, Germany). Fetal bovine serum (FBS) was purchased from Pan-Biotech (Aidenbach, Germany) or Sigma. Succinimidyl [^{3}H]propionate ([^{3}H]**3.11**, molar activity: 105 Ci/mmol) was purchased from Novandi (Södertälje, Sweden). Fura-2 AM and Pluronic F-127 were obtained from Calbiochem/Merck Biosciences (Beeston, UK). GppNHP was purchased from Jena Biosciences (Jena, Germany). The syntheses of *N*-Boc-γ-aminobutyric acid succinimidyl ester[56] and compound **3.21**[5]were described previously. The radioligand [^{3}H]**1.7** (molar activity: 2.41 TBq/mmol) was prepared according to a described procedure.[13] Compound **3.1**,[13] **3.5**,[31] and **3.11**[57] were prepared according to the reported procedures. 5-TAMRA-azide (**3.12**) was purchased from Carl Roth (Karlsruhe, Germany). Millipore water was consistently used for the preparation of stock solutions, buffers, and aqueous eluents for HPLC. Polypropylene reaction vessels with screw cap (1.5 and 2 mL) from Sarstedt (Nümbrecht, Germany) were used for small-scale reactions (e.g., activation of Fmoc-protected amino acids) and to keep stock solutions.

NMR spectroscopy. NMR spectra were recorded on an AVANCE 600 instrument with cryogenic probe (^{1}H: 600 MHz; ^{13}C: 150 MHz) (Bruker, Karlsruhe, Germany). NMR spectra were calibrated based on the solvent residual peaks (^{1}H-NMR, DMSO-d_6: δ = 2.50 ppm; ^{13}C-NMR, DMSO-d_6: δ = 39.50 ppm), and data are reported as follows: ^{1}H-NMR: chemical shift δ in ppm (multiplicity [s = singlet, d = doublet, t = triplet, m = multiplet, and br s = broad singlet], integral, coupling constant *J* in Hz); ^{13}C NMR: chemical shift δ in ppm.

Mass spectroscopy. High-resolution mass spectrometry (HRMS) was performed with an Agilent 6540 UHD accurate-mass Q-TOF LC/MS system coupled to an Agilent 1290 analytical HPLC system (Agilent Technologies. Santa Clara, CA) using an ESI source and the following LC method: column: Luna Omega C18, 1.6 µm, 50 × 2.1 mm (Phenomenex, Aschaffenburg, Germany), column temperature: 40 °C, solvent/linear gradient: 0−4 min: 0.1% aqueous HCOOH/acetonitrile supplemented with 0.1% HCOOH 95:5−2:98, 4−5 min: 2:98, flow: 0.6 mL/min.

Preparative HPLC. Preparative HPLC was performed with a system from Knauer (Berlin, Germany) consisting of two K-1800 pumps and a K-2001 detector. A Gemini NX-C18, 5 µm, 250 mm × 21 mm (Phenomenex, Aschaffenburg, Germany) was used as stationary phase at a flow rate of 20 mL/min using mixtures of 0.1% aqueous TFA and acetonitrile as the mobile phase. A detection wavelength of 220 nm was used throughout. Collected fractions were lyophilized using a Scanvac CoolSafe 100-9 freeze dryer (Labogene, Allerød, Denmark) equipped with a RZ 6 rotary vane vacuum pump (Vacuubrand, Wertheim, Germany).

Analytical HPLC. Analytical HPLC analysis was performed with a system from Agilent Technologies composed of a 1290 Infinity binary pump equipped with a degasser, a 1290 Infinity autosampler, a 1290 Infinity thermostated column compartment, a 1260 Infinity diode array detector, and a 1260 Infinity fluorescence detector. A Kinetex-XB C18, 2.6 µm, 100 × 3 mm (Phenomenex) served as stationary phase at a flow rate of 0.6 mL/min. Detection was performed at 220 nm and the temperature of the column compartment was set to 25 °C. Mixtures of acetonitrile (A) and 0.04% aqueous TFA (B) were used as mobile phase. The following linear gradients were applied: compounds **3.6**-**3.9**, **3.10a**, **3.10b** and **3.19**-**3.20**: 0-14 min: A/B 10:90-30:70, 14-15 min: 30:70-95:5, 15-18 min: 95:5 (isocratic); compounds **3.13**-**3.16** and **3.18**: 0-14 min: A/B 20:80-40:60, 14-15 min: 40:60-95:5, 15-18 min: 95:5 (isocratic); compound **3.17**: 0-14 min: A/B 25:75-45:55, 14-15 min: 45:55-95:5, 15-18 min: 95:5 (isocratic). The injection volume was 20 µL. Retention (capacity) factors *k* were calculated from the retention times t_R according to $k = (t_R - t_0)/t_0$ (t_0 = dead time, 0.76 min for the used system and column).

General procedure for solid phase peptide synthesis. Peptides were synthesized manually by SPPS according to the Fmoc strategy. A H-Leu-2-ClTrt resin was used as solid phase and DMF/NMP 4:1 v/v was used as solvent. 5-mL NORM-JECT syringes (B. Braun-Melsungen, Melsungen, Germany), equipped with a 35-µm polypropylene frit (Roland Vetter Laborbedarf, Ammerbuch, Germany), were used as reaction vessels. The resin was allowed to swell in solvent for 30 min at rt. Fmoc-amino acids (except for **3.1**, **3.2**, **2.24**, and **3.4**), used in 5-fold

excess, were preactivated with HOBt/HBTU/DIPEA (5/4.9/10 equiv.) in solvent (about 2.2 mL/mmol amino acid) for at least 5 min before addition to the resin. The Fmoc-protected unnatural amino acids **3.1**, **3.2**, **2.24**, and **3.4** were used in 3-fold excess and were preactivated with HBTU/HOBt/DIPEA (3/3/6 equiv.) in anhydrous solvent (about 1.6 mL/mmol amino acid) for 5-10 min prior to addition to the resin. Amino acid coupling was carried out on a shaker (Heidolph Multi Reax; Heidolph Instruments, Schwabach, Germany) covered with a thermostat controlled (35 °C) box. In the case of standard amino acids, "double" coupling (2 × 45 min) was performed. **3.1**, **3.2**, **2.24**, and **3.4** were attached by a single coupling procedure (35 °C, 16 h). After coupling of an Fmoc-amino acid, the resin was washed with solvent (4 ×) followed by Fmoc deprotection using 20% piperidine in solvent (2 × 10 min at rt) and subsequent washing of the resin with solvent (6 × ca. 1 mL). After coupling of the last amino acid, final Fmoc deprotection and, in the case of **3.6**-**3.9**, **3.10a**, and **3.10b**, subsequent treatment with 10 equivalents of succinimidyl 4-pentynoic acid (**3.5**) (peptides **3.6**-**3.8**, **3.10a**, and **3.10b**) or with 10 equivalents of *N*-Boc-γ-aminobutyric acid succinimidyl ester (peptide **3.9**) in solvent in the presence of DIPEA (10 equiv.) at 35 °C for 30 min, the resin was washed with solvent (6 ×) and CH_2Cl_2 (3 ×) (treated with potassium carbonate). Peptides were cleaved off the resin using CH_2Cl_2/TFA 3:1 v/v (2 × 20 min at rt). The liquids (2 × ca. 2 mL) were collected in a 100-mL round bottom flask and the resin was washed once with CH_2Cl_2/TFA 3:1 v/v (2 mL). The volatiles of the combined liquids were removed by evaporation, TFA/H_2O 95:5 v/v (2 mL per 100 mg resin) was added to the residue and the mixture was stirred at rt for 5 h. The volatiles were removed by evaporation followed by the addition of H_2O (ca. 50 mL) and lyophilization to obtain the crude peptide, which was subjected to purification by preparative HPLC.

Compound characterization. Peptides **3.6**-**3.9** and **3.10a** were characterized by HRMS, ^{1}H-, ^{13}C-, and 2D-NMR spectroscopy (2D: ^{1}H-COSY, HSQC, HMBC), and RP-HPLC. Compounds **3.13** and **3.18** were characterized by HRMS, ^{1}H-NMR spectroscopy, and RP-HPLC. **3.10b**, **3.14**-**3.17**, **3.19**, and **3.20** were characterized by HRMS and RP-HPLC. HPLC purities of all target compounds were ≥ 97% (UV detection, 220 nm).

3.4.2 Experimental protocols and analytical data

***N*$^{\alpha}$-(Pent-4-ynoyl)-β,β-(3-aza)pent-1,5-diyl-Ala-Pro-*N*$^{\omega}$-[(4-aminobutyl)aminocarbonyl]Arg-Arg-Pro-Tyr-Ile-Leu tetrakis(hydrotrifluoroacetate) (3.6).** Peptide **3.6** was synthesized on a H-Leu-2-ClTrt resin (60 mg, 0.79 mmol/g) according to the general procedure. Purification by preparative HPLC (gradient: 0-30 min: acetonitrile/0.1% aqueous TFA 15:85-35:65, t_R = 9 min) yielded **3.6** as a

white fluffy solid (8.8 mg, 11%). ^{1}H-NMR (600 MHz, DMSO-d_6): δ (ppm) 0.80 (t, 3H, *J* 7.6 Hz), 0.84 (d, 6H, *J* 6.5 Hz), 0.90 (d, 3H, *J* 6.7 Hz), 1.00-1.09 (m, 1H), 1.29-1.44 (m, 3H), 1.44-1.59 (m, 12H), 1.59-1.74 (m, 5H), 1.74-1.97 (m, 9H), 2.02-2.11 (m, 1H), 2.32-2.37 (m, 4H), 2.65-2.72 (m, 1H), 2.74-2.77 (t, 1H, 2.3 Hz), 2.77-2.90 (m, 5H), 3.01-3.16 (m, 4H), 3.18-3.33 (m, 4H), 3.46-3.60 (m, 3H), 3.68-3.74 (m, 1H), 4.17-4.26 (m, 3H, quantified via spectrum with additional D_2O), 4.29-4.36 (m, 2H, quantified via spectrum with additional D_2O), 4.37-4.50 (m, 3H, quantified via spectrum with additional D_2O), 6.58-6.63 (m, 2H), 6.72-7.20 (br s, 2H, interfering with next listed signal), 6.97-7.01 (m, 2H), 7.20-7.56 (br s, 2H), 7.58-7.65 (br s, 1H), 7.67 (t, 1H, *J* 5.3 Hz), 7.73 (d, 1H, *J* 8.9 Hz), 7.76-7.85 (br s, 3H), 7.89 (d, 1H, *J* 7.9 Hz), 7.95 (d, 1H, *J* 7.5 Hz), 8.08 (d, 1H, *J* 7.3 Hz), 8.19 (t, 2H, *J* 7.2 Hz), 8.29-8.41 (m, 1H), 8.47 (s, 2H), 8.72-8.85 (d, 1H, *J* 8.8 Hz), 9.06 (s, 1H), 9.20 (br s, 1H), 10.67 (s, 1H), 12.51 (s, 1H). ^{13}C-NMR (150 MHz, DMSO-d_6): δ (ppm) 10.91, 14.23, 15.12, 21.22, 22.84, 24.10, 24.16, 24.26, 24.37, 24.40, 24.49, 24.55, 25.04, 25.96 (2 carbon atoms), 28.39, 28.77, 29.06, 29.36, 33.74, 35.49, 36.37, 37.12, 38.47, 38.64, 39.73, 40.49 (2 carbon atoms), 42.74, 42.99, 46.73, 47.28, 49.86, 50.14, 51.99, 53.67, 54.12, 56.36, 59.18, 59.45, 71.37, 83.67,113.80 (TFA), 114.77 (2 carbon atoms), 115.77 (TFA), 117.74 (TFA), 119.71 (TFA), 127.61, 130.12 (2 carbon atoms), 153.73, 153.91, 155.76, 156.81, 158.70 (q, *J* 32 Hz) (TFA), 168.75, 169.46, 170.48, 170.62, 170.90, 171.22, 171.26, 171.44, 173.82. HRMS (ESI): *m/z* $[M+4H]^{4+}$ calcd. for $[C_{60}H_{101}N_{17}O_{12}]^{4+}$ 312.9449, found: 312.9459. RP-HPLC (220 nm): > 99% (t_R = 8.1 min, *k* = 9.7). $C_{60}H_{97}N_{17}O_{12} \cdot C_8H_4F_{12}O_8$ (1248.54 + 456.09).

***N*$^{\alpha}$-(Pent-4-ynoyl)-Lys-Pro-Arg-Arg-Pro-Tyr-Ile-Leu tris(hydrotrifluoroacetate) (3.7).** Peptide **3.7** was synthesized on a H-Leu-2-ClTrt resin (60 mg, 0.79 mmol/g) according to the general procedure. Purification by preparative HPLC (gradient: 0-30 min: acetonitrile/0.1% aqueous TFA 15:85-35:65, t_R = 11 min) yielded **3.7** as a white fluffy solid (26.1 mg, 38%). ^{1}H-NMR (600 MHz, DMSO-d_6): δ (ppm) 0.80 (t, 3H, *J* 7.5 Hz), 0.83 (d, 6H, *J* 6.5 Hz), 0.89 (d, 3H, *J* 6.6 Hz), 1.01-1.09 (m, 1H), 1.30-1.72 (m, 19H), 1.73-1.93 (m, 6H), 1.93-2.07 (m, 2H), 2.24-2.40 (m, 4H), 2.65-2.71 (m, 1H), 2.71-2.79 (m, 3H), 2.82-2.89 (m, 1H), 3.01-3.15 (m, 4H), 3.46-3.54 (m, 2H), 3.55-3.61 (m, 1H), 3.63-3.69 (m, 1H), 4.18-4.24 (m, 3H), 4.30-4.36 (m, 2H), 4.38-4.43 (m, 1H), 4.43-4.51 (m, 2H), 6.58-6.63 (m, 2H), 6.68-7.20 (br s, 4H, interfering with next listed signal), 6.98-7.01 (m, 2H), 7.20-7.59 (br s, 4H), 7.64 (t, 1H, *J* 5.5 Hz), 7.68 (t, 1H, *J* 5.7 Hz), 7.71-7.83 (m, 4H), 7.89 (d, 1H, *J* 8.0 Hz), 7.95 (d, 1H, *J* 7.5 Hz), 8.06 (d, 1H, *J* 8.0 Hz), 8.14 (d, 1H, *J* 8.0 Hz), 8.16-8.21 (d, 1H, *J* 7.9 Hz), 9.20 (s, 1H), 12.52 (s, 1H). ^{13}C-NMR (150 MHz, DMSO-d_6): δ (ppm) 10.91, 14.14, 15.12, 21.21, 21.96, 22.84, 24.10, 24.17, 24.26,

24.46, 25.03, 26.65, 28.38, 28.92, 29.07, 29.12, 30.56 (2 carbon atoms), 33.75, 36.37, 37.12, 38.67, 39.78, 40.37, 40.49, 46.73, 46.87, 49.84, 50.03, 50.13, 52.00, 54.13, 56.35, 59.16, 59.24, 71.29, 83.72, 113.86 (TFA), 114.77 (2 carbon atoms), 115.83 (TFA), 117.81 (TFA), 119.78 (TFA), 127.62, 130.12 (2 carbon atoms), 155.75, 156.78 (2 carbon atoms), 158.51 (q, *J* 32 Hz) (TFA), 169.46, 170.04, 170.22, 170.64, 170.90, 171.19, 171.28, 171.55, 173.82. HRMS (ESI): *m/z* $[M+3H]^{3+}$ calcd. for $[C_{54}H_{90}N_{15}O_{11}]^{3+}$ 374.8976, found: 374.8982. RP-HPLC (220 nm): > 99% (t_R = 8.8 min, *k* = 10.6). $C_{54}H_{87}N_{15}O_{11} \cdot C_6H_3F_9O_6$ (1122.38 + 342.07).

***N*$^{\alpha}$-(Pent-4-ynoyl)-D-Lys-Pro-Arg-Arg-Pro-Tyr-Ile-Leu tris(hydrotrifluoroacetate) (3.8).** Peptide **3.8** was synthesized on a H-Leu-2-ClTrt resin (60 mg, 0.79 mmol/g) according to the general procedure. Purification by preparative HPLC (gradient: 0-30: min acetonitrile/0.1% aqueous TFA 15:85-35:65, t_R = 11 min) yielded **3.8** as a white fluffy solid (7.1 mg, 10%). ^{1}H-NMR (600 MHz, DMSO-d_6): δ (ppm) 0.80 (t, 3H, *J* 7.5 Hz), 0.84 (d, 6H, *J* 6.5 Hz), 0.90 (d, 3H, *J* 6.6 Hz), 1.01-1.09 (m, 1H), 1.21-1.31 (m, 1H), 1.31-1.38 (m, 1H), 1.38-1.59 (m, 13H), 1.59-1.72 (m, 5H), 1.75-1.90 (m, 5H), 1.93-2.06 (m, 2H), 2.26-2.42 (m, 4H), 2.65-2.72 (m, 1H), 2.72-2.79 (m, 3H), 2.84-2.90 (m, 1H), 3.01-3.14 (m, 4H), 3.28-3.41 (m, 1H), 3.46-3.54 (m, 1H, overlaying with water peak, identified as one integral by additional D_2O spectrum), 3.54-3.61 (m, 1H, overlaying with water peak, identified as one integral by additional D_2O spectrum), 3.69-3.75 (m, 1H, overlaying with water peak, identified as one integral by additional D_2O spectrum), 4.15-4.24 (m, 3H), 4.28-4.36 (m, 2H), 4.36-4.51 (m, 3H), 6.59-6.63 (m, 2H), 6.68-7.17 (br s, 4H, interfering with next listed signal), 6.97-7.00 (m, 2H 7.17-7.54 (br s, 4H), 7.56-7.62 (m, 1H), 7.67 (t, 1H, *J* 5.8 Hz), 7.69-7.79 (m, 4H), 7.82 (d, 1H, *J* 8.0 Hz), 7.85-7.93 (m, 2H), 8.16-8.21 (m, 1H), 8.24 (d, 1H, *J* 7.2 Hz), 9.20 (s, 1H), 12.51 (s, 1H). ^{13}C-NMR (150 MHz, DMSO-d_6): δ (ppm) 10.91, 14.17, 15.12, 21.22, 22.03, 22.84, 24.09, 24.17, 24.26, 24.47, 25.13, 26.75, 28.24, 28.60, 29.05, 29.09, 30.56 (2 carbon atoms), 33.73, 36.37, 37.11, 38.64, 39.78, 40.38, 40.51, 46.70, 46.85, 49.96, 50.13, 50.42, 52.08, 54.12, 56.36, 59.21, 59.59, 71.33, 83.68, 113.96 (TFA), 114.78 (2 carbon atoms), 115.94 (TFA), 117.91 (TFA), 119.89 (TFA), 127.63, 130.11 (2 carbon atoms), 155.75, 156.76 (2 carbon atoms), 158.21 (q, *J* 32 Hz) (TFA), 169.64, 170.34, 170.64, 170.69, 170.90, 171.22, 171.28, 171.32, 172.08. HRMS (ESI): *m/z* $[M+3H]^{3+}$ calcd. for $[C_{54}H_{90}N_{15}O_{11}]^{3+}$ 374.8976, found: 374.8986. RP-HPLC (220 nm): 99% (t_R = 8.9 min, *k* = 10.7). $C_{54}H_{87}N_{15}O_{11} \cdot C_6H_3F_9O_6$ (1122.38 + 342.07).

***N*$^{\alpha}$-(4-Aminobutanoyl)-2-(prop-2-ynyl)-Gly-β,β-(3-aza)pent-1,5-diyl-Ala-Pro-Arg-Arg-Pro-Tyr-Ile-Leu tetrakis(hydrotrifluoroacetate) (3.9).** Peptide **3.9** was synthesized on a H-

Leu-2-ClTrt resin (60 mg, 0.79 mmol/g) according to the general procedure. Purification by preparative HPLC (gradient: 0-30 min: acetonitrile/0.1% aqueous TFA 18:82-38:62, t_R = 10 min) yielded **3.9** as a white fluffy solid (16.1 mg, 20%). ^{1}H-NMR (600 MHz, DMSO-d_6): δ (ppm) 0.73-0.90 (m, 12H), 1.02-1.12 (m, 1H), 1.19-1.65 (m, 13H), 1.65-1.92 (m, 13H), 1.92-1.98 (m, 1H), 1.98-2.09 (m, 1H), 2.18-2.31 (m, 2H), 2.37-2.58 (m, 2Hm, interfering with solvent peak, identified via HSQC and HMBC), 2.72-2.84 (m, 5H), 2.88-3.15 (m, 6H), 3.17-3.28 (m, 2H, interfering with water signal, quantified by D_2O spectrum), 3.47-3.55 (m, 2H), 3.55-3.62 (m, 1H), 3.62-3.70 (m, 1H), 3.97-4.11 (m, 1H), 4.11-4.31 (m, 3H), 4.31-4.43 (m, 3H), 4.43-4.55 (m, 2H), 6.43-8.99 (m, 22H, interfering with next two listed signals), 6.57-6.66 (m, 2H), 6.96-7.02 (m, 2H), 9.23 (s, 1H). The proton signal of the carboxylic acid group was not apparent. ^{13}C-NMR (150 MHz, DMSO-d_6): δ (ppm) 10.98, 15.27, 21.88, 22.24, 22.94, 23.34, 24.06, 24.27, 24.39, 24.46 (2 carbon atoms), 24.59, 24.72, 25.42, 28.25, 28.43, 28.78, 29.28, 31.83, 35.70, 36.59 (2 carbon atoms), 38.46, 40.13 (interfering with solvent peak, identified by HSQC), 40.42, 41.98 (identified by HSQC), 42.91, 43.13, 46.76, 47.18, 49.89, 51.31, 52.09, 52.69, 53.89, 57.35, 59.45 (2 carbon atoms), 59.65, 72.86, 80.48, 114.75 (2 carbon atoms), 116.22 (TFA), 118.22 (TFA), 127.98, 129.99 (2 carbon atoms), 155.75, 157.02, 157.08, 158.25 (TFA), 158.43 (TFA), 168.46, 169.87, 169.98, 170.05, 170.88, 171.01, 171.30, 171.36 (2 carbon atoms), 176.22. HRMS (ESI): *m/z* $[M+4H]^{4+}$ calcd. for $[C_{59}H_{99}N_{17}O_{12}]^{4+}$ 309.4409, found: 309.4420. RP-HPLC (220 nm): 98% (t_R = 7.7 min, k = 9.1). $C_{59}H_{95}N_{17}O_{12} \cdot C_8H_4F_{12}O_8$ (1234.52 + 456.09).

***N*$^{\alpha}$-(Pent-4-ynoyl)-β,β-(3-aza)pent-1,5-diyl-Ala-Pro-*N*$^{\omega}$-[(4-aminobutyl)aminocarbonyl]Arg-Arg-Pro-β,β-dimethyl-L-Tyr-Ile-Leu tetrakis(hydrotrifluoroacetate) (3.10a) and *N*$^{\alpha}$-(pent-4-ynoyl)-β,β-(3-aza)pent-1,5-diyl-Ala-Pro-*N*$^{\omega}$-[(4-aminobutyl)aminocarbonyl]Arg-Arg-Pro-β,β-dimethyl-D-Tyr-Ile-Leu tetrakis(hydrotrifluoroacetate) (3.10b).** Peptides **3.10a** and **3.10b**, representing diastereomers, were synthesized on a H-Leu-2-ClTrt resin (130 mg, 0.79 mmol/g) according to the general procedure. The unavailability of enantiomerically pure Fmoc-*ß,ß*-dimethyl-L-Tyr(*t*Bu)-OH (this Fmoc amino acid was only available as racemic mixture) necessitated the synthesis of both diastereomers, which were separated by preparative HPLC (gradient: 0-40 min: acetonitrile/0.1% aqueous TFA 15:85-40:60, t_R (**3.10a**) = 17 min, t_R (**3.10b**) = 20 min). Lyophilization of the eluates yielded **3.10a** and **3.10b** as white fluffy solids (**3.10a**: 60.3 mg, 34%; **3.10b**: 37.2 mg, 21%). ^{1}H-NMR of **3.10a** (600 MHz, DMSO-d_6): δ (ppm) 0.78 (t, 3H, *J* 7.3 Hz), 0.82 (t, 6H, *J* 6.9 Hz), 0.90 (d, 3H, *J* 6.6 Hz), 0.96-1.05 (m, 1H), 1.23 (s, 3H), 1.25 (s,

3H), 1.31-1.44 (m, 3H), 1.44-1.60 (m, 12H), 1.60-1.99 (m, 14H), 2.02-2.11 (m, 1H), 2.28-2.40 (m, 4H), 2.73-2.89 (m, 5H), 3.03-3.14 (m, 4H), 3.19-3.27 (m, 3H), 3.27-3.32 (m, 1H), 3.38-3.46 (br s, 1H, quantified via spectrum with additional D_2O), 3.51-3.57 (m, 2H, quantified via spectrum with additional D_2O), 3.67-3.74 (m, 1H), 4.08-4.14 (m, 1H), 4.19-4.27 (m, 2H), 4.29-4.34 (m, 1H), 4.35-4.40 (m, 1H), 4.40-4.48 (m, 2H), 4.60-4.65 (m, 1H), 6.58-6.65 (m, 2H), 6.85-7.20 (br s, 2H, interfering with next listed signal), 7.09-7.14 (m, 2H), 7.21-7.50 (m, 3H), 7.55-7.66 (m, 2H), 7.68 (t, 1H, *J* 5.4 Hz), 7.80 (s, 3H), 7.98 (d, 1H, *J* 7.4 Hz), 8.04-8.15 (m, 2H), 8.19 (d, 1H, *J* 8.7 Hz), 8.33-8.42 (m, 1H), 8.42-8.52 (br s, 2H), 8.70-8.81 (m, 1H), 9.06 (s, 1H), 9.17 (s, 1H), 10.67 (s, 1H), 12.49 (s, 1H). ^{13}C-NMR of **3.10a** (150 MHz, DMSO-d_6): δ (ppm) 10.85, 14.22, 15.11, 21.09, 22.95, 24.16-24.55 (these interfering peaks were identified as 8 carbon atoms via HSQC), 25.04, 25.95, 26.97, 28.41 (2 carbon atoms), 28.52, 28.76, 29.35, 33.73, 35.49, 36.67, 38.47, 38.64, 39.60 (interfering with solvent peak, identified by HSQC), 40.17, 40.46, 40.51, 42.74, 43.00, 46.72, 47.27, 49.80, 49.97, 51.98, 53.65, 56.60, 59.25, 59.43, 59.77, 71.36, 83.67, 114.05 (TFA), 114.26 (2 carbon atoms), 116.03 (TFA), 118.00 (TFA), 119.99 (TFA), 127.44 (2 carbon atoms), 136.22, 153.74, 153.90, 155.27, 156.82, 158.71 (q, *J* 32 Hz) (TFA), 168.72, 169.35, 169.84, 170.47, 170.59, 170.74, 171.26, 171.44, 173.85. HRMS (ESI): *m/z* $[M+4H]^{4+}$ calcd. for $[C_{62}H_{105}N_{17}O_{12}]^{4+}$ 319.9527, found: 319.9537 (**3.10a**); 319.9542 (**3.10b**). RP-HPLC (220 nm): **3.10a**: 97% (t_R = 8.9 min, *k* = 10.7), **3.10b**: 98% (t_R = 10.4 min, *k* = 12.7). $C_{62}H_{101}N_{17}O_{12} \cdot C_8H_4F_{12}O_8$ (1276.60 + 456.09).

***N*$^{\alpha}$-(3-(1-*N*-((1-Carboxylato-2-(6-(dimethylamino)-3-(dimethyliminio)-3*H*-xanthen-9-yl)phen-5-yl)1-oxomethyl)aminoprop-3-yl-1*H*-1,2,3-triazol-4-yl)propanoyl)-β,β-(3-aza)pent-1,5-diyl-Ala-Pro-*N*$^{\omega}$-[(4-(*N*-propanoyl)aminobutyl)aminocarbonyl]Arg-Arg-Pro-Tyr-Ile-Leu tris(hydrotrifluoroacetate) (3.13).** Peptide **3.6** (6.2 mg, 3.9 µmol) was dissolved in anhydrous DMF (100 µL) and a solution of succinimidyl propionate (**3.11**) (0.40 mg, 2.3 µmol) and DIPEA (35 µmol, 6.1 µL) in anhydrous DMF (30 µL) was added. The mixture was stirred at rt for 2 h. 10% aqueous TFA (30 µL) and 0.1% aqueous TFA/acetonitrile 85:15 v/v (1000 µL) were added and the product of the propionylation reaction was isolated by preparative RP-HPLC (gradient: 0-30 min: acetonitrile/0.1% aqueous TFA 20:80-40:60, t_R = 14 min). Lyophilization of the eluate yielded a white fluffy solid (2.9 mg, 45%). The propionylation product (2.9 mg, 1.8 µmol) and azide **3.12** (1.3 mg, 2.5 µmol) were dissolved in NMP/PBS 1:1 v/v (180 µL). A solution of $CuSO_4 \cdot 5\ H_2O$ (0.77 mg, 3.1 µmol) in NMP/PBS 1:1 v/v (60 µL) (note: $CuSO_4$ was first dissolved in 30 µL of PBS and then 30 µL of NMP were added) and a solution of sodium ascorbate (1.8 mg, 8.9 µmol) in PBS (30 µL) were added. After

stirring at rt in the dark for 2 h, the mixture was diluted with 800 µL of 0.1% aqueous TFA/acetonitrile 85:15 v/v followed by isolation of the product by preparative HPLC (gradient: 0-40 min: acetonitrile/0.1% aqueous TFA 25:75-55:45, t_R = 11 min). Lyophilization of the eluate afforded **3.13** as a purple fluffy solid (2.95 mg, 77%). ^{1}H-NMR (600 MHz, DMSO-d_6): δ (ppm) 0.79 (t, 3H, *J* 7.4 Hz), 0.85 (d, 6H, *J* 6.6 Hz), 0.90 (d, 3H, *J* 6.6 Hz), 0.97 (t, 3H, *J* 7.5 Hz), 1.01-1.08 (m, 1H), 1.20-1.44 (m, 7H), 1.44-1.58 (m, 8H), 1.58-1.74 (m, 5H), 1.74-1.85 (m, 5H), 1.85-2.01 (m, 4H), 2.02-2.08 (m, 3H), 2.08-2.15 (m, 2H), 2.45-2.57 (m, 3H, signals overlaying with solvent peak, identified by COSY), 2.63-2.70 (m, 1H, D_2O), 2.70-2.89 (m, 5H, D_2O), 2.95-3.08 (m, 6H, D_2O), 3.11-3.28 (m, 15H, D_2O), 3.29-3.37 (m, 2H, D_2O), 3.40-3.48 (m, 1H, D_2O), 3.48-3.58 (m, 2H, D_2O), 3.64-3.72 (m, 1H, D_2O), 4.18-4.27 (m, 3H), 4.30-4.36 (m, 2H), 4.34-4.50 (m, 5H), 6.39-6.57 (br s, 1H), 6.58-6.63 (m, 2H),6.63-6.88 (br s, 2H), 6.89-7.13 (m, 7H), 7.16-7.43, (br s, 2H), 7.14-7.66 (m, 3H), 7.66-7.79 (m, 2H), 7.84-7.93 (m, 2H), 7.97 (d, 1H, *J* 7.4 Hz), 8.07 (d, 1H, *J* 7.5 Hz), 8.15-8.22 (m, 2H), 8.22-8.32 (br s, 2H), 8.32-8.50 (br s, 2H), 8.54-8.78 (m, 2H), 8.88-9.12 (m, 2H), 9.17 (s, 1H), 10.10 (s, 1H), 12.51 (s, 1H), 13.41 (s, 1H). HRMS (ESI): *m/z* $[M+3H]^{3+}$ calcd. for $[C_{91}H_{132}N_{23}O_{17}]^{3+}$ 606.3385, found: 606.3392. RP-HPLC (220 nm): 99% (t_R = 7.0 min, *k* = 8.2). $C_{91}H_{129}N_{23}O_{17} \cdot C_6H_3F_9O_6$ (1817.18 + 342.07).

***N*$^{\alpha}$-(3-(1-*N*-((1-Carboxylato-2-(6-(dimethylamino)-3-(dimethyliminio)-3*H*-xanthen-9-yl)phen-5-yl)1-oxomethyl)aminoprop-3-yl-1*H*-1,2,3-triazol-4-yl)propanoyl)-*N*$^{\omega}$-(propanoyl)-Lys-Pro-Arg-Arg-Pro-Tyr-Ile-Leu bis(hydrotrifluoroacetate) (3.14).** Peptide **7** (8.9 mg, 6.1 µmol) was dissolved in anhydrous DMF (100 µL) and a solution of **3.11** (0.62 mg, 3.7 µmol) and DIPEA (55 µmol, 10.5 µL) in anhydrous DMF (30 µL) was added. The mixture was stirred at rt for 2 h. 10% aqueous TFA (30 µL) and 0.1% aqueous TFA/acetonitrile 85:15 v/v (1000 µL) were added and the product of the propionylation reaction was isolated by preparative RP-HPLC (gradient: 0-30 min: acetonitrile/0.1% aqueous TFA 18:82-38:62, t_R = 15 min). Lyophilization of the eluate afforded a white fluffy solid (4.2 mg, 49%). The propionylation product (2.1 mg, 1.5 µmol) and azide **3.12** (1.0 mg, 2.0 µmol) were dissolved in NMP/PBS 1:1 v/v (180 µL). A solution of $CuSO_4 \cdot 5\ H_2O$ (0.62 mg, 2.5 µmol) in NMP/PBS 1:1 v/v (60 µL) (note: $CuSO_4$ was first dissolved in 30 µL of PBS and then 30 µL of NMP were added) and a solution of sodium ascorbate (1.4 mg, 7.1 µmol) in PBS (30 µL) were added. After stirring at rt in the dark for 2 h, the mixture was diluted with 800 µL of 0.1% aqueous TFA/acetonitrile 85:15 v/v followed by isolation of the product by preparative HPLC (gradient: 0-40 min: acetonitrile/0.1% aqueous TFA 25:75-55:45, t_R = 13 min). Lyophilization of the

eluate afforded **3.14** as a purple fluffy solid (2.9 mg, 99%). HRMS (ESI): *m/z* $[M+2H]^{2+}$ calcd. for $[C_{85}H_{121}N_{21}O_{16}]^{2+}$ 845.9645, found: 845.9653. RP-HPLC (220 nm): > 99% (t_R = 7.9 min, k = 9.4). $C_{85}H_{119}N_{21}O_{16} \cdot C_4H_2F_6O_4$ (1691.02 + 228.05).

***N*$^{\alpha}$-(3-(1-*N*-((1-Carboxylato-2-(6-(dimethylamino)-3-(dimethyliminio)-3*H*-xanthen-9-yl)phen-5-yl)1-oxomethyl)aminoprop-3-yl-1*H*-1,2,3-triazol-4-yl)propanoyl)-*N*$^{\omega}$-(propanoyl)-D-Lys-Pro-Arg-Arg-Pro-Tyr-Ile-Leu bis(hydrotrifluoroacetate) (3.15).** Compound **3.15** was prepared from peptide **3.8** (4.5 mg, 3.1 µmol), **13.1** (0.32 mg, 1.8 µmol) and **3.12** (1.5 mg, 2.9 µmol) according to the procedure used for the synthesis of **3.14**. The product of the propionylation reaction, resulting from the treatment of **3.8** with **3.11**, was obtained as a white fluffy solid (3.1 mg, 2.2 µmol, 71%). Peptide **3.15**, resulting from the "click" reaction between the propionylation product and **3.12**, was obtained as a purple fluffy solid (2.61 mg, 61%). HRMS (ESI): *m/z* $[M+2H]^{2+}$ calcd. for $[C_{85}H_{121}N_{21}O_{16}]^{2+}$ 845.9645, found: 845.9655. RP-HPLC (220 nm): > 99% (t_R = 7.8 min, k = 9.3). $C_{85}H_{119}N_{21}O_{16} \cdot C_4H_2F_6O_4$ (1691.02 + 228.05).

***N*$^{\alpha}$-[(4-(*N*-Propanoyl)aminobutanoyl)]-2-(1-(1-*N*-((1-carboxylato-2-(6-(dimethylamino)-3-(dimethyliminio)-3*H*-xanthen-9-yl)phen-5-yl)1-oxomethyl)aminoprop-3-yl-1*H*-1,2,3-triazol-4-yl)methyl)-Gly-β,β-(3-aza)pent-1,5-diyl-Ala-Pro-Arg-Arg-Pro-Tyr-Ile-Leu tris(hydrotrifluoroacetate) (3.16).** Peptide **3.9** (5.0 mg, 3.0 µmol) was dissolved in anhydrous DMF (100 µL) and a solution of **3.11** (0.36 mg, 2.1 µmol) and DIPEA (32 µmol, 5.5 µL) in anhydrous DMF (30 µL) was added. The mixture was stirred at rt for 2 h. 10% aqueous TFA (30 µL) and 0.1% aqueous TFA/acetonitrile 85:15 v/v (1000 µL) were added and the product of the propionylation reaction was isolated by preparative RP-HPLC (gradient: 0-30 min: acetonitrile/0.1% aqueous TFA 20:80-40:60, t_R = 14 min). Lyophilization of the eluate yielded a white fluffy (1.5 mg, 31%). The propionylation product (1.5 mg, 0.92 µmol) and **3.12** (0.66 mg, 1.3 µmol) were dissolved in NMP/PBS 1:1 v/v (180 µL). A solution of $CuSO_4 \cdot 5\ H_2O$ (0.41 mg, 1.6 µmol) in NMP/PBS 1:1 v/v (60 µL) (note: $CuSO_4$ was first dissolved in 30 µL of PBS and then 30 µL of NMP were added) and a solution of sodium ascorbate (0.92 mg, 4.6 µmol) in PBS (30 µL) were added. After stirring at rt in the dark for 2 h, the mixture was diluted with 800 µL of 0.1% aqueous TFA/acetonitrile 85:15 v/v and the product was isolated by preparative HPLC (gradient: 0-40 min: acetonitrile/0.1% aqueous TFA 25:75-55:45, t_R = 10 min). Lyophilization of the eluate afforded **3.16** as a purple fluffy solid (0.78 mg, 40%). HRMS

(ESI): *m/z* $[M+3H]^{3+}$ calcd. for $[C_{90}H_{130}N_{23}O_{17}]^{3+}$ 601.6666, found: 601.6675. RP-HPLC (220 nm): > 99% (t_R = 6.4 min, k = 7.4). $C_{90}H_{127}N_{23}O_{17} \cdot C_6H_3F_9O_6$ (1803.15 + 342.07).

24-(5-(3-Azidopropyl)amino-5-oxopent-1-yn-1-yl)-5,5,27,27-tetramethyl-16-oxa-20-aza-12-azoniaheptacyclo-[15.11.0.03,15.04,12.06,11.020,28.021,26]octacosa-1(28),2,4(12),6-(11),7,9,21(26),22,24-nonaene-8-sulfonate (3.17). Compound **3.21** (15.0 mg, 19.2 µmol) was dissolved in anhydrous DMF (600 µL). DIPEA (10 µL, 58 µmol) and a solution of 3-azidopropylamine (1) (6.2 mg, 29 µmol) in anhydrous DMF (80µL) were added and the mixture was stirred at room temperature in the dark for 1 h. 10% aqueous TFA (30 µL)and 0.1% aqueous TFA/acetonitrile 85:15 v/v (700 µL) were added, and the solution was subjected to preparative RP-HPLC (Kinetex-XB C18 column, mobile phase: 0−40 min: 0.1% aqueous TFA/acetonitrile 80:20 to 50:50, t_R = 24 min), yielding **3.17** as a purple fluffy solid (5.8 mg, 54%). HRMS (ESI): *m/z* $[M+1H]^{1+}$ calcd. for $[C_{37}H_{41}N_6O_5S]^+$ 681.2854, found: 681.2867. RP-HPLC (220 nm): 98% (t_R = 5.7 min, k = 6.5). $C_{37}H_{40}N_6O_5S$ (680.82).

***N*$^{\alpha}$-(3-(*N*-(1-(8-Sulfonato-5,5,27,27-tetramethyl-16-oxa-20-aza-12-azoniaheptacyclo[15.11.0.03,15.04,12.06,11.020,28.021,26]octacosa-1(28),2,4(12),6(11),7,9,21(26),22,24-nonaen-24-yl)-5-oxopentyn-5-yl)-1-aminoprop-3-yl-1*H*-1,2,3-triazol-4-yl)propanoyl)-β,β-(3-aza)pent-1,5-diyl-Ala-Pro-*N*$^{\omega}$-[(4-(*N*-propanoyl)aminobutyl)aminocarbonyl]Arg-Arg-Pro-β,β-dimethyl-L-Tyr-Ile-Leu tris(hydrotrifluoroacetate) (3.18).** Peptide **3.10a** (16.3 mg, 9.4 µmol) was dissolved in anhydrous DMF (170 µL) and a solution of **3.11** (1.0 mg, 6.0 µmol) and DIPEA (91 µmol, 15.8 µL) in anhydrous DMF (30 µL) was added. The mixture was stirred at rt for 2 h. 10% aqueous TFA (30 µL) and 0.1% aqueous TFA/acetonitrile 85:15 v/v (1000 µL) were added and the product of the propionylation reaction was isolated by preparative RP-HPLC (gradient: 0-40 min: acetonitrile/0.1% aqueous TFA 18:82-43:57, t_R = 17 min). Lyophilization of the eluate yielded a white fluffy solid (6.0 mg, 38%). The propionylation product (2.3 mg, 1.4 µmol) and azide **3.17** (1.2 mg, 1.7 µmol) were dissolved in NMP/PBS 1:1 v/v (180 µL). A solution of $CuSO_4 \cdot 5\ H_2O$ (0.60 mg, 2.4 µmol) in NMP/PBS 1:1 v/v (60 µL) (note: $CuSO_4$ was first dissolved in 30 µL of PBS and then 30 µL of NMP were added) and a solution of sodium ascorbate (1.4 mg, 6.9 µmol) in PBS (30 µL) were added. After stirring at rt in the dark for 2 h, the mixture was diluted with 800 µL of 0.1% aqueous TFA/acetonitrile 85:15 v/v followed by purification of the product by preparative HPLC (gradient: 0-40 min: acetonitrile/0.1% aqueous TFA 20:80-50:50, t_R = 19 min) affording **3.18** as a purple fluffy solid (1.3 mg, 39%). ^{1}H NMR

(600 MHz, DMSO-d_6): δ (ppm) 0.78 (t, 3H, *J* 7.4 Hz), 0.83 (t, 6H, *J* 7.7 Hz), 0.90 (d, 3H, *J* 6.6 Hz), 0.97 (t, 3H, *J* 7.7 Hz), 0.99-1.05 (m, 1H), 1.19-1.32 (m, 7H), 1.32-1.45 (m, 6H), 1.45-1.61 (m, 15H), 1.61-1.82 (m, 17H), 1.82-1.99 (m, 8H), 1.99-2.07 (m, 3H), 2.37-2.39 (m, 2H), 2.52-2.58 (m, 2H), 2.68 (t, 2H, *J* 7.1 Hz), 2.72-2.91 (m, 5H), 2.99-3.04 (m, 2H), 3.04-3.17 (m, 7H), 3.20-3.45 (3H, overlaying with water peak, identified and quantified via spectrum with additional D_2O), 3.53-3.60 (m, 2H), 3.64-3.72 (m, 1H), 3.83-3.97 (m, 2H), 4.09-4.14 (m, 1H), 4.19-4.27 (m, 2H), 4.27-4.40 (m, 6H), 4.44-4.54 (m, 2H), 4.60-4.68 (m, 3H), 6.52 (s, 2H), 6.58-6.64 (m, 2H), 6.68-7.04 (br s, 2H), 7.09-7.15 (m, 2H), 7.15-7.41 (m, 5H), 7.41-7.47 (m, 2H), 7.48-7.54 (m, 2H), 7.58-7.63 (d, 1H, *J* 8.3 Hz), 7.70-7.77 (m, 2H), 7.85 (s, 1H), 7.88 (s, 1H), 7.95-8.02 (m, 2H), 8.06-8.14 (m, 3H), 8.15-8.27 (m, 2H), 8.32-8.45 (br s, 1H), 8.52-8.63 (br s, 1H), 8.93-9.04 (br s, 1H), 9.13 (s, 1H), 9.84 (br s, 1H), 12.47 (br s, 1H). HRMS (ESI): *m/z* $[M+3H]^{3+}$ calcd. for $[C_{102}H_{148}N_{23}O_{18}S]^{3+}$ 672.0370, found: 672.0381. RP-HPLC (220 nm): > 99% (t_R = 7.7 min, *k* = 9.1). $C_{102}H_{145}N_{23}O_{18}S \cdot C_6H_3F_9O_6$ (2013.49 + 342.07).

***N*$^{\alpha}$-(3-(1-*N*-((1-Carboxylato-2-(6-(dimethylamino)-3-(dimethyliminio)-3*H*-xanthen-9-yl)phen-5-yl)1-oxomethyl)aminoprop-3-yl-1*H*-1,2,3-triazol-4-yl)propanoyl)-β,β-(3-aza)pent-1,5-diyl-Ala-Pro-*N*$^{\omega}$-[(4-aminobutyl)aminocarbonyl]Arg-Arg-Pro-Tyr-Ile-Leu tetrakis(hydrotrifluoroacetate) (3.19).** Peptide **3.6** (1.5 mg, 0.88 µmol) and azide **3.12** (0.68 mg, 1.3 µmol) were dissolved in NMP/PBS 1:1 v/v (140 µL). A solution of $CuSO_4 \cdot 5\ H_2O$ (0.42 mg, 1.7 µmol) in NMP/PBS 1:1 v/v (50 µL) (note: $CuSO_4$ was first dissolved in 25 µL of PBS and then 25 µL of NMP were added) and a solution of sodium ascorbate (0.95 mg, 4.8 µmol) in PBS (25 µL) were added. After stirring at rt in the dark for 2 h, the mixture was diluted with 0.1% aqueous TFA/acetonitrile 85:15 v/v (800 µL) followed by isolation of the product by preparative HPLC (gradient: 0-40 min: acetonitrile/0.1% aqueous TFA 18:82-48:52, t_R = 17 min). Lyophilization of the eluate afforded **3.19** as a purple fluffy solid (1.2 mg, 61%). HRMS (ESI): *m/z* $[M+4H]^{4+}$ calcd. for $[C_{88}H_{129}N_{23}O_{16}]^{4+}$ 440.9992, found: 441.0005. RP-HPLC (220 nm): 97% (t_R = 12.5 min, *k* = 15.4). $C_{88}H_{125}N_{23}O_{16} \cdot C_8H_4F_{12}O_8$ (1765.14 + 456.09).

***N*$^{\alpha}$-(3-(*N*-(1-(8-Sulfonato-5,5,27,27-tetramethyl-16-oxa-20-aza-12-azoniaheptacyclo[15.11.0.03,15.04,12.06,11.020,28.021,26]octacosa-1(28),2,4(12),6(11),7,9,21(26),22,24-nonaen-24-yl)-5-oxopentyn-5-yl)-1-aminoprop-3-yl-1*H*-1,2,3-triazol-4-yl)propanoyl)-β,β-(3-aza)pent-1,5-diyl-Ala-Pro-*N*$^{\omega}$-[(4-aminobutyl)aminocarbonyl]Arg-Arg-Pro-β,β-dimethyl-L-Tyr-Ile-Leu-OH tetrakis(hydrotrifluoroacetate) (3.20).** Peptide **3.10a** (6.7 mg, 3.9 µmol) and azide **3.17** (3.4

mg, 5.0 µmol) were dissolved in NMP/PBS 1:1 v/v (300 µL). A solution of $CuSO_4 \cdot 5\ H_2O$ (1.8 mg, 7.4 µmol) in NMP/PBS 1:1 v/v (100 µL) (note: $CuSO_4$ was first dissolved in 50 µL of PBS and then 50 µL of NMP were added) and a solution of sodium ascorbate (4.2 mg, 21 µmol) in PBS (50 µL) were added. After stirring at rt in the dark for 2 h, the mixture was diluted with 0.1% aqueous TFA/acetonitrile 85:15 v/v (800 µL) followed by isolation of the product by preparative HPLC (gradient: 0-40 min: acetonitrile/0.1% aqueous TFA 18:82-48:52, t_R = 18 min). Lyophilization of the eluate afforded **3.20** as a purple fluffy solid (3.2 mg, 34%). HRMS (ESI): *m/z* $[M+4H]^{4+}$ calcd. for $[C_{99}H_{145}N_{23}O_{17}S]^{3+}$ 490.2730, found: 490.2745. RP-HPLC (220 nm): 99% (t_R = 13.3 min, k = 16.5). $C_{99}H_{141}N_{23}O_{17}S \cdot C_8H_4F_{12}O_8$ (1957.42 + 456.09).

3.4.3 Synthesis of [^{3}H]3.13 and [^{3}H]3.18

A solution of succinimidyl [^{3}H]propionate (molar activity: 3.89 TBq/mmol, purchased from Novandi, Södertälje, Sweden) (55.5 MBq, 0.75 mL, 14.3 nmol) in n-heptane/ethyl acetate 3:2 v/v was transferred from the delivered ampule into a 1.5-mL polypropylene reaction vessel with screw cap, and the solvent was removed in a vacuum concentrator (30 °C, ca. 30 min). A solution of the precursor peptide **3.19** (0.35 mg, 166.4 nmol) or **3.20** (0.35 mg, 152.2 nmol) and DIPEA (1 µL, 5.73 µmol) in DMF/NMP 75:25 v/v (55 µL) was added, immediately followed by vortexing for 20 s. Subsequently, the vessel was shaken at rt for 2 h. The mixture was acidified by the addition of 2% aqueous TFA (32 µL), followed by the addition of acetonitrile/H_2O 1:9 v/v (280 µL). [^{3}H]**3.13** and [^{3}H]**3.18** were isolated using a HPLC system from Waters (Eschborn, Germany) consisting of two pumps 510, a pump control module, a manual injector (loop size: 200 µL), a 486 UV/vis detector, and a Flow-one Beta series A-500 radiodetector (Packard, Meriden, USA) (the latter was disconnected during the purification process). A Luna C18(2) column (3 µm, 150 mm × 4.6 mm, Phenomenex, Aschaffenburg, Germany) was used as stationary phase at a flow rate of 0.8 mL/min. Mixtures of acetonitrile supplemented with 0.04% TFA (A) and 0.05% aqueous TFA (B) were used as mobile phase. The following linear gradient was applied: 0-20 min: A/B 10:90-44:56, 20-25 min: 44:56-95:5, 25-30 min: 95:5 (isocratic). Four ([^{3}H]**3.13**) and three ([^{3}H]**3.18**) injections were applied. The fractions containing [^{3}H]**3.13** (t_R = 17.7 min) or [^{3}H]**3.18** (t_R = 18.0 min) were collected and combined in a 2-mL polypropylene reaction vessel with screw cap. The volume of the combined eluates was reduced by evaporation in a vacuum concentrator to approximately 300 µL. Ethanol (450 µL) was added resulting in a mixing ratio of EtOH/H_2O 6:4 v/v and a total volume of 750 µL (preliminary stock solution). To determine the radiochemical purity and to prove the identity of [^{3}H]**3.13** and [^{3}H]**3.18**, 2 µL of the preliminary stock solution were added to 100 µL of a 15

µM solution of **3.13** ("cold" analog of [^{3}H]**3.13**) or **3.18** ("cold" analog of [^{3}H]**3.18**) in A/B 1:9 affording the sample to be analyzed using the aforementioned HPLC system, column and solvents. The following linear gradient was applied: 0-20 min: A/B 10:90-45:55, 20-30 min: 45:55-95:5, 30-38 min: 95:5 (isocratic). The radiochemical purity was > 99% in both cases (t_R (**3.13**/[^{3}H]**3.13**) = 18.0 min; t_R (**3.18**/[^{3}H]**3.18**) = 18.5 min). To quantify the activity of the two radioligands and to determine the molar concentration, 2 × 2 µL of the preliminary stock solution were added to 998 µL of DMSO/H_2O 3:7 v/v, and 4 × 10 µL of these dilutions were counted in 3 mL of liquid scintillator (Rotiscint Eco Plus, Carl Roth, Karlsruhe, Germany) with a Tri-Carb 3100TR liquid scintillation counter (PerkinElmer). The activity concentration was adjusted to 18.5 MBq/mL by the addition of EtOH/H_2O 6:4 v/v ([^{3}H]**3.13**: 296 µL; [^{3}H]**3.18**: 604 µL), resulting in a final concentration of 4.76 µM for both stock solutions. Radiochemical yields: [^{3}H]**3.13**, 13.7 MBq (0.371 mCi), 35%; [^{3}H]**3.18**, 13.8 MBq (0.372 mCi), 45%. Molar activity: As the supplier of the labeling reagent succinimidyl [^{3}H]propionate (Novandi, Södertälje, Sweden) provides a precisely determined molar activity and due the fact that [^{3}H]**3.13** and [^{3}H]**3.18** each bear exactly one tritiated propionyl residue originating from the labeling reagent, the molar activities of [^{3}H]**3.13** and [^{3}H]**3.18** were defined to be equal to the molar activity of the labeling reagent, amounting to 3.44 TBq/mmol (it is assumed that under the mild reaction conditions the carbon-tritium bonds remained intact). The molar activity of the labeling reagent succinimidyl [^{3}H]propionate was determined by LC-MS analysis. Coinjection of "cold" succinimidyl propionate allowed the quantification of the incorporated tritium (Novandi).

3.4.4 Chemical stability

The chemical stability of peptides **3.13** and **3.18** was investigated in PBS (adjusted to pH = 7.4) at 22 °C in the dark. The incubation was started by the addition of 15 µL of a 1 mM stock solution (solvent: DMSO) to 135 µL of PBS to yield a concentration of 100 µM. After periods of 0, 6, 24 and 48 h, an aliquot (25 µL) was removed and added to 25 µL of acetonitrile/0.04% aq. TFA 1:9 v/v to obtain a peptide solution with a concentration of 50 µM. 20 µL of this solution were subjected to analytical RP-HPLC analysis using the same system and conditions as described under *Analytical HPLC* with the following gradient: 0-14 min: acetonitrile/0.04% aq. TFA 20:80-40:60, 14-15 min: 40:60-95:5, 15-20 min: 95:5 (isocratic). A 1:1 mixture of PBS and acetonitrile/0.04% aq. TFA 1:9 v/v (20 µL) was analyzed to obtain the blank chromatogram.

3.4.5 Stability in human plasma

The proteolytic stabilities of **3.13** and **3.18** were investigated in human blood plasma/PBS (136.9 mM NaCl, 2.68 mM KCl, 5.62 mM Na_2HPO_4, 1.09 mM NaH_2PO_4 and 1.47 mM KH_2PO_4, pH = 7.4) 1:2 v/v according to a described procedure[38] with the following modifications: 5 mM stock solutions in EtOH/10 mM aq. HCl 1:1 v/v were used for the addition of the peptides to plasma/PBS 1:2 v/v. As the RP-HPLC purity of 1-methyl-D-Trp, used as internal standard (IS), was < 95%, the compound was purified by preparative HPLC to give a purity of > 99%. The concentration of the peptides in plasma/PBS 1:2 v/v was 40 µM (recovery determination) or 80 µM (stability tests). Samples were analyzed using the same RP-HPLC system and conditions as described under *Analytical HPLC* with the following gradient: 0-6 min: acetonitrile/0.04% aq. TFA 10:90-21:79, 6-12 min: 21:79-40:60, 12-13 min: 40:60-95:5, 13-16 min: 95:5 (isocratic). Data analysis was based on UV detection at 220 nm. Reference samples, representing 100% recovery, were prepared in quadruplicate. Recovery ratios were obtained by dividing the recovery of the peptide by the recovery of IS for each individual sample (n = 4). The obtained recoveries and the recovery ratios are summarized in Table A3.2, Appendix.

3.4.6 Excitation spectra, emission spectra, and fluorescence quantum yields

Excitation and emission spectra of **3.13** and **3.18** were recorded with a Cary Eclipse spectrofluorimeter (Varian, Mulgrave, Victoria, Australia) using polystyrene cuvettes (10 mm × 10 mm, reference 1961, Kartell, Noviglio, Italy). Sample solutions (solvent: PBS (pH = 7.4) and PBS supplemented with 1% BSA, concentration of **3.13** and **3.18**: 1 µM, sample volume: 2 mL) were prepared in the cuvettes. Excitation spectra (shown in Figure A3.6, Appendix) were recorded with spectral bandwidths of 5 nm (excitation slit) and 10 nm (emission slit). The spectral bandwidth applied for the emission spectra was 10 nm (excitation slit) and 5 nm (emission slit). Net spectra were obtained by subtracting the respective reference spectrum of a vehicle sample.

The fluorescence quantum yield of compounds **3.13** and **3.18** was determined in PBS and PBS supplemented with 1% BSA via an absolute method using an Ulbricht sphere with an inaccuracy of ca. 3% (Hamamatsu C9920−02 system equipped with a Spectralon integrating sphere) at room temperature (23 ± 1 °C). The optical density at the excitation wavelength of the sample was < 0.1 (optical path length: 1 cm). Samples were measured in a 10 mm × 10 mm quartz cuvette.

3.4.7 Cell culture

Mammalian cells were cultured in T75 or T175 culture flasks (Sarstedt). Chinese hamster ovary (CHO) cells stably expressing $hNTS_1R$[49] were cultured in DMEM/HAM's F12 (Sigma, Taufkirchen, Germany) medium (1:1) supplemented with 7.5% FBS, L-glutamine (Sigma) (630 µg/mL) and hygromycin B (Carl Roth, Karlsruhe, Germany) (250 µg/mL). HT-29 colon carcinoma cells (DSMZ-no. ACC 299) were grown in antibiotic-free RPMI-1640 medium (Sigma) supplemented with 7.5% FBS. Both cell lines were cultured in a humidified atmosphere (95% air and 5% CO_2) at 37 °C. Insect *Spodoptera frugiperda* (*Sf9*) cells (Invitrogen Life Technologies, Schwerte, Germany) were maintained as a suspension culture in serum-free insect cell growth medium EX-CELL 420 (Sigma-Aldrich) at 27 °C in a non-humidified environment. Cell viability was assessed by the exclusion of 0.2% trypan blue (Sigma-Aldrich), and the cell density was determined with TC10™ Automated Cell Counter (Bio-Rad Laboratories, Sundyberg, Sweden).

3.4.8 Molecular cloning and baculovirus generation

All enzymes and reagents used for cloning were obtained from Thermo Fisher Scientific (Vilnius, Lithuania) unless stated otherwise. Plasmids used to prepare baculoviruses, were generated using standard restriction cloning techniques. The $hNTS_1R$-Nluc sequence from pcDNA3.1-hNTS1-NlucC (obtained from Missouri cDNA Research Center, Rolla, MO) (note: NlucC, fused to the C-terminus of $hNTS_1R$, stands for the C-terminal fragment of Nluc consisting of 11 amino acids) was digested with *Hind*III and *Mss*I to insert into the pIMACE-CMVintP10 vector[39] that was digested with *Hind*III and *Sca*I. Restriction digests were gel purified using the FavorPrep Gel/PCR Purification Kit (Favorgen, Vienna, Austria), ligated by T4 DNA ligase (Thermo Fisher Scientific) at 22 °C for 1 h to obtain the plasmid pIMACE-CMVintP10-$hNTS_1R$-Nluc, and transformed into DH5α *E. coli* (made competent in house). After selection with gentamycin (MP Biomedicals, Eschwege, Germany), plasmids were extracted from overnight bacterial cultures (FavorPrep Plasmid DNA Extraction Kit). To create NTS_1R baculoviruses pIMACE-CMVintP10-NTS_1R-Nluc was directly used for transposition into DH10MultiBac (Geneva Biotech, Pregny-Chambésy, Switzerland) according to described standard procedures.[58]

3.4.9 CHO-$hNTS_1R$ cell membrane preparations

CHO-$hNTS_1R$ cells were grown on 175-cm^2 culture dishes (Ref. 83.3903, Sarstedt) to ca. 90% confluency. After washing two times with cold PBS (4 °C), the cells were scraped off in Tris

buffer (50 mM Tris HCl, 1 mM EDTA, pH = 7.4) and centrifuged at 200g at rt for 5 min. The cell pellet was resuspended in the aforementioned Tris buffer supplemented with SIGMAFAST protein inhibitor cocktail (Sigma) (1 tablet in 100 mL buffer). Under cooling in ice-water, cells were disrupted with an Ultra-turrax (IKA, Staufen, Germany) applying six 5-second treatments with breaks of 30 seconds in between. The resulting homogenate was centrifuged at 1500g at 4 °C for 15 min. The supernatant was then centrifuged with an Optima XPN-80 ultracentrifuge (Beckmann Coulter, Brea, CA) at 119,000g at 4 °C for 30 min. The pellet was resuspended in Tris buffer (50 mM Tris HCl, 1 mM EDTA, pH = 7.4) buffer followed by aliquoting and storing at -80 °C. The protein concentration was determined according to the Bradford method[59] in transparent 96-well plates (Greiner Cellstar 655180, Greiner Bio-One, Frickenhausen, Germany) using bovine serum albumin as standard. The protein concentration amounted to 1.3 ± 0.1 mg/mL (mean value ± SEM from three different sample dilutions).

3.4.10 Buffers used for binding and functional assays

DPBS1 (high-content imaging, flow cytometry, radiochemical assays): Dulbecco's phosphate-buffered saline with calcium and magnesium (1.8 mM $CaCl_2$, 2.68 mM KCl, 1.47 mM KH_2PO_4, 3.98 mM $MgSO_4$, 137 mM NaCl, 8.06 mM Na_2HPO_4, pH = 7.4) supplemented with 0.1% BSA (HCI, FC) or 1% BSA (radiochemical assays) and 0.1 mg/mL bacitracin. For high-content imaging and flow cytometric binding studies, *DPBS* was filtrated using 0.2 µm NY syringe filters (Phenomenex).

DPBS2 (fluorescence anisotropy): Dulbecco's phosphate-buffered saline with calcium and magnesium supplemented with 0.1% Pluronic F-127 and cOmplete EDTA-free Protease Inhibitor Cocktail (Roche).

NTS_2R binding buffer: Tris buffer (50 mM TrisHCl, 1 mM EDTA, pH = 7.4) supplemented with 0.1% BSA.

Fura-2 assay buffer: HEPES buffer (120 mM NaCl, 5 mM KCl, 2 mM $MgCl_2$, 1.5 mM $CaCl_2$, 25 mM HEPES and 10 mM glucose at pH = 7.4) supplemented with 2% BSA and 2.5 mM Probenecid (Sigma).

3.4.11 Radiochemical competition binding assay with [^{3}H]1.7

NTS_1R radioligand competition binding experiments with [^{3}H]**1.7** (molar activity: 2.41 TBq/mmol) and the peptides **3.6**-**3.9**, **3.10a**, **3.10b**, **3.13**-**3.16**, and **3.18** were performed with intact $hNTS_1R$-expressing human HT-29 colon carcinoma cells at 23 ± 1 °C using a previously reported protocol.[13] The K_d value of [^{3}H]**1.7** amounted to 0.41 ± 0.08 nM (mean value ± SEM

from two independent saturation binding experiments, each performed in triplicate). Cells were seeded one day before the assay, yielding a confluency of at least 90% on the day of the experiment. Total binding data (including total binding in the absence of competitor) were plotted as dpm values against log(concentration competitor) and analyzed by a four-parameter logistic equation (log(inhibitor) vs response – variable slope, GraphPad Prism 5, GraphPad Software, San Diego, CA) to obtain pIC_{50} values. Individual pIC_{50} values were converted to pK_i values according to the Cheng-Prusoff equation[60] (logarithmic form). To plot average data from individual binding experiments, data were normalized (100% = "top" of the four-parameter logistic fit, 0% = unspecifically bound radioligand).

NTS_2R radioligand competition binding experiments were performed at homogenates of HEK293T cells transiently transfected with the $hNTS_2R$ according to a reported procedure,[49] but using [^{3}H]**1.7** as radioligand instead of [^{3}H]**1.3**. Samples contained 6-10 µg of total soluble protein. Unspecific binding was determined in the presence of **1.3** (10 µM). Experiments were performed in triplicate and data were processed as reported.[49] The K_d value of [^{3}H]**1.7** amounted to 0.75 ± 0.05 nM at a receptor density of B_{max} = 1000 ± 60 fmol/mg protein (mean value ± SEM from four independent saturation binding experiments, each performed in triplicate).

3.4.12 Fura-2 Ca^{2+} assay

$CHO\text{-}hNTS_1R$ cells were seeded in T175 culture flasks 3-4 days prior to the experiment. On the day of the experiment, cells of a confluent T175 flask were detached by trypsinization and centrifuged at rt at 200 g for 5 min. After discarding the medium, cells were resuspended in 10 mL of assay buffer followed by adjustment of the cell concentration to 1.3×10^6 cells per mL. Per 1×10^6 cells (corresponds to 0.77 mL of the cell suspension), 0.25 mL of loading suspension (assay buffer (1 mL), Pluronic F-127 (20% in DMSO, 5 µL) and Fura-2 AM (1 mM in DMSO, 4 µL) were added and the cell suspension was gently stirred at rt in the dark for 30 min. After centrifugation at rt at 200 g for 5 min, the supernatant was discarded, the cells were resuspended in assay buffer (10 mL), and the suspension was gently stirred at rt in the dark for further 30 min. Afterwards, the cell density was adjusted to 1×10^6 cells per mL by the addition of assay buffer to obtain the cell suspension to be used for the assay. For the Fura-2 assay (performed in agonist mode), a 10-fold concentrated (relative to the final concentration) solution of the compound of interest (20 µL) in assay buffer was added to the empty wells of a white 96-well plate (Brand 781605, Wertheim, Germany). To determine the maximal response, **1.3** was used instead (final concentration: 10 nM). To obtain blank controls, neat assay buffer (20 µL) was filled into the wells. After prefilling the plate, it was subjected to a preheated (37 °C)

CLARIOstar Plus Microplatereader (BMG Labtech, Ortenberg, Germany) equipped with two reagent injectors. In a single well, fluorescence (excitation = 335/380 nm, emission = 510 nm, gain = 1300/1100) was recorded for two read cycles (1.5 s). Using one of the injectors, 180 µL of cell suspension (gently stirred using a magnetic stirrer) were injected (flow rate: 100 µL/s) into the well immediately followed by continued measurement of the fluorescence for 44 cycles (66s). This process was conducted for all sample wells. Fluorescence signals were converted into ratios ($signal_{excitation335nm}$ divided by $signal_{excitation380nm}$) and the highest ratio of each well ($ratio_{max}$) was determined. Triplicate mean values of $ratio_{max}$ were normalized based on the response ($ratio_{max}$) obtained for 10 nM **1.3** (100% = response elicited by 10 nM **1.3**, 0% = response in the absence of agonist (blank control)) and the normalized data were plotted in % against log(concentration of agonist, M) followed by analysis according to a four-parameter logistic fit (log(agonist) vs. response - variable slope, GraphPad Prism 5) to obtain pEC_{50} and E_{max} values (the latter correspond to the upper curve plateau). All experiments were performed in triplicate.

3.4.13 High-content imaging binding experiments

CHO-hNTS_1R or HT-29 cells were seeded one day prior to the experiment into the inner 60 wells of a black clear-bottom 96-well plate (Greiner 655090, Greiner Bio-One) at a concentration of 25,000 cells/well and 35,000 cells/well, respectively. On the day of the assay, the medium was removed by suction and the cells were washed with *DPBS1* (50 µL). After this step, *DPBS1* (180 or 200 µL) containing the nuclear dye Hoechst H33342 (2 µg/mL) was added. This solution also contained the fluorescent ligand (kinetic studies, competition binding experiments), or the fluorescent ligand was added separately (saturation binding experiments). In the case of competition binding experiments, the non-labeled receptor ligands were also added separately (details given below). All samples were incubated at 23 ± 1 °C in the dark under gentle shaking (incubation times are specified below). The final volume per well was 200 µL. Shortly before subjecting the plate to the plate reader for image acquisition, the liquid was removed by suction and *DPBS1* (100 µL) was added. Images were acquired using an IX Micro plate reader (Molecular Devices, Sunnyvale, CA) using a 20× Plan Fluor ELWD objective, a Xenon lamp light source and DAPI and TRITC excitation / emission filter cubes for imaging nuclear and fluorescent ligand staining respectively. 2×2 pixel binning from the CCD camera acquisition was used to generate the images for analysis (0.645 mm / image pixel: 449 × 335 mm image size). Two sites/well were measured throughout. Images were analyzed by granularity analysis (2-3 µm diameter granules; MetaXpress 5.3, Molecular Devices, San

Diego, CA) and the integrated intensity (pixel intensity × granule area) per cell was used as the raw measurement of fluorescent ligand binding. Saturation binding experiments were performed with HT-29 and CHO-hNTS_1R cells, kinetic and competition experiments only with CHO-hNTS_1R cells. All experiments were performed in triplicate. For all kind of experiments, unspecific binding was determined in the presence of 1 µM **1.3**.

Saturation binding experiments. The wells were prefilled with *DPBS1* (180 µL) containing Hoechst H33342 (determination of total binding) or Hoechst H33342 and **1.3** (determination of unspecific binding), followed by the addition of 20 µL of a 10-fold concentrated (relative to the final concentration) solution of **3.13** or **3.18** in *DPBS1*. The samples were incubated for 2 h, followed by the washing step and image acquisition. A concentration range of 0.07-100 nM (**3.13**) or 0.15-150 nM (**3.18**) was used. Specific binding data, obtained by subtracting triplicate mean values of unspecific binding from triplicate mean values of total binding, were plotted against the fluorescent ligand concentration and analyzed by a two-parameter equation describing hyperbolic single-site binding (one site, specific binding, GraphPad Prism 5) to obtain K_d values.

Association experiments. After the initial washing step, 200 µL of *DPBS1* containing the fluorescent ligand **3.13** or **3.18** (2.5 nM) and Hoechst H33342 were added to determine total binding. To determine unspecific binding, the same solution, but additionally containing **1.3**, was added. Samples were incubated for different periods of time. The samples of the different time points were prepared in reversed order (longest incubation time first, shortest incubation time last) so that the cells of all samples could be washed and measured approximately at the same time (note: the measurement time for 60 wells was < 5 min). The studied time span was 1-180 min for both fluorescent ligands. Specific binding data, obtained by subtracting triplicate mean values of unspecific binding from triplicate mean values of total binding, were plotted against the time and analyzed by a three-parameter equation describing an exponential rise to a maximum (one-phase association, Y_0 constrained to zero, GraphPad Prism 5) to yield the observed association rate constant k_{obs}. To calculate mean values in %, specific binding data were normalized based on the corresponding B_{eq} value.

Dissociation experiments. After initial washing of the cells, 200 µL of *DPBS1* containing the fluorescent ligand **3.13** or **3.18** (2.5 nM) and Hoechst H33342 were added to the wells (determination of total binding). To determine unspecific binding, the same solution, but additionally containing **1.3**, was added. All samples were preincubated for 90 min, followed by removal of the liquid by suction and addition of 200 µL of *DPBS1* containing **1.3** (1 µM) to initiate the dissociation process. The samples of the different time points were prepared at

different times in reversed order (longest incubation time first, shortest incubation time last) so that the cells of all samples could be measured approximately at the same time. The studied dissociation times were 1-240 min. The plate was directly subjected to the plate reader (no washing step). Specific binding data, obtained by subtracting triplicate mean values of unspecific binding from triplicate mean values of total binding, were plotted against the time and analyzed by a three-parameter equation describing an incomplete monophasic exponential decline (one phase decay, GraphPad Prism 5) to obtain k_{off} values. The mean ± SEM of the plateau values from individual experiments proved to be throughout significantly different from zero (one-tailed t-test, $P < 0.05$). To calculate mean values in %, binding data were normalized based on specifically bound ligand (B) at t = 0 (B_0).

Calculation of association rate constants (k_{on}) and kinetically derived dissociation constants K_d(kin). The association rate constants were calculated from k_{obs} mean values, k_{off} mean values, and the fluorescent ligand concentration used for the association experiments ([FL]) according to the equation $k_{on} = (k_{obs} - k_{off})/[FL]$. The kinetically derived dissociation constants K_d(kin) were calculated from k_{on} and k_{off} mean values according to $K_d(kin) = k_{off}/k_{on}$.

Competition binding experiments. After initial washing of the cells, 180 µL of *DPBS1* containing the fluorescent ligand (used final concentrations corresponded to the K_d values obtained from equilibrium saturation binding experiments: 1.1 nM (**3.13**) or 1.3 nM (**3.18**)) and Hoechst H33342 were added, followed by the addition of 20 µL of a 10-fold concentrated (relative to the final concentration) solution of the compound of interest (**1.3** or **1.5**), 20 µL of neat *DPBS1* (determination of total binding), or 20 µL of a 10 µM solution of **1.3** (determination of unspecific binding). Samples were incubated for 90 min, followed by the washing step and image acquisition. Total binding fluorescence intensities (including total binding in the absence of competitor) were plotted against log(concentration competitor) and analyzed by a four-parameter logistic equation (log(inhibitor) vs response – variable slope, GraphPad Prism 5) to obtain pIC_{50} values. Individual pIC_{50} values were converted to pK_i values according to the Cheng-Prusoff equation[60] (logarithmic form). To plot average data from individual binding experiments, data were normalized (100% = "top" of the four-parameter logistic fit, 0% = unspecifically bound fluorescent ligand).

3.4.14 Flow cytometric binding experiments

Flow cytometry-based NTS_1R binding studies were performed with intact CHO-hNTS_1R (all kind of experiments) and HT-29 cells (only saturation binding) using a BD FACSCanto II (Becton Dickinson, Heidelberg, Germany), equipped with an Argon laser (488 nm) and a red

diode laser (640 nm), and a BD High Throughput Sampler (HTS unit) for microtiter plates. Saturation and competition binding experiments were performed in triplicate in 96-well polypropylene plates (Brand 701330, Wertheim, Germany) using the HTS unit for sample injection. Association and dissociation experiments were performed in duplicate in 5-mL polypropylene tubes (VWR, Radnor, USA) using the standard injection port of the flow cytometer. The following gain settings for forward and sideward scatter were applied: FSC, 0 V; SSC, 252 V. Fluorescence was recorded using the PE-channel (excitation: 488 nm, emission: 585 ± 21) nm with a PMT gain of 330-400 V. For measurements using the HTS unit, 45 µL of the sample were injected with a speed of 1.5 µL/s. For measurements, requiring the use of the standard injection port, the medium flow rate (60 µL/min) was used. Measurements were stopped after 30 seconds (HTS unit) or after counting of 500-3000 gated events (standard injection port).

Cells were seeded in T75 culture flasks 3-4 days (CHO-hNTS$_1$R cells) or 5-6 days (HT-29 cells) prior to the experiment. On the day of the experiment, cells were detached by trypsinization, suspended in *DPBS1* and centrifuged at 200 g at rt for 5 min. The cell pellet was re-suspended in binding buffer and the cell density was adjusted to 1.5×10^5 to 2.5×10^5 cells/mL (CHO-hNTS1R cells) or 1.0×10^6 cells/mL (HT-29 cells). Unspecific binding was determined in the presence of 1 µM **1.3**.

Saturation binding experiments. A 96-well polypropylene plate was prefilled with 200 µL of cell suspension. For total binding, H_2O (2 µL) and DMSO/H_2O 2:8 v/v (2 µL) containing the fluorescent ligand (100-fold concentrated compared to the final concentration) were added. To determine unspecific binding, a 100 µM solution of **1.3** in H_2O (2 µL) and DMSO/H_2O 2:8 v/v (2 µL) containing the fluorescent ligand (100-fold concentrated) were added. Samples were incubated at 23 ± 1 °C in the dark under gentle shaking for 2 h followed by measurement via the HTS unit. Specific binding data, obtained by subtracting triplicate mean values of unspecific binding from triplicate mean values of total binding, were plotted against the fluorescent ligand concentration and analyzed by a two-parameter equation describing hyperbolic single-site binding (one site, specific binding, GraphPad Prism 5) to obtain K_d values.

Association experiments. 5-mL polypropylene tubes were prefilled with 2000 µL of cell suspension and H_2O (20 µL) was added (determination of total binding). To start the association, a 100 nM solution of the fluorescent ligand in DMSO/H_2O 2:8 v/v (20 µL) was added (final concentration of **3.13** and **3.18**: 1 nM). After short mixing, the tube was placed in the injection port of the flow cytometer and the data of the first (20 s), second (40 s) and third (60s) time point were acquired. Additional measurements were conducted within different

periods of time (2-180 min). When not placed in the injection port, the sample tube was gently shaken in the dark at 23 ± 1 °C. To determine unspecific binding, a 100 µM solution of **1.3** in H_2O (20 µL) and a 100 nM solution of the fluorescent ligand in DMSO/H_2O 2:8 v/v (20 µL) were added. Specific binding data, obtained by subtracting triplicate mean values of unspecific binding from triplicate mean values of total binding, were plotted against the time and analyzed by a three-parameter equation describing an exponential rise to a maximum (one-phase association, Y_0 constrained to zero, GraphPad Prism 5) to yield the observed association rate constant k_{obs}. To calculate mean values in %, specific binding data were normalized based on the corresponding B_{eq} value.

Dissociation experiments. 5-mL polypropylene tubes were prefilled with 2000 µL of cell suspension. For the determination of total binding, the preincubation was started by the addition of H_2O (20 µL) and a 1 µM solution of **3.13** or **3.18** in DMSO/H_2O 2:8 v/v (20 µL) (final fluorescent ligand concentration: 10 nM). To determine unspecific binding, a 100 µM solution of **1.3** in H_2O (20 µL) and a 1 µM solution of **3.13** or **3.18** in DMSO/H_2O 2:8 v/v were added. The samples were gently shaken in the dark at 23 ± 1 °C for 90 min. The dissociation process was initiated by the addition of a 2.5 mM solution of **1.3** in H_2O (20 µL) (final concentration: approximately 25 µM). After different periods of time (1-240 min), sample aliquots were measured by placing the tube in the injection port of the flow cytometer. Specific binding data, obtained by subtracting triplicate mean values of unspecific binding from triplicate mean values of total binding, were plotted against the time and analyzed by a three-parameter equation describing an incomplete monophasic exponential decline (one phase decay, GraphPad Prism 5) to obtain k_{off} values. The mean ± SEM of the plateau values from individual experiments proved to be throughout significantly different from zero (one-tailed t-test, $P < 0.05$). To calculate mean values in %, binding data were normalized based on the specifically bound ligand (B) at t = 0 (B_0).

Calculation of association rate constants (k_{on}) and kinetically derived dissociation constants K_d(kin). The k_{on} and K_d(kin) values were calculated as described for high-content imaging binding experiments.

Competition binding experiments. A 96-well polypropylene plate was prefilled with 200 µL of cell suspension. 2 µL of H_2O (for the determination of total binding in the absence of competitor), 2 µL of a 100 µM solution of **1.3** in H_2O (determination of unspecific binding), or 2 µL of a 100-fold concentrated solution (compared to the final concentration) of the compound of interest (**1.3** or **1.5**; used at varying concentrations) in DMSO/H_2O 2:8 v/v were added and the plate was shortly shaken. Subsequently, 2 µL of a 260 nM solution of **3.13** or a 310 nM

solution of **3.18** in DMSO/H_2O 2:8 v/v were added to each well and the plate was gently shaken in the dark at 23 ± 1 °C for 90 min followed by measurement via the HTS unit. The final concentrations of **3.13** and **3.18** corresponded to their K_d values determined by equilibrium saturation binding: 2.6 nM (**3.13**) or 3.1 nM (**3.18**). Data were analyzed as described for HCI competition binding experiments.

3.4.15 Fluorescence anisotropy binding experiments

FA-based NTS_1R binding studies with **3.13** and **3.18** were performed at $hNTS_1R$ displaying budded baculovirus particles (termed BBVs below), which were obtained from Sf9 insect cells following the procedure reported for the preparation of neuropeptide Y Y_1R displaying BBVs.[61] The obtained viruses were collected by centrifugation at 1600g for 10 min, and the virus titer was determined with an image-based cell-size estimation assay as described elsewhere.[62] The viruses were amplified using a multiplicity of infection (MOI) between 0.01 and 0.1 until a high-titer baculovirus stock (virus concentration of at least 1.0×10^8 infectious viral particles/mL) was acquired. To produce BBV preparations with a high receptor density, Sf9 cells with a density of 1.9×10^6 cells/mL were infected with an MOI of 3 and the BBVs were collected by centrifugation 63 h after the infection, when the cell viability was < 30%. The BBVs were concentrated 40-fold by centrifugation at 48,000g at 4 °C for 40 min, washed with ice-cold DPBS, resuspended, and homogenized using a 0.3 mm diameter needle (Sterican, B. Braun, Melsungen, Germany). Aliquots of the BBV preparations were stored at −90 °C until use.

FA measurements were performed with a Synergy NEO multimode plate reader (BioTek, Winooski, VT) and black, half-area, flat bottom polystyrene NBS (nonbinding surface) 96-well plates (product no. 3993; Corning, Corning, NY). Polarizing excitation (530 ± 15 nm) and dual emission (590 ± 17.5 nm) filters with a dichroic mirror were used, allowing the simultaneous detection of parallelly and perpendicularly polarized fluorescence emission after polarizing beam splitter. All measurements were performed at 27 °C. For all experiments, *DPBS2* was used as binding buffer. Saturation binding, association and dissociation experiments were performed in duplicate (total binding) and singlet (unspecific binding). Competition binding experiments were carried out in triplicate. The final total volume per well was 100 µL. On the day of the experiment, frozen preparations of $hNTS_1R$ displaying BBVs were thawed and thoroughly resuspended, followed by further dilution required for the respective experiment.

Saturation binding, association, and dissociation experiments. 25 µL of a 4-fold concentrated (compared to the final concentration) solution of **3.13** or **3.18** (final concentrations

were 0.3 and 1 nM for both ligands) and 25 µL of *DPBS2* were premixed in the 96-well plate followed by the addition of 50 µL of BBV suspension (used in six different concentrations; each was combined with the two ligand concentrations) to start the association. To determine unspecific binding, 25 µL of a 4 µM solution of **1.5** in *DPBS2* was added instead of neat *DPBS2*. For blank measurements, 50 µL of *DPBS2* were mixed with 50 µL of BBV suspension. Due to the very fast association of both fluorescent ligands, separate measurements were performed for the individual combinations of fluorescent ligand and BBV concentrations (each measurement comprised 4 wells: 2× total binding, 1× unspecific binding, 1× blank). This enabled shorter time intervals between the read cycles (the measuring time for one cycle, comprising 4 wells, was 6 s; 100 read cycles were carried out). The time span between the addition of the ligands to the wells using a multichannel pipette and the start of the measurement was 7 s (no shaking carried out). It was taken into account for data analysis. After 10 min of reading (within this time period a stable signal was reached for all combinations of ligand and BBV concentrations), the plate was removed and 5 µL of a 21 µM solution of **1.5** in *DPBS2* (final concentration: 1 µM) were added to start the dissociation. Immediately after the addition of **1.5**, FA signals were measured for 10 min (within this time period, the dissociation was complete and a plateau was reached, respectively). Fluorescence intensities were processed as previously reported[61] using the in-house developed software Aparecium 2.0.20 (http://www.gpcr.ut.ee/software.html).[63] Prior to the calculation of fluorescence anisotropy values, the parallel and perpendicular fluorescence intensities were blank-corrected based on the data obtained from wells containing BBVs, but no fluorescent ligand. The FA signals at 10 min were used to analyze equilibrium saturation binding using a previously presented user-defined GraphPad Prism-compatible binding model (https://github.com/laasfeld/FPoLi-GPCR)[63] to obtain K_d values. The association rate constant k_{on} and the K_d(kin) values were obtained by fitting the binding data with a reported model[63] with k_{off} constrained to the value derived from the dissociation section of the respective experiment. Mean K_d(kin) values ± SEM were calculated from individual K_d(kin) values. The NTS_1R concentrations of the BBV stocks (two batches were used), obtained from the global data analysis, amounted to 1.4 and 10.0 nM.

Competition binding experiments. 25 µL of a 1.2 nM solution of **3.13** or **3.18** in *DPBS2* and 25 µL of a 4-fold concentrated (compared to the final concentration) solution of the compound of interest (used at varying concentrations) in *DPBS2* were premixed in a 96-well plate. To determine total binding, 50 µL of the BBV suspension (used at one fixed dilution corresponding to a receptor concentration of 1.0 nM) were added. To determine total binding in the absence of competitor, 25 µL of neat *DPBS2* were added instead of *DPBS2* containing the competing

ligand. Unspecific binding was determined by the addition of 25 µL of a 4 µM solution of **1.5** in *DPBS2* (final concentration: 1 µM). For blank measurements, 50 µL of *DPBS2* were mixed with 50 µL of BBV suspension. The incubation time was 90 min. Anisotropy data of total binding (including total binding in the absence of competitor) were plotted against log(concentration competitor) and analyzed by a four-parameter logistic equation (log(inhibitor) vs response – variable slope, GraphPad Prism 5) to obtain pIC_{50} values. Individual pIC_{50} values were converted to pK_i values according to the Cheng-Prusoff equation[60] (logarithmic form). To plot average data from individual binding experiments, data were normalized (100% = "top" of the four-parameter logistic fit, 0% = unspecifically bound fluorescent ligand). It should be noted that in the case of FA, data fitting by a four-parameter logistic equation and conversion of the resulting pIC_{50} values to pK_i values according to the Cheng-Prusoff equation represents an approximation since it assumes abundance of the ligands relative to the amount of receptor, which may be violated in the case of FA assay, especially when measuring high-affinity unlabeled ligands.

3.4.16 Radiochemical NTS_1R binding assays with [^{3}H]3.13 and [^{3}H]3.18

Binding of both ligands, [^{3}H]**3.13** and [^{3}H]**3.18**, was studied at adherent and suspended intact CHO-hNTS_1R cells, and binding of [^{3}H]**3.13** was additionally studied using CHO-hNTS_1R cell membrane preparations (saturation and competition binding, kinetic studies). Furthermore, saturation binding experiments were performed with both ligands at intact adherent HT-29 cells. All experiments were performed in triplicate except for dissociation experiments with suspended cells (performed in duplicate). All samples were incubated at 23 ± 1 °C in the dark under gentle shaking (incubation times are outlined below). *DPBS1* served as binding buffer throughout. In the case of experiments performed with cell suspensions, CHO-hNTS_1R cells were seeded in T75 culture flasks 3-4 days prior to the experiment. On the day of the experiment, cells were detached by trypsinization, suspended in *DPBS1* and centrifuged at 200g at rt for 5 min. Cells were resuspended in binding buffer and the cell density was adjusted to 1.5×10^5 to 2.5×10^5 cells/mL. Samples involving suspended cells or membrane preparations were prepared and incubated in 96-well polypropylene plates (Brand 701330, Wertheim, Germany) or in 50-mL polypropylene falcon tubes (Sarstedt), and the same filtration procedure for separating free radioligand from cell- or membrane bound radioligand was applied for all kind of binding experiments: after completed incubation, cells or cell membranes were collected on GF/C filter mats (0.26 mm; Whatman, Maidstone, UK) (pretreated with 0.3% polyethyleneimine for 30 min) using an in-house manufactured harvester for 96-well plates

(precision engineering workshop of the University of Regensburg, Regensburg, Germany), and the wells of the plate and the cells on the filter mat were immediately washed twice with ice-cold PBS (2 × 200 µL) (note: when samples were incubated in falcon tubes, 200-µL aliquots were transferred to the wells of a 96-well polypropylene plate after the incubation period, immediately followed by the filtration procedure). Filter pieces for each well were punched out and transferred into 1450-401 96-well sample plates (PerkinElmer, Rodgau, Germany), followed by the addition of Rotiscint Routine (Carl Roth, Karlsruhe, Germany) (200 µL). The plates were sealed with transparent sealing tape (Greiner EASYseal, part no. 676001, Greiner Bio-One) and shaken in the dark overnight before measurement of the radioactivity (dpm) using a MicroBeta2 plate counter equipped with six pairs of photomultiplier tubes (PerkinElmer).

For experiments involving adherent cells, CHO-hNTS_1R (25,000 cells per well) or HT-29 (35,000 cells per well) cells were seeded one day prior to the experiment in white 96-well plates with clear bottom (VWR 732-3740). On the day of the experiment, the medium was aspirated and the cells (confluency: 70-90%) were washed with PBS (200 µL) followed by covering with *DPBS1* (160 µL) and the addition of the ligands as outlined below. After completed incubation, the liquid was aspirated and the wells were washed twice with ice-cold PBS (200 µL) followed by the addition of lysis solution (urea (8 M), acetic acid (3 M) and Triton-X (1%) in water) (25 µL). After shaking for at least 20 min, liquid scintillator (UltimaGold, PerkinElmer) (200 µL) was added and the plates were sealed with a transparent sealing tape (permanent seal for microplates, PerkinElmer, prod. no. 1450−461). The sealed plates were turned upside down several times to achieve complete mixing of scintillator and lysis solution and were kept in the dark for at least 3 h before measurement of the radioactivity (dpm) with the MicroBeta2 plate counter.

Saturation binding experiments. A 96-well polypropylene plate was prefilled with cell suspension (160 µL) or 96-well white/clear bottom plates with adherent cells were prefilled with *DPBS1* (160 µL) after initial washing of the cells. For the determination of total binding, *DPBS1* (20 µL) and a 10-fold concentrated (relative to the final concentration) solution of [^{3}H]**3.13** or [^{3}H]**3.18** in *DPBS1* (20 µL) were added. To determine unspecific binding, a 10 µM solution of **1.3** (final concentration: 1 µM) *in DPBS1* (20 µL) was added instead of neat *DPBS1*. Samples were incubated for 2 h followed by cell harvesting (cell suspensions) or cell lysis (adherent cells) and further processing as described afore. Specific binding data, obtained by subtracting triplicate dpm mean values of unspecific binding from triplicate dpm mean values of total binding, were plotted against the free radioligand concentration and analyzed by a two-parameter equation describing hyperbolic single-site binding (one site, specific binding,

GraphPad Prism 5) to obtain K_d values. The free concentration of [^{3}H]**3.13** or [^{3}H]**3.18** (nM) was calculated by subtracting the amount of specifically bound [^{3}H]**3.13** or [^{3}H]**3.18** (nM) (calculated from specifically bound radioligand in dpm, the molar activity and the volume per well) from the total concentration of [^{3}H]**3.13** or [^{3}H]**3.18**.

Association experiments. Cell suspensions: After prefilling a 96-well polypropylene plate with cell suspension (160 µL), 20 µL of *DPBS1* (determination of total binding) or 20 µL of a 10 µM solution of **1.3** (final concentration: 1 µM) in *DPBS1* (determination of unspecific binding) were added. To start the association, 20 µL of an 18 nM solution of [^{3}H]**3.13** or 20 µL of a 12 nM solution of [^{3}H]**3.18** in *DPBS1* (final concentrations: 1.8 or 1.2 nM) were added. The samples of the different time points were prepared in reversed order (longest incubation time first, shortest incubation time last) so that the cells of all samples could be harvested simultaneously. The timespan for sample incubation was 1-180 min. **Adherent cells:** 96-well white/clear bottom plates with adherent cells were prefilled with *DPBS1* (160 µL) after initial washing of the cells. 20 µL of *DPBS1* (determination of total binding) or 20 µL of a 10 µM solution of **1.3** in *DPBS1* (final concentration: 1 µM) (determination of unspecific binding) were added. To start the association, 20 µL of a 13 nM solution of [^{3}H]**3.13** or 20 µL of an 11 nM solution of [^{3}H]**3.18** in *DPBS1* (final concentrations: 1.3 or 1.1 nM) were added. When the incubation time was reached, all liquid was removed by suction followed by washing (2 × ice-cold PBS) and cell lysis. The samples of the different time points were prepared in reversed order (longest incubation time first, shortest incubation time last) so that the cells of all samples could be washed and lysed simultaneously. This did not apply for the first four time points (1, 3, 5, 8 min). These samples were prepared and processed individually during the incubation of the samples of the longer time points (note: lysis solution was not directly added after washing of the cells; it was added when the incubation of all samples had been finished). The timespan for the association was 1-180 min. **Data processing (cell suspensions and adherent cells):** Specific binding data, obtained by subtracting triplicate dpm mean values of unspecific binding from triplicate dpm mean values of total binding, were plotted against the time. Data describing the first association phase were fitted by a one phase association fit (Y_0 constrained to zero, GraphPad Prism 5) followed by a biphasic fit (two phase association, Y_0 constrained to zero, $k_{obs(fast)}$ constrained to the k_{obs} value of the initial monophasic fit, GraphPad Prism 5) affording $k_{obs(slow)}$ values. To calculate mean values in %, specific binding data were normalized based on the corresponding plateau value (set to 100%) obtained for the biphasic fit.

Dissociation experiments. Cell suspensions: Initially, dissociation experiments with [^{3}H]**3.13** and [^{3}H]**3.18** using cell suspensions were performed in 96-well polypropylene plates. The plates

were prefilled with cell suspension (160 µL) followed by the addition of 20 µL of *DPBS1* (determination of total binding) or 20 µL of a 10 µM solution of **1.3** (final concentration: 1 µM) in *DPBS1* (determination of unspecific binding). 20 µL of a 50 or 90 nM ([^{3}H]**3.13**) or 20 µL of a 50 or 60 nM ([^{3}H]**3.18**) solution were added to start the preincubation period of 90 min. The dissociation process was initiated by the addition of a 250 µM solution of **1.3** in *DPBS1* (20 µL) (final concentration: approximately 25 µM). The samples of the different time points were prepared at different times in reversed order (longest incubation time first, shortest incubation time last) so that the cells of all samples could be harvested simultaneously. The studied dissociation times were 1-240 min. As these dissociation experiments did not yield useful (reproducible) results, dissociation experiments were performed using 50-mL falcon tubes as sample container. These were prefilled with 5000 µL of cell suspension followed by the addition of *DPBS1* (50 µL) and a 500 nM solution of [^{3}H]**3.13** or [^{3}H]**3.18** (final concentration: 5 nM) in *DPBS1* (50 µL). To determine unspecific binding, a 100 µM solution of **1.3** (final concentration: 1 µM) in *DPBS1* (50 µL) was added instead of neat *DPBS1*. The samples were preincubated for 90 min. The dissociation was initiated by the addition of 50 µL of a 2.5 mM solution of **1.3** in *DPBS1* (final concentration: 25 µM). As this kind of dissociation experiment is laborious with respect to the separation of bound from free radioligand, only a few time points (10, 30, 60, 90, 120, 150, and 180 min) were studied. After the indicated incubation periods, three 200-µL aliquots were removed and transferred into a 96-well polypropylene plate immediately followed by cell harvesting and further processing as described afore (filter pieces were collected in one 1450-401 96-well sample plate). Note that the experimental setup necessitated an individual filtration process for each incubation time.
Adherent cells: The inner 60 wells of two white 96-well plates with clear bottom were prefilled with *DPBS1* (160 µL) after initial washing of the cells. The preincubation was started by the addition of *DPBS1* (20 µL) and a 50 nM solution of [^{3}H]**3.13** or [^{3}H]**3.18** (final concentrations: 5 nM) in *DPBS1* (20 µL). To determine unspecific binding, a 10 µM solution of **1.3** (final concentration: 1 µM) in *DPBS1* (20 µL) was added instead of neat *DPBS1*. The samples were incubated for 90 min followed by removal of all liquid by suction and the addition of a 1 µM solution of **1.3** in *DPBS1* (200 µL) to initiate the dissociation. The samples of the different time points were prepared at different times in reversed order (longest incubation time first, shortest incubation time last) so that the cells of all samples could be washed and lysed at approximately the same time. This did not apply for the four shortest time points (1, 3, 5 and 8 min). These samples were prepared and processed individually during the incubation of the samples of the longer time points (note: lysis solution was not directly added after washing of the cells; it was

added when the incubation of all samples had been finished). The timespan for the dissociation was 1-180 min

Specific binding data, obtained by subtracting triplicate mean values of unspecific binding from triplicate mean values of total binding, were plotted against the time and analyzed by a three-parameter equation, describing an incomplete monophasic exponential decline (one phase decay, GraphPad Prism 5) to obtain k_{off} values. The mean ± SEM of the plateau values from individual experiments proved to be throughout significantly different from zero (one-tailed t-test, $P < 0.05$). To calculate mean values in %, binding data were normalized based on the specifically bound ligand (B) at t = 0 (B_0).

Calculation of association rate constants (k_{on}) and kinetically derived dissociation constants K_d(kin). The association rate constants $k_{on(fast)}$ were calculated from $k_{obs(fast)}$ mean values, k_{off} mean values, and the radioligand concentration used for the association experiments ([RL]) according to the equation $k_{on(fast)} = (k_{obs(fast)} - k_{off})/[RL]$. To note, the calculation of $k_{on(slow)}$ from $k_{obs(slow)}$ gave no reasonable values since the k_{off} mean value was nearly equal to the individual $k_{obs(slow)}$ values. The kinetically derived dissociation constants K_d(kin) were calculated from $k_{on(fast)}$ and k_{off} mean values according to $K_d(kin) = k_{off}/k_{on(fast)}$.

Competition binding experiments. A 10-fold concentrated solution (compared to the final concentration) of [^{3}H]**3.13** or [^{3}H]**3.18** in *DPBS1* (20 µL) was added to 160 µL of cell suspension (final radioligand concentrations: 1.8 and 1.2 nM, respectively) or to the adherent cells covered with 160 µL of *DPBS1* (final radioligand concentrations: 1.3 and 1.1 nM, respectively), followed by the addition of a 10-fold concentrated solution (compared to the final concentration) of the compound of interest in *DPBS1* (20 µL). Total binding in the absence of competitor was determined by adding *DPBS1* (20 µL) instead of competitor, and unspecific binding was determined by the addition of a 10 µM solution of **1.3** (final concentration: 1 µM) in *DPBS1* (20 µL) instead of competitor. Samples were incubated for 90 min followed by cell harvesting or cell lysis and further processing as described afore. Data were analyzed as described for HCI competition binding experiments.

3.4.17 Saturation and competition binding, association, and dissociation experiments with [^{3}H]3.13 at membranes of CHO-hNTS$_1$R cells

On the day of the experiment, membrane aliquots (150 µL) were thawn and *DPBS1* (300 µL) was added. The suspension was centrifuged at 9000g at 4 °C for 5 min followed by discarding the supernatant and resuspending in *DPBS1* supplemented with saponin (100 µg/mL) and GppNHp (50 µM) (approximately 2 mL). The membrane dilution was homogenized using a 0.4

mm diameter needle (Sterican, B. Braun, Melsungen, Germany). Experiments were performed as the saturation and competition binding, association, and dissociation experiments with suspended CHO-hNTS_1R cells, using 20 µL of the membrane dilution in *DPBS1* (soluble protein content: 98 µg/mL) instead of 160 µL of the cell suspension. To reach a volume of 160 µL, 140 µL of *DPBS1* with saponin and GppNHp were added to each well prior to addition of the ligands. Data were processed and analyzed as described for HCI binding assays. As the plateau mean value from individual dissociation experiments (one phase decay fit, GraphPad Prism 5) was not significantly different from zero ($P > 0.05$, unpaired one-tailed t-test), data were reanalyzed with the plateau value constrained to zero to obtain k_{off} values.

3.4.18 Confocal microscopy

Confocal microscopy was performed with a Celldiscoverer 7 (Zeiss, Jena, Germany). The used objective was 50× magnification with water (1.2 NA) (Zeiss). Experiments were performed at 23 ± 1 °C. One day prior to the experiment, CHO-hNTS_1R cells were seeded into a black clear-bottom 96-well plate (Greiner 655090) at a concentration of 25,000 cells/well. Shortly before image acquisition, the medium of one well was removed by suction and the cells were washed with *DPBS1* (50 µL), followed by the addition of *DPBS1* (200 µL) containing Hoechst H33342 (2 µg/mL) and **3.13** or **3.18** (each 5 nM). The plate was immediately transferred to the instrument and a series of 30 images (1-30 min) was acquired using the following settings: sequential laser excitation (405 nm nuclei, 561 nm **3.13**/**3.18**), emission (410-540 nm band pass, nuclei, 565-700 nm long pass **3.13**/**3.18**), with a pinhole set to 1 Airy unit for the longer wavelength. For the determination of unspecific binding, **1.3** (1 µM) was added to the solution containing Hoechst H33342 and **3.13** or **3.18**.

3.4.19 Calculation of Propagated Errors

Propagated errors (applying to specifically bound fluorescent ligand or radioligand (saturation binding), association rate constants k_{on} (except for FA assays), and kinetically derived dissociation constants K_d(kin) (except for FA assays) were calculated as described elsewhere.[56]

3.5 References

1. Maillard, J.; Klehs, K.; Rumble, C.; Vauthey, E.; Heilemann, M.; Furstenberg, A. Universal quenching of common fluorescent probes by water and alcohols. *Chem. Sci.* **2020**, *12*, 1352-1362.
2. Song, L.; Varma, C. A.; Verhoeven, J. W.; Tanke, H. J. Influence of the triplet excited state on the photobleaching kinetics of fluorescein in microscopy. *Biophys. J.* **1996**, *70*, 2959-2968.
3. Torimura, M.; Kurata, S.; Yamada, K.; Yokomaku, T.; Kamagata, Y.; Kanagawa, T.; Kurane, R. Fluorescence-quenching phenomenon by photoinduced electron transfer between a fluorescent dye and a nucleotide base. *Anal. Sci.* **2001**, *17*, 155-160.
4. Koide, Y.; Urano, Y.; Hanaoka, K.; Terai, T.; Nagano, T. Evolution of group 14 rhodamines as platforms for near-infrared fluorescence probes utilizing photoinduced electron transfer. *ACS Chem. Biol.* **2011**, *6*, 600-608.
5. Archipowa, N.; Wittmann, L.; Köckenberger, J.; Ertl, F. J.; Gleixner, J.; Keller, M.; Heinrich, M. R.; Kutta, R. J. Characterization of fluorescent dyes frequently used for bioimaging: Photophysics and photocatalytical reactions with proteins. *J. Phys. Chem. B* **2023**, *127*, 9532-9542.
6. Vincent, J. P.; Mazella, J.; Kitabgi, P. Neurotensin and neurotensin receptors. *Trends Pharmacol. Sci.* **1999**, *20*, 302-309.
7. Faure, M. P.; Gaudreau, P.; Shaw, I.; Cashman, N. R.; Beaudet, A. Synthesis of a biologically active fluorescent probe for labeling neurotensin receptors. *J. Histochem. Cytochem.* **1994**, *42*, 755-763.
8. Faure, M. P.; Alonso, A.; Nouel, D.; Gaudriault, G.; Dennis, M.; Vincent, J. P.; Beaudet, A. Somatodendritic internalization and perinuclear targeting of neurotensin in the mammalian brain. *J. Neurosci.* **1995**, *15*, 4140-4147.
9. Betancur, C.; Canton, M.; Gully, D.; Vela, G.; Pelaprat, D.; Rostene, W. Characterization and distribution of binding sites for a new neurotensin receptor antagonist ligand, [3H]SR 48692, in the guinea pig brain. *J. Pharmacol. Exp. Ther.* **1995**, *273*, 1450-1458.
10. Betancur, C.; Canton, M.; Burgos, A.; Labeeuw, B.; Gully, D.; Rostene, W.; Pelaprat, D. Characterization of binding sites of a new neurotensin receptor antagonist, [3H]SR 142948A, in the rat brain. *Eur. J. Pharmacol.* **1998**, *343*, 67-77.
11. Maes, V.; Hultsch, C.; Kohl, S.; Bergmann, R.; Hanke, T.; Tourwe, D. Fluorescein-labeled stable neurotensin derivatives. *J. Pept. Sci.* **2006**, *12*, 505-508.

12. Deng, H.; Wang, H.; Wang, M.; Li, Z.; Wu, Z. Synthesis and evaluation of 64Cu-DOTA-NT-Cy5.5 as a dual-modality PET/fluorescence probe to image neurotensin receptor-positive tumor. *Mol. Pharmaceutics* **2015**, *12*, 3054-3061.
13. Keller, M.; Kuhn, K. K.; Einsiedel, J.; Hübner, H.; Biselli, S.; Mollereau, C.; Wifling, D.; Svobodová, J.; Bernhardt, G.; Cabrele, C.; Vanderheyden, P. M. L.; Gmeiner, P.; Buschauer, A. Mimicking of arginine by functionalized N^{ω}-carbamoylated arginine as a new broadly applicable approach to labeled bioactive peptides: High affinity angiotensin, neuropeptide Y, neuropeptide FF, and neurotensin receptor ligands as examples. *J. Med. Chem.* **2016**, *59*, 1925-1945.
14. Antoine, T.; Ott, D.; Ebell, K.; Hansen, K.; Henry, L.; Becker, F.; Hannus, S. Homogeneous time-resolved G protein-coupled receptor-ligand binding assay based on fluorescence cross-correlation spectroscopy. *Anal. Biochem.* **2016**, *502*, 24-35.
15. Heine, P.; Witt, G.; Gilardi, A.; Gribbon, P.; Kummer, L.; Pluckthun, A. High-throughput fluorescence polarization assay to identify ligands using purified G protein-coupled receptor. *SLAS Discovery* **2019**, *24*, 915-927.
16. Keller, M.; Mahuroof, S. A.; Hong Yee, V.; Carpenter, J.; Schindler, L.; Littmann, T.; Pegoli, A.; Hübner, H.; Bernhardt, G.; Gmeiner, P.; Holliday, N. D. Fluorescence labeling of neurotensin(8–13) via arginine residues gives molecular tools with high receptor affinity. *ACS Med. Chem. Lett.* **2020**, *11*, 16-22.
17. Vogt, H.; Shinkwin, P.; Huber, M. E.; Staffen, N.; Hubner, H.; Gmeiner, P.; Schiedel, M.; Weikert, D. Development of a Fluorescent Ligand for the Intracellular Allosteric Binding Site of the Neurotensin Receptor 1. *ACS Pharmacol. Transl. Sci.* **2024**, *7*, 1533-1545.
18. Bohn, B. Flow cytometry: a novel approach for the quantitative analysis of receptor--ligand interactions on surfaces of living cells. *Mol. Cell. Endocrinol.* **1980**, *20*, 1-15.
19. Sklar, L. A.; Edwards, B. S.; Graves, S. W.; Nolan, J. P.; Prossnitz, E. R. Flow cytometric analysis of ligand-receptor interactions and molecular assemblies. *Annu. Rev. Biophys. Biomol. Struct.* **2002**, *31*, 97-119.
20. Stoddart, L. A.; White, C. W.; Nguyen, K.; Hill, S. J.; Pfleger, K. D. Fluorescence- and bioluminescence-based approaches to study GPCR ligand binding. *Br. J. Pharmacol.* **2016**, *173*, 3028-3037.
21. Rinken, A.; Lavogina, D.; Kopanchuk, S. Assays with detection of fluorescence anisotropy: Challenges and possibilities for characterizing ligand binding to GPCRs. *Trends Pharmacol. Sci.* **2018**, *39*, 187-199.

22. Way, G. P.; Sailem, H.; Shave, S.; Kasprowicz, R.; Carragher, N. O. Evolution and impact of high content imaging. *SLAS Discovery* **2023**, *28*, 292-305.
23. Gratz, L.; Muller, C.; Pegoli, A.; Schindler, L.; Bernhardt, G.; Littmann, T. Insertion of nanoluc into the extracellular loops as a complementary method to establish BRET-based binding assays for GPCRs. *ACS Pharmacol. Transl. Sci.* **2022**, *5*, 1142-1155.
24. White, J. F.; Noinaj, N.; Shibata, Y.; Love, J.; Kloss, B.; Xu, F.; Gvozdenovic-Jeremic, J.; Shah, P.; Shiloach, J.; Tate, C. G.; Grisshammer, R. Structure of the agonist-bound neurotensin receptor. *Nature* **2012**, *490*, 508-513.
25. Egloff, P.; Hillenbrand, M.; Klenk, C.; Batyuk, A.; Heine, P.; Balada, S.; Schlinkmann, K. M.; Scott, D. J.; Schutz, M.; Pluckthun, A. Structure of signaling-competent neurotensin receptor 1 obtained by directed evolution in Escherichia coli. *PNAS Nexus* **2014**, *111*, E655-662.
26. Krumm, B. E.; Lee, S.; Bhattacharya, S.; Botos, I.; White, C. F.; Du, H.; Vaidehi, N.; Grisshammer, R. Structure and dynamics of a constitutively active neurotensin receptor. *Sci. Rep.* **2016**, *6*, 38564.
27. Alshoukr, F.; Rosant, C.; Maes, V.; Abdelhak, J.; Raguin, O.; Burg, S.; Sarda, L.; Barbet, J.; Tourwe, D.; Pelaprat, D.; Gruaz-Guyon, A. Novel neurotensin analogues for radioisotope targeting to neurotensin receptor-positive tumors. *Bioconjugate Chem.* **2009**, *20*, 1602-1610.
28. Wu, Z.; Li, L.; Liu, S.; Yakushijin, F.; Yakushijin, K.; Horne, D.; Conti, P. S.; Li, Z.; Kandeel, F.; Shively, J. E. Facile preparation of a thiol-reactive (18)F-labeling agent and synthesis of (18)F-DEG-VS-NT for PET imaging of a neurotensin receptor-positive tumor. *J. Nucl. Med.* **2014**, *55*, 1178-1184.
29. de Visser, M.; Janssen, P. J.; Srinivasan, A.; Reubi, J. C.; Waser, B.; Erion, J. L.; Schmidt, M. A.; Krenning, E. P.; de Jong, M. Stabilised 111In-labelled DTPA- and DOTA-conjugated neurotensin analogues for imaging and therapy of exocrine pancreatic cancer. *Eur. J. Nucl. Med. Mol. Imaging* **2003**, *30*, 1134-1139.
30. Unruh, J. R.; Gokulrangan, G.; Wilson, G. S.; Johnson, C. K. Fluorescence properties of fluorescein, tetramethylrhodamine and Texas Red linked to a DNA aptamer. *Photochem. Photobiol.* **2005**, *81*, 682-690.
31. Schindler, L.; Moosbauer, J.; Schmidt, D.; Spruss, T.; Gratz, L.; Ludeke, S.; Hofheinz, F.; Meister, S.; Echtenacher, B.; Bernhardt, G.; Pietzsch, J.; Hellwig, D.; Keller, M. Development of a neurotensin-derived (68)Ga-labeled PET ligand with high in vivo stability for imaging of NTS(1) receptor-expressing tumors. *Cancers* **2022**, *14*, 4922.

32. Einsiedel, J.; Hubner, H.; Hervet, M.; Harterich, S.; Koschatzky, S.; Gmeiner, P. Peptide backbone modifications on the C-terminal hexapeptide of neurotensin. *Bioorg. Med. Chem. Lett.* **2008**, *18*, 2013-2018.
33. Kitabgi, P.; De Nadai, F.; Rovere, C.; Bidard, J. N. Biosynthesis, maturation, release, and degradation of neurotensin and neuromedin N. *Ann. N.Y. Acad. Sci.* **1992**, *668*, 30-42.
34. Bruehlmeier, M.; Garayoa, E. G.; Blanc, A.; Holzer, B.; Gergely, S.; Tourwe, D.; Schubiger, P. A.; Blauenstein, P. Stabilization of neurotensin analogues: effect on peptide catabolism, biodistribution and tumor binding. *Nucl. Med. Biol.* **2002**, *29*, 321-327.
35. Nock, B. A.; Nikolopoulou, A.; Reubi, J. C.; Maes, V.; Conrath, P.; Tourwe, D.; Maina, T. Toward stable N4-modified neurotensins for NTS1-receptor-targeted tumor imaging with 99mTc. *J. Med. Chem.* **2006**, *49*, 4767-4776.
36. Maina, T.; Nikolopoulou, A.; Stathopoulou, E.; Galanis, A. S.; Cordopatis, P.; Nock, B. A. [99mTc]Demotensin 5 and 6 in the NTS1-R-targeted imaging of tumours: Synthesis and preclinical results. *Eur. J. Nucl. Med. Mol. Imaging* **2007**, *34*, 1804-1814.
37. Mascarin, A.; Valverde, I. E.; Mindt, T. L. Structure-activity relationship studies of amino acid substitutions in radiolabeled neurotensin conjugates. *ChemMedChem* **2016**, *11*, 102-107.
38. Schindler, L.; Bernhardt, G.; Keller, M. Modifications at Arg and Ile give neurotensin(8-13) derivatives with high stability and retained NTS(1) receptor affinity. *ACS Med. Chem. Lett.* **2019**, *10*, 960-965.
39. Gleixner, J.; Kopanchuk, S.; Gratz, L.; Tahk, M. J.; Laasfeld, T.; Veiksina, S.; Horing, C.; Gattor, A. O.; Humphrys, L. J.; Muller, C.; Archipowa, N.; Kockenberger, J.; Heinrich, M. R.; Kutta, R. J.; Rinken, A.; Keller, M. Illuminating neuropeptide Y Y(4) receptor binding: Fluorescent cyclic peptides with subnanomolar binding affinity as novel molecular tools. *ACS Pharmacol. Transl. Sci.* **2024**, *7*, 1142-1168.
40. Lefkowitz, R. J.; Williams, L. T. Catecholamine binding to the beta-adrenergic receptor. *Proc. Natl. Acad. Sci. U. S. A.* **1977**, *74*, 515-519.
41. Kusayama, T.; Oka, J.; Yabana, H.; Adachi-Akahane, S.; Nagao, T. Binding of a catechol derivative of denopamine (T-0509) and N-tert-butylnoradrenaline (Colterol) to beta 1- and beta 2-adrenoceptors. *Biol. Pharm. Bull.* **1994**, *17*, 1023-1027.
42. Wang, S. Z.; Edmundson, R.; Zhu, S. Z.; el-Fakahany, E. E. Selective enhancement of antagonist ligand binding at muscarinic M2 receptors by heparin due to receptor uncoupling. *Eur. J. Pharmacol.* **1996**, *296*, 113-118.

43. Azzi, M.; Pineyro, G.; Pontier, S.; Parent, S.; Ansanay, H.; Bouvier, M. Allosteric effects of G protein overexpression on the binding of beta-adrenergic ligands with distinct inverse efficacies. *Mol. Pharmacol.* **2001**, *60*, 999-1007.
44. Milligan, G.; Kellett, E.; Dacquet, C.; Dubreuil, V.; Jacoby, E.; Millan, M. J.; Lavielle, G.; Spedding, M. S 14506: novel receptor coupling at 5-HT(1A) receptors. *Neuropharmacology* **2001**, *40*, 334-344.
45. Devlin, M. G.; Christopoulos, A. Modulation of cannabinoid agonist binding by 5-HT in the rat cerebellum. *J. Neurochem.* **2002**, *80*, 1095-1102.
46. Croy, C. H.; Schober, D. A.; Xiao, H.; Quets, A.; Christopoulos, A.; Felder, C. C. Characterization of the novel positive allosteric modulator, LY2119620, at the muscarinic M(2) and M(4) receptors. *Mol. Pharmacol.* **2014**, *86*, 106-115.
47. DeVree, B. T.; Mahoney, J. P.; Velez-Ruiz, G. A.; Rasmussen, S. G.; Kuszak, A. J.; Edwald, E.; Fung, J. J.; Manglik, A.; Masureel, M.; Du, Y.; Matt, R. A.; Pardon, E.; Steyaert, J.; Kobilka, B. K.; Sunahara, R. K. Allosteric coupling from G protein to the agonist-binding pocket in GPCRs. *Nature* **2016**, *535*, 182-186.
48. Tyler, B. M.; Douglas, C. L.; Fauq, A.; Pang, Y. P.; Stewart, J. A.; Cusack, B.; McCormick, D. J.; Richelson, E. In vitro binding and CNS effects of novel neurotensin agonists that cross the blood-brain barrier. *Neuropharmacology* **1999**, *38*, 1027-1034.
49. Einsiedel, J.; Held, C.; Hervet, M.; Plomer, M.; Tschammer, N.; Hubner, H.; Gmeiner, P. Discovery of highly potent and neurotensin receptor 2 selective neurotensin mimetics. *J. Med. Chem.* **2011**, *54*, 2915-2923.
50. Maschauer, S.; Einsiedel, J.; Hubner, H.; Gmeiner, P.; Prante, O. (18)F- and (68)Ga-Labeled neurotensin peptides for PET imaging of neurotensin receptor 1. *J. Med. Chem.* **2016**, *59*, 6480-6492.
51. Granier, C.; van Rietschoten, J.; Kitabgi, P.; Poustis, C.; Freychet, P. Synthesis and characterization of neurotensin analogues for structure/activity relationship studies. Acetyl-neurotensin-(8--13) is the shortest analogue with full binding and pharmacological activities. *Eur. J. Biochem.* **1982**, *124*, 117-124.
52. Lang, C.; Maschauer, S.; Hubner, H.; Gmeiner, P.; Prante, O. Synthesis and evaluation of a (18)F-labeled diarylpyrazole glycoconjugate for the imaging of NTS1-positive tumors. *J. Med. Chem.* **2013**, *56*, 9361-9365.
53. Tontson, L.; Kopanchuk, S.; Rinken, A. Characterization of 5-HT_{1A} receptors and their complexes with G-proteins in budded baculovirus particles using fluorescence anisotropy of Bodipy-FL-NAN-190. *Neurochem. Int.* **2014**, *67*, 32-38.

54. Rinken, A. Formation of the functional complexes of m2 muscarinic acetylcholine receptors with GTP-binding regulatory proteins in solution. *J. Biochem.* **1996**, *120*, 193-200.
55. Pinkerton, A. B.; Peddibhotla, S.; Yamamoto, F.; Slosky, L. M.; Bai, Y.; Maloney, P.; Hershberger, P.; Hedrick, M. P.; Falter, B.; Ardecky, R. J.; Smith, L. H.; Chung, T. D. Y.; Jackson, M. R.; Caron, M. G.; Barak, L. S. Discovery of beta-arrestin biased, orally bioavailable, and CNS penetrant neurotensin receptor 1 (NTR1) allosteric modulators. *J. Med. Chem.* **2019**, *62*, 8357-8363.
56. Gleixner, J.; Gattor, A. O.; Humphrys, L. J.; Brunner, T.; Keller, M. [(3)H]UR-JG102-A radiolabeled cyclic peptide with high affinity and excellent selectivity for the neuropeptide Y Y(4) receptor. *J. Med. Chem.* **2023**, *66*, 13788-13808.
57. Keller, M.; Pop, N.; Hutzler, C.; Beck-Sickinger, A. G.; Bernhardt, G.; Buschauer, A. Guanidine-acylguanidine bioisosteric approach in the design of radioligands: Synthesis of a tritium-labeled N(G)-propionylargininamide ([3H]-UR-MK114) as a highly potent and selective neuropeptide Y Y1 receptor antagonist. *J. Med. Chem.* **2008**, *51*, 8168-8172.
58. Allikalt, A.; Veiksina, S.; Tahk, M. J.; Vevers, E.; Laaneväli, E.; Rinken, A.; Kopanchuk, S. MultiBacMam technology for studying the downstream cAMP signaling pathway of M2 muscarinic acetylcholine receptor. In *Muscarinic Receptor: From Structure to Animal Models*, Myslivecek, J.; Jakubik, J., Eds., Springer, 2024; Vol. 211.
59. Bradford, M. M. A rapid and sensitive method for the quantitation of microgram quantities of protein utilizing the principle of protein-dye binding. *Anal. Biochem.* **1976**, *72*, 248-254.
60. Cheng, Y.-C.; Prusoff, W. H. Relationship between the inhibition constant (K_I) and the concentration of inhibitor which causes 50 per cent inhibition (IC50) of an enzymatic reaction. *Biochem. Pharmacol.* **1973**, *22*, 3099-3108.
61. Muller, C.; Gleixner, J.; Tahk, M. J.; Kopanchuk, S.; Laasfeld, T.; Weinhart, M.; Schollmeyer, D.; Betschart, M. U.; Ludeke, S.; Koch, P.; Rinken, A.; Keller, M. Structure-based design of high-affinity fluorescent probes for the neuropeptide Y Y(1) receptor. *J. Med. Chem.* **2022**, *65*, 4832-4853.
62. Veiksina, S.; Tahk, M. J.; Laasfeld, T.; Link, R.; Kopanchuk, S.; Rinken, A. Fluorescence anisotropy-based assay for characterization of ligand binding dynamics to GPCRs: The case of Cy3B-labeled ligands binding to MC(4) receptors in budded baculoviruses. *Methods Mol. Biol.* **2021**, *2268*, 119-136.

63. Veiksina, S.; Kopanchuk, S.; Rinken, A. Budded baculoviruses as a tool for a homogeneous fluorescence anisotropy-based assay of ligand binding to G protein-coupled receptors: The case of melanocortin 4 receptors. *Biochim. Biophys. Acta* **2014**, *1838*, 372-381.

Appendix Chapter 3

A3.1 Figures A3.1-A3.17

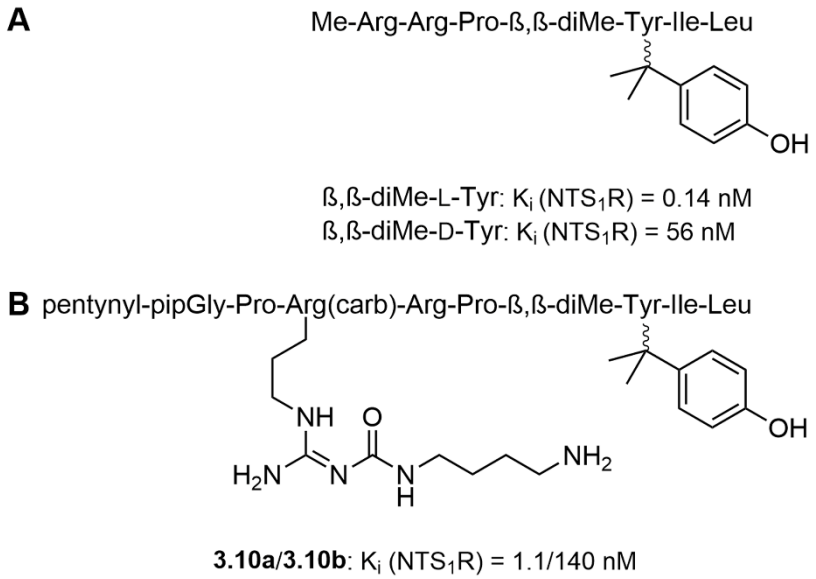


Figure A3.1. (A) Structures and NTS_1R binding affinities of reported NT(8-13) derivatives containing either β,β-dimethyl-L-tyrosine or β,β-dimethyl-D-tyrosine in position 11 (compound **48** and **49**, respectively, in Schindler *et al.*[1]). (B) Structures and NTS_1R binding affinities of **3.10a** and **3.10b**.

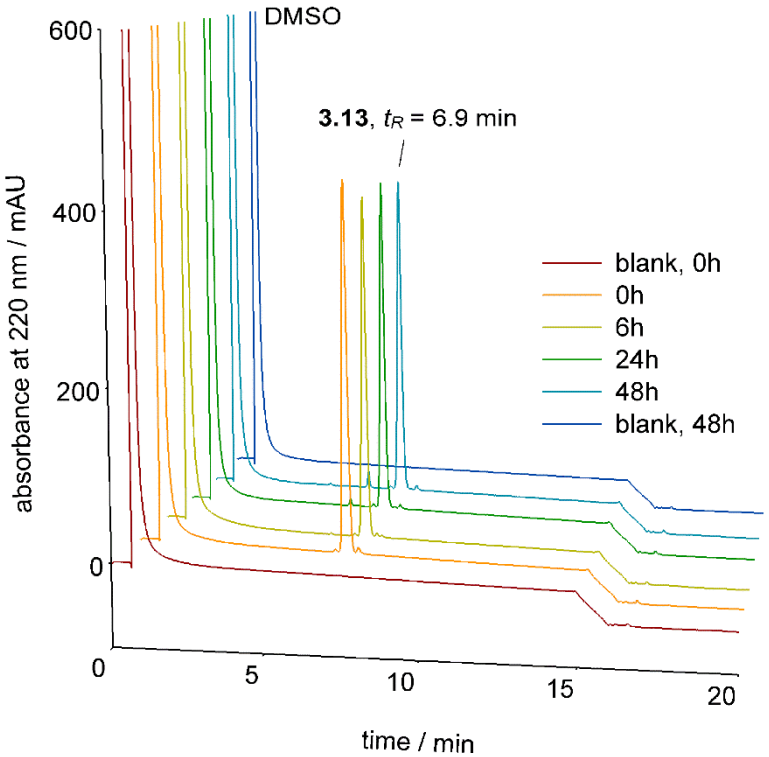


Figure A3.2. Investigation of the chemical stability of **3.13** in PBS (pH = 7.4). Shown are the chromatograms of the RP-HPLC after incubation for up to 48 hours. **3.13** exhibited high stability. After 48 h, a minor decomposition product (t_R = 5.7 min) was observed.

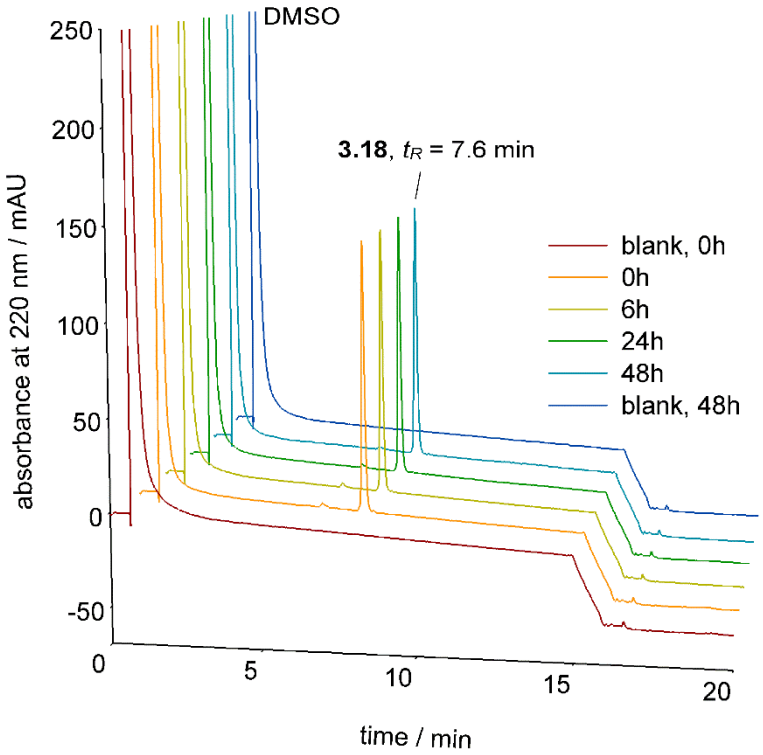


Figure A3.3. Investigation of the chemical stability of **3.18** in PBS (pH = 7.4). Shown are the chromatograms of the RP-HPLC after incubation for up to 48 hours. **3.18** showed no decomposition.

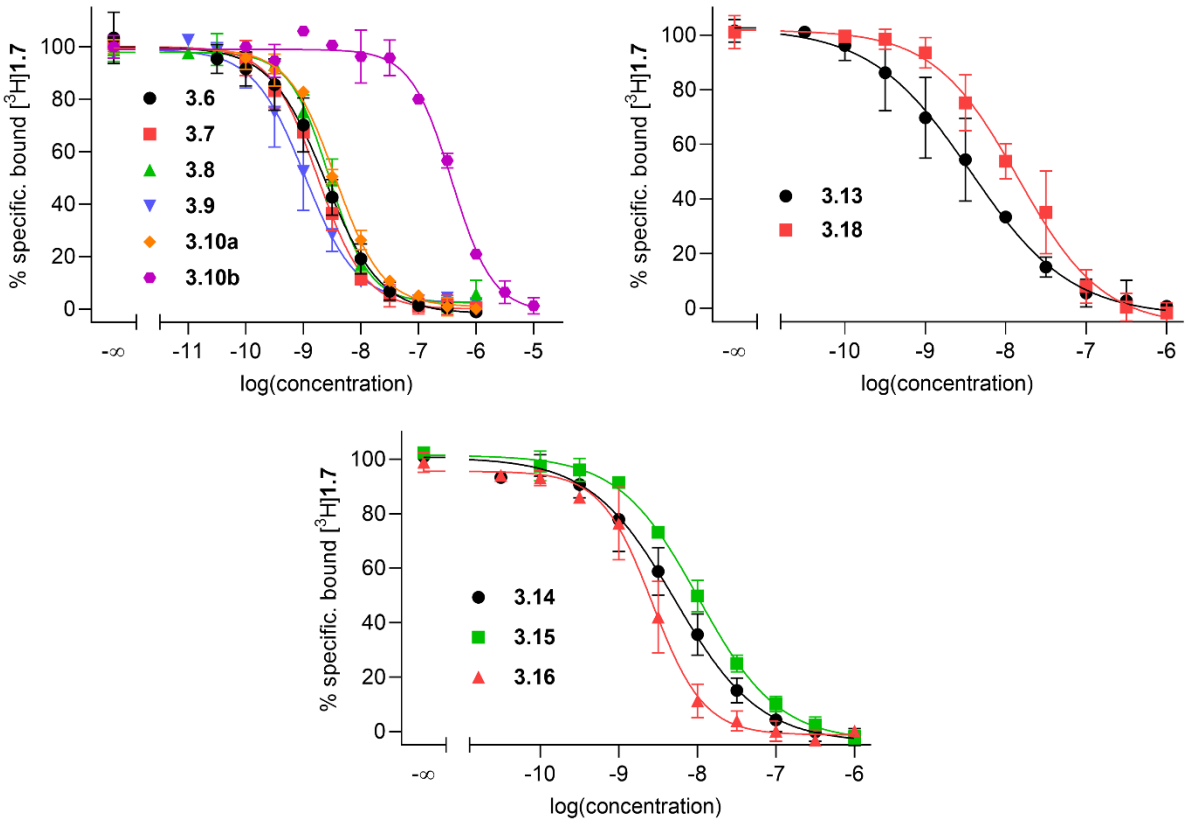


Figure A3.4. Radioligand displacement curves from competition binding experiments with [^{3}H]**1.7** (K_d = 0.41 nM,[1] c = 1 nM) and **3.6-3.9**, **3.10a**, **3.10b**, **3.13-3.16** or **3.18** at intact HT-29 cells. Data represent mean values ± SEM from at least three independent experiments performed in triplicate. For pK_i values, see Table 3.1.

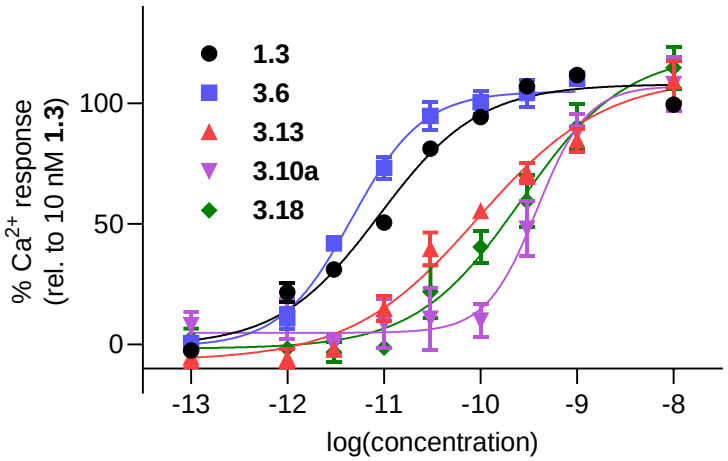


Figure A3.5. Concentration response curves of **1.3**, **3.6**, **3.10a**, **3.13**, and **3.18**, obtained from a Fura-2 Ca^{2+} assay performed with CHO-hNTS_1R cells. Mean values ± SEM from at least three independent experiments (performed in triplicate).

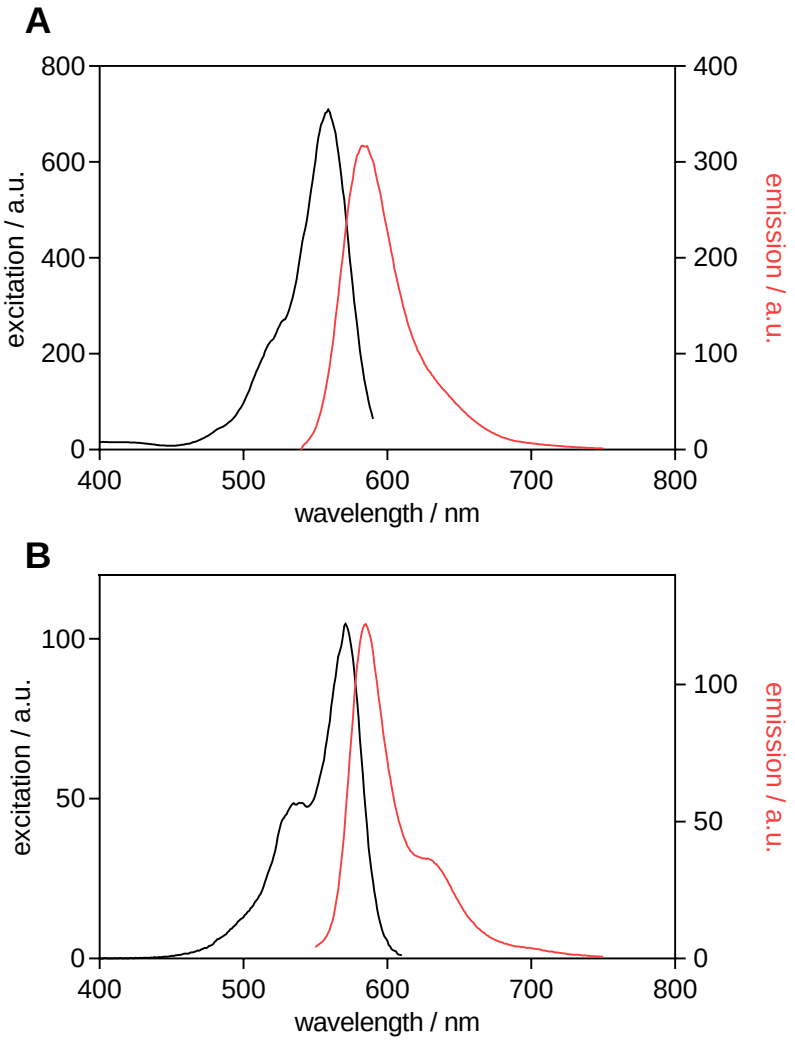


Figure A3.6. Excitation and corrected emission spectra of **3.13** (A) and **3.18** (B) recorded in PBS (pH = 7.4) supplemented with 1% BSA, at 22 °C. The concentration of both ligands was 1 µM.

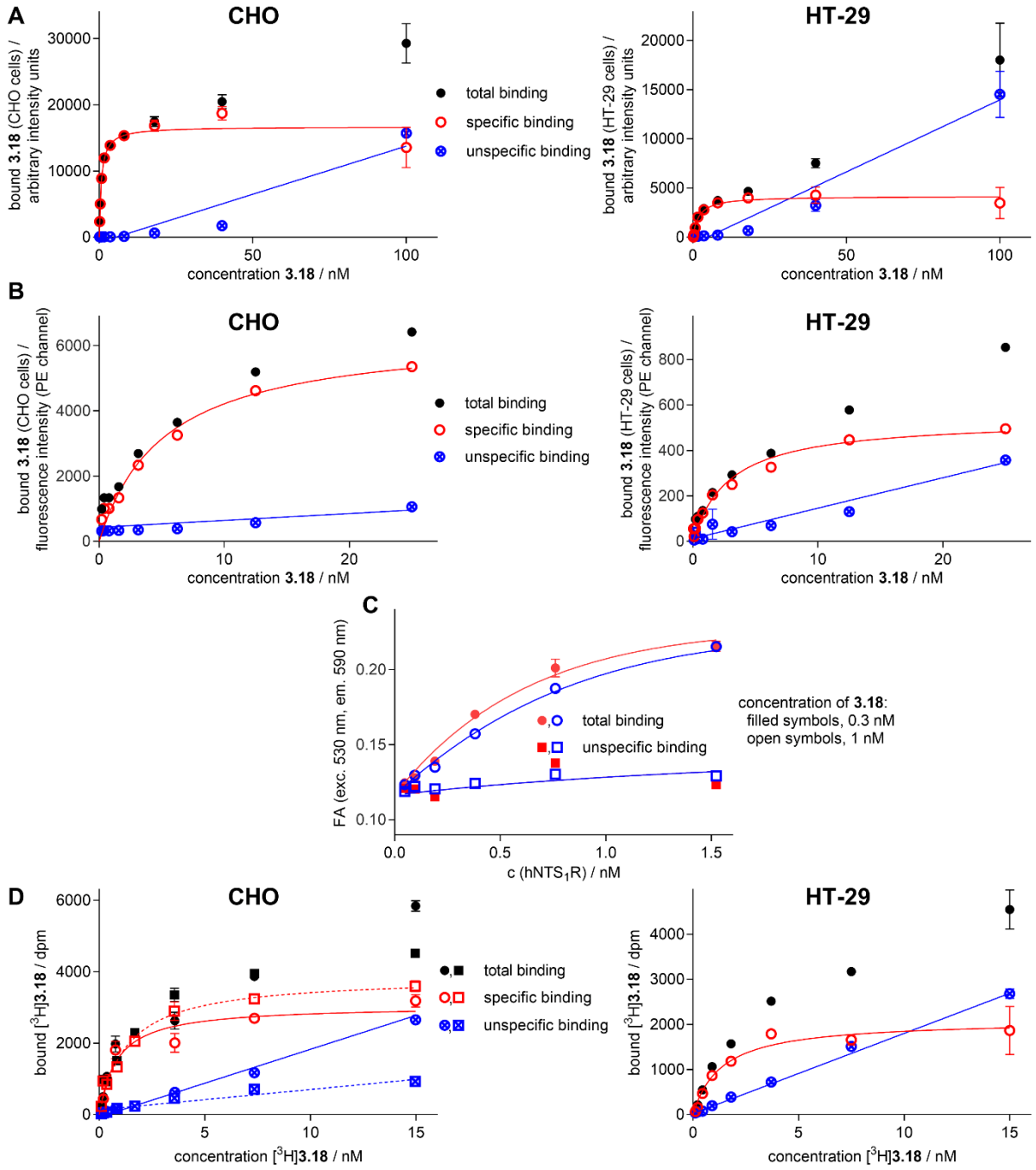


Figure A3.7. NTS_1R equilibrium binding of **3.18** and [^{3}H]**3.18** studied by different methods. (A) Binding isotherms (specific binding, open symbols) of **3.18** obtained from high-content imaging (HCI) binding experiments performed at intact CHO-hNTS_1R and HT-29 cells (incubation: 90 min at 23 °C). (B) Binding isotherms (specific binding, open symbols) of **3.18** obtained from flow cytometric (FC) saturation binding experiments performed at intact CHO-hNTS_1R and HT-29 cells (incubation: 90 min at 23 °C). (C) Binding isotherms (total binding, circles) of **3.18** obtained from FA-based binding experiments using fixed concentrations of **3.18** (0.3 or 1 nM) and increasing amounts of NTS_1R-displaying BBVs (depicted data represent snapshots at 10 min incubation at 27 °C). (D) Binding isotherms of [^{3}H]**3.18** from radiochemical saturation binding experiments performed at intact CHO-hNTS_1R cells (adherent and in suspension) and at adherent HT-29 cells (incubation: 90 min at 23 °C). Circles represent adherent cells, squares represent suspended cells. Unspecific binding was determined in the presence of 1 µM **1.3** (A, B, and D) or 1 µM **1.5** (C). K_d values are presented in Table 3.3. Data represent mean values ± SEM (total and unspecific binding) or calculated values ± propagated error (specific binding) from representative experiments performed in triplicate (A, B, and D) or duplicate (C).

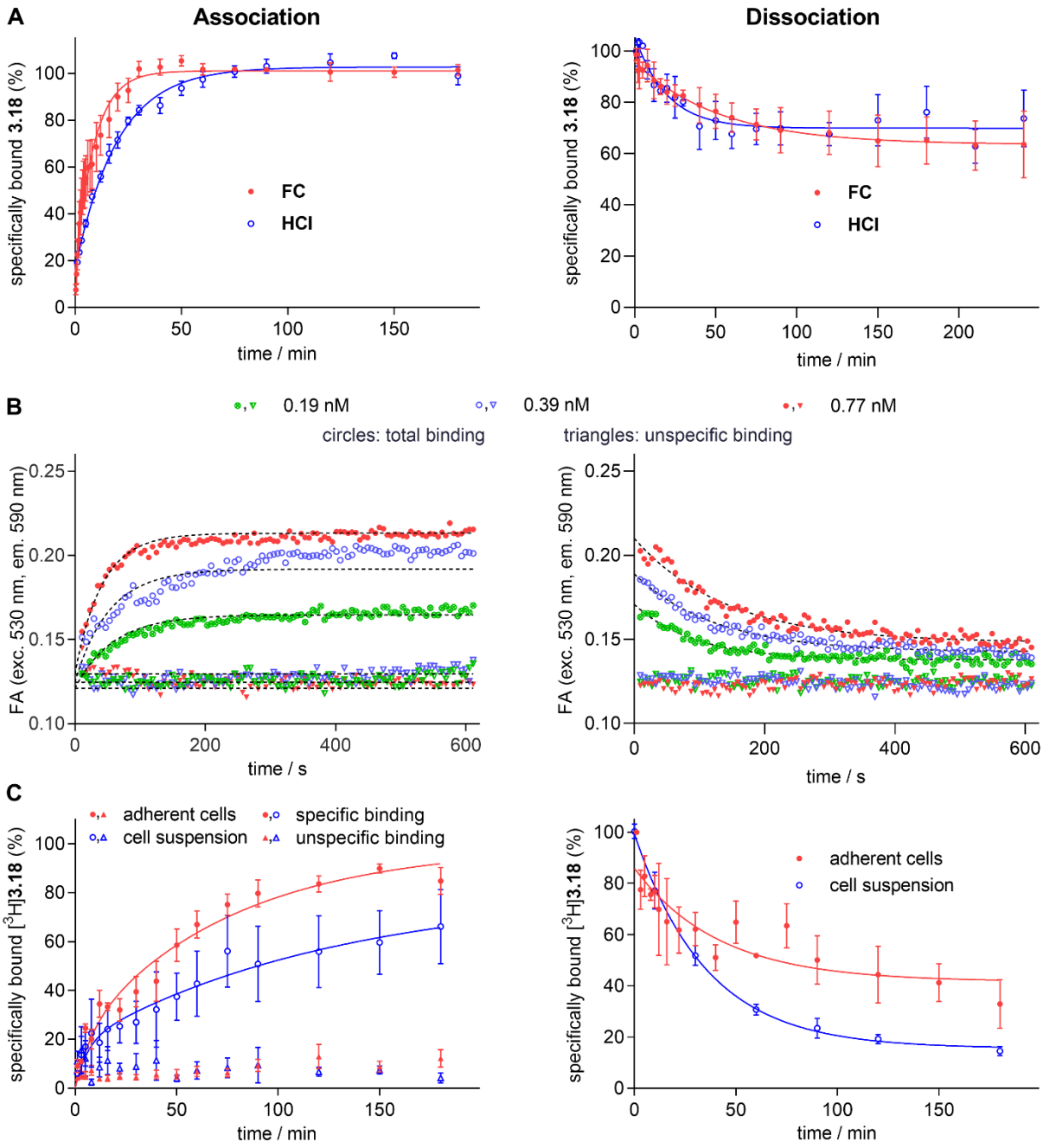


Figure A3.8. Binding kinetics of **3.18** and [^{3}H]**3.18** at NTS$_1$R studied by different methods. (A) Association and dissociation of **3.18** studied by HCI and FC at live adherent CHO-hNTS$_1$R cells (HCI) or suspended CHO-hNTS$_1$R cells (FC) at 23 °C. Concentrations of **3.18** used for the association: 2.5 nM (HCI) and 1 nM (FC); concentrations of **3.18** used during the preincubation period (90 min) of dissociation experiments: 2.5 nM (HCI) and 10 nM (FC). (B) Association and dissociation of **3.18** (0.3 nM) determined in an FA-based assay for three different NTS$_1$R concentrations (green, blue, and red symbols) at 27 °C using NTS$_1$R-displaying BBVs. Total binding is represented by circles and unspecific binding is represented by triangles. Following the association for up to 180 min did not reveal a second association phase (data not shown). (C) Association and dissociation of [^{3}H]**3.18** studied at live adherent CHO-hNTS$_1$R cells and suspended CHO-hNTS$_1$R cells at 23 °C. Concentrations of [^{3}H]**3.18** used for the association: 1.1 nM (adherent cells) and 1.2 nM (cell suspension); concentrations of [^{3}H]**3.18** used during the preincubation period (90 min) of dissociation experiments: 5.5 nM (adherent cells) and 5 nM (cell suspension). For the biphasic association, unspecific binding is shown to demonstrate that both association phases account for binding to NTS$_1$R. Proportion of fast/slow kinetic components (association): 16%/84% (adherent cells), 19%/81% (suspended cells). In the case of dissociation experiments performed with suspended cells, less times were studied because these experiments were laborious due to the use of 50 mL falcon tubes instead of 96-well plates (in this case, a separate work-up process with the cell harvester had to be carried out for each timepoint).
Dissociation and association rate constants are presented in Table 3.3. Data represent mean values ± SEM from at least three independent experiments performed in triplicate (A (HCI), C (association, dissociation at adherent cells)) or duplicate (A (FC), B, C (dissociation with cell suspensions)).

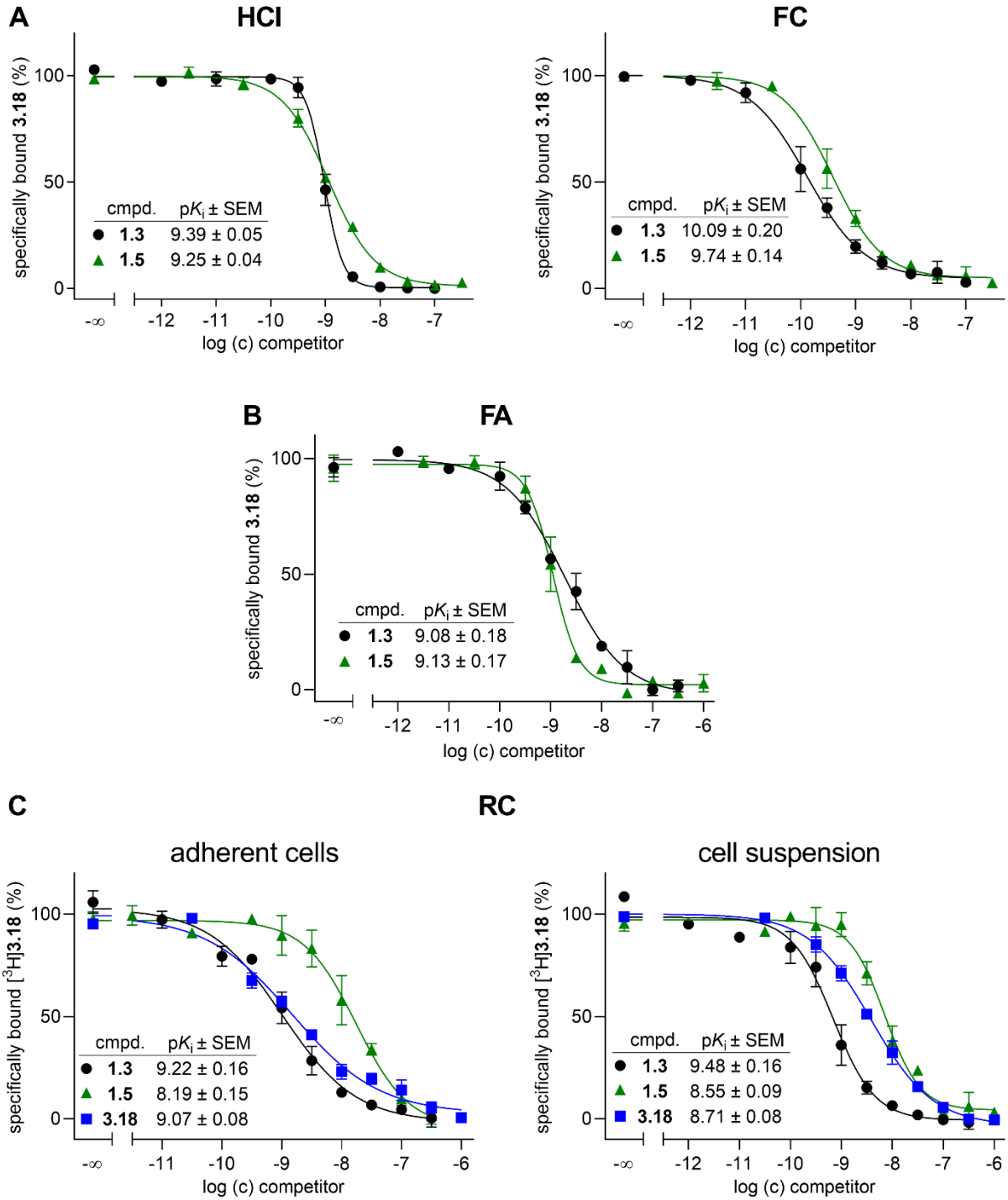


Figure A3.9. Displacement curves and corresponding pK_i values from competition binding studies performed with **3.18** or [^{3}H]**3.18** and **1.3** and **1.5** using different types of binding assays (A: high-content imaging and flow cytometry; B: fluorescence anisotropy; C: radiochemical binding assay). Used concentrations of **3.18**: 1.3 nM (A (HCl)), 3.1 nM (A (FC)), 0.3 nM (B). Used concentrations of [^{3}H]**3.18** (C): 1.1 nM (adherent cells), 1.2 nM (cell suspension). Incubation times: 90 min (A, B, C). Incubation temperatures: 23 °C (A, C), 27 °C (B). Data represent mean value ± SEM from at least three individual experiments performed in triplicate.

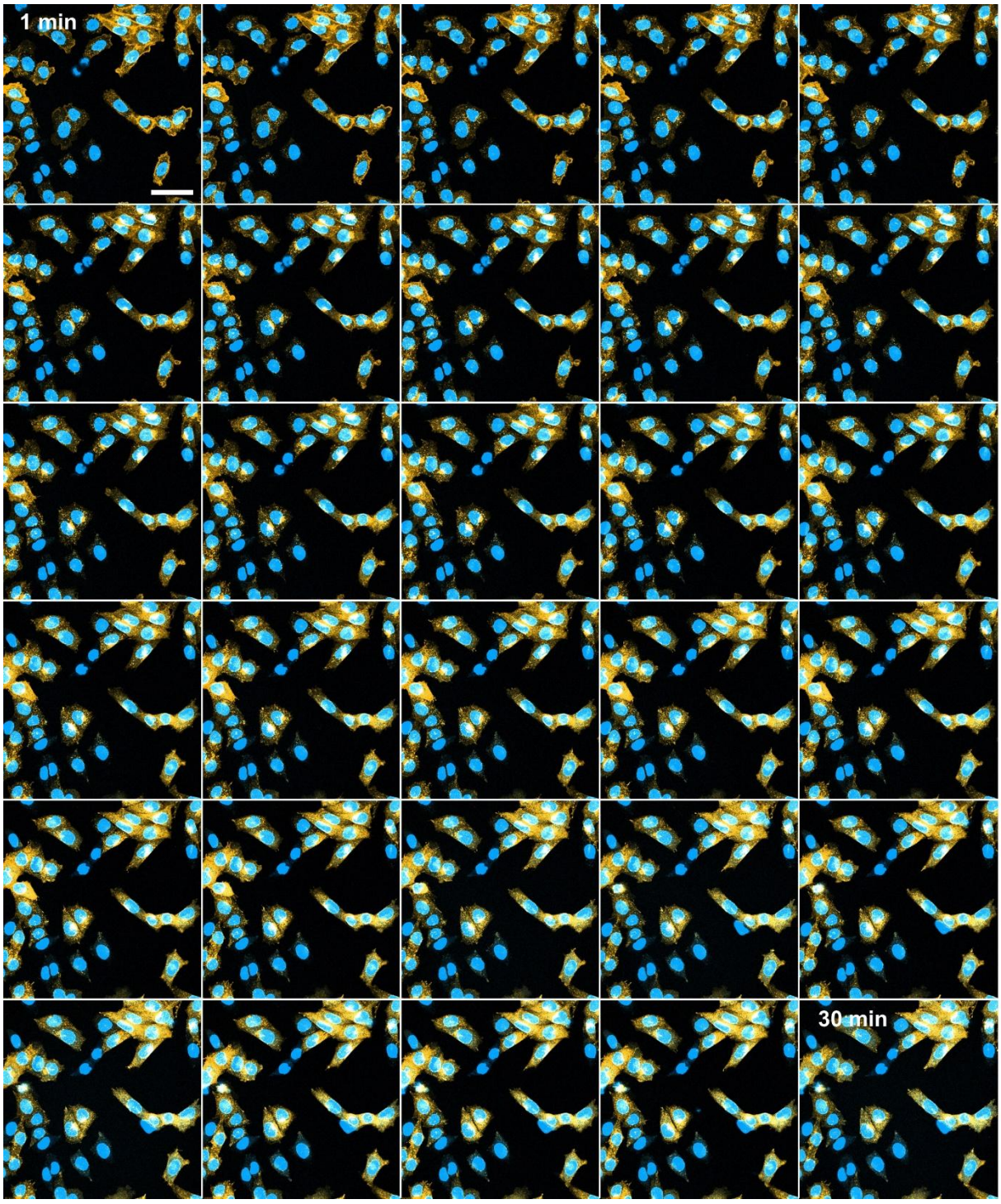


Figure A3.10. Fluorescence images (acquired with a Zeiss Celldiscoverer 7) of a binding experiment performed with the fluorescent NT(6-13) derivative **3.13** (5 nM) at intact CHO-hNTS_1R cells (temperature: 23 °C). 30 images were acquired over a period of 30 min. Shown are merge fluorescence of **3.13** (orange) and nuclei (blue). Scale bar: 50 µm. Unspecific binding of this experiment is shown in Figure A3.12.

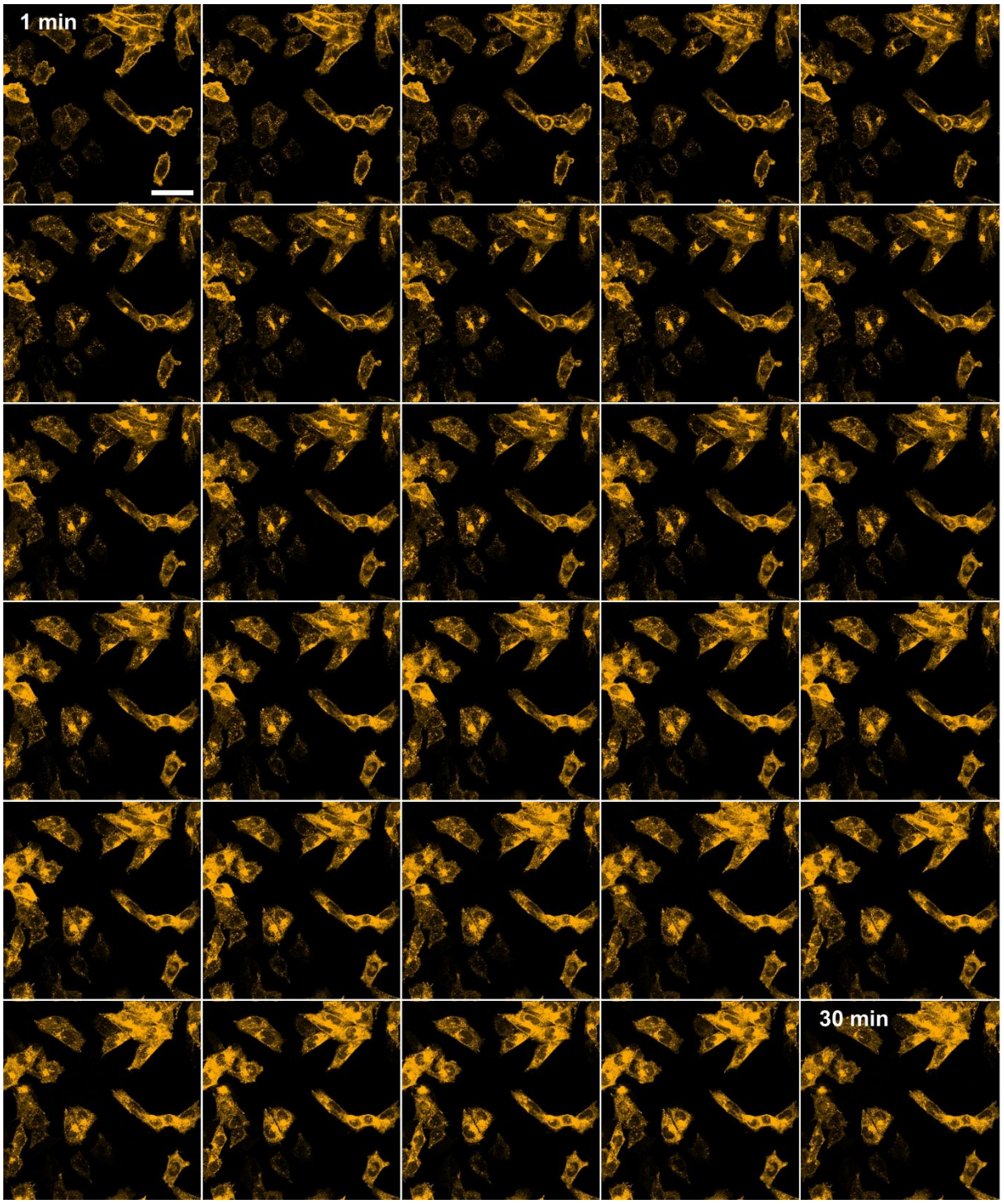


Figure A3.11. Same images as shown in Figure A3.10, but without nuclei fluorescence.

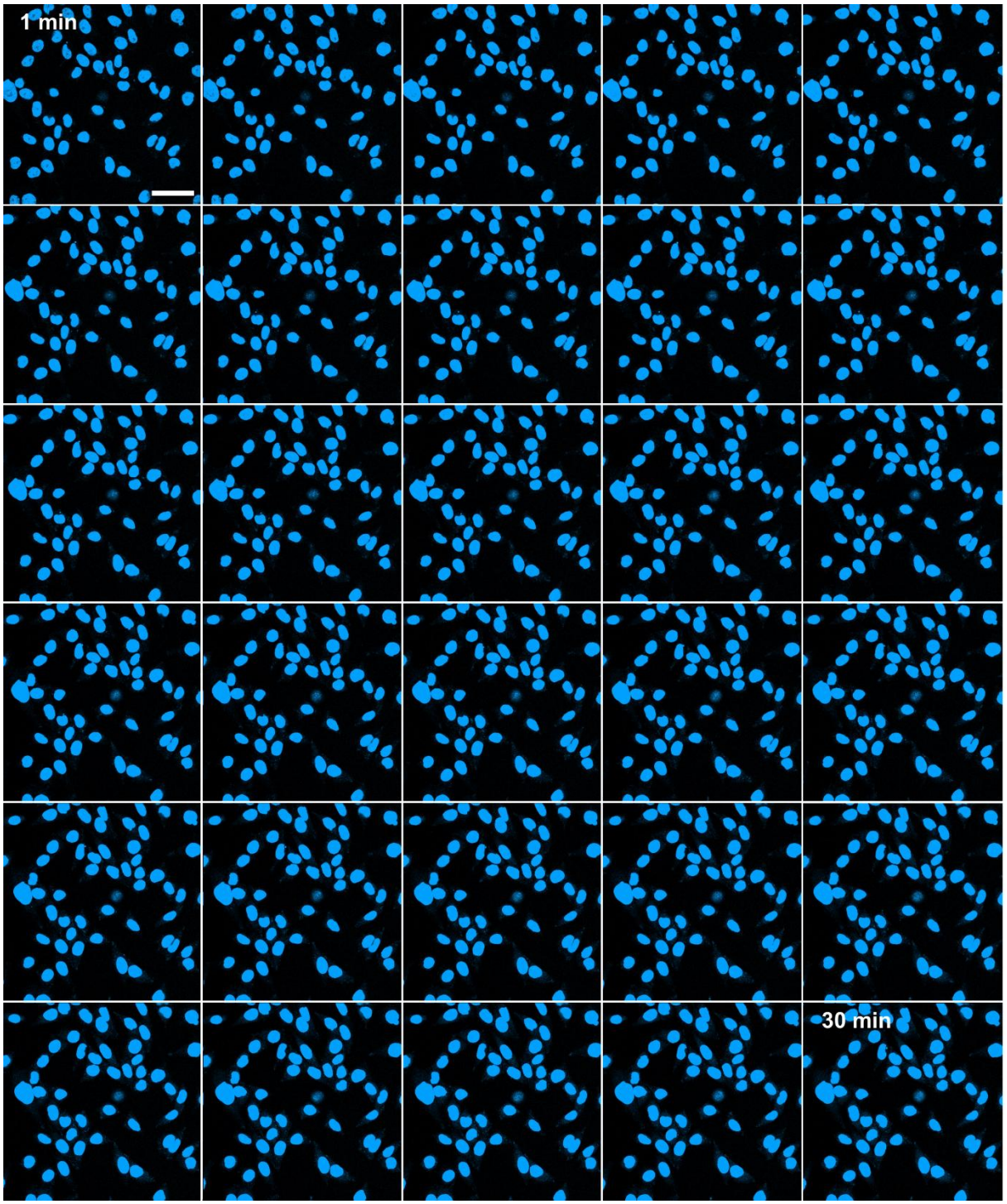


Figure A3.12. Fluorescence images (acquired with a Zeiss Celldiscoverer 7) of adherent CHO-hNTS$_1$R cells, which were incubated with **3.13** (5 nM) in the presence of 1 µM **1.3** at 23 °C (determination of unspecific binding). 30 images were acquired over a period of 30 min. Shown are merge fluorescence of **3.13** (orange) and nuclei (blue). Scale bar: 50 µm. Total binding of this experiment is shown in Figures A3.10 and A3.11.

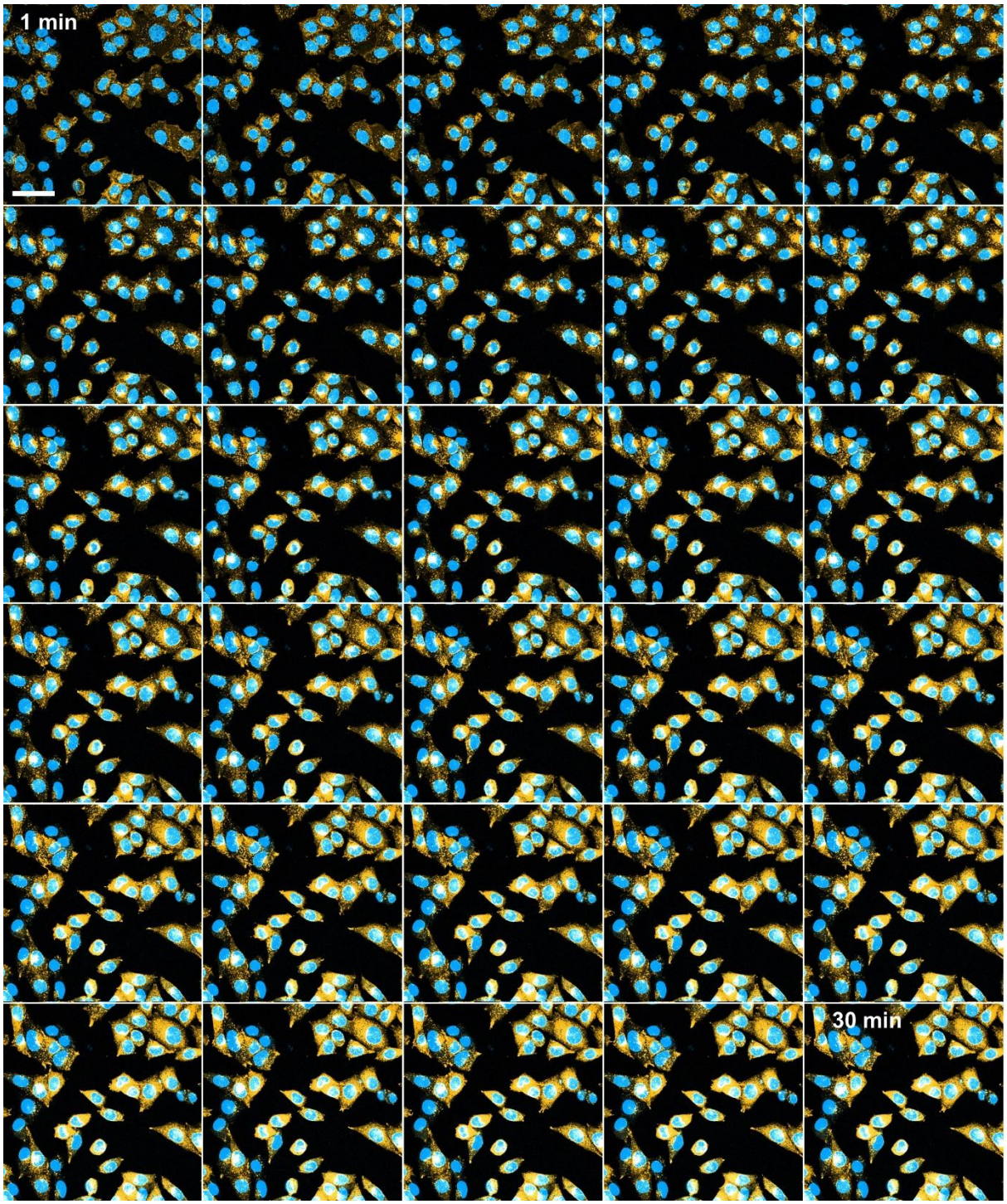


Figure A3.13. Fluorescence images (acquired with a Zeiss Celldiscoverer 7) of a binding experiment performed with the fluorescent NT(6-13) derivative **3.18** (5 nM) at intact CHO-hNTS_1R cells (temperature: 23 °C). 30 images were acquired over a period of 30 min. Shown are merge fluorescence of **3.18** (orange) and nuclei (blue). Scale bar: 50 µm. Unspecific binding of this experiment is shown in Figure A3.15.

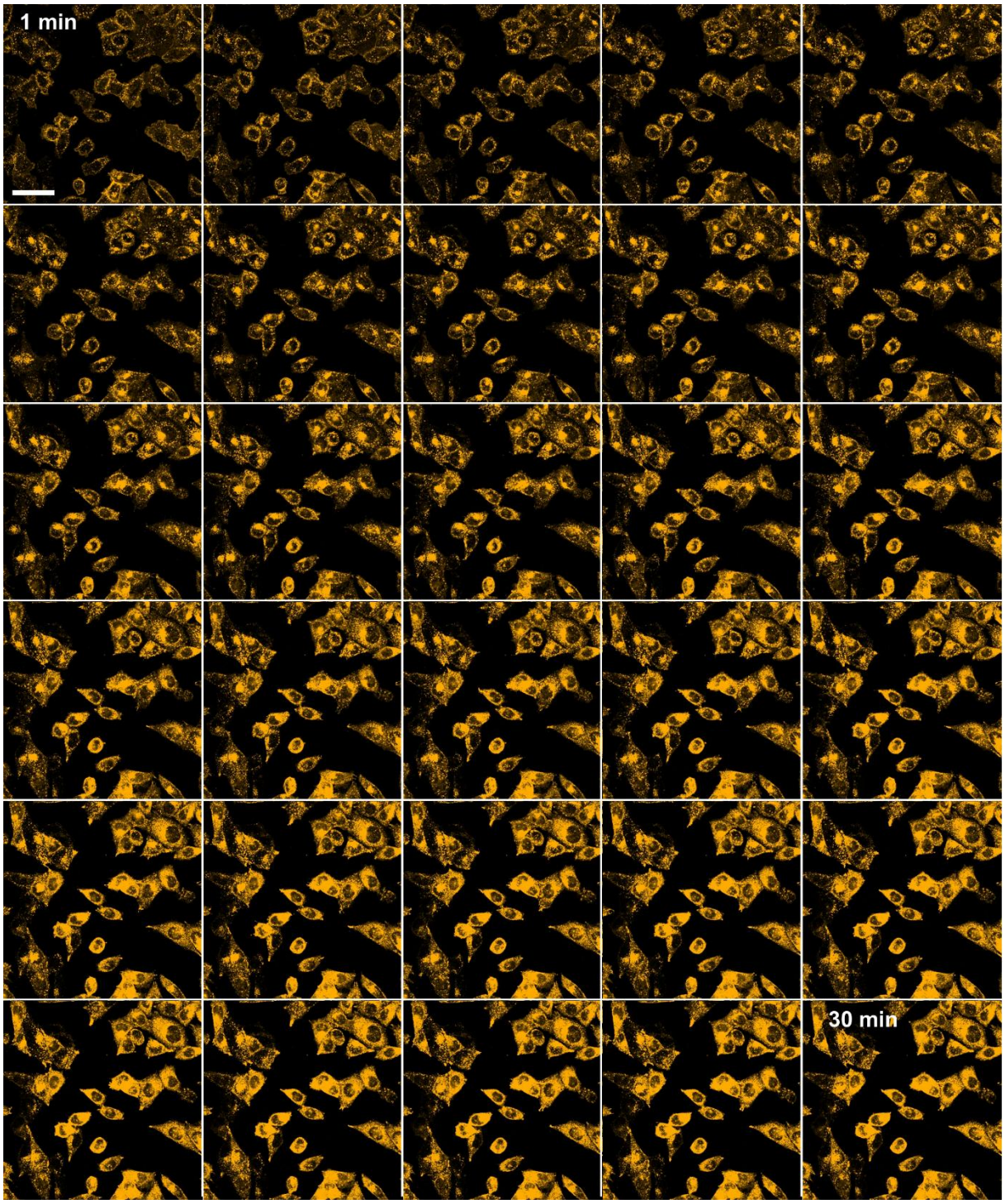


Figure A3.14. Same images as shown in Figure A3.13, but without nuclei fluorescence.

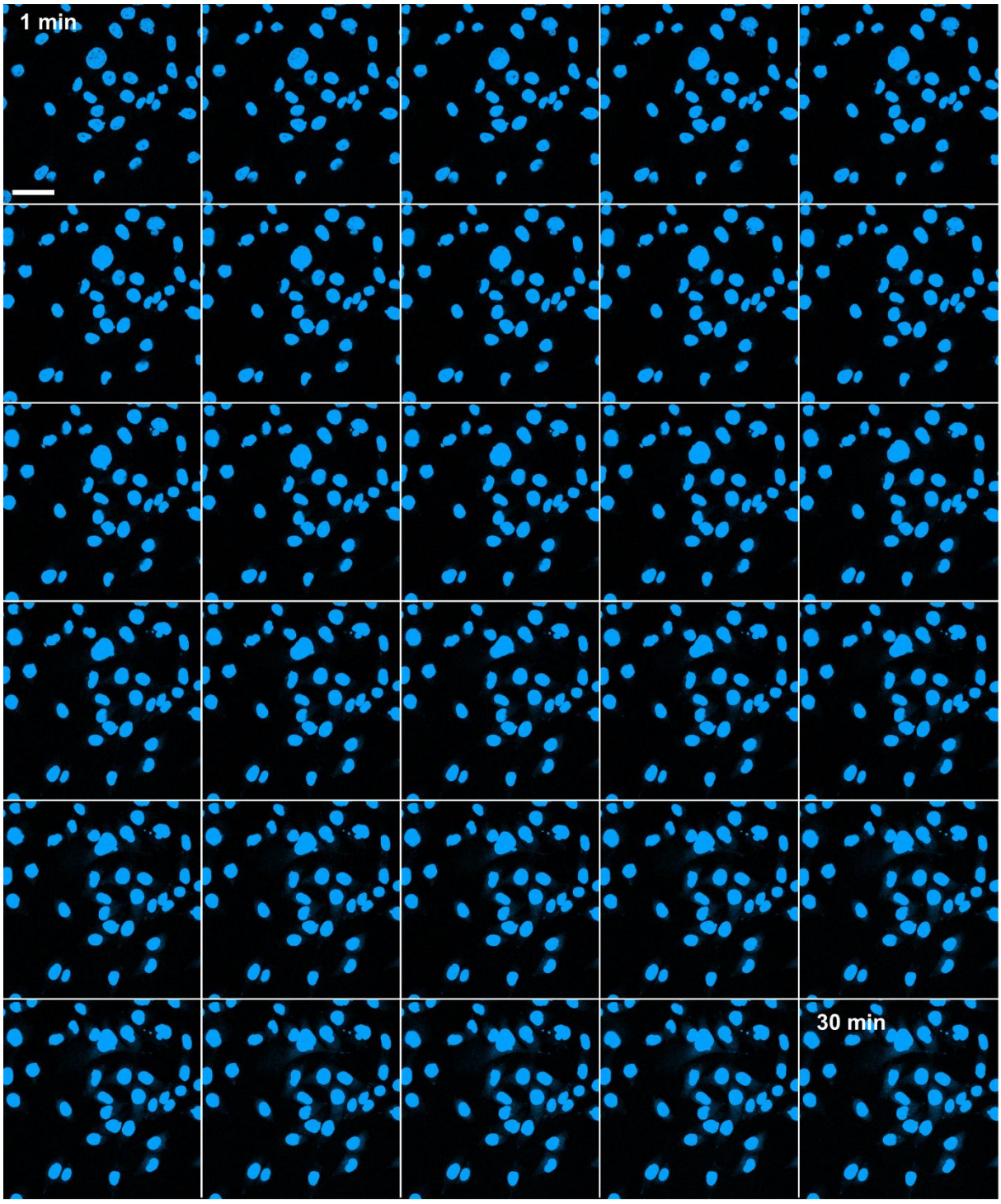


Figure A3.15. Fluorescence images (acquired with a Zeiss Celldiscoverer 7) of adherent CHO-hNTS$_1$R cells, which were incubated with **3.18** (5 nM) in the presence of 1 µM **1.3** at 23 °C (determination of unspecific binding). 30 images were acquired over a period of 30 min. Shown are merge fluorescence of **3.18** (orange) and nuclei (blue). Scale bar: 50 µm. Total binding of this experiment is shown in Figures A3.13 and A3.14.

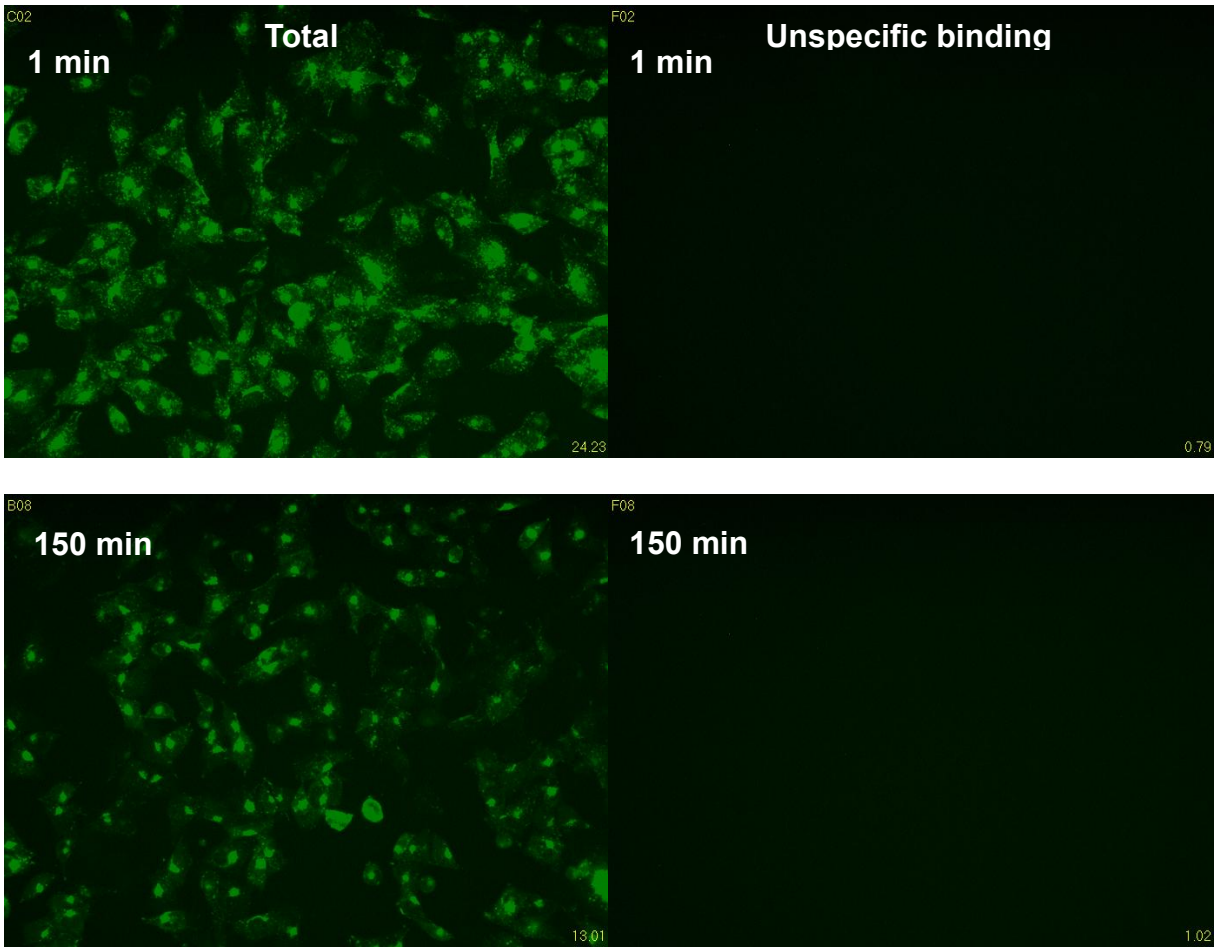


Figure A3.16. Representative fluorescence images acquired with an IX Micro Confocal plate reader of a high-content imaging dissociation experiment performed with **3.13** at intact adherent CHO-hNTS$_1$R cells in a 96-well plate at 22 ± 1 °C. Unspecific binding was determined in the presence of 1 µM **1.3**. Shown are representative wells after 1 min and 150 min of dissociation. Fluorescence detected at 150 min represents the plateau of the dissociation curve shown in Figure 3.4A.

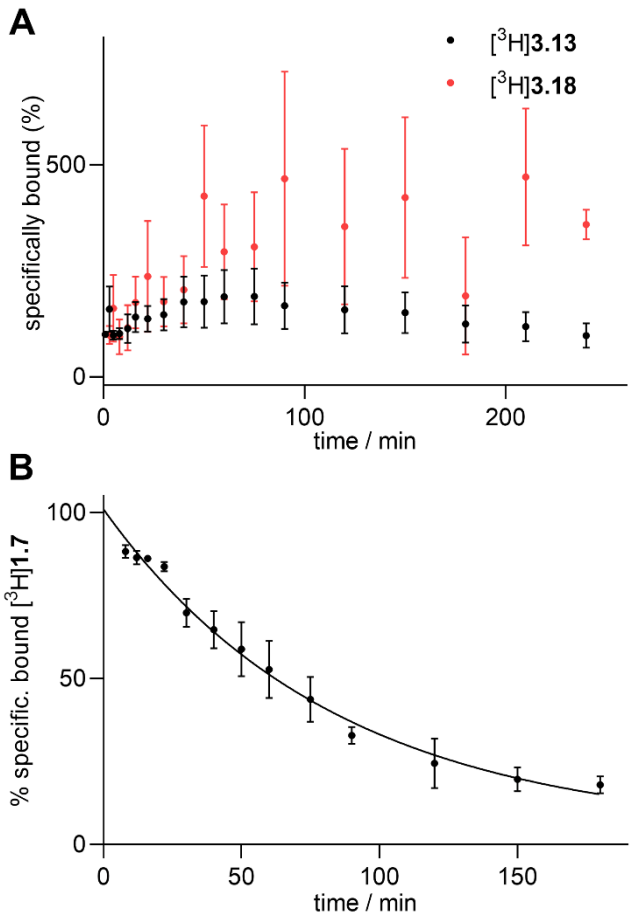
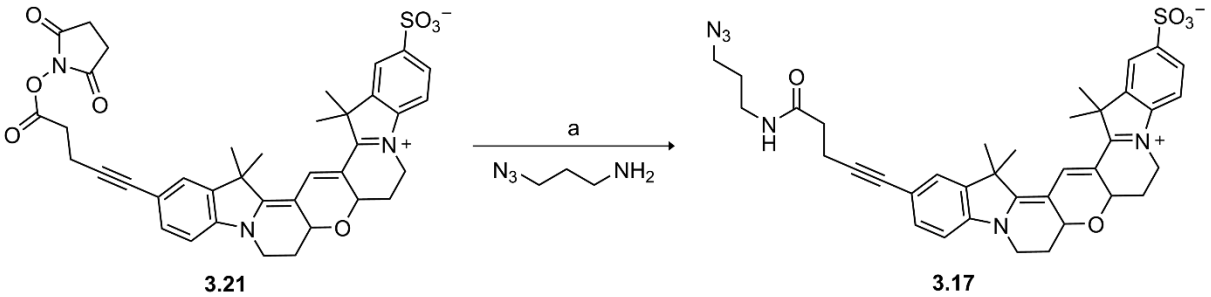


Figure A3.17. Data obtained from dissociation experiments performed with [^{3}H]**3.13**, [^{3}H]**3.18** and [^{3}H]**1.7** in 96-well PP plates at CHO-hNTS$_1$R cells suspended in D-PBS with 1% BSA. All experiments were performed at 23 ± 1 °C. The dissociation was initiated by the addition of **1.3** (final concentration: 25 µM). Unspecific binding (not shown) was determined by the addition of 1 µM **1.3** during the preincubation. (A) Data obtained for [^{3}H]**3.13** and [^{3}H]**3.18**. Used radioligand concentrations during the preincubation period (90 min): 5 or 9 nM ([^{3}H]**3.13**) and 5 or 6 nM ([^{3}H]**3.18**). Data represent mean values ± SEM from nine independent experiments performed in triplicate (carried out by three different operators). The first timepoint of each experiment (1 min) was set to 100 %. The results of the individual experiments were not reproducible and gave no trend. (B) Dissociation of [^{3}H]**1.7**. The radioligand concentration used for the preincubation period (90 min) was 2 nM. Data represent mean values ± SEM from three independent experiments performed in triplicate. The fit (one phase decay, GraphPad Prism 5) was extrapolated to t = 0 min.

A3.2 Scheme A3.1

Scheme A3.1. Synthesis of the azido-functionalized fluorescent dye **3.17**.



3.21 **3.17**

Reagents and conditions: (a) DIPEA, DMF, room temperature (rt), 1 h, 54%.

A3.3 Tables A3.1 and A3.2

Table A3.1. Stabilities of **3.13** and **3.18** in human plasma/PBS 1:2 v/v (37 °C).

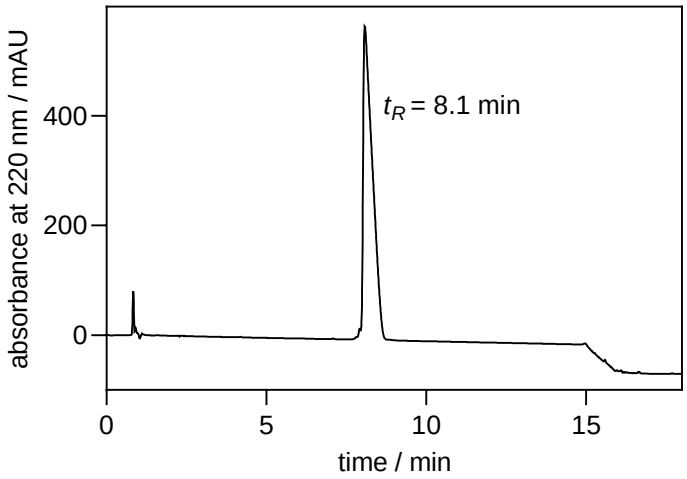
compd.	% intact compound in plasma after the specified incubation times				
	30 min	2 h	6 h	24 h	48 h
3.13	> 99	> 99	> 99	86 ± 4	58 ± 5
3.18	n.d.	95 ± 6	90 ± 6	82 ± 4	52 ± 4

Table A3.2. Recoveries of **3.13** and **3.18** from human plasma/PBS 1:2 v/v and ratios of compound-recovery over recovery of internal standard (1-methyl-D-tryptophan).

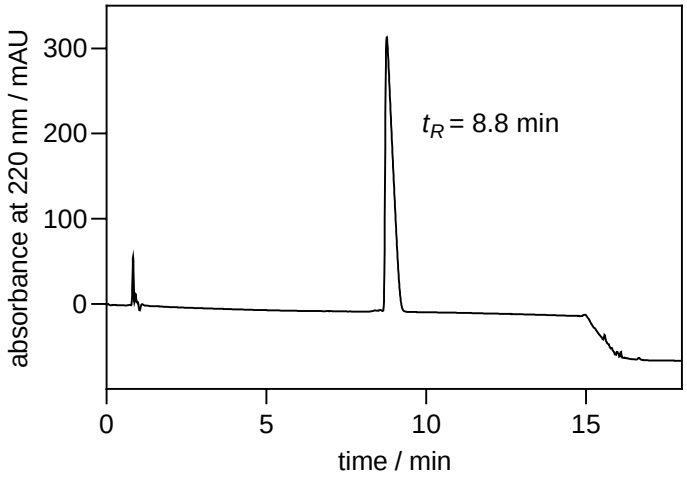
compd.	recovery compd. (%)[a]	recovery 1-methyl-D-tryptophan (%)[a]	ratio[b]
3.13	75	80	0.93
	102	98	1.04
	109	91	1.11
	104	98	1.06
			(1.03 ± 0.03)
3.18	98	108	0.91
	72	71	1.01
	65	63	1.03
	70	69	1.01
			(0.99 ± 0.02)

[a]Recoveries of the peptides and of the internal standard from human plasma/PBS 1:2 v/v using a peptide concentration of 40 µM and an internal standard concentration of 10 µM (four independent experiments). [b]Ratios of peptide recovery over recovery of internal standard calculated for individual experiments, as well as mean recovery ratios ± SEM (given in parenthesis).

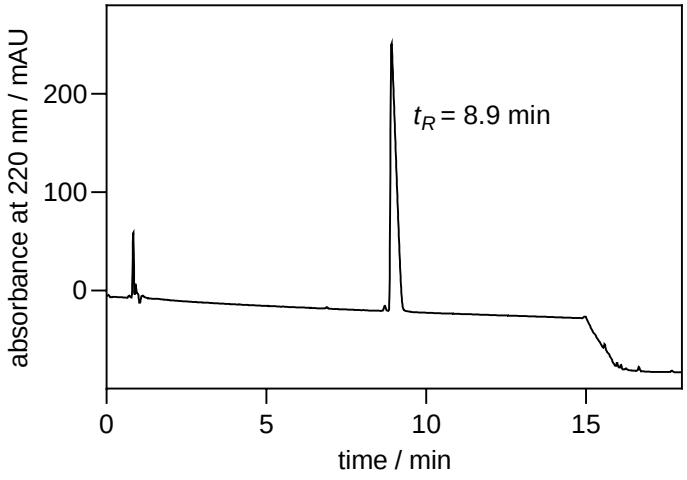
A3.4 RP-HPLC chromatograms of 3.6-3.9, 3.10a, 3.10b and 3.13-3.20 (purity controls)



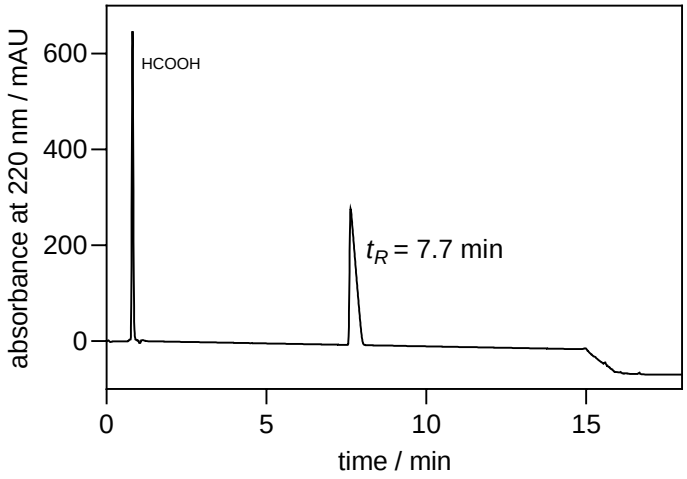
RP-HPLC analysis of compound **3.6**



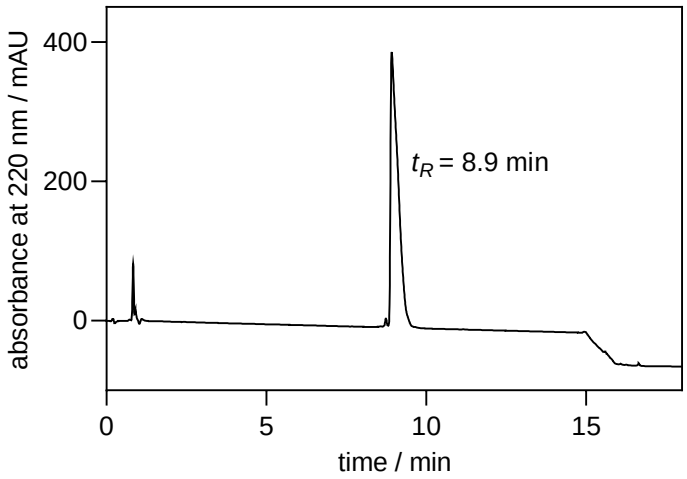
RP-HPLC analysis of compound **3.7**



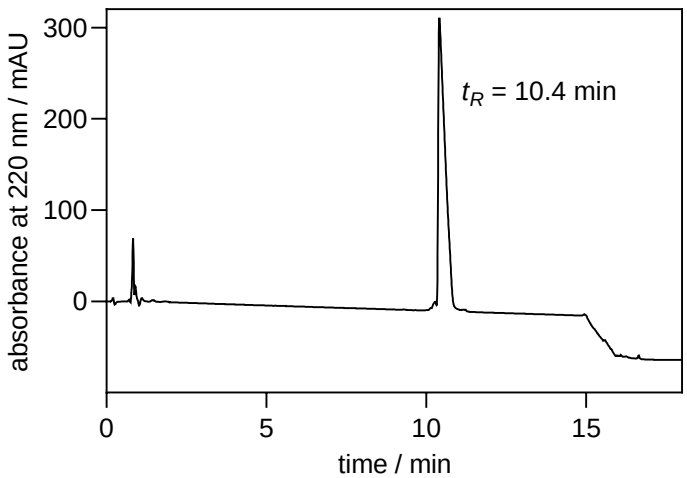
RP-HPLC analysis of compound **3.8**



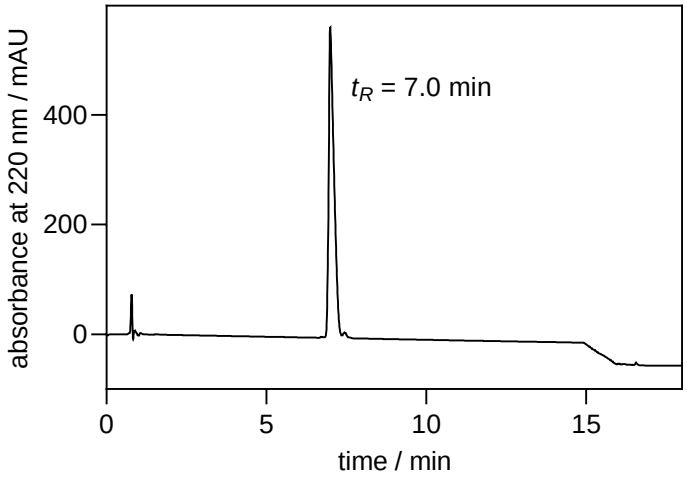
RP-HPLC analysis of compound **3.9**



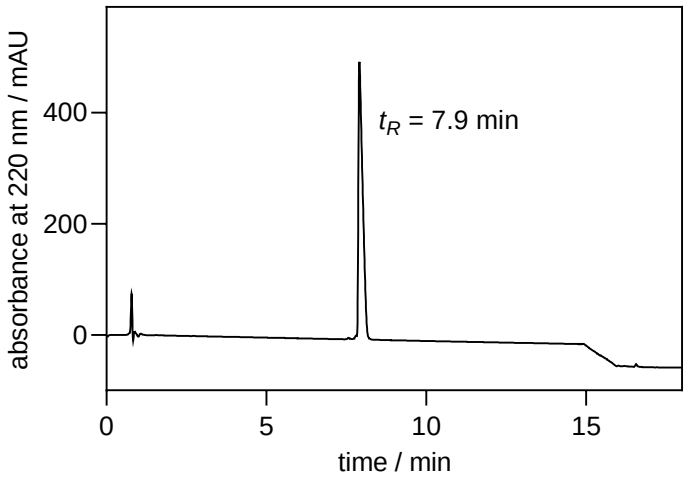
RP-HPLC analysis of compound **3.10a**



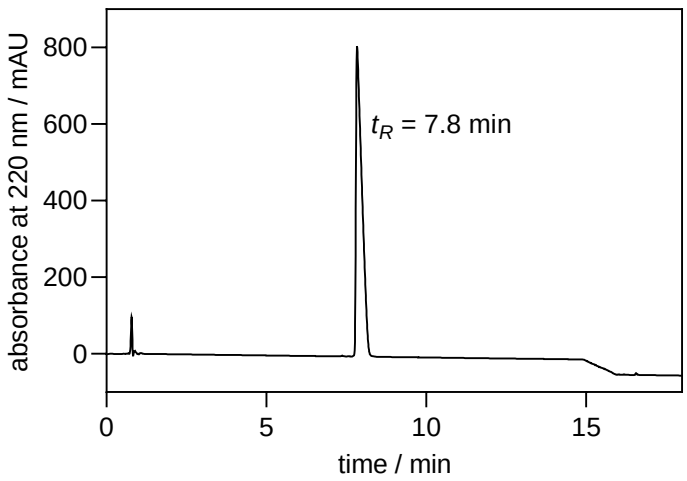
RP-HPLC analysis of compound **3.10b**



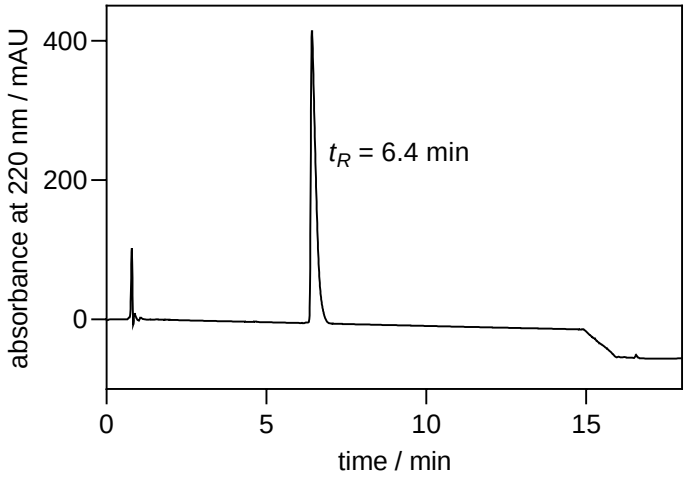
RP-HPLC analysis of compound **3.13**



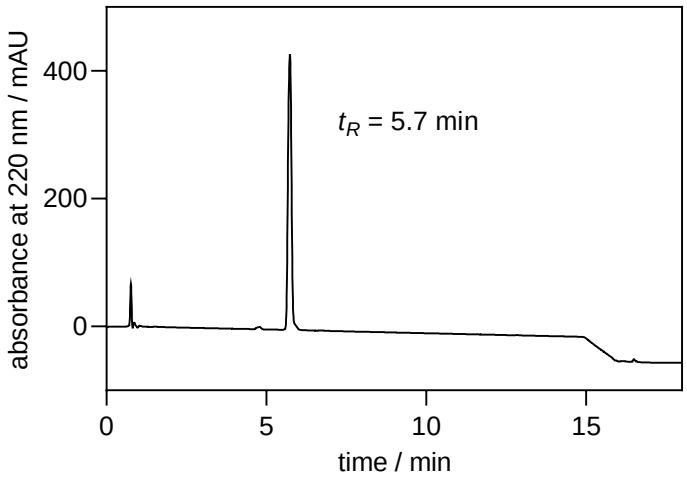
RP-HPLC analysis of compound **3.14**



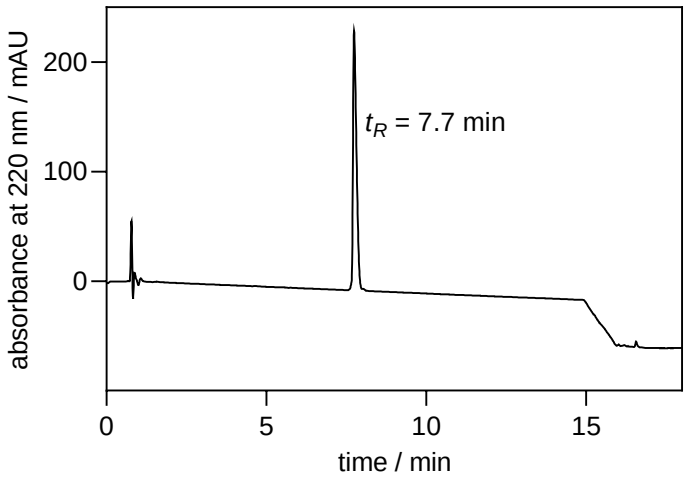
RP-HPLC analysis of compound **3.15**



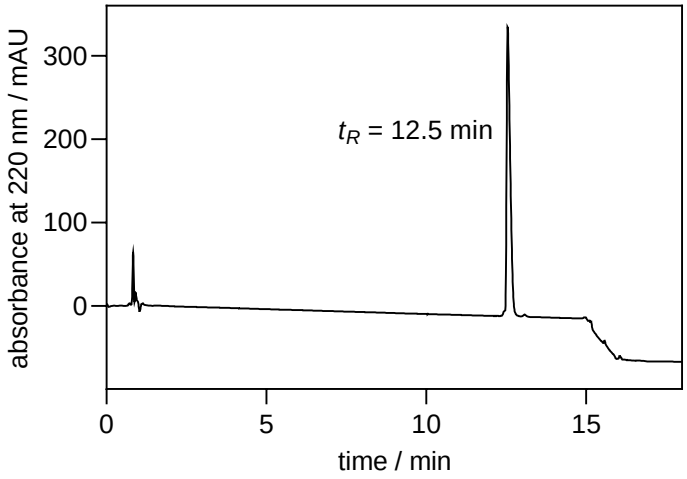
RP-HPLC analysis of compound **3.16**



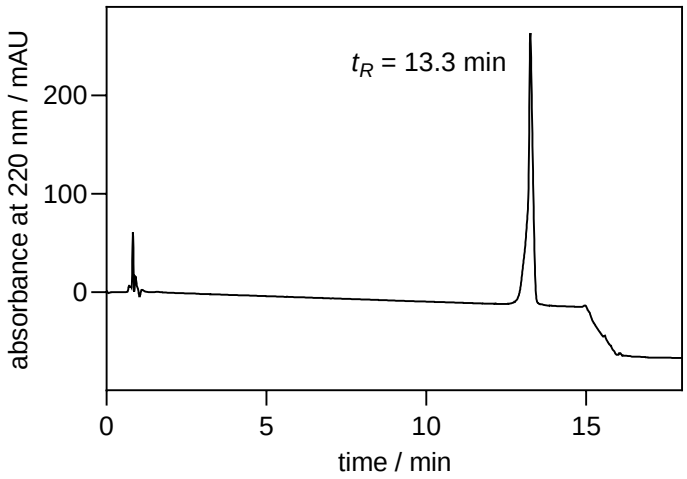
RP-HPLC analysis of compound **3.17**



RP-HPLC analysis of compound **3.18**

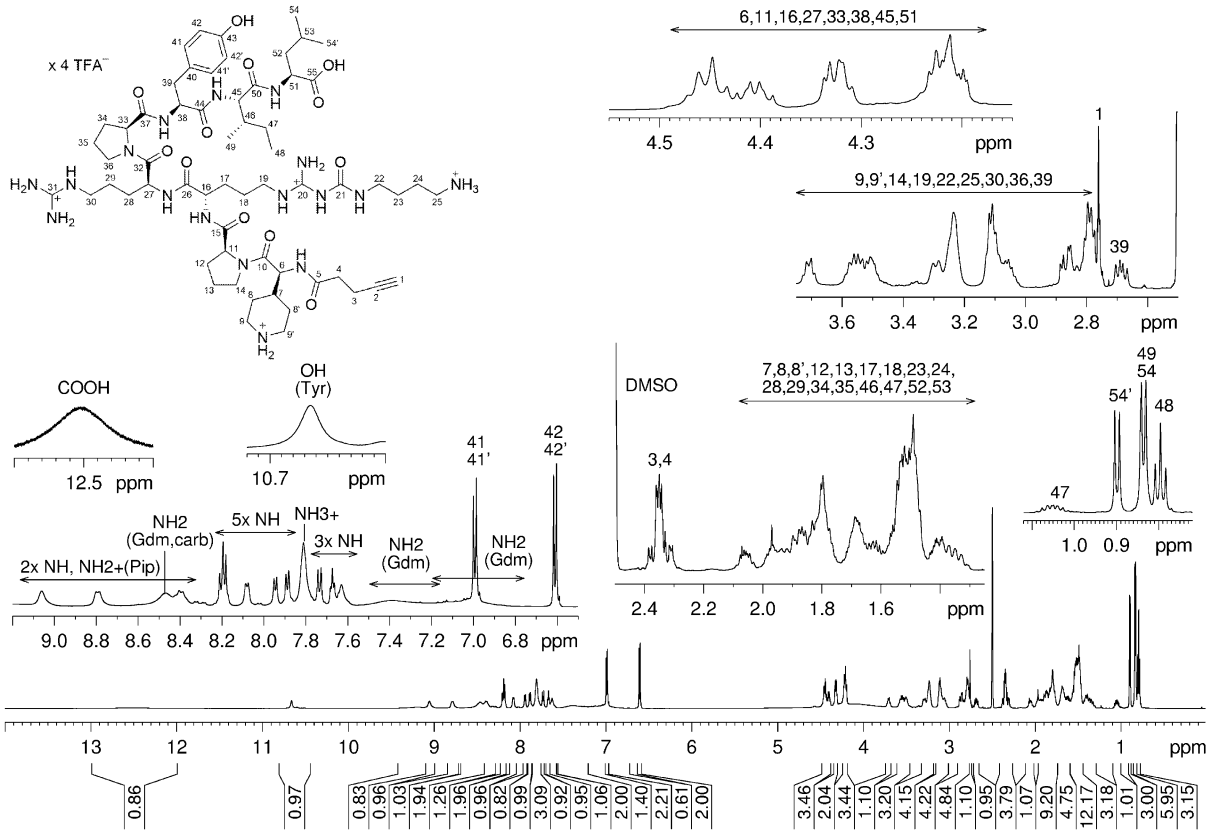


RP-HPLC analysis of compound **3.19**

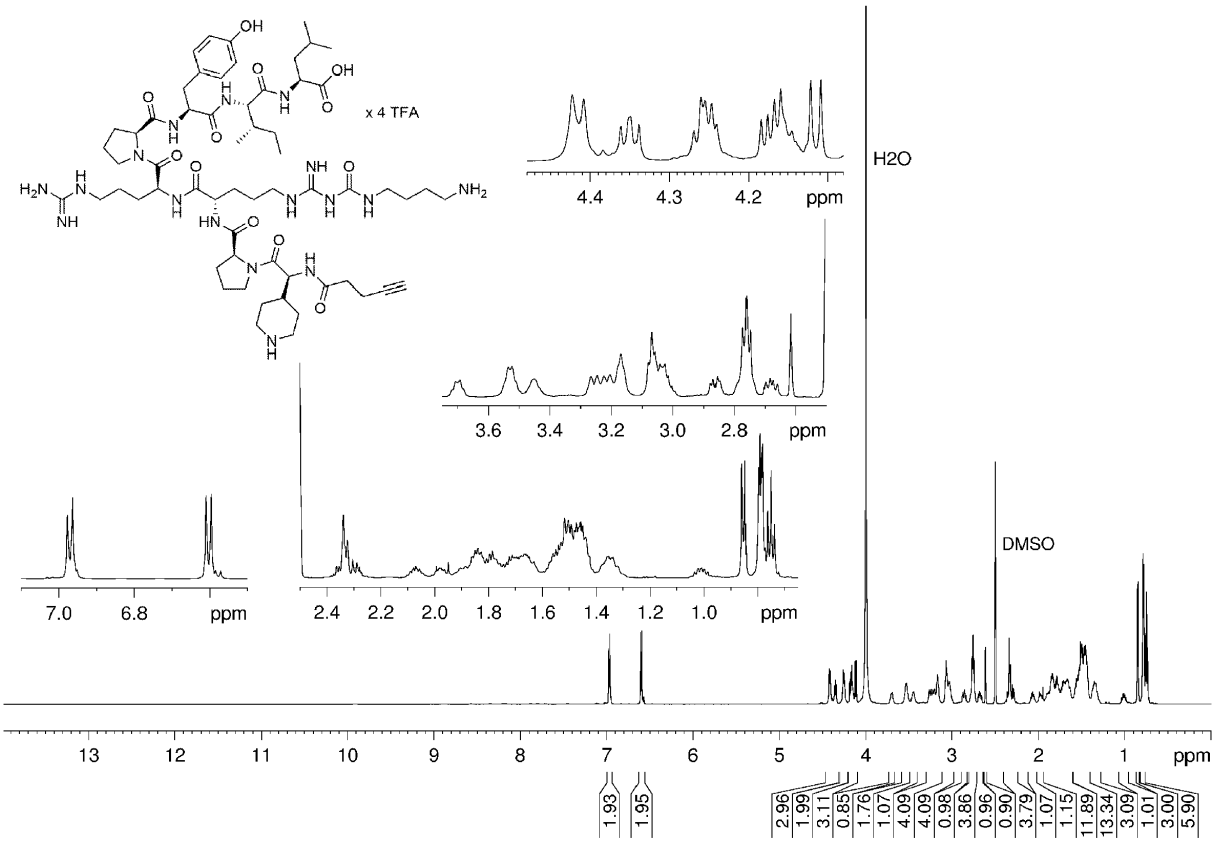


RP-HPLC analysis of compound **3.20**

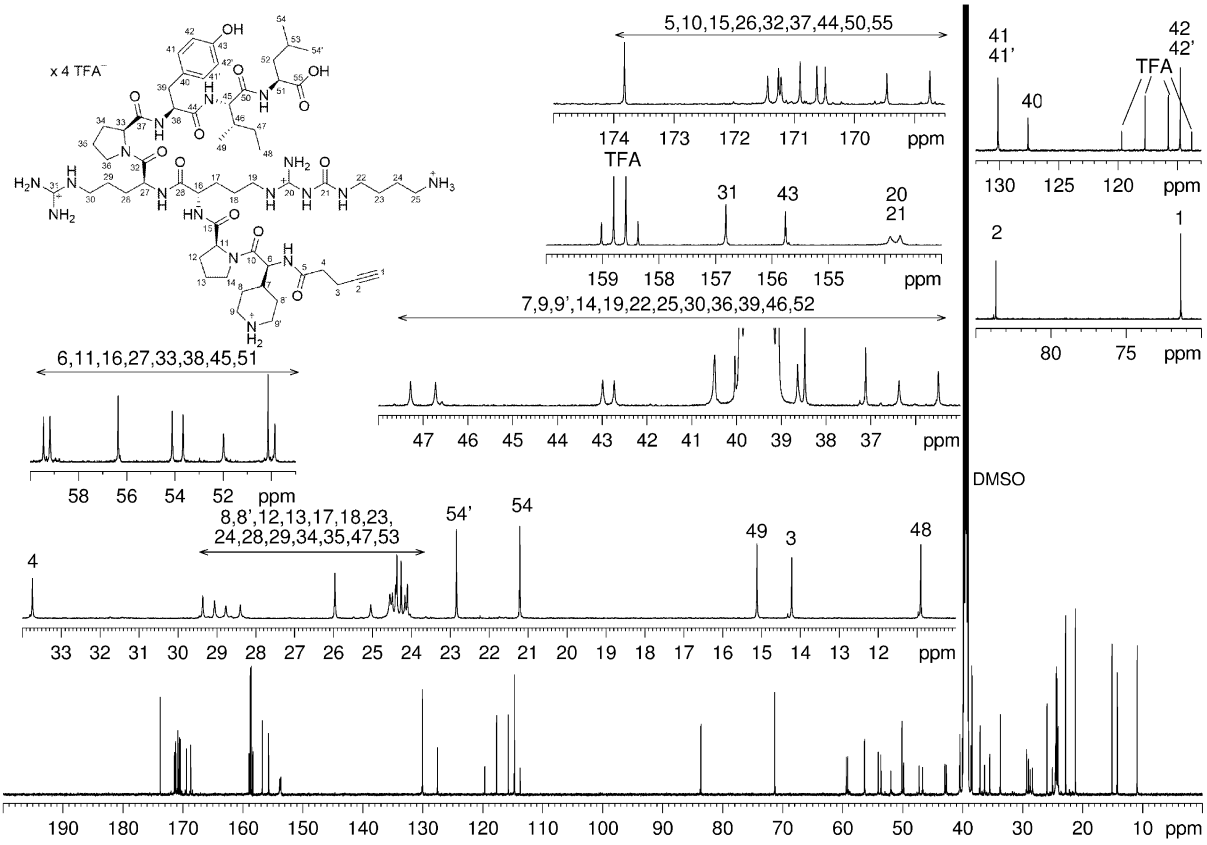
A3.5 ^{1}H-NMR spectra of compounds 3.6-3.9, 3.10a, 3.13, and 3.18, and ^{13}C-NMR spectra of compounds 3.6-3.9 and 3.10a in DMSO-d_6 and DMSO-d_6/D_2O 4:1



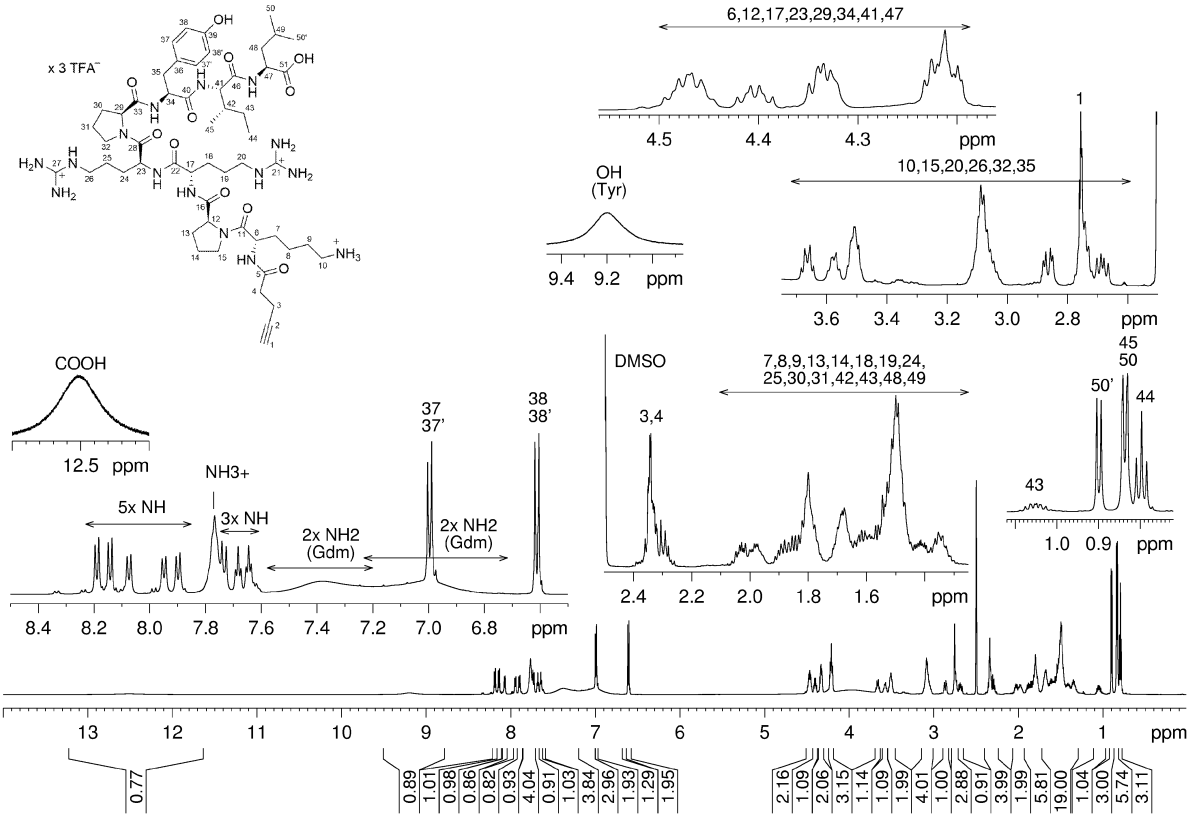
^{1}H-NMR spectrum (600 MHz, DMSO-d_6) of compound **3.6**



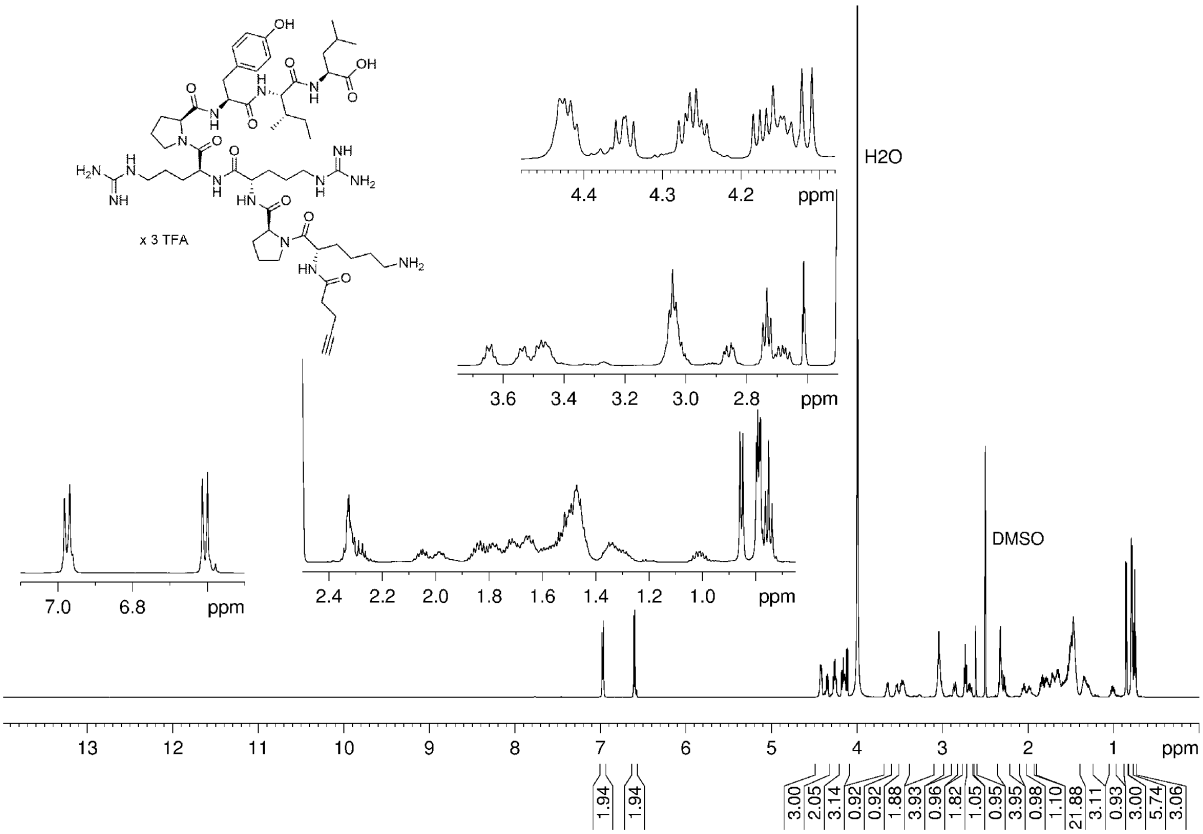
^{1}H-NMR spectrum (600 MHz, DMSO-d_6/D_2O 4:1 v/v) of compound **3.6**



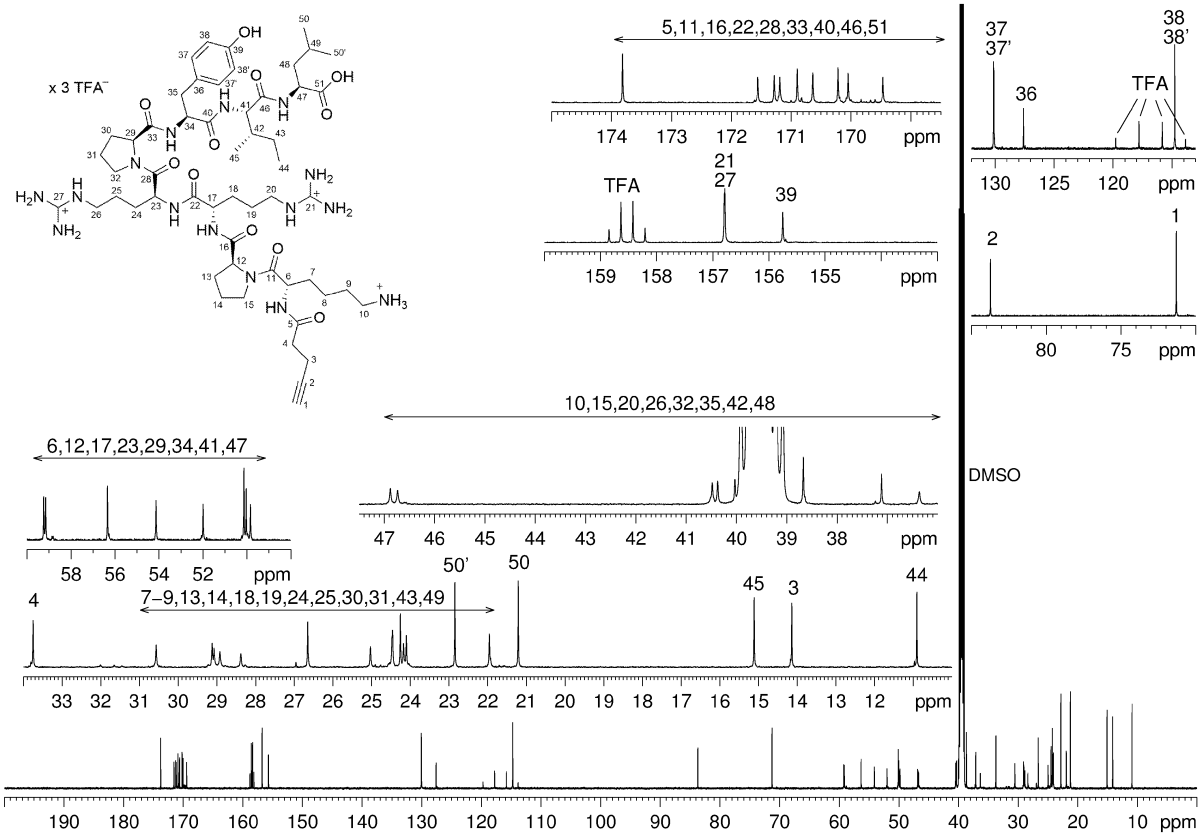
^{13}C-NMR spectrum (150 MHz, DMSO-d_6) of compound **3.6**



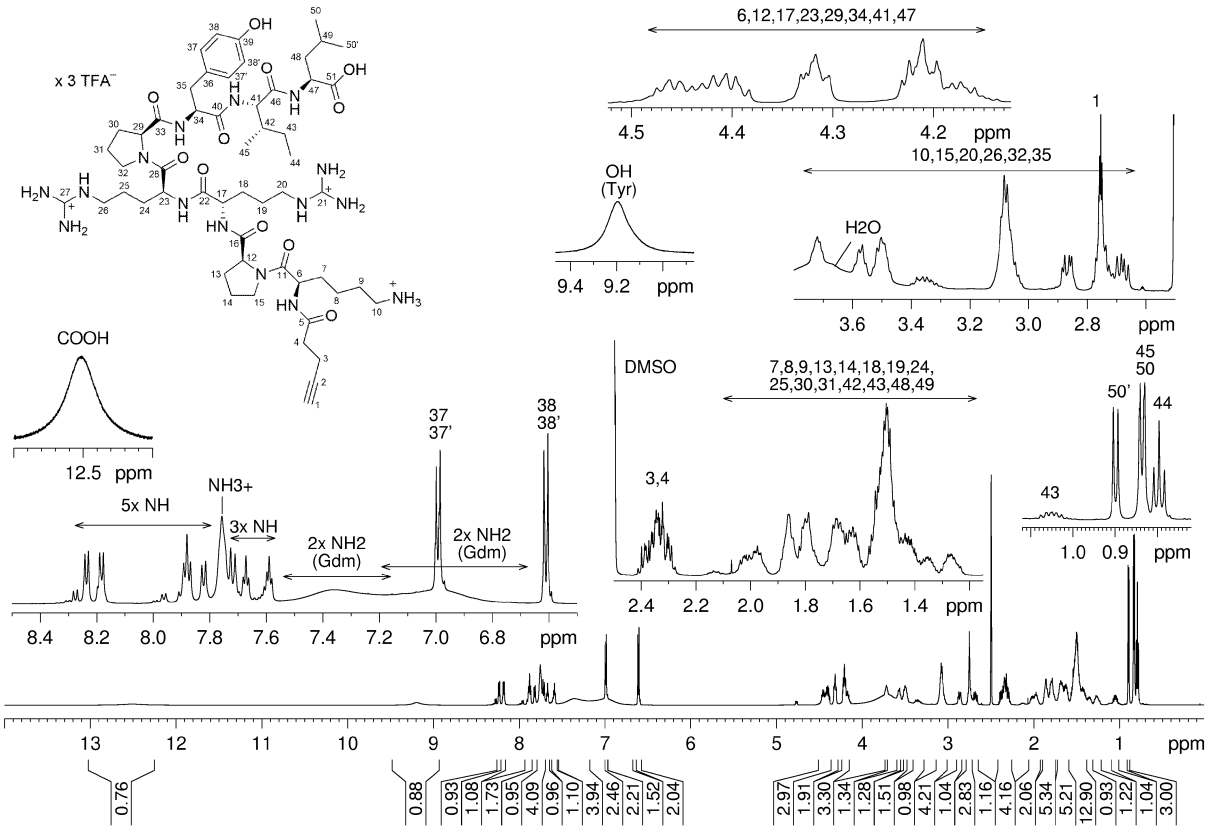
^{1}H-NMR spectrum (600 MHz, DMSO-d_6) of compound **3.7**



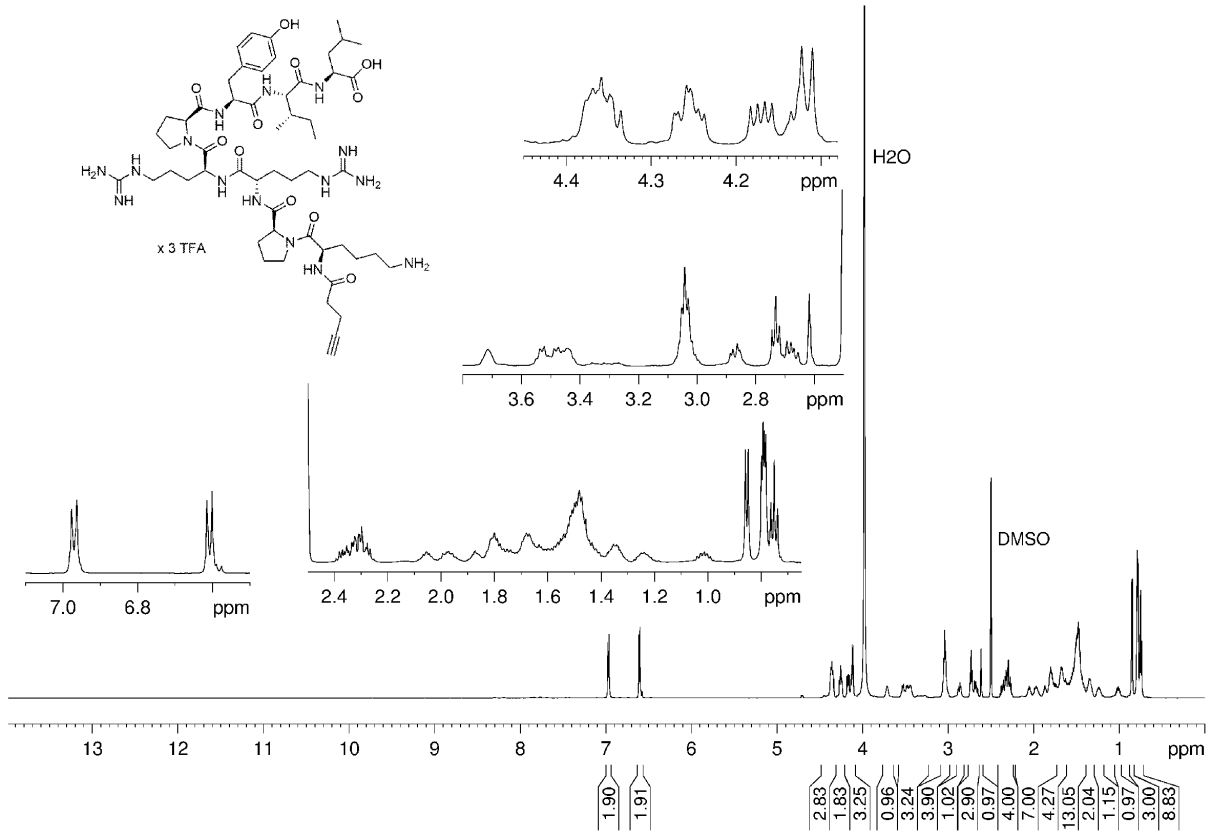
^{1}H-NMR spectrum (600 MHz, DMSO-d_6/D_2O 4:1 v/v) of compound **3.7**



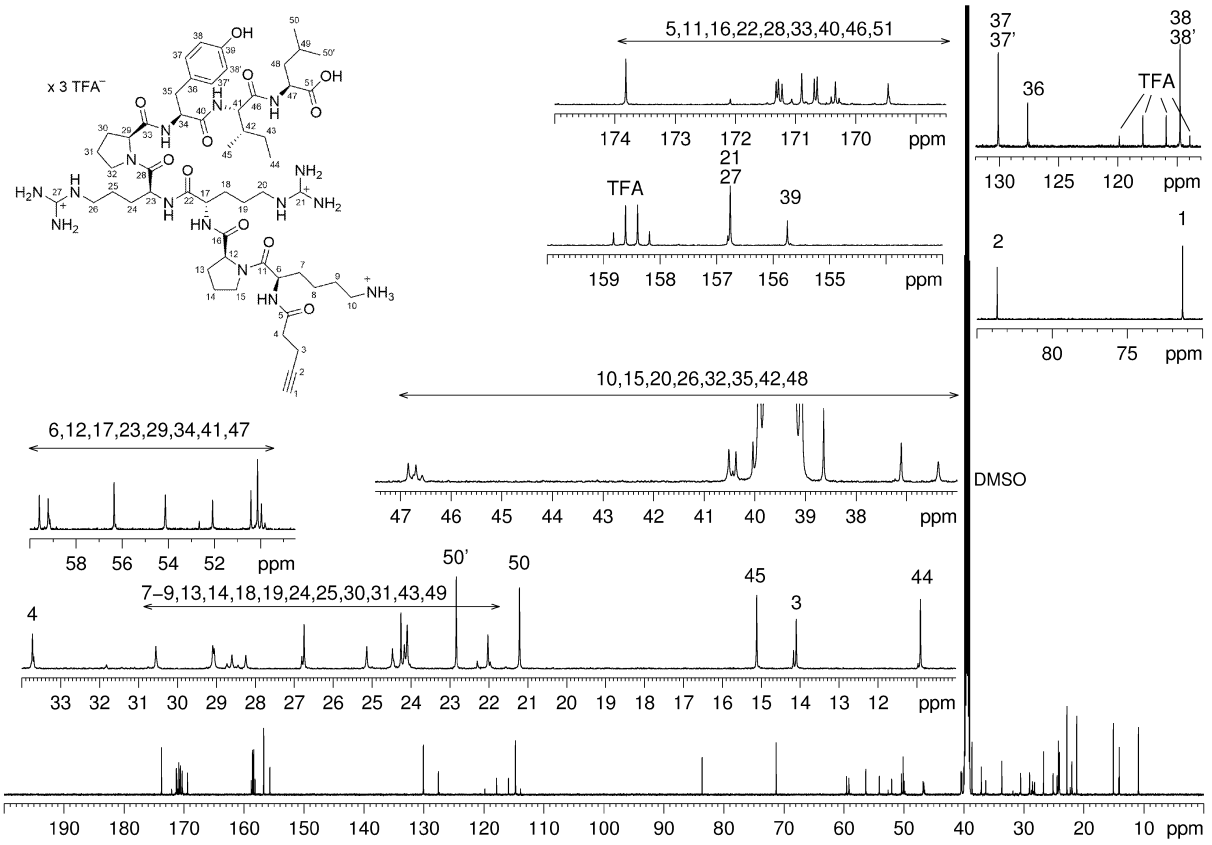
^{13}C-NMR spectrum (150 MHz, DMSO-d_6) of compound **3.7**



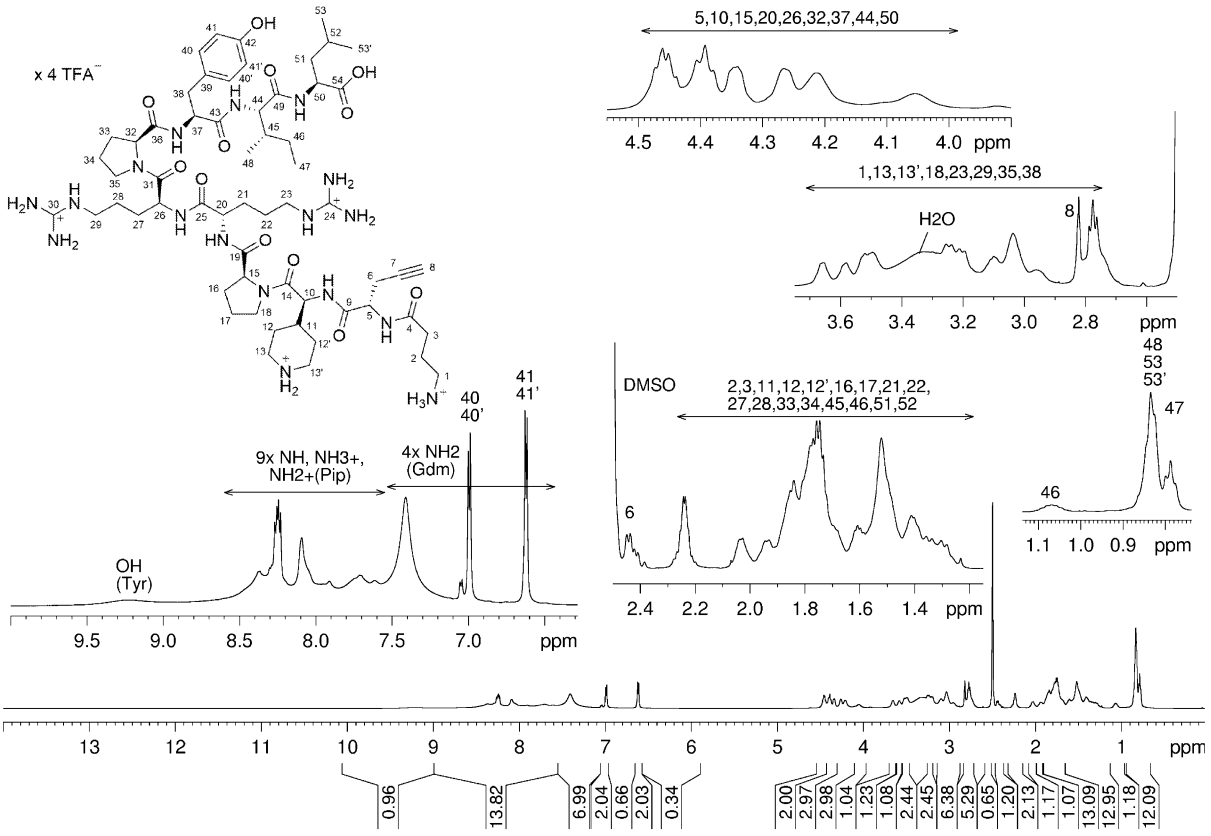
^{1}H-NMR spectrum (600 MHz, DMSO-d_6) of compound **3.8**



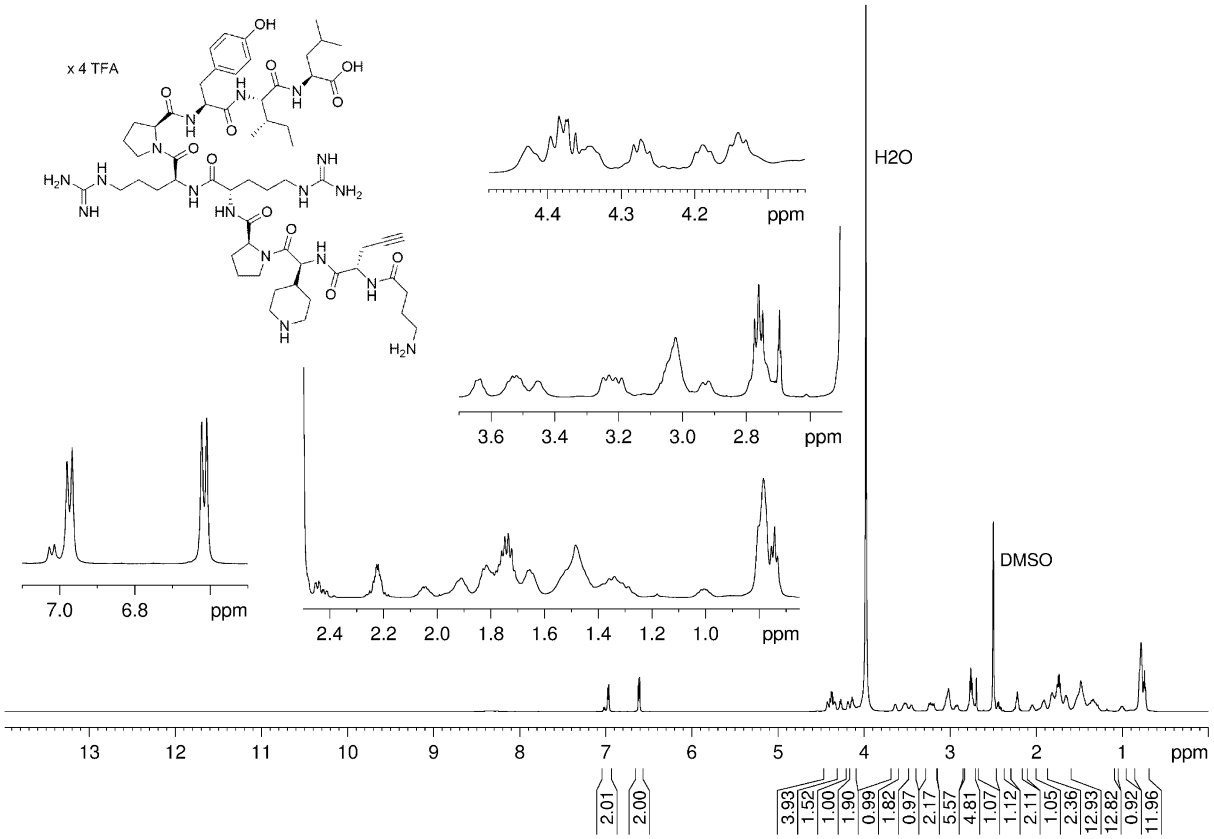
^{1}H-NMR spectrum (600 MHz, DMSO-d_6/D_2O 4:1 v/v) of compound **3.8**



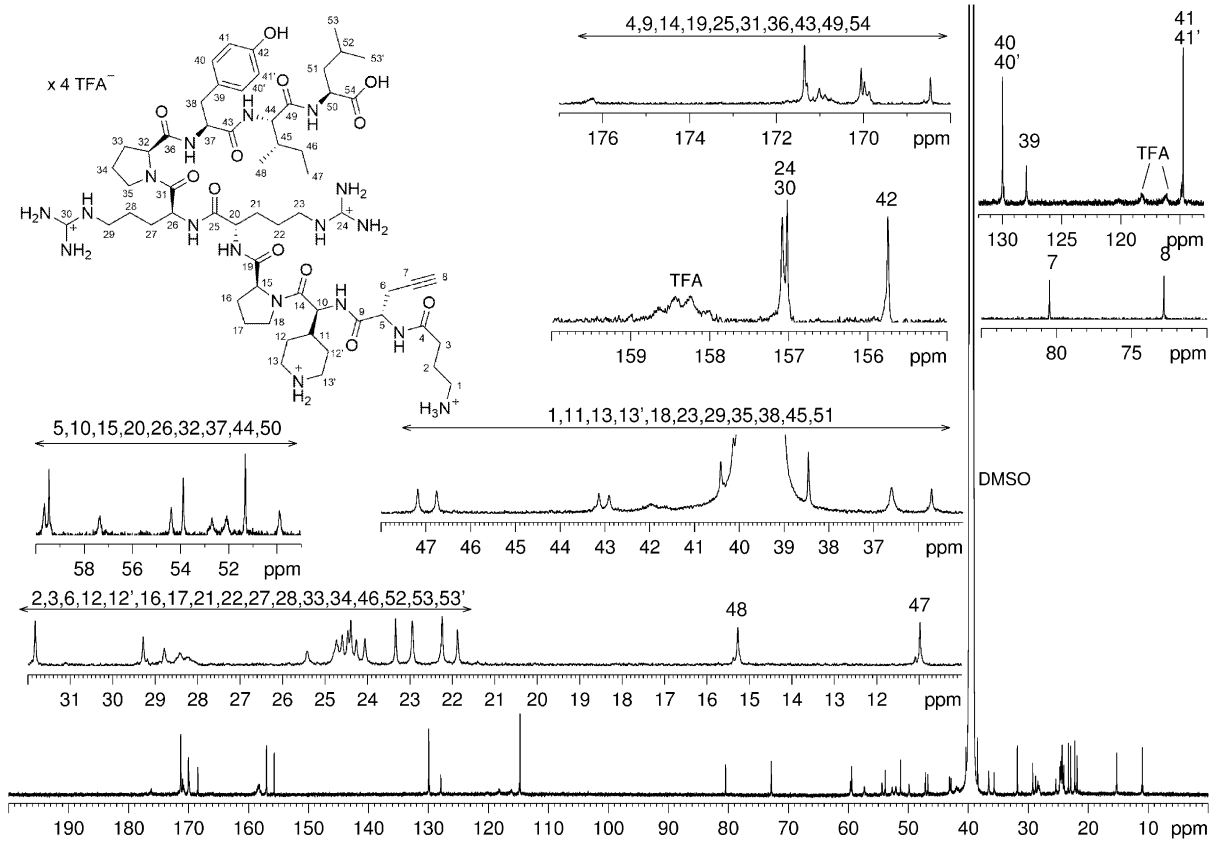
^{13}C-NMR spectrum (150 MHz, DMSO-d_6) of compound **3.8**



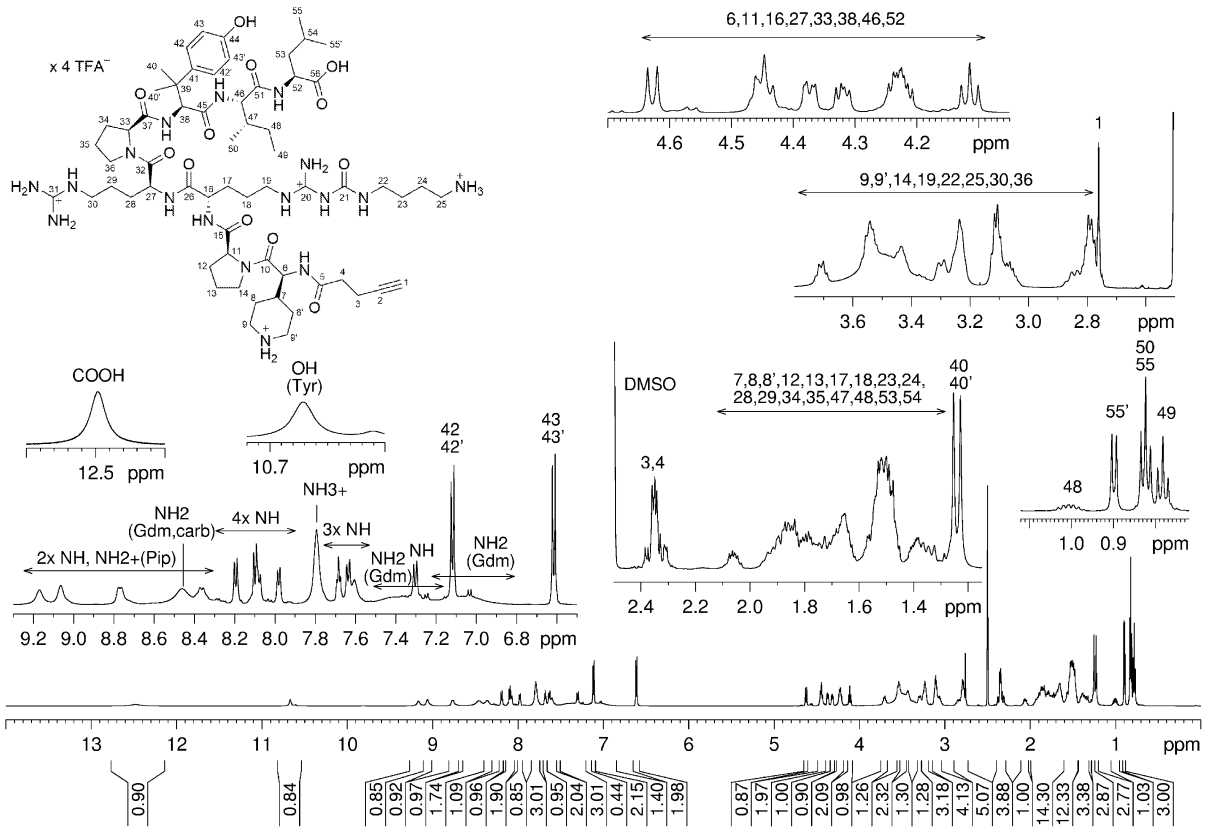
^{1}H-NMR spectrum (600 MHz, DMSO-d_6) of compound **3.9**



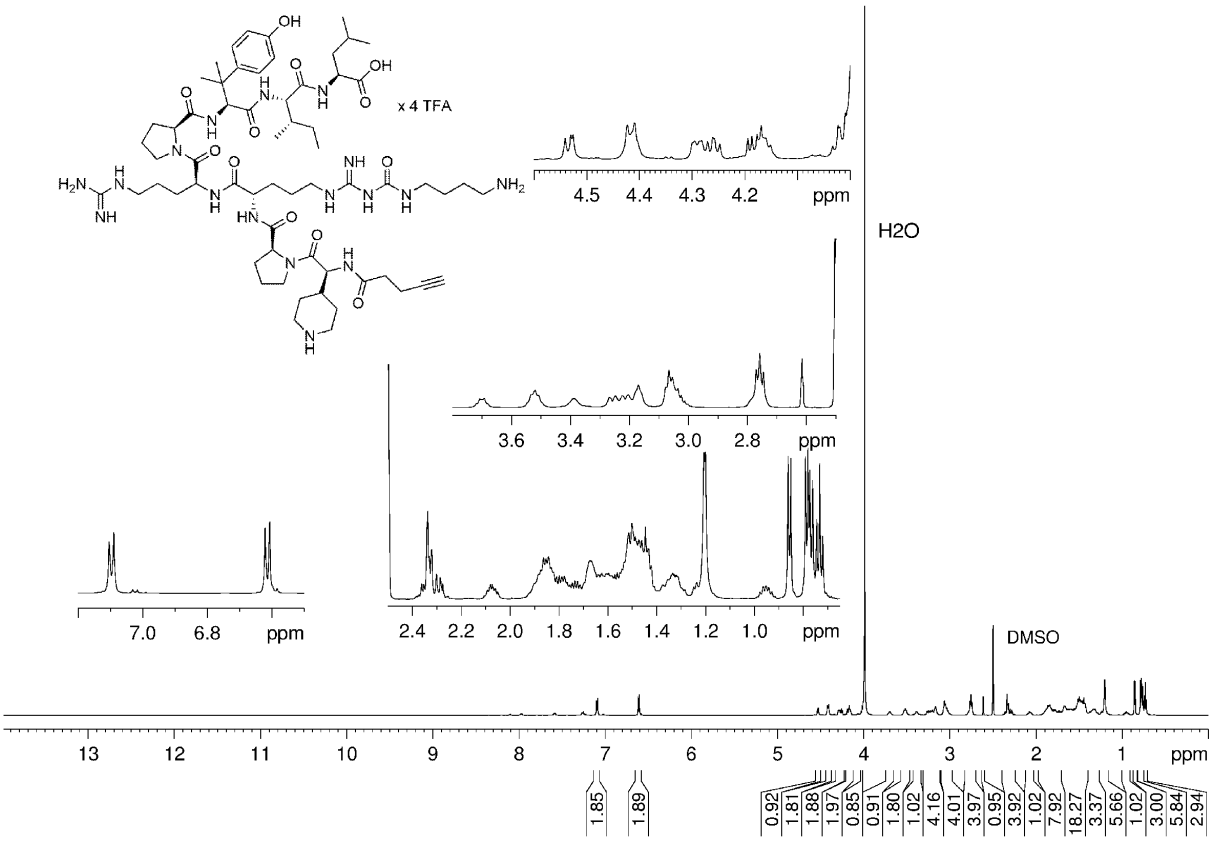
^{1}H-NMR spectrum (600 MHz, DMSO-d_6/D_2O 4:1 v/v) of compound **3.9**



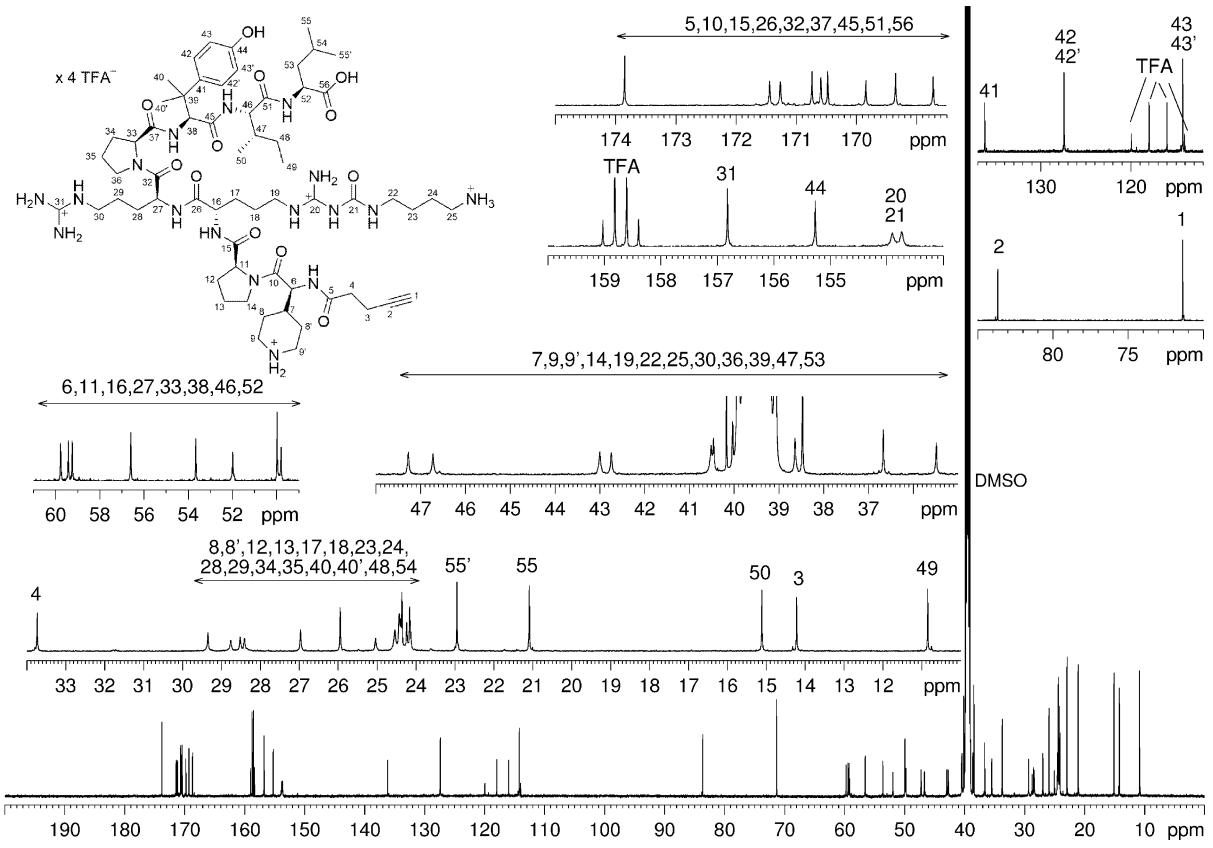
^{13}C-NMR spectrum (150 MHz, DMSO-d_6) of compound **3.9**



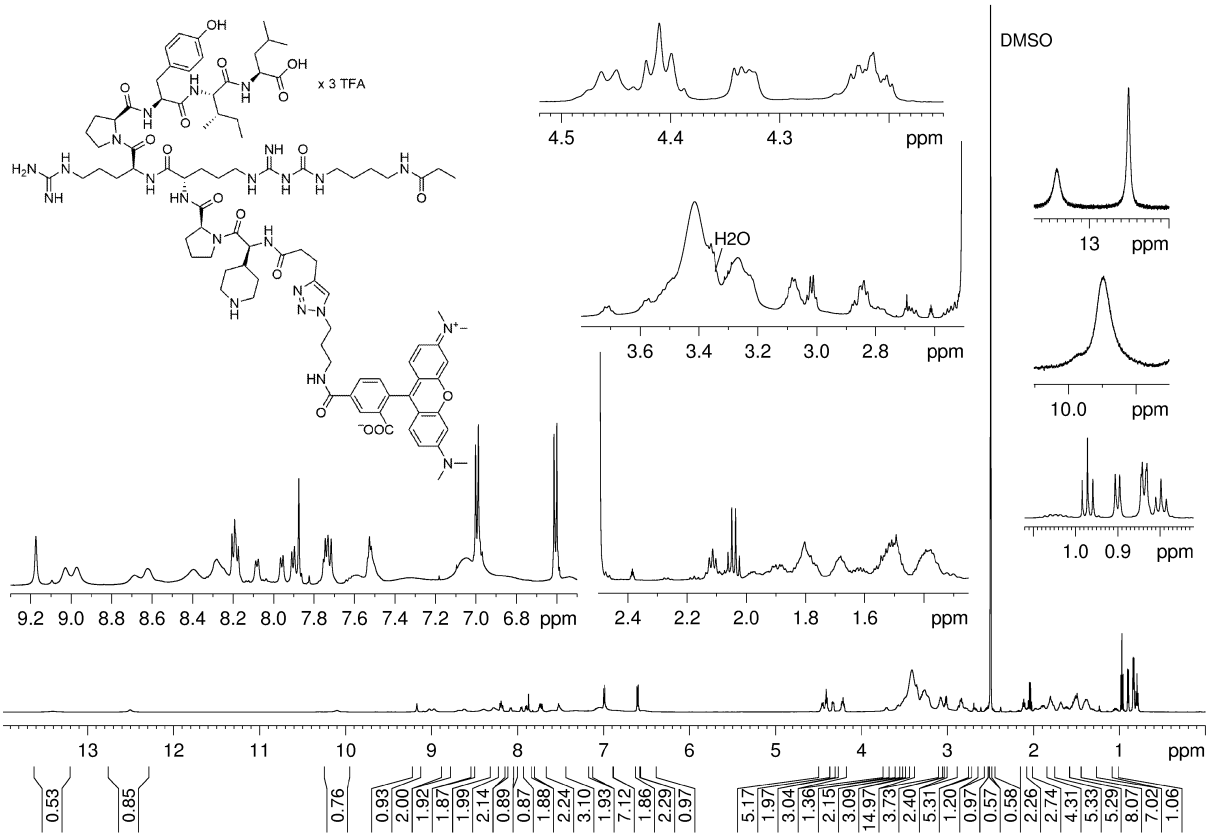
^{1}H-NMR spectrum (600 MHz, DMSO-d_6) of compound **3.10a**



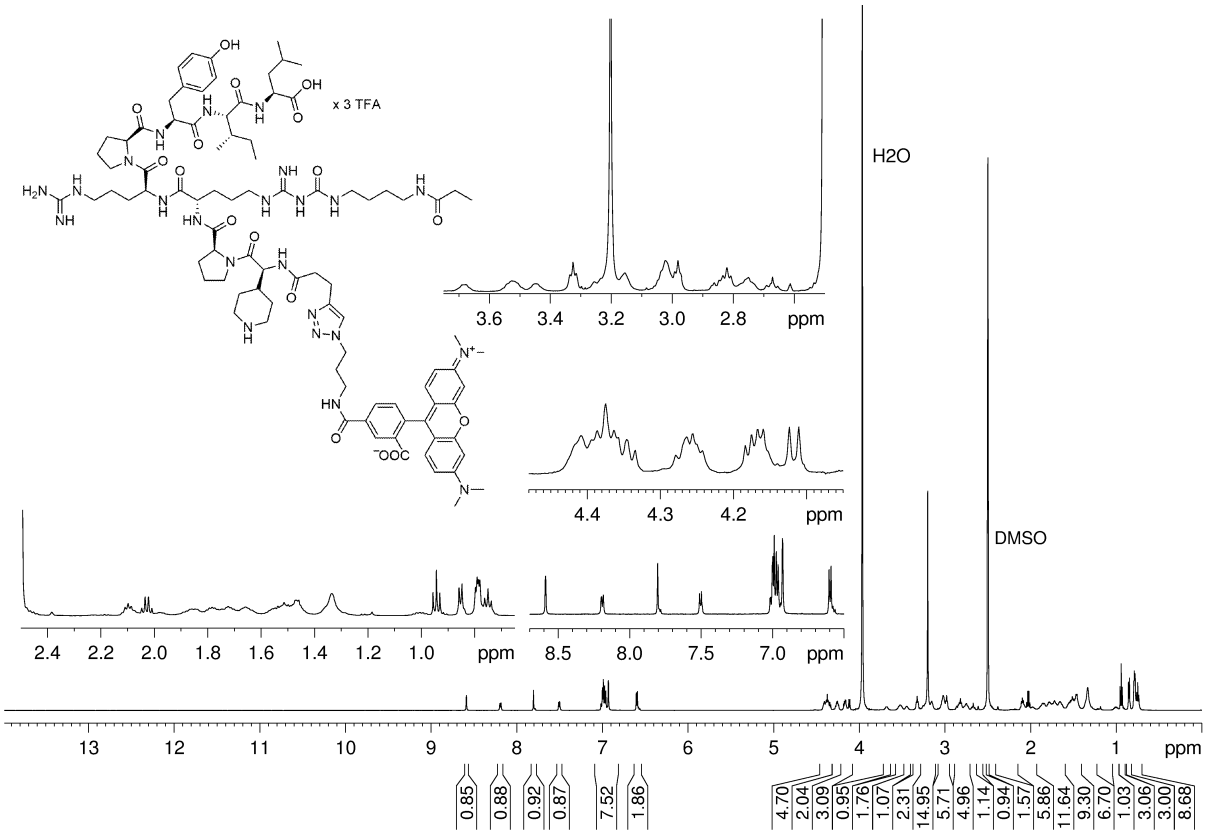
^{1}H-NMR spectrum (600 MHz, DMSO-d_6/D_2O 4:1 v/v) of compound **3.10a**



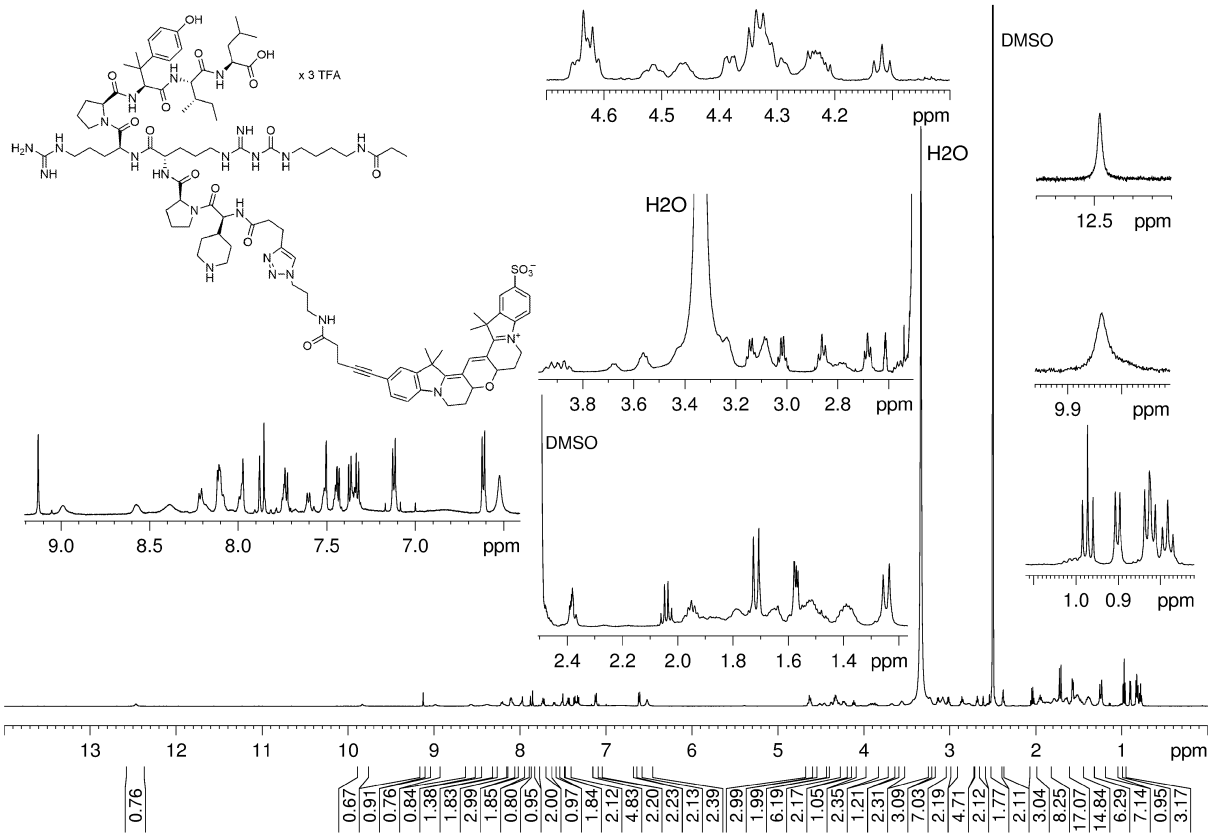
^{13}C-NMR spectrum (150 MHz, DMSO-d$_6$) of compound **3.10a**



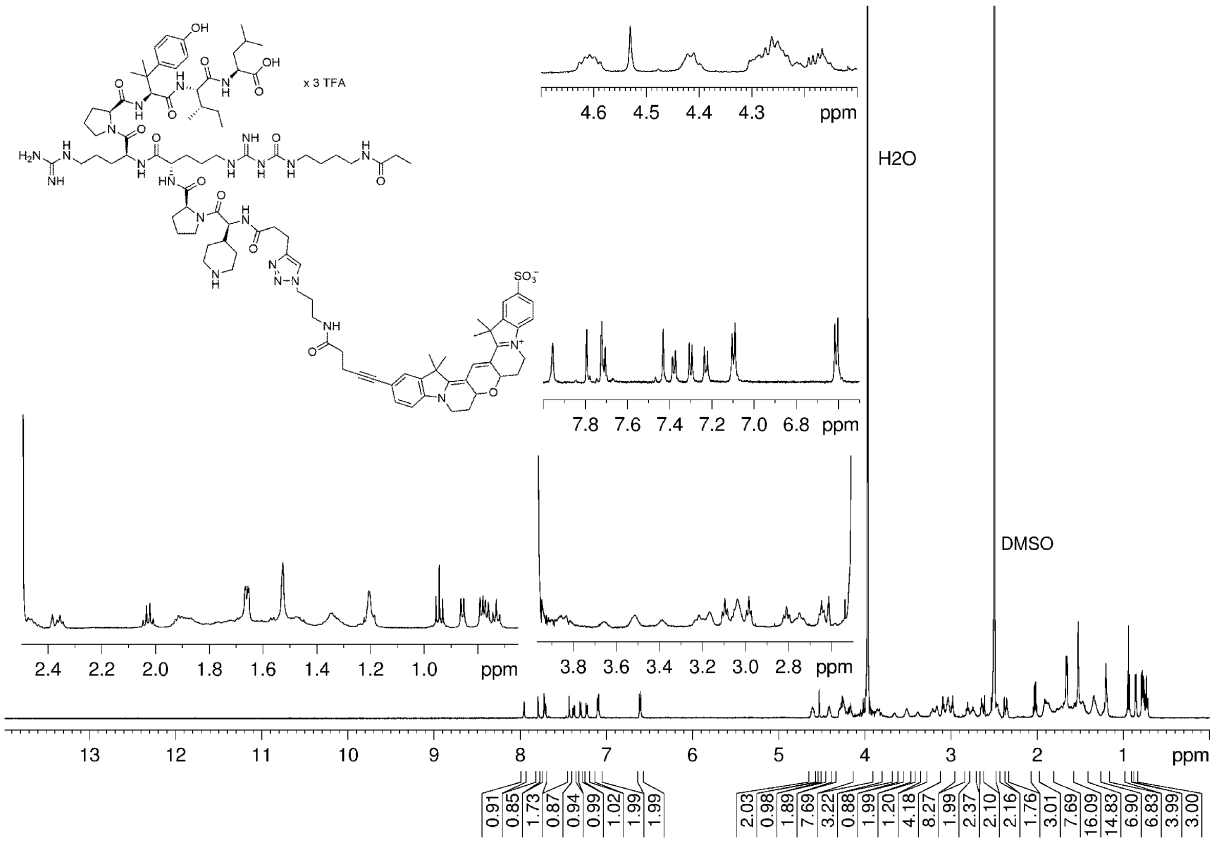
^{1}H-NMR spectrum (600 MHz, DMSO-d$_6$) of compound **3.13**



^{1}H-NMR spectrum (600 MHz, DMSO-d_6/D_2O 4:1 v/v) of compound **3.13**



^{1}H-NMR spectrum (600 MHz, DMSO-d_6) of compound **3.18**



^{1}H-NMR spectrum (600 MHz, DMSO-d_6/D_2O 4:1 v/v) of compound **3.18**

A3.6 References

(1) Schindler, L.; Moosbauer, J.; Schmidt, D.; Spruss, T.; Gratz, L.; Ludeke, S.; Hofheinz, F.; Meister, S.; Echtenacher, B.; Bernhardt, G.; Pietzsch, J.; Hellwig, D.; Keller, M. Development of a Neurotensin-Derived ^{68}Ga-Labeled PET Ligand with High In Vivo Stability for Imaging of NTS_1 Receptor-Expressing Tumors. *Cancers* **2022**, *14*, 4922.

Chapter 4

High-affinity and proteolytically stable peptidic fluorescent NTS_1R ligands

---

This chapter was published in *Journal of Medicinal Chemistry* in collaboration with cooperation partners after the submission of the thesis (reused with permissions from ACS, Copyright 2025):

Ertl, F. J., Friedel, A., Schmid, E. J., Höring, C., Archipowa, N., Koch, P., Maschauer, S., Kutta, R. J., Prante, O., and Keller, M. (2025) High-affinity and proteolytically stable peptidic fluorescent NTS1R ligands. *J. Med. Chem. 68*, 19482-19502. https://doi.org/10.1021/acs.jmedchem.5c01701

Contributions of the co-authors to the work presented in this chapter: Elena J. Schmid performed the synthesis of the peptide **2.2**. Carina Höring established the Fura-2 Ca^{2+} assay. Nataliya Archipowa and Roger-Jan Kutta recorded the absorption, emission, and excitation spectra and determined fluorescence lifetimes and quantum yields. Anna Friedel performed biomolecular imaging experiments. Max Keller initiated and planned the project. Max Keller, Olaf Prante, Pierre Koch, Simone Maschauer, and Roger-Jan Kutta supervised the research.

Note: The compounds assigned with **2.2** in Chapter 2 and **3.1**, **3.4**, and **3.13** in Chapter 3 are also part of Chapter 4. To avoid an assignment of several numbers to the same compound, the numbers **2.2**, **3.1**, **3.4**, and **3.13** are also used in this chapter, which had been submitted as revised manuscript prior to submission of this thesis. Instead of reorganizing the compound numbers, the numbers designating the same compounds as **2.2**, **3.1**, **3.4**, and **3.13** in the submitted revised manuscript were omitted in Chapter 4 resulting in gaps in compound numbering, i.e., **4.2**, **4.6**, **4.12**, and **4.13** are missing.

4.1 Introduction

The neurotensin receptor 1 (NTS_1R), a class A G-protein coupled receptor (GPCR), is one of three receptors of the neurotensin receptor family. The hexapeptide neuromedin N (**1.1**) and the tridecapeptide neurotensin (NT, **1.2**) represent endogenous NTS_1R agonists (Figure 4.1A). The bioactivity of neurotensin is conferred by the C-terminal hexapeptide sequence, NT(8-13) (**1.3**).[1] Thus, **1.3** has served as a lead structure for the development of various NTS_1R ligands including radio- and fluorescence labeled analogs. In healthy tissues, the NTS_1R is mainly expressed in the brain and gastrointestinal tract.[2,3] With regard to neoplastic diseases, the NTS_1R is (over)expressed, e.g., in pancreatic adenocarcinoma, prostate and colon carcinoma, and in about one third of primary breast cancer tumors.[4-9] Therefore, the NTS_1R is considered a promising target for tumor diagnostics and treatment using metabolically stable, appropriately radiolabeled NTS_1R ligands.[10]

Besides radioligands, fluorescently labeled NTS_1R ligands also represent useful tool compounds which can substitute radioligands, e.g., in competition binding assays needed to determine binding affinities of new NTS_1R ligands. Advantages of fluorescent probes over radioligands are mild safety issues, unproblematic waste disposal, and accessibility to a broad range of methods such as flow cytometry, high-content imaging, fluorescence anisotropy or NanoBRET, most of them being compatible with multi-mode plate reader measurements. Moreover, fluorescent probes can be used to study receptor-ligand binding by fluorescence microscopy. Unlike radiochemical assays, most fluorescence-based techniques allow for measurement under homogeneous conditions, meaning that a separation of bound from free ligand is not required.

To date, several fluorescent NTS_1R ligands, all derived from **1.3**, have been reported (e.g., **4.1**, **3.13**, **4.3**, and **4.4**, Figure 4.1B). These probes were characterized by high-content imaging, flow cytometry, fluorescence anisotropy, NanoBRET, or fluorescence microscopy.[11-16] Among the reported fluorescently labeled NTS_1R ligands, compounds **4.1**, **3.13**, and **4.3** exhibit the highest binding affinities (K_i = 0.76-1.1 nM) allowing an application as probes for cell-based binding assays.

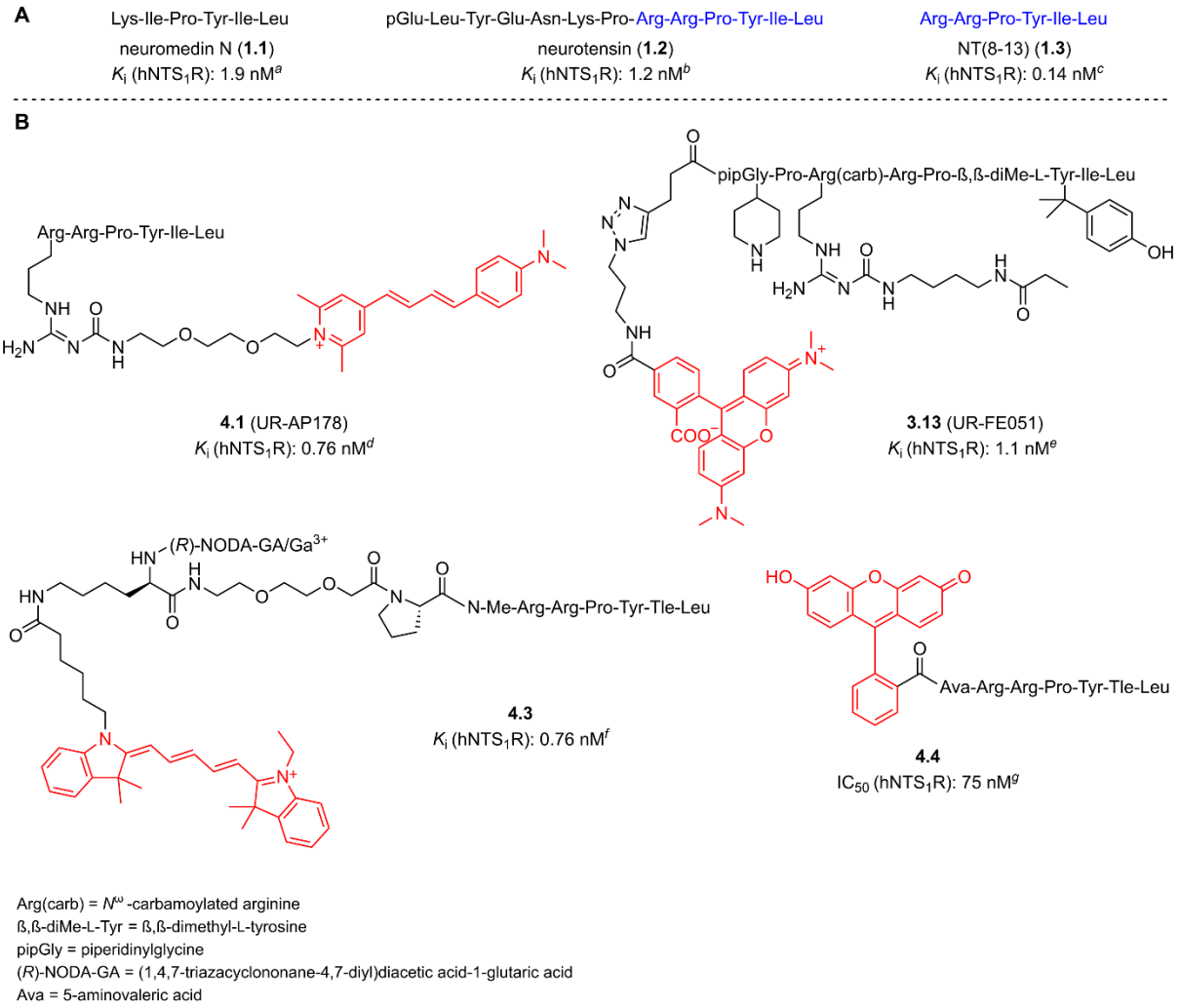


Figure 4.1. (A) Peptide sequences and NTS_1R binding affinities of the endogenous NTS_1R ligands neuromedin N (**1.1**) and neurotensin (**1.2**), and the lead compound NT(8-13) (**1.3**). (B) Reported fluorescent NTS_1R ligands with binding affinities in the low nanomolar range. Fluorescent dyes are shown in red. [a]Skrzydelski *et al.*[17] [b]Granier *et al.*[18] [c]Keller *et al.*[12] [d]Keller *et al.*[13] [e]Ertl *et al.*[16] [f]Renard *et al.*[14] [g]Maes *et al.*[11]

Yet, there is interest in fluorescently labeled NTS_1R ligands with even higher binding affinity since this comes along with reduced unspecific binding and potentially with longer residence time, which is particularly advantageous for fluorescence-based imaging of receptor expression, e.g., in tumor tissue.

The design of the novel fluorescently labeled NT(8-13)-derivatives in this study was guided by different reported studies. First, Leu[13] is replaced by (trimethylsilyl)alanine (TMSAla) in the synthesized NT(8-13) analogs because Fanelli and coworkers reported that this structural modification leads to markedly increased NTS_1R binding affinity of hexapeptides derived from **1.3** (see compounds **4.5** and **2.2**, Figure 4.2).[19]

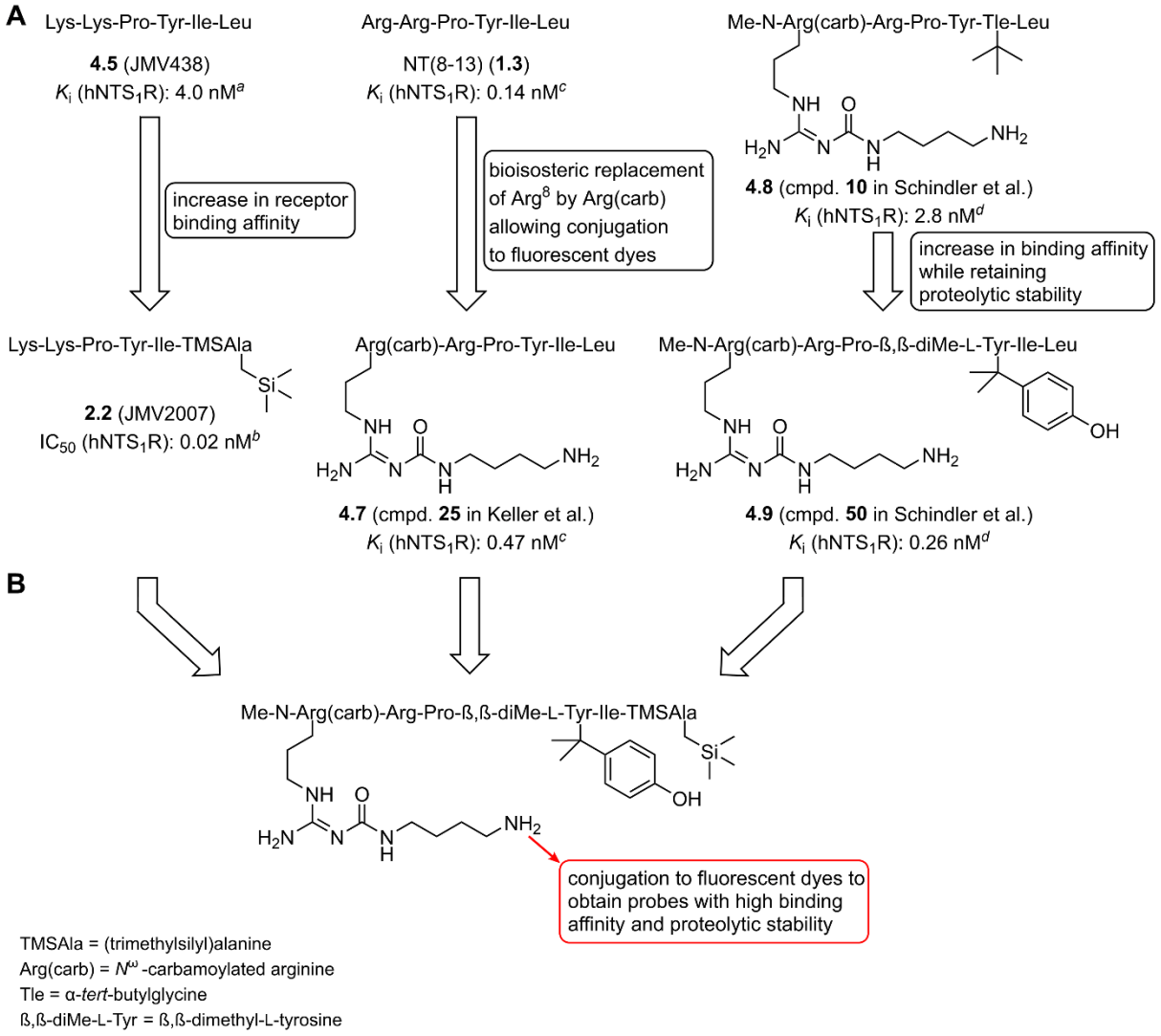


Figure 4.2. (A) Schematic presentation of reported amino acid replacements in NT(8-13) (**1.3**) or NT(8-13) derivatives useful to increase NTS_1R binding affinity (replacement of Leu^{13} by TMSAla), for peptide conjugation (replacement of Arg^8 by an amino-functionalized carbamoylated arginine), and to achieve proteolytic stability (methylation of the N-terminus and replacement of Tyr^{11} by β,β-dimethyl-L-Tyr). (B) Aim of the present study: combination of approaches shown in A in one molecule followed by the synthesis of fluorescently labeled NTS_1R ligands. [a]Vivancos *et al.*[20] [b]Fanelli *et al.*[19] [c]Keller *et al.*[12] [d]Schindler *et al.*[21]

Second, Arg^8 is bioisosterically exchanged by an amino-functionalized N^{ω}-carbamoylated arginine (Arg(carb)) (e.g., compound **4.7**, Figure 4.2).[12] Attachment of fluorescent dyes to the side chain of this carbamoylated arginine was previously demonstrated to be well tolerated with respect to NTS_1R binding.[13,16] Third, the N-terminus is methylated and Tyr^{11} is replaced by β,β-dimethyltyrosine, in order to obtain proteolytically stable peptides. The N-terminal methylation was reported to prevent N-terminal degradation by proteases[22] and the incorporation of β,β-dimethyl-Tyr was recently shown to result in an effective stabilization of the C-terminus against proteolytic cleavage (see compounds **4.8** and **4.9**, Figure 4.2).[21] Notably, the replacement of Tyr^{11} by β,β-dimethyl-Tyr represents a favorable alternative to the replacement of Ile^{12} by α-

tert-butylglycine (standard modification for the stabilization of the C-terminus), since NTS_1R binding is affected by the latter but not by the former modification.[21]

For fluorescence labeling of the peptides, the rhodamine-based dye 5-TAMRA and the indolinium-type cyanine dye sulfo-Cy5 were used. The precursor compounds and the labeled peptides were characterized in a radiochemical NTS_1R competition binding assay. The labeled probes were also studied in a functional NTS_1R Ca^{2+} assay and were photophysically characterized (fluorescent quantum yields and fluorescence lifetimes). Moreover, NTS_1R binding of the fluorescent ligands was investigated by flow cytometry (saturation binding, kinetic studies, and competition binding), confocal microscopy, and in tumor sections using a biomolecular imager.

4.2 Results and discussion

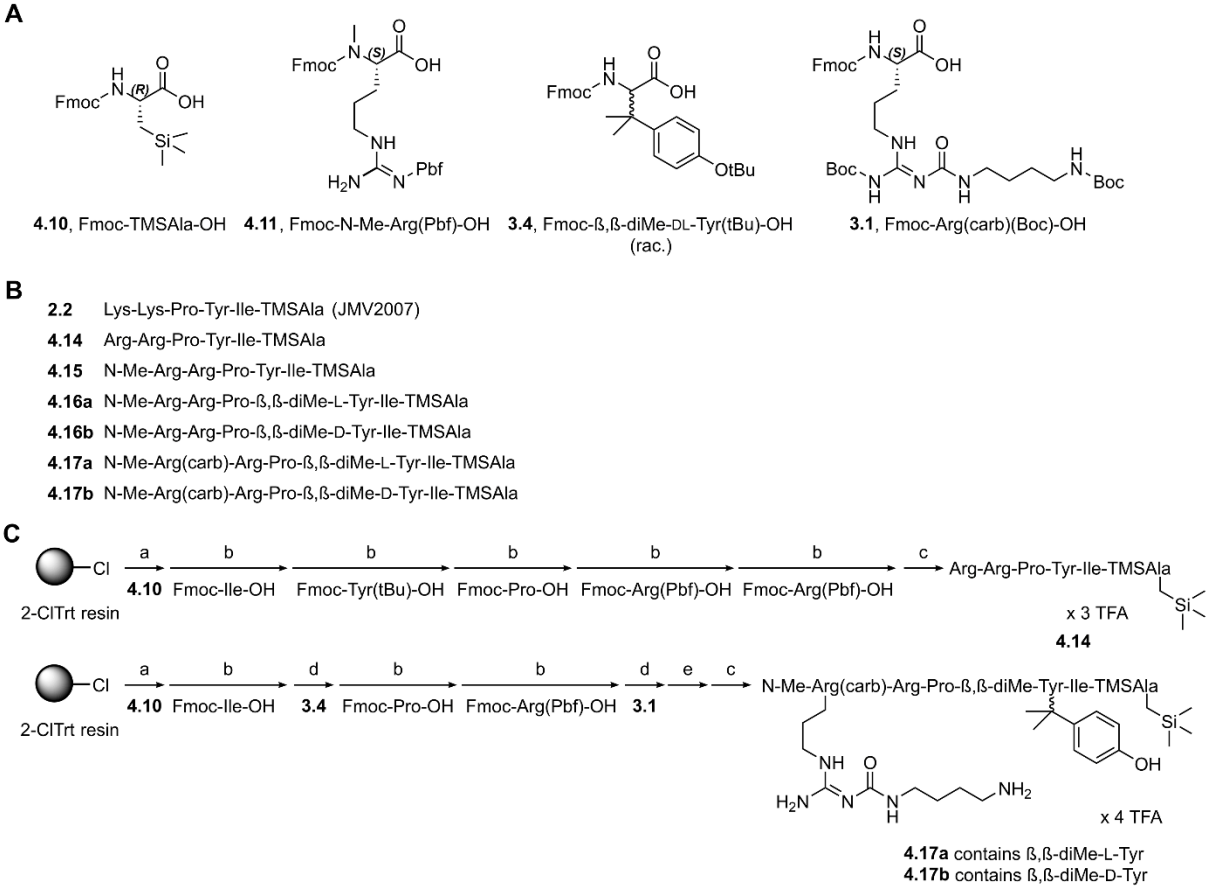
4.2.1 Synthesis

The unnatural, Fmoc-protected amino acids (**3.1**, **3.4**, **4.10**, **4.11**) used for the peptide synthesis are shown in Scheme 4.1A. N^{α}-methylated Fmoc/Pbf-protected arginine (**4.11**) and racemic Fmoc/tBu-protected β,β-dimethyl-Tyr (**3.4**) were commercially available (note: the desired L-configured stereoisomer of **3.4** was not available as a pure enantiomer). The Fmoc/Boc-protected amino-functionalized, carbamoylated arginine (**3.1**) was prepared as reported.[12] The Fmoc-protected TMSAla (**4.10**) was synthesized according to a published procedure yielding (*R*)-**4.10** with a reported ee of 98%.[23] Here, this asymmetric synthesis, using (1*R*,2*R*,5*R*)-2-hydroxy-3-pinanone (**4.23**) as chiral auxiliary (see Scheme A4.1, Appendix), gave (*R*)-**10** with an ee of 86% (determined with capillary electrophoresis, electropherograms shown in the Appendix).

All peptides (**2.2**, **4.14**-**4.17b**; sequences shown in Scheme 4.1B) were synthesized by solid-phase peptide synthesis (SPPS) on a 2-ClTrt resin. Peptide **4.14** represents the NT(8-13) derivative containing TMSAla instead of Leu^{13}. To our best knowledge, this peptide has not been described to date. Peptide **4.15** represents the N-terminally methylated congener of **4.14** and in **4.16** Tyr^{11} is additionally replaced by β,β-dimethyl-Tyr (**4.16a**: β,β-dimethyl-L-Tyr, **4.16b**: β,β-dimethyl-D-Tyr). Finally, **4.17**, representing the precursor for fluorescence labeling, contains the N^{α}-methylated, amino-functionalized N^{ω}-carbamoylated arginine in position 8, β,β-dimethyl-L-Tyr (**4.17a**) or β,β-dimethyl-D-Tyr (**4.17b**) in position 11, and TMSAla in position 13 (note: the amino acid positions in the synthesized hexapeptides were assigned with the numbers corresponding to the respective amino acid positions in NT(8-13)). For **4.14** and **4.17**,

the solid-phase synthesis is exemplarily illustrated in Scheme 4.1C. Regarding the separation of the diastereomers **4.16a** and **4.16b** as well as **4.17a** and **4.17b**, this could be conveniently achieved by achiral preparative RP-HPLC. The assignment of the absolute configuration to β,β-dimethyl-Tyr in **4.16a**-**4.17b** was carried out as recently reported for structurally related NT(8−13) derivatives.[16] This approach is based on NT(8-13) analogs also containing β,β-dimethyl-L-Tyr or β,β-dimethyl-D-Tyr in position 11, for which the configuration was assigned using CD spectroscopy (structures shown in Figure A4.1A, Appendix).[21] As described by Ertl *et al.*,[16] the elution order in RP-HPLC and the NTS_1R binding affinities served as criteria for the assignment. Derivatives containing β,β-dimethyl-L-Tyr consistently elute first (RP-HPLC) and show markedly higher NTS_1R binding affinities compared to the analogs containing β,β-dimethyl-D-Tyr (see Figure A4.1, Appendix).

Scheme 4.1. Structures of the unnatural amino acids **3.1**, **3.4**, **4.10**, and **4.11**, sequences of the synthesized peptides **2.2** and **4.14-4.17b**, and exemplary schematic presentation of the syntheses of **4.14** and **4.17**.

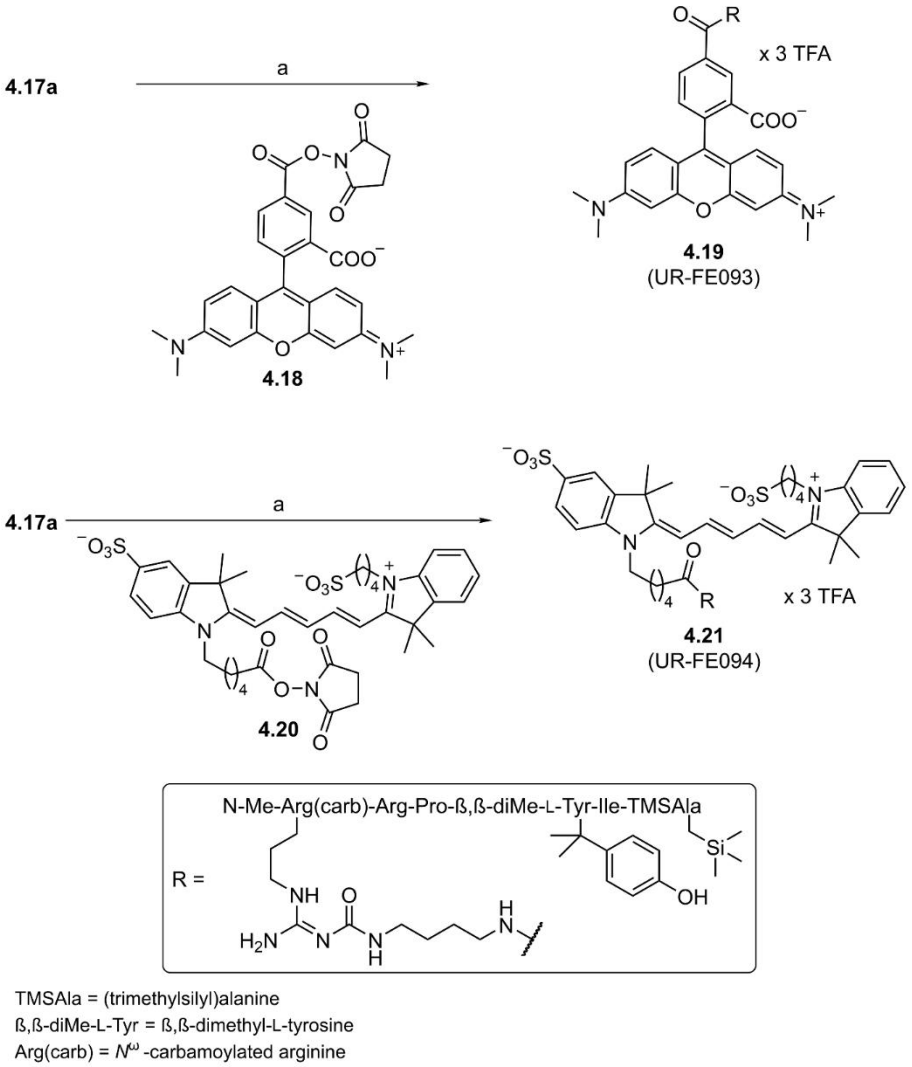


(A) Structures of used unnatural amino acids. (B) Amino acid sequences of the synthesized NT(8-13) derivatives. Overall yields for SPPS: 13-52%. (C) SPPS shown for **4.14** and **4.17**. Reagents and conditions: (a) anchoring of **4.10** to a 2-ClTrt resin: **4.10**/DIPEA (1/2.5 equiv.), CH_2Cl_2, rt, overnight, Fmoc deprotection: 20% piperidine in DMF/NMP 4:1 v/v, rt, 2 x 10 min; (b) amino acid coupling: Fmoc-amino acid/HOBt/HBTU/DIPEA (5/5/4.9/10 equiv.), DMF/NMP 4:1 v/v, 35 °C, 2 × 45 min ("double" coupling), Fmoc deprotection: as under (a); (c) (1) TFA/CH_2Cl_2 1:3 v/v, rt, 2 × 20 min; (2) TFA/H_2O 95:5 v/v, rt, 5 h; (d) **3.1** or **3.4**/HOBt/HBTU/DIPEA (3/3/2.95/6 equiv.), DMF/NMP 4:1 v/v, 35 °C, 16 h ("single" coupling), Fmoc deprotection: as under (a); (e) N-terminal methylation according to reported procedures:[21,24] (1) 2-nitrobenzenesulfonylchloride/collidine (3/5 equiv.), CH_2Cl_2, rt, 2 h; (2) MTBD/methyl-4-nitrobenzenesulfonate (4/5 equiv.), DMF, rt, 30 min; (3) DBU/2-mercaptoethanol (5/10 equiv.), DMF, rt, 30 min. The separation of the diastereomers **4.17a** and **4.17b** was performed by achiral preparative RP-HPLC. The wavy bond in **4.17a/b** indicates either configuration, L or D.

The fluorescently labeled peptides **4.19** and **4.21** were obtained by treatment of the precursor **4.17a** with the succinimidyl ester of the 5-TAMRA dye (**4.18**) or sulfo-Cy5 dye (**4.20**) in the presence of a base (Scheme 4.2). The fluorophores were chosen based on different criteria. Both dyes are commercially available at low to moderate costs and filter sets matching the excitation and emission wavelengths of these dyes are available for most instruments used for fluorescence detection. A favorable feature of the 5-TAMRA dye is its high photostability,[25]

whereas the sulfo-Cy5 dye is excitable at higher wavelengths (> 600 nm) which is advantageous with respect to an application at cells and tissues. Moreover, both dyes contain a negatively charged acid function conveying increased polarity and solubility.

Scheme 4.2. Synthesis of the fluorescently labeled peptides **4.19** and **4.21**.



Reagents and conditions: (a) DIPEA, DMF/NMP 4:1 v/v, rt, 1 h; 40% (**4.19**), 30% (**4.21**).

4.2.2 Chemical and proteolytic stability

The chemical stability of the fluorescently labeled ligands **4.19** and **4.21** was studied in phosphate-buffered saline (PBS, pH = 7.4) at room temperature over 48 h. Both compounds showed excellent stability (Figure A4.2 and Figure A4.3, Appendix). In the case of **4.21**, adsorption of the fluorescent ligand to the vessel (visible by eye) resulted in a moderate decrease (ca. 33%) in peptide concentration over 48 h (cf. Figure A4.3, Appendix). The adsorption as the cause for the decrease in concentration is also supported by the fact that no additional peak

was observed in the RP-HPLC chromatograms. The proteolytic stability of **4.15**, **4.17a**, **4.19**, and **4.21** was investigated in human plasma at 37 °C over 48 h. **1.3**, studied as a control, showed very low plasma stability (complete degradation after 30 min, Table 4.1). The NT(8-13) analog **4.15**, being N-terminally methylated and containing TMSAla instead of Leu^{13} (cf. Scheme 4.1B), showed moderate proteolytic stability (ca. 50% intact peptide after 48 h). In contrast, the labeling precursor **4.17a** and the fluorescent ligands **4.19** and **4.21**, containing β,β-dimethyl-L-Tyr in position 11, exhibited high proteolytic stability (Table 4.1). The apparent low degradation of peptide **4.21** (10% after 48 h) can be attributed to the adsorption of **4.21** to the vessel material as also observed in the case of stability studies in PBS (discussed above). These results show that replacement of Leu^{13} by TMSAla as the only C-terminal modification of the NT(8-13) sequence is not sufficient to achieve high proteolytic stability. Consequently, the results confirm that N-terminal methylation in combination with the incorporation of β,β-dimethyl-Tyr in position 11 is highly effective in terms of proteolytic stability of NT(8-13) derivatives.

Table 4.1. Stabilities of **1.3**, **4.15**, **4.17a**, **4.19**, and **4.21** in human plasma/PBS 1:2 v/v (37 °C).

compd.	% intact compound in plasma after the specified incubation times[a]					
	10 min	30 min	2 h	6 h	24 h	48 h
1.3	17 ± 1	< 1	< 1	< 1	n.d.	n.d.
4.15	n.d.	n.d.	83 ± 1	80 ± 1	65 ± 1	47 ± 1
4.17a	n.d.	n.d.	> 99	> 99	> 99	> 99
4.19	n.d.	n.d.	> 99	95 ± 2	93 ± 2	97 ± 1
4.21	n.d.	n.d.	97 ± 1	93 ± 1	90 ± 1	90 ± 2

[a]The initial concentration of the peptide in human plasma/PBS (1:2 v/v) was 80 µM. Data represent mean values ± SEM from two or three independent experiments (SEM not given when no degradation was observed).

4.2.3 Neurotensin receptor binding studied in radiochemical competition binding assays

NTS_1R binding affinities were determined in a radioligand competition binding assay as reported[12] using intact HT-29 colon carcinoma cells which express NTS_1R endogenously, but no NTS_2R.[12] The tritium-labeled NT(8-13) analog [^{3}H]UR-MK300 ([^{3}H]**1.7**, structure shown in Figure A4.4, Appendix) was used as radioligand. The obtained K_i values of **2.2**, **4.14**-**4.17b**, **4.19**, and **4.21** are presented in Table 4.2 and competition binding curves are shown in Figure A4.5A (Appendix). The previously described peptide **2.2**, containing two lysines, exhibited high NTS_1R binding affinity with a K_i value of 0.055 nM (Table 4.2) confirming the reported high binding affinity (IC_{50} = 0.02 nM[19]). Peptide **4.14**, containing TMSAla instead of Leu^{13} as the only structural difference compared to **1.3**, displayed similar binding affinity as **2.2**. This

confirmed the former observation that replacement of Arg^8 and Arg^9 by Lys^8 and Lys^9 does not affect NTS_1R binding.[20,26-29] N-methylation of **4.14** (peptide **4.15**) had no impact on NTS_1R binding as shown in Table 4.2. This finding is consistent with a previously reported N^{α}-methyl scan of **1.3**.[22] Replacement of Tyr^{11} by β,β-dimethyl-L-Tyr in **4.15**, resulting in **4.16a**, did also not affect binding to the NTS_1R (K_i of **4.16a**: 0.050 nM). Likewise, replacement of Arg^8 in **4.16a** by the amino-functionalized N^{ω}-carbamoylated arginine (peptide **4.17a**) did not influence the NTS_1R binding affinity (K_i of **4.17a**: 0.055 nM). As stated before, the peptides containing β,β-dimethyl-D-Tyr (**4.16b** and **4.17b**) showed markedly lower binding affinities (Table 4.2). The fluorescently labeled peptides **4.19** and **4.21**, bearing a bulky fluorescent dye at the side chain of Arg^8, exhibited only slightly higher K_i values (K_i = 0.14 and 0.094 nM, respectively) compared to the precursor **4.17a**. This confirms that conjugation of NT(8-13) derivatives via an N^{ω}-carbamoylated arginine, incorporated in position 8, is a favorable approach in terms of preserving high NTS_1R binding affinity. As a consequence, **4.19** and **4.21** bind to the NTS_1R with similar binding affinity as **1.3** (K_i = 0.093 nM).

In addition to NTS_1R binding, NTS_2R binding affinities were determined for the fluorescent ligands **4.19** and **4.21** in a radiochemical competition binding assay using membranes of HEK293T-hNTS_2R cells[21] and [^{3}H]**1.7** as radioligand (competition binding curves see Figure A4.5B, Appendix). With pK_i values of 9.11 and 9.14, respectively, both probes bind with slightly lower affinity to NTS_2R than to NTS_1R (Table 4.2).

4.2.4 NTS_1R agonism

The agonistic potencies of **1.3** and the fluorescently labeled NTS_1R ligands **4.19** and **4.21** were determined in a Fura-2 Ca^{2+} assay using HT-29 cells (concentration-response curves shown in Figure A4.6, Appendix). Peptides **4.19** and **4.21** proved to be full agonists with potencies comparable to that of **1.3** (Table 4.2). The pEC_{50} values were consistently circa one log unit lower than the corresponding pK_i values, which can be explained by the non-equilibrium conditions in the case of the Fura-2 Ca^{2+} assay: as the signal occurs immediately after addition of the agonist, the receptor occupancy at the time of the readout is considerably lower than the hypothetical receptor occupancy that would be achieved in equilibrium for the respective concentrations of receptor and receptor ligand. An impairment of the optical readout of the assay by the 5-TAMRA label, whose absorption spectrum (λ_{max} = 555-558 nm, cf. Table 4.3) largely overlaps with the emission spectrum of the Fura-2 Ca^{2+} complex (λ_{max} = 505 nm[30]), can be excluded based on the results of previous studies using a 5-TAMRA dummy ligand.[31]

Table 4.2. NTS_1R binding affinities and agonistic potencies and NTS_2R binding affinities of **4.19** and **4.21**.

compd.	NTS_1R		NTS_2R
	$pK_i \pm SEM / K_i$ [nM][a]	$pEC_{50} \pm SEM / EC_{50}$ [nM][b]	$pK_i \pm SEM / K_i$ [nM][c]
1.3	10.03 ± 0.03 / 0.093	8.96 ± 0.07 / 1.2	9.23[16] / 0.62[16]
2.2	10.28 ± 0.06 / 0.055	n.d.	n.d.
4.14	10.10 ± 0.02 / 0.079	n.d.	n.d.
4.15	10.43 ± 0.1 / 0.041	n.d.	n.d.
4.16a	10.30 ± 0.05 / 0.050	n.d.	n.d.
4.16b	7.91 ± 0.06 / 12	n.d.	n.d.
4.17a	10.39 ± 0.2 / 0.055	n.d.	n.d.
4.17b	8.42 ± 0.1 / 4.2	n.d.	n.d.
4.19	9.86 ± 0.09 / 0.14	9.00 ± 0.09 / 1.1	9.11 ± 0.02 / 0.78
4.21	10.04 ± 0.06 / 0.094	8.89 ± 0.09 / 1.4	9.14 ± 0.07 / 0.75

[a]Determined by radioligand competition binding with [^{3}H]**1.7**[12] at HT-29 colon carcinoma cells. [b]Determined in a Fura-2 Ca^{2+} assay at HT-29 cells. [c]Determined by radioligand competition binding with [^{3}H]**1.7**[12] at membranes of HEK293T-hNTS_1R cells. Data represent mean values ± SEM (pK_i, pEC_{50}) or mean values (K_i, EC_{50}) from at least three independent experiments performed in triplicate. n.d. not determined.

4.2.5 Photophysical characterization

The absorption of the first electronic transition and the emission spectrum of both compounds are their corresponding mirror images indicating a rather constrained molecular scaffold both in the electronic ground and first excited state (Figure A4.7A and A4.7C, Appendix). However, in the presence of BSA (1% w/w) the spectral distributions shift. In the case of **4.19**, the spectra blue-shift, while in the case of **4.21** the spectra red-shift. This already indicates an interaction with the protein's surface. Further, while in the case of **4.21** the excitation spectrum always resembles the corresponding absorption spectrum with or without BSA, the excitation spectrum of **4.19** recorded in the absence of BSA already shows a blueshift compared to the corresponding absorption spectrum. This indicates a significant structural rearrangement of the molecular framework in the excited state compared to the ground state. The impact of BSA in form of interactions to the chromophore is further manifested in altered fluorescence quantum yields and lifetimes (Table 4.3). Each chromophoric system shows a prolonged excited singlet state lifetime in the presence of BSA. To note, the emission decay is biexponential and the second lifetime is of small amplitude (cf. Figure A4.7B and A4.7D, Appendix), which may arise either from small impurities or an equilibrium between different conformers. Interestingly, while **4.19** shows a decreased fluorescence quantum yield, **4.21** shows an increased fluorescence quantum yield. In the case of **4.19**, this may indicate a deactivation process

induced by the interaction with the protein. An electron transfer from a redox active amino acid to the chromophore or the hindrance for structural changes in the excited state, which could result in a brighter emissive configuration, may represent two potential explanations. This will be addressed by transient absorption spectroscopy and presented elsewhere. In the case of **4.21**, the emissive character of the electronically excited chromophore is apparently inversely effected. Here, the data suggest a situation in which, in the excited state, the molecule undergoes structural changes forming a less emissive configuration that is hindered when attached to the protein's surface. Also, in this case the transient absorption will inform on the mechanistic scenario in more detail, which will be presented elsewhere. The observed changes in quantum yield are in accordance with reported studies on 5-TAMRA-labeled and sulfo-Cy5-labeled fluorescent GPCR ligands.[13,31-33]

Table 4.3. Maxima of the absorption, excitation, and emission spectra, fluorescence lifetimes and fluorescence quantum yields of **4.19** and **4.21** in PBS in the presence or absence of BSA (1% w/w).

compd.	λ_{abs} / λ_{ex} / λ_{em} [nm] | Δ[eV][a]		τ_{fl} [ns][b]		Φ (%)	
	PBS	PBS + 1% BSA	PBS	PBS + 1% BSA	PBS	PBS + 1% BSA
4.19	558 / 552 / 583 | 0.12	555 / 553 / 578 | 0.097	2.7	3.5	41	34
4.21	647 / 648 / 665 | 0.049	650 / 651 / 669 | 0.051	1.4	2.7	29	39

[a]Calculated based on λ_{ex} and λ_{em}. [b]Only the main component of a bi-exponential fit with a contribution > 90% is presented.

4.2.6 Investigation of NTS_1R binding of 4.19 and 4.21 by flow cytometry

The flow cytometric binding experiments were carried out at 23 °C using a BD FACSCanto II cytometer equipped with an argon laser (488 nm) and a red laser (640 nm). Saturation binding experiments with **4.19** and **4.21** were performed at live human HT-29 colon carcinoma cells and stably transfected CHO-hNTS_1R cells. For both ligands, specific binding was saturable (Figure 4.3A; Figure A4.8, Appendix), however, the apparent K_d values determined at CHO-hNTS_1R cells were higher (10-20-fold) compared to the apparent K_d values obtained from HT-29 cells (Table 4.4) which were in good agreement with the K_i values determined by competition binding with [^{3}H]**1.7** at HT-29 cells (Table 4.2). The higher K_d values determined at CHO-hNTS_1R cells can be explained by the markedly higher NTS_1R expression in CHO-hNTS_1R cells (ca. 300,000 receptors/cell) compared to HT-29 cells (ca. 45,000 receptors/cell).[12] As the studied ligands **4.19** and **4.21** show subnanomolar binding affinities, a high receptor concentration in saturation binding experiments leads to ligand depletion and consequently results in higher apparent K_d values.[34] This effect can be reduced by using less

cells in the experiment. Typically, for this kind of flow cytometric analysis, cell densities ≥ 100,000 cells/mL are used to obtain a reasonable number of gated events (≥ 2,000), required for the calculation of representative fluorescence intensity mean values, within a reasonable measuring time. To explore the influence of the receptor concentration and associated to this the effect of ligand depletion on the discrepancy between the apparent K_d and the true K_d, additional saturation binding experiments were performed with CHO-hNTS$_1$R cells using a considerably lower cell density of 15,000 cells/mL. These conditions resulted in 200-300 gated events, just high enough to enable a statistically reasonable data analysis. The apparent K_d values of **4.19** and **4.21** obtained from these saturation binding experiments were markedly lower (> factor 10) than the apparent K_d values obtained from saturation binding studies using 150,000 cells/mL (Table 4.4, Figure A4.8, Appendix) and similar to the K_d values determined at HT-29 cells. The apparent K_d values determined at low receptor concentrations (HT-29 cells, CHO-hNTS$_1$R cells at a density of 15,000 cells/mL) should better resemble the true K_d, although the latter is potentially even lower than the experimentally determined dissociation constants.

Noteworthy, the excitation laser line (640 nm) used for the excitation of the sulfo-Cy5 dye in **4.21** is close to its absorption maximum (647/650 nm, see Table 4.3). In contrast, the excitation of the 5-TAMRA label in **4.19** by the 488 nm argon laser is not ideal with respect to its absorption maximum (558/555 nm, Table 4.3). This is also reflected by the markedly lower B_{max} values obtained from saturation binding experiments with **4.19** compared to **4.21** (Figure 4.3A).

Kinetic binding studies, performed at HT-29 cells, revealed notable differences between **4.19** and **4.21**. While **4.21** showed a monophasic association, the 5-TAMRA-labeled ligand **4.19** displayed a clear biphasic association (two-phase association favored over one-phase association according to the *F*-test, $P < 0.005$, GraphPad Prism 5) (Figure 4.3B). The proportion of the fast and slow association phase was 42:58 (based on the fit to the data shown in Figure 4.3B). The observed association rate constants k_{obs} and the calculated association rate constants k_{on} are shown in Table 4.4. The $k_{on(bi,slow)}$ value, calculated from $k_{obs(bi,slow)}$, k_{off}, and the concentration of **4.19** used for the association studies, was negative. This could be due to internalization of ligand-receptor complex during the association process (cf. Figure 4.6), but could also be attributed to the low ratios of total over unspecific binding in the case of **4.19** particularly during the initial phase of the association (discussed in more detail below). As the $k_{on(bi,slow)}$ was negative, precluding a calculation of the kinetically derived dissociation constant K_d(kin), the association data of **4.19** were additionally fitted with a monophasic exponential fit

covering the whole association process. This enabled the calculation of a K_d(kin) value which comprises the entire association (see below).

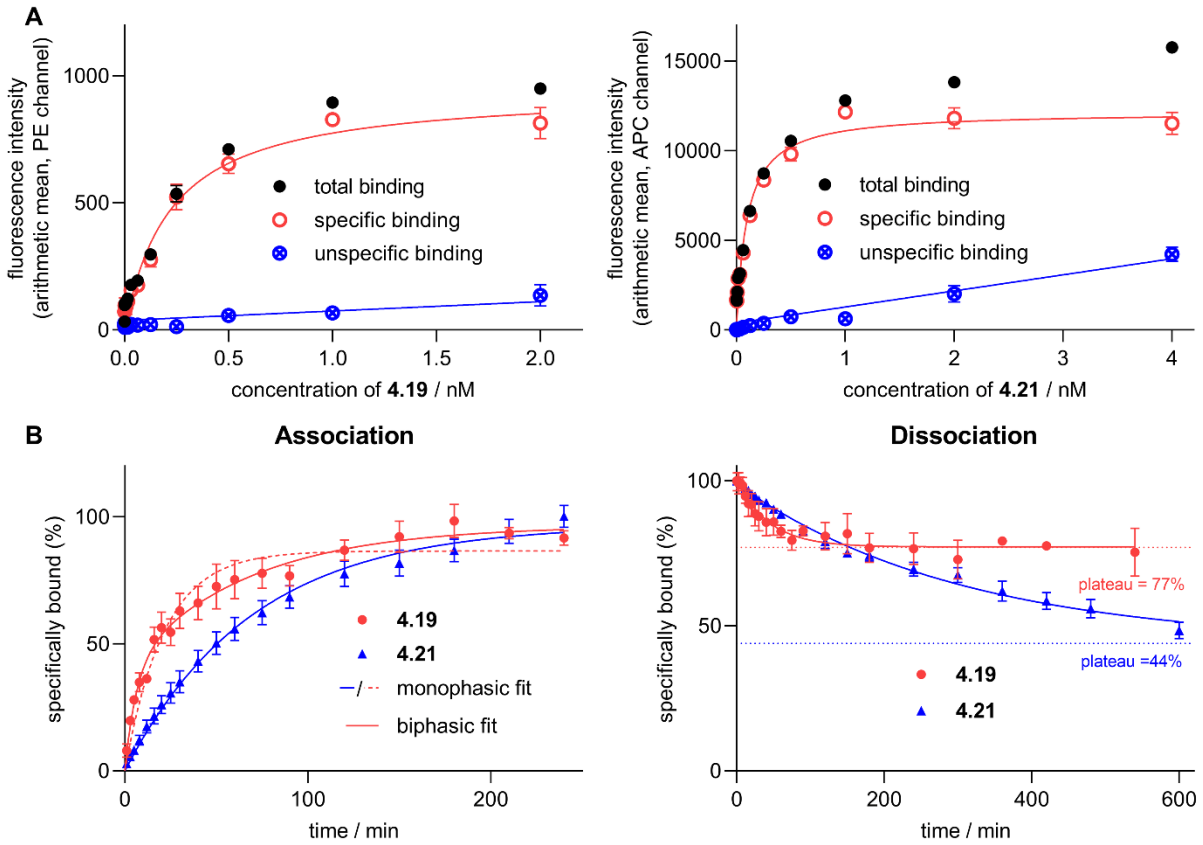


Figure 4.3. NTS$_1$R equilibrium binding and kinetic studies of **4.19** and **4.21** determined by flow cytometry at intact HT-29 cells. (A) Representative binding isotherms (specific binding, open symbols) of **4.19** and **4.21** obtained from saturation binding experiments (incubation: 120 min at 23 °C). Unspecific binding was determined in the presence of 1 µM **1.3**. K_d values are presented in Table 4.4. Data represent mean values ± SEM (total and unspecific binding) or calculated values ± propagated error (specific binding) from a representative experiment performed in triplicate. (B) Association and dissociation of **4.19** and **4.21** studied at 23 °C. Concentrations of **4.19** and **4.21** used for the association: 1 nM and 0.1 nM, respectively; concentrations of **4.19** and **4.21** used for the preincubation period (**4.19**: 120 min, **4.21**: 180 min) of dissociation experiments: 1 nM and 0.25 nM, respectively. Dissociation and association rate constants are presented in Table 4.4. Data represent mean values ± SEM from at least three independent experiments performed in triplicate.

The fact that one ligand shows a monophasic and the other ligand a biphasic association for the same cellular system suggests that the biphasic association cannot be explained by the existence of two subpopulations of NTS$_1$R (e.g., one coupled to and the other uncoupled from G-protein). It should be mentioned that for the association studies of **4.19**, a fluorescent ligand concentration corresponding to 9-fold the K_d value of **4.19** had to be used since with lower ligand concentrations, correlating with lower receptor occupancies, the difference between total und unspecific binding was too low for a reliable data analysis. This was particularly due to the aforementioned mismatch of the excitation wavelength and the absorption maximum of the 5-

TAMRA dye in **4.19**. In contrast, for association studies with **4.21**, a ligand concentration corresponding to 3-fold the K_d value could be used because of the optimal excitation of the sulfo-Cy5 dye in **4.21** with the red laser (640 nm) resulting in the detection of high fluorescence intensities. It is noteworthy that, in the case of experiments with **4.19**, the excitation with 488 nm light gave a high autofluorescence of the cells which also affected data analysis. The excitation of the cells with 640 nm (used for **4.21**) resulted in very low autofluorescence. The different ligand concentrations used for the association experiments might be the reason for the observed differences in the association kinetics of **4.19** and **4.21** (biphasic vs. monophasic). Moreover, it could be explained by the internalization of ligand-receptor complex (as confirmed by confocal microscopy, see below), occurring already during the association process. Upon internalization, ligand-dependent differences could occur with respect to changes of fluorescent properties in the cell interior and retrafficking of ligand-receptor complex or free receptor to the plasma membrane.

Dissociation studies at HT-29 cells, initiated by adding an excess of **1.3**, gave monophasic dissociation curves revealing an incomplete dissociation (plateau significantly higher than zero, $P < 0.05$, t-test) as also previously reported for fluorescently labeled NT(8-13) derivatives.[13,16] The plateau values amounted to 77% (**4.19**) and 44% (**4.21**). This can be explained by the NTS_1R agonism of **19** and **21** (cf. Figure A4.6, Appendix) meaning that the ligand-receptor complex is internalized, potentially followed by intracellular dissociation of the fluorescent ligand from the receptor. The k_{off} values of **4.19** and **4.21** differed by a factor of 7 (k_{off} = 0.021 min^{-1} vs. 0.0033 min^{-1}, see Table 4.4). Compared to previously described fluorescently labeled NT(8-13) derivatives, **4.19** and **4.21** show a slower dissociation from NTS_1R which is favorable for imaging of NTS_1R expression in cells or tissues. The kinetically derived dissociation constants K_d(kin) (Table 4.4) were calculated according to $K_d(kin) = k_{off}/k_{on}$. In the case of **4.19**, the K_d(kin) was calculated from $k_{on,mono}$ and $k_{on(bi,fast)}$ yielding K_d(kin) values of 1.2 and 0.13 nM, respectively. The value of 0.13 nM is in excellent agreement with the K_d obtained from saturation binding (Table 4.4). Likewise, the K_d(kin) value obtained for **4.21** is in good agreement with the K_d from saturation binding studies (0.030 nM vs. 0.046 nM), indicating a binding process largely following the law of mass action. Yet, the determined kinetic parameters of **4.19** and **4.21** must be interpreted with care since both ligands induce receptor endocytosis (cf. Figure 4.6 and 4.7) and show an incomplete dissociation. Moreover, as discussed before, flow cytometric kinetic studies with the 5-TAMRA-labeled ligand **4.19** were compromised by the non-optimal excitation and higher autofluorescence compared to **4.21**.

Table 4.4. NTS_1R binding data of **4.19** and **4.21** determined by flow cytometry at HT-29 and CHO-$hNTS_1R$ cells.

compd.	saturation binding		binding kinetics (HT-29 cells)			
	apparent K_d [nM]					
	HT-29 cells	CHO-$hNTS_1R$ cells	k_{obs} [min^{-1}]	k_{on} [$nM^{-1}min^{-1}$][a]	k_{off} [min^{-1}]	K_d(kin) [nM][b]
4.19	0.11 ± 0.04	1.2 ± 0.3[c] 0.034 ± 0.009[d]	$k_{obs,mono}$ = 0.039 ± 0.005 $k_{obs(bi,fast)}$ = 0.19 ± 0.03 $k_{obs(bi,slow)}$ = 0.016 ± 0.003	$k_{on,mono}$ = 0.017 ± 0.01 $k_{on(bi,fast)}$ = 0.16 ± 0.04 $k_{on(bi,slow)}$ = -0.0055 ± 0.01	0.021 ± 0.007	1.2 ± 1.3 0.13 ± 0.07 n.a.
4.21	0.046 ± 0.02	0.88 ± 0.1[c] 0.022 ± 0.005[d]	0.014 ± 0.002	0.11 ± 0.02	0.0033 ± 0.0002	0.030 ± 0.007

[a]Association rate constant ± propagated error calculated from k_{off}, k_{obs}, and the ligand concentration used for the association experiments. [b]Kinetically derived dissociation constant ± propagated error calculated from k_{off} and k_{on} values. K_d, k_{obs}, and k_{off} values represent mean values ± SEM from at least three independent experiments; k_{on} and K_d(kin) values represent calculated values ± propagated error. [c]Experiments performed with a cell density of 150,000 cells/mL. [d]Experiments performed with a cell density of 15,000 cells/mL. n.a. not applicable

To investigate the suitability of **4.19** and **4.21** to serve as probes for the determination of NTS_1R binding affinities of unlabeled NTS_1R ligands, the K_i values of reported NTS_1R ligands (**1.3**, SR48692 (**1.4**), SR142948 (**1.5**), UR-MK300 (**1.7**)) were determined in flow cytometric competition binding studies at HT-29 cells using **4.19** or **4.21** as labeled probe (displacement curves shown in Figure 4.4).

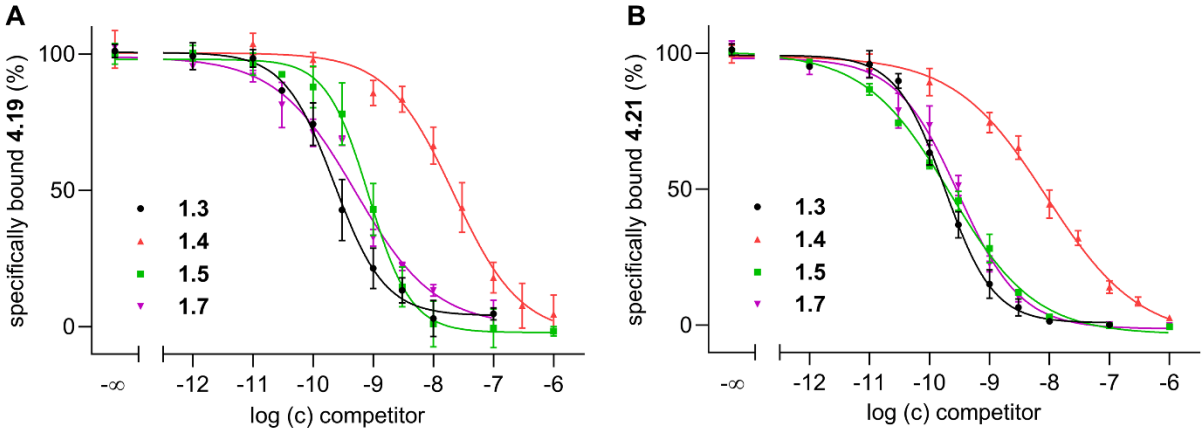


Figure 4.4. Displacement curves from flow cytometric competition binding studies using **4.19** (A) or **4.21** (B) as a labeled probe and **1.3**, **1.4**, **1.5**, or **1.7** as competitors. Experiments were performed at intact HT-29 cells at 23 °C. The concentrations of **4.19** and **4.21** were 0.3 nM and 0.1 nM, respectively. Incubation times: 120 min (A) and 180 min (B). Data represent mean values ± SEM from at least three individual experiments performed in triplicate.

Although the dissociation kinetics of **4.19** and **4.21**, indicating long-lasting binding, is not ideal in terms of competition binding experiments, the pK_i values obtained for the reference ligands were generally in good agreement with reported data (Table 4.5).

Table 4.5. NTS_1R binding affinities of reported NTS_1R ligands determined by flow cytometry at HT-29 cells using **4.19** and **4.21** as labeled probes.

compd.	pK_i		
	4.19	**4.21**	literature
1.3	10.20 ± 0.2	10.25 ± 0.09	9.85[12], 9.62[28], 9.54[35], 9.00[18], 9.55[16], 10.09[16]
1.4	8.25 ± 0.1	8.49 ± 0.2	8.07[36]
1.5	9.70 ± 0.1	10.14 ± 0.08	8.96[12], 9.24[16], 9.74[16], 9.00[37]
1.7	9.85 ± 0.1	10.05 ± 0.1	9.33[12]

Reported K_i values were converted to pK_i values. Data represent mean values ± SEM from at least three individual experiments performed in triplicate.

The Hill coefficients of the displacement curves (4-parameter logistic fit) were not significantly different from -1 (two-tailed *t*-test, $P > 0.05$) except for **1.4** and **1.5** studied with **4.21** (Hill

coefficients: -0.63 ± 0.02 and -0.55 ± 0.06, respectively; mean values ± SEM). The low slope factors might be attributed to the (pseudo)irreversible binding of **4.21** (cf. Figure 4.3B) or to the internalization and putative externalization of NTS_1R induced by the fluorescent agonists, potentially resulting in a retarded displacement of fluorescent ligand. However, for the other competitors (**1.3**, **1.7**) and for all competitors studied with **4.19**, also showing (pseudo)irreversible binding, the Hill coefficients were not significantly lower than unity, which contradicts the aforementioned hypothesis. Since slope factors different from unity could also arise from the existence of ligand-dependent multiple conformational receptor states,[38,39] the low slopes observed for **1.4** and **1.5** could be caused by the preference of different receptor conformations of the used NTS_1R ligands: whereas the agonist **4.21** prefers the active conformation, the antagonists do not discriminate between receptor states or even prefer the inactive conformation.[40,41]

4.2.7 Cooperativity between 4.21 and the allosteric NTS_1R modulator SBI-553

In recent years, several allosteric NTS_1R modulators, targeting an intracellular binding site, have been reported.[42-45] In vivo studies suggested that allosteric potentiators of NTS_1R binding of neurotensin can potentially be used as therapeutics for the treatment of pain.[45] A prominent example is the positive allosteric modulator SBI-553 (structure shown in Figure 4.5A) which was demonstrated to potentiate binding of radiolabeled neurotensin or NT(8-13).[42,44] To explore if SBI-553 also enhances binding of fluorescently labeled NT(8-13) derivatives such as **4.21**, the effect of SBI-553 on NTS_1R binding of **4.21** was studied by flow cytometry using HT-29 tumor cells. For these experiments, **4.21** was used at a concentration of 0.01 nM, corresponding to approximately one fifth of its K_d, and these samples were titrated with SBI-553. As previously observed in the radiochemical assays, SBI-553 clearly enhanced NTS_1R binding of **4.21** (Figure 4.5B). However, in contrast to the reported studies, a biphasic CEC of SBI-553 was obtained, yielding a pEC_{50}(high) of 10.37 and a pEC_{50}(low) of 7.28. The latter is in excellent agreement with the reported pEC_{50} value of SBI-553 of 7.30[44] and with the described EC_{50} value of 140 nM.[42] To note, in contrast to the pEC_{50}(low), the pEC_{50}(high) was not well reproducible in the individual experiments which is reflected by the high SEM of 0.40 (cf. Figure 4.5). The E_{max} observed for SBI-553 (E_{max} = 88%) was lower than the reported E_{max} of 140%[42] and 242%.[44]

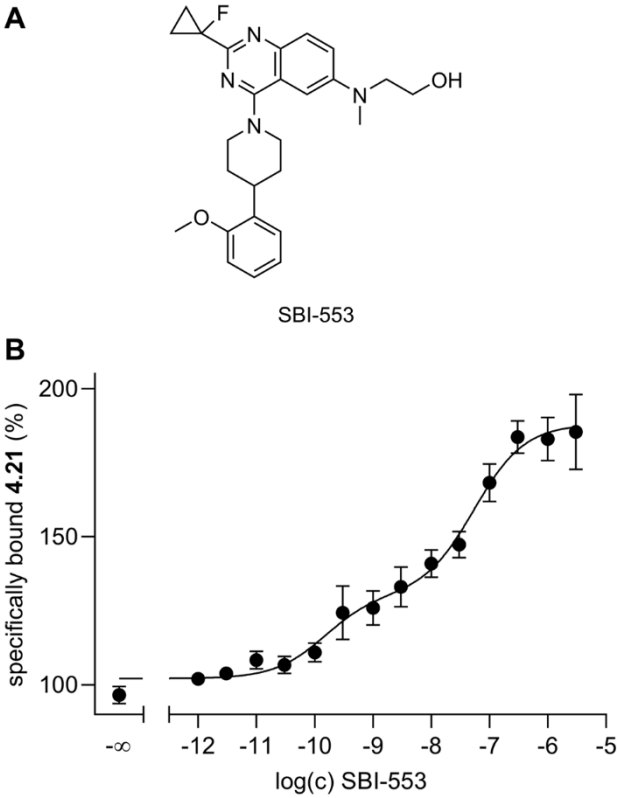


Figure 4.5. (A) Structure of the allosteric NTS_1R modulator SBI-553. (B) Effect of SBI-553 on NTS_1R binding of the fluorescent NT(8-13) derivative **4.21** determined in a flow cytometric binding assay performed with intact HT-29 cells at 23 °C. Cells were pre-incubated with SBI-553 for 30 min prior to the addition of **4.21** and continued incubation for 180 min. SBI-553 enhanced binding of **21** in a biphasic manner (fraction high/low: 0.33/0.67). 100% specifically bound **21** corresponds to specific binding of **21** in the absence of SBI-553. Data represent mean values ± SEM from six individual experiments performed in triplicate. pEC_{50}(high) = 10.37 ± 0.40. pEC_{50}(low) = 7.28 ± 0.16. E_{max} = 88 ± 8% (difference between lower and upper plateau).

It is a matter of speculation why SBI-553 shows a biphasic CEC when studied with the fluorescent ligand **4.21**. The major differences compared to the reported radiochemical assays[42,44] are the type of labeled ligand (radiolabeled vs. fluorescently labeled), the use of intact cells (in contrast to membrane preparations in the reported studies), and a measurement under equilibrium conditions in the present study (flow cytometry). Supposedly, the biphasic course of the CEC of SBI-553 can be attributed to one or more of these differences in the technical setup of the binding assays. The elucidation of the underlying mechanisms requires further studies. Likewise, the lower E_{max} compared to the reported E_{max} values[42,44] could also arise from the different assay parameters.

4.2.8 Confocal Microscopy

Binding of **4.19** and **4.21** to both HT-29 cells, natively expressing NTS_1R, and stably transfected CHO-hNTS_1R cells, overexpressing the NTS_1R, was studied by confocal microscopy at 22 °C using a confocal laser scanning microscope. In all cases, a marked difference between total und unspecific binding was found (Figure 4.6 and 4.7; Figure A4.9 and A4.10, Appendix), showing that the NTS_1R expression can be visualized with both fluorescent ligands, even at low receptor expression levels (HT-29 cells, Figure 4.6 and 4.7).

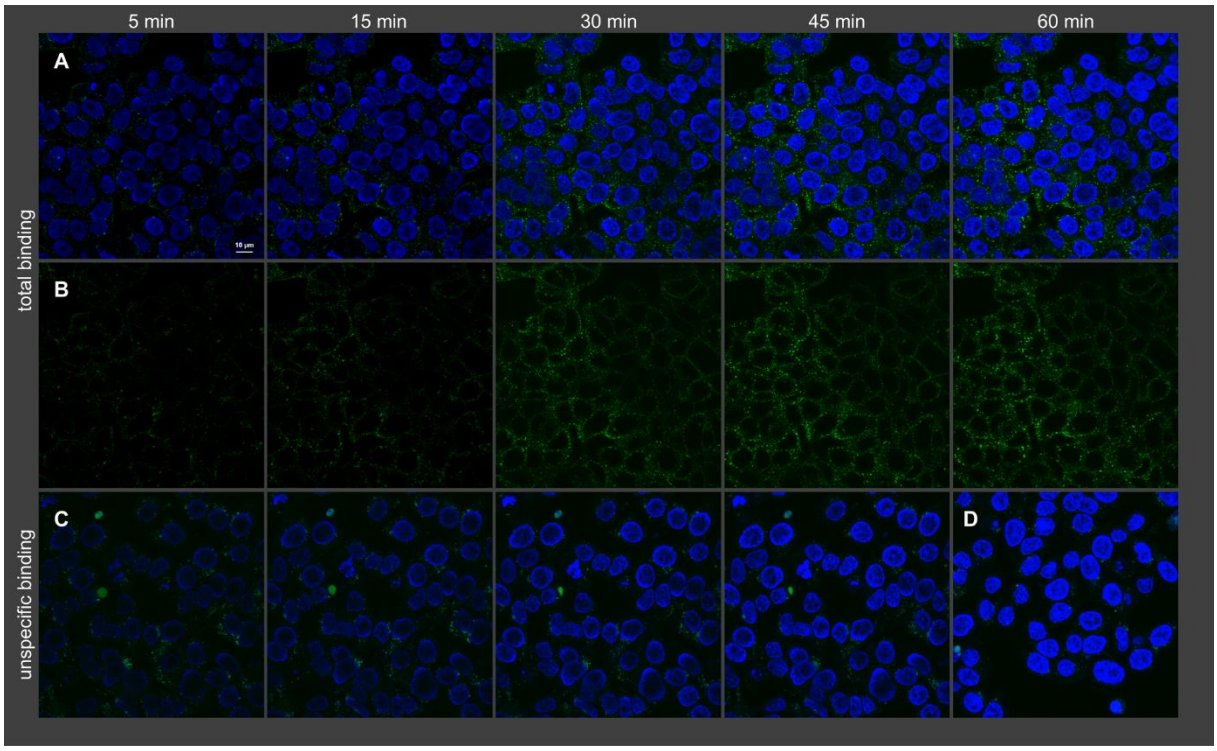


Figure 4.6. Visualization of binding of **4.19** (2 nM) to intact HT-29 cells (temperature: 22 °C) by confocal microscopy. Shown is total binding (A, B), unspecific binding (C), and autofluorescence (D). Nuclei were stained with Hoechst H33342 (2 µg/mL). (A) Merged fluorescence of **4.19** (green) and nuclei (blue). (B) Fluorescence of **4.19**, without nuclei. (C) Merged fluorescence of **4.19** and nuclei acquired in the presence of 1 µM **1.3**.

The excitation with 561 nm (**4.19**) resulted in higher autofluorescence compared to an excitation with 633 nm (**4.21**). This was only observable when using HT-29 cells (cf. Figure 4.6D and 4.7D) because the lower receptor expression in these cells compared to CHO-hNTS_1R cells (cf. Figure A4.9D and A4.10D, Appendix) necessitates higher laser power and higher detector gain (see experimental section). As becomes obvious from Figure 4.6C and 4.7C, showing unspecific binding of **4.19** and **4.21**, respectively, the 5-TAMRA-labeled ligand **4.19** exhibited considerably higher unspecific binding compared to the sulfo-Cy5-labeled probe **4.21**.

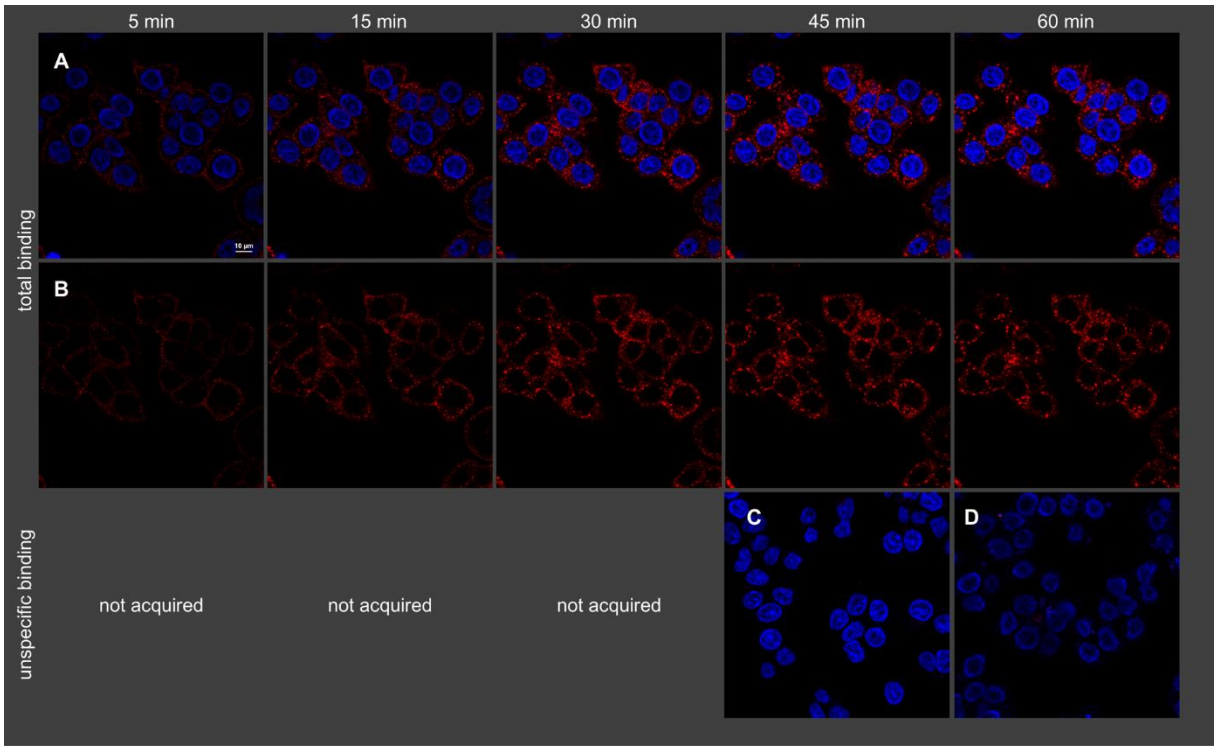


Figure 4.7. Visualization of binding of **4.21** (2 nM) to intact HT-29 cells (temperature: 22 °C) by confocal microscopy. Shown is total binding (A, B), unspecific binding (C), and autofluorescence (D). Nuclei were stained with Hoechst H33342 (2 µg/mL). (A) Merged fluorescence of **4.21** (red) and nuclei (blue). (B) Fluorescence of **4.21**, without nuclei. (C) Merged fluorescence of **4.21** and nuclei acquired in the presence of 1 µM **1.3**. Note: as no unspecific binding of **4.21** was observed, images of unspecific binding were only acquired after 45 min.

The microscopic studies with **4.19** and **4.21** revealed that the NTS_1R is internalized by endocytosis upon binding of the fluorescent ligands, occurring already during the association process (Figure 4.6 and 4.7; Figure A4.9 and A4.10, Appendix). The intracellular fluorescent ligand appeared to be located in vesicles. The internalization rates were estimated by defining an outer ROI, representing the total cellular fluorescence, and an inner ROI, representing the intracellular fluorescence, and quantification of fluorescence (Figure A4.11, Appendix). This analysis suggests that the fraction of internalized ligand only slightly increases over the studied time (5-60 min). This could be explained by recycling of NTS_1R to the plasma membrane after internalization as also suggested by previous studies of fluorescently labeled NT(8-13) analogs.[13] It should be noted that the determined internalization rate represents only a rough estimation due to the visual definition of the ROIs and potentially biased fluorescence intensities caused by changes in the photophysical properties of the fluorescent ligands in the intracellular environment.

4.2.9 Biomolecular imaging of NTS_1R expression in cells and tumor tissue

In another approach, the suitability of **4.19** and **4.21** to serve as probes for the investigation of NTS_1R expression in living cells and tumor tissue was studied using an Azure Sapphire Biomolecular Imager. For these experiments, HT-29 cells, showing a low NTS_1R expression,[12] and HT-29 tumors subcutaneously grown in nude mice were used. Saturation binding experiments with the sulfo-Cy5-labeled ligand **4.21** at adherent HT-29 cells gave satisfactory fluorescence images revealing low unspecific binding of **4.21** (Figure 4.8A). Based on the fluorescence intensities, saturation binding curves could be generated (Figure 4.8B) yielding a K_d value of 1.7 ± 1 nM (mean value ± SEM from four individual experiments performed in triplicate), which was higher than the K_d value obtained from flow cytometric saturation binding experiments at suspended HT-29 cells (cf. Table 4.4).

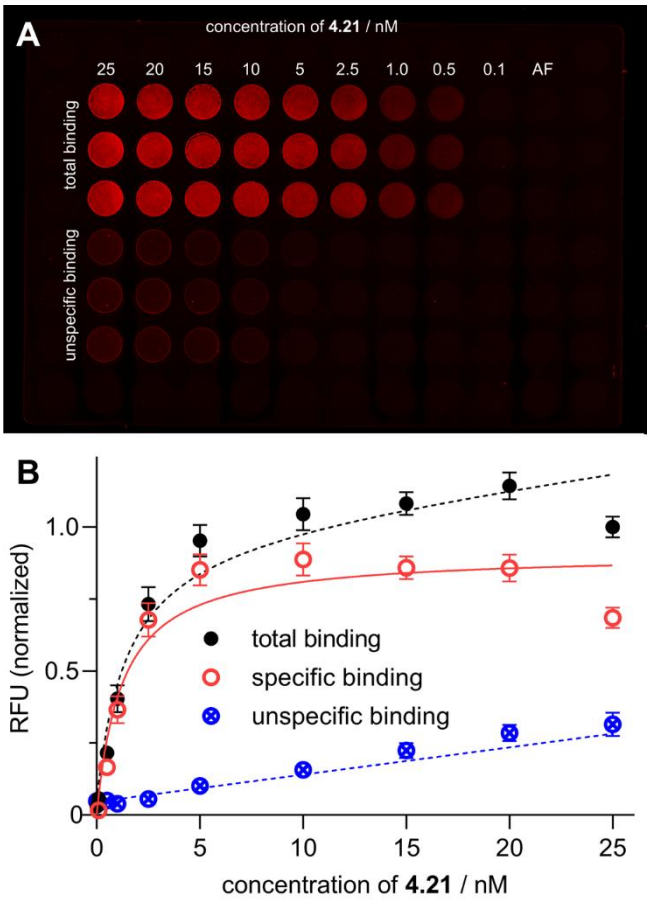


Figure 4.8. (A) Fluorescence image of a 96-well plate with adherent HT-29 cells acquired with an Azure Sapphire Biomolecular Imager (laser: 658 nm; pixel size: 20 µm) 2 h after incubation with **4.21** at rt. Unspecific binding was determined in the presence of **1.5** (1 µM). Shortly before image acquisition, cells were washed three times with cold buffer. (B) Fluorescent intensities from A plotted against the concentration of **4.21**. Specific binding was calculated from total and unspecific binding. Data represent means ± SEM (total and unspecific binding) or calculated values ± propagated error (specific binding) from four independent experiments performed in triplicates.

This discrepancy could be explained by a lower sensitivity of the biomolecular imaging technique compared to the flow cytometric analysis, meaning that cell-bound fluorescence is underestimated for low ligand concentrations in the case of biomolecular imaging. Moreover, a higher adsorption of **4.21** to the plate material (polystyrene) and the required washing step in the case of the biomolecular imaging could account for the higher K_d value compared to flow cytometric experiment which uses polypropylene plates and allows a measurement under equilibrium conditions (no washing required).

In contrast to **4.21**, the fluorescence images obtained from the same experiment performed with the 5-TAMRA-labeled ligand **4.19** were not suited for the determination of a K_d value due to high autofluorescence and high unspecific binding (Figure A4.12, Appendix).

Using the same biomolecular imager, visualization of NTS_1R expression in HT-29 tumors was explored by imaging 10 µm cryosections of tumor tissue after incubation with **4.19** and **4.21**. As observed for the saturation binding experiment with HT-29 cells, a detection of NTS_1R expression in the tumor was possible with the red-emitting probe **4.21** (Figure 4.9), but failed when using the 5-TAMRA-labeled ligand **4.19** as probe, mainly due to high autofluorescence relative to specific binding (Figure A4.13, Appendix). The regions of the tumor sections showing high unspecific binding of **4.21** (Figure 4.9) likely represent necrotic tumor tissue. It should be noted that the HT-29 tumors originated from a former research project and had been stored for more than eight years at -80 °C.[12] This long-term storage might have led to partial unfolding or degradation of the receptor protein.

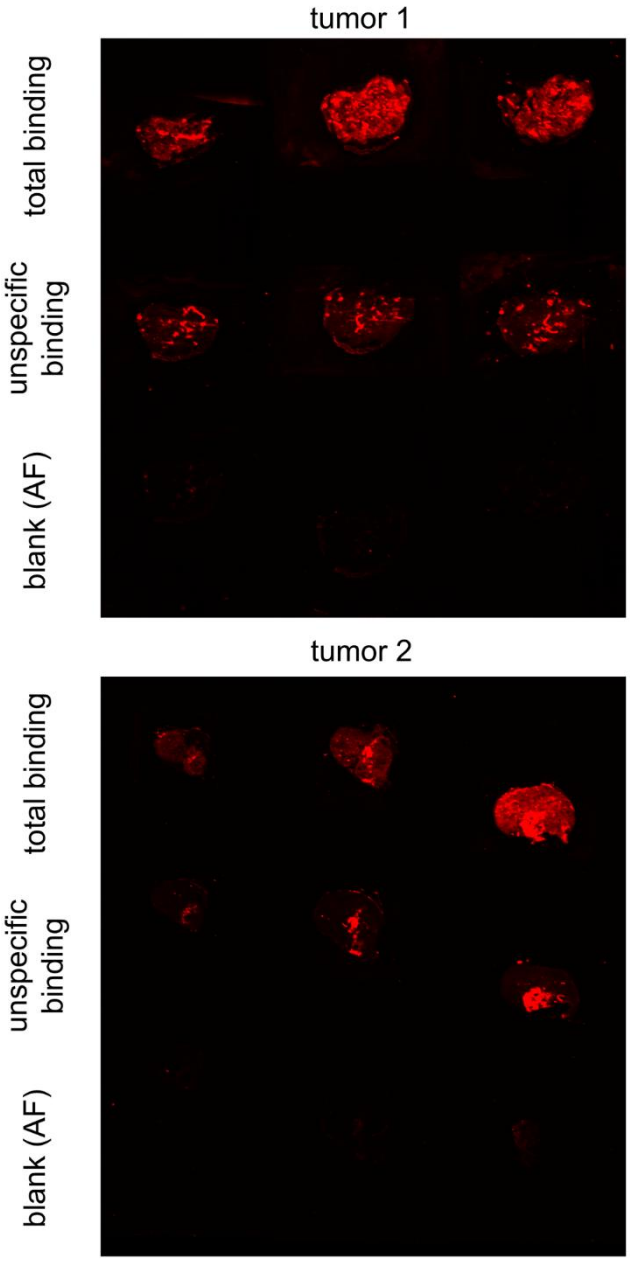


Figure 4.9. Fluorescence images of cryosections (10 µm) of a HT-29 tumor acquired after incubation with **4.21** (5 nM) at rt for 60 min with an Azure Sapphire FL Biomolecular Imager (laser: 658 nm; pixel size: 20 µm). Unspecific binding was determined in the presence of **1.5** (5 µM). Blank samples were incubated with neat buffer to determine background signals. Shortly before image acquisition, tumor sections were washed three times with cold buffer.

4.3 Conclusion

N-terminal methylation and the replacement of Arg^{8}, Tyr^{11}, and Leu^{13} in **1.3** by an amino-functionalized carbamoylated arginine, β,β-dimethyl-L-Tyr, and TMSAla, respectively, resulted in a NT(8-13) analog (**4.17a**, UR-FE083-I) that was used as a precursor for the preparation of a 5-TAMRA-labeled (**4.19**, UR-FE093) and a sulfo-Cy5-labeled (**4.21**, UR-FE094) NTS_1R ligand. Both fluorescent ligands show subnanomolar NTS_1R binding affinities with K_i values of 0.14 nM and 0.094 nM. The high binding affinity allows an application of these probes for flow cytometric binding assays using cells with low NTS_1R expression levels, which was demonstrated for non-transfected HT-29 cells natively expressing the NTS_1R.

The fluorescent peptides **4.19** and **4.21** display high in vitro proteolytic stability ($t_{1/2}$ >> 48 h, human plasma), which is favorable with respect to binding studies in living cells potentially featuring proteolytic activities. **4.19** and **4.21** are anticipated to exhibit also high stability in vivo since recently described NT(8-13)-derived PET ligands, containing an N-terminal methyl group and β,β-dimethyl-L-Tyr in position 11, showed high in vivo stability in mice.[21]

Fluorescence imaging of receptor expression in tissues represents an attractive alternative to autoradiography that requires radiolabeled receptor ligands. The present study reveals that the 5-TAMRA-labeled ligand **4.19** is not suited for fluorescence-based imaging of the NTS_1R expression in tumor tissue. This shows that the 5-TAMRA label, although characteristic of high photostability,[25] does not meet the demands for this kind of imaging in particular due to the excitation wavelength of < 600 nm, resulting in interfering autofluorescence. Contrarily, the near-infrared sulfo-Cy5-labeled probe **4.21**, differing from **4.19** only with respect to the fluorescent dye, turned out to be an excellent molecular tool for NTS_1R imaging in tumor tissue sections with high signal-to-noise ratio (used excitation: 658 nm), suggesting its application in tumor tissue screening procedures. As **4.19** and **4.21** display also high NTS_2R binding affinity, they can potentially serve as probes for NTS_2R binding studies using cellular systems solely expressing NTS_2R.

One of the major challenges with respect to the in vivo use of labeled peptidic NTS_1R ligands has been the development of tracers which exhibit both high proteolytic stability and high NTS_1R binding affinity (K_i < 1 nM). With the development of the amine-functionalized precursor **4.17a**, which can be conjugated to various molecular labels, the present study paved the way to the future synthesis and use of high-affinity and proteolytically stable probes for the NTS_1R with a functionality of choice.

4.4 Experimental section

4.4.1 General experimental conditions

Materials. The protected amino acids Fmoc-Tyr(tBu)-OH, Fmoc-Arg(Pbf)-OH, and glycine *tert*-butyl ester hydrochloride (**4.22**) were purchased from Carbolution Chemicals (St. Ingbert, Germany). Fmoc-N-Me-Arg(Pbf)-OH (**4.11**), Fmoc-Lys(Boc)-OH, Fmoc-Pro-OH, Fmoc-Ile-OH, and HBTU were from Merck (Darmstadt, Germany). Racemic Fmoc-β,β-dimethyl-Tyr(*t*Bu)-OH (**3.4**) and 2-ClTrt resin were obtained from Iris Biotech (Marktredwitz, Germany). HOBt, 7-methyl-1,5,7-triazabicyclo[4.4.0]dec-5-ene (MTBD), methyl-4-nitrobenzenesulfonate, 2-mercaptoethanol, and 1-methyl-D-Trp were from Sigma-Aldrich (Taufkirchen, Germany). Collidine, 2-nitrobenzenesulfonylchloride, 1,8-diazabicyclo [5.4.0] undec-7-ene (DBU), NMP and DMF for peptide synthesis, anhydrous DMF and NMP, dichloromethane, piperidine, and TFA were purchased from Fisher Scientific (Schwerte, Germany). (1*R*,2*R*,5*R*)-2-Hydroxy-3-pinanone (**4.23**) and (iodomethyl)trimethylsilane (**4.25**) were from TCI (Eschborn, Germany). DIPEA was obtained from ABCR (Karslruhe, Germany). Acetonitrile (HPLC gradient grade) was from VWR (Ismaning, Germany). **1.3** was synthesized via SPPS in-house. **1.4** and **1.5** were purchased from Tocris Bioscience (Bristol, UK). SBI-553 was from Biocat (Heidelberg, Germany). Bacitracin, HEPES, and bovine serum albumin (BSA) were obtained from Serva (Heidelberg, Germany). Fetal bovine serum (FBS) was purchased from Pan-Biotech (Aidenbach, Germany). Fura-2 AM and Pluronic F-127 were obtained from Calbiochem/Merck Biosciences (Beeston, UK). The radioligand [^{3}H]**1.7** (molar activity: 2.41 TBq/mmol) and its unlabeled analog **1.7** were prepared according to a described procedure.[12] Compounds **3.1**[12] and **4.10**[23] were prepared according to the reported procedures. 5-TAMRA succinimidyl ester (**4.18**) was purchased from Carl Roth (Karlsruhe, Germany). Sulfo-Cyanine5 NHS ester (S0586, **4.20**) was obtained from FEW Chemicals (Bitterfeld, Germany). Millipore water was consistently used for the preparation of stock solutions, buffers, and aqueous eluents for HPLC. Polypropylene reaction vessels with screw cap (1.5 and 2 mL) from Sarstedt (Nümbrecht, Germany) were used for small-scale reactions (e.g., activation of Fmoc-protected amino acids) and to keep stock solutions.

NMR spectroscopy. NMR spectra were recorded on an AVANCE 600 instrument with cryogenic probe (^{1}H: 600 MHz; ^{13}C: 150 MHz) and an AVANCE 400 instrument (^{1}H: 400 MHz; ^{13}C: 100 MHz) (Bruker, Karlsruhe, Germany). NMR spectra were calibrated based on the solvent residual peaks (^{1}H-NMR, DMSO-d_6: δ = 2.50 ppm, $CDCl_3$: δ = 7.26 ppm; ^{13}C-NMR, DMSO-d_6: δ = 39.50 ppm, $CDCl_3$: δ = 77.16 ppm) and data are reported as follows: ^{1}H-

NMR: chemical shift δ in ppm (multiplicity [s = singlet, d = doublet, t = triplet, m = multiplet, br s = broad singlet], integral, coupling constant *J* in Hz); ^{13}C NMR: chemical shift δ in ppm.

Mass spectrometry. High-resolution mass spectrometry (HRMS) was performed with an Agilent 6540 UHD accurate-mass Q-TOF LC/MS system coupled to an Agilent 1290 analytical HPLC system (Agilent Technologies. Santa Clara, CA) using an ESI source and the following LC method: column: Agilent Zorbax Eclipse Plus C18, 1.8 µm, 50 × 2.1 mm, column temperature: 40 °C, solvent/linear gradient: 0−4 min: 0.1% aqueous HCOOH/acetonitrile supplemented with 0.1% HCOOH 95:5−2:98, 4−5 min: 2:98, flow: 0.6 mL/min.

Preparative HPLC. Preparative HPLC was performed with a system from Knauer (Berlin, Germany) consisting of two K-1800 pumps and a K-2001 detector (in the following referred to as "system 1") or with a Prep 150 LC system from Waters (Eschborn, Germany) comprising a Waters 2545 binary gradient module, a Waters 2489 UV/vis detector, and a Waters fraction collector III (in the following referred to as "system 2"). A Gemini NX-C18, 5 µm, 250 mm × 21 mm (Phenomenex, Aschaffenburg, Germany) was used as stationary phase at a flow rate of 20 mL/min using mixtures of 0.1% aqueous TFA and acetonitrile as the mobile phase. A detection wavelength of 220 nm was used throughout. Collected fractions were lyophilized using a Scanvac CoolSafe 100-9 freeze dryer (Labogene, Allerød, Denmark) equipped with a RZ 6 rotary vane vacuum pump (Vacuubrand, Wertheim, Germany).

Analytical HPLC. Analytical HPLC analysis was performed with a system from Agilent Technologies composed of a 1290 Infinity binary pump equipped with a degasser, a 1290 Infinity autosampler, a 1290 Infinity thermostated column compartment, a 1260 Infinity diode array detector, and a 1260 Infinity fluorescence detector. A Kinetex-XB C18, 2.6 µm, 100 × 3 mm (Phenomenex) served as stationary phase at a flow rate of 0.6 mL/min. Detection was performed at 220 nm and the temperature of the column compartment was set to 25 °C. Mixtures of acetonitrile (A) and 0.04% aqueous TFA (B) were used as mobile phase. The following linear gradients were applied: compounds **2.2** and **4.14**-**4.17b**: 0-14 min: A/B 10:90-30:70, 14-15 min: 30:70-95:5, 15-18 min: 95:5 (isocratic); compounds **4.10**, **4.24**, **4.26**, and **4.27**: 0-20 min: A/B 10:90-90:10, 20-21 min: 90:10-95:5, 21-25 min: 95:5 (isocratic); compounds **4.19** and **4.21**: 0-14 min: A/B 20:80-40:60, 14-15 min: 40:60-95:5, 15-18 min: 95:5 (isocratic). The injection volume was 20 µL. Retention (capacity) factors *k* were calculated from the retention times t_R according to $k = (t_R - t_0)/t_0$ (t_0 = dead time, 0.76 min for the used system and column).

General procedure for solid phase peptide synthesis. Peptides were synthesized manually by SPPS on a 2-ClTrt resin according to the Fmoc strategy. 5-mL NORM-JECT syringes (B.

Braun-Melsungen, Melsungen, Germany), equipped with a 35-µm polypropylene frit (Roland Vetter Laborbedarf, Ammerbuch, Germany), were used as reaction vessels. DMF/NMP 4:1 v/v was used as solvent for all amino acid coupling and Fmoc deprotection steps. Prior to the coupling of the first amino acid (**4.10**), the 2-ClTrt resin (loading: 1.60 mmol/g) was allowed to swell in CH_2Cl_2 for 30 min at rt followed by washing of the resin with CH_2Cl_2 (2 ×). Amino acid **4.10** was attached to the resin according to a reported procedure.[46] The loading of the resulting Fmoc-TMSAla-2-ClTrt resin, which was used for the synthesis of peptides **2.2** and **4.14-4.17b**, amounted to 1.00 mmol/g (determined photometrically via absorbance at 304 nm in DMF according to a reported protocol[47]). Fmoc deprotection of the Fmoc-TMSAla-2-ClTrt resin was carried out using 20% piperidine in solvent (2 × 10 min at rt) followed by washing with solvent (6 × ca. 1 mL). The following Fmoc-amino acids (except for **3.1**, **3.4**, and **4.11**), used in 5-fold excess, were preactivated with HOBt/HBTU/DIPEA (5/4.9/10 equiv.) in solvent (about 2.2 mL/mmol amino acid) for at least 5 min before addition to the resin. The Fmoc-protected unnatural amino acids **3.1**, **3.4**, and **4.11** were used in 3-fold excess and were preactivated with HOBt/HBTU/DIPEA (3/3/6 equiv.) in anhydrous solvent (about 1.6 mL/mmol amino acid) for 5-10 min prior to addition to the resin. Amino acid coupling was carried out on a shaker (Heidolph Multi Reax; Heidolph Instruments, Schwabach, Germany) covered with a thermostat controlled (35 °C) box. In the case of standard amino acids, "double" coupling (2 × 45 min) was performed. **3.1**, **3.4**, and **4.11** were attached by a single coupling procedure (35 °C, 16 h). After coupling of an Fmoc-amino acid, the resin was washed with solvent (4 ×) followed by Fmoc deprotection using 20% piperidine in solvent (2 × 10 min at rt) and subsequent washing of the resin with solvent (6 × ca. 1 mL). After coupling of the last amino acid and final Fmoc deprotection, the resin was washed with solvent (6 ×) and CH_2Cl_2 (3 ×) (treated with potassium carbonate). Peptides were cleaved off the resin using CH_2Cl_2/TFA 3:1 v/v (2 × 20 min at rt). The liquids (2 × ca. 2 mL) were collected in a 100-mL round bottom flask and the resin was washed once with CH_2Cl_2/TFA 3:1 v/v (2 mL). The volatiles of the combined liquids were removed by evaporation, TFA/H_2O 95:5 v/v (2 mL per 100 mg resin) was added to the residue and the mixture was stirred at rt for 5 h. The volatiles were removed by evaporation followed by the addition of H_2O (ca. 50 mL) and lyophilization to obtain the crude peptide, which was subjected to purification by preparative HPLC.

Compound characterization. Amino acid **4.7**, peptides **4.14-4.17b**, and compounds **4.24** and **4.26** were characterized by HRMS, ^{1}H-, ^{13}C-, and 2D-NMR spectroscopy (2D: ^{1}H-COSY, HSQC, HMBC), and RP-HPLC. Compounds **4.19** and **4.21** were characterized by HRMS, ^{1}H-

NMR spectroscopy, and RP-HPLC. **2.2** and **4.27** were characterized by HRMS and RP-HPLC. HPLC purities of all target compounds were ≥ 97% (UV detection, 220 nm).

4.4.2 Experimental protocols and analytical data

Lys-Lys-Pro-Tyr-Ile-β-trimethylsilyl-Ala tris(hydrotrifluoroacetate) (2.2).[19] Peptide **2.2** was synthesized on a Fmoc-TMSAla-2-ClTrt resin (50 mg, 1.00 mmol/g) according to the general procedure. Purification by preparative RP-HPLC (system 2, gradient: 0-30 min: acetonitrile/0.1% aqueous TFA 22:78-27:73, t_R = 7 min) yielded **2.2** as a white fluffy solid (29.4 mg, 52%). HRMS (ESI): *m/z* $[M+3H]^{3+}$ calcd. for $[C_{38}H_{69}N_8O_8Si]^{3+}$ 264.4997, found: 264.5001. RP-HPLC (220 nm): > 99% (t_R = 8.6 min, *k* = 10.3). $C_{38}H_{66}N_8O_8Si \cdot C_6H_3F_9O_6$ (794.10 + 342.07).

Arg-Arg-Pro-Tyr-Ile-β-trimethylsilyl-Ala tris(hydrotrifluoroacetate) (4.14). Peptide **4.14** was synthesized on a Fmoc-TMSAla-2-ClTrt resin (75 mg, 1.00 mmol/g) according to the general procedure. Purification by preparative RP-HPLC (system 1, gradient: 0-25 min: acetonitrile/0.1% aqueous TFA 15:85-45:55, t_R = 13 min) yielded **4.14** as a white fluffy solid (34.1 mg, 38%). ^{1}H-NMR (600 MHz, DMSO-d_6): δ (ppm) 0.00 (s, 9H), 0.76-0.85 (m, 6H), 0.91-0.98 (m, 1H), 0.98-1.08 (m, 2H), 1.35-1.44 (m, 1H), 1.44-1.62 (m, 5H), 1.64-1.76 (m, 4H), 1.77-1.90 (m, 3H), 1.93-2.03 (m, 1H), 2.62-2.70 (m, 1H), 2.80-2.93 (m, 1H), 3.03-3.12 (m, 4H), 3.54-3.61 (m, 2H, interfering with the water signal, quantified in the spectrum acquired after the addition of D_2O), 3.81-3.84 (m, 1H, interfering with the water signal, quantified in the spectrum acquired after the addition of D_2O), 4.18-4.26 (m, 2H), 4.31-4.36 (m, 1H), 4.37-4.43 (m, 1H), 4.44-4.53 (m, 1H), 6.59-6.64 (m, 2H), 6.84-7.28 (br s, 4H, interfering with next listed signal), 6.99-7.03 (m, 2H), 7.28-7.65 (br s, 4H), 7.73 (d, 1H, *J* 9.2 Hz), 7.81 (t, 1H, 5.5 Hz), 7.86 (t, 1H, *J* 6.2 Hz), 7.94 (d, 1H, *J* 8.1 Hz), 8.13-8.29 (m, 4H), 8.67 (d, 1H, *J* 7.3 Hz), 9.23 (s, 1H), 12.45 (s, 1H). ^{13}C-NMR (150 MHz, DMSO-d_6): δ (ppm) 0.00 (3 carbon atoms), 10.89, 15.13, 19.28, 24.03, 24.09, 24.17, 24.61, 28.21, 28.42, 29.10, 36.43, 37.27, 40.16, 40.53, 46.85, 48.63, 50.46, 51.69, 54.28, 56.32, 59.15, 113.96 (TFA), 114.85 (2 carbon atoms), 115.93 (TFA), 117.90 (TFA), 119.88 (TFA), 127.80, 130.11 (2 carbon atoms), 155.79, 156.92, 156.94, 158.88 (q, *J* 32 Hz) (TFA), 168.31, 169.24, 170.54, 170.75, 171.37, 174.61. HRMS (ESI): *m/z* $[M+3H]^{3+}$ calcd. for $[C_{38}H_{69}N_{12}O_8Si]^{3+}$ 283.1705, found: 283.1716. RP-HPLC (220 nm): > 99% (t_R = 9.0 min, *k* = 10.8). $C_{38}H_{66}N_{12}O_8Si \cdot C_6H_3F_9O_6$ (847.11 + 342.07).

***N*$^{\alpha}$-Methyl-Arg-Arg-Pro-Tyr-Ile-β-trimethylsilyl-Ala tris(hydrotrifluoroacetate) (4.15).** Peptide **4.15** was synthesized on a Fmoc-TMSAla-2-ClTrt resin (75 mg, 1.00 mmol/g) according to the general procedure. Purification by preparative HPLC (system 1, gradient: 0-25 min: acetonitrile/0.1% aqueous TFA 15:85-45:55, t_R = 14 min) yielded **4.15** as a white fluffy solid (40.3 mg, 44%).^{1}H-NMR (600 MHz, DMSO-d_6): δ (ppm) 0.00 (s, 9H), 0.76-0.86 (m, 6H), 0.91-0.98 (m, 1H), 0.98-1.07 (m, 2H), 1.38-1.48 (m, 3H), 1.51-1.59 (m, 3H), 1.66-1.76 (m, 4H), 1.79-1.87 (m, 3H), 1.94-2.04 (m, 1H), 2.46-2.48 (m, 3H), 2.62-2.69 (m, 1H), 2.82-2.88 (m, 1H), 3.06-3.15 (m, 4H), 3.55-3.60 (m, 2H, interfering with the water signal, quantified in the spectrum acquired after the addition of D_2O), 3.78-3.81 (m, 1H, interfering with the water signal, quantified in the spectrum acquired after the addition of D_2O), 4.17-4.28 (m, 2H), 4.32-4.36 (m, 1H), 4.38-4.43 (m, 1H), 4.52-4.57 (m, 1H), 6.60-6.63 (m, 2H), 6.82-7.29 (br s, 4H, interfering with next listed signal), 7.00-7.02 (m, 2H), 7.29-7.65 (br s, 4H), 7.71-7.75 (m, 1H), 7.84-7.90 (m, 2H), 7.93 (d, 1H, *J* 8.1 Hz), 8.20 (d, 1H, *J* 7.9 Hz), 8.87 (d, 1H, *J* 7.3 Hz), 8.95 (s, 1H), 9.04-9.70 (m, 2H), 12.46 (s, 1H). ^{13}C-NMR (150 MHz, DMSO-d_6): δ (ppm) 0.00 (3 carbon atoms), 10.89, 15.13, 19.28, 23.92, 24.03, 24.18, 24.62, 26.99, 28.12, 29.09, 31.16, 36.42, 37.27, 40.08, 40.44, 46.86, 48.63, 50.58, 54.27, 56.32, 59.16, 59.92, 113.94 (TFA), 114.85 (2 carbon atoms), 115.91 (TFA), 117.88 (TFA), 119.86 (TFA), 127.80, 130.11 (2 carbon atoms), 155.78, 156.93 (2 carbon atoms), 158.91 (q, *J* 33 Hz) (TFA), 167.00, 169.06, 170.54, 170.74, 171.33, 174.60. HRMS (ESI): *m/z* $[M+3H]^{3+}$ calcd. for $[C_{39}H_{71}N_{12}O_8Si]^{3+}$ 287.8424, found: 287.8434. RP-HPLC (220 nm): > 99% (t_R = 9.2 min, *k* = 11.1). $C_{39}H_{68}N_{12}O_8Si \cdot C_6H_3F_9O_6$ (861.13 + 342.07).

***N*$^{\alpha}$-Methyl-Arg-Arg-Pro-β,β-dimethyl-L-Tyr-Ile-β-trimethylsilyl-Ala tris(hydrotrifluoroacetate) (4.16a) and *N*$^{\alpha}$-methyl-Arg-Arg-Pro-β,β-dimethyl-D-Tyr-Ile-β-trimethylsilyl-Ala tris(hydrotrifluoroacetate) (4.16b).** Peptides **4.16a** and **4.16b**, representing diastereomers, were synthesized on a Fmoc-TMSAla-2-ClTrt resin (50 mg, 1.00 mmol/g) according to the general procedure. The unavailability of enantiomerically pure Fmoc-β,β-dimethyl-L-Tyr(*t*Bu)-OH (this Fmoc amino acid was only available as racemic mixture) necessitated the synthesis of both diastereomers, which were separated by preparative HPLC (system 1, gradient: 0-25 min: acetonitrile/0.1% aqueous TFA 15:85-45:55, t_R (**4.16a**) = 14 min, t_R (**4.16b**) = 16 min). Lyophilization of the eluates yielded **4.16a** and **4.16b** as white fluffy solids (**4.16a**: 23.0 mg, 37%; **4.16b**: 21.1 mg, 34%). ^{1}H-NMR of **4.16a** (600 MHz, DMSO-d_6): δ (ppm) 0.00 (s, 9H), 0.73-0.85 (m, 6H), 0.90-1.04 (m, 3H), 1.19-1.30 (m, 6H), 1.33-1.42 (m, 1H), 1.42-1.50 (m, 2H), 1.50-1.61 (m, 3H), 1.61-1.84 (m, 7H), 1.84-1.95 (m, 1H), 2.48 (s, 3H),

3.04-3.17 (m, 4H), 3.48-3.53 (m, 1H, interfering with the water signal, quantified in the spectrum acquired after the addition of D_2O), 3.55-3.59 (m, 1H, interfering with the water signal, quantified in the spectrum acquired after the addition of D_2O), 3.82 (s, 1H, interfering with the water signal, quantified in the spectrum acquired after the addition of D_2O), 4.14 (t, 1H, *J* 8.4 Hz), 4.14-4.24 (m, 1H), 4.36-4.43 (m, 1H), 4.52-4.58 (m, 1H), 4.60-4.69 (m, 1H), 6.59-6.65 (m, 2H), 6.93-7.30 (br s, 4H, interfering with next listed signal), 7.11-7.14 (m, 2H), 7.30-7.81 (m, 6H), 7.84-7.94 (m, 2H), 8.08 (d, 1H, *J* 7.8 Hz), 8.92 (d, 1H, *J* 8.0 Hz), 8.95 (s, 1H), 9.04-9.41 (m, 2H), 12.42 (s, 1H). ^{13}C-NMR of **4.16a** (150 MHz, DMSO-d_6): δ (ppm) 0.00 (3 carbon atoms), 10.94, 15.13, 19.22, 23.92, 24.11, 24.14, 24.45, 24.55, 26.99, 27.09, 28.13, 28.63, 31.16, 37.08, 40.06, 40.16, 40.43, 46.86, 48.68, 50.51, 56.43, 59.25, 59.88, 59.91, 114.07 (TFA), 114.34 (2 carbon atoms), 116.05 (TFA), 118.02 (TFA), 120.00 (TFA), 127.42 (2 carbon atoms), 136.42, 155.26, 156.90, 156.95, 158.83 (q, *J* 32 Hz) (TFA), 167.05, 169.35, 169.42, 170.43, 170.56, 174.66. ^{1}H-NMR of **4.16b** (600 MHz, DMSO-d_6): δ (ppm) 0.00 (s, 9H), 0.71-0.82 (m, 6H), 0.88-1.03 (m, 3H), 1.17-1.34 (m, 8H), 1.40-1.49 (m, 2H), 1.49-1.64 (m, 5H), 1.64-1.85 (m, 5H), 2.47 (s, 3H), 3.01-3.17 (m, 4H), 3.41-3.50 (m, 1H, interfering with the water signal, quantified in the spectrum acquired after the addition of D_2O), 3.51-3.58 (m, 1H, interfering with the water signal, quantified in the spectrum acquired after the addition of D_2O), 3.80 (s, 1H, interfering with the water signal, quantified in the spectrum acquired after the addition of D_2O), 4.10 (q, 1H, *J* 7.3 Hz), 4.13-4.19 (m, 1H), 4.35-4.42 (m, 1H), 4.47-4.54 (m, 1H), 4.87 (d, 1H, *J* 9.9 Hz), 6.57-6.67 (m, 2H), 6.74-7.26 (br s, 4H, interfering with next listed signal), 7.14-7.17 (m, 2H), 7.26-7.59 (br s, 4H), 7.62 (d, 1H, *J* 8.5 Hz), 7.69 (d, 1H, *J* 9.8 Hz), 7.79-7.90 (m, 2H), 8.19 (d, 1H, *J* 7.0 Hz), 8.85 (d, 1H, *J* 7.1 Hz), 8.94 (s, 1H), 9.00-9.56 (m, 2H), 12.43 (s, 1H). ^{13}C-NMR of **4.16b** (150 MHz, DMSO-d_6): δ (ppm) 0.00 (3 carbon atoms), 11.09, 15.26, 19.25, 23.84, 23.99, 24.01, 24.15, 24.55, 26.53, 26.97, 28.02, 29.40, 31.14, 37.09, 40.09, 40.43, 41.00, 46.71, 49.31, 50.60, 56.41, 59.15, 59.49, 59.86, 114.06 (TFA), 114.35 (2 carbon atoms), 116.03 (TFA), 118.02 (TFA), 120.00 (TFA), 127.29 (2 carbon atoms), 136.86, 155.38, 156.92 (2 carbon atoms), 158.74 (q, *J* 32 Hz) (TFA), 166.95, 168.97, 169.40, 170.17, 170.84, 174.48. HRMS (ESI): *m/z* $[M+3H]^{3+}$ calcd. for $[C_{41}H_{75}N_{12}O_8Si]^{3+}$ 297.1861, found: 297.1866 (**4.16a**), 297.1866 (**4.16b**). RP-HPLC (220 nm): **4.16a**: 99% (t_R = 10.7 min, *k* = 13.1), **4.16b**: 97% (t_R = 12.2 min, *k* = 15.1). $C_{41}H_{72}N_{12}O_8Si \cdot C_6H_3F_9O_6$ (889.19 + 342.07).

N^{α}-Methyl-N^{ω}-[(4-aminobutyl)aminocarbonyl]Arg-Arg-Pro-β,β-dimethyl-L-Tyr-Ile-β-trimethylsilyl-Ala tetrakis(hydrotrifluoroacetate) (4.17a) and N^{α}-methyl-N^{ω}-[(4-aminobutyl)aminocarbonyl]Arg-Arg-Pro-β,β-dimethyl-D-Tyr-Ile-β-trimethylsilyl-Ala tetrakis(hydrotrifluoroacetate) (4.17b). Peptides **4.17a** and **4.17b**, representing diastereomers, were synthesized on a Fmoc-TMSAla-2-ClTrt resin (150 mg, 1.00 mmol/g) according to the general procedure with the following modification: after coupling of the last amino acid and Fmoc-deprotection, the resin was washed with CH_2Cl_2 (5 ×), a solution of 2-nitrobenzenesulfonylchloride (100 mg, 0.45 mmol) and collidine (100 µL, 0.75 mmol) in CH_2Cl_2 (3.5 mL) was added and the mixture was shaken at rt for 2 h. The resin was washed with DMF (5 ×) and a solution of MTBD (87 µL, 0.6 mmol) and methyl-4-nitrobenzenesulfonate (163 mg, 0.75 mmol) in DMF (4.2 mL) was added followed by shaking at rt for 30 min. After washing the resin with DMF (3 ×), a solution of DBU (112 µL, 0.75 mmol) and 2-mercaptoethanol (104 µL, 1.5 mmol) in DMF (3.5 mL) was added and the mixture was shaken at rt for 30 min. The resin was washed with DMF (5 ×) followed by cleavage from the resin as described in the general procedure for SPPS. The unavailability of enantiomerically pure Fmoc-β,β-dimethyl-L-Tyr(*t*Bu)-OH (only available as racemic mixture) necessitated the synthesis of both diastereomers, which were separated by preparative RP-HPLC (system 1, gradient: 0-25 min: acetonitrile/0.1% aqueous TFA 15:85-45:55, t_R (**4.17a**) = 12 min, t_R (**4.17b**) = 14 min). Lyophilization of the eluates yielded **4.17a** and **4.17b** as white fluffy solids (**4.17a**: 30.1 mg, 14%; **4.17b**: 27.8 mg, 13%). ^{1}H-NMR of **4.17a** (600 MHz, DMSO-d_6): δ (ppm) 0.00 (s, 9H), 0.72-0.89 (m, 6H), 0.90-1.04 (m, 3H), 1.18-1.31 (m, 6H), 1.33-1.42 (m, 1H), 1.43-1.61 (m, 9H), 1.62-1.94 (m, 8H), 2.47 (s, 3H), 2.73-2.83 (m, 2H), 3.03-3.18 (m, 4H), 3.21-3.30 (m, 2H), 3.46-3.54 (m, 1H), 3.54-3.63 (m, 1H), 3.76-3.91 (m, 1H), 4.12 (t, 1H, *J* 7.1 Hz), 4.16-4.25 (m, 1H), 4.36-4.43 (m, 1H), 4.48-4.59 (m, 1H), 4.66 (d, 1H, *J* 9.6 Hz), 6.57-6.65 (m, 2H), 6.71-7.28 (br s, 2H, interfering with next listed signal), 7.11-7.14 (m, 2H), 7.28-7.70 (m, 5H), 7.71-7.99 (m, 4H), 8.06 (d, 1H, *J* 7.9 Hz), 8.52 (s, 2H), 8.68-9.15 (m, 3H), 9.17 (s, 1H), 10.78 (s, 1H), 12.41 (s, 1H). One exchangeable proton (NH) of the presumably 4-fold protonated molecule was not apparent. ^{13}C-NMR of **4.17a** (150 MHz, DMSO-d_6): δ (ppm) 0.00 (3 carbon atoms), 10.95, 15.14, 19.25, 23.43, 24.11, 24.16, 24.38, 24.54 (2 carbon atoms), 25.99, 27.00 (2 carbon atoms), 28.16, 28.64, 32.16, 37.08, 38.49, 38.64, 40.06, 40.14, 40.43, 46.86, 48.71, 50.50, 56.45, 59.25, 59.88 (2 carbon atoms), 114.12 (TFA), 114.35 (2 carbon atoms), 116.10 (TFA), 118.08 (TFA), 120.06 (TFA), 127.42 (2 carbon atoms), 136.40, 153.93 (2 carbon atoms), 155.27, 156.94, 158.90 (q, *J* 32 Hz) (TFA), 167.14, 169.32, 169.39, 170.42, 170.58, 174.69. ^{1}H-NMR of **4.17b** (600 MHz, DMSO-d_6): δ (ppm) 0.00 (s, 9H), 0.70-0.82 (m, 6H),

0.87-1.02 (m, 3H), 1.19-1.35 (m, 8H), 1.44-1.65 (m, 11H), 1.65-1.83 (m, 5H), 2.47 (s, 3H), 2.75-2.83 (m, 2H), 3.04-3.16 (m, 4H), 3.21-3.30 (m, 2H), 3.43-3.50 (m, 1H), 3.50-3.58 (m, 1H), 3.81 (s, 1H), 4.11 (q, 1H, *J* 7.6 Hz), 4.15 (t, 1H, *J* 7.4 Hz), 4.36-4.41 (m, 1H), 4.49-4.55 (m, 1H), 4.86 (d, 1H, *J* 9.8 Hz), 6.57-6.65 (m, 2H), 6.73-7.32 (br s, 2H, interfering with next listed signal), 7.14-7.17 (m, 2H), 7.32-7.72 (m, 5H), 7.72-8.04 (m, 4H), 8.17 (d, 1H, *J* 7.0 Hz), 8.53 (s, 2H), 8.87 (d, 1H, *J* 7.3 Hz), 8.96 (s, 1H), 9.05-9.23 (m, 2H), 10.88 (s, 1H), 12.43 (s, 1H). One exchangeable proton (NH) of the presumably 4-fold protonated molecule was not apparent. ^{13}C-NMR of **4.17b** (150 MHz, DMSO-d_6): δ (ppm) 0.00 (3 carbon atoms), 11.09, 15.26, 19.26, 23.37, 23.99, 24.02, 24.20, 24.39, 24.55, 25.99, 26.48, 26.91, 28.10, 29.32, 31.14, 37.10, 38.49, 38.66, 40.11, 40.44, 40.98, 46.71, 49.26, 50.59, 56.39, 59.17, 59.55, 59.81, 114.07 (TFA), 114.37 (2 carbon atoms), 116.04 (TFA), 118.01 (TFA), 119.98 (TFA), 127.29 (2 carbon atoms), 136.86, 153.94 (2 carbon atoms), 155.40, 156.97, 158.97 (q, *J* 32 Hz) (TFA), 166.92, 168.99, 169.34, 170.19, 170.81, 174.50. HRMS (ESI): *m/z* $[M+3H]^{3+}$ calcd. for $[C_{46}H_{85}N_{14}O_9Si]^{3+}$ 335.2126, found: 335.2135 (**4.17a**), 335.2132 (**4.17b**). RP-HPLC (220 nm): **4.17a**: 97% (t_R = 9.5 min, *k* = 11.5), **4.17b**: 99% (t_R = 10.9 min, *k* = 13.3). $C_{46}H_{82}N_{14}O_9Si \cdot C_8H_4F_{12}O_8$ (1003.34 + 456.09).

***N*$^{\alpha}$-Methyl-*N*$^{\omega}$-{[4-(*N*-{1-carboxylato[2-(6-(dimethylamino)-3-(dimethyliminio))-3*H*-xanthen-9-yl]phen-5-yl}carbonyl)-aminobutyl]aminocarbonyl}Arg-Arg-Pro-β,β-dimethyl-L-Tyr-Ile-β-trimethylsilyl-Ala tris(hydrotrifluoroacetate) (4.19).** Peptide **4.17a** (3.4 mg, 2.3 µmol) and DIPEA (4.7 µL, 27 µmol) were dissolved in DMF/NMP 4:1 v/v (100 µL) followed by the addition of a solution of 5-TAMRA succinimidyl ester **4.18** (1.1 mg, 2.1 µmol) in DMF/NMP 4:1 v/v (30 µL). After stirring at room temperature in the dark for 1 h, the mixture was diluted with 10% aqueous TFA (14 µL) and acetonitrile/0.1% aqueous TFA 20:80 v/v (1 mL). Isolation by preparative RP-HPLC (system 1, gradient: 0-35 min: acetonitrile/0.1% aqueous TFA 20:80-60:40, t_R = 16 min) gave **4.19** as a purple fluffy solid (1.6 mg, 40%) ^{1}H-NMR (600 MHz, DMSO-d_6): δ (ppm) 0.00 (s, 9H), 0.73-0.83 (m, 6H), 0.92-1.03 (m, 3H), 1.22-1.29 (m, 6H), 1.34-1.41 (m, 1H), 1.49-1.61 (m, 9H), 1.62-1.68 (m, 1H), 1.68-1.86 (m, 6H), 1.86-1.96 (m, 1H), 2.45-2.48 (m, 3H), 3.07-3.18 (m, 6H), 3.27 (s, 12H), 3.33-3.36 (m, 2H, interfering with the water signal, quantified in the spectrum acquired after the addition of D_2O), 3.51-3.52 (m, 1H, interfering with the water signal, quantified in the spectrum acquired after the addition of D_2O), 3.58-3.59 (m, 1H, interfering with the water signal, quantified in the spectrum acquired after the addition of D_2O), 3.81-3.84 (m, 1H, interfering with the water signal, quantified in the spectrum acquired after the addition of D_2O), 4.13 (t,

1H, *J* 7.8 Hz), 4.18-4.23 (m, 1H), 4.39-4.44 (m, 1H), 4.54-4.60 (m, 1H), 4.66 (d, 1H, *J* 9.1 Hz), 6.31-6-72 (br s, 1H, interfering with next listed signal), 6.59-6.64 (m, 2H), 6.82-7.17 (m, 9H), 7.18-7.48 (br s, 2H, interfering with next listed signal), 7.39 (d, 1H, *J* 9.3 Hz), 7.48-7.62 (m, 3H), 7.68 (t, 1H, *J* 5.1 Hz), 8.08 (d, 1H, *J* 7.6 Hz), 8.28 (d, 1H, *J* 7.6 Hz), 8.47 (s, 2H), 8.61-8.74 (m, 1H), 8.81-9.24 (m, 6H), 10.30 (s, 1H), 12.40 (s, 1H), 13.40 (s, 1H). HRMS (ESI): *m/z* $[M+3H]^{3+}$ calcd. for $[C_{71}H_{105}N_{16}O_{13}Si]^{3+}$ 472.5933, found: 472.5942. RP-HPLC (220 nm): 99% (t_R = 8.8 min, *k* = 10.6). $C_{71}H_{102}N_{16}O_{13}Si \cdot C_6H_3F_9O_6$ (1415.78 + 342.07).

***N*$^{\alpha}$-Methyl-*N*$^{\omega}$-{[4-(*N*-{6-3*H*-[2-(5-3*H*-(1-(4-sulfonatobutyl)-3,3-dimethyl)indol-2-ylidenepent-1,3-dienyl)-3,3-dimethyl-5-sulfo]indol-1-ium-1-yl}hexanoyl)-aminobutyl]aminocarbonyl}Arg-Arg-Pro-β,β-dimethyl-L-Tyr-Ile-β-trimethylsilyl-Ala tris(hydrotrifluoroacetate) (4.21).** Peptide **4.17a** (3.3 mg, 2.3 µmol) and DIPEA (4.6 µL, 26 µmol) were dissolved in DMF/NMP 4:1 v/v (100 µL) followed by the addition of the sulfo-Cy5 succinimidyl ester **4.20** (1.1 mg, 2.1 µmol) in DMF/NMP 4:1 v/v (30 µL). After stirring at room temperature in the dark for 1 h, the mixture was diluted with 10% aqueous TFA (14 µL) and 0.1% acetonitrile/aqueous TFA 20:80 v/v (1 mL). Isolation by preparative RP-HPLC (system 1, gradient: 0-35 min: acetonitrile/0.1% aqueous TFA 20:80-60:40, t_R = 17 min) gave **4.21** as a purple fluffy solid (1.4 mg, 30%). ^{1}H-NMR (600 MHz, DMSO-d_6): δ (ppm) 0.00 (s, 9H), 0.73-0.83 (m, 6H), 0.91-1.01 (m, 3H), 1.21-1.29 (m, 6H), 1.28-1.44 (m, 8H), 1.48-1.59 (m, 7H), 1.63-1.71 (m, 15H), 1.71-1.84 (m, 9H), 1.85-1.95 (m, 1H), 2.04 (t, 2H, *J* 6.4 Hz), 2.46-2.48 (m, 3H), 2.64 (t, 2H, *J* 6.8 Hz), 2.98-3.03 (m, 2H), 3.06-3.14 (m, 4H, interfering with the water signal, quantified in the spectrum acquired after the addition of D_2O), 3.22-3.26 (m, 2H, interfering with the water signal, quantified in the spectrum acquired after the addition of D_2O), 3.55-3.57 (m, 2H, interfering with the water signal, quantified in the spectrum acquired after the addition of D_2O), 3.80-3.84 (m, 1H, interfering with the water signal, quantified in the spectrum acquired after the addition of D_2O), 4.03-4.09 (m, 2H), 4.10-4.16 (m, 3H), 4.17-4.23 (m, 1H), 4.39-4.44 (m, 1H), 4.52-4.58 (m, 1H), 4.64 (d, 1H, *J* 9.3 Hz), 6.24 (d, 1H, *J* 13.7 Hz), 6.39 (d, 1H, *J* 14.0 Hz), 6.53-6.65 (m, 3H), 6.68-7.06 (br s, 2H), 7.09-7.16 (m, 2H), 7.20-7.32 (m, 3H), 7.32-7.58 (m, 7H), 7.61-7.67 (m, 2H), 7.78 (t, 1H, *J* 5.5 Hz), 7.81-7.84 (m, 1H), 8.08 (d, 1H, *J* 7.7 Hz), 8.25-8.48 (m, 4H), 8.74-9.05 (m, 4H), 9.06-9.18 (m, 1H), 9.99 (s, 1H), 12.40 (s, 1H). HRMS (ESI): *m/z* $[M+3H]^{3+}$ calcd. for $[C_{81}H_{126}N_{16}O_{16}S_2Si]^{3+}$ 557.2937, found: 557.2943. RP-HPLC (220 nm): 99% (t_R = 10.1 min, *k* = 12.3). $C_{81}H_{123}N_{16}O_{16}S_2Si \cdot C_6H_3F_9O_6$ (1669.18 + 342.07).

4.4.3 Capillary electrophoresis

Capillary electrophoresis was performed with an Agilent 7100 CE system using a bare fused silica capillary with an inner diameter of 0.05 mm and a length of 72 cm (G1600-62211, Agilent). 50 mM α-cyclodextrin (Honeywell, Charlotte, United States) in a 125 mM sodium phosphate buffer (pH = 7.0) served as electrolyte solution. Injections were performed hydrodynamically applying a pressure of 100 mbar for 10 s. The temperature of the capillary housing was set to 30 °C. A voltage of 20 kV was applied for 35 min and the detection was performed at 220 nm.

4.4.4 Chemical stability

The chemical stability of peptides **4.19** and **4.21** was investigated in PBS (adjusted to pH = 7.4) at 22 °C in the dark. The incubation was started by the addition of 3 µL of a 5 mM stock solution (solvent: DMSO) to 147 µL of PBS to yield a concentration of 100 µM. After periods of 0, 6, 24, and 48 h, an aliquot (25 µL) was removed and added to 25 µL of acetonitrile/0.04% aq. TFA 2:8 v/v to obtain a peptide solution with a concentration of 50 µM. 20 µL of this solution were subjected to analytical RP-HPLC analysis using the same system and conditions as described under *Analytical HPLC*. A 1:1 mixture of PBS and acetonitrile/0.04% aq. TFA 2:8 v/v (20 µL) was analyzed to obtain the blank chromatogram.

4.4.5 Stability in human plasma

The proteolytic stabilities of **1.3**, **4.15**, **4.17a**, **4.19**, and **4.21** were investigated in human blood plasma/PBS 1:2 v/v according to a described procedure.[16] Samples were analyzed using the RP-HPLC system and conditions as described under *Analytical HPLC* with the following gradient: 0-6 min: acetonitrile/0.04% aq. TFA 10:90-21:79, 6-12 min: 21:79-40:60, 12-13 min: 40:60-95:5, 13-16 min: 95:5 (isocratic). Data analysis was based on UV detection at 220 nm. Reference samples, representing 100% recovery, were prepared in quadruplicate. Recovery ratios were obtained by dividing the recovery of the peptide by the recovery of IS for each individual sample (n = 3-5). The obtained recoveries and the recovery ratios are summarized in Table A4.1, Appendix.

4.4.6 Excitation spectra, emission spectra, and fluorescence quantum yields

Absorption spectra were recorded with a referenced single beam spectrometer (Cary 60, Agilent) and the emission and excitation spectra were recorded in an orthogonal configuration in an emission spectrometer (Fluorolog, Horiba) setting the slits to 1 nm for excitation and

emission detection. The fluorescence decays were recorded with a self-constructed Time Correlated Single Photon Counting (TCSPC) setup[48] with single detection wavelength at room temperature. The sample was excited along a 10 mm pathlength at λ_{ex} = 280 nm and the emission was recorded orthogonally to this along a 2 mm pathlength at λ_{obs} as indicated in the Figure A4.7, Appendix. The optical density of the sample was set to ca. 0.1 at the excitation wavelength over 10 mm pathlength. The fluorescence quantum yields of compounds **4.19** and **4.21** were determined in PBS and PBS supplemented with 1% BSA via an absolute method using an Ulbricht sphere with an inaccuracy of ca. 3% (Hamamatsu C9920−02 system equipped with a Spectralon integrating sphere) at room temperature using a 10 mm × 10 mm quartz cuvette. The optical density at the excitation wavelength of the sample was < 0.1 along an optical path length of 1 cm.

4.4.7 Cell culture

Mammalian cells were cultured in T75 or T175 culture flasks (Sarstedt). Chinese hamster ovary (CHO) cells stably expressing $hNTS_1R$[28] were cultured in DMEM/HAM's F12 (Sigma, Taufkirchen, Germany) medium (1:1) supplemented with 7.5% FBS, L-glutamine (Sigma) (630 µg/mL), and hygromycin B (Carl Roth, Karlsruhe, Germany) (250 µg/mL). HT-29 colon carcinoma cells (DSMZ-no. ACC 299) were grown in antibiotic-free RPMI-164 medium (Sigma) supplemented with 7.5% FBS or in MEM Earles medium supplemented with 10% FBS, 1% L-glutamine, 1% NEAA, and 1% pyruvate. HEK293T-$hNTS_2R$ cells were cultured in Dulbecco's modified Eagle's medium (Sigma-Aldrich) supplemented with 10% FBS, L-glutamine (2 mM) and Penicillin-Streptomycin (100 IU/mL and 0.1 mg/mL, respectively) (Sigma-Aldrich). All cell lines were cultured in a humidified atmosphere (95% air and 5% CO_2) at 37 °C.

4.4.8 Buffers used for binding and functional assays

DPBS: Dulbecco's phosphate-buffered saline with calcium and magnesium (1.8 mM $CaCl_2$, 2.68 mM KCl, 1.47 mM KH_2PO_4, 3.98 mM $MgSO_4$, 137 mM NaCl, 8.06 mM Na_2HPO_4, pH = 7.4) supplemented with 0.1% BSA (flow cytometry) or 1% BSA (radiochemical assays) and 0.1 mg/mL bacitracin. For flow cytometric binding studies, *DPBS* was filtrated using 0.2 µm nylon syringe filters (Phenomenex).

Fura-2 assay buffer: HEPES buffer (120 mM NaCl, 5 mM KCl, 2 mM $MgCl_2$, 1.5 mM $CaCl_2$, 25 mM HEPES, and 10 mM glucose at pH = 7.4) supplemented with 2% BSA and 2.5 mM Probenecid (Sigma).

4.4.9 Radiochemical competition binding assays with [^{3}H]1.7

NTS_1R radioligand competition binding experiments with [^{3}H]**1.7** (molar activity: 2.41 TBq/mmol) and the peptides under study were performed with intact $hNTS_1R$-expressing human HT-29 colon carcinoma cells at 23 ± 1 °C using a previously reported protocol.[12] The K_d value of the radioligand for the used batch of [^{3}H]**1.7** was determined recently (K_d = 0.41 nM).[21] Cells were seeded one day before the assay, yielding a confluency of at least 90% on the day of the experiment. Total binding data (including total binding in the absence of competitor) were plotted as dpm values against log(concentration competitor) and analyzed by a four-parameter logistic equation (log(inhibitor) vs response – variable slope, GraphPad Prism 5, GraphPad Software, San Diego, CA) to obtain pIC_{50} values. Individual pIC_{50} values were converted to pK_i values according to the Cheng-Prusoff equation[49] (logarithmic form). To plot average data from individual binding experiments, data were normalized (100% = "top" of the four-parameter logistic fit, 0% = unspecifically bound radioligand).

NTS_2R radioligand competition binding experiments with [^{3}H]**1.7** were performed with membranes of HEK293T-$hNTS_2R$.[21] Membrane preparations were prepared using a recently reported protocol for membrane preparations of CHO-$hNTS_1R$ cells.[16] The protein concentration amounted to 1.8 ± 0.2 mg/mL (mean value ± SEM from three different sample dilutions). NTS_2R saturation and competition binding experiments with [^{3}H]**1.7** were carried out as described for saturation and competition binding studies with [^{3}H]**1.7** at membrane preparations of CHO-$hNTS_1R$ cells.[16] The soluble protein concentration in the assays was 135 µg/mL. The K_d value of [^{3}H]**1.7** amounted to 3.1 ± 0.2 nM (mean value ± SEM from three independent experiments, each performed in triplicate). The concentration of [^{3}H]**1.7** in the competition binding assays was 5 nM. Data from competition binding assays were processed as the data from the NTS_1R binding assays.

4.4.10 Fura-2 Ca^{2+} assay

The Fura-2 Ca^{2+} assay was conducted as previously described[16] with the following modifications: HT-29 cells were used in place of CHO-$hNTS_1R$ cells and 1 µM **1.3** was used to determine the maximal response. Measurements were performed in black 96-well plates (Greiner 655076, Greiner Bio-One, Frickenhausen, Germany) and a measurement for one well comprised 40 cycles (instead of 44 cycles) with a cycle duration of 1.4 s (total time: 56 s).

4.4.11 Flow cytometric binding experiments

Flow cytometry-based NTS_1R binding studies were performed with intact HT-29 (all kind of experiments) and CHO-hNTS_1R cells (only saturation binding) using a BD FACSCanto II flow cytometer (Becton Dickinson, Heidelberg, Germany), equipped with an Argon laser (488 nm), a red diode laser (640 nm), and a BD High Throughput Sampler (HTS unit) for microtiter plates. Saturation and competition binding experiments were performed in triplicate in 96-well polypropylene plates (Brand 701330, Wertheim, Germany) using the HTS unit for sample injection. Association and dissociation experiments were performed in triplicate in 5-mL polypropylene tubes (VWR, Radnor, USA), from which samples were directly injected into the flow cytometer. The following gain settings for forward and sideward scatter were applied: FSC, 0 V; SSC, 252 V. Fluorescence was recorded using the PE channel (excitation: 488 nm, emission: 585 ± 21 nm) with a PMT gain of 400-500 V (**4.19**) or the APC channel (excitation: 640 nm, emission: 660 ± 10 nm) with a PMT gain of 380-580 V (**4.21**). For measurements using the HTS unit, 45 µL of the sample were injected with a speed of 1.5 µL/s. For measurements, using an injection from 5-mL sample tubes, the medium flow rate (60 µL/min) was used. Measurements were stopped after 30 seconds (HTS unit) or after counting of 10000 gated events (injection from sample tubes).

Cells were seeded in T75 culture flasks 3-4 days (CHO-hNTS_1R cells) or 5-6 days (HT-29 cells) prior to the experiment. On the day of the experiment, cells were detached by trypsinization, suspended in *DPBS* and centrifuged at 200 g at rt for 5 min. The cell pellet was re-suspended in binding buffer and the cell density was adjusted to 1.5×10^4 or 1.5×10^5 cells/mL (CHO-hNTS1R cells) or 5.0×10^5 cells/mL (HT-29 cells). Unspecific binding was determined in the presence of 1 µM **1.3**.

Saturation binding experiments. A 96-well polypropylene plate was prefilled with 200 µL of cell suspension. For total binding, H_2O (2 µL) and DMSO/H_2O 2:8 v/v (2 µL) containing the fluorescent ligand (100-fold concentrated compared to the final concentration) were added. To determine unspecific binding, a 100 µM solution of **1.3** in H_2O (2 µL) and DMSO/H_2O 2:8 v/v (2 µL) containing the fluorescent ligand (100-fold concentrated) were added. Samples were incubated at 23 ± 1 °C in the dark under gentle shaking for 2 h followed by measurement via the HTS unit. Specific binding data, obtained by subtracting triplicate mean values of unspecific binding from triplicate mean values of total binding, were plotted against the fluorescent ligand concentration and analyzed by a two-parameter equation describing hyperbolic single-site binding (one site, specific binding, GraphPad Prism 5) to obtain K_d values.

Association experiments. 5-mL polypropylene tubes were prefilled with 2000 µL of cell suspension and H_2O (20 µL) was added (determination of total binding). To start the association, a 100-fold concentrated solution (compared to the final concentration) of the fluorescent ligand in DMSO/H_2O 2:8 v/v (20 µL) was added (final concentrations: **4.19**: 1 nM, **4.21**: 0.1 nM). The sample tubes were gently shaken in the dark at 23 ± 1 °C. Measurements were conducted within different periods of time (1-240 min) by placing the tubes in the injection port of the cytometer. To determine unspecific binding, samples were set up as in the case of total binding, but instead of 20 µL of H_2O 20 µL of a 100 µM solution of **1.3** in H_2O were added. It should be noted that this experimental setup corresponds to a pseudo first-order measurement as the concentration of the free ligand, being markedly higher than the receptor concentration, can be considered constant by approximation during the association reaction. Specific binding data of **4.21**, obtained by subtracting triplicate mean values of unspecific binding from triplicate mean values of total binding, were plotted against the time and analyzed by a three-parameter equation describing an exponential rise to a maximum (one-phase association, Y_0 constrained to zero, GraphPad Prism 5) to yield the observed association rate constant k_{obs}. To calculate mean values in %, specific binding data were normalized based on the corresponding B_{eq} value. Since specific binding data of **4.19** indicated a biphasic association, data of **4.19** were analyzed using a five-parameter two-phase association fit (two-phase association, Y_0 constrained to zero, GraphPad Prism 5) to obtain the observed association rate constants $k_{obs(bi,fast)}$ and $k_{obs(bi,slow)}$ for the fast and slow phase of the association, respectively. To calculate mean values in % (cf. Figure 4.3B), specific binding data were normalized based on the corresponding B_{eq} values from the two-phase association fit (set to 100%). In addition to this analysis, the whole specific binding data of **4.19** were analyzed by a three-parameter equation describing an exponential rise to a maximum (one-phase association, Y_0 constrained to zero, GraphPad Prism 5) to yield the observed association rate constant $k_{obs(mono)}$.

Dissociation experiments. 5-mL polypropylene tubes were prefilled with 2000 µL of cell suspension. For the determination of total binding, the preincubation was started by the addition of H_2O (20 µL) and a 100 nM solution of **4.19** or a 25 nM solution of **4.21** in DMSO/H_2O 2:8 v/v (20 µL) (final fluorescent ligand concentration: 1 nM (**4.19**) or 0.25 nM (**4.21**)). To determine unspecific binding, a 100 µM solution of **1.3** in H_2O (20 µL) and a 100 nM solution of **4.19** or a 25 nM solution of **4.21** in DMSO/H_2O 2:8 v/v (20 µL) were added. The samples were gently shaken in the dark at 23 ± 1 °C for 120 min (**4.19**) or for 180 min (**4.21**). The dissociation process was initiated by the addition of a 2.5 mM solution of **1.3** in H_2O (20 µL) (final concentration: approximately 25 µM). After different periods of time (1-300 min (**4.19**)

or 5-600 min (**4.21**)), sample aliquots were measured by placing the tube in the injection port of the flow cytometer. Specific binding data, obtained by subtracting triplicate mean values of unspecific binding from triplicate mean values of total binding, were plotted against the time and analyzed by a three-parameter equation describing an incomplete monophasic exponential decline (one phase decay, GraphPad Prism 5) to obtain k_{off} values. For both fluorescent ligands, the mean ± SEM of the plateau values from individual experiments proved to be significantly different from zero (one-tailed t-test, $P < 0.05$). To calculate mean values in %, binding data were normalized based on the specifically bound ligand measured immediately before the start of the dissociation.

Calculation of association rate constants (k_{on}) and kinetically derived dissociation constants K_d(kin). The association rate constants were calculated from k_{obs} mean values, k_{off} mean values, and the fluorescent ligand concentration used for the association experiments ([FL]) according to the equation $k_{on} = (k_{obs} - k_{off})/[FL]$. The kinetically derived dissociation constants K_d(kin) were calculated from the respective k_{on} value and the k_{off} mean value according to $K_d(kin) = k_{off}/k_{on}$.

Competition binding experiments. A 96-well polypropylene plate was prefilled with 200 µL of cell suspension. 2 µL of DMSO/H_2O 2:8 v/v (for the determination of total binding in the absence of competitor), 2 µL of a 100 µM solution of **1.3** in H_2O (determination of unspecific binding), or 2 µL of a 100-fold concentrated solution (compared to the final concentration) of the compound of interest (**1.3**, **1.4**, **1.5** or **1.7**; used at varying concentrations) in DMSO/H_2O 2:8 v/v were added and the plate was shortly shaken. Subsequently, 2 µL of a 30 nM solution of **4.19** or a 10 nM solution of **4.21** in DMSO/H_2O 2:8 v/v were added to each well and the plate was gently shaken in the dark at 23 ± 1 °C for 120 min (**4.19**) or 180 min (**4.21**) followed by measurement via the HTS unit. The final concentrations of **4.19** and **4.21** corresponded to their 3-fold or 2-fold K_d values determined by equilibrium saturation binding (K_d = 0.11 nM (**4.19**) or 0.046 nM (**4.21**)). Total binding fluorescence intensities (including total binding in the absence of competitor) were plotted against log (concentration inhibitor) and analyzed by a four-parameter logistic equation (log(inhibitor) vs response-variable slope, GraphPad Prism 5) to obtain pIC_{50} values. Individual pIC_{50} values were converted to pK_i values according to the Cheng-Prusoff equation[49] (logarithmic form). To plot average data from individual binding experiments, data were normalized (100% = "top" of the four-parameter logistic fit, 0% = unspecifically bound fluorescent ligand).

Binding experiments with SBI-553. A 96-well polypropylene plate was prefilled with 200 µL of cell suspension. 2 µL of DMSO/H_2O 2:8 v/v (determination of total binding in the absence

of SBI-553) or 2 µL of a 100-fold concentrated solution (compared to the final concentration) of SBI-553 (used at varying concentrations) in DMSO/H_2O 2:8 v/v (determination of total binding in the presence of SBI-553) were added and the plate was incubated at 23 ± 1 °C for 30 min. Subsequently, 2 µL of a 1 nM solution of **4.21** in DMSO/H_2O 2:8 v/v (final concentration: 0.01 nM) were added. To determine unspecific binding, 2 µL of a 100 µM solution of **1.3** in H_2O and 2 µL of a 1 nM solution of **4.21** in DMSO/H_2O 2:8 v/v were added. The plate was then gently shaken in the dark at 23 ± 1 °C for 180 min followed by measurement via the HTS unit. Total binding fluorescence intensities (including total binding in the absence of the allosteric modulator) were plotted against log (concentration SBI-553). As the data clearly indicated a biphasic course, data were analyzed by a five-parameter two sites - fit logIC_{50} (GraphPad Prism 5) to obtain pIC_{50} (corresponding to pEC_{50}) values for the high- and low-affinity state (the biphasic fit was favored over the four-parameter logistic fit according to the *F*-test, $P < 0.05$, GraphPad Prism 5). To plot average data from individual binding experiments, data were normalized (100% = lower plateau of the initial biphasic fit, 0% = unspecifically bound fluorescent ligand). The differences between the lower and upper plateaus of the individual experiments gave the E_{max} values which were averaged to give the E_{max} mean ± SEM.

4.4.12 Confocal microscopy

Confocal microscopy was performed with a Zeiss LSM 710 confocal laser scanning microscope (Zeiss, Jena, Germany). The objective was 63× magnification with oil (1.4 NA). One day prior to the experiment, CHO-hNTS_1R (30,000 to 35,000 cells per chamber) and HT-29 cells (45,000 to 50,000 cells per chamber) were seeded in Nunc LabTekTM II cover glasses with 8 chambers (Thermo Fisher Scientific). On the day of the experiment, the confluency of the cells was 60-80%. After removal of the culture medium, cells were washed with Leibovitz's L15 medium (200 µL) and covered with L15 medium (150 µL) containing Hoechst H33342 (Sigma-Aldrich) (2 µg/mL). To study total binding, L15 medium (150 µL) containing Hoechst H33342 (2 µg/mL) and **4.19** or **4.21** (final concentration: 2 nM) was added. To determine unspecific binding, L15 medium (150 µL) containing Hoechst H33342 (2 µg/mL), **1.3** (final concentration: 1 µM) and **4.19** or **4.21** was added. The first image was acquired 5 min after addition of the fluorescent ligand. The pinhole was set to 1.0 Airy unit. Laser powers and gains for the investigation of **4.19**: 405 nm, 2% (gain: 700 V); 561 nm, 8% (gain: 800 V) (CHO-hNTS_1R cells) or 10% (gain: 850 V) (HT-29 cells). Laser powers and gains for the study of **4.21**: 405 nm, 2% (gain: 650 V (HT-29 cells) or 750 V (CHO-hNTS_1R cells)); 633 nm, 20% (gain: 1050 V) (CHO-hNTS_1R cells) or 40% (gain: 1100 V) (HT-29 cells). The following filter

settings for fluorescence detection were applied: 410-549 nm (Hoechst H33342, experiments with **4.19**), 410-585 nm (Hoechst H33342, experiments with **4.21**), 562-649 nm (**4.19**), and 638-759 nm (**4.21**).

4.4.13 Biomolecular imaging

Saturation binding studies at HT-29 cells. HT-29 cells were seeded one day prior to the experiment (1.0×10^5 cells/well) in black clear bottom 96-well plates (Greiner 655090, Greiner Bio-One). After washing the cells with Leibovitz's L-15 Medium (Thermo Fisher Scientific, Waltham, MA, USA), 100 µL of L-15 containing **4.19** or **4.21** in various concentrations (0.1-100 nM (**4.19**) or 0.1-25 nM (**4.21**), each in triplicates) followed by incubation at rt in the dark for 2 h. To determine unspecific binding, **1.5** (1 µM; Sigma-Aldrich) was added to the samples. For the determination of the autofluorescence only L-15 was added to the cells. In addition, CellTag™ 520 or 700 Stain (LI-COR Biotechnology, Bad Homburg, Germany) was added to each well (final concentrations: 1 µM and 0.2 µM, respectively). After incubation, the plate was set on ice, the cells were washed three times with ice-cold DPBS (Sigma-Aldrich), the buffer was removed, and fluorescence images were acquired using the Sapphire FL Biomolecular Imager (520 nm and 658 nm laser; pixel size: 20 µm; Azure Biosystems, Dublin, CA, USA). The following bandpass filters were used for fluorescence detection: 565/24 nm (**4.19**) or 710/40 nm (**4.21**). Fluorescence intensities for each well were normalized to the respective CellTag fluorescence. Specific binding data, obtained by subtracting triplicate mean values of unspecific binding from triplicate mean values of total binding, were plotted against the ligand concentration and K_d values were obtained by fitting of the data with a two-parameter equation describing hyperbolic single-site binding (one site, total and unspecific binding, GraphPad Prism 9). Four independent experiments were performed in triplicate.

Fluorescent imaging of tumor slices. NMRI (nu/nu) mice were bred in the animal facility of the University of Regensburg. Animal experiments were approved by the local veterinary authorities (district government) according to the European guidelines and national regulations of the German animal protection act (notification from 12th of May, 2011, "Propagation of tumor cells in nude mice", to the Regierung der Oberpfalz, Department 621, veterinary services). HT-29 tumor slices (10 µm) were prepared from HT-29 tumors (subcutaneously grown in NMRI nude (nu/nu) mice) using a cryostat microtome HM 500 O (Microm, Walldorf, Germany) and thaw-mounted on HistoBond® adhesive glass slides (Marienfeld, Lauda-Königshofen, Germany). Tumor slices used for the determination of total binding were covered with buffer (DPBS supplemented with 1.8 mM $CaCl_2$ and 3.98 mM $MgCl_2$) at rt for 15 min.

Tumor slices used for the determination of unspecific binding were preincubated with buffer containing **1.5** (5 µM in buffer). The tumor slices were then incubated with **4.19** (10 nM) or **4.21** (5 nM) in buffer to determine total binding. For the determination of unspecific binding, the samples contained additionally **1.5** (5 µM). Tumor slices were incubated with neat buffer to determine background signals (autofluorescence). After 1 h of incubation, the tumor slices were washed three times with ice-cold buffer, once with cold water, and were allowed to dry prior to acquisition of fluorescence images as described under *Saturation binding studies at HT-29 cells*. Data analysis was performed using the Aida Image Analyzer (v.5.1, Elysia-raytest GmbH, Straubenhardt, Germany).

4.4.14 Calculation of Propagated Errors

Propagated errors (applying to specifically bound fluorescent ligand (saturation binding)), association rate constants k_{on}, and kinetically derived dissociation constants K_d(kin) were calculated as described elsewhere.[50]

4.5 References

1. Carraway, R.; Leeman, S. E. The isolation of a new hypotensive peptide, neurotensin, from bovine hypothalami. *J. Biol. Chem.* **1973**, *248*, 6854-6861.
2. Vita, N.; Laurent, P.; Lefort, S.; Chalon, P.; Dumont, X.; Kaghad, M.; Gully, D.; Le Fur, G.; Ferrara, P.; Caput, D. Cloning and expression of a complementary DNA encoding a high affinity human neurotensin receptor. *FEBS Lett.* **1993**, *317*, 139-142.
3. Vincent, J. P.; Mazella, J.; Kitabgi, P. Neurotensin and neurotensin receptors. *Trends Pharmacol. Sci.* **1999**, *20*, 302-309.
4. Reubi, J. C.; Waser, B.; Friess, H.; Buchler, M.; Laissue, J. Neurotensin receptors: A new marker for human ductal pancreatic adenocarcinoma. *Gut* **1998**, *42*, 546-550.
5. Yin, X.; Wang, M.; Wang, H.; Deng, H.; He, T.; Tan, Y.; Zhu, Z.; Wu, Z.; Hu, S.; Li, Z. Evaluation of neurotensin receptor 1 as a potential imaging target in pancreatic ductal adenocarcinoma. *Amino Acids* **2017**, *49*, 1325-1335.
6. He, T.; Wang, M.; Wang, H.; Tan, H.; Tang, Y.; Smith, E.; Wu, Z.; Liao, W.; Hu, S.; Li, Z. Evaluation of neurotensin receptor 1 as potential biomarker for prostate cancer theranostic use. *Eur. J. Nucl. Med. Mol. Imaging* **2019**, *46*, 2199-2207.
7. Morgat, C.; Brouste, V.; Chastel, A.; Velasco, V.; Macgrogan, G.; Hindie, E. Expression of neurotensin receptor-1 (NTS(1)) in primary breast tumors, cellular distribution, and association with clinical and biological factors. *Breast Cancer Res. Treat.* **2021**, *190*, 403-413.
8. Szarynska, M.; Olejniczak-Keder, A.; Podplonska, K.; Prahl, A.; Ilowska, E. Bradykinin and neurotensin analogues as potential compounds in colon cancer therapy. *Int. J. Mol. Sci.* **2023**, *24*.
9. Pan, M.; Chen, Q.; Yao, S. Recent advances in small molecular PET tracers for pancreatic cancer diagnosis: preclinical stage. *Mini-Rev. Med. Chem.* **2025**, *25*, 745-759.
10. Maschauer, S.; Prante, O. Radiopharmaceuticals for imaging and endoradiotherapy of neurotensin receptor-positive tumors. *J. Labelled Compd. Radiopharm.* **2018**, *61*, 309-325.
11. Maes, V.; Hultsch, C.; Kohl, S.; Bergmann, R.; Hanke, T.; Tourwe, D. Fluorescein-labeled stable neurotensin derivatives. *J. Pept. Sci.* **2006**, *12*, 505-508.
12. Keller, M.; Kuhn, K. K.; Einsiedel, J.; Hübner, H.; Biselli, S.; Mollereau, C.; Wifling, D.; Svobodová, J.; Bernhardt, G.; Cabrele, C.; Vanderheyden, P. M. L.; Gmeiner, P.; Buschauer, A. Mimicking of arginine by functionalized N^{ω}-carbamoylated arginine as a new broadly applicable approach to labeled bioactive peptides: High affinity angiotensin,

neuropeptide Y, neuropeptide FF, and neurotensin receptor ligands as examples. *J. Med. Chem.* **2016**, *59*, 1925-1945.

13. Keller, M.; Mahuroof, S. A.; Hong Yee, V.; Carpenter, J.; Schindler, L.; Littmann, T.; Pegoli, A.; Hübner, H.; Bernhardt, G.; Gmeiner, P.; Holliday, N. D. Fluorescence labeling of neurotensin(8–13) via arginine residues gives molecular tools with high receptor affinity. *ACS Med. Chem. Lett.* **2020**, *11*, 16-22.
14. Renard, E.; Dancer, P. A.; Portal, C.; Denat, F.; Prignon, A.; Goncalves, V. Design of bimodal ligands of neurotensin receptor 1 for positron emission tomography imaging and fluorescence-guided surgery of pancreatic cancer. *J. Med. Chem.* **2020**, *63*, 2426-2433.
15. Gratz, L.; Muller, C.; Pegoli, A.; Schindler, L.; Bernhardt, G.; Littmann, T. Insertion of nanoluc into the extracellular loops as a complementary method to establish BRET-based binding assays for GPCRs. *ACS Pharmacol. Transl. Sci.* **2022**, *5*, 1142-1155.
16. Ertl, F. J.; Kopanchuk, S.; Dijon, N. C.; Veiksina, S.; Tahk, M. J.; Laasfeld, T.; Schettler, F.; Gattor, A. O.; Hubner, H.; Archipowa, N.; Kockenberger, J.; Heinrich, M. R.; Gmeiner, P.; Kutta, R. J.; Holliday, N. D.; Rinken, A.; Keller, M. Dually labeled neurotensin NTS(1)R ligands for probing radiochemical and fluorescence-based binding assays. *J. Med. Chem.* **2024**, *67*, 16664-16691.
17. Skrzydelski, D.; Lhiaubet, A. M.; Lebeau, A.; Forgez, P.; Yamada, M.; Hermans, E.; Rostene, W.; Pelaprat, D. Differential involvement of intracellular domains of the rat NTS1 neurotensin receptor in coupling to G proteins: A molecular basis for agonist-directed trafficking of receptor stimulus. *Mol. Pharmacol.* **2003**, *64*, 421-429.
18. Granier, C.; van Rietschoten, J.; Kitabgi, P.; Poustis, C.; Freychet, P. Synthesis and characterization of neurotensin analogues for structure/activity relationship studies. Acetyl-neurotensin-(8--13) is the shortest analogue with full binding and pharmacological activities. *Eur. J. Biochem.* **1982**, *124*, 117-124.
19. Fanelli, R.; Besserer-Offroy, E.; Rene, A.; Cote, J.; Tetreault, P.; Collerette-Tremblay, J.; Longpre, J. M.; Leduc, R.; Martinez, J.; Sarret, P.; Cavelier, F. Synthesis and characterization in vitro and in vivo of (l)-(trimethylsilyl)alanine containing neurotensin analogues. *J. Med. Chem.* **2015**, *58*, 7785-7795.
20. Vivancos, M.; Fanelli, R.; Besserer-Offroy, E.; Beaulieu, S.; Chartier, M.; Resua-Rojas, M.; Mona, C. E.; Previti, S.; Remond, E.; Longpre, J. M.; Cavelier, F.; Sarret, P. Metabolically stable neurotensin analogs exert potent and long-acting analgesia without hypothermia. *Behav. Brain Res.* **2021**, *405*, 113189.

21. Schindler, L.; Moosbauer, J.; Schmidt, D.; Spruss, T.; Gratz, L.; Ludeke, S.; Hofheinz, F.; Meister, S.; Echtenacher, B.; Bernhardt, G.; Pietzsch, J.; Hellwig, D.; Keller, M. Development of a neurotensin-derived (68)Ga-labeled PET ligand with high in vivo stability for imaging of NTS(1) receptor-expressing tumors. *Cancers* **2022**, *14*, 4922.
22. Schindler, L.; Bernhardt, G.; Keller, M. Modifications at Arg and Ile give neurotensin(8-13) derivatives with high stability and retained NTS(1) receptor affinity. *ACS Med. Chem. Lett.* **2019**, *10*, 960-965.
23. Rene, A.; Vanthuyne, N.; Martinez, J.; Cavelier, F. (L)-(Trimethylsilyl)alanine synthesis exploiting hydroxypinanone-induced diastereoselective alkylation. *Amino Acids* **2013**, *45*, 301-307.
24. Miller, S. C.; Scanlan, T. S. Site-selective N-methylation of peptides on solid support. *J. Am. Chem. Soc.* **1997**, *119*, 2301-2302.
25. Archipowa, N.; Wittmann, L.; Kockenberger, J.; Ertl, F. J.; Gleixner, J.; Keller, M.; Heinrich, M. R.; Kutta, R. J. Characterization of fluorescent dyes frequently used for bioimaging: Photophysics and photocatalytical reactions with proteins. *J. Phys. Chem. B* **2023**, *127*, 9532-9542.
26. Lugrin, D.; Vecchini, F.; Doulut, S.; Rodriguez, M.; Martinez, J.; Kitabgi, P. Reduced peptide bond pseudopeptide analogues of neurotensin: Binding and biological activities, and in vitro metabolic stability. *Eur. J. Pharmacol.* **1991**, *205*, 191-198.
27. Cusack, B.; McCormick, D. J.; Pang, Y. P.; Souder, T.; Garcia, R.; Fauq, A.; Richelson, E. Pharmacological and biochemical profiles of unique neurotensin 8-13 analogs exhibiting species selectivity, stereoselectivity, and superagonism. *J. Biol. Chem.* **1995**, *270*, 18359-18366.
28. Einsiedel, J.; Held, C.; Hervet, M.; Plomer, M.; Tschammer, N.; Hubner, H.; Gmeiner, P. Discovery of highly potent and neurotensin receptor 2 selective neurotensin mimetics. *J. Med. Chem.* **2011**, *54*, 2915-2923.
29. Previti, S.; Vivancos, M.; Remond, E.; Beaulieu, S.; Longpre, J. M.; Ballet, S.; Sarret, P.; Cavelier, F. Insightful backbone modifications preventing proteolytic degradation of neurotensin analogs improve NTS1-induced protective hypothermia. *Front. Chem.* **2020**, *8*, 406.
30. Grynkiewicz, G.; Poenie, M.; Tsien, R. Y. A new generation of Ca2+ indicators with greatly improved fluorescence properties. *J. Biol. Chem.* **1985**, *260*, 3440-3450.
31. Muller, C.; Gleixner, J.; Tahk, M. J.; Kopanchuk, S.; Laasfeld, T.; Weinhart, M.; Schollmeyer, D.; Betschart, M. U.; Ludeke, S.; Koch, P.; Rinken, A.; Keller, M.

Structure-based design of high-affinity fluorescent probes for the neuropeptide Y Y(1) receptor. *J. Med. Chem.* **2022**, *65*, 4832-4853.

32. Kockenberger, J.; Fischer, O.; Konopa, A.; Bergwinkl, S.; Muhlich, S.; Gmeiner, P.; Kutta, R. J.; Hubner, H.; Keller, M.; Heinrich, M. R. Synthesis, characterization, and application of muscarinergic M(3) receptor ligands linked to fluorescent dyes. *J. Med. Chem.* **2022**, *65*, 16494-16509.
33. She, X. K.; Pegoli, A.; Gruber, C. G.; Wifling, D.; Carpenter, J.; Hübner, H.; Chen, M. Y.; Wan, J. F.; Bernhardt, G.; Gmeiner, P.; Holliday, N. D.; Keller, M. Red-emitting dibenzodiazepinone derivatives as fluorescent dualsteric probes for the muscarinic acetylcholine M2 receptor. *J. Med. Chem.* **2020**, *63*, 4133-4154.
34. Carter, C. M. S.; Ies, C. R. L. D.; Charlton, S. J. Miniaturized receptor binding assays: Complications arising from ligand depletion. *J. Biomol. Screening* **2007**, *12*, 255-266.
35. Maschauer, S.; Einsiedel, J.; Hubner, H.; Gmeiner, P.; Prante, O. (18)F- and (68)Ga-Labeled neurotensin peptides for PET imaging of neurotensin receptor 1. *J. Med. Chem.* **2016**, *59*, 6480-6492.
36. Pugsley, T. A.; Akunne, H. C.; Whetzel, S. Z.; Demattos, S.; Corbin, A. E.; Wiley, J. N.; Wustrow, D. J.; Wise, L. D.; Heffner, T. G. Differential effects of the nonpeptide neurotensin antagonist, SR 48692, on the pharmacological effects of neurotensin agonists. *Peptides* **1995**, *16*, 37-44.
37. Lang, C.; Maschauer, S.; Hubner, H.; Gmeiner, P.; Prante, O. Synthesis and evaluation of a (18)F-labeled diarylpyrazole glycoconjugate for the imaging of NTS1-positive tumors. *J. Med. Chem.* **2013**, *56*, 9361-9365.
38. Prinz, H. Hill coefficients, dose-response curves and allosteric mechanisms. *J. Biol. Chem.* **2010**, *3*, 37-44.
39. Bindslev, N. *Drug-acceptor interactions: modeling theoretical tools to test and evaluate experimental equilibirum effects, open access e-book*; 1st ed., Taylor & Francis Group: 2017, DOI: 10.4324/9781315159782.
40. Deluigi, M.; Klipp, A.; Klenk, C.; Merklinger, L.; Eberle, S. A.; Morstein, L.; Heine, P.; Mittl, P. R. E.; Ernst, P.; Kamenecka, T. M.; He, Y.; Vacca, S.; Egloff, P.; Honegger, A.; Pluckthun, A. Complexes of the neurotensin receptor 1 with small-molecule ligands reveal structural determinants of full, partial, and inverse agonism. *Sci. Adv.* **2021**, *7*.
41. Lu, X.; Shi, X.; Fan, J.; Li, M.; Zhang, Y.; Lu, S.; Xu, G.; Chen, Z. Mechanistic elucidation of activation/deactivation signal transduction within neurotensin receptor 1

triggered by 'Driver Chemical Groups' of modulators: A comparative molecular dynamics simulation. *Pharmaceutics* **2023**, *15*.

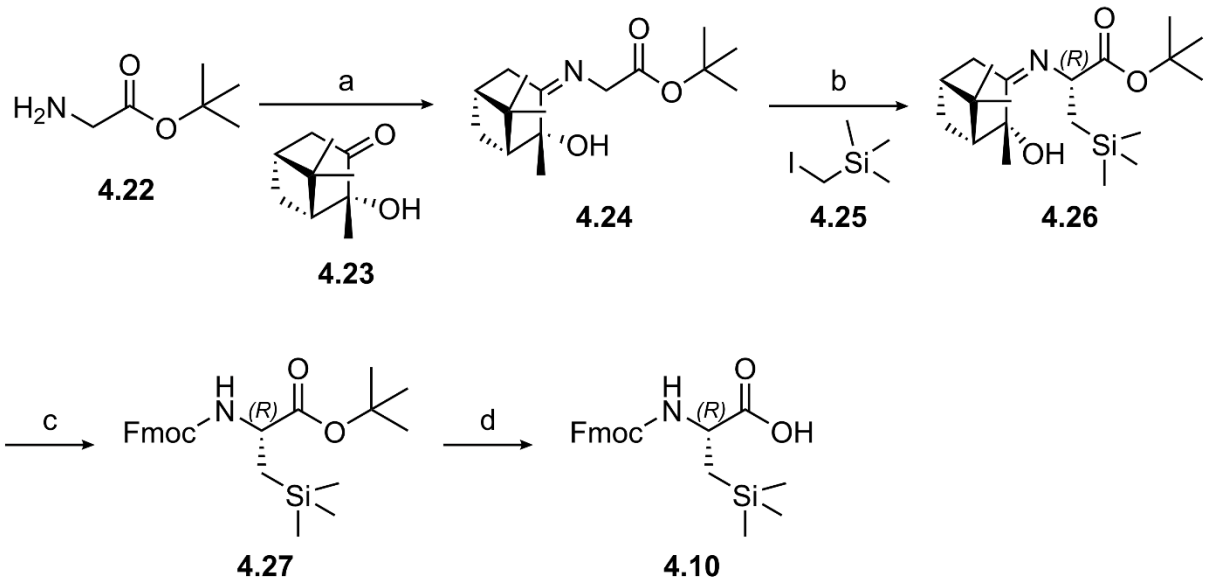
42. Pinkerton, A. B.; Peddibhotla, S.; Yamamoto, F.; Slosky, L. M.; Bai, Y.; Maloney, P.; Hershberger, P.; Hedrick, M. P.; Falter, B.; Ardecky, R. J.; Smith, L. H.; Chung, T. D. Y.; Jackson, M. R.; Caron, M. G.; Barak, L. S. Discovery of beta-arrestin biased, orally bioavailable, and CNS penetrant neurotensin receptor 1 (NTR1) allosteric modulators. *J. Med. Chem.* **2019**, *62*, 8357-8363.
43. Slosky, L. M.; Bai, Y.; Toth, K.; Ray, C.; Rochelle, L. K.; Badea, A.; Chandrasekhar, R.; Pogorelov, V. M.; Abraham, D. M.; Atluri, N.; Peddibhotla, S.; Hedrick, M. P.; Hershberger, P.; Maloney, P.; Yuan, H.; Li, Z.; Wetsel, W. C.; Pinkerton, A. B.; Barak, L. S.; Caron, M. G. beta-Arrestin-biased allosteric modulator of NTSR1 selectively attenuates addictive behaviors. *Cell* **2020**, *181*, 1364-1379 e1314.
44. Vogt, H.; Shinkwin, P.; Huber, M. E.; Staffen, N.; Hubner, H.; Gmeiner, P.; Schiedel, M.; Weikert, D. Development of a fluorescent ligand for the intracellular allosteric binding site of the neurotensin receptor 1. *ACS Pharmacol. Transl. Sci.* **2024**, *7*, 1533-1545.
45. Guo, R.; Chen, O.; Zhou, Y.; Bang, S.; Chandra, S.; Li, Y.; Chen, G.; Xie, R. G.; He, W.; Xu, J.; Zhou, R.; Song, S.; Person, K. L.; Moore, M. N.; Alwin, A. R.; Spasojevic, I.; Jackson, M. R.; Olson, S. H.; Caron, M. G.; Slosky, L. M.; Wetsel, W. C.; Barak, L. S.; Ji, R. R. Arrestin-biased allosteric modulator of neurotensin receptor 1 alleviates acute and chronic pain. *Cell* **2025**, *188*, 1-18.
46. Fanelli, R.; Chastel, A.; Previti, S.; Hindie, E.; Vimont, D.; Zanotti-Fregonara, P.; Fernandez, P.; Garrigue, P.; Lamare, F.; Schollhammer, R.; Balasse, L.; Guillet, B.; Remond, E.; Morgat, C.; Cavelier, F. Silicon-containing neurotensin analogues as radiopharmaceuticals for NTS(1)-positive tumors imaging. *Bioconjugate Chem.* **2020**, *31*, 2339-2349.
47. Gude, M.; Ryf, J.; White, P. D. An accurate method for the quantitation of Fmoc-derivatized solid phase supports. *Lett. Pept. Sci.* **2002**, *9*, 203-206.
48. Kutta, R. J. - Blitzlichtphotolyse - Untersuchung zu LOV-Domänen und photochromen Systemen. Doctoral Thesis, University of Regensburg, Regensburg, Germany, 2012 (https://epub.uni-regensburg.de/24528/1/Dissertation_main_online.pdf).
49. Cheng, Y.-C.; Prusoff, W. H. Relationship between the inhibition constant (K_I) and the concentration of inhibitor which causes 50 per cent inhibition (IC50) of an enzymatic reaction. *Biochem. Pharmacol.* **1973**, *22*, 3099-3108.

50. Gleixner, J.; Gattor, A. O.; Humphrys, L. J.; Brunner, T.; Keller, M. [(3)H]UR-JG102-A radiolabeled cyclic peptide with high affinity and excellent selectivity for the neuropeptide Y Y(4) receptor. *J. Med. Chem.* **2023**, *66*, 13788-13808.

Appendix Chapter 4

A4.1 Synthesis of Fmoc-L-(trimethylsilyl)alanine ((*R*)-4.10)

Scheme A4.1. Asymmetric synthesis of (*R*)-**4.10** according to a reported procedure.[1]



Reagents and conditions: (a) (1) Et_3N, toluene, rt, 1h; (2) **4.23**, $Et_2O \cdot BF_3$, toluene, reflux, 4 h; (b) (1) LDA, THF, -78 °C, 40 min; (2) **4.25**, -78 °C, 8 h; (3) -10 °C, overnight; (c) (1) 15% aqueous citric acid solution/THF 75:25 (v/v), rt, 3 days; (2) FmocOSu, Et_3N, ethyl acetate, rt, 6 h; (d) TFA, rt, 1 h.

Experimental protocols and analytical data

***Tert*-butyl 2-(((1*R*,2*R*,5*R*,*Z*)-2-hydroxy-2,6,6-trimethylbicyclo[3.1.1]heptan-3-ylidene)amino)acetate (4.24).**[1] Compound **4.24** was synthesized according to the reported procedure[1] using 3.0 g of glycine *tert*-butyl ester hydrochloride (**4.22**) (17.9 mmol) and 2.0 g of (1*R*,2*R*,5*R*)-2-hydroxy-3-pinanone (**4.23**) (11.9 mmol). Purification was slightly adapted using light petroleum/diethyl ether with 1% Et_3N (3:1 (v/v) to 1:1 (v/v)) as eluent mixture. **4.24** was obtained as yellow oil (0.97 g, 29%). ^{1}H-NMR (400 MHz, $CDCl_3$): δ (ppm) 0.86 (s, 3H), 1.32 (s, 3H), 1.48 (s, 9H), 1.51 (s, 3H), 1.56 (d, 1H, *J* 10.7 Hz), 1.99-2.10 (m, 2H), 2.29-2.37 (m, 1H), 2.41-2.54 (m, 2H), 2.55-2.70 (br s, 1H), 4.02-4.13 (m, 2H). ^{13}C-NMR (100 MHz, $CDCl_3$): δ (ppm) 22.90, 27.32, 28.12 (4 carbon atoms), 28.29, 33.62, 38.28, 38.55, 50.26, 53.45, 76.50, 81.30, 169.31, 179.63. HRMS (ESI): *m/z* $[M+H]^+$ calcd. for $[C_{16}H_{28}NO_3]^+$ 282.2064, found: 282.2067. RP-HPLC (220 nm): 97% (t_R = 5.5 min, *k* = 6.2). $C_{16}H_{27}NO_3$ (281.40).

***Tert*-butyl (*R*)-2-(((1*R*,2*R*,5*R*,*Z*)-2-hydroxy-2,6,6-trimethylbicyclo[3.1.1]heptan-3-ylidene)amino)-3-(trimethylsilyl)propanoate (4.26).**[1] Compound **4.26** was synthesized according to the reported procedure[1] using 1.5 g of **4.24** (5.2 mmol) and 1.4 mL of (iodomethyl)trimethylsilane (**4.25**) (9.4 mmol). Purification was slightly adapted using light petroleum/diethyl ether with 1% Et_3N (6:1 (v/v) to 2:1 (v/v)) as eluent mixture. **4.26** was obtained as yellow oil (0.64 g, 34%). ^{1}H-NMR (400 MHz, $CDCl_3$): δ (ppm) 0.02 (s, 9H), 0.86 (s, 3H), 1.21-1.25 (m, 2H), 1.33 (s, 3H), 1.44 (s, 9H), 1.48 (s, 3H), 1.56 (d, 1H, *J* 10.7 Hz), 1.98-2-05 (m, 1H), 2.05-2.10 (m, 1H), 2.28-2.37 (m, 1H), 2.45-2.59 (m, 2H), 2.62 (s, 1H), 4.15-4.21 (m, 1H). ^{13}C-NMR (100 MHz, $CDCl_3$): δ (ppm) 0.00 (3 carbon atoms), 21.35, 22.97, 27.50, 28.14 (3 carbon atoms), 28.32, 28.39, 33.15, 38.37, 38.50, 50.26, 60.56, 76.63, 81.21, 172.28, 177.71. HRMS (ESI): *m/z* $[M+H]^+$ calcd. for $[C_{20}H_{38}NO_3Si]^+$ 368.2616, found: 268.2622. RP-HPLC (220 nm): 86% (t_R = 10.7 min, *k* = 13.1). $C_{20}H_{37}NO_3Si$ (367.61).

***Tert*-butyl (*R*)-2-((((9*H*-fluoren-9-yl)methoxy)carbonyl)amino)-3-(trimethylsilyl)propanoate (4.27).**[1] Compound **4.27** was synthesized according to the reported procedure[1] using 0.64 g of **4.26** (1.7 mmol) and 0.76 g of FmocOSu (2.3 mmol). **4.27** was obtained as yellow oil (0.56 g, 76%). HRMS (ESI): *m/z* $[M+Na]^+$ calcd. for $[C_{25}H_{33}NNaO_4Si]^+$ 462.2072, found: 462.2083. RP-HPLC (220 nm): 94% (t_R = 18.6 min, *k* = 23.5). $C_{25}H_{33}NO_4Si$ (439.63).

(*R*)-2-((((9*H*-Fluoren-9-yl)methoxy)carbonyl)amino)-3-(trimethylsilyl)propanoic acid (4.10).[1] Compound **4.10** was synthesized according to the reported procedure[1] using 0.56 g of **4.27** (1.3 mmol). **4.10** was obtained as crystalline foam (0.41g, 85%). ^{1}H-NMR (400 MHz, $CDCl_3$): δ (ppm) 0.07 (s, 9H), 0.95-1.04 (m, 1H), 1.17-1.25 (m, 1H), 4.22 (t, 1H, *J* 7.1 Hz), 4.38-4.44 (m, 2H), 5.13 (d, 1H, *J* 8.7 Hz), 7.30 (t, 2H, *J* 7.8 Hz), 7.39 (t, 2H, *J* 7.1 Hz), 7.59 (t, 2H, *J* 7.7 Hz), 7.76 (t, 2H, *J* 7.4 Hz), 7.92-8.98 (br s, 1H). The proton signal of the carboxylic acid was not apparent. ^{13}C-NMR (100 MHz, $CDCl_3$): δ (ppm) 0.00 (3 carbon atoms), 21.04, 47.28, 51.24, 67.20, 120.13 (2 carbon atoms), 125.16, 125.23, 127.22 (2 carbon atoms), 127.87 (2 carbon atoms), 141.45 (2 carbon atoms), 143.80 (2 carbon atoms), 155.95, 178.95. HRMS (ESI): *m/z* $[M+H]^+$ calcd. for $[C_{21}H_{26}NO_4Si]^+$ 384.1626, found: 384.1630. RP-HPLC (220 nm): > 93% (t_R = 13.9 min, *k* = 17.3). $C_{21}H_{25}NO_4Si$ (383.52).

A4.2 Figures A4.1-A4.13

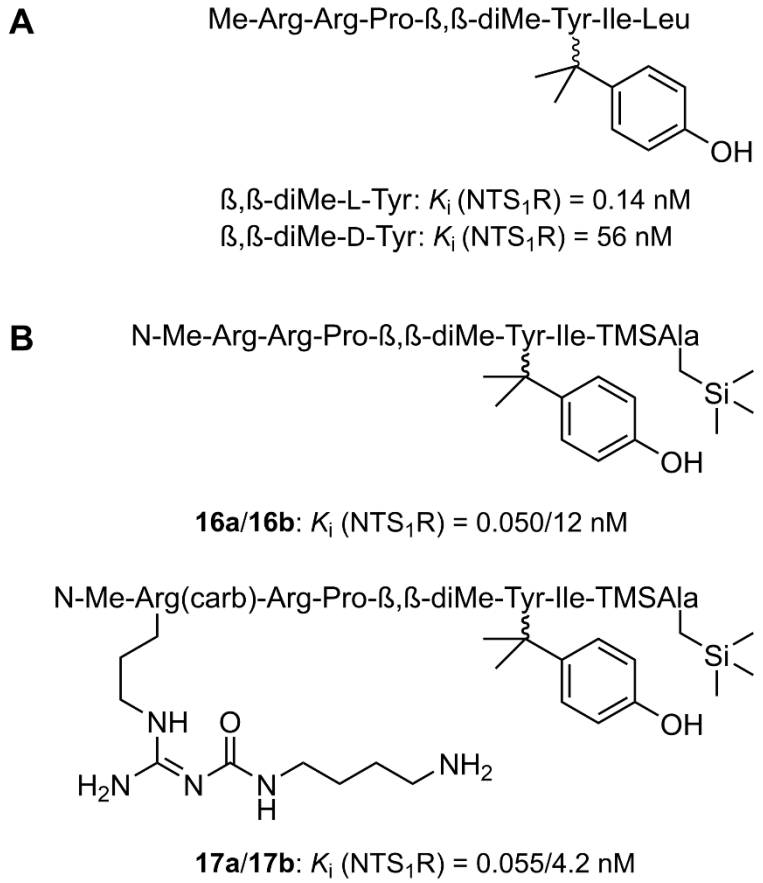


Figure A4.1. (A) Structures and NTS_1R binding affinities of reported NT(8-13) derivatives containing either β,β-dimethly-L-Tyr or β,β-dimethly-D-Tyr in position 11 (compound **48** and **49**, respectively, in Schindler *et al.*[2]). (B) Structures and NTS_1R binding affinities of the diastereomeric pairs **4.16a**/**4.16b** and **4.17a**/**4.17b**.

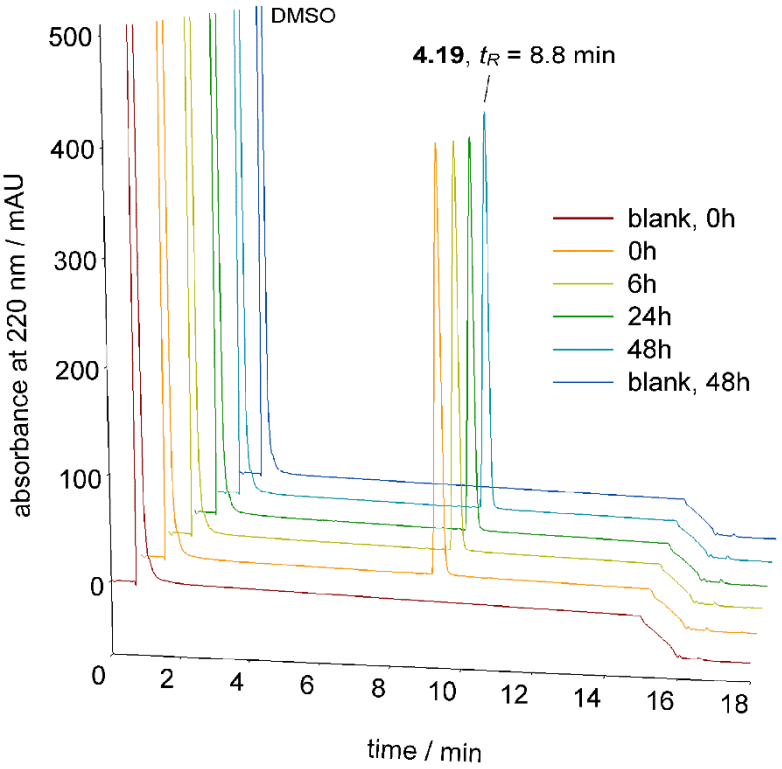


Figure A4.2. Investigation of the chemical stability of **4.19** in PBS (pH = 7.4). Shown are the chromatograms of the RP-HPLC after incubation for up to 48 hours. **4.19** showed no decomposition.

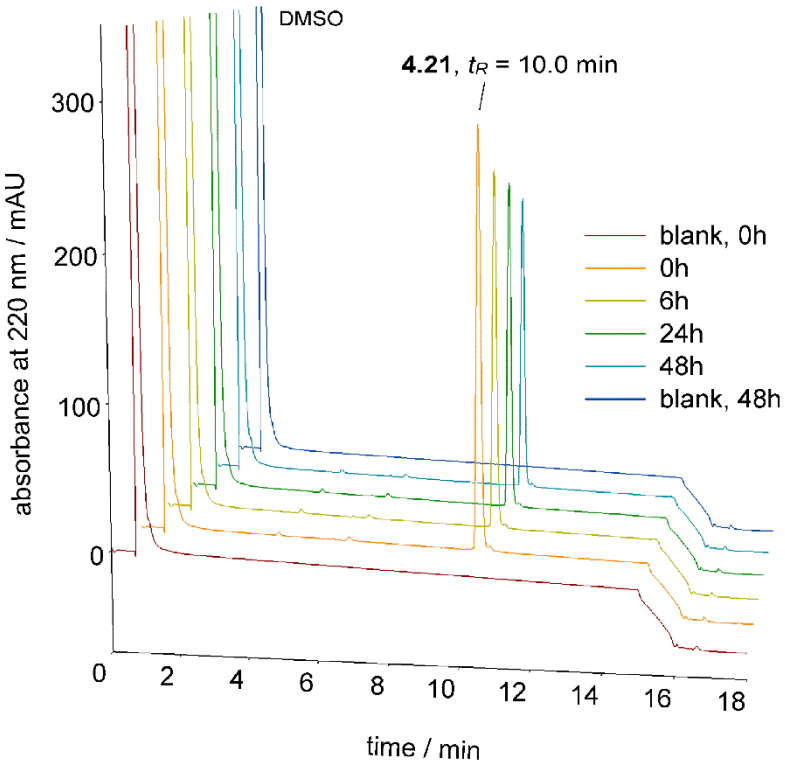
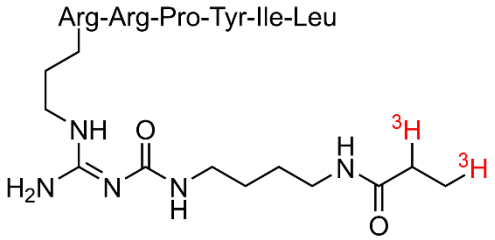


Figure A4.3. Investigation of the chemical stability of **4.21** in PBS (pH = 7.4). Shown are the chromatograms of the RP-HPLC after incubation for up to 48 hours. **4.21** showed no decomposition. The slight decrease in peak height over time is caused by adsorption of **4.21** to the vessel.



[^{3}H]UR-MK300

Figure A4.4. Structure of [^{3}H]**1.7** ([^{3}H]MK300) used for the NTS_1R and NTS_2R competition binding studies.[3] Note that the tritium atoms in the [^{3}H]propionyl residue do not represent the quantity of tritium isotopes. They only indicate that tritium is present in the respective position.

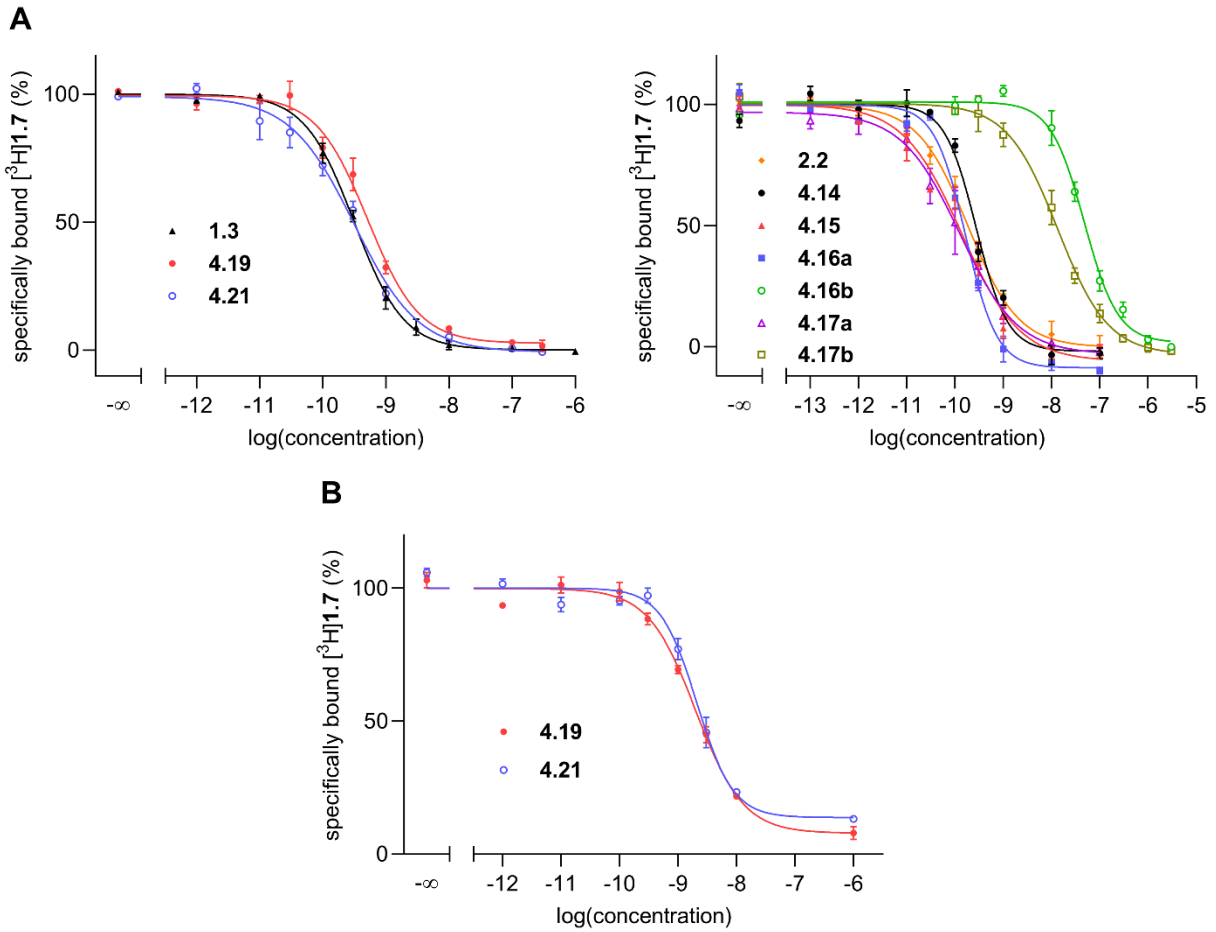


Figure A4.5. (A) Radioligand displacement curves from competition binding experiments with [^{3}H]**1.7** (K_d = 0.41 nM,[2] c = 1 nM) and **1.3**, **2.2**, **4.14-4.17b**, **4.19** or **4.21** at intact HT-29 cells. (B) Radioligand displacement curves from competition binding experiments with [^{3}H]**1.7** (K_d = 3.1 nM, c = 5 nM) and **4.19** or **4.21** at membranes of HEK293T-$hNTS_2R$ cells. Data represent mean values ± SEM from at least three independent experiments performed in triplicate. All slope factors (data not shown) were not significantly different from -1 (two-tailed *t* test based on the SEM, $P > 0.05$). For pK_i and K_i values see Table 4.2.

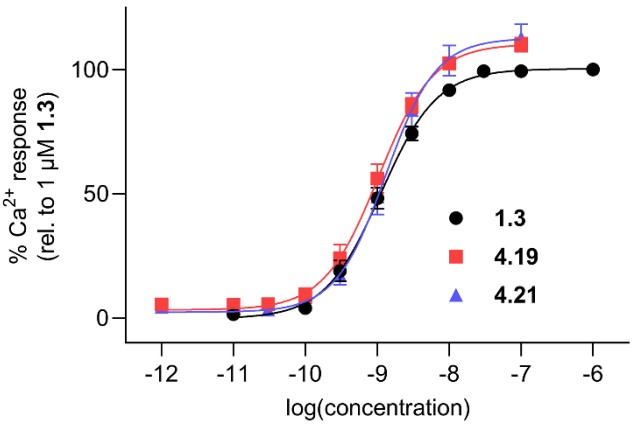


Figure A4.6. Concentration response curves of **1.3**, **4.19**, and **4.21** obtained from a Fura-2 Ca^{2+} assay performed with HT-29 cells. Mean values ± SEM from at least three independent experiments (performed in triplicate). For pEC_{50} and EC_{50} values see Table 4.2.

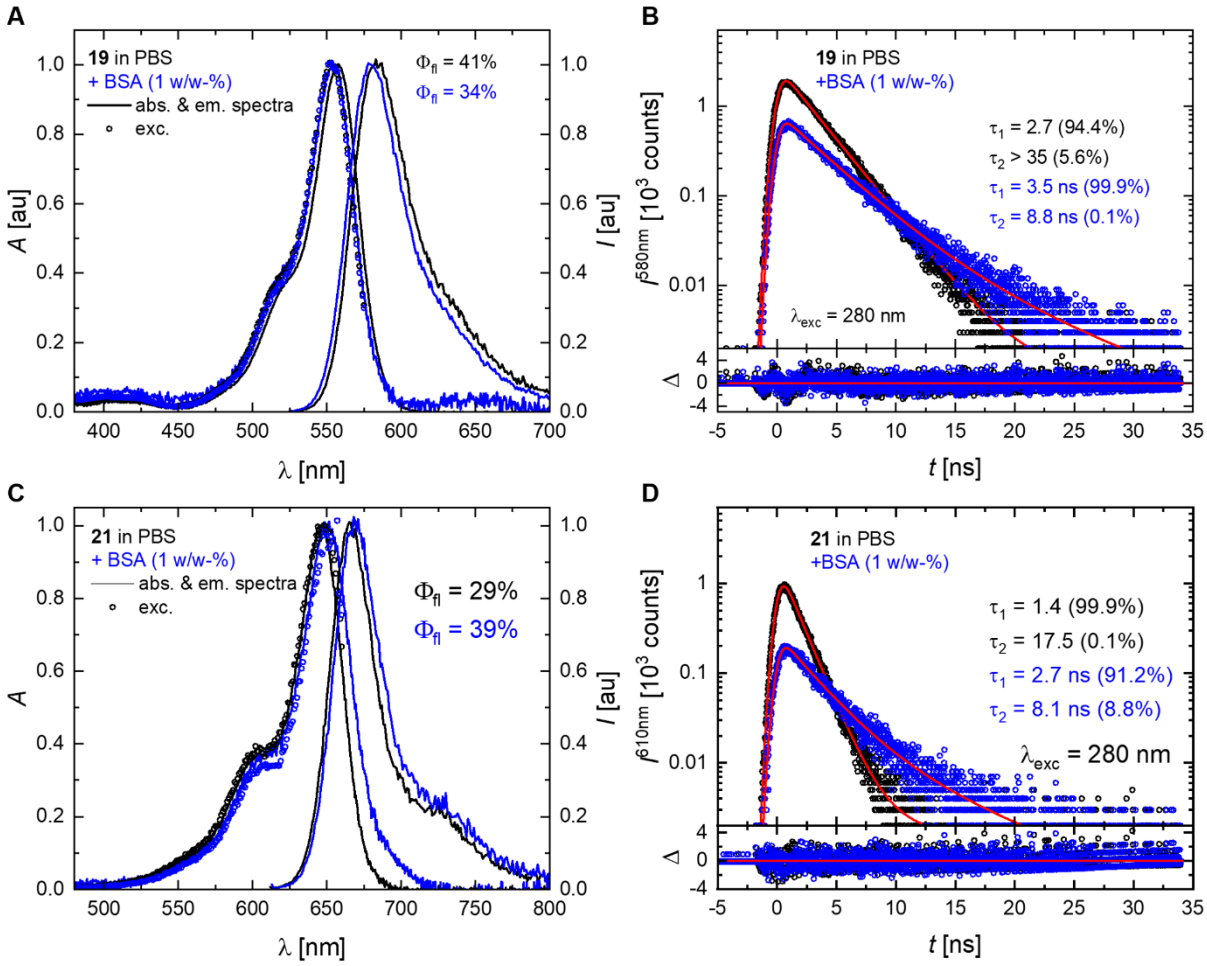


Figure A4.7. Absorption, emission, and excitation spectra (A, C) as well as emission lifetimes (B, C) of **4.19** and **4.21** in PBS in the absence (black) and presence of BSA (1% w/w, blue).

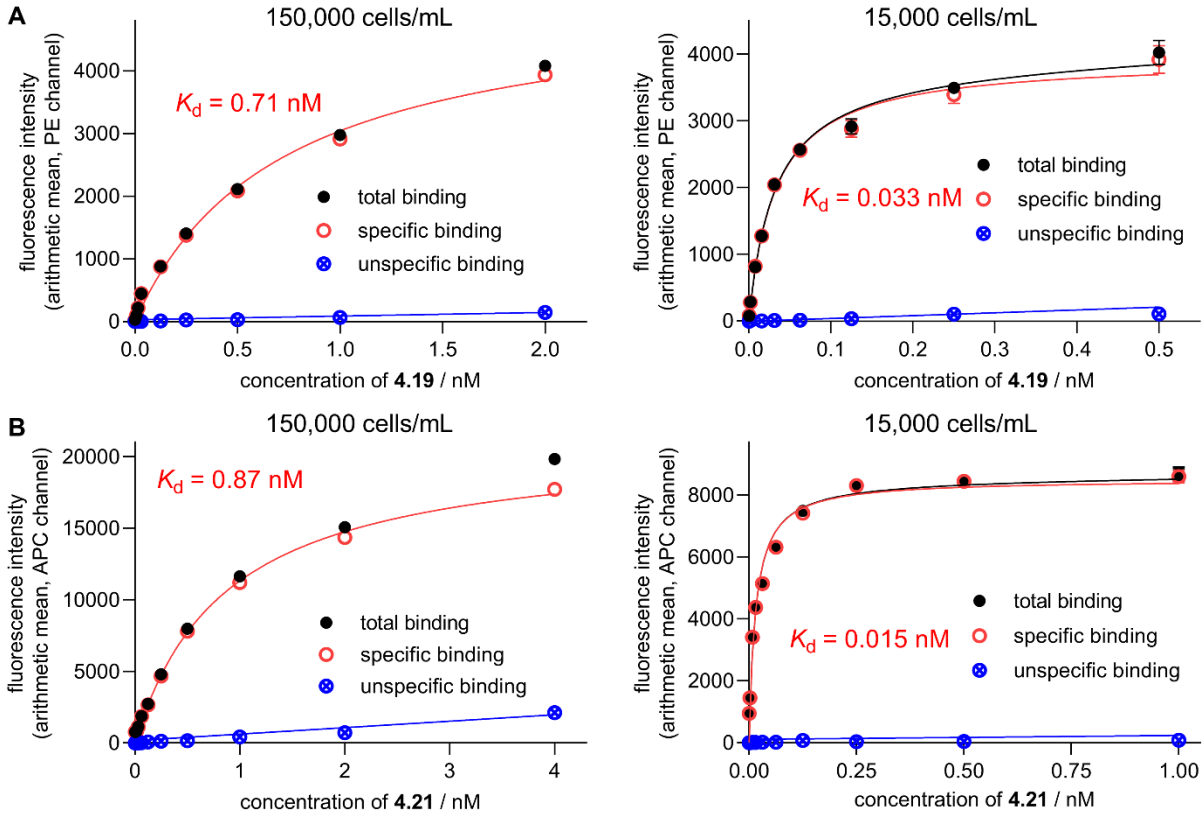


Figure A4.8. Representative binding isotherms (specific binding, open symbols) of **4.19** (A) and **4.21** (B) obtained from flow cytometric saturation binding experiments performed at intact CHO-hNTS$_1$R cells using different cell densities (150,000 or 15,000 cells/mL) (incubation: 120 min at 23 °C). Unspecific binding was determined in the presence of 1 µM **1.3**. K_d values are presented in Table 4.4. Data represent mean values ± SEM (total and unspecific binding) or calculated values ± propagated error (specific binding) from representative experiments performed in triplicate.

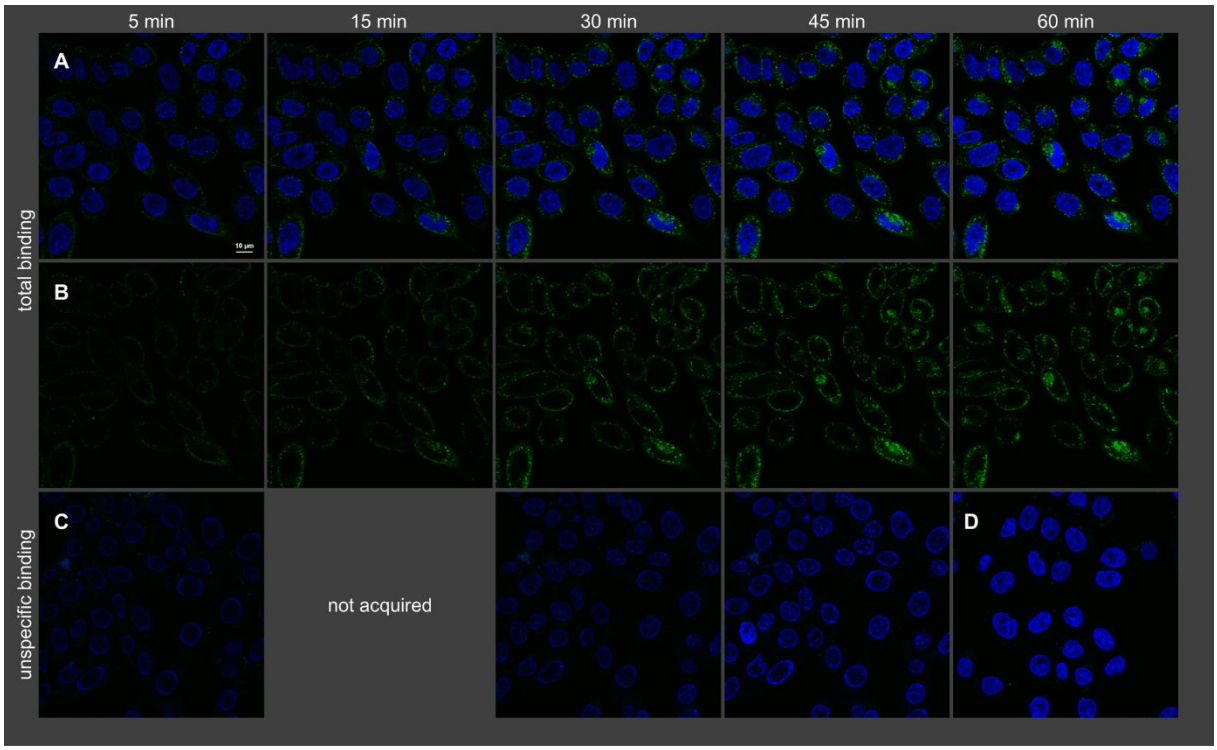


Figure A4.9. Visualization of binding of **4.19** (2 nM) to intact CHO-hNTS$_1$R cells (temperature: 22 °C) by confocal microscopy. Shown is total binding (A, B), unspecific binding (C), and autofluorescence (D). Nuclei were stained with Hoechst H33342 (2 µg/mL). (A) Merged fluorescence of **4.19** (green) and nuclei (blue). (B) Fluorescence of **4.19**, without nuclei. (C) Merged fluorescence of **4.19** and nuclei acquired in the presence of 1 µM **1.3**.

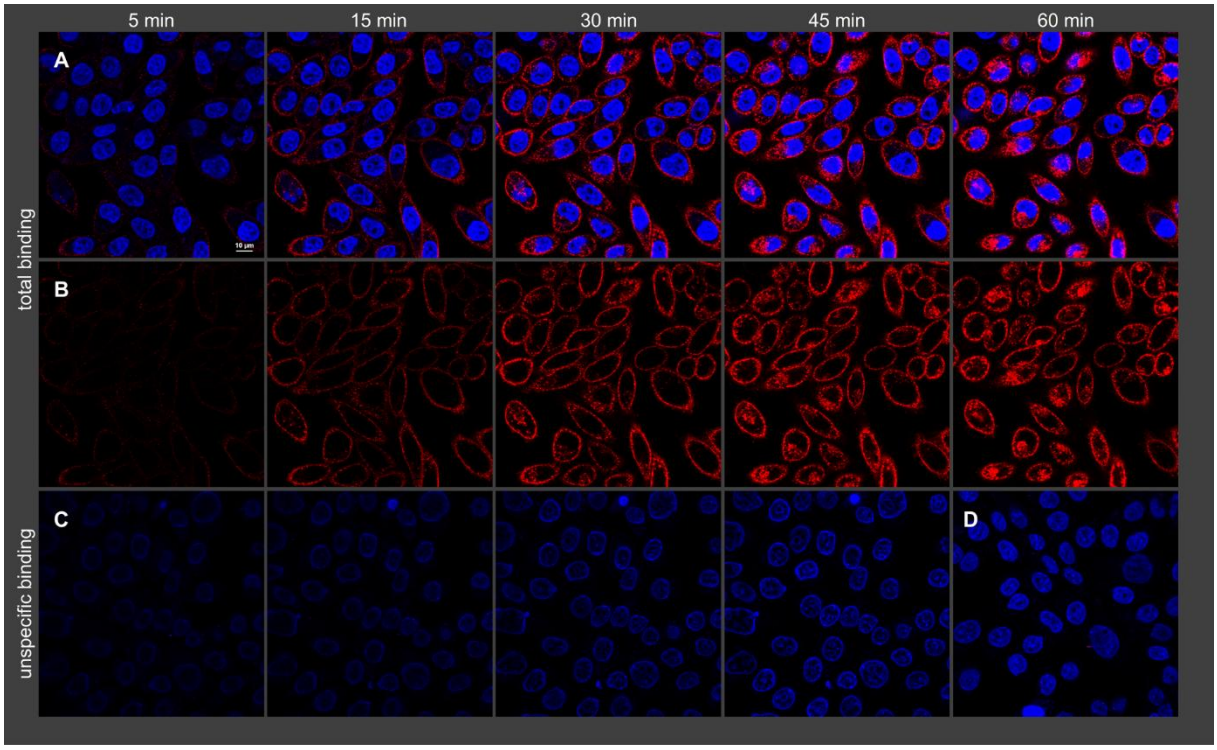


Figure A4.10. Visualization of binding of **4.21** (2 nM) to intact CHO-hNTS$_1$R cells (temperature: 22 °C) by confocal microscopy. Shown is total binding (A, B), unspecific binding (C), and autofluorescence (D). Nuclei were stained with Hoechst H33342 (2 µg/mL). (A) Merged fluorescence of **4.21** (red) and nuclei (blue). (B) Fluorescence of **4.21**, without nuclei. (C) Merged fluorescence of **4.21** and nuclei acquired in the presence of 1 µM **1.3**.

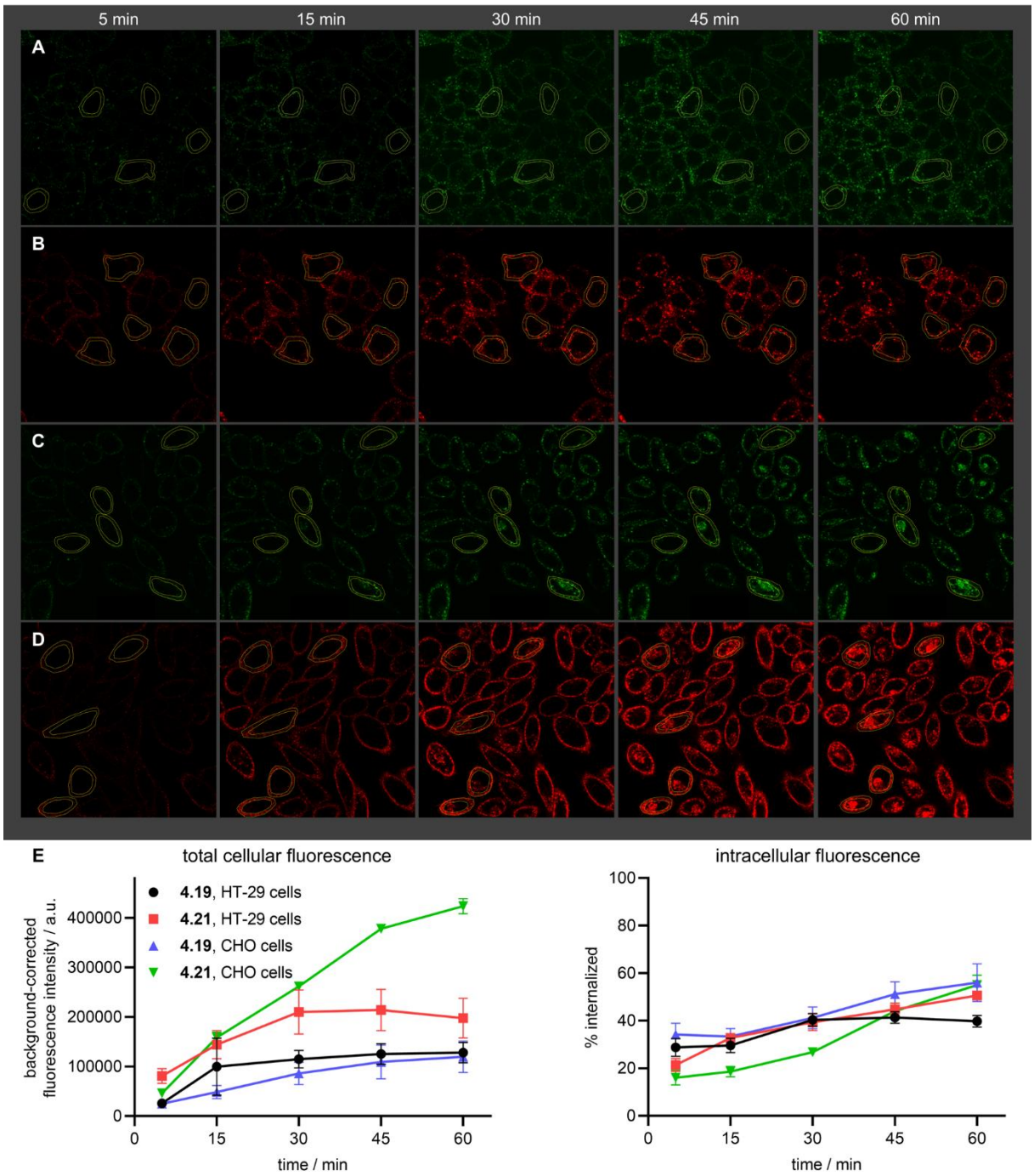


Figure A4.11. Estimation of total cellular fluorescence and intracellular fluorescence based on the confocal microscopy images shown in Figure 4.6 (**4.19**, HT-29 cells) (A), Figure 4.7 (**4.21**, HT-29 cells) (B), Figure A4.9 (**4.19**, CHO cells) (C), and Figure A4.10 (**4.21**, CHO cells) (D). For each image series, two regions of interest (ROI) were defined for five individual cells (yellow line). The outer ROI includes the entire cell and the inner ROI represents the inside of the cell. The ROIs were visually defined based on the 5 min time point. (E) Graphical presentation of the total cellular fluorescence (outer ROIs, mean values ± SEM) and the intracellular fluorescence (inner ROIs, mean values ± SEM), representing internalized fluorescent ligand, calculated as % of total cellular fluorescence. Fluorescence densities were determined with ImageJ.[4] Fluorescence densities were background-corrected according to: *corrected fluorescence density = fluorescence density of the ROI defining total and intracellular fluorescence* – (*background mean fluorescence of the background ROI* × *area of the ROI defining total and intracellular fluorescence*). Background ROIs are not depicted. Note that the intensities of the total fluorescence can not be directly compared for the two cell lines since different settings (laser power, detector gain) were used.

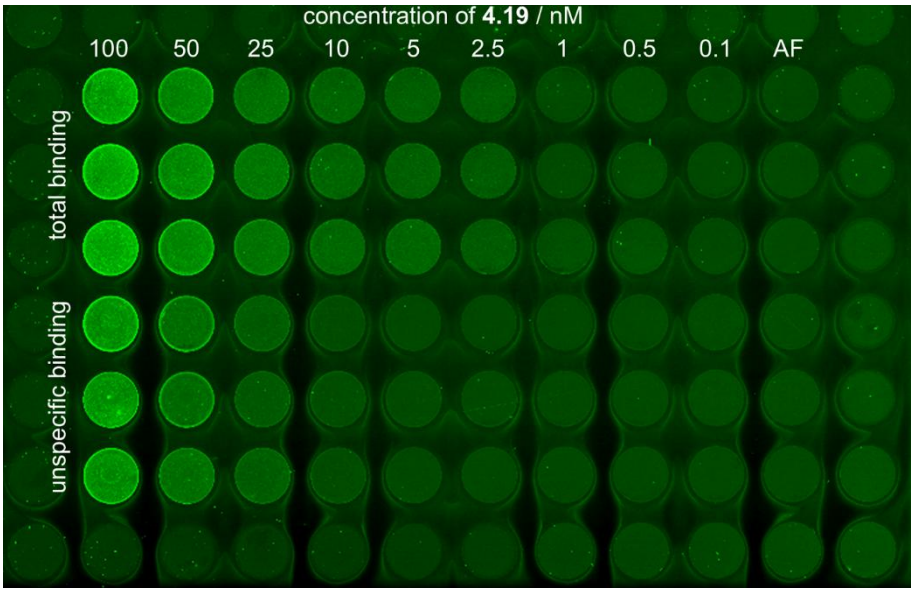


Figure A4.12. Fluorescence image of a 96-well plate with adherent HT-29 cells acquired with an Azure Sapphire Biomolecular Imager (laser: 520 nm; pixel size: 20 µm) 2 h after incubation with **4.19** at rt. Unspecific binding was determined in the presence of **1.5** (1 µM). Shortly before image acquisition, cells were washed three times with cold buffer.

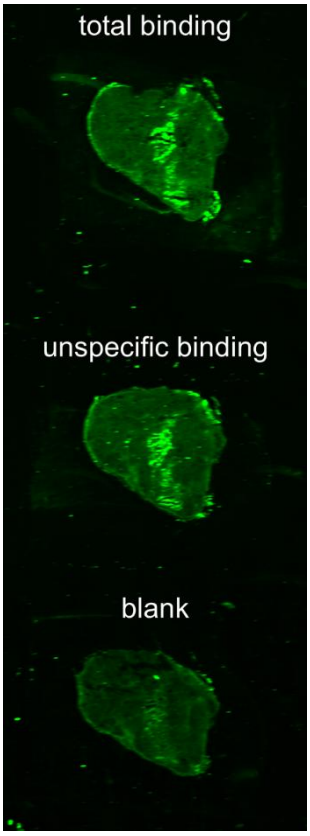


Figure A4.13. Fluorescence images of cryosections (10 µm) of a HT-29 tumor (the same tumor was used for experiments with **4.21**; see tumor 2 in Figure 4.8) acquired after incubation with **4.19** (10 nM) at rt for 60 min with an Azure Sapphire FL Biomolecular Imager (laser: 520 nm; pixel size: 20 µm). Unspecific binding was determined in the presence of **1.5** (5 µM). Blank samples were incubated with neat buffer to determine background signals. Shortly before image acquisition, tumor sections were washed three times with cold buffer.

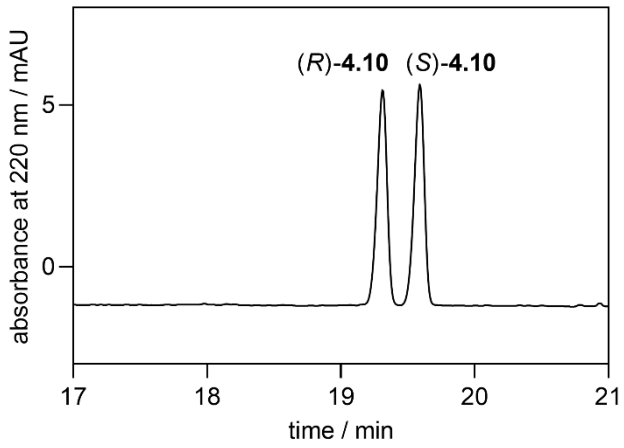
A4.3 Table A4.1

Table A4.1. Recoveries of **1.3**, **4.15**, **4.17a**, **4.19**, and **4.21** from human plasma/PBS 1:2 v/v and ratios of compound-recovery over recovery of internal standard (1-methyl-D-tryptophan).

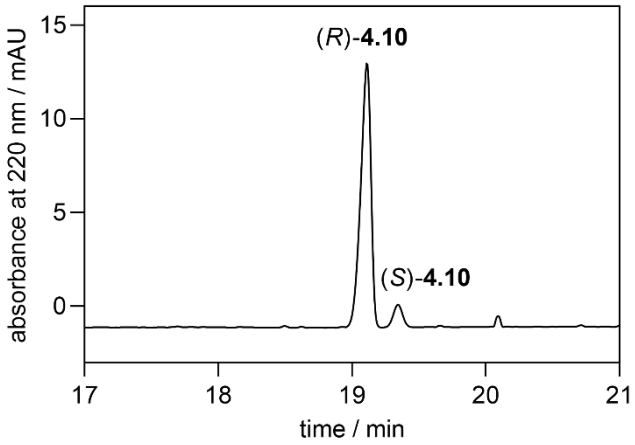
compd.	recovery compd. (%)[a]	recovery 1-methyl-D-tryptophan (%)[a]	ratio[b]
1.3	100	101	1.00
	91	97	0.93
	92	90	1.03
	96	94	1.01
	92	89	1.03
			(1.00 ± 0.02)
4.15	95	94	1.00
	91	93	0.99
	87	86	1.01
	96	97	0.99
	90	91	0.99
			(1.00 ± 0.004)
4.17a	50	50	1.00
	84	81	1.04
	76	84	0.91
	76	78	0.97
	94	94	1.01
			(0.99 ± 0.02)
4.19	97	93	1.05
	110	109	1.02
	104	106	0.99
	117	110	1.06
			(1.03 ± 0.02)
4.21	101	102	0.99
	77	69	1.12
	93	87	1.07
			(1.06 ± 0.04)

[a]Recoveries of the peptides and of the internal standard from human plasma/PBS 1:2 v/v using a peptide concentration of 40 µM and an internal standard concentration of 10 µM (four independent experiments). [b]Ratios of peptide recovery over recovery of internal standard calculated for individual experiments, as well as mean recovery ratios ± SEM (given in parenthesis).

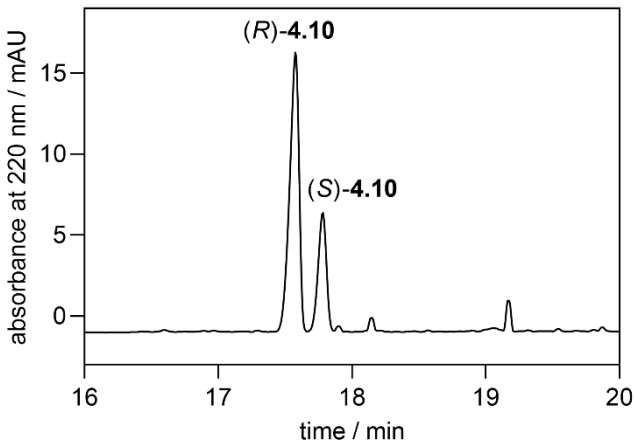
A4.4 Electropherograms of the CE analysis of (*R*,*S*)-4.10 and (*R*)-4.10



Section of the electropherogram of the CE analysis of (*R*,*S*)-**4.10** showing the separated signals of the enantiomers

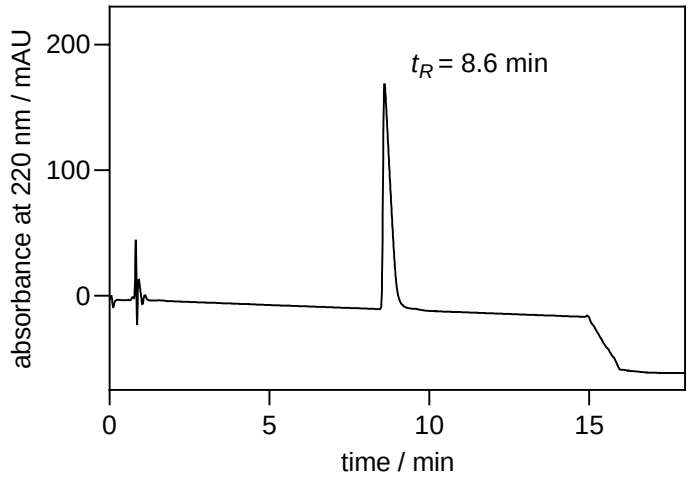


Section of the electropherogram of the CE analysis of (*R*)-**4.10** showing the signal of (*R*)-**4.10** and the minor enantiomer (*S*)-**4.10** (7%)

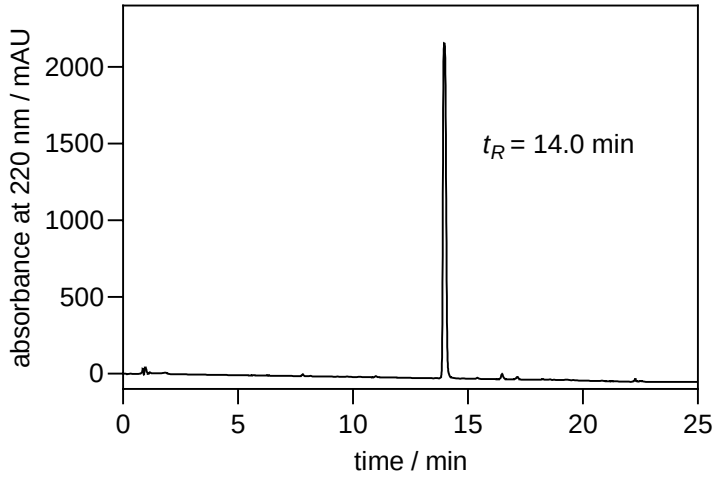


Section of the electropherogram of the CE analysis of (*R*)-**4.10** spiked with (*R*,*S*)-**4.10** showing the signals of (*R*)-**4.10** and (*S*)-**4.10**

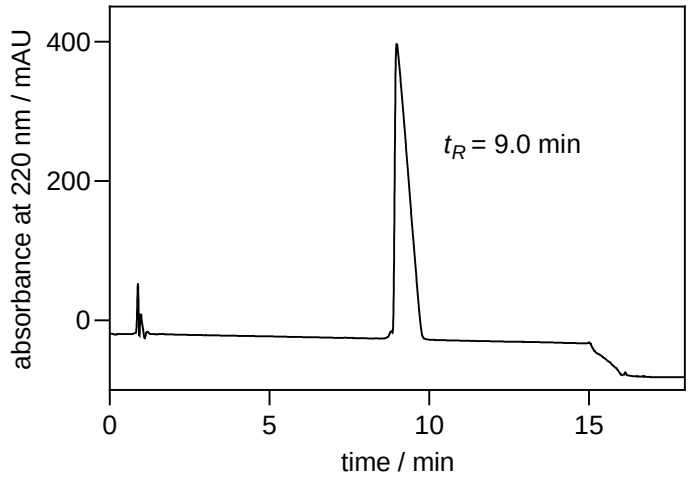
A4.5 RP-HPLC chromatograms of 2.2, 4.10, 4.14-4.17b, 4.19, and 4.21 (purity controls)



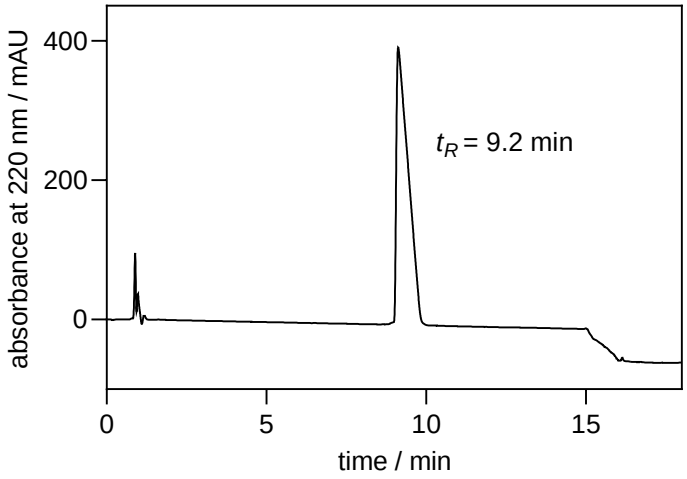
RP-HPLC analysis of compound **2.2**



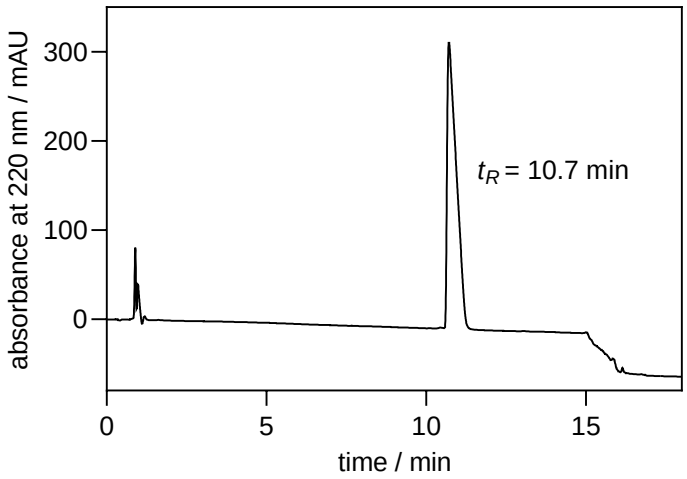
RP-HPLC analysis of compound **4.10**



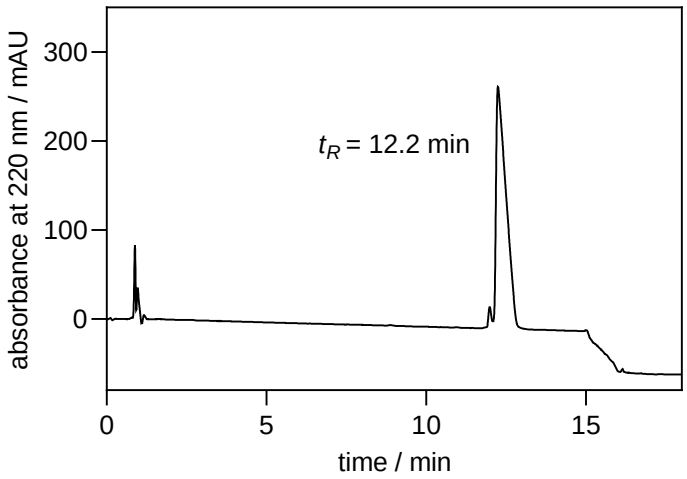
RP-HPLC analysis of compound **4.14**



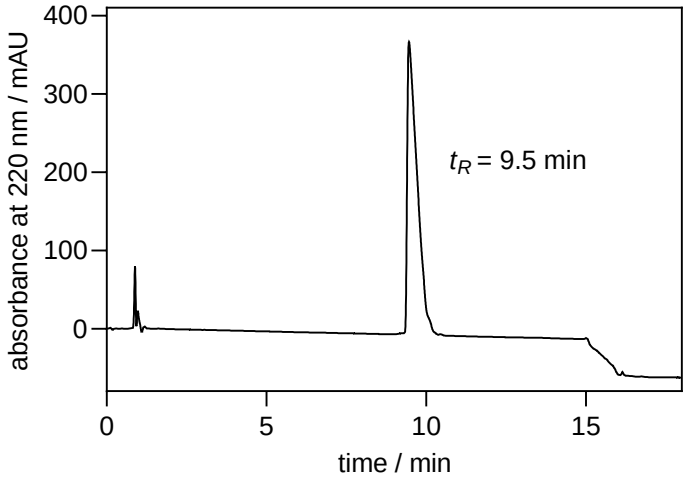
RP-HPLC analysis of compound **4.15**



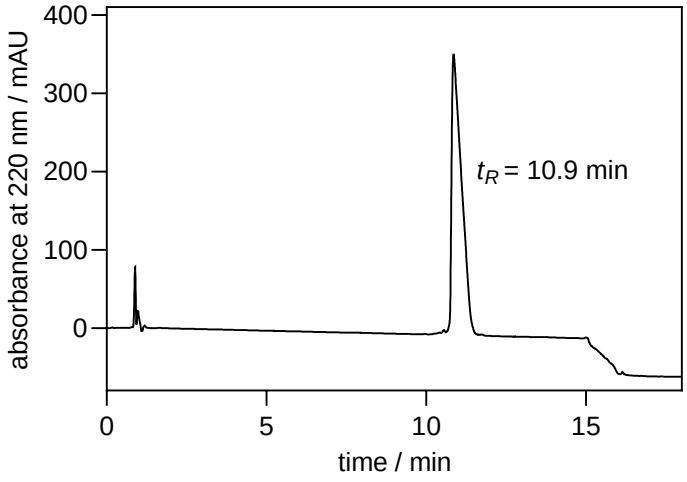
RP-HPLC analysis of compound **4.16a**



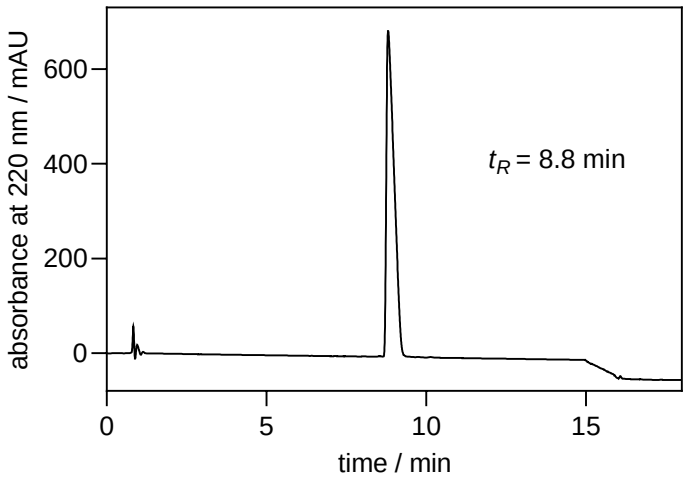
RP-HPLC analysis of compound **4.16b**



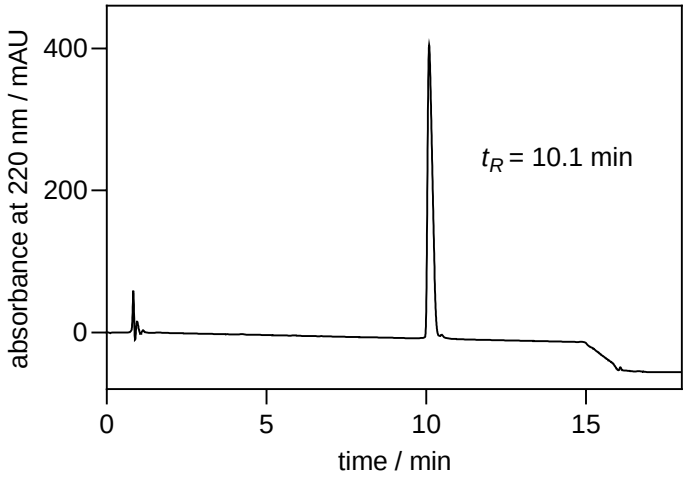
RP-HPLC analysis of compound **4.17a**



RP-HPLC analysis of compound **4.17b**

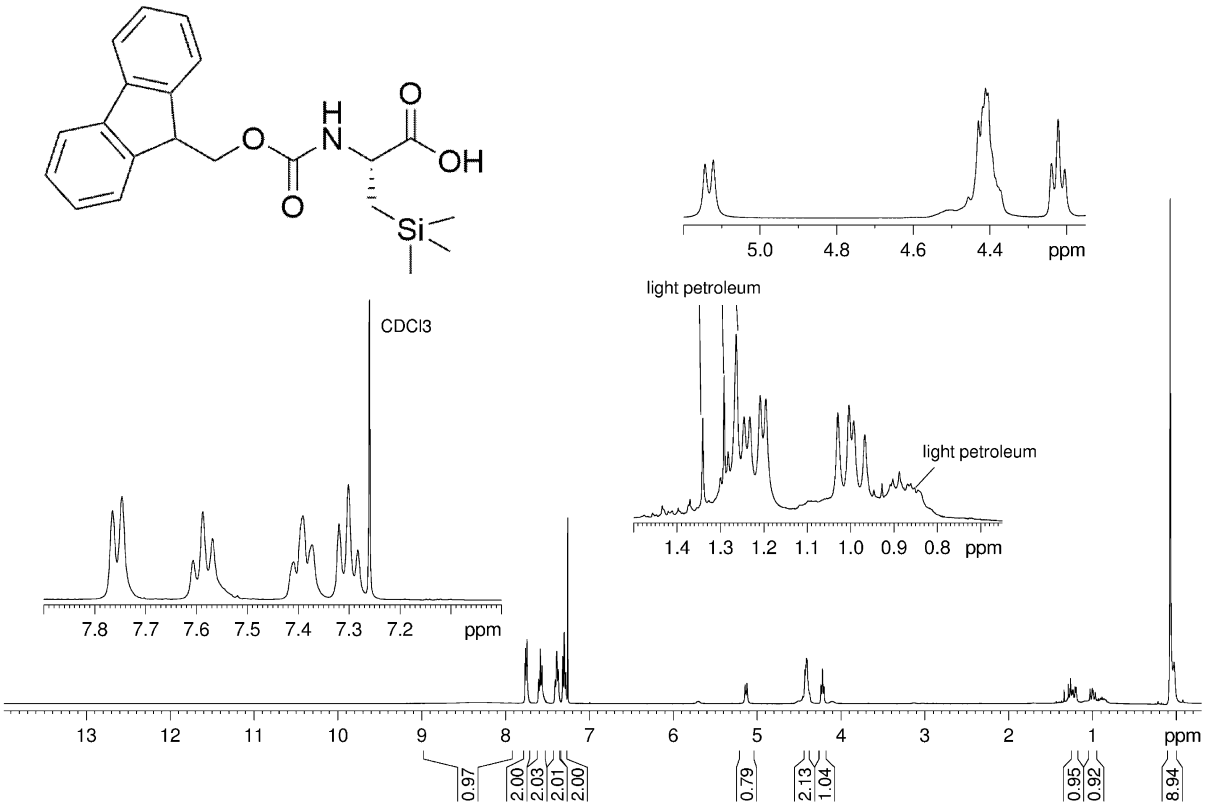


RP-HPLC analysis of compound **4.19**

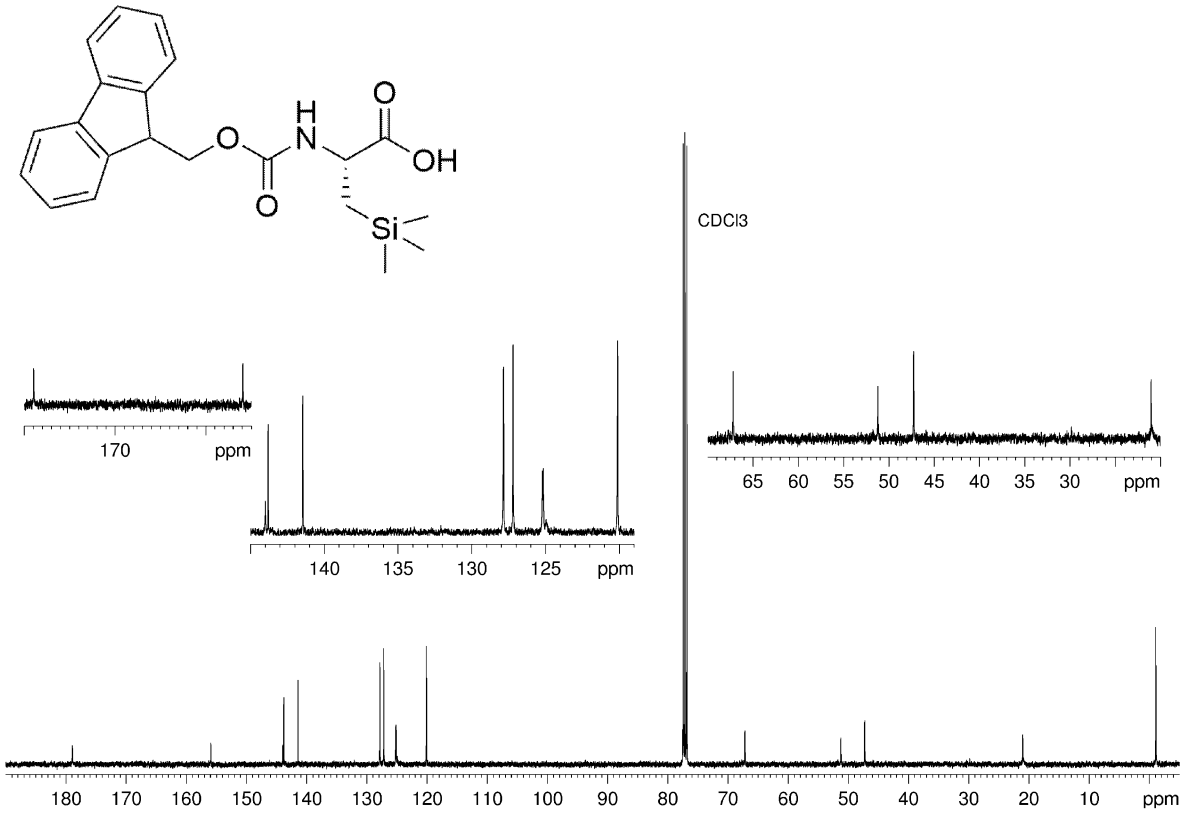


RP-HPLC analysis of compound **4.21**

A4.6 ^{1}H-NMR spectrum and ^{13}C-NMR spectrum of compound 4.10 in $CDCl_3$

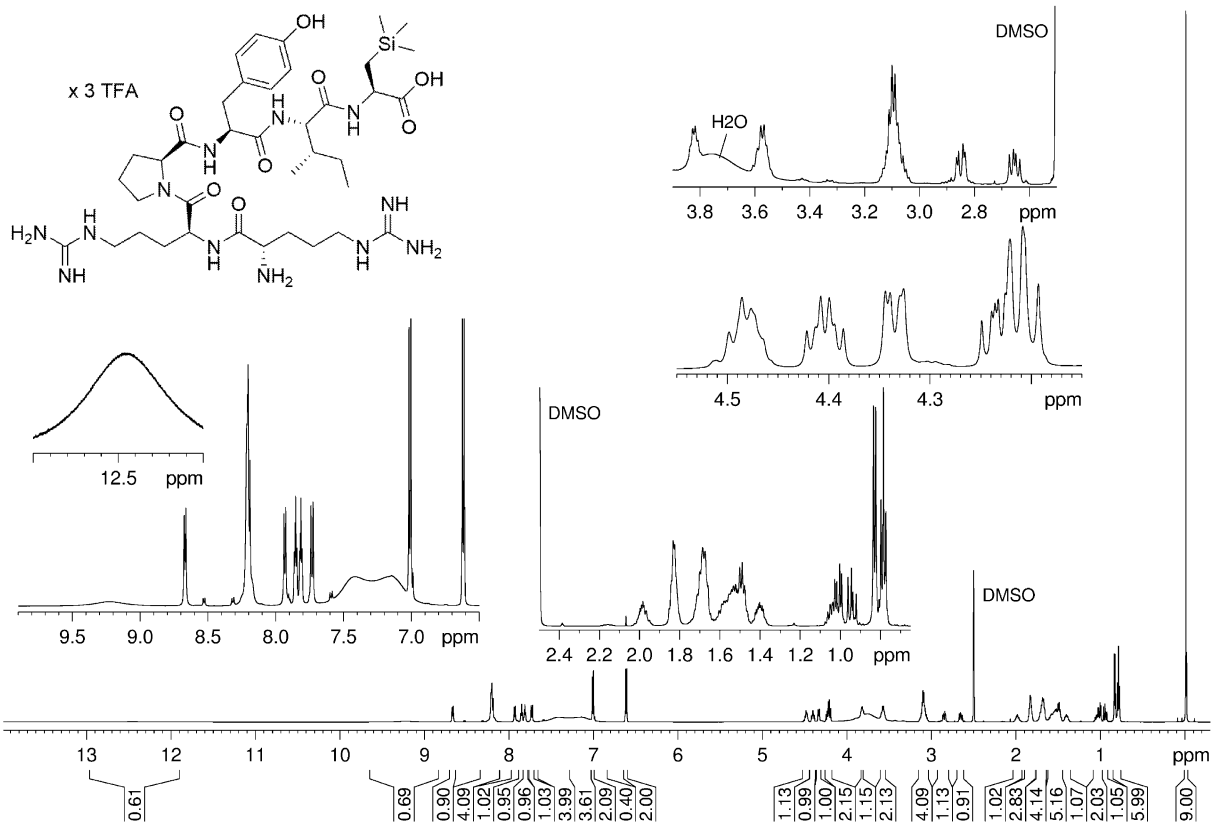


^{1}H-NMR spectrum (400 MHz, $CDCl_3$) of compound **4.10**

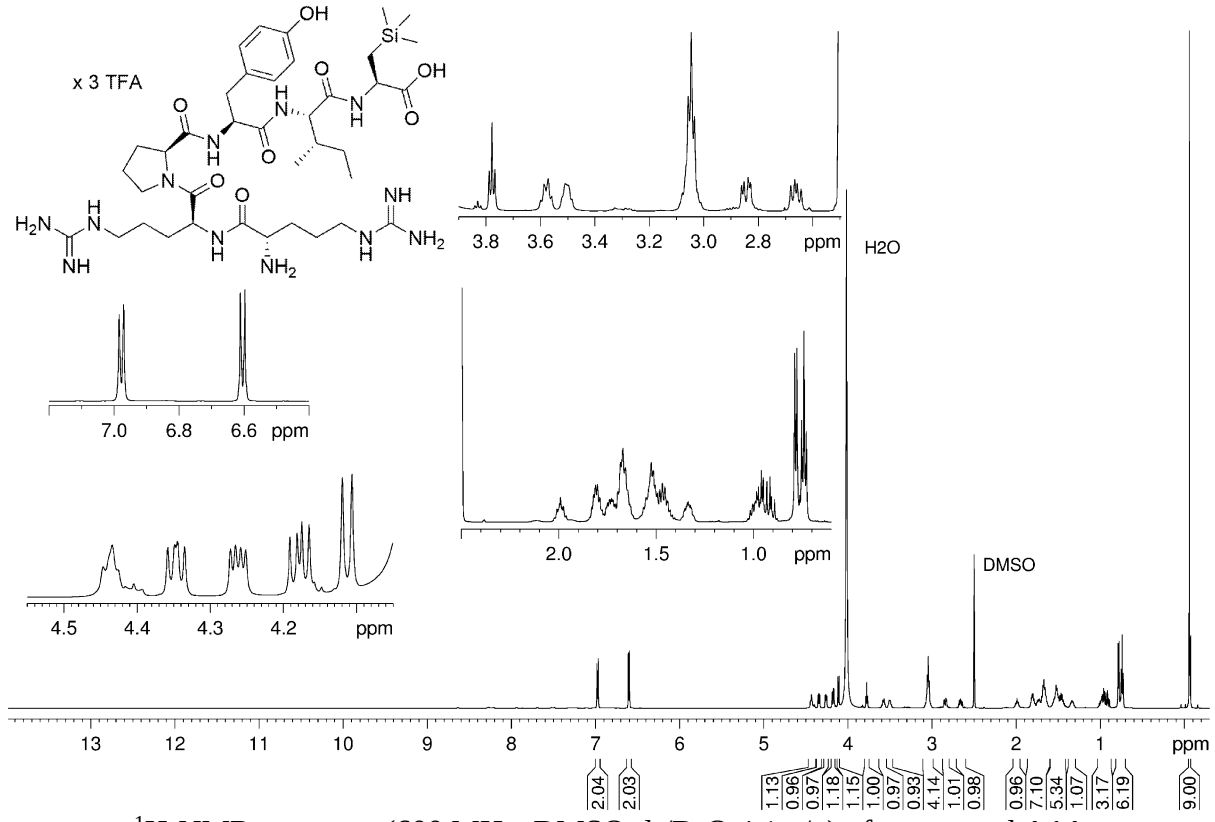


^{13}C-NMR spectrum (100 MHz, $CDCl_3$) of compound **4.10**

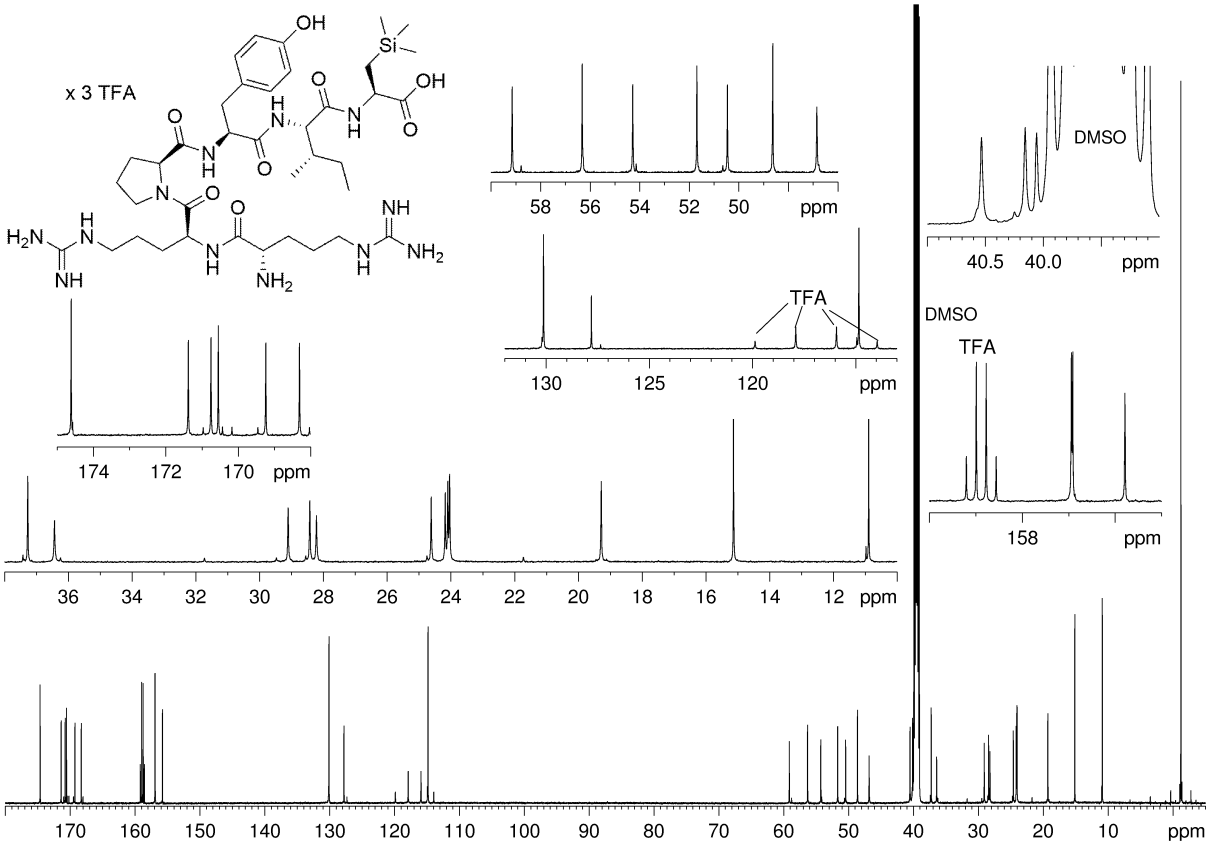
A4.7 ^{1}H-NMR spectra of compounds 4.14-4.17b, 4.19, and 4.21 and ^{13}C-NMR spectra of compounds 4.14-4.17b in DMSO-d_6 and DMSO-d_6/D_2O 4:1 v/v



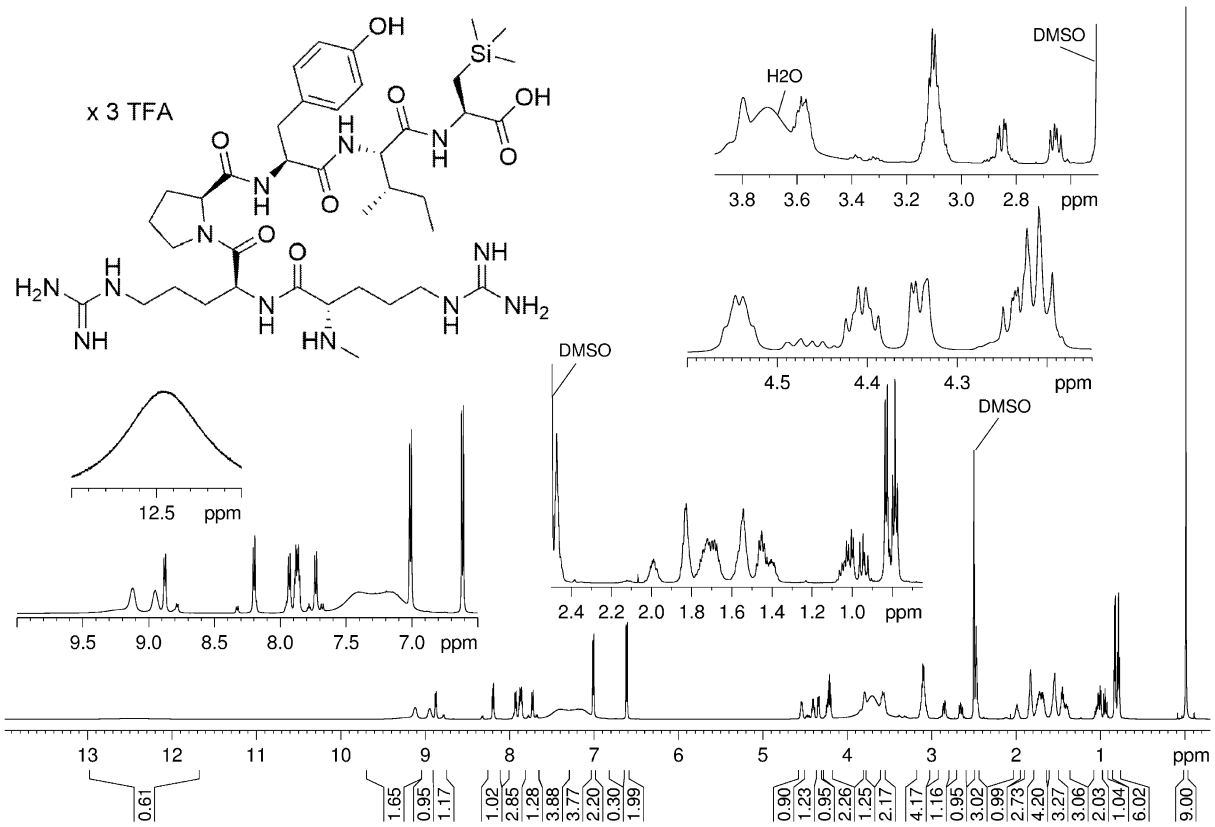
^{1}H-NMR spectrum (600 MHz, DMSO-d_6) of compound **4.14**



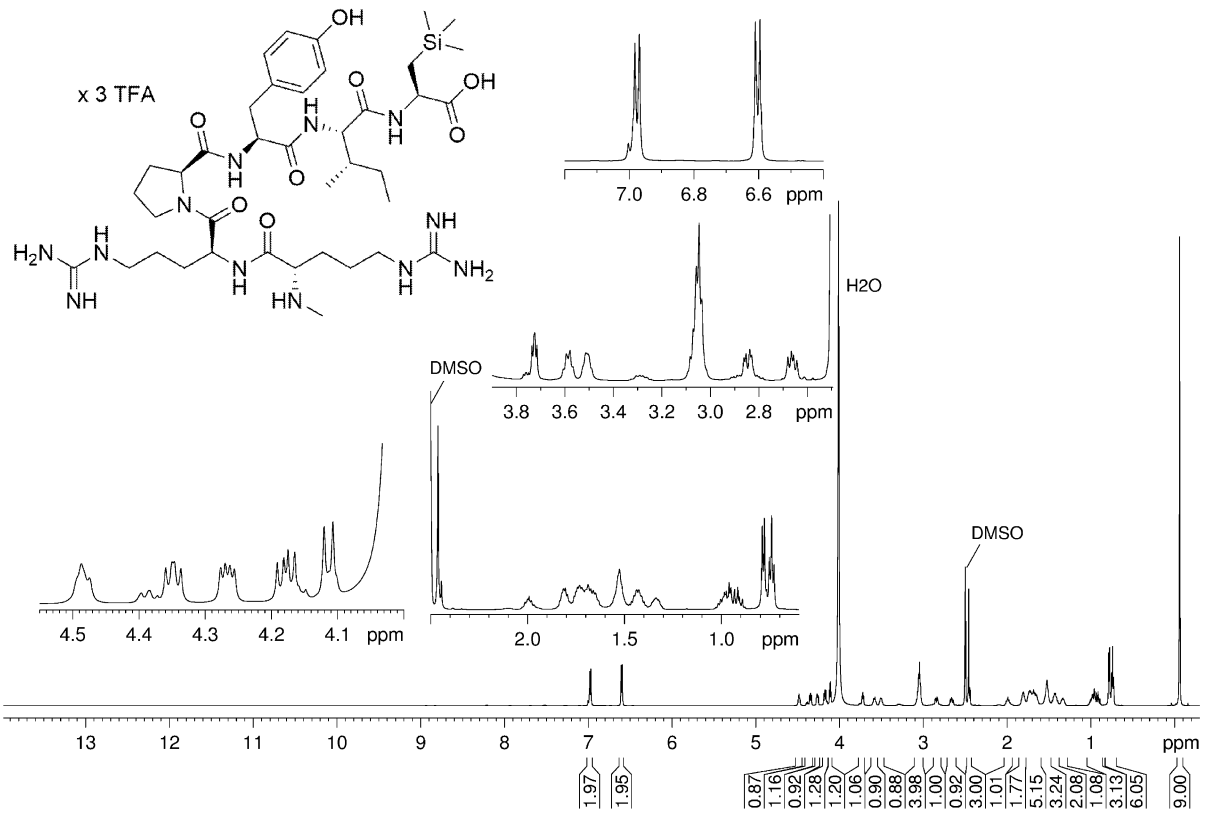
^{1}H-NMR spectrum (600 MHz, DMSO-d_6/D_2O 4:1 v/v) of compound **4.14**



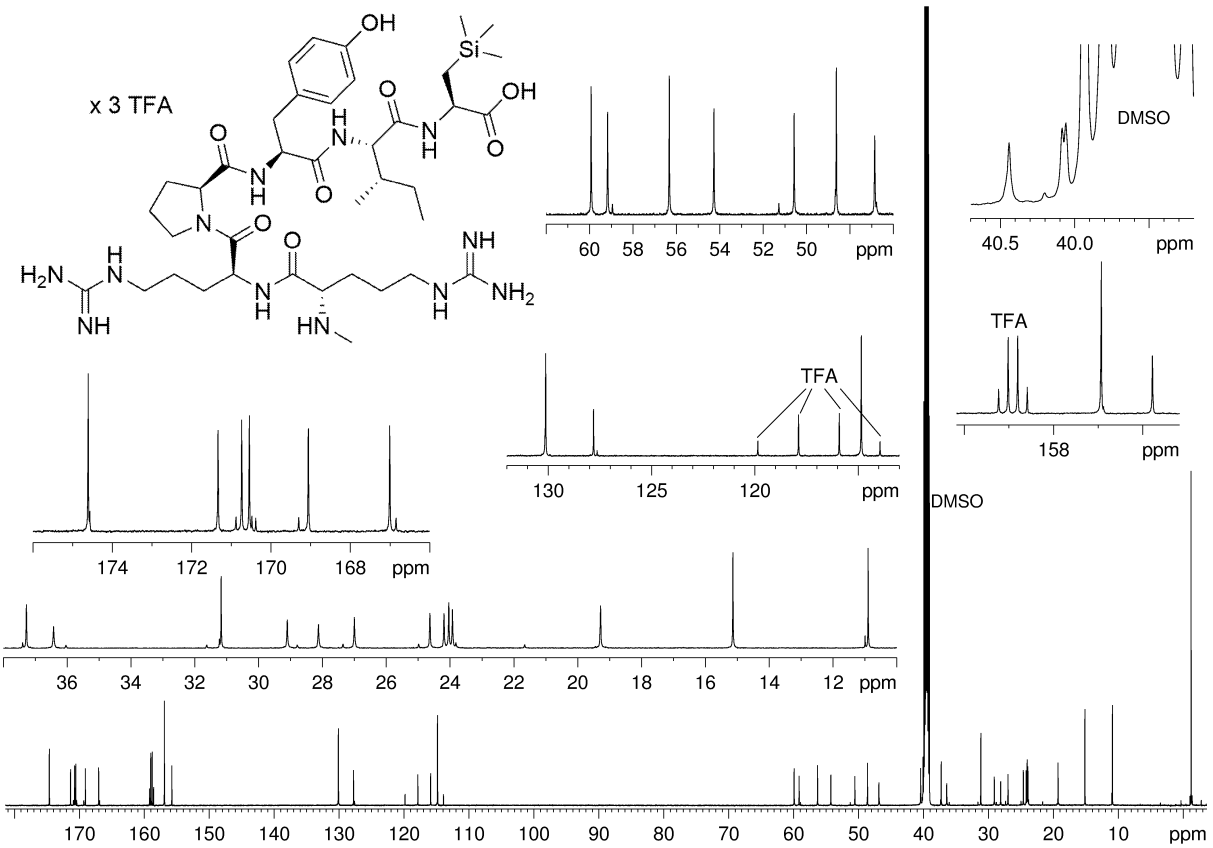
^{13}C-NMR spectrum (150 MHz, DMSO-d_6) of compound **4.14**



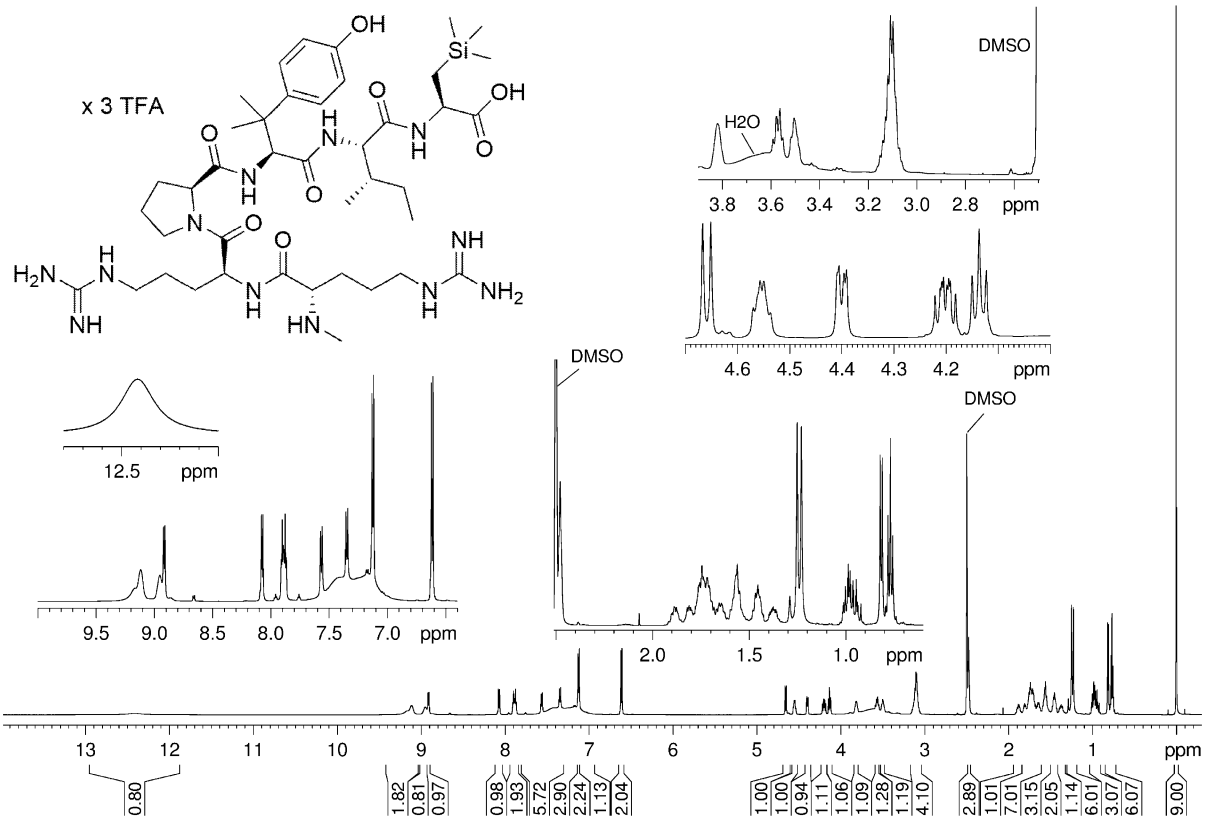
^{1}H-NMR spectrum (600 MHz, DMSO-d_6) of compound **4.15**



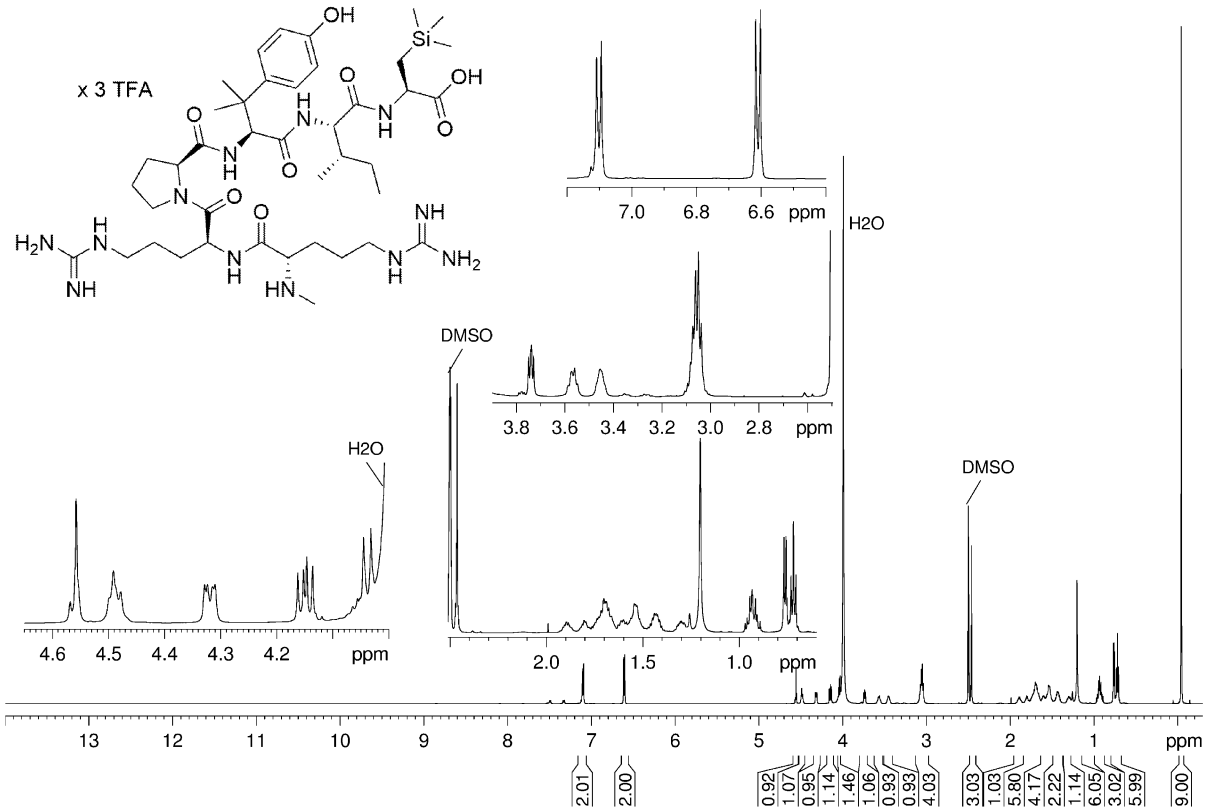
^{1}H-NMR spectrum (600 MHz, DMSO-d_6/D_2O 4:1 v/v) of compound **4.15**



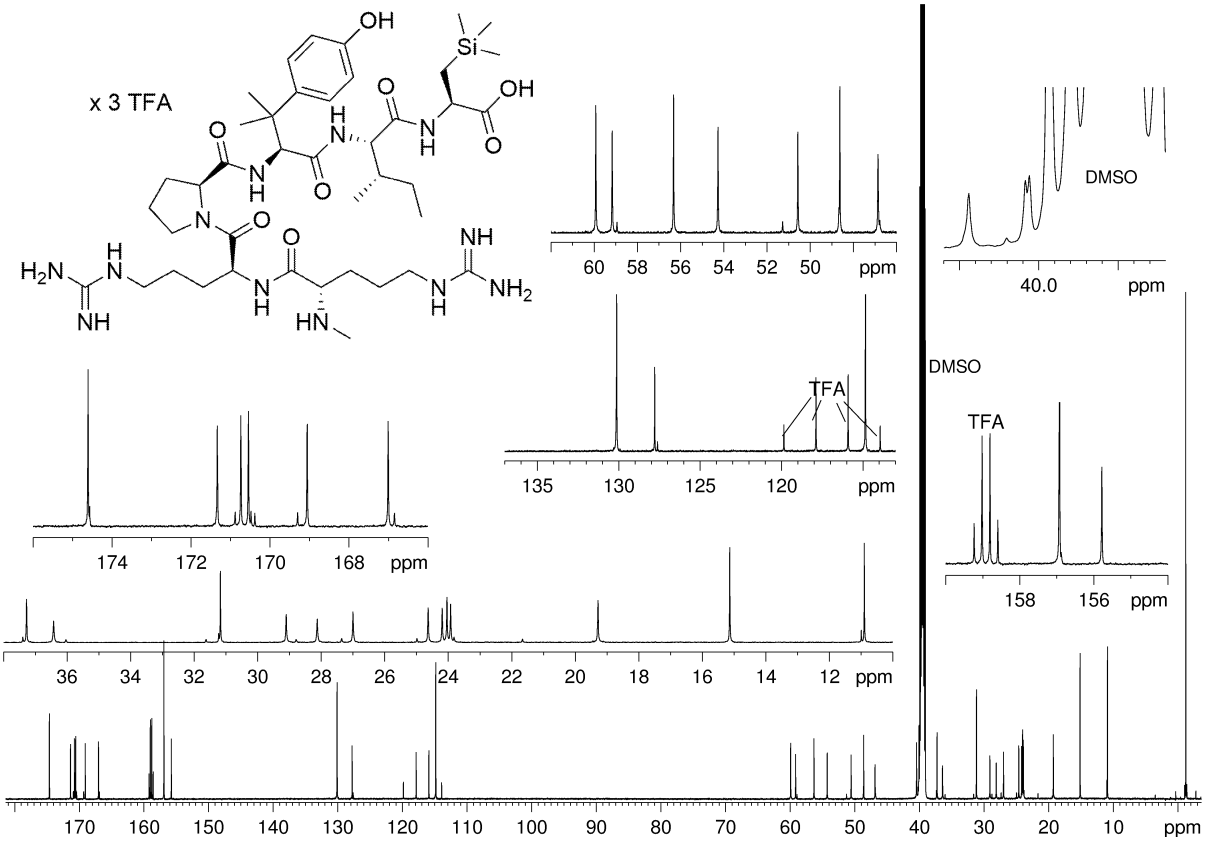
^{13}C-NMR spectrum (150 MHz, DMSO-d_6) of compound **4.15**



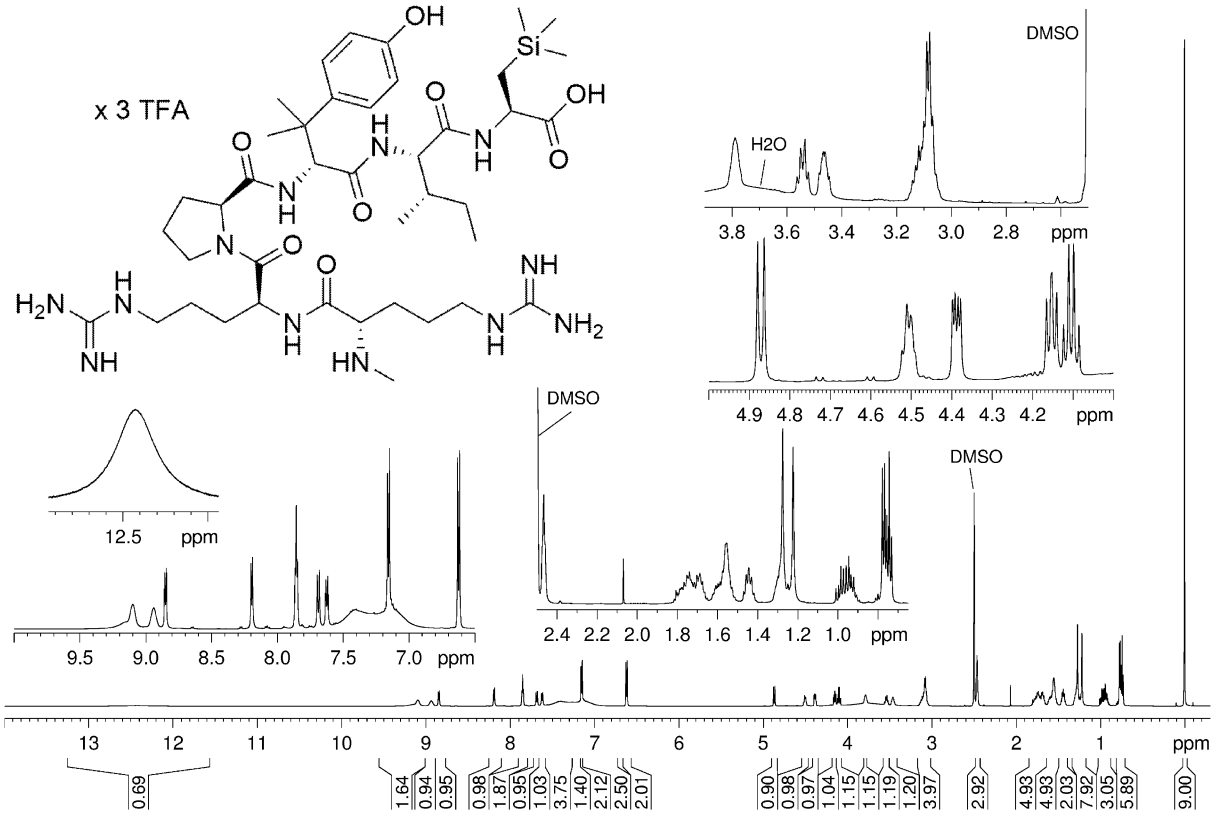
^{1}H-NMR spectrum (600 MHz, DMSO-d_6) of compound **4.16a**



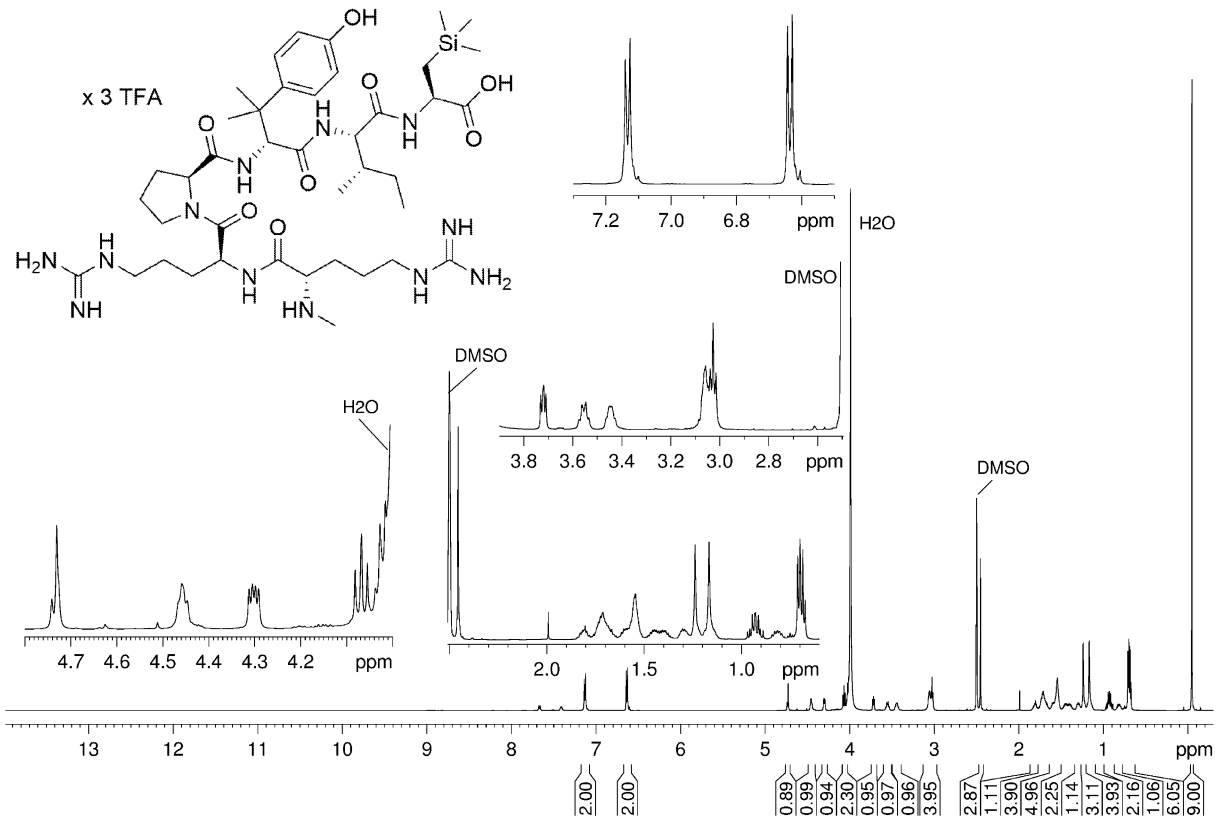
^{1}H-NMR spectrum (600 MHz, DMSO-d_6/D_2O 4:1 v/v) of compound **4.16a**



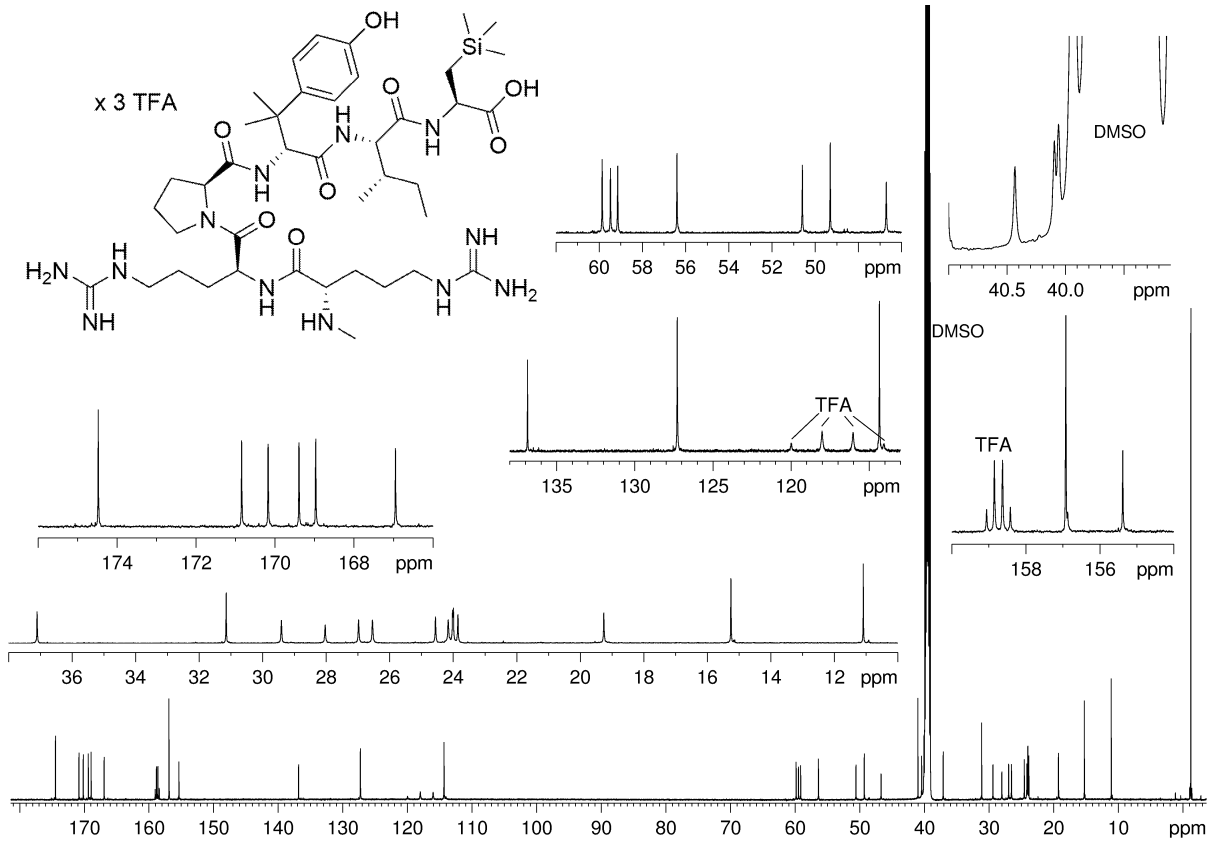
^{13}C-NMR spectrum (150 MHz, DMSO-d_6) of compound **4.16a**



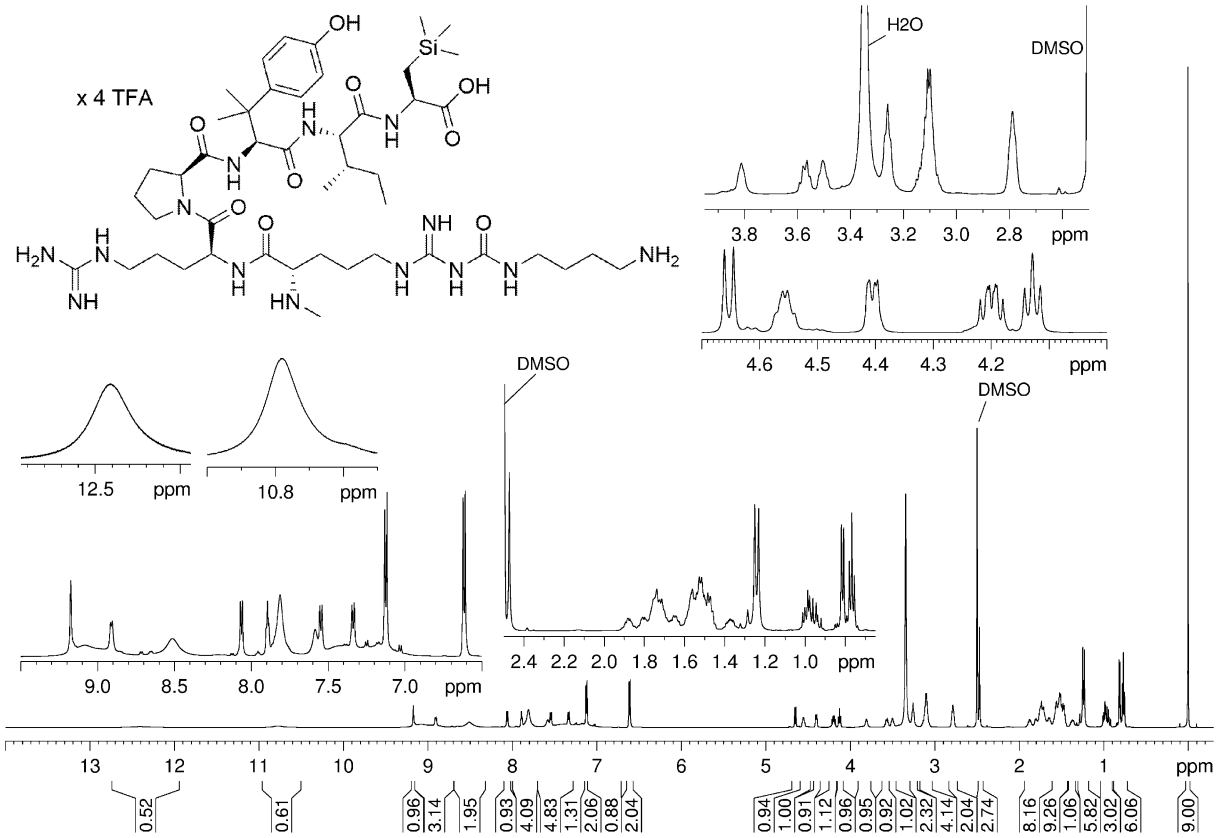
^{1}H-NMR spectrum (600 MHz, DMSO-d_6) of compound **4.16b**



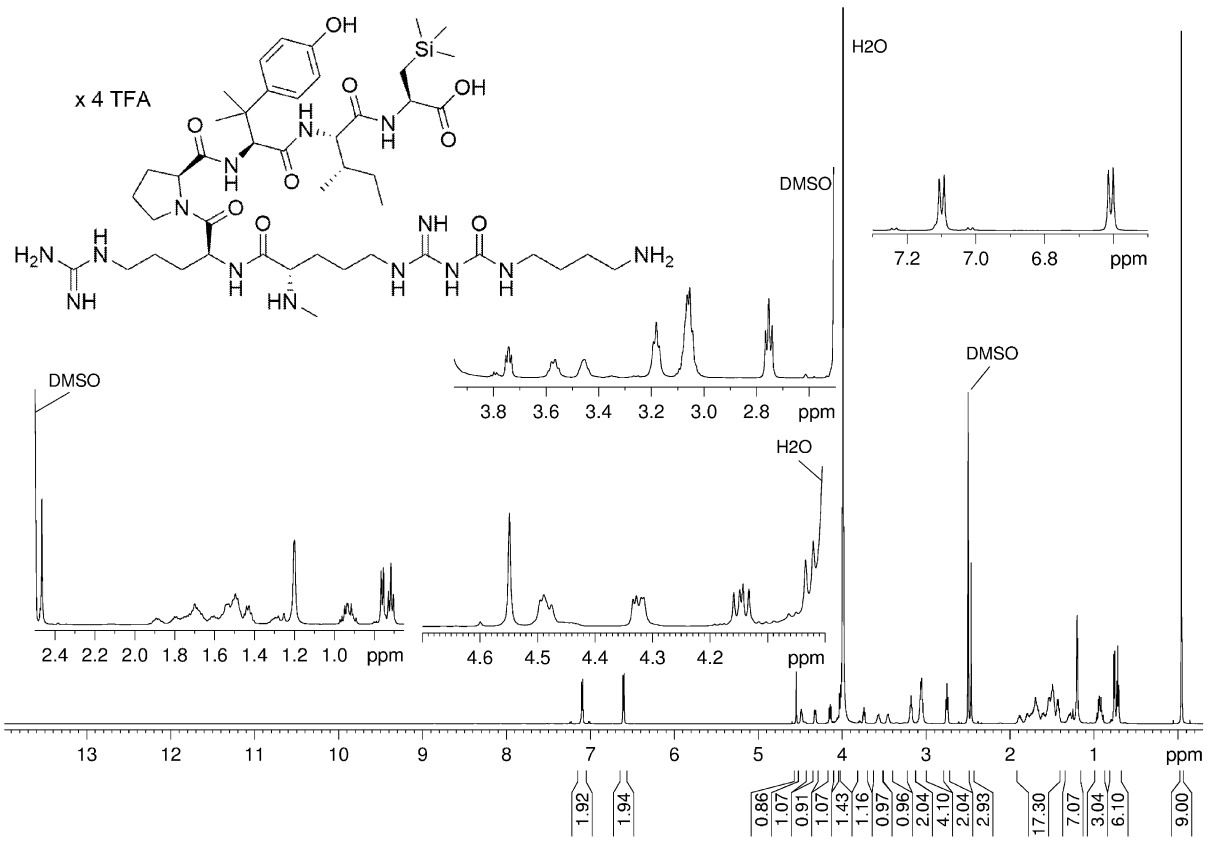
^{1}H-NMR spectrum (600 MHz, DMSO-d_6/D_2O 4:1 v/v) of compound **4.16b**



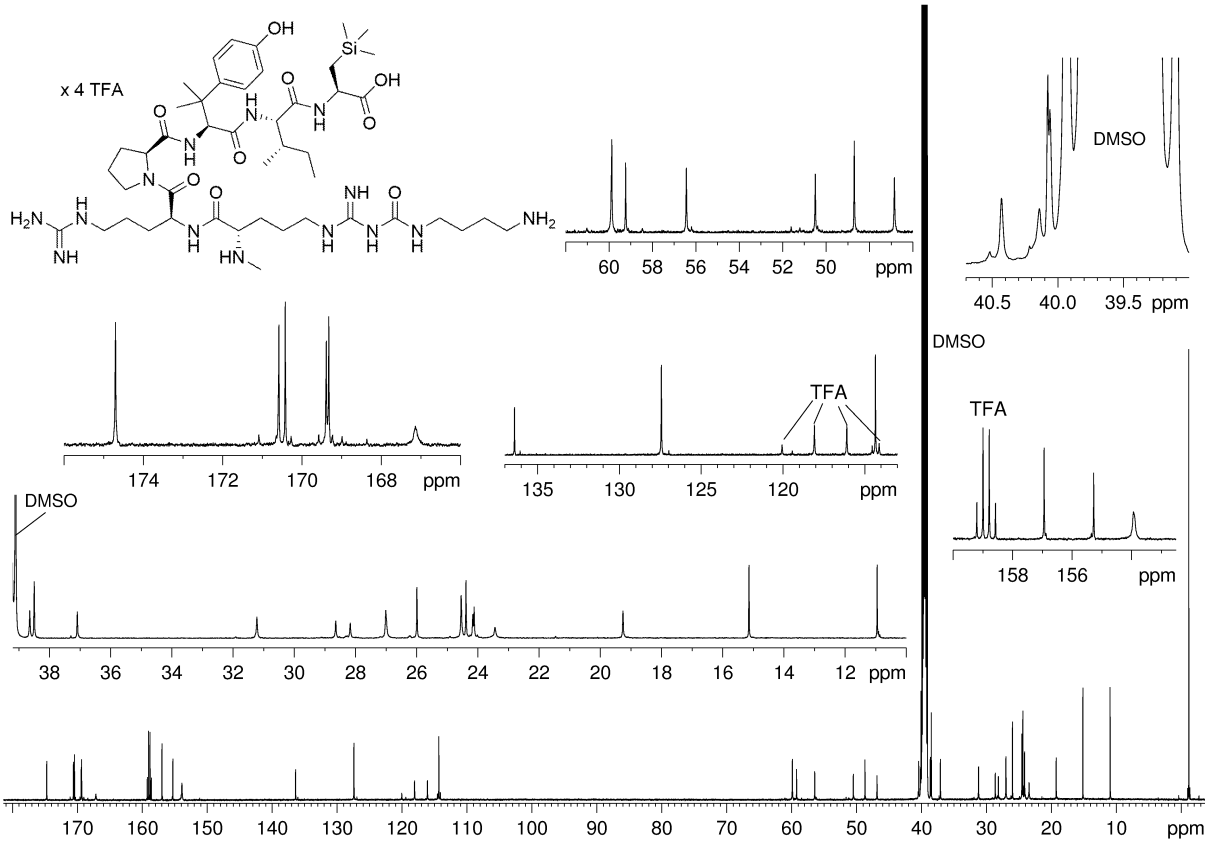
^{13}C-NMR spectrum (150 MHz, DMSO-d_6) of compound **4.16b**



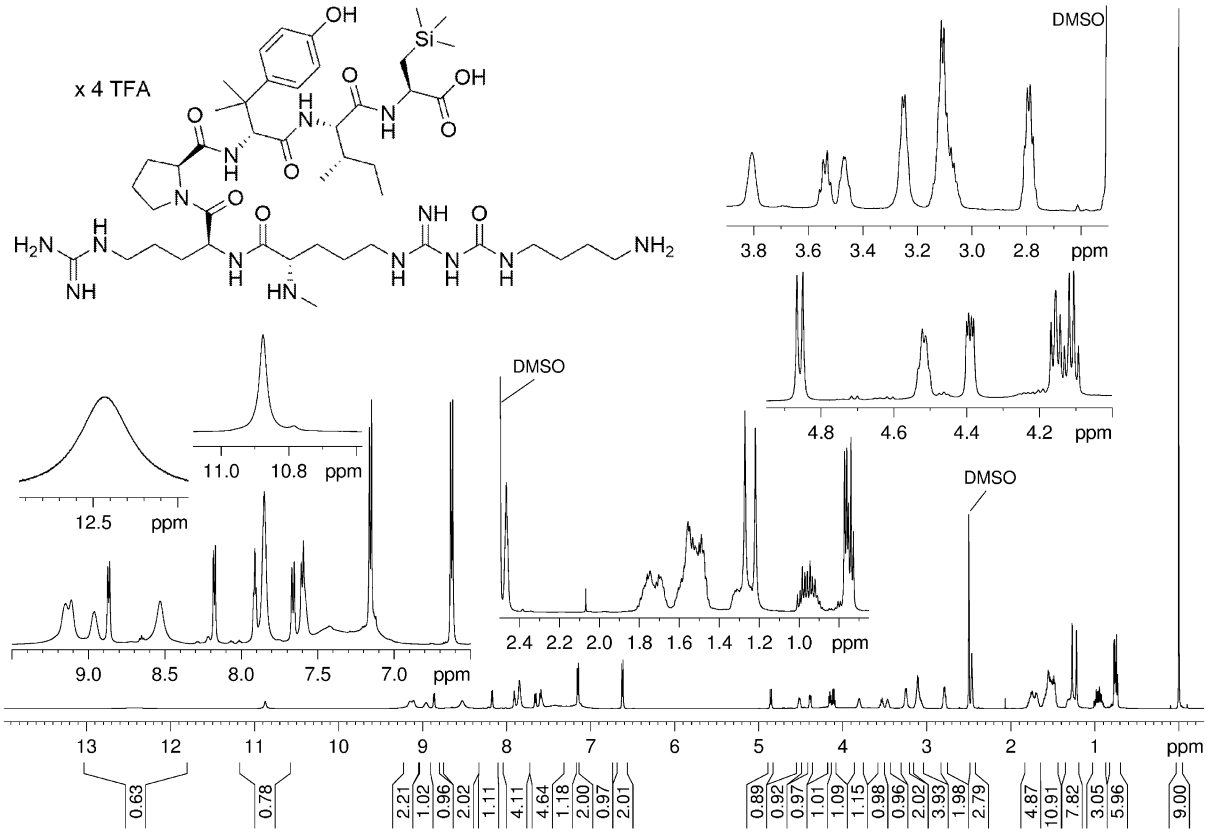
^{1}H-NMR spectrum (600 MHz, DMSO-d_6) of compound **4.17a**



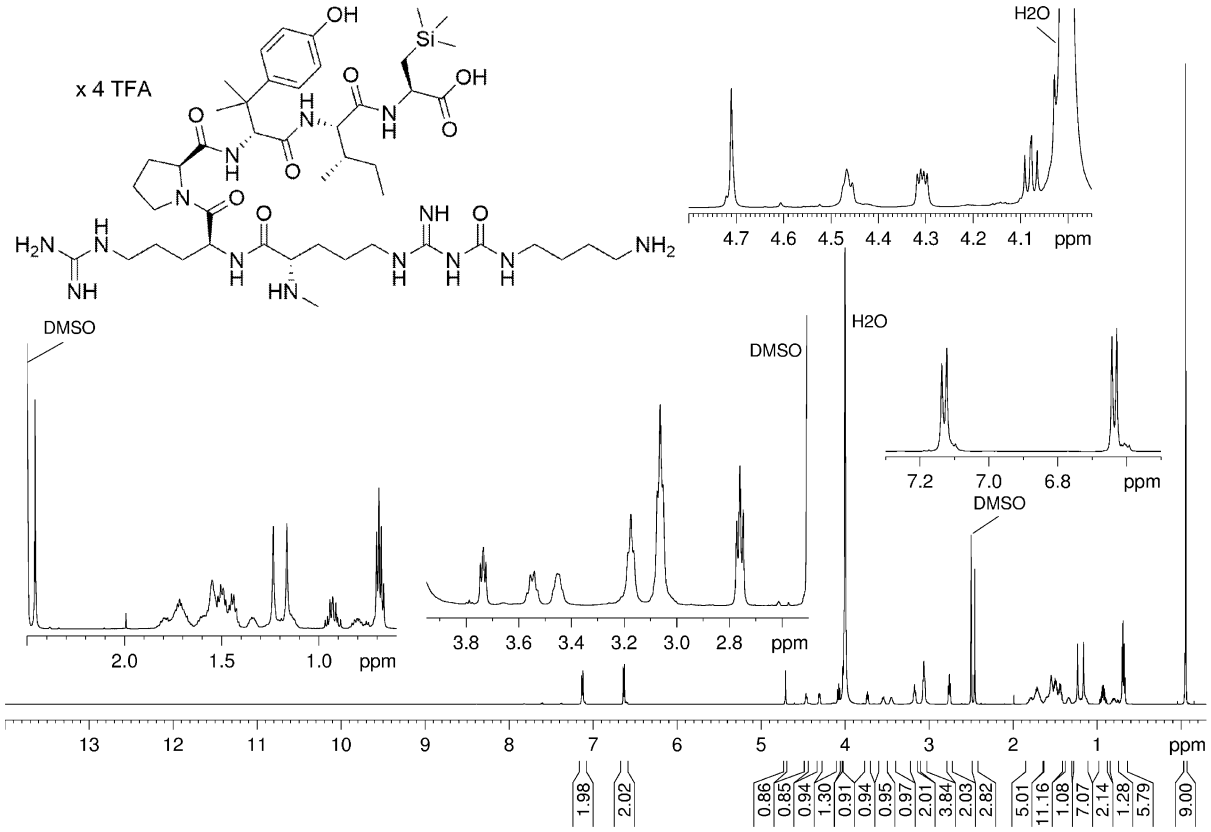
^{1}H-NMR spectrum (600 MHz, DMSO-d_6/D_2O 4:1 v/v) of compound **4.17a**



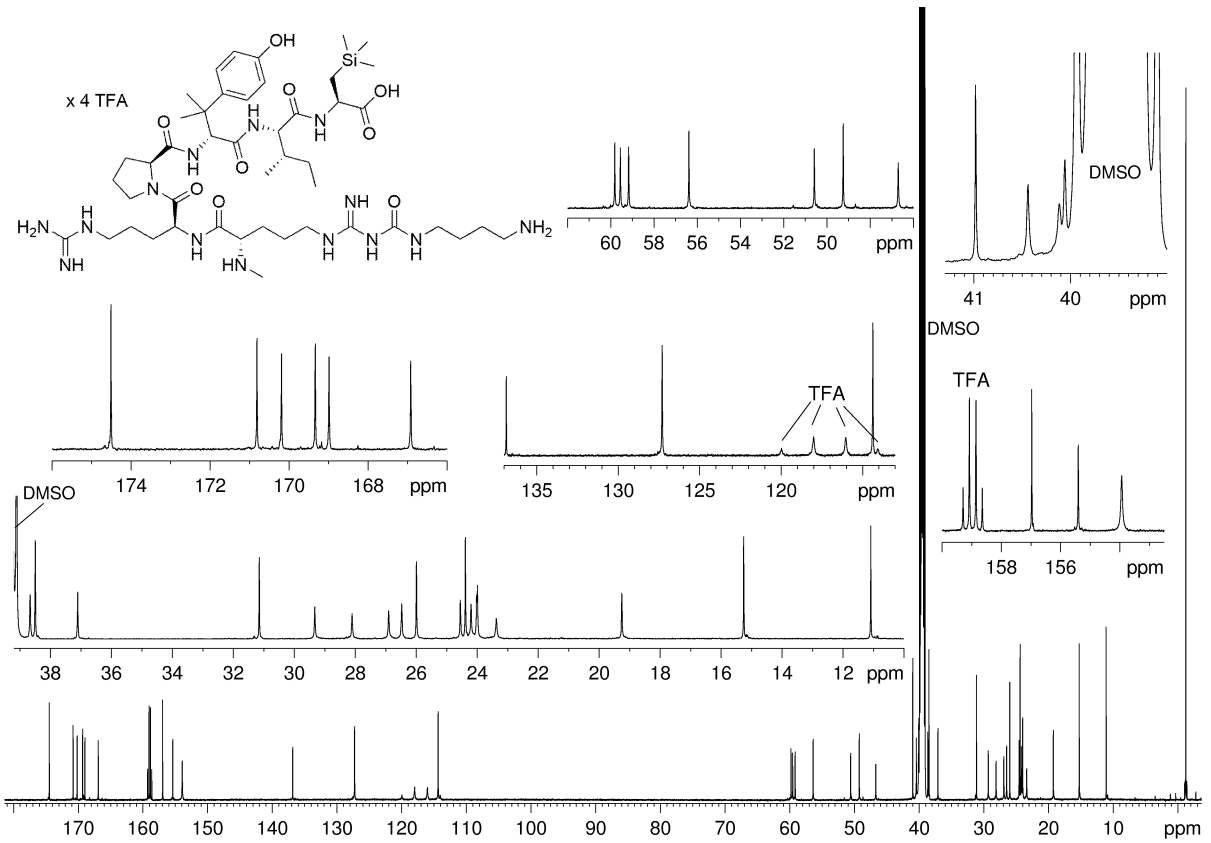
^{13}C-NMR spectrum (150 MHz, DMSO-d_6) of compound **4.17a**



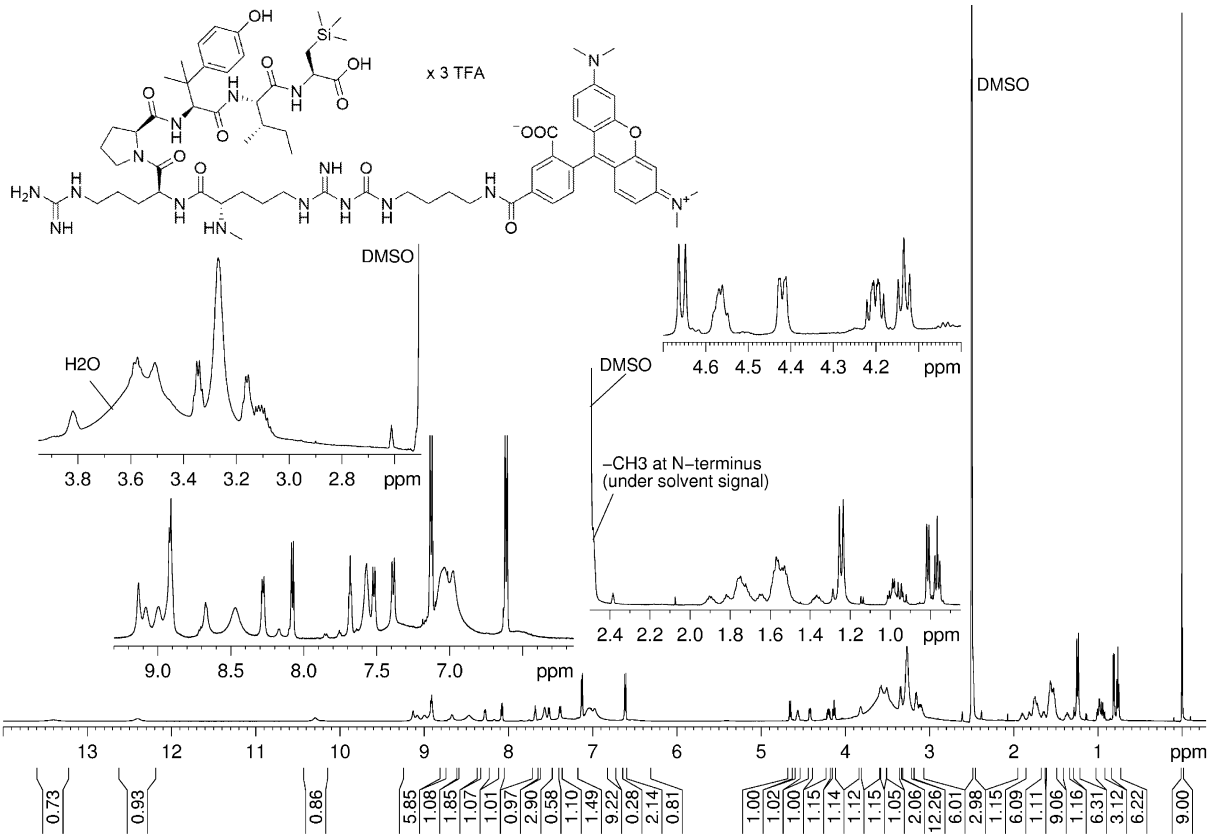
^{1}H-NMR spectrum (600 MHz, DMSO-d_6) of compound **4.17b**



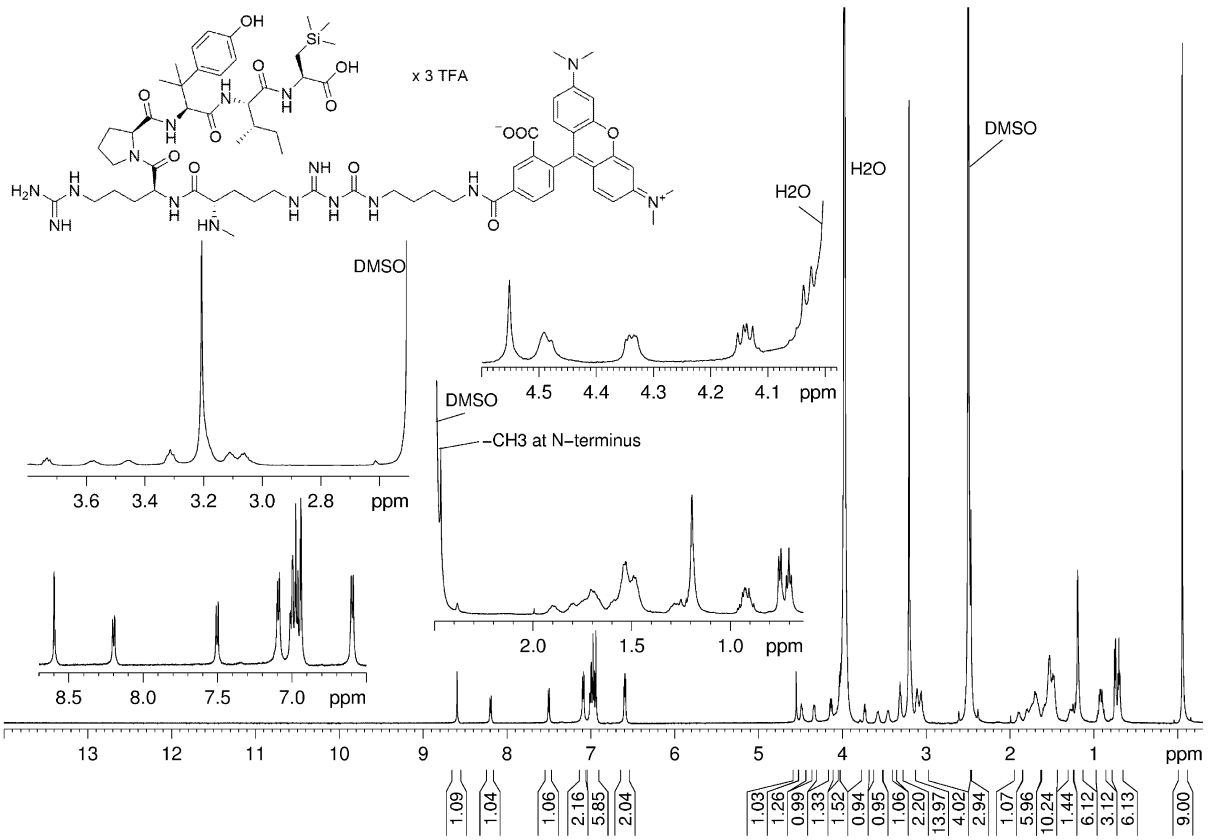
^{1}H-NMR spectrum (600 MHz, DMSO-d_6/D_2O 4:1 v/v) of compound **4.17b**



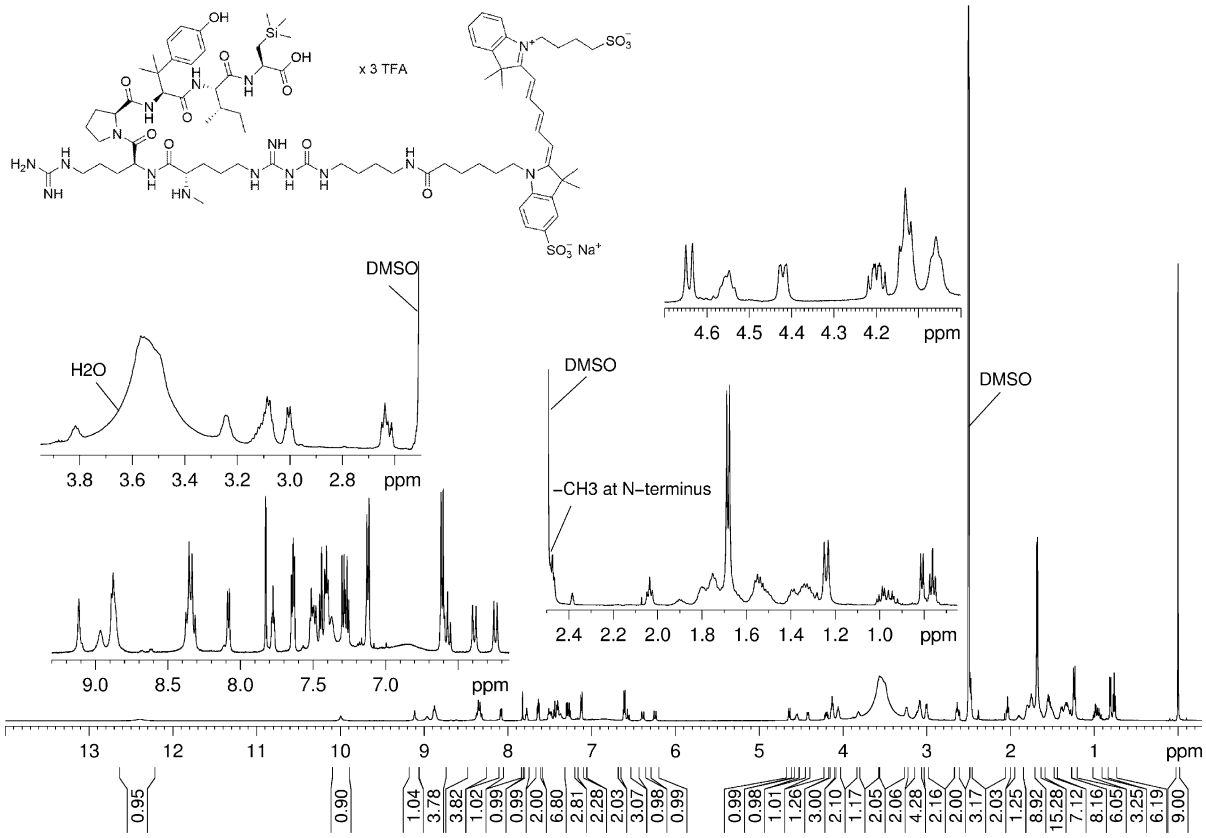
^{13}C-NMR spectrum (150 MHz, DMSO-d_6) of compound **4.17b**



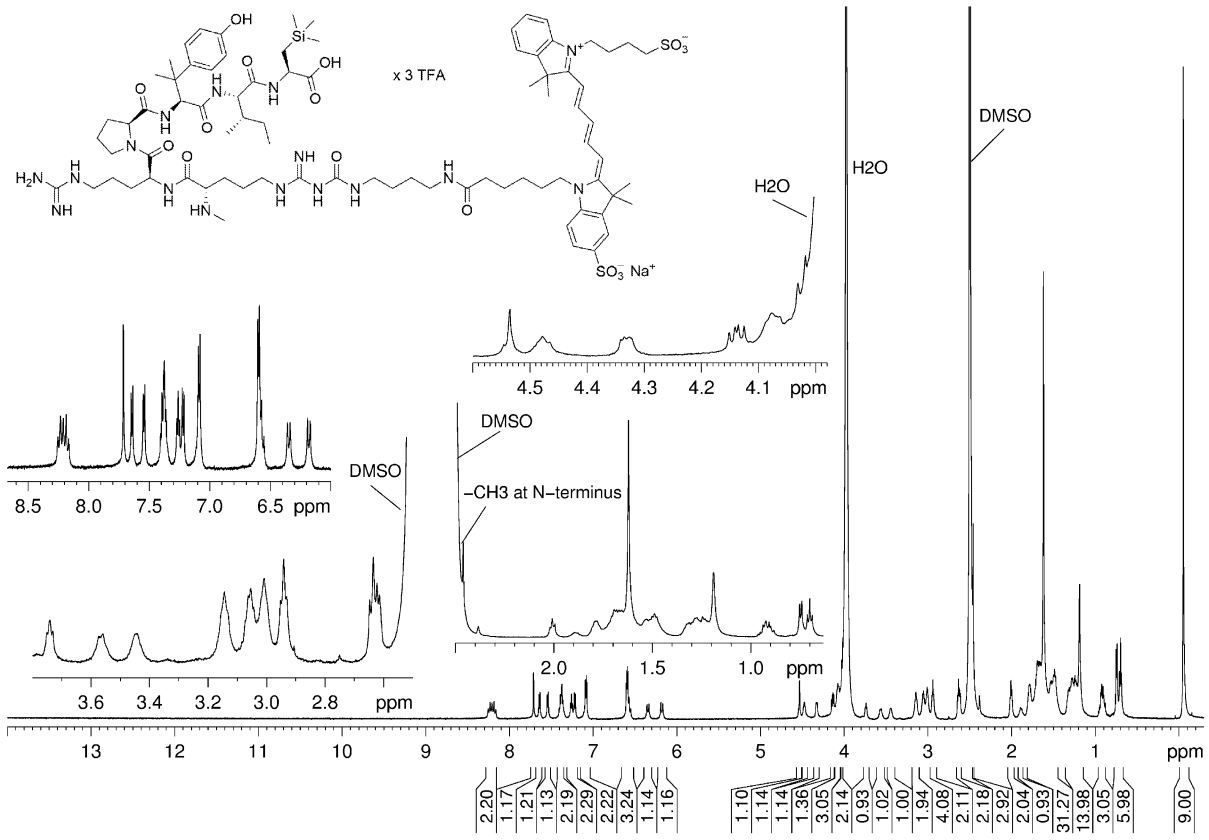
^{1}H-NMR spectrum (600 MHz, DMSO-d_6) of compound **4.19**



^{1}H-NMR spectrum (600 MHz, DMSO-d_6/D_2O 4:1 v/v) of compound **4.19**



^{1}H-NMR spectrum (600 MHz, DMSO-d_6) of compound **4.21**



^{1}H-NMR spectrum (600 MHz, DMSO-d_6/D_2O 4:1 v/v) of compound **4.21**

A4.8 References

(1) René, A., Vanthuyne, N., Martinez, J., Cavelier, F. (L)-(Trimethylsilyl)alanine synthesis exploiting hydroxypinanone-induced diastereoselective alkylation. *Amino acids* **2013**, *45*, 301-307.

(2) Schindler, L.; Moosbauer, J.; Schmidt, D.; Spruss, T.; Grätz, L.; Ludeke, S.; Hofheinz, F.; Meister, S.; Echtenacher, B.; Bernhardt, G.; Pietzsch, J.; Hellwig, D.; Keller, M. Development of a neurotensin-derived ^{68}Ga-labeled PET ligand with high in vivo stability for imaging of NTS_1 receptor-expressing tumors. *Cancers* **2022**, *14*, 4922.

(3) Keller, M., Kuhn, K. K., Einsiedel, J., Hübner, H., Biselli, S., Mollereau, C., Wifling, D., Svobodovà, J., Bernhardt, G., Cabrele, C., Vanderheyden, P. M. L., Gmeiner, P., Buschauer, A. Mimicking of arginine by functionalized N^{ω}-carbamoylated arginine as a new broadly applicable approach to labeled bioactive peptides: High affinity angiotensin, neuropeptide Y, neuropeptide FF, and neurotensin receptor ligands as examples. *J. Med. Chem.* **2016**, *59*, 1925-1945.

(4) Schneider, C. A., Rasband, W. S:, Eliceiri, K. W. NIH Image to ImageJ: 25 years of image analysis. *Nat. Methods* **2012**, *9*, 671-675.

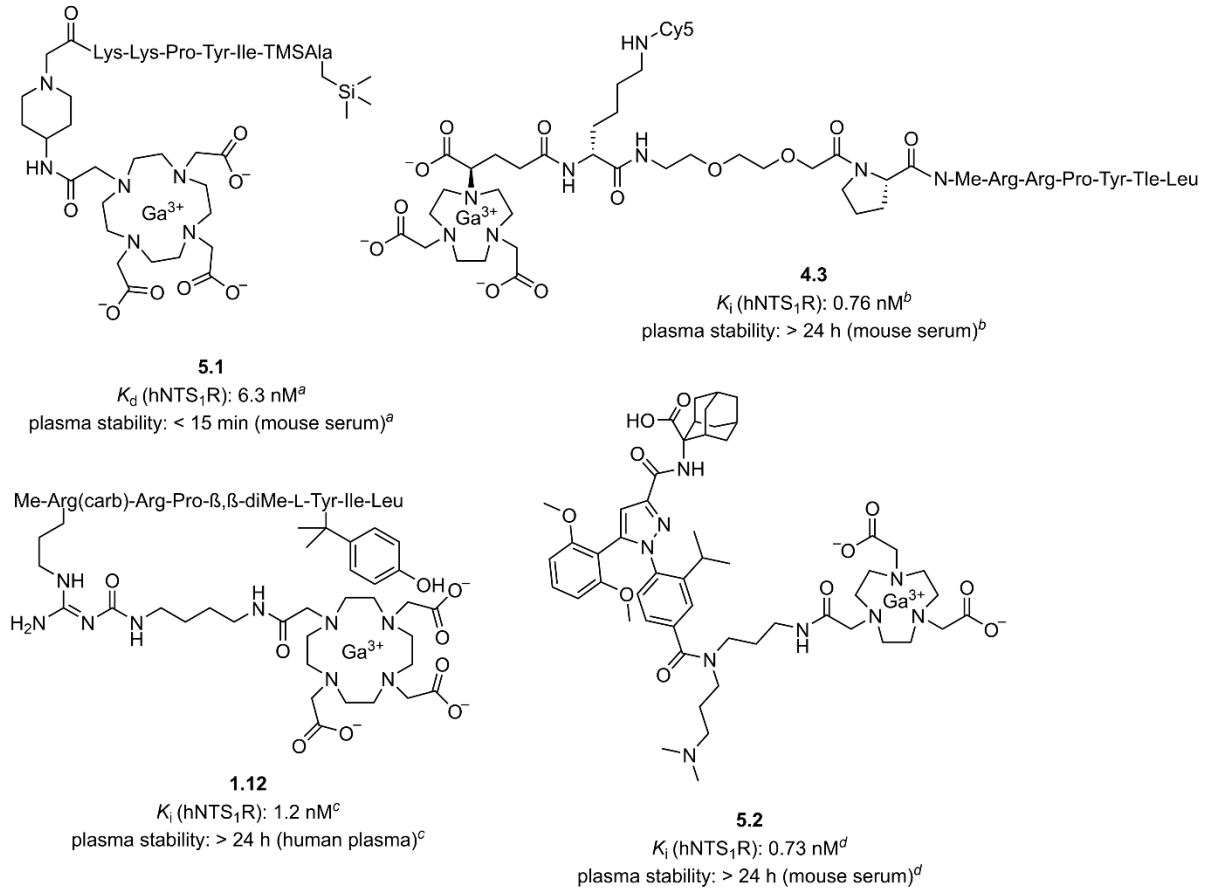
Chapter 5

Development of proteolytically stable peptidic NTS_1R PET ligands with subnanomolar binding affinity

5.1 Introduction

Over the past fifteen years, a steady increase in incidence and prevalence of neuroendocrine tumors could be observed.[1,2] Although it may seem alarming at the first sight, the rising numbers can be partly attributed to a positive development: improved diagnostic methods and novel radiopharmaceuticals enable earlier detection and the identification of asymptomatic progressions.[2] For example, the peptide receptor radionuclide therapy (PRRT) provides radionuclide-labeled somatostatin receptor ligands for imaging and therapy of neuroendocrine tumors expressing somatostatin receptors.[3] Another interesting target is the neurotensin 1 receptor (NTS_1R), which is also (over)expressed in various malignant tumors.[4-10] Therefore, the NTS_1R represents a potential target for tumor visualization and cancer treatment giving rise to the development of new radiotherapeutics.

Imaging of tumor tissue can be achieved by positron emission tomography (PET) which utilizes a positron-emitting isotope such as ^{68}Ga or ^{64}Cu. An advantage of PET ligands containing cations of these radiometals is their convenient synthesis: in only one reaction step, the isotopes are easily incorporated in a chelator moiety such as DOTA. Generally, high receptor binding affinity and proteolytic stability are among the most important requirements a useful PET ligand must meet. So far, in the case of the NTS_1R, this has been achieved with agonistic peptidic ligands and non-peptidic antagonists. Noteworthy, in the following, only NTS_1R PET ligands containing $^{68}Ga^{3+}$ are presented since the present study also aimed for ^{68}Ga-labeled, NTS_1R-targeting PET tracers. Peptidic PET ligands such as compound **5.1** (Figure 5.1) are prone to rapid enzymatic degradation resulting in short half-lives.[11] Schindler *et al.*[12] and Renard *et al.*[13] have overcome this issue by an N-terminal methylation and stabilization of the C-terminus by the incorporation of a dimethylated tyrosine (β,β-diMe-L-Tyr) and an α-*tert* butylglycine (Tle), respectively. This resulted in high proteolytic stability while retaining the receptor binding affinity in a low nanomolar range (compounds **1.12** and **4.3**, Figure 5.1). Compound **5.2**, derived from the NTS_1R antagonist SR142948 (**1.5**), exhibits subnanomolar binding affinity and high stability against degrading enzymes.[14] In addition, antagonists offer low kidney and liver uptake which is advantageous compared to agonists.[15]



Arg(carb) = N^{ω}-carbamoylated arginine
Tle = α-*tert* butylglycine
ß,ß-diMe-L-Tyr = ß,ß-dimethyl-L-tyrosine
TMSAla = (trimethylsilyl)alanine

Figure 5.1. Structures, K_i values and in vitro plasma or serum stabilities of reported NTS_1R PET ligands showing high NTS_1R binding affinity (K_i < 10 nM). [a]Fanelli *et al.*[11] [b]Renard *et al.*[13] [c]Schindler *et al.*[12] [d]Renard *et al.*[14]

The NT(8-13) derived fluorescent NTS_1R ligands presented in Chapter 4 show high in vitro plasma stability and subnanomolar NTS_1R binding affinity (K_i < 0.14 nM). These tool compounds were conveniently accessible by conjugation of fluorescent dyes to the newly developed precursor peptide **4.17a** (see Chapter 4). Therefore, **4.17a** was utilized to synthesize potential NTS_1R PET ligands containing natural Ga^{3+} incorporated in a chelator. Worth mentioning, the fluorescent ligands introduced in Chapter 4 are quickly internalized by binding to the NTS_1R and show a slow dissociation from the receptor. This is a favorable feature particularly for PET ligands, which, when used in vivo, should exhibit a high retention in NTS_1R-expressing tumor tissue. The herein presented potential PET ligands were studied with respect to their in vitro buffer and plasma stabilities, NTS_1R binding affinities, and agonistic potencies. Finally, a ^{68}Ga-labeled PET ligand was prepared and studied in terms of hydrophilicity (determination of $logD_{7.4}$) and in vitro plasma stability.

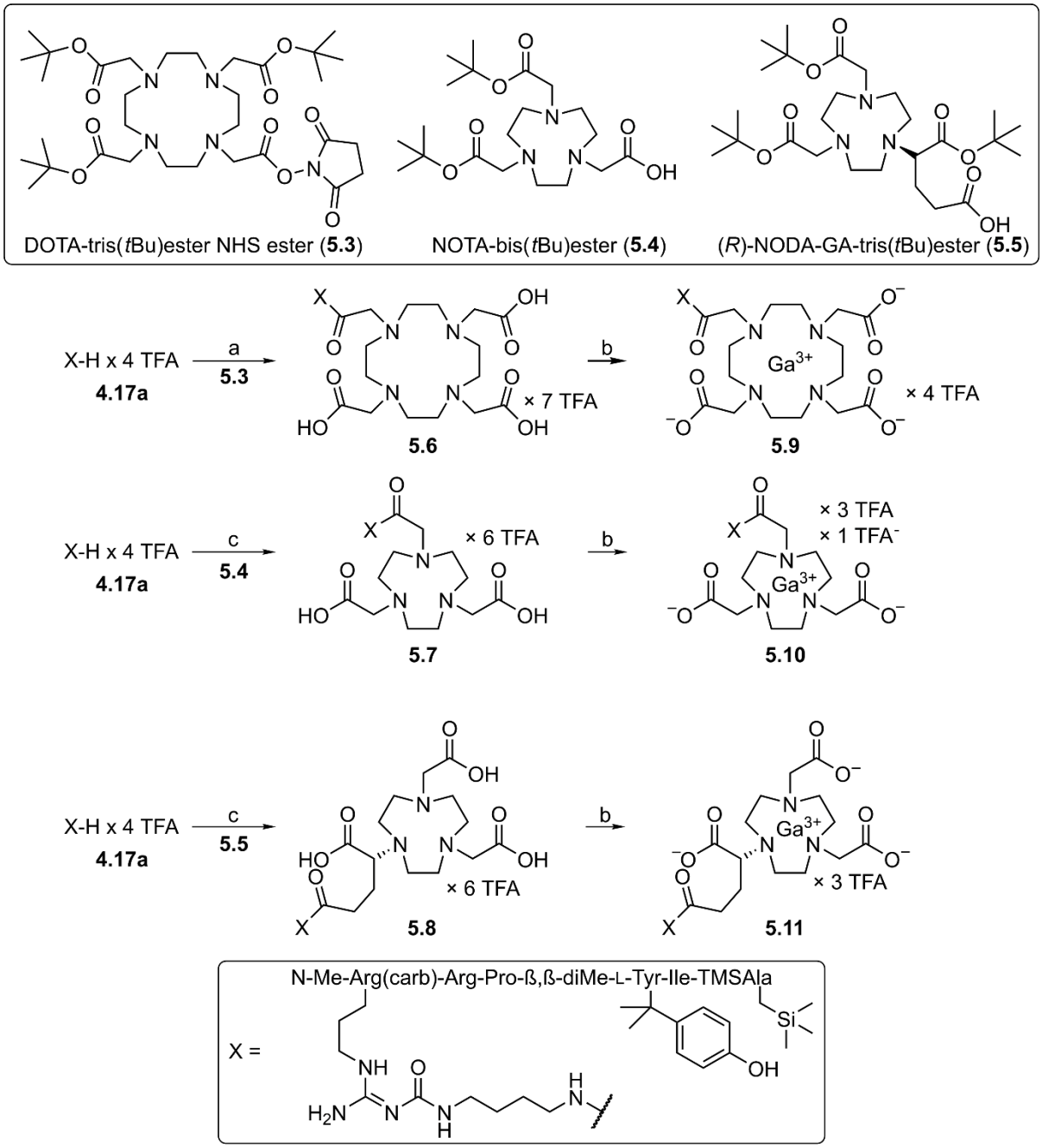
5.2 Results and discussion

5.2.1 Synthesis

The synthesis of precursor **4.17a** via solid-phase peptide synthesis (SPPS) is described in Chapter 4. Treatment of **4.17a** with the succinimidyl ester of tris-*t*Bu-protected DOTA (**5.3**) yielded the *t*Bu-protected precursor of **5.6**. As bis-*t*Bu-protected NOTA (**5.4**) and tris-*t*Bu-protected (*R*)-NODA-GA (**5.5**) were not available as an activated carboxylic acid species (see Scheme 5.1), **5.4** and **5.5** were incubated with HOBt, HBTU, and DIPEA for 10 min at 35 °C followed by addition to peptide **4.17a**. All protected intermediates were isolated by preparative RP-HPLC and subsequently deprotected using 80% aqueous TFA (Scheme 5.1). Subsequent purification by preparative RP-HPLC gave the chelator-conjugated peptides **5.6**-**5.8** with satisfactory purities (> 98%, RP-HPLC).

The "cold" PET ligands **5.9**-**5.11** were synthesized by incubation of **5.6**-**5.8** with an excess of $Ga(NO_3)_3$ in a HEPES buffer (pH = 4.2) at 100 °C for 30 min (Scheme 5.1) according to a reported protocol.[12] Complete conversion was confirmed by LC-HRMS. Due to similar retention times of peptide **5.6** and its Ga^{3+}-occupied derivative **5.9** (the same applied to **5.8** and its analog **5.11**) in RP-HPLC using 0.04% aqueous TFA and acetonitrile as mobile phase, the conversion and product purity were additionally confirmed using 0.05% formic acid and methanol as eluents, enabling a separation of precursor peptide (empty chelator) and product (Ga^3+-occupied chelator). The NOTA-conjugated compounds **5.7** and **5.10** were separable using both mobile phases (see RP-HPLC chromatograms under A5.3 and A5.4, Appendix).

Scheme 5.1. Synthesis of the "cold" NTS_1R PET ligands **5.9**-**5.11**.



TMSAla = (trimethylsilyl)alanine
ß,ß-diMe-L-Tyr = ß,ß-dimethyl-L-tyrosine
Arg(carb) = N^{ω} -carbamoylated arginine

Reagents and conditions: (a) (1) DIPEA, DMF, rt, 90 min; (2) TFA/H_2O 80:20 v/v, rt, 16 h, 73%; (b) $Ga(NO_3)_3 \times H_2O$, HEPES buffer (0.2 M, pH = 4.2), 100 °C, 30 min, 99% (**5.9**), 99% (**5.10**), 99% (**5.11**); (c) (1) **5.4** or **5.5**/HOBt/HBTU/DIPEA (0.9/0.9/0.9/1.8 equiv.), DMF/NMP 4:1 v/v, rt, 2 h; (2) TFA/H_2O 80:20 v/v, rt, 16 h, 42% (**5.7**), 54% (**5.8**).

5.2.2 Chemical stability of 5.6-5.11

The stability of the "cold" PET ligands **5.9**-**5.11** was studied in phosphate-buffered saline (PBS, pH = 7.4) at room temperature over 48 h. **5.11** showed excellent stability in PBS (Figure A5.6, Appendix). The DOTA-conjugated peptide **5.9** exhibited high stability with a minor decomposition observable after 24 h of incubation (Figure A5.4, Appendix). Since both Ga^{3+}-occupied compounds (**5.9**, **5.11**) show the same retention time in RP-HPLC (using 0.04% aqueous TFA and acetonitrile as eluents) as their corresponding "empty" precursors **5.6** and **5.8**, respectively, the sample of the last timepoint (48 h) was additionally analyzed using 0.05% aqueous formic acid and methanol as eluents, allowing a separation (as shown under A5.4, Appendix). **5.9** and **5.11** showed no release of Ga^{3+} during the incubation in PBS (data not shown). In the case of the NOTA-conjugated peptide **5.10** a new major peak appeared (after 48 h, 78% of total integrated peak area, t_R= 9.9 min), i.e., only 22% of **5.10** (t_R= 9.5 min) remained after 48 h (Figure A5.5, Appendix). An obvious explanation for this observation would be a release or exchange of Ga^{3+} by a different metal ion such as Zn^{2+}. However, LC-HRMS analysis of the same samples led to the detection of only one species corresponding to the Ga^{3+}-occupied NOTA-conjugated peptide **5.10** (signals corresponding to the precursor **5.7** or derivatives of **5.10** containing metal ions other than Ga^{3+} were not detected). This led to the conclusion that both peaks detected by RP-HPLC correspond to the same molecular mass and thus the same compound. To further investigate this phenomenon, the stability of the precursor peptides **5.6**-**5.8** (empty chelators) was also studied in PBS over 48 h. For these peptides, only minor decompositions were observed and the RP-HPLC purities remained > 95% after 48 h (Figure A5.1-A5.3, Appendix). The fact that compound **5.7** (t_R= 10.7 min), the precursor of the Ga^{3+}-occupied peptide **5.10**, showed high stability and a different retention time than both **5.10** and the observed 'degradation product', confirms that Ga^{3+} was not liberated from **5.10** and that the peptide-chelator conjugate is stable as such under the used conditions. A possible explanation for the observation of two species with the same mass could lie in the coordination behavior of Ga^{3+}: it prefers to form octahedral complexes with six donor atoms which are available in both DOTA- and (*R*)-NODA-GA-conjugated peptides. Since the NOTA-conjugated compound **5.10** offers only five donor atoms (one carboxylic acid is converted to an amide bond during the conjugation to the peptide), the sixth position of Ga^{3+} can be occupied, e.g., by water as reported for a Ga^{3+}-DTPA complex and a Ga^{3+}-Dpaa complex[16,17] or, in the case of **5.10**, by TFA^- due to purification by preparative RP-HPLC using 0.1% aqueous TFA as eluent. During the incubation in PBS, the sixth coordination site of Ga^{3+}, initially occupied by TFA^-, is likely replaced by phosphate anions (HPO_4^{2-} or $H_2PO_4^-$), reported to be capable of coordinating to

Ga^{3+} (Figure 5.2).[18-20] The TFA^--phosphate exchange is most likely the reason for the two peaks observed in the RP-HPLC chromatograms: the initial peak (t_R = 9.5 min) represents the NOTA-Ga^{3+} complex with one TFA^- counterion bound, and the second peak (t_R = 9.9 min), appearing during the incubation in PBS, represents the NOTA-Ga^{3+} complex with a bound phosphate anion. Obviously, the concentration of 0.04% (v/v) TFA in the aqueous HPLC eluent is not sufficient to achieve a replacement of the phosphate anion by TFA^- within the time of sample preparation and analysis (< 1 h). Increasing the TFA concentration in the injection solution from 0.04% to 0.5% followed by HPLC analysis under the same conditions as before, resulted in a chromatogram showing only one peak of **5.10** (t_R = 9.5 min) (data not shown), which corresponds to the peak detected in the HPLC purity control (Appendix A5.3). This confirms the aforementioned coordination of phosphate, which can be displaced by TFA^- in the presence of an excess of TFA, to the Ga^{3+}-complex. As mentioned before, the HRMS analysis of the two species of **5.10** observed after incubation in PBS gave the mass of **5.10** for both complexes. This shows that the counterion at the Ga^{3+} metal ion is released during HRMS analysis. The strong complexation of Ga^{3+} by the chelator NOPO, a NOTA derivative in which the carboxylic acid functions have been changed to phosphinates, also confirms the coordination of phosphate to **5.10** during incubation in PBS.[21-23]

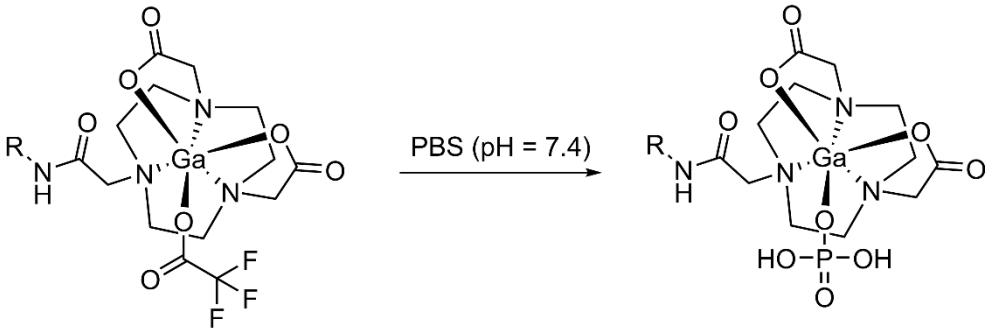


Figure 5.2. Schematic illustration of the proposed ligand exchange in PBS. The structures represent the NOTA chelator of **5.10**. Structures were drawn according to Mitran *et al.*[24]

5.2.3 Proteolytic stability of 5.9-5.11

To evaluate the proteolytic stability, the potential NTS_1R PET ligands **5.9**-**5.11** were incubated in human plasma/PBS 1:2 v/v at 37 °C for 48 h according to previously described procedures.[12,25,26] The peptides **5.9**-**5.11** exhibited high proteolytic stability with at least 95% of remaining intact peptide after 48 h of incubation (Table 5.1). This shows that the N-terminus methylation and the incorporation of β,β-dimethyl-Tyr in position 11 markedly enhanced the proteolytic stability compared to **1.3** (NT(8-13)). In the case of **5.10**, it is worth mentioning that, in contrast to the stability studies in neat PBS, no additional peak was detected by RP-HPLC analysis although the samples contained a considerable amount (ca. 67%) of PBS. Obviously, the presence of plasma proteins prevents the putative coordination of phosphate to Ga^{3+} in **5.10** or the phosphate ion dissociates from **5.10** during the work-up procedure following the incubation in plasma/PBS.

Table 5.1. Stabilities of **5.9**-**5.11** in human plasma/PBS 1:2 v/v (37 °C).

compd.	% intact compound in plasma after the specified incubation times[a]			
	2 h	6 h	24 h	48 h
5.9	> 99	> 99	> 99	> 99
5.10	> 99	98 ± 1	96 ± 1	97 ± 1
5.11	> 99	> 99	> 99	> 99

[a]The initial concentration of the peptide in human plasma/PBS (1:2 v/v) was 80 µM. Data represent mean values ± SEM from two or three independent experiments (SEM not given when no degradation was observed).

5.2.4 Determination of NTS_1R binding

NTS_1R binding affinities were determined in a radioligand competition binding assay as described in Chapter 4. Competition binding curves are presented in Figure 5.3 and pK_i and K_i values are shown in Table 5.2. Conjugation of the precursor peptide **4.17a** to the different chelators (**5.6**-**5.8**) did only marginally affect NTS_1R binding compared to **4.17a** (K_i = 0.13-0.31 nM vs. 0.055 nM). Insertion of Ga^{3+} in **5.6**-**5.8**, which resulted in the potential PET ligands **5.9**-**5.11**, had almost no effect on NTS_1R binding affinities.

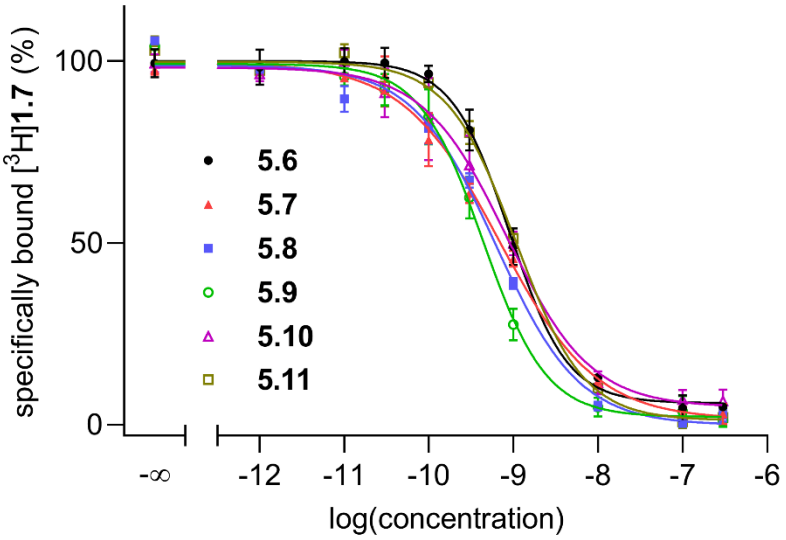


Figure 5.3. Radioligand displacement curves from competition binding experiments with [^{3}H]**1.7** ([^{3}H]UR-MK300) (K_d = 0.41 nM,[12] c = 1 nM) and **5.6**-**5.11** at intact HT-29 cells. Data represent mean values ± SEM from at least three independent experiments performed in triplicate. For pK_i and K_i values see Table 5.2.

Table 5.2. NTS_1R binding affinities and NTS_1R agonistic potencies.

compd.	pK_i ± SEM[a] / K_i [nM][a]	pEC_{50} ± SEM[b] / EC_{50} [nM][b]
1.3	10.03[c] / 0.093[c]	8.96[c] / 1.2[c]
4.17a	10.39[c] / 0.055[c]	n.d.
5.6	9.60 ± 0.06 / 0.26	n.d.
5.7	9.73 ± 0.1 / 0.20	n.d.
5.8	9.74 ± 0.04 / 0.18	n.d.
5.9	9.92 ± 0.1 / 0.13	8.65 ± 0.06 / 2.3
5.10	9.69 ± 0.1 / 0.23	8.84 ± 0.04 / 1.5
5.11	9.52 ± 0.2 / 0.31	8.77 ± 0.03 / 1.7

[a]Determined by radioligand competition binding with [^{3}H]**1.7**[27] at HT-29 colon carcinoma cells. [b]Determined in a Fura-2 Ca^{2+} assay at HT-29 cells. [c]Data taken from Table 4.2, Chapter 4. Data represent mean values ± SEM (pK_i, pEC_{50}) or mean values (K_i, EC_{50}) from at least three independent experiments performed in triplicate. n.d. = not determined.

5.2.5 NTS_1R agonism

The agonistic potencies of **1.3** and the "cold" PET ligands **5.9**-**5.11** were investigated in a Fura-2 Ca^{2+} assay as described in Chapter 4. The obtained concentration-response curves are presented in Figure 5.4.

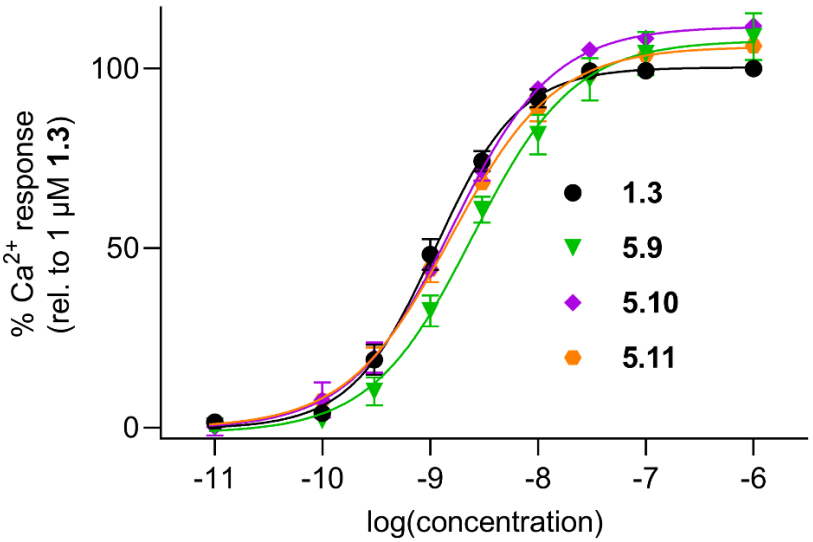


Figure 5.4. Concentration-response curves of **1.3** and **5.9**-**5.11** determined in a Fura-2 Ca^{2+} assay.

The functional assay revealed that compounds **5.9**-**5.11** are full agonists with slightly lower pEC_{50} values compared to **1.3** (Table 5.2). The discrepancy between the binding affinities determined in the radiochemical competition binding assays and the agonistic potencies (pEC_{50} values ca. one log-unit lower than the respective pK_i values) can be explained by the non-equilibrium conditions in the Fura-2 Ca^{2+} assay. This is outlined in more detail in Chapter 4.

5.2.6 Synthesis of [^{68}Ga]**5.9**

Since $^{68}Ga^{3+}$ and the DOTA chelator form thermodynamically highly stable complexes, the ^{68}Ga-labeled PET ligand was prepared for the DOTA-conjugated peptide **5.9**. The insertion of radioactive gallium into the precursor **5.6** was carried out with [^{68}Ga]$GaCl_3$ in HEPES buffer (pH = 5.5) and subsequent purification using a reversed-phase C18 cartridge and EtOH/0.01% aqueous TFA 80:20 v/v as eluent yielded [^{68}Ga]**5.9** with excellent radiochemical purity (Figure A5.7, Appendix). The radiochemical yield amounted to 73%. Dilution of the eluate with PBS (pH = 7.4) afforded the stock solution of [^{68}Ga]**5.9** which was used for the following experiments.

5.2.7 Distribution coefficient $logD_{7.4}$ and proteolytic stability of [^{68}Ga]**5.9**

The determination of the distribution coefficient $logD_{7.4}$ of [^{68}Ga]**5.9** in n-octanol/PBS 1:1 yielded a value of -3.32 being similar to the $logD_{7.4}$ (-3.06) reported for the NTS_1R PET ligand **1.12**.[12] With a $logD_{7.4}$ < -3, [^{68}Ga]**5.9** represents a very hydrophilic NTS_1R ligand, which is expected to be strongly renally excreted when used in vivo.

Furthermore, the proteolytic stability of [^{68}Ga]**5.9** in human plasma was studied (note: due to the short half-life of ^{68}Ga ($t_{1/2}$ = 68 min), the longest timepoint studied was 3 h). [^{68}Ga]**5.9** exhibited high stability – no additional radiopeaks were observed after 3 h – which confirms the aforementioned high stability of the "cold" analog **5.9** (Figure A5.8, Appendix).

5.3 Conclusion

Conjugation of different chelators – DOTA, NOTA, and (*R*)-NODA-GA – to the reported precursor **4.17a** led to the peptides **5.6**-**5.8** which represent precursors for the insertion of various metal ions. The synthesized potential NTS_1R PET ligands **5.9**-**5.11**, containing natural gallium, showed NTS_1R binding affinities in the subnanomolar range (K_i = 0.13-0.31 nM) and exhibited high proteolytic stability in human plasma ($t_{1/2}$ >> 48 h). Insertion of the positron-emitting radionuclide $^{68}Ga^{3+}$ in compound **5.6** gave the NTS_1R PET ligand [^{68}Ga]**5.9** which was studied in terms of hydrophilicity and plasma stability. The very hydrophilic PET tracer ($logD_{7.4}$ = -3.32) showed high stability in human plasma over a time period of 3 h.

The chelator-conjugated NTS_1R ligands **5.6**-**5.8** represent versatile precursors with a theranostic potential allowing the incorporation of different kinds of radioactive metal ions such as ^{68}Ga, ^{64}Cu, or ^{111}In for PET or SPECT imaging, respectively, to visualize NTS_1R-positive tumors. Incorporation of a β^--emitter like ^{177}Lu or an α-emitting isotope such as ^{225}Ac can give potential NTS_1R ligands for tumor therapy. In future studies, the cellular uptake of [^{68}Ga]**5.9** in tumor cells will be determined. Furthermore, the promising NTS_1R PET ligand [^{68}Ga]**5.9** should be studied in vivo (mouse tumor models) to evaluate its biodistribution and suitability for PET tumor imaging.

5.4 Experimental section

5.4.1 General experimental conditions

Materials. DMF (anhydrous) and TFA were purchased from Fisher Scientific (Schwerte, Germany). DIPEA was obtained from ABCR (Karslruhe, Germany). DOTA-tris(tBu)ester succinimidyl ester (**5.3**), (*R*)-NODA-GA-tris(tBu)ester (**5.4**) and NOTA-bis(tBu)ester (**5.5**) were purchased from CheMatech (Dijon, France). Ultrapure 4-(2-hydroxyethyl)-1-piperazineethanesulfonic acid (HEPES) was obtained from Gerbu (Heidelberg, Germany). Gallium(III)nitrate hydrate was from Sigma-Aldrich (Taufkirchen, Germany). Acetonitrile (HPLC gradient grade) was from VWR (Ismaning, Germany). NT(8-13) (**1.3**) was synthesized via SPPS in-house. Bacitracin, HEPES, and bovine serum albumin (BSA) were obtained from Serva (Heidelberg, Germany). Fetal bovine serum (FBS) was purchased from Pan-Biotech (Aidenbach, Germany). The radioligand [^{3}H]**1.7** (molar activity: 2.41 TBq/mmol) was prepared according to a described procedure.[27] The synthesis of compound **4.17a** is described in Chapter 4. Millipore water was consistently used for the preparation of stock solutions, buffers, and aqueous eluents for HPLC. Polypropylene reaction vessels with screw cap (1.5 and 2 mL) from Sarstedt (Nümbrecht, Germany) were used for small-scale reactions and to keep stock solutions.

NMR spectroscopy. NMR spectra of compounds **5.6**-**5.11** were recorded and analyzed as described in Chapter 4.

Mass spectroscopy. High-resolution mass spectrometry (HRMS) was performed as described in Chapter 4.

Preparative HPLC. Preparative HPLC and lyophilization were performed using the same systems as described in Chapter 4.

Analytical HPLC. Analytical HPLC analysis was performed using the same system, column, flow rate, detection wavelength, eluents and column temperature as described in Chapter 4. For purity controls, the following linear gradient was applied: 0-14 min: acetonitrile/0.04% aqueous TFA 10:90-30:70, 14-15 min: 30:70-95:5, 15-18 min: 95:5 (isocratic). Retention (capacity) factors *k* were calculated as described in Chapter 4. To verify the insertion of Ga^{3+}, the aforementioned eluents were replaced by methanol and 0.05% aqueous formic and the following gradient was applied: 0-14 min: methanol/0.05% aqueous formic acid 20:80-40:60, 14-15 min: 40:60-95:5, 15-18 min: 95:5 (isocratic).

General procedure for the incorporation of Ga^{3+}. The chelator-conjugated peptides **5.6**-**5.8** (1 equiv.) were dissolved in HEPES buffer (0.2 M, pH = 4.2) to give a concentration of 4 mM. The solution of the peptide was preheated at 60 °C for 5 min. After the addition of a solution of $Ga(NO_3)_3 \times H_2O$ (3 equiv., 0.4 M) in 10 mM aqueous HCl, the mixture was shaken at 100 °C for 30 min followed by dilution with 0.1% aqueous TFA/acetonitrile 90:10 v/v and purification by preparative RP-HPLC.

Compound characterization. Compounds **5.6**-**5.11** were characterized by HRMS, ^{1}H-NMR spectroscopy, and RP-HPLC. HPLC purities of all target compounds were ≥ 95% (UV detection, 220 nm).

5.4.2 Experimental protocols and analytical data

***N*$^{\alpha}$-Methyl-*N*$^{\omega}$-{[4-(*N*-{2-[4,7,10-tris(carboxymethyl)-1,4,7,10-tetraazacyclododecan-1-yl]acetyl})aminobutyl]aminocarbonyl}Arg-Arg-Pro-β,β-dimethyl-L-Tyr-Ile-β-trimethylsilyl-Ala heptakis(hydrotrifluoroacetate) (5.6).** Peptide **4.17a** (7.0 mg, 4.8 µmol) was dissolved in anhydrous DMF/NMP 4:1 v/v (150 µL) followed by the addition of DIPEA (8.9 µL, 52 µmol). A solution of DOTA tris(*tert*-butyl) succinimidyl ester (**5.3**, 3.5 mg, 4.3 µmol) in DMF/NMP 4:1 v/v (50 µL) was added and the mixture was stirred at room temperature for 90 min. 10% aqueous TFA (28 µL) and 0.1% aqueous TFA/acetonitrile 80:20 v/v (1 mL) were added and the solution was subjected to preparative RP-HPLC (gradient: 0-35 min: acetonitrile/0.1% aqueous TFA 20:80-60:40, t_R = 17 min). Lyophilization of the eluate yielded the protected intermediate as a white fluffy solid. TFA/H_2O 80:20 v/v (2 mL) was added and the mixture was stirred at room temperature overnight. On the next day, the volatiles were evaporated and the crude product was taken up in H_2O (100 mL) followed by lyophilization. Isolation by preparative RP-HPLC (gradient: 0-25 min: acetonitrile/0.1% aqueous TFA 15:85-45:55, t_R = 13 min) and lyophilization of the eluate yielded **5.6** as a white fluffy solid (6.5 mg, 62%).^{1}H-NMR (600 MHz, DMSO-d_6): δ (ppm) 0.01 (s, 9H), 0.73-0.84 (m, 6H), 0.90-1.03 (m, 3H), 1.21-1.29 (m, 6H), 1.33-1.46 (m, 5H), 1.48-1.60 (m, 5H), 1-62-1.84 (m, 7H), 1-86-19.5 (m, 1H), 2.48 (s, 3H), 3.08-3.18 (m, 13H), 3.21-3.33 (m, 10H), 3.50-3.53 (m, 2H, interfering with the water signal, quantified in the spectrum acquired after the addition of D_2O), 3.57-3.59 (m, 2H, interfering with the water signal, quantified in the spectrum acquired after the addition of D_2O), 3.80-3.87 (m, 6H, interfering with the water signal, quantified in the spectrum acquired after the addition of D_2O), 4.13 (t, 2H, *J* 8.2 Hz), 4.17-4.26 (m, 2H), 4.39-4.44 (m, 1H), 4.53-4.60 (m, 1H), 4.65 (d, 1H, *J* 10.0 Hz), 6.57-6.65 (m, 2H), 6.71-7.11 (br s, 2H), 7.12-7.15 (m,

2H), 7.15-7.48 (m, 4H), 7.51 (d, 1H, *J* 8.4 Hz), 7.64 (t, 1H, *J* 5.1 Hz), 8.08 (d, 1H, *J* 7.5 Hz), 8.40 (s, 2H), 8.78-9.05 (m, 3H), 9.13 (s, 1H), 9.28 (s, 1H), 11.00-13.33 (m, 4H). 6 exchangeable protons (NH) of the presumably 7-fold protonated molecule were not apparent. HRMS (ESI): *m/z* $[M+4H]^{4+}$ calcd. for $[C_{62}H_{112}N_{18}O_{16}Si]^{4+}$ 348.2063, found: 348.2069. RP-HPLC (220 nm): 99% (t_R = 9.6 min, *k* = 11.6). $C_{62}H_{108}N_{18}O_{16}Si \cdot C_{14}H_7F_{21}O_{14}$ (1389.74 + 798.16).

N^{α}-Methyl-N^{ω}-{[4-(*N*-{2-[4,7-bis(carboxymethyl)-1,4,7-triazacyclononan-1-yl]acetyl})aminobutyl]aminocarbonyl}Arg-Arg-Pro-β,β-dimethyl-L-Tyr-Ile-β-trimethylsilyl-Ala hexakis(hydrotrifluoroacetate) (5.7). Peptide **4.17a** (6.5 mg, 4.5 µmol) was dissolved in anhydrous DMF/NMP 4:1 v/v (150 µL) followed by the addition of DIPEA (8.3 µL, 49 µmol). NOTA bis(*tert*-butyl) ester (**5.4**, 1.7 mg, 4.1 µmol) was preactivated with HOBt (0.55 mg, 4.1 µmol), HBTU (1.5 mg, 4.1 µmol) and DIPEA (1.4 µL, 8.2 µmol) in anhydrous DMF/NMP 4:1 v/v (100 µL) at 35°C for 10 min. After combining both solutions, the mixture was stirred at room temperature for 1 h. Since monitoring by RP-HPLC still showed substantial amounts of starting material (**4.17a**), additional **5.4** was added (1.7 mg, 4.1 µmol; activated as described before). After stirring for one more hour, 10% aqueous TFA (28 µL) and 0.1% aqueous TFA/acetonitrile 80:20 v/v (1 mL) were added and the solution was subjected to preparative RP-HPLC (gradient: 0-35 min: acetonitrile/0.1% aqueous TFA 20:80-60:40, t_R = 18 min). Lyophilization of the eluate yielded the protected intermediate as a white fluffy solid. TFA/H_2O 80:20 v/v (2 mL) was added and the mixture was stirred at room temperature overnight. On the next day, the volatiles were evaporated and the crude product was taken up in H_2O (100 mL) and followed by lyophilization. Isolation by preparative RP-HPLC (gradient: 0-25 min: acetonitrile/0.1% aqueous TFA 15:85-45:55, t_R = 14 min) and lyophilization of the eluate yielded **5.7** as a white fluffy solid (3.3 mg, 37%). ^{1}H-NMR (600 MHz, DMSO-d_6): δ (ppm) 0.01 (s, 9H), 0.93-0.84 (m, 6H), 0.91-1.03 (m, 3H), 1.18-1.29 (m, 7H), 1.31-1.96 (m, 20H), 2.48 (s, 3H), 2.86-3.13 (m, 17H), 3.24-3.28 (m, 2H), 3.46-3.54 (m, 3H, interfering with the water signal, quantified in the spectrum acquired after the addition of D_2O), 3.61-3.63 (m, 4H, interfering with the water signal, quantified in the spectrum acquired after the addition of D_2O), 3.80-3.82 (m, 1H, interfering with the water signal, quantified in the spectrum acquired after the addition of D_2O), 4.13 (t, 2H, *J* 8.4 Hz), 4.17-4.24 (m, 2H), 4.39-4.44 (m, 1H), 4.53-4.59 (m, 1H), 4.65 (d, 1H, *J* 9.9 Hz), 6.56-6.64 (m, 2H), 6.65-7.10 (br s, 2H), 7.10-7.14 (m, 2H), 7.14-7.48 (m, 3H), 7.51 (d, 1H, *J* 8.8 Hz), 7.61 (t, 1H, *J* 5.3 Hz), 7.82-8.12 (m, 2H), 8.13-8.69 (m, 2H), 8.77-9.05 (m, 3H), 9.05-9.24 (m, 1H), 11.05-12.57 (m, 3H). 3 exchangeable protons (NH) of the presumably 6-fold protonated molecule were not apparent. HRMS (ESI):

m/z $[M+4H]^{4+}$ calcd. for $[C_{58}H_{105}N_{17}O_{14}Si]^{4+}$ 322.9444, found: 322.9449. RP-HPLC (220 nm): 98% (t_R = 10.7 min, *k* = 13.1). $C_{58}H_{101}N_{17}O_{14}Si \cdot C_{12}H_6F_{18}O_{12}$ (1288.64 + 684.14).

***N*$^{\alpha}$-Methyl-*N*$^{\omega}$-{[4-(*N*-{4-[4,7-bis(carboxymethyl)-1,4,7-triazacyclononan-1-yl]-(*R*)-4-carboxybutanoyl})aminobutyl]aminocarbonyl}Arg-Arg-Pro-β,β-dimethyl-L-Tyr-Ile-β-trimethylsilyl-Ala hexakis(hydrotrifluoroacetate) (5.8).** Peptide **4.17a** (6.8 mg, 4.7 µmol) was dissolved in anhydrous DMF/NMP 4:1 v/v (150 µL) followed by the addition of DIPEA (8.7 µL, 51 µmol). (*R*)-NODA-GA tris(*tert*-butyl) ester (**5.5**, 2.3 mg, 4.2 µmol) was preactivated with HOBt (0.57 mg, 4.2 µmol), HBTU (1.6 mg, 4.2 µmol) and DIPEA (1.4 µL, 8.5 µmol) in anhydrous DMF/NMP 4:1 v/v (100 µL) at 35°C for 10 min. After combining both solutions, the mixture was stirred at room temperature for 2 h. 10% aqueous TFA (28 µL) and 0.1% aqueous TFA/acetonitrile 80:20 v/v (1 mL) were added and the solution was subjected to preparative RP-HPLC (gradient: 0-35 min: acetonitrile/0.1% aqueous TFA 20:80-60:40, t_R = 21 min). Lyophilization of the eluate yielded the protected intermediate as a white fluffy solid. TFA/H_2O 80:20 v/v (2 mL) was added and the mixture was stirred at room temperature overnight. On the next day, the volatiles were evaporated and the crude product was taken up in H_2O (100 mL) followed by lyophilization. Isolation by preparative RP-HPLC (gradient: 0-25 min: acetonitrile/0.1% aqueous TFA 15:85-45:55, t_R = 14 min) and lyophilization of the eluate yielded **5.8** as a white fluffy solid (4.3 mg, 45%). ^{1}H-NMR (600 MHz, DMSO-d_6): δ (ppm) 0.01 (s, 9H), 0.73-0.83 (m, 6H), 0.91-1.03 (m, 3H), 1.21-1.29 (m, 6H), 1.34-1.44 (m, 5H), 1.47-1.60 (m, 5H), 1-62-1.96 (m, 10H), 2.14-2.25 (m, 2H), 2.48 (s, 3H), 2.72-2.79 (m, 1H), 2.89-2.99 (m, 4H), 3.01-3.15 (m, 11H), 3.23-3.28 (m, 2H), 3.46-3.51 (m, 2H), 3.55-3.61 (m, 2H), 3.78-3.83 (m, 4H), 4.13 (t, 2H, *J* 8.4 Hz), 4.18-4.23 (m, 2H), 4.40-4.43 (m, 1H), 4.54-4.59 (m, 1H), 4.65 (d, 1H, *J* 9.8 Hz), 6.59-6.64 (m, 2H), 6.71-7.11 (br s, 2H), 7.11-7.14 (m, 2H), 7.15-7.42 (m, 3H), 7.42-7.74 (m, 4H), 7.80 (t, 1H, *J* 5.7 Hz), 8.08 (d, 1H, *J* 7.9 Hz), 8.42 (s, 2H), 8.83-9.20 (m, 5H), 10.32 (s, 1H), 12.12-12.85 (m, 4H). 2 exchangeable protons (NH) of the presumably 6-fold protonated molecule were not apparent. HRMS (ESI): *m/z* $[M+3H]^{3+}$ calcd. for $[C_{61}H_{108}N_{17}O_{14}Si]^{3+}$ 454.2638, found: 454.2645. RP-HPLC (220 nm): 98% (t_R = 10.4 min, *k* = 12.7). $C_{61}H_{105}N_{17}O_{16}Si \cdot C_{12}H_6F_{18}O_{12}$ (1360.70 + 684.14).

***N*$^{\alpha}$-Methyl-*N*$^{\omega}$-{[4-(N-{2-[gallium(III)-4,7,10-tris(carboxymethyl)-1,4,7,10-tetraazacyclododecan-1-yl]acetyl})aminobutyl]aminocarbonyl}Arg-Arg-Pro-β,β-dimethyl-L-Tyr-Ile-β-trimethylsilyl-Ala tetrakis(hydrotrifluoroacetate) (5.9).** Compound

5.9 was prepared from the DOTA-conjugated peptide **5.6** (6.1 mg, 2.8 µmol) according to the general procedure for Ga^{3+}-incorporation. Purification by preparative RP-HPLC (gradient: 0-25 min: acetonitrile/0.1% aqueous TFA 15:85-45:55, t_R = 14 min) followed by lyophilization of the eluate afforded **5.9** as a white fluffy solid (5.3 mg, 99%). ^{1}H-NMR (600 MHz, DMSO-d_6): δ (ppm) 0.01 (s, 9H), 0.73-0.84 (m, 6H), 0.90-1.03 (m, 3H), 1.19-1.29 (m, 6H), 1.34-1.47 (m, 5H), 1.47-1.61 (m, 5H), 1.62-1.67 (m, 1H), 1.67-1.85 (m, 6H), 1.85-1.95 (m, 1H), 2.45-2.49 (m, 3H), 3.04-3.18 (m, 8H), 3.22-3.36 (m, 12H), 3.46-3.54 (m, 3H), 3.54-3.62 (m, 3H), 3.62-3.70 (m, 4H), 3.70-3.78 (m, 4H), 3.78-3.87 (m, 1H), 4.13 (t, 1H, *J* 8.0 Hz), 4.18-4.23 (m, 1H), 4.39-4.44 (m, 1H), 4.53-4.59 (m, 1H), 4.65 (d, 1H, *J* 9.6 Hz), 6.58-6.64 (m, 2H), 6.87-7.23 (br s, 2H, interfering with next listed signal), 7.11-7.15 (m, 2H), 7.23-7.62 (m, 5H), 7.76 (t, 1H, *J* 5.7 Hz), 8.05-8.11 (m, 1H), 8.35 (t, 1H, *J* 5.6 Hz), 8.48 (s, 2H), 8.88-8.99 (m, 2H), 8.99-9.28 (m, 3H), 10.46 (s, 1H), 12.41 (s, 1H), 13.33 (s, 1H). HRMS (ESI): *m/z* $[M+4H]^{4+}$ calcd. for $[C_{62}H_{109}GaN_{18}O_{16}Si]^{4+}$ 364.6818, found: 364.6824. RP-HPLC (220 nm): 99% (t_R = 9.6 min, *k* = 11.6). $C_{62}H_{105}GaN_{18}O_{16}Si \cdot C_8H_4F_{12}O_8$ (1456.44 + 456.09).

***N*$^{\alpha}$-Methyl-*N*$^{\omega}$-{[4-(*N*-{2-[gallium(III)-trifluoroacetate-4,7-bis(carboxymethyl)-1,4,7-triazacyclononan-1-yl]acetyl})aminobutyl]aminocarbonyl}Arg-Arg-Pro-β,β-dimethyl-L-Tyr-Ile-β-trimethylsilyl-Ala tris(hydrotrifluoroacetate) (5.10).** Compound **5.10** was prepared from the NOTA-conjugated peptide **5.7** (2.0 mg, 0.99 µmol) according to the general procedure for Ga^{3+}-incorporation. Purification by preparative RP-HPLC (gradient: 0-25 min: acetonitrile/0.1% aqueous TFA 15:85-45:55, t_R = 14 min) followed by lyophilization of the eluate afforded **5.10** as a white fluffy solid (1.8 mg, 99%). ^{1}H-NMR (600 MHz, DMSO-d_6): δ (ppm) 0.01 (s, 9H), 0.74-0.83 (m, 6H), 0.92-1.02 (m, 3H), 1.22-1.29 (m, 6H), 1.33-1.41 (m, 1H), 1.45-1.59 (m, 9H), 1.62-1.84 (m, 7H), 1.86-1.95 (m, 1H), 2.46-2.49 (m, 3H), 2.90-3.14 (m, 10H), 3.25-3.40 (m, 10H), 3.49-3.53 (m, 1H, interfering with the water signal, quantified in the spectrum acquired after the addition of D_2O), 3.57-3.66 (m, 5H, interfering with the water signal, quantified in the spectrum acquired after the addition of D_2O), 3.81-3.83 (m, 1H, interfering with the water signal, quantified in the spectrum acquired after the addition of D_2O), 4.12-4.15 (m, 3H, interfering with the water signal, quantified in the spectrum acquired after the addition of D_2O), 4.19-4.22 (m, 1H, interfering with the water signal, quantified in the spectrum acquired after the addition of D_2O), 4.39-4.44 (m, 1H), 4.53-4.60 (m, 1H), 4.65 (t, 1H, *J* 9.5 Hz), 6.57-6.65 (m, 2H), 6.70-7.11 (br s, 2H), 7.11-7.14 (m, 2H), 7.14-7.47 (m, 3H), 7.47-7.63 (m, 2H), 7.66 (t, 1H, *J* 5.3 Hz), 8.08 (d, 1H, *J* 8.0 Hz), 8.46 (s, 2H), 8.78-9.24 (m, 5H), 10.30 (s, 1H), 10.66 (t, 1H, *J* 5.5 Hz), 12.41 (s, 1H). HRMS (ESI): *m/z* $[M+3H]^{3+}$ calcd.

for $[C_{58}H_{102}GaN_{17}O_{16}Si]^{3+}$ 452.5600, found: 452.5587. RP-HPLC (220 nm): 99% (t_R = 9.5 min, k = 11.5). $C_{58}H_{99}GaN_{17}O_{14}Si^{+} \cdot C_2F_3O_2^{-} \cdot C_6H_3F_9O_6$ (1356.34 + 113.02 + 342.07).

***N*$^{\alpha}$-Methyl-*N*$^{\omega}$-({4-[*N*-(gallium(III)-{4-[4,7-bis(carboxymethyl)-1,4,7-triazacyclononan-1-yl]-(*R*)-4-carboxybutanoyl})]aminobutyl}aminocarbonyl)Arg-Arg-Pro-β,β-dimethyl-L-Tyr-Ile-β-trimethylsilyl-Ala tris(hydrotrifluoroacetate) (5.11).** Compound **5.11** was prepared from the (*R*)-NODA-GA-conjugated peptide **5.8** (3.5 mg, 1.7 µmol) according to the general procedure for Ga^{3+}-incorporation. Purification by preparative RP-HPLC (gradient: 0-25 min: acetonitrile/0.1% aqueous TFA 15:85-45:55, t_R = 14 min) followed by lyophilization of the eluate afforded **5.11** as a white fluffy solid (3.0 mg, 99%). ^{1}H-NMR (600 MHz, DMSO-d_6): δ (ppm) 0.01 (s, 9H), 0.74-0.84 (m, 6H), 0.91-1.03 (m, 3H), 1.21-1.29 (m, 6H), 1.33-1.45 (m, 5H), 1.46-1.61 (m, 5H), 1.61-1.94 (m, 9H), 2.08-2.19 (m, 1H), 2.33-2.45 (m, 2H), 2.46-2.49 (m, 3H), 2.66-2.85 (m, 3H), 2.97-3.16 (m, 12H), 3.20-3.29 (m, 4H), 3.32-3.40 (m, 2H), 3.41-3.46 (m, 1H), 3.50-3.60 (m, 5H, interfering with the water signal, quantified in the spectrum acquired after the addition of D_2O), 3.80-3.83 (m, 1H, interfering with the water signal, quantified in the spectrum acquired after the addition of D_2O), 4.13 (t, 1H, *J* 8.2 Hz, interfering with the water signal, quantified in the spectrum acquired after the addition of D_2O), 4.18-4.22 (m, 1H, interfering with the water signal, quantified in the spectrum acquired after the addition of D_2O), 4.40-4.44 (m, 1H), 4.54-4.59 (m, 1H), 4.63-4.68 (d, 1H, *J* 9.4 Hz), 6.58-6.65 (m, 2H), 6.72-7.11 (br s, 2H), 7.11-7.16 (m, 2H), 7.16-7.58 (m, 5H), 7.65 (t, 1H, *J* 5.6 Hz), 7.89 (t, 1H, *J* 5.4 Hz), 8.08 (d, 1H, 7.8 Hz), 8.43 (s, 2H), 8.84-9.00 (m, 3H), 9.00-9.24 (m, 2H), 10.02 (s, 1H), 12.40 (s, 1H). HRMS (ESI): *m/z* $[M+3H]^{3+}$ calcd. for $[C_{61}H_{105}GaN_{17}O_{16}Si]^{3+}$ 476.2311, found: 476.2315. RP-HPLC (220 nm): 99% (t_R = 10.4 min, k = 12.7). $C_{61}H_{102}GaN_{17}O_{16}Si \cdot C_6H_3F_9O_6$ (1427.40 + 342.07).

5.4.3 Cell culture

HT-29 colon carcinoma cells (DSMZ-no. ACC 299) were grown as described in Chapter 4.

5.4.4 NTS_1R binding assay

NTS_1R radioligand competition binding experiments with [^{3}H]**1.7** (molar activity: 2.41 TBq/mmol) and the peptides **5.6**-**5.11** were performed with intact $hNTS_1R$-expressing human

HT-29 colon carcinoma cells as described in Chapter 4. Data were analyzed as reported in Chapter 4.

5.4.5 Fura-2 Ca^{2+} assay

NTS_1R agonistic potencies of **5.9**-**5.11** were determined as described under *Fura-2 Ca^{2+} assay* in Chapter 4.

5.4.6 Chemical stability

The chemical stability of **5.6**-**5.11** was investigated as described under *Chemical stability* in Chapter 4.

5.4.7 Stability in human plasma

The proteolytic stability of **5.9**-**5.11** was investigated as described under *Stability in human plasma* in Chapter 4. Obtained recoveries and calculated recovery ratios are shown in Table A5.1 (Appendix).

5.4.8 Radiosynthesis of [^{68}Ga]**5.9**

The preparation of the PET tracer [^{68}Ga]**5.9** was performed according to a reported procedure[12] with the following modifications: A 0.11 mM solution of the precursor **5.6** in ultrapure H_2O (100 µL) was used. After the synthesis and cooling to rt, the acidic solution of the crude material was subjected to a C18 cartridge (Sep-Pak C18 Plus Short Cartridge, 55-105 µm, Waters, Milford, MA, USA). A washing step with H_2O (12 mL) was followed by elution of the product with EtOH/0.04% aqueous TFA 80:20 v/v (1.2 mL). The eluate was diluted with PBS (9 mL, pH = 7.4) and the activity and purity were determined (final activity = 234.9 MBq). 77 µL of this solution were added to 923 µL of PBS (pH = 7.4) to obtain the final "stock" solution which was used for experiments [^{68}Ga]**5.9**. The quality control of the PET ligand was performed by RP-HPLC analysis using a system from Agilent Technologies consisting of an 1100 Series quaternary pump equipped with a 1260 Infinity degasser, an 1100 Series Autosampler, an 1100 Series Thermostated Column Compartment, an 1100 Series Diode Array Detector, and a GABI Star radiometric detector (Raytest Isotopenmessgeräte GmbH, Straubenhardt, Germany). A

linear gradient was applied: 0–9 min: acetonitrile/0.01% aqueous TFA 95:5–55:45, 9–12 min: 55:45–5:95, 12–16 min: 5:95. UV detection was performed at 220 nm.

5.4.9 Determination of the distribution coefficient $logD_{7.4}$

To determine the distribution coefficient $logD_{7.4}$ of [^{68}Ga]**5.9**, 100 µL of the "stock" solution were added to n-octanol (500 µL) and PBS (400 µL, pH = 7.4) in a 1.8-mL HPLC vial (Agilent, article number 5188-6535) with a screw cap equipped with a septum (VWR, article number 548-0027). The mixture was vortexed for 2 min and two 100 µL aliquots of the upper n-octanol phase were withdrawn followed by the determination of their activities with a Canberra Genie 2000 system (Canberra, Rüsselsheim, Germany) with the Gamma Acquisition & Analysis Software Genie 2000 3.4.1. Samples of the lower, aqueous phase were obtained by holding the vial upside down and taking a 100-150 µL aliquot by using a syringe with a needle. Two 10 µL aliquots from the aliquot of the aqueous phase were subjected to activity measurements using the aforementioned Canberra Genie 2000 system. Three individual $logD_{7.4}$ determinations were carried out. The decay-corrected counts per minute (cpm) values were averaged (n = 3) and transformed to a distribution coefficient $logD_{7.4}$ according to $logD_{7.4} = \log(A_{octanol}/A_{aqueous})$, where $A_{octanol}$ is the mean of the decay-corrected cpm values obtained for samples of the n-octanol phase, and $A_{aqueous}$ is the mean of the decay-corrected cpm values obtained for samples of the aqueous phase.

5.4.10 Stability of [^{68}Ga]5.9 in human plasma

To study the plasma stability, 300 µL of the "stock" solution of [^{68}Ga]**5.9** were combined with 150 µL of human plasma in 1.5 mL polypropylene vessel. The mixture was incubated at 37 °C under shaking (450 rpm). After 60, 120, and 180 min, a 100 µL aliquot was withdrawn and 10% aqueous TFA (100 µL) was added to precipitate proteins. After vortexing for 1 min, the sample was centrifuged at 16,100 g for 10 min at 10 °C. For the first two timepoints (60 and 120 min), 50 µL of the supernatant were injected into the same HPLC system as under *Radiosynthesis of [^{68}Ga]**5.9*** (same gradient was applied as well). In the case of the third timepoint (180 min), 100 µL of the supernatant were injected due to the decreasing activity and signal-to-noise over time.

5.5 References

1. Oberg, K.; Castellano, D. Current knowledge on diagnosis and staging of neuroendocrine tumors. *Cancer Metastasis Rev.* **2011**, *30 Suppl 1*, 3-7.
2. Dasari, A.; Shen, C.; Halperin, D.; Zhao, B.; Zhou, S.; Xu, Y.; Shih, T.; Yao, J. C. Trends in the incidence, prevalence, and survival outcomes in patients with neuroendocrine tumors in the United States. *JAMA Oncol.* **2017**, *3*, 1335-1342.
3. Morgat, C.; MacGrogan, G.; Brouste, V.; Velasco, V.; Sevenet, N.; Bonnefoi, H.; Fernandez, P.; Debled, M.; Hindie, E. Expression of gastrin-releasing peptide receptor in breast cancer and its association with pathologic, biologic, and clinical parameters: A study of 1,432 primary tumors. *J. Nucl. Med.* **2017**, *58*, 1401-1407.
4. Maoret, J. J.; Pospai, D.; Rouyer-Fessard, C.; Couvineau, A.; Laboisse, C.; Voisin, T.; Laburthe, M. Neurotensin receptor and its mRNA are expressed in many human colon cancer cell lines but not in normal colonic epithelium: Binding studies and RT-PCR experiments. *Biochem. Biophys. Res. Commun.* **1994**, *203*, 465-471.
5. Reubi, J. C.; Waser, B.; Friess, H.; Buchler, M.; Laissue, J. Neurotensin receptors: A new marker for human ductal pancreatic adenocarcinoma. *Gut* **1998**, *42*, 546-550.
6. Reubi, J. C.; Waser, B.; Schaer, J. C.; Laissue, J. A. Neurotensin receptors in human neoplasms: High incidence in Ewing's sarcomas. *Int. J. Cancer* **1999**, *82*, 213-218.
7. Bossard, C.; Souaze, F.; Jarry, A.; Bezieau, S.; Mosnier, J. F.; Forgez, P.; Laboisse, C. L. Over-expression of neurotensin high-affinity receptor 1 (NTS1) in relation with its ligand neurotensin (NT) and nuclear β-catenin in inflammatory bowel disease-related oncogenesis. *Peptides* **2007**, *28*, 2030-2035.
8. He, T.; Wang, M.; Wang, H.; Tan, H.; Tang, Y.; Smith, E.; Wu, Z.; Liao, W.; Hu, S.; Li, Z. Evaluation of neurotensin receptor 1 as potential biomarker for prostate cancer theranostic use. *Eur. J. Nucl. Med. Mol. Imaging* **2019**, *46*, 2199-2207.
9. Morgat, C.; Brouste, V.; Chastel, A.; Velasco, V.; Macgrogan, G.; Hindie, E. Expression of neurotensin receptor-1 (NTS(1)) in primary breast tumors, cellular distribution, and association with clinical and biological factors. *Breast Cancer Res. Treat.* **2021**, *190*, 403-413.
10. Szarynska, M.; Olejniczak-Keder, A.; Podplonska, K.; Prahl, A.; Ilowska, E. Bradykinin and neurotensin analogues as potential compounds in colon cancer therapy. *Int. J. Mol. Sci.* **2023**, *24*.
11. Fanelli, R.; Chastel, A.; Previti, S.; Hindie, E.; Vimont, D.; Zanotti-Fregonara, P.; Fernandez, P.; Garrigue, P.; Lamare, F.; Schollhammer, R.; Balasse, L.; Guillet, B.;

Remond, E.; Morgat, C.; Cavelier, F. Silicon-containing neurotensin analogues as radiopharmaceuticals for NTS(1)-positive tumors imaging. *Bioconjugate Chem.* **2020**, *31*, 2339-2349.

12. Schindler, L.; Moosbauer, J.; Schmidt, D.; Spruss, T.; Gratz, L.; Ludeke, S.; Hofheinz, F.; Meister, S.; Echtenacher, B.; Bernhardt, G.; Pietzsch, J.; Hellwig, D.; Keller, M. Development of a neurotensin-derived (68)Ga-labeled PET ligand with high in vivo stability for imaging of NTS(1) receptor-expressing tumors. *Cancers (Basel)* **2022**, *14*.
13. Renard, E.; Dancer, P. A.; Portal, C.; Denat, F.; Prignon, A.; Goncalves, V. Design of bimodal ligands of neurotensin receptor 1 for positron emission tomography imaging and fluorescence-guided surgery of pancreatic cancer. *J. Med. Chem.* **2020**, *63*, 2426-2433.
14. Renard, E.; Moreau, M.; Bellaye, P. S.; Guillemin, M.; Collin, B.; Prignon, A.; Denat, F.; Goncalves, V. Positron emission tomography imaging of neurotensin receptor-positive tumors with (68)Ga-labeled antagonists: The chelate makes the difference again. *J. Med. Chem.* **2021**, *64*, 8564-8578.
15. Maschauer, S.; Prante, O. Radiopharmaceuticals for imaging and endoradiotherapy of neurotensin receptor-positive tumors. *J. Labelled Compd. Radiopharm.* **2018**, *61*, 309-325.
16. Price, T. W.; Gallo, J.; Kubicek, V.; Bohmova, Z.; Prior, T. J.; Greenman, J.; Hermann, P.; Stasiuk, G. J. Amino acid based gallium-68 chelators capable of radiolabeling at neutral pH. *Dalton Trans.* **2017**, *46*, 16973-16982.
17. Wallin, M.; Turner, P.; Katsifis, A.; Yang, M.; Chan, H. K. Crystal structure of aqua-(2-[2-(2-[bis-(carboxyl-ato-kappaO-meth-yl)amino-kappaN]eth-yl(carboxyl-ato-kappaO-meth-yl)amino-kappaN)eth-yl](carb-oxy-meth-yl)aza-niumylacetato)-gallium(III) trihydrate. *Acta Crystallogr., Sect. E: Crystallogr. Commun.* **2018**, *74*, 1054-1057.
18. Hsien, M. C.; Kao, H. M.; Lii, K. H. Synthesis, crystal structure, and solid-state NMR spectroscopy of (4-HAP)2[Ga4O(PO4)4(H2O)4] (AP = aminopyridine), a gallophosphate containing discrete double-four-ring units. *Chem. Mater.* **2001**, *13*, 2584-2588.
19. Lin, Z. E.; Zhang, J.; Sun, Y. Q.; Yang, G. Y. Ga(2,2'-bipy)(HPO(4))(H(2)PO(4)): First layered inorganic-organic hybrid gallium phosphate with a neutral framework. *Inorg. Chem.* **2004**, *43*, 797-801.
20. Wang, G. M.; Li, J. H.; Wei, L.; Zhang, X.; Bao, Z. Z. Concise template syntheses of gallium phosphates driven by direct alkylation of aliphatic and aromatic precursors by methanol. *RSC Adv.* **2015**, *5*, 74811-74820.

21. Simecek, J.; Zemek, O.; Hermann, P.; Notni, J.; Wester, H. J. Tailored Gallium(III) chelator NOPO: Synthesis, characterization, bioconjugation, and application in preclinical Ga-68-PET imaging. *Mol. Pharmacol.* **2014**, *11*, 3893-3903.
22. Holub, J.; Meckel, M.; Kubicek, V.; Rosch, F.; Hermann, P. Gallium(III) complexes of NOTA-bis (phosphonate) conjugates as PET radiotracers for bone imaging. *Contrast Media Mol. Imaging* **2015**, *10*, 122-134.
23. Davey, P. R. W. J.; Forsyth, C. M.; Paterson, B. M. Crystallographic and computational characterisation of the potential PET tracer 1,4,7-triazacyclononane-1,4,7-tri(methylenephosphonato)gallium(III). *Chemistryselect* **2022**, *7*.
24. Mitran, B.; Thisgaard, H.; Rinne, S.; Dam, J. H.; Azami, F.; Tolmachev, V.; Orlova, A.; Rosenstrom, U. Selection of an optimal macrocyclic chelator improves the imaging of prostate cancer using cobalt-labeled GRPR antagonist RM26. *Sci. Rep.* **2019**, *9*, 17086.
25. Schindler, L.; Bernhardt, G.; Keller, M. Modifications at Arg and Ile give neurotensin(8-13) derivatives with high stability and retained NTS(1) receptor affinity. *ACS Med. Chem. Lett.* **2019**, *10*, 960-965.
26. Ertl, F. J.; Kopanchuk, S.; Dijon, N. C.; Veiksina, S.; Tahk, M. J.; Laasfeld, T.; Schettler, F.; Gattor, A. O.; Hubner, H.; Archipowa, N.; Kockenberger, J.; Heinrich, M. R.; Gmeiner, P.; Kutta, R. J.; Holliday, N. D.; Rinken, A.; Keller, M. Dually labeled neurotensin NTS(1)R ligands for probing radiochemical and fluorescence-based binding assays. *J. Med. Chem.* **2024**, *67*, 16664-16691.
27. Keller, M.; Kuhn, K. K.; Einsiedel, J.; Hubner, H.; Biselli, S.; Mollereau, C.; Wifling, D.; Svobodova, J.; Bernhardt, G.; Cabrele, C.; Vanderheyden, P. M.; Gmeiner, P.; Buschauer, A. Mimicking of arginine by functionalized N(omega)-carbamoylated arginine as a new broadly applicable approach to labeled bioactive peptides: High affinity angiotensin, neuropeptide Y, neuropeptide FF, and neurotensin neceptor ligands as examples. *J. Med. Chem.* **2016**, *59*, 1925-1945.

Appendix Chapter 5

A5.1 Figures A5.1-A5.8

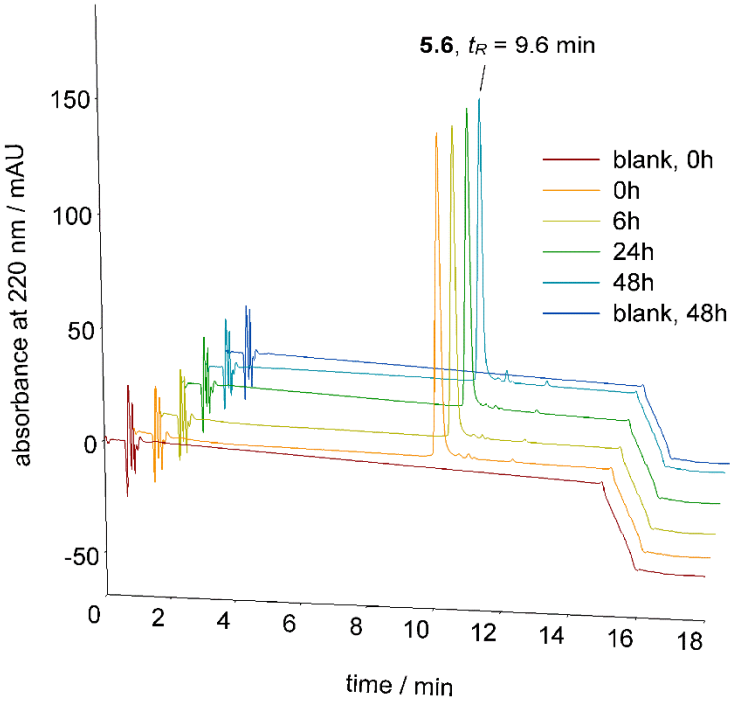


Figure A5.1. Investigation of the chemical stability of **5.6** in PBS (pH = 7.4). Shown are the chromatograms of the RP-HPLC after incubation for up to 48 hours. **5.6** exhibited high stability. Over 48 h, two minor impurities (< 5%) that were already present in the beginning increased (t_R = 10.6 min and t_R =11.9 min).

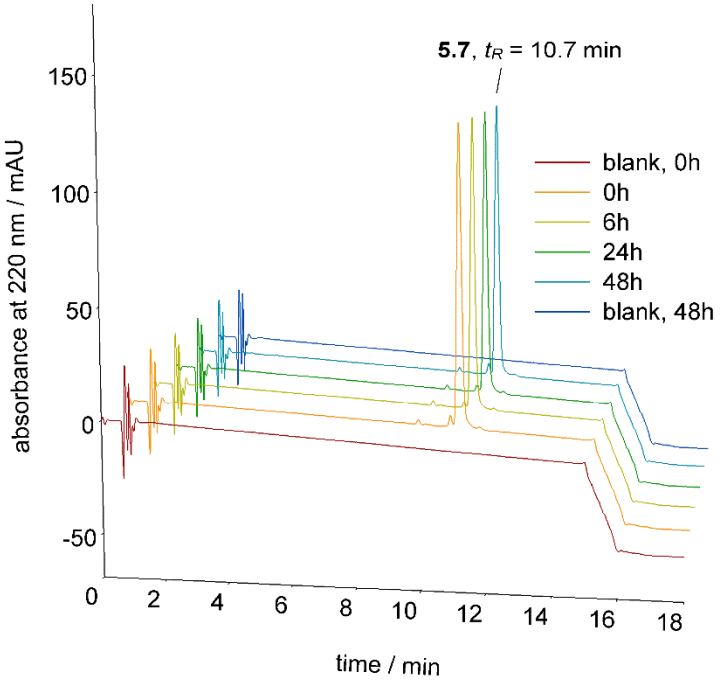


Figure A5.2. Investigation of the chemical stability of **5.7** in PBS (pH = 7.4). Shown are the chromatograms of the RP-HPLC after incubation for up to 48 hours. **5.7** showed no decomposition.

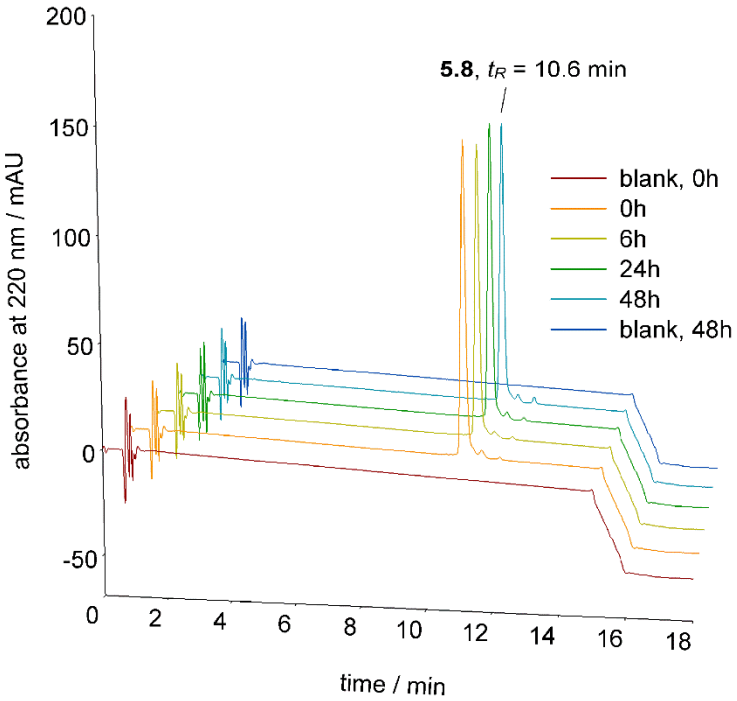


Figure A5.3. Investigation of the chemical stability of **5.8** in PBS (pH = 7.4). Shown are the chromatograms of the RP-HPLC after incubation for up to 48 hours. **5.8** exhibited high stability. Over 48 h, two minor impurities (< 5%) that were already present in the beginning increased (t_R = 11.2 min and t_R =11.8 min).

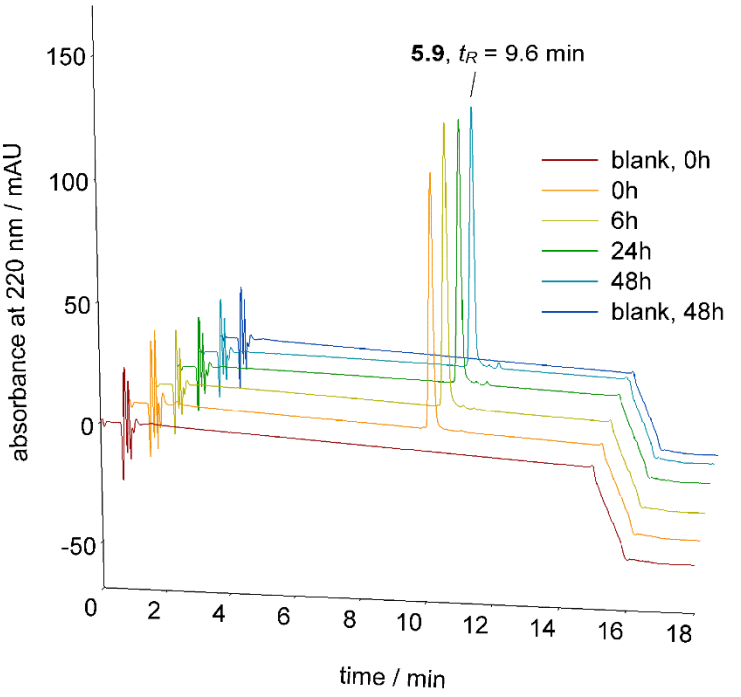


Figure A5.4. Investigation of the chemical stability of **5.9** in PBS (pH = 7.4). Shown are the chromatograms of the RP-HPLC after incubation for up to 48 hours. **5.9** exhibited high stability. After 48 h, two minor decomposition products (t_R = 10.2 min and t_R =10.6 min) were observed.

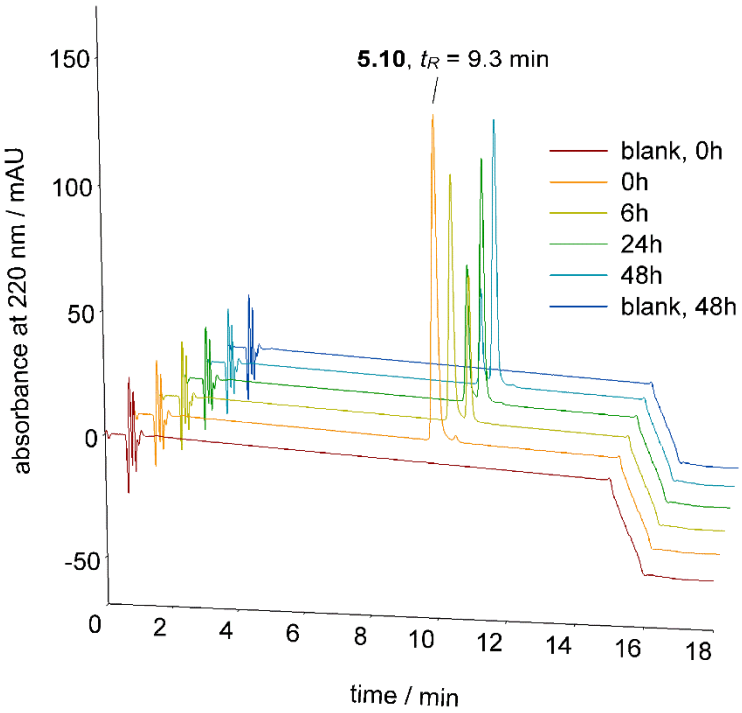


Figure A5.5. Investigation of the chemical stability of **5.10** in PBS (pH = 7.4). Shown are the chromatograms of the RP-HPLC after incubation for up to 48 hours. The reduction of the peak at 9.3 min and the appearance of the second peak at t_R = 9.9 min is most likely due to a ligand exchange (see discussion and Figure 5.2 under *Chemical stability of **5.6**-**5.11***).

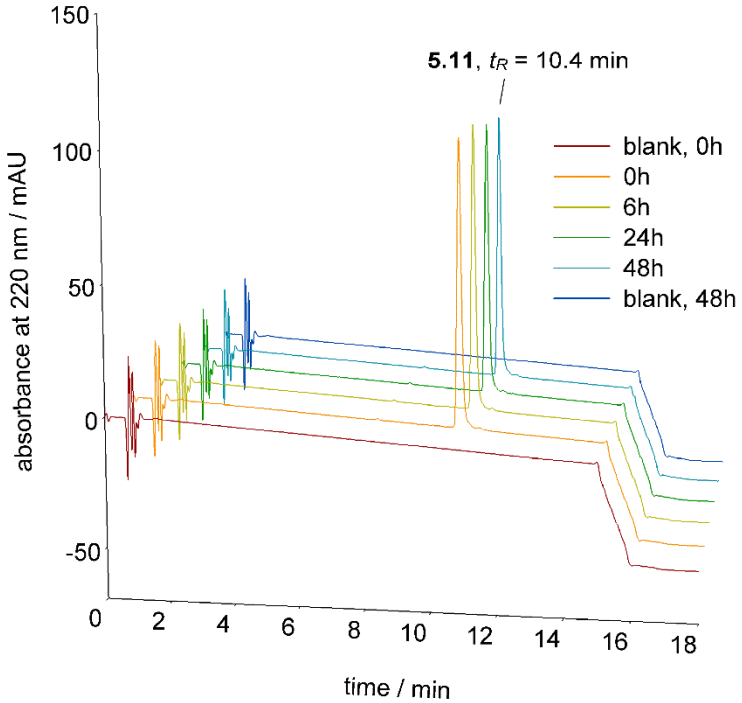


Figure A5.6. Investigation of the chemical stability of **5.11** in PBS (pH = 7.4). Shown are the chromatograms of the RP-HPLC after incubation for up to 48 hours. **5.11** showed no decomposition.

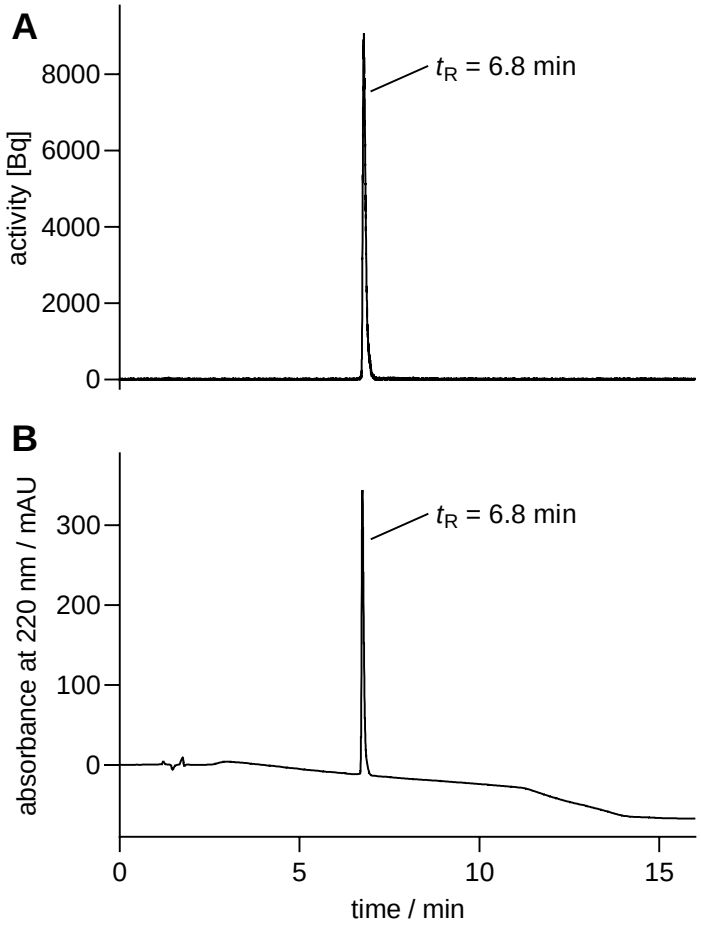


Figure A5.7. (A) RP-HPLC chromatogram of the quality control of [^{68}Ga]**5.9** after radiosynthesis. Shown is radiodetection. Note: the low amount of injected [^{68}Ga]**5.9** did not allow a detection of the compound by the UV detector (data not shown). (B) RP-HPLC chromatogram of the cold analog **5.9** with UV-detection.

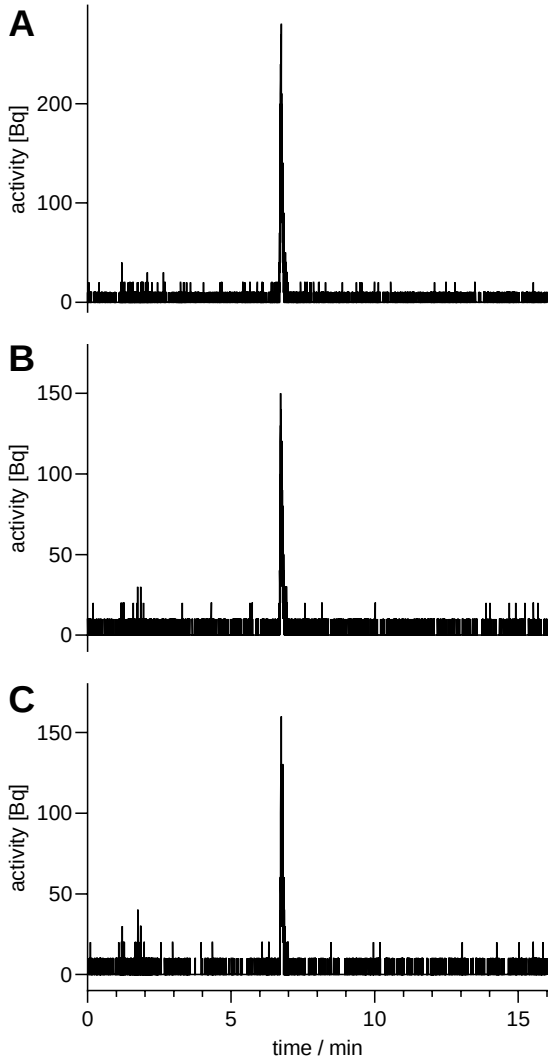


Figure A5.8. Radiochromatograms of the RP-HPLC analysis of [^{68}Ga]**5.9** after incubation in human plasma after 1 h (A), 2 h (B), and 3 h (C) at 37 °C.

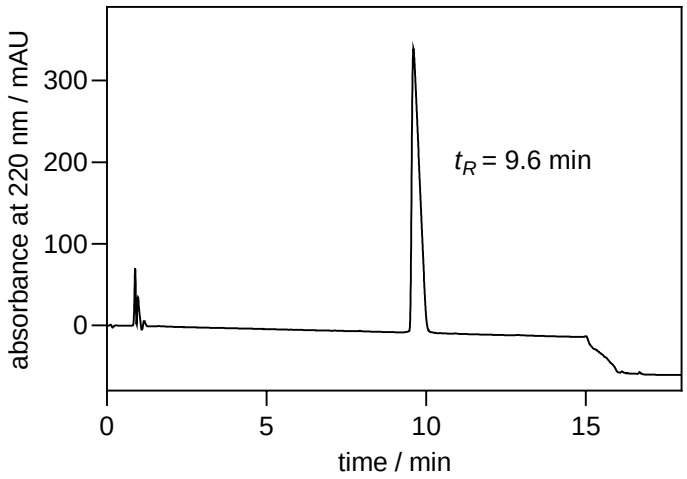
A5.2 Table A5.1

Table A5.1. Recoveries of **5.9**-**5.11** from human plasma/PBS 1:2 v/v and ratios of compound-recovery over recovery of internal standard (1-methyl-D-tryptophan).

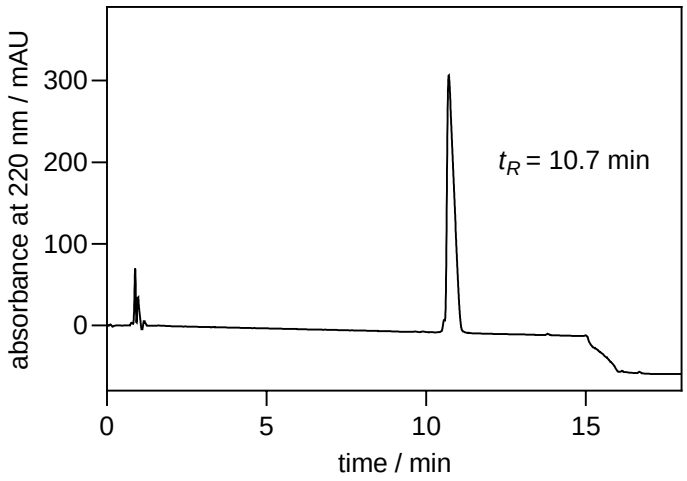
compd.	recovery compd. (%)[a]	recovery 1-methyl-D-tryptophan (%)[a]	ratio[b]
5.9	87 90 88 92 90	96 99 98 100 100	0.91 0.91 0.89 0.91 0.91 (0.91 ± 0.003)
5.10	91 87 91 94 95	90 86 91 90 90	1.01 1.02 1.00 1.04 1.06 (1.03 ± 0.01)
5.11	109 108 99 103 109	107 100 100 99 109	1.02 1.08 0.99 1.04 1.00 (1.03 ± 0.02)

[a]Recoveries of the peptides and of the internal standard from human plasma/PBS 1:2 v/v using a peptide concentration of 40 µM and an internal standard concentration of 10 µM (four independent experiments). [b]Ratios of peptide recovery over recovery of internal standard calculated for individual experiments, as well as mean recovery ratios ± SEM (given in parenthesis).

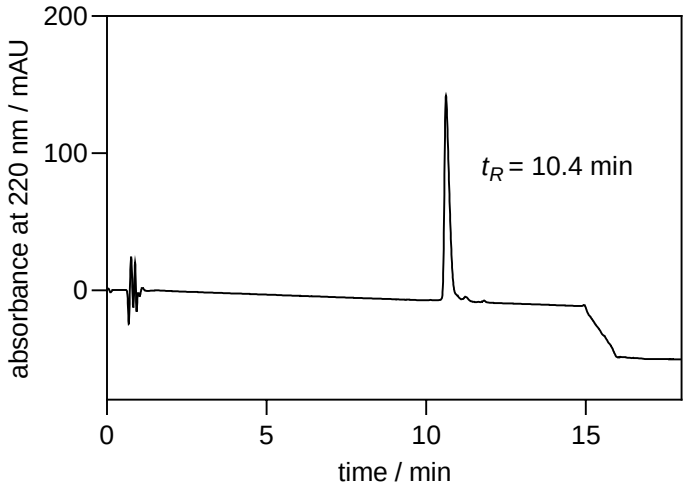
A5.3 RP-HPLC chromatograms of compounds 5.6-5.11 (purity controls)



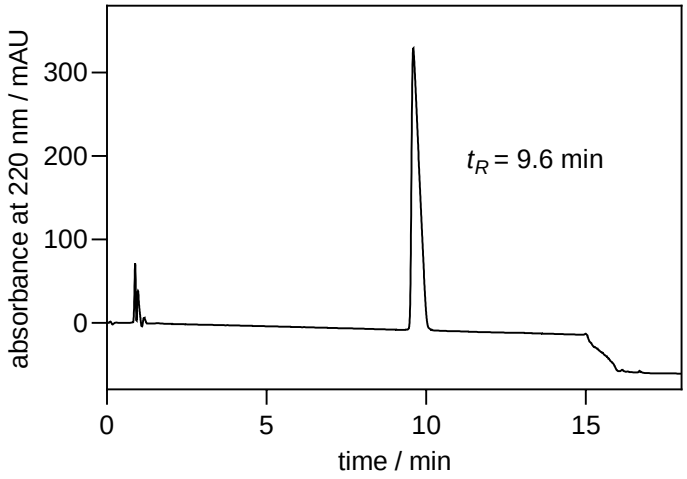
RP-HPLC analysis of compound **5.6**



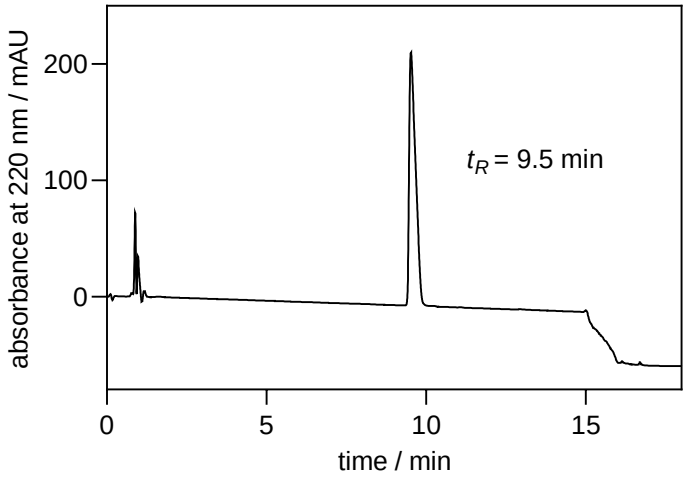
RP-HPLC analysis of compound **5.7**



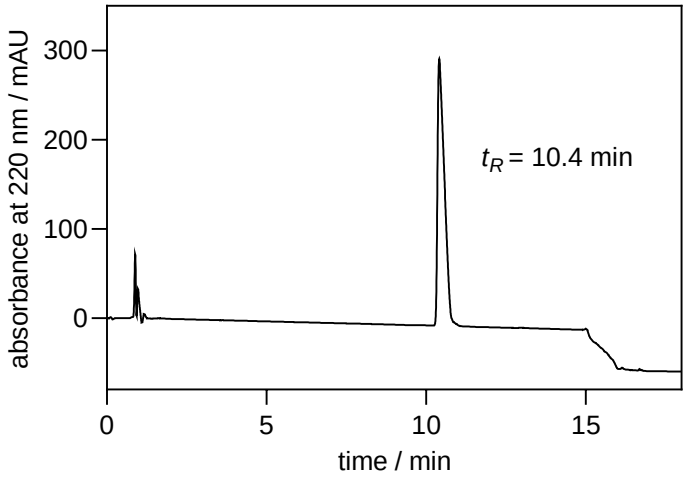
RP-HPLC analysis of compound **5.8**



RP-HPLC analysis of compound **5.9**

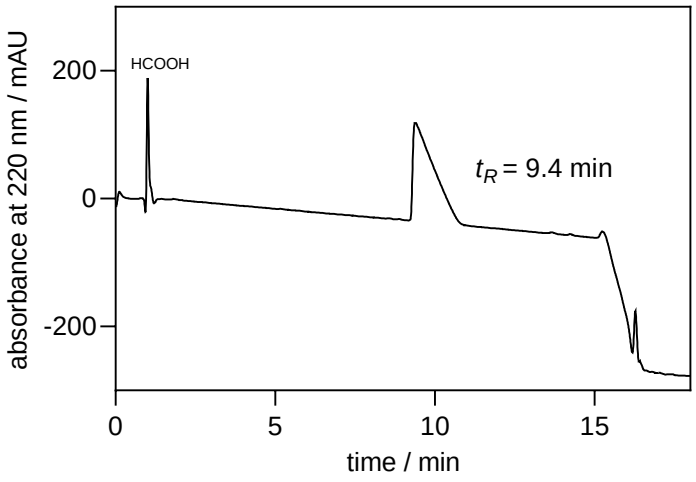


RP-HPLC analysis of compound **5.10**

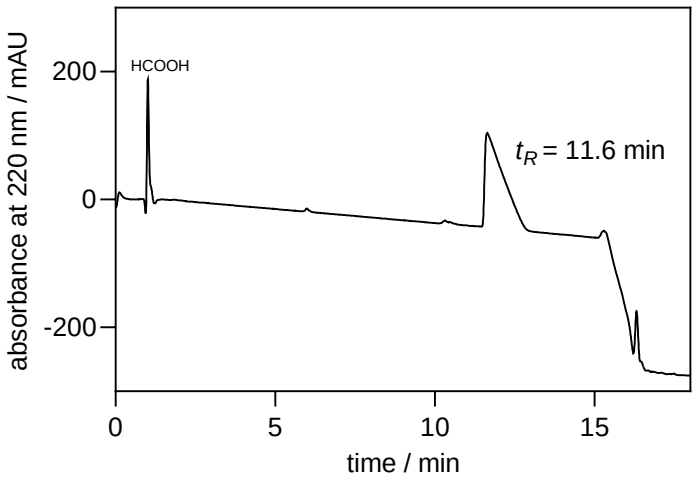


RP-HPLC analysis of compound **5.11**

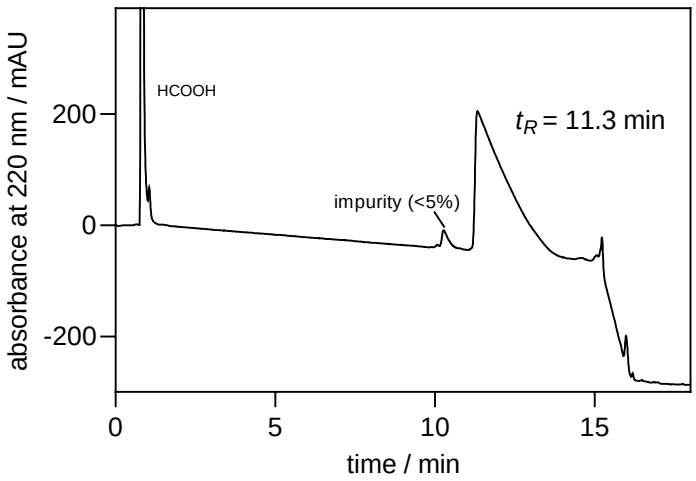
A5.4 RP-HPLC chromatograms of compounds 5.6-5.11 using methanol and 0.05% aqueous formic acid as eluents (control of the Ga^{3+} insertion)



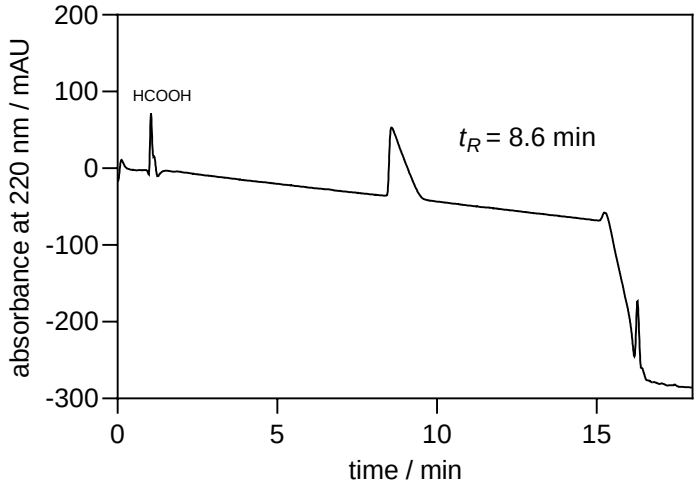
RP-HPLC analysis of compound **5.6**



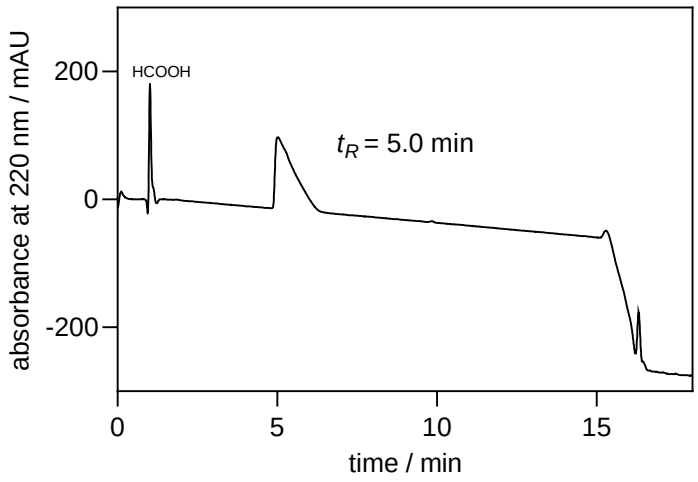
RP-HPLC analysis of compound **5.7**



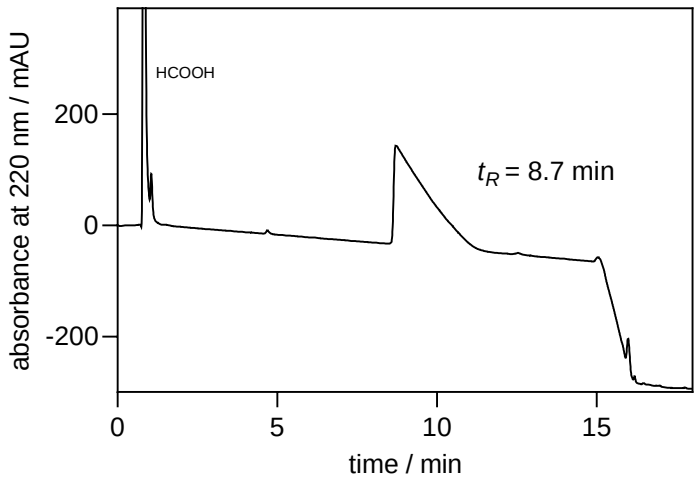
RP-HPLC analysis of compound **5.8**



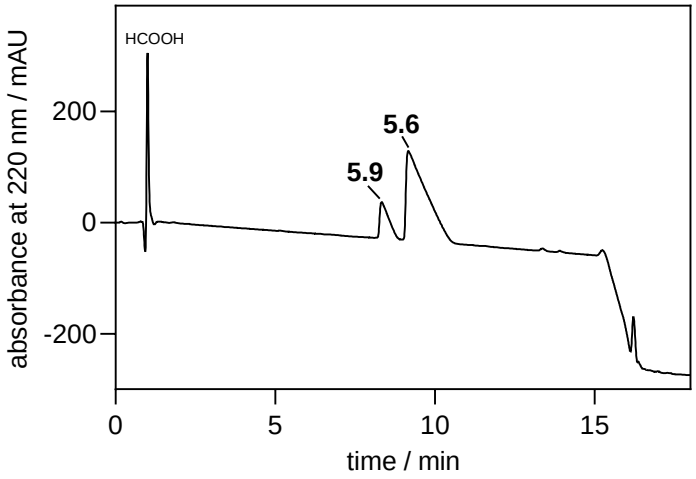
RP-HPLC analysis of compound **5.9**



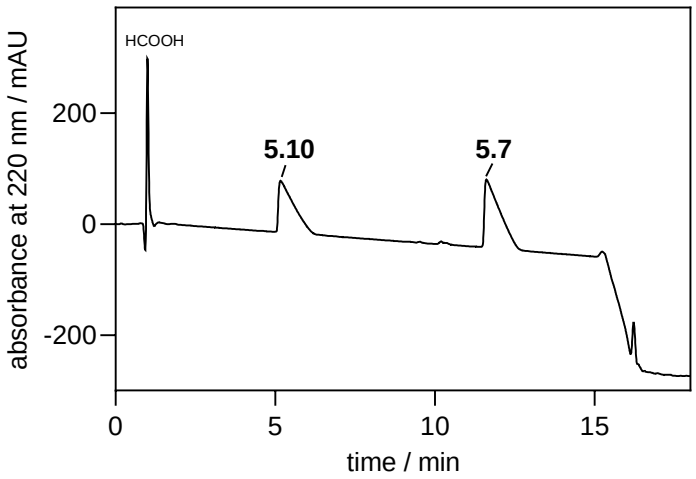
RP-HPLC analysis of compound **5.10**



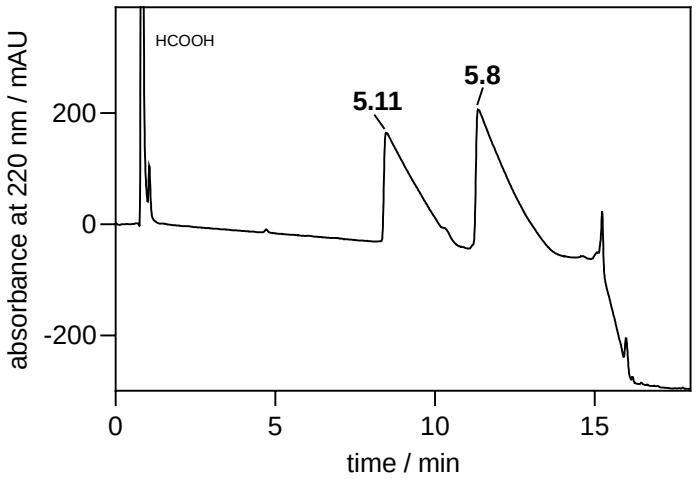
RP-HPLC analysis of compound **5.11**



RP-HPLC analysis of compound **5.6**
co-injected with **5.9**

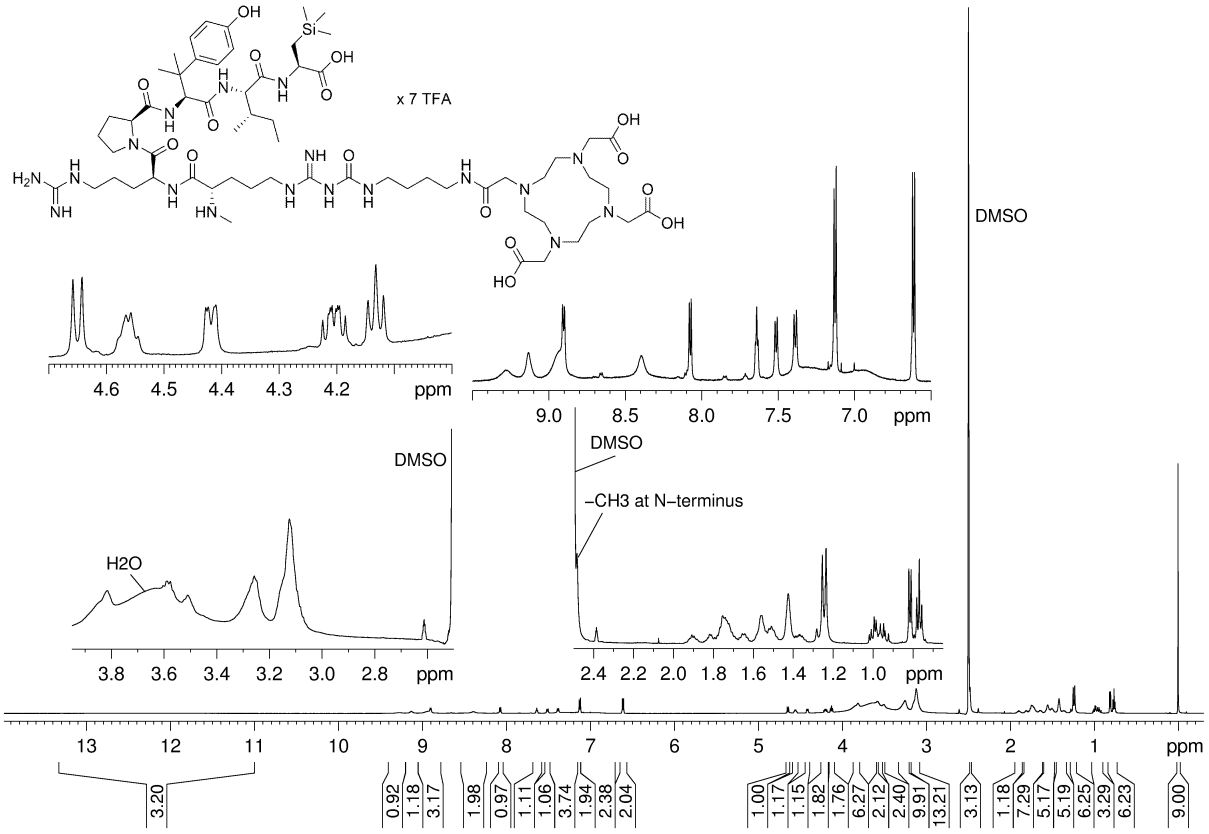


RP-HPLC analysis of compound **5.7**
co-injected with **5.10**

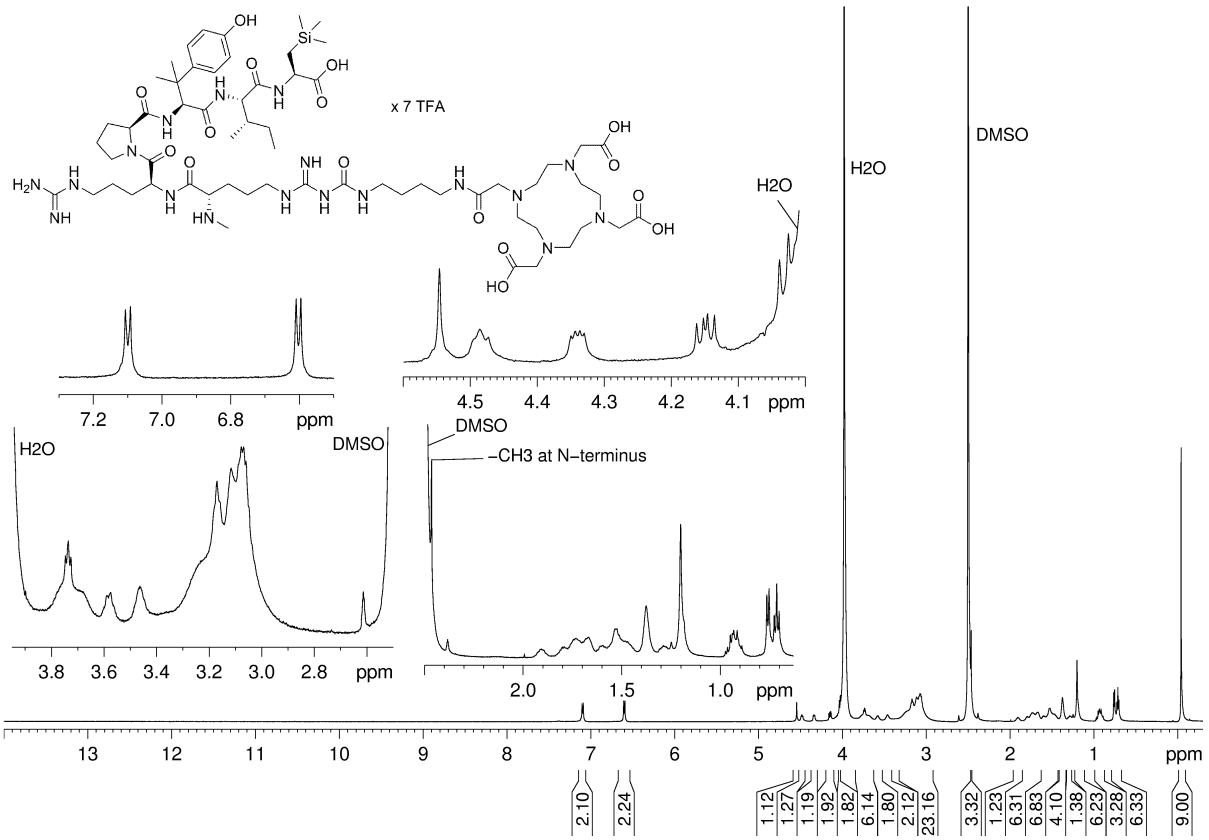


RP-HPLC analysis of compound **5.8**
co-injected with **5.11**

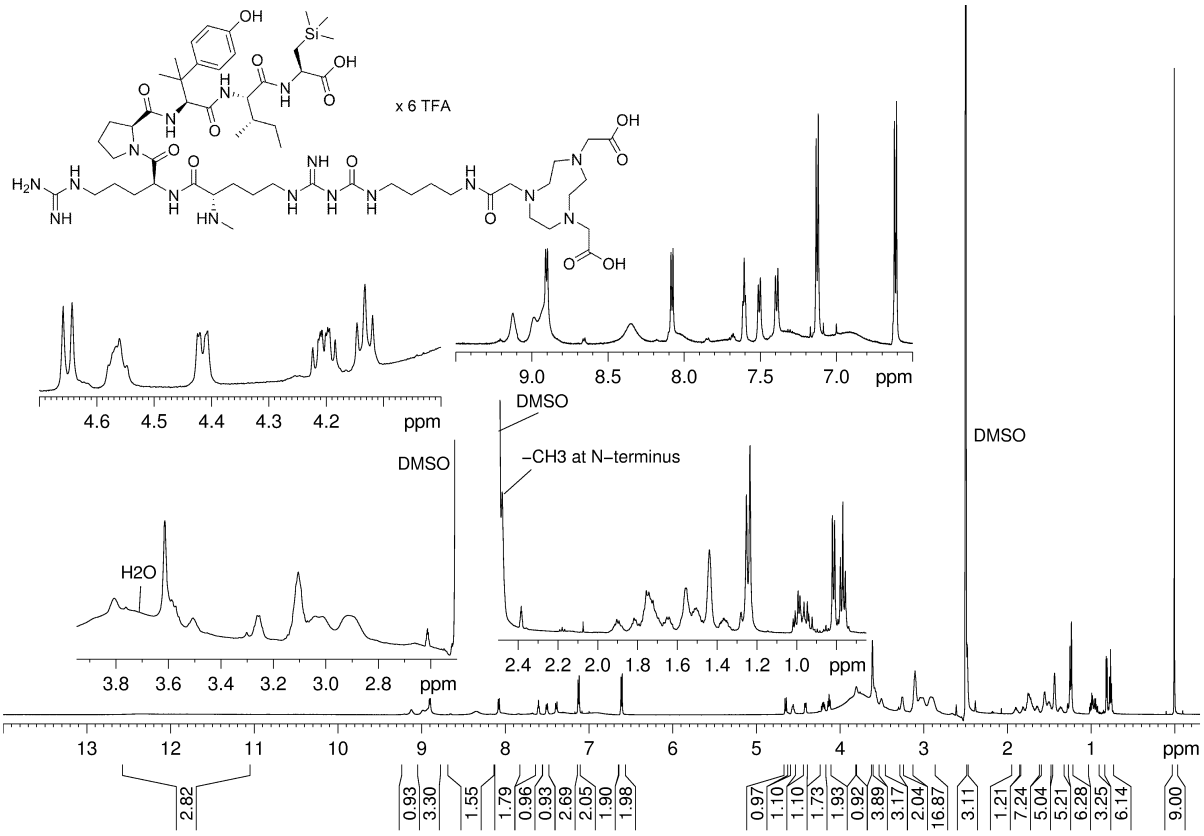
A5.5 ^{1}H-NMR spectra of compounds 5.6-5.11



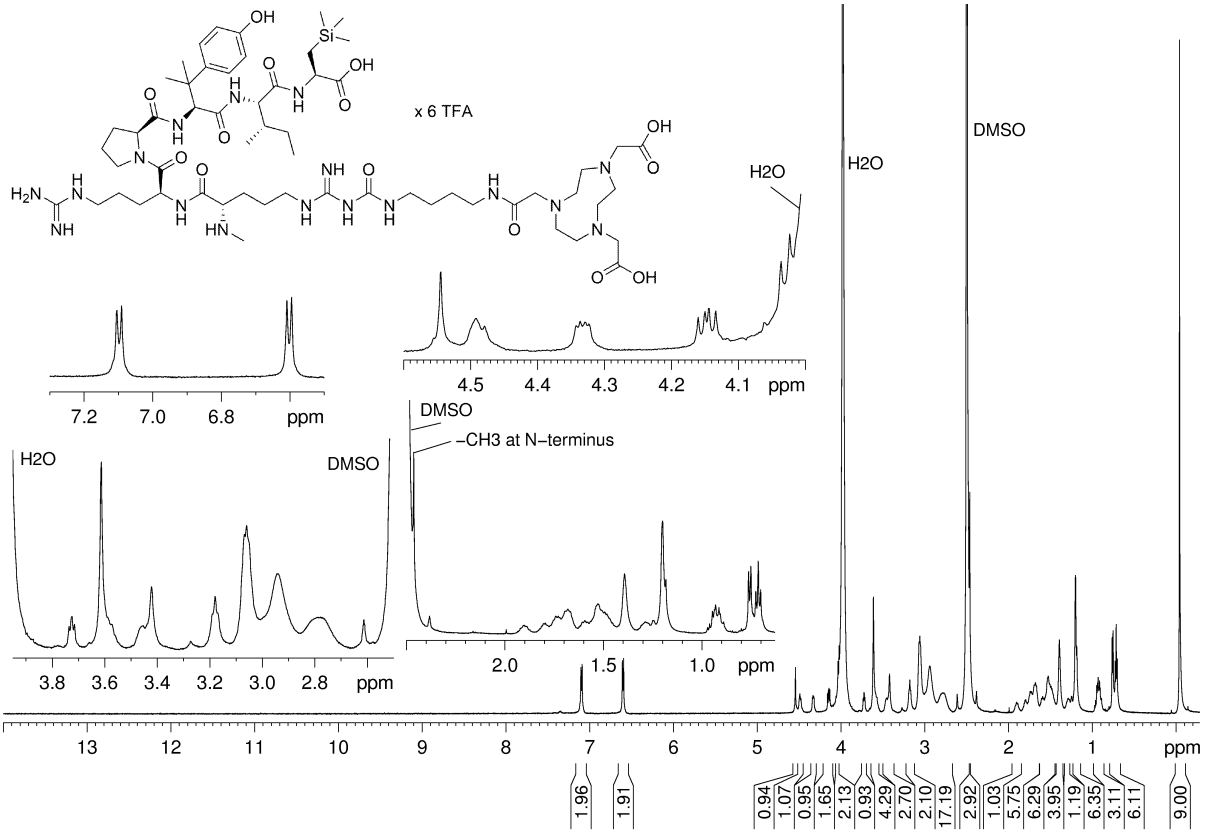
^{1}H-NMR spectrum (600 MHz, DMSO-d_6) of compound **5.6**



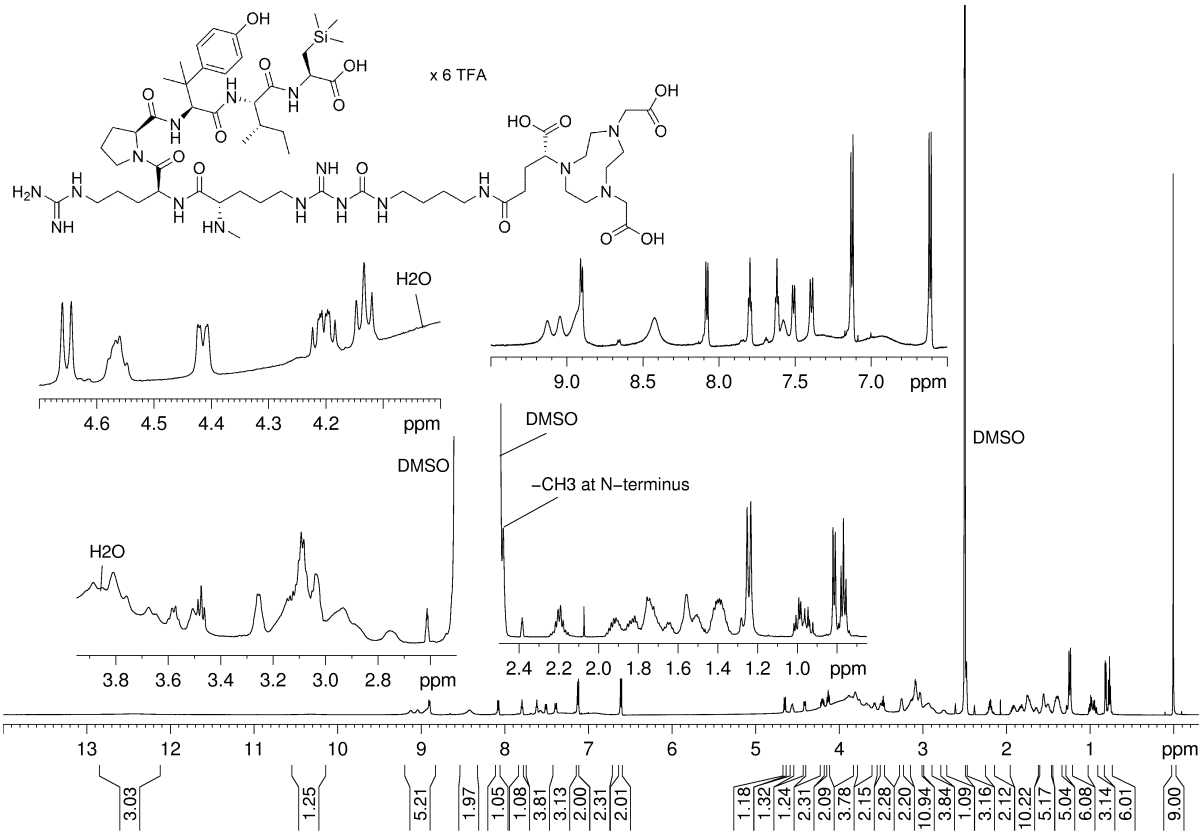
^{1}H-NMR spectrum (600 MHz, DMSO-d_6/D_2O 4:1 v/v) of compound **5.6**



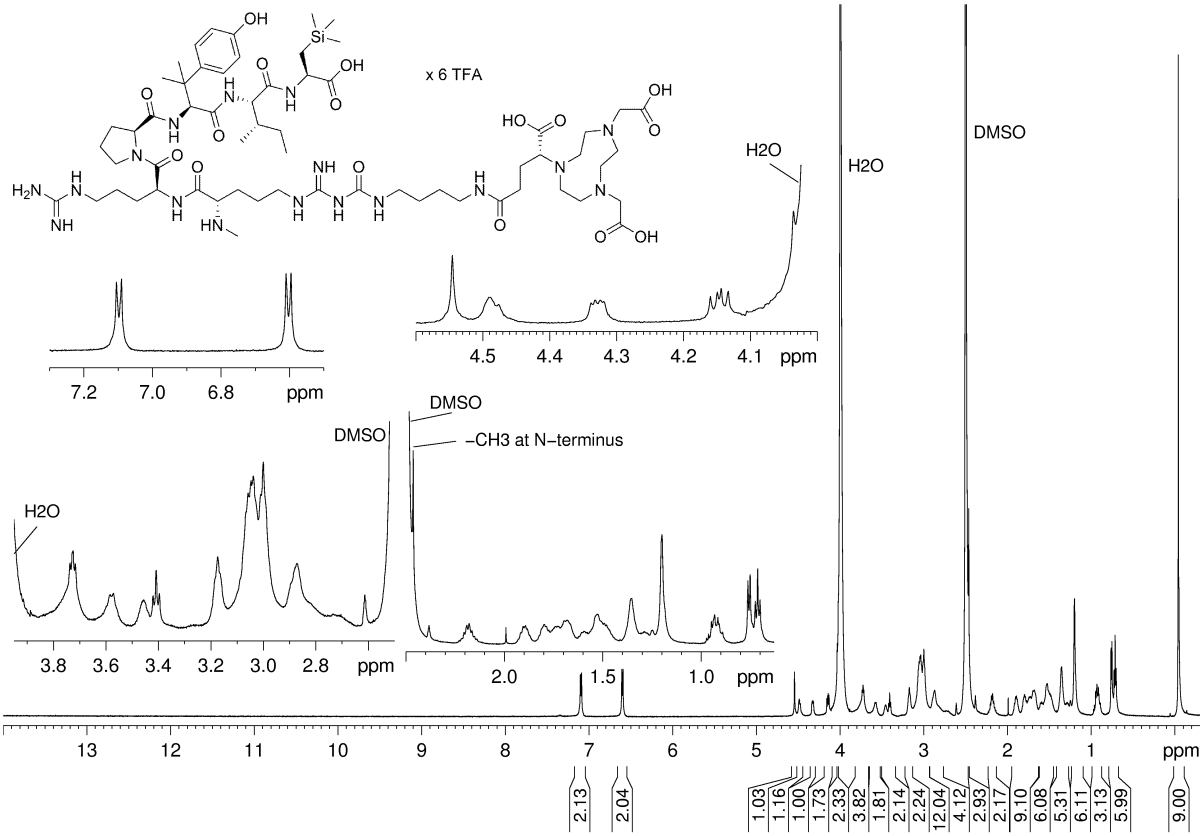
^{1}H-NMR spectrum (600 MHz, DMSO-d_6) of compound **5.7**



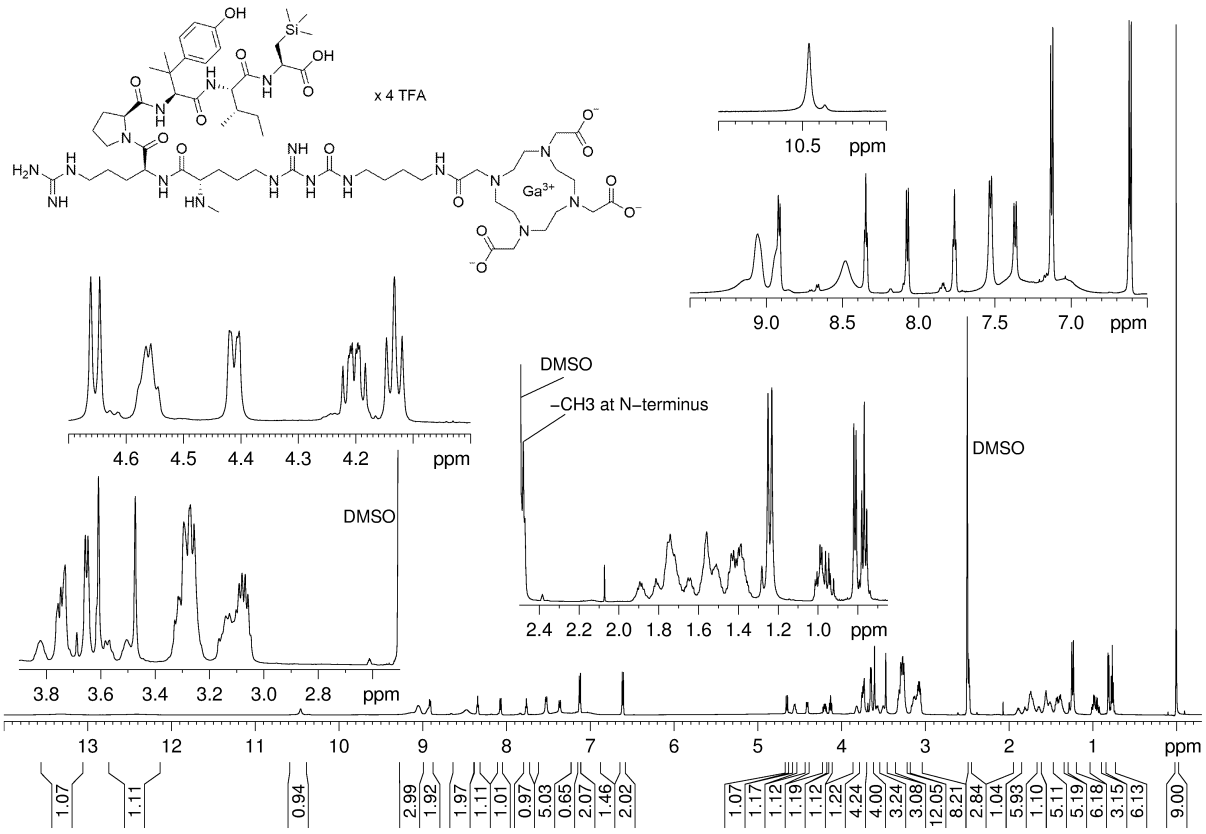
^{1}H-NMR spectrum (600 MHz, DMSO-d_6/D_2O 4:1 v/v) of compound **5.7**



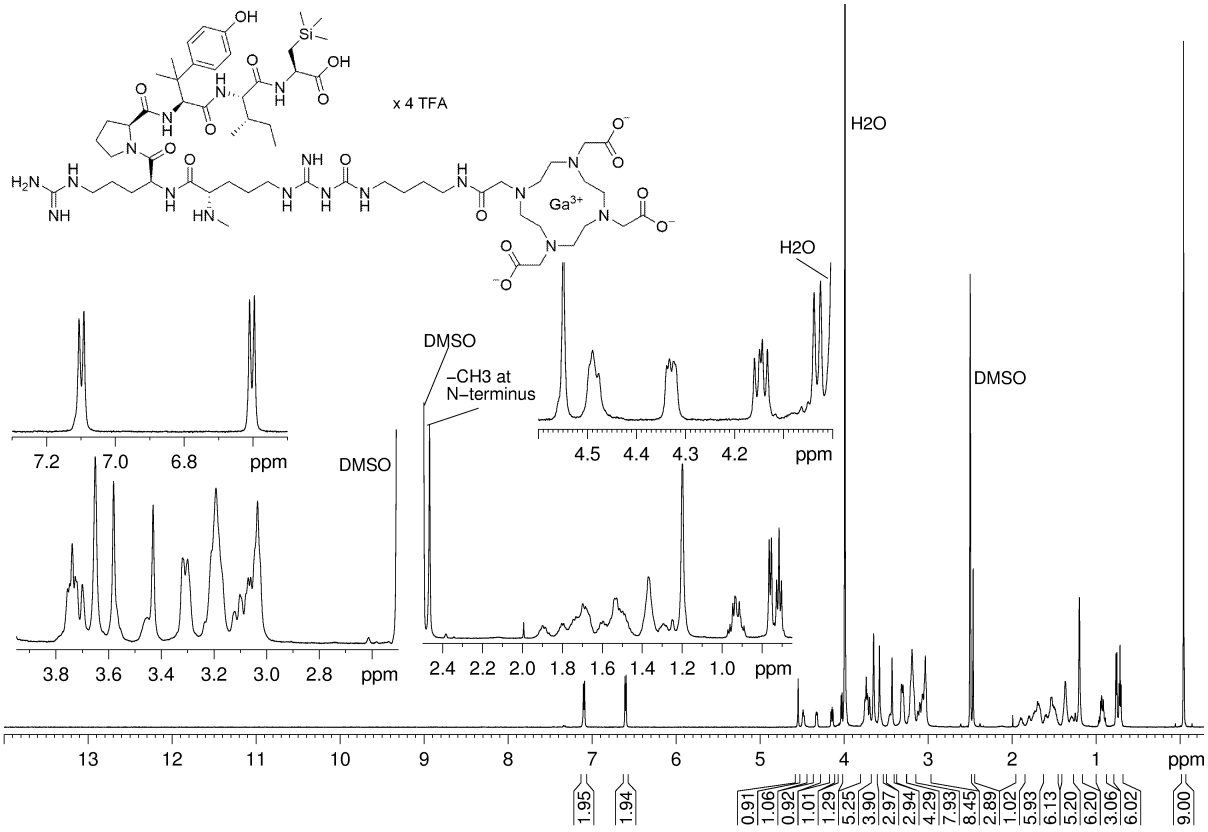
^{1}H-NMR spectrum (600 MHz, DMSO-d_6) of compound **5.8**



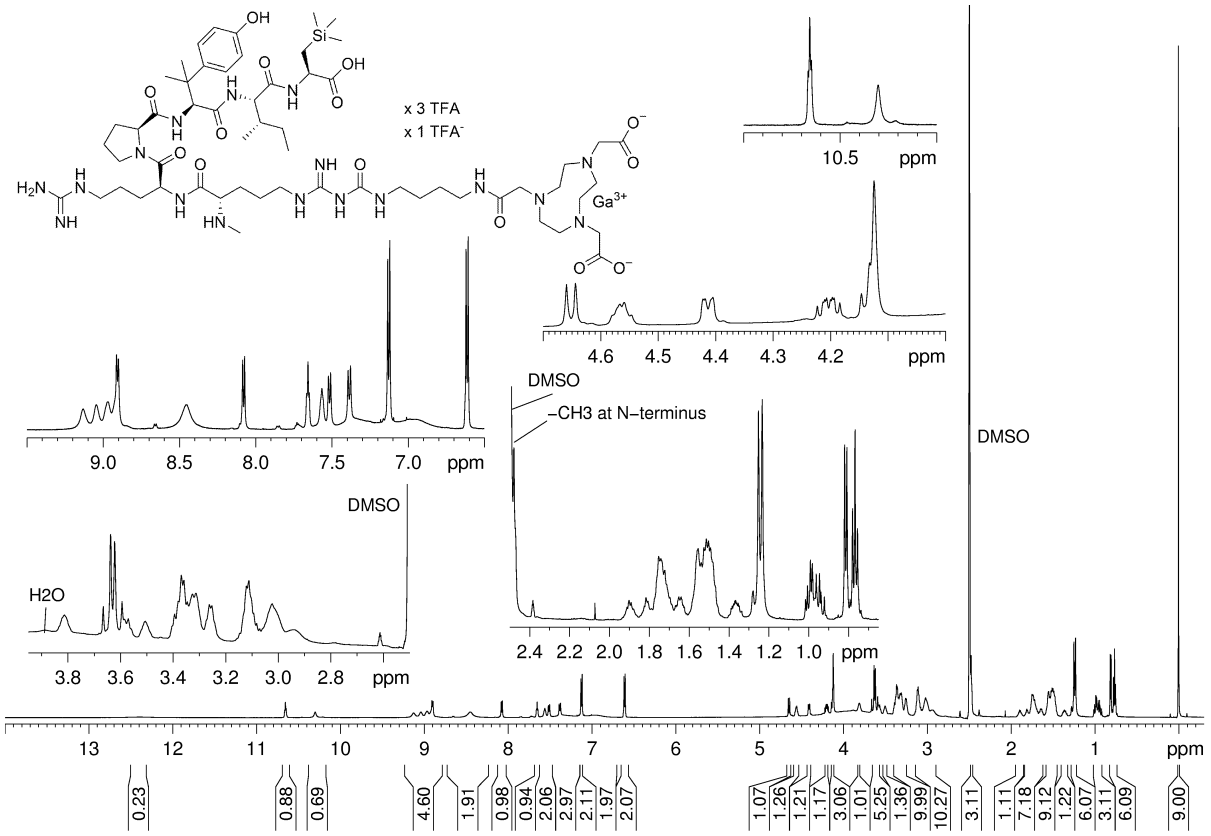
^{1}H-NMR spectrum (600 MHz, DMSO-d_6/D_2O 4:1 v/v) of compound **5.8**



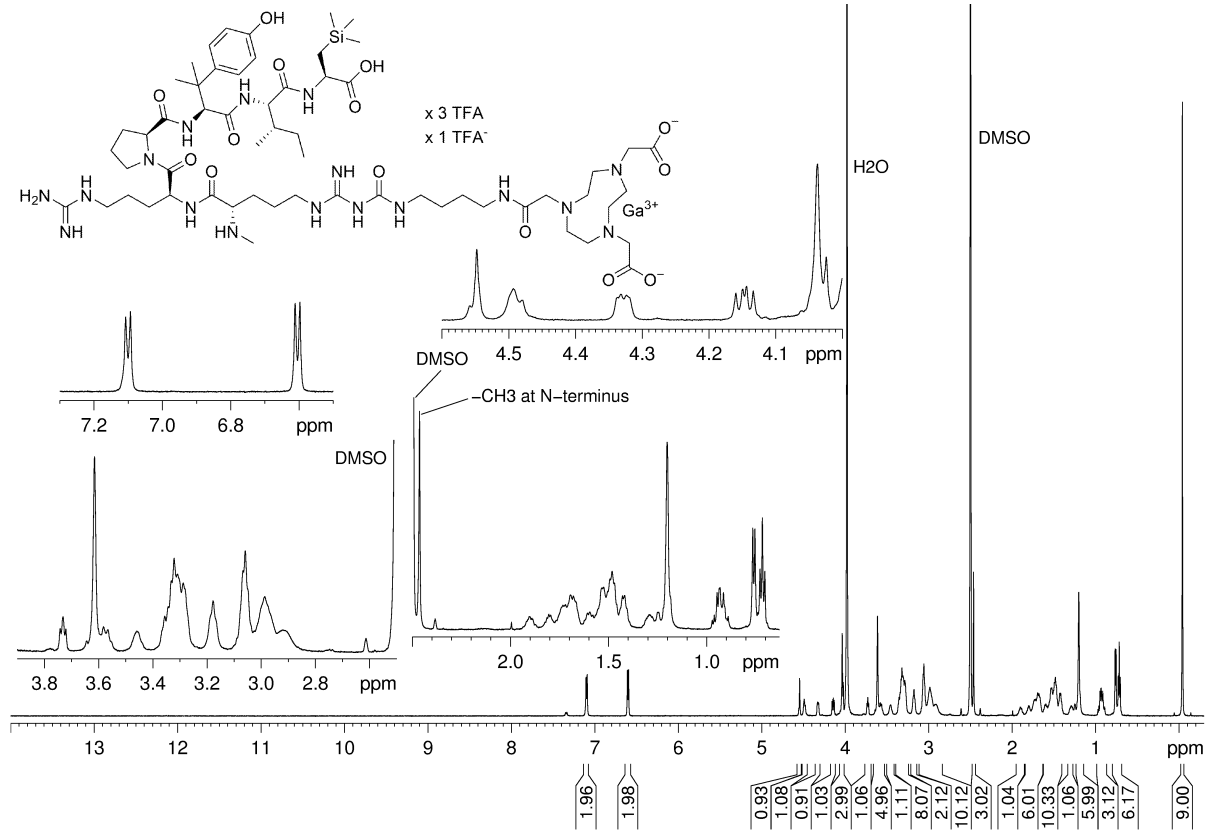
^{1}H-NMR spectrum (600 MHz, DMSO-d_6) of compound **5.9**



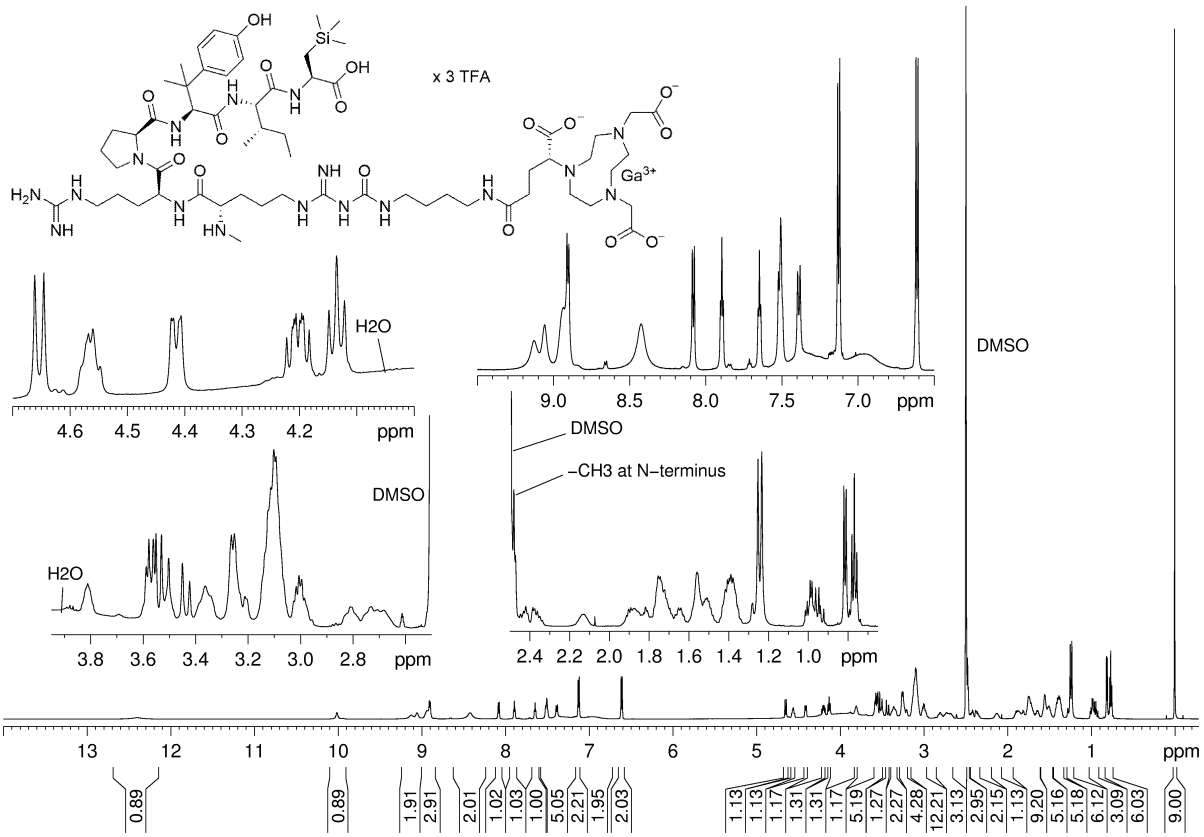
^{1}H-NMR spectrum (600 MHz, DMSO-d_6/D_2O 4:1 v/v) of compound **5.9**



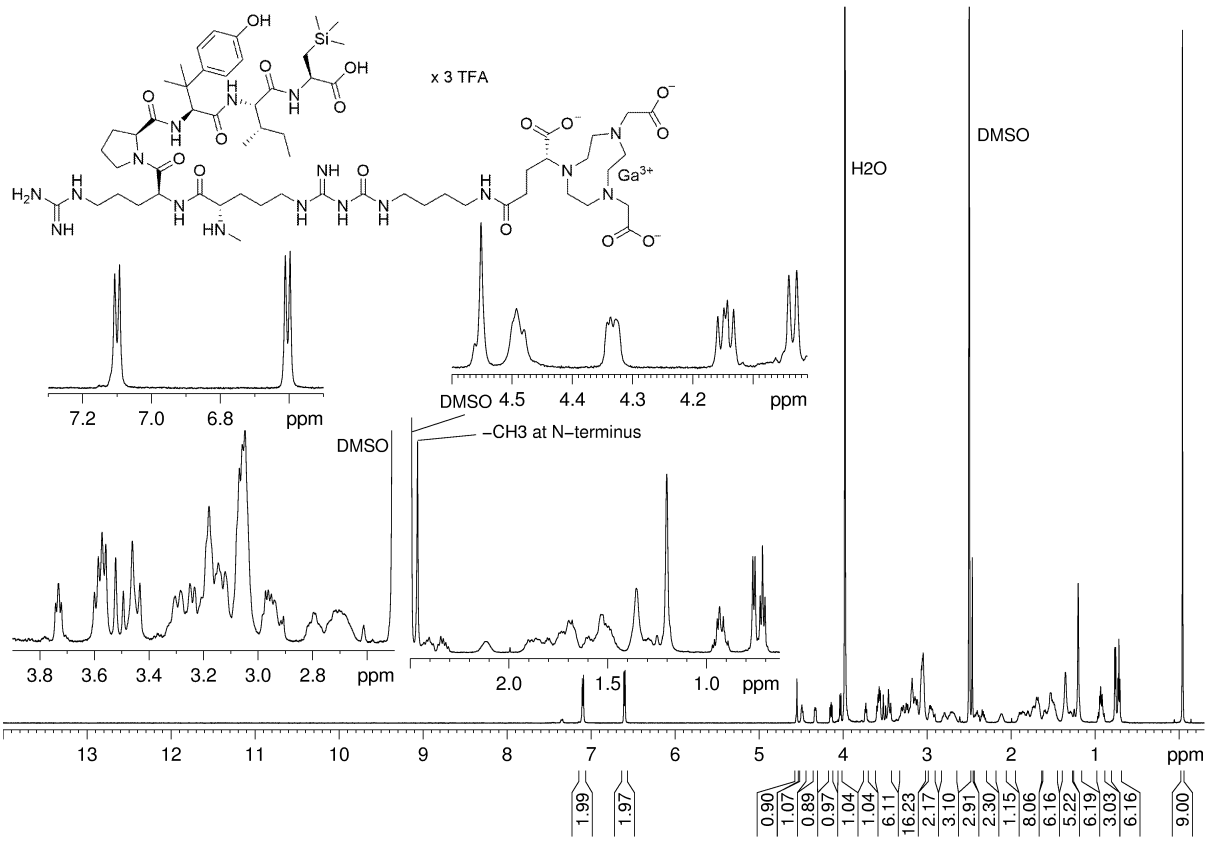
^{1}H-NMR spectrum (600 MHz, DMSO-d_6) of compound **5.10**



^{1}H-NMR spectrum (600 MHz, DMSO-d_6/D_2O 4:1 v/v) of compound **5.10**



^{1}H-NMR spectrum (600 MHz, DMSO-d_6) of compound **5.11**



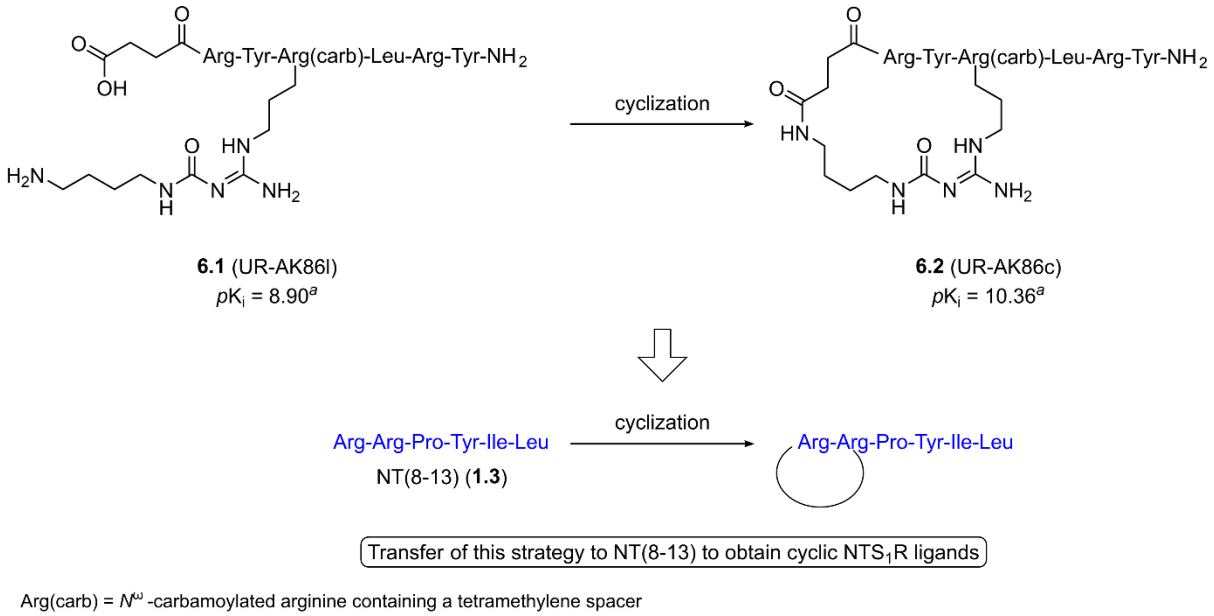
^{1}H-NMR spectrum (600 MHz, DMSO-d_6/D_2O 4:1 v/v) of compound **5.11**

Chapter 6

Design and synthesis of macrocyclic peptidic NTS_1R ligands

6.1 Introduction

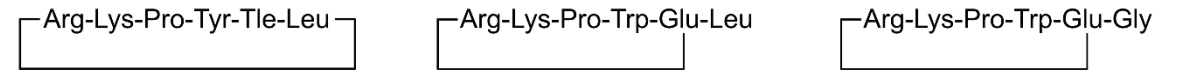
Rigidization of molecules is a well-known approach to improve drug-target interactions of a drug candidate. For instance, flexible ligands with rotable bonds will bind in a particular, active conformation to a receptor, whereas the other possible conformations might remain inactive or even trigger unwanted responses. By locking a molecule exactly into this active conformation, the affinity and selectivity can be increased. Additionally, rigid structures are less prone to enzymatical degradation which gives very stable drugs exhibiting longer-lasting effects.[1-4] This approach can also be applied to peptides, a compound class with considerable conformational flexibility due to the high number of rotable bonds. Moreover, their amide bonds are prone to hydrolytic cleavage by proteases, reducing their bioavailability and consequently their bioactivity.[5-10] One possible strategy for the rigidization of peptides is cyclization of linear peptides which can result in an improvement of the aforementioned properties.[11-23] The work of Konieczny *et al.*[17] should be emphasized at this point, as their study served as main inspiration for the work presented in this chapter. They showed that the cyclization product **6.2** exhibited an approximately 30-fold increase in Y_4R binding affinity compared to its linear precursor peptide **6.1**, resulting in subnanomolar K_i values (Figure 6.1). The cyclization, which is based on an amide bond formation between a reported amino-functionalized N^{ω}-carbamoylated arginine (Arg(carb), Figure 6.1)[24] and a succinylated N-terminus, was executed in solution. With **6.2** as lead compound, Gleixner *et al.*[25,26] synthesized several labeled Y_4R ligands such as a radioligand with a subnanomolar K_d value of 0.11 nM[25] and multiple fluorescently labeled ligands with Y_4R binding affinities in the subnanomolar range.[26] Both types of probes represent excellent molecular tools. As the Y_4R and the neurotensin receptor 1 (NTS_1R), both members of the family of class A G-protein coupled receptors (GPCRs), are targeted by arginine-containing peptidic endogenous ligands, the aim was to transfer the mentioned cyclization approach to peptidic NTS_1R ligands.



Arg(carb) = N^{ω}-carbamoylated arginine containing a tetramethylene spacer

Figure 6.1. Structures of the linear Y_4R ligand **6.1** and its cyclization product **6.2** with enhanced Y_4R binding affinity, which guided the design of cyclic NTS_1R ligands. [a]Konieczny *et al.*[17]

Neurotensin, a 13 amino acid long peptide, is the endogenous agonist acting on the NTS_1R. This tridecapeptide can be truncated to the C-terminal hexapeptide NT(8-13) (**1.3**, amino acid sequence shown in Figure 6.1) while fully retaining NTS_1R binding affinity.[27] Therefore, **1.3** serves as a lead compound for the design of NTS_1R ligands. So far, several cyclic peptides binding to the NTS_1R have been reported, which showed decreased binding affinities with K_i values ranging from the two-digit nanomolar to the micromolar range (most promising peptides **6.3**-**6.5** are shown in Figure 6.2).[28-31] The proteolytic stability was only evaluated in one study where a cyclic compound exhibited high stability towards degrading enzymes and additionally the ability to cross the blood-brain barrier.[32]



6.3 (cmpd. **16** from Sefler et al.)
K_i ($mNTS_1R$): 410 nM[a]
K_i ($hNTS_1R$): 1070 nM[b]
K_i ($rNTS_1R$): > 100 µM[c]

6.4 (cmpd. **2** from Sefler et al.)
K_i ($mNTS_1R$): 16 nM[a]
K_i ($hNTS_1R$): 190 nM[c]

6.5 (cmpd. **4** from Sefler et al.)
K_i ($mNTS_1R$): 250 nM[a]
K_i ($hNTS_1R$): 470 nM[c]

Tle = α-*tert*-butylglycine

Figure 6.2. Structures and NTS_1R binding affinities of the reported cyclic peptides **6.3**-**6.5**. [a]Sefler *et al.*[28] [b]Akunne *et al.*[29] [c]De Zhang *et al.*[31]

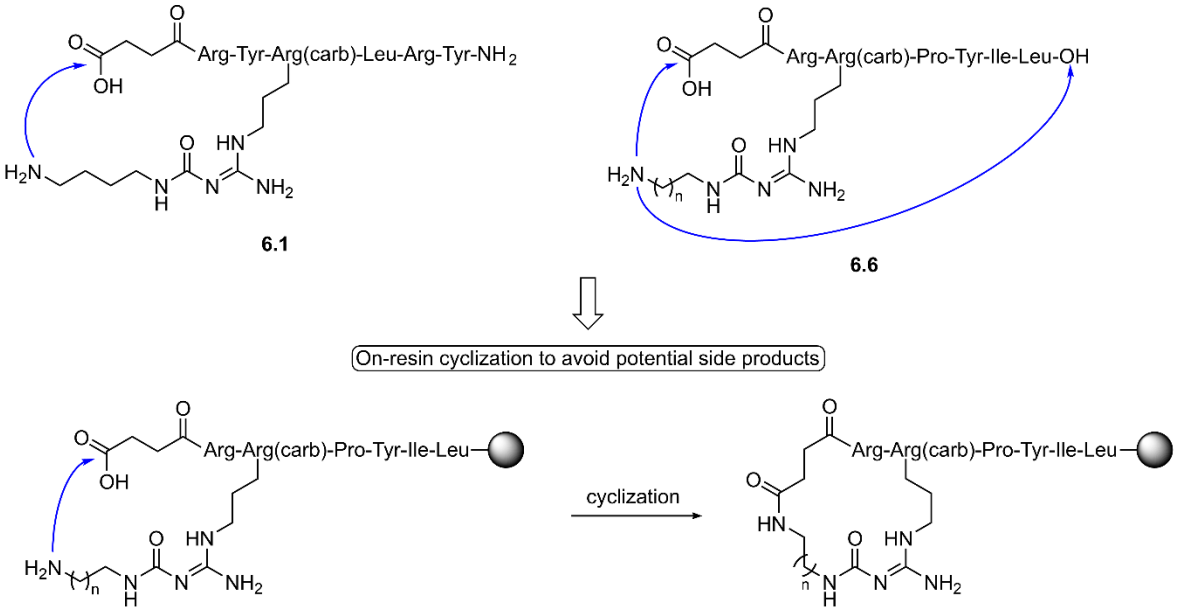
However, these affinities are insufficient for the design of labeled probes intended for the use as molecular tools. A common feature among the ligands from these approaches is the large cyclic structure which in some cases also includes the C-terminus. The resulting loss of binding

affinity seems obvious since crystal structures revealed that one of the main interactions between **1.3** and the NTS_1R is the formation of a salt bridge of the free C-terminus of **1.3** with an arginine residue located in the lower part of the binding pocket of the NTS_1R.[33-35] Consequently, the approach from Konieczny *et al.*,[17] using an amino-functionalized N^{ω}-carbamoylated arginine and a succinylated N-terminus, was pursued to obtain cyclic NTS_1R ligands by head-to-side chain cyclization. The new cyclic peptides were studied in terms of NTS_1R binding in a radiochemical competition binding assays.

6.2 Results and discussion

6.2.1 Cyclization approach

The reported cyclic Y_4R ligands contain a C-terminal carboxamide, allowing a cyclization of the linear precursor peptides (e.g., **6.1** in Figure 6.3) in solution.[17] As the NT(8-13) derivatives exhibit a free C-terminus, this approach was not considered for the synthesis of the cyclic NTS_1R ligands. Due to the free C-terminus, cyclization of the linear precursor peptide **6.6** (Figure 6.3) via the amino-functionalized arginine in position 9 would likely result in an unwanted side product. Conversion of the C-terminal carboxylic acid to an amide was not considered since this was reported to strongly impede NTS_1R binding.[36]



Arg(carb) = N^{ω}-carbamoylated arginine containing a tetramethylene spacer

Figure 6.3. Schematic illustration comparing the structures of the linear Y_4R ligand **6.1** and the potential linear NTS_1R ligand **6.6** showing the unsuitability of running the cyclization reaction in solution. The size of the macrocycle can be varied by different linker lengths (n).

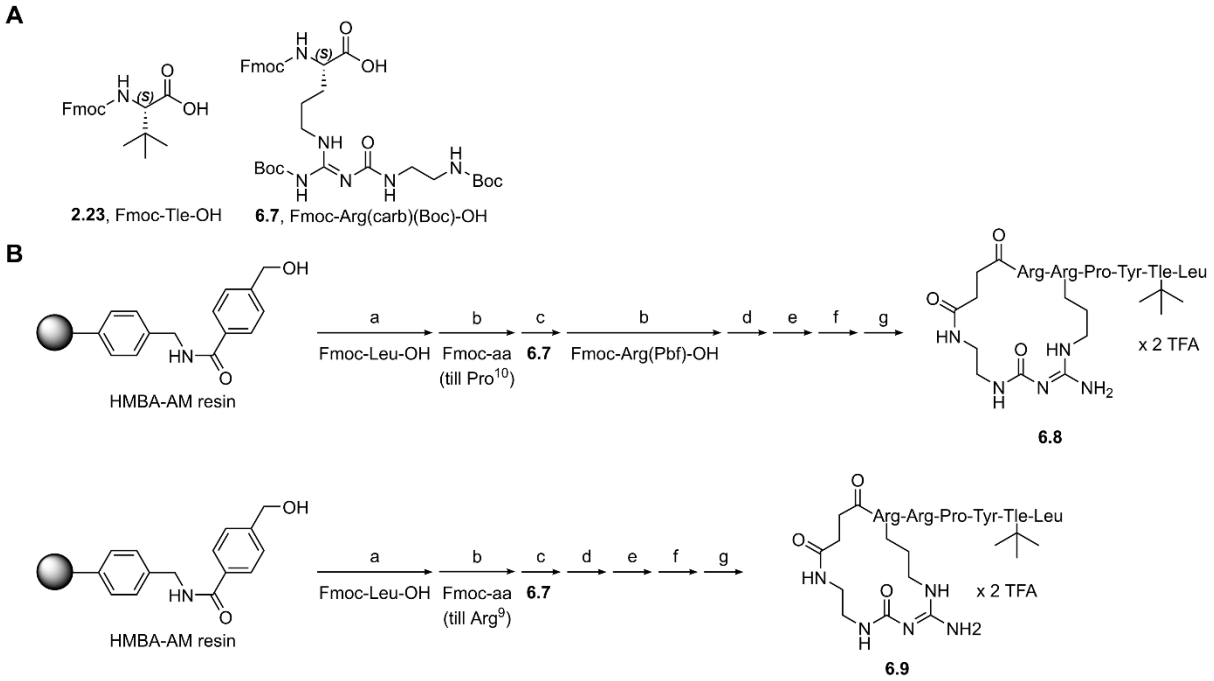
Thus, on-resin cyclization (illustrated in Figure 6.3) was chosen as a promising strategy. While the carboxylic acid at the C-terminus of the NT(8-13) derivative remains protected through resin attachment, side-chains of the incorporated amino acids, including the important primary amine in the side-chain of the functionalized arginine, can be deprotected allowing the selective cyclization followed by cleavage of the cyclic peptide from the resin. The use of Fmoc-protected amino acids with acid-labile side-chain protecting groups such as Pbf or *tert*-butyl requires cleavage cocktails with high TFA concentrations to yield the free side-chains of the amino acids. Therefore, an HMBA-AM resin was chosen to synthesize cyclic NTS_1R ligands. In this resin, the 4-(hydroxymethyl)benzamide (HMBA) linker is base-labile and resistant to

strong acidic conditions, i.e., the anchored peptide is not cleaved off during acidic side chain deprotection.[37-41] This enabled the on-resin cyclization of the herein presented NTS_1R ligands, in which either Arg^8 or Arg^9 was exchanged by an amino-functionalized N^{ω}-carbamoylated arginine to obtain different sizes of macrocycles. Cyclization via the side chains of the other amino acids (Pro^{10}, Tyr^{11}, Ile^{12} or Leu^{13}) was not considered, since this is synthetically highly challenging and would very likely result in a marked decrease in NTS_1R binding affinity.

6.2.2 Synthesis

Fmoc-protected, standard amino acids and unnatural amino acids (**2.23** and **6.7**, see Scheme 6.1A) were used to synthesize **6.8** and **6.9** (sequences shown in Scheme 6.1B) by solid-phase peptide synthesis (SPPS) (synthesis shown in Scheme 6.1B). The attachment of the first amino acid, Fmoc-Leu-OH, to the HMBA-AM resin was performed using 1-(mesitylene-2-sulfonyl)-3-nitro-1,2,4-triazole (MSNT) and 1-methylimidazole in dichloromethane to prevent potential racemization.[37,42] In compound **6.8**, Arg^9 was replaced by the amino-functionalized N^{ω}-carbamoylated arginine resulting from **6.7**, whereas in **6.9** Arg^8 was replaced by the same carbamoylated arginine. In comparison to the unnatural amino acid Arg(carb) (Figure 6.1 and 6.3), the linker in the side-chain of **6.7** is shorter by two methylene groups. This resulted in a smaller macrocycle (compared to the use of a carbamoylated arginine with a tetramethylene linker), which was considered favorable since it was assumed that the binding pocket of NTS_1R provides rather limited space. The amino-functionalized carbamoylated arginine enabled a cyclization via the succinyl residue at the N-terminus according to the aforementioned strategy.[17,25,26] Furthermore, Tle (**2.23**) was incorporated instead of Ile^{12}, contributing to proteolytic stability.[8,43-46]

Scheme 6.1. Structures of the unnatural amino acids **2.23** and **6.7** (A) and schematic illustration of the synthesis of **6.8** and **6.9** (B).



(A) Structures of used unnatural amino acids. (B) SPPS of peptides **6.8** and **6.9**. Reagents and conditions: (a) anchoring of Fmoc-Leu-OH to an HMBA-AM resin: Fmoc-Leu-OH/MSNT/1-methylimidazole (5/5/3.75 equiv.), CH_2Cl_2, rt, 2 × 1 h, Fmoc deprotection: 20% piperidine in DMF/NMP 4:1 v/v, rt, 2 × 10 min; (b) amino acid coupling: Fmoc-amino acid or **2.23**/HOBt/HBTU/DIPEA (5/5/4.9/10 equiv.), DMF/NMP 4:1 v/v, 35 °C, 2 × 45 min ("double" coupling), Fmoc deprotection: as under (a); (c) **6.7**/HOBt/HBTU/DIPEA (3/3/2.95/6 equiv.), DMF/NMP 4:1 v/v, 35 °C, 16 h ("single" coupling), Fmoc deprotection: as under (a); (d) succinic anhydride/DIPEA (10/10 equiv.), DMF/NMP 4:1 v/v, 35 °C, 30 min; (e) TFA/H_2O 95:5 v/v, rt, 1 × 4 h (**6.8**) or 2 × 2 h (**6.9**); (f) HOBt/PyBOP/DIPEA (5/5/10 equiv.), DMF/NMP 4:1 v/v, rt, overnight; (g) 0.1 M NaOH/dioxane 1:3 v/v, rt, 2 × 30 min.

After coupling of the last amino acid and Fmoc deprotection, the succinyl moiety at the N-terminus was introduced using succinic anhydride and DIPEA. The addition of 95% aqueous TFA resulted in the removal of acid-labile side-chain protecting groups such as the *tert*-butyl group of the tyrosine, the Pbf group of the natural arginine, and, more importantly, the Boc group of the unnatural arginine **6.7**. Using PyBOP, HOBt, and DIPEA, the cyclization was carried out, while the peptide remained attached to the resin according to reported procedures.[17,25,26] The peptides were cleaved off the resin using a mixture of 0.1 M NaOH and dioxane as the HMBA linker is base-labile. RP-HPLC runs of the crude products of **6.8** and **6.9** showed only one peak originating from the cyclized peptides. This was confirmed by HR-MS analysis of the purified peptides (purity > 96%) which revealed only the mass corresponding to the cyclized products. The linear peptides were not isolated or detected, which leads to the conclusion that the on-resin cyclization worked. Worth mentioning are the extremely low yields. The final yields of **6.8** and **6.9** were below 1%. This could be explained by an incomplete cleavage of the peptide from the resin, by the formation of oligomers (intermolecular amide

bond formation), or by other side reactions. However, these assumptions are contrary to recent publications reporting that peptides can be easily cleaved off the HMBA-AM linker with 0.1 M NaOH and that the linkage of the peptide to the HMBA-AM resin is strongly resistant to high TFA concentrations.[37-41] Therefore, other reasons such as insufficient amino acid coupling could be an explanation for the low yields. This needs to be further elucidated in future studies, especially if an upscaling of the reaction is intended.

6.2.3 Determination of NTS_1R binding affinities

NTS_1R binding affinities of peptides **6.8** and **6.9** were determined in a published radioligand competition binding assay using [^{3}H]**1.7** ([^{3}H]UR-MK300, structure shown in Figure 1.2, Chapter 1) as radioligand and intact hNTS_1R-expressing HT-29 colon carcinoma cells (competition binding curves shown in Figure 6.4). Corresponding pK_i and K_i values are shown in Table 6.1.

Table 6.1. NTS_1R binding affinities of **6.8** and **6.9**.

compound	NTS_1R
	pK_i ± SEM[a] / K_i [nM][a]
1.3	9.85[b] / 0.14[b]
6.8	6.97 ± 0.10 / 112
6.9	7.99 ± 0.08 / 11

[a]Determined by radioligand competition binding with [^{3}H]**1.7**[24] at HT-29 colon carcinoma cells. [b]Keller *et al.* (reported K_i value of 0.14 nM was converted to pK_i).[24] Data represent mean values ± SEM (pK_i) or mean values (K_i) from at least three independent experiments performed in triplicate.

Compared to **1.3**, **6.8**, and **6.9** showed a marked decrease in NTS_1R binding affinity by almost three or two log units, respectively (cf. Table 6.1). **6.8** exhibited a 10-fold higher binding affinity than **6.9** indicating that the ring size, which depends on the position of the carbamoylated arginine (position 8 vs. 9), had a significant impact on the binding affinity; the larger macrocycle in **6.8** led to a more pronounced reduction in binding affinity. A possible explanation can be stated by looking at the binding mode of **1.3** at the NTS_1R, revealing that Arg^9 shows more interactions and is deeper located in the binding pocket than Arg^8.[33] Accordingly, **6.8** does not properly fit into the binding pocket resulting in a reduction of attractive interactions with NTS_1R.

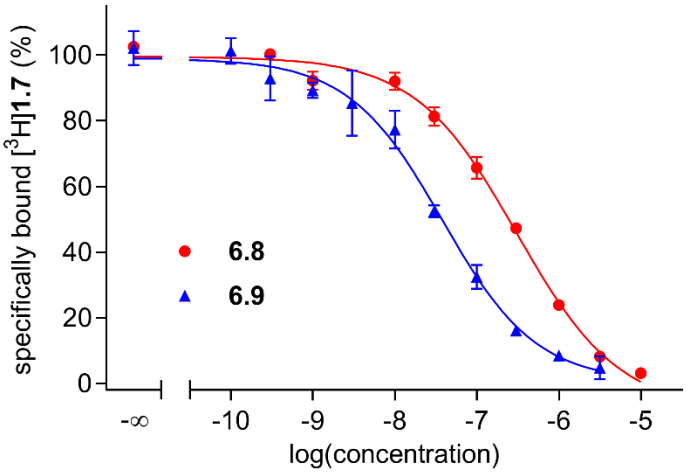


Figure 6.4. Radioligand displacement curves from competition binding experiments with [^{3}H]**1.7** (K_d = 0.41 nM,[47] c = 1 nM) and **6.8** or **6.9** at intact HT-29 cells. Data represent mean values ± SEM from at least three independent experiments performed in triplicate. For pK_i and K_i values, see Table 6.1.

6.3 Conclusion

Transferring the cyclization approach from peptidic Y_4R ligands[17] to NTS_1R ligands resulted in the cyclic peptides **6.8** and **6.9**. As a cyclization reaction in solution was inappropriate, an on-resin cyclization was performed. Despite very low yields, both peptides were obtained in amounts allowing a characterization in binding assays. Since **6.8** and **6.9** exhibited low receptor NTS_1R binding affinities with K_i values of 112 and 11 nM, respectively, these compounds do not represent lead structures for further modification such as functionalization with different labels (radionuclides or fluorescent dyes). Furthermore, proteolytic stabilities, one of the main reasons for cyclization, were not evaluated, as future studies with **6.8** and **6.9** are unlikely.

6.4 Experimental section

6.4.1 General

Materials. The protected amino acids Fmoc-Tyr(tBu)-OH and Fmoc-Arg(Pbf)-OH were purchased from Carbolution Chemicals (St. Ingbert, Germany). Fmoc-Pro-OH, Fmoc-Leu-OH Fmoc-α-*tert*-butylglycine-OH (**2.23**) and HBTU were from Merck (Darmstadt, Germany). HMBA-AM resin was obtained from Iris Biotech (Marktredwitz, Germany). HOBt was from Sigma-Aldrich (Taufkirchen, Germany). NMP and DMF for peptide synthesis, anhydrous DMF and NMP, dichloromethane, piperidine and TFA were purchased from Fisher Scientific (Schwerte, Germany). 1-(Mesitylene-2-sulfonyl)-3-nitro-1,2,4-triazole (MSNT), 1-methylimidazole and DIPEA were obtained from ABCR (Karslruhe, Germany). Acetonitrile (HPLC gradient grade) was from VWR (Ismaning, Germany). NT(8-13) (**1.3**) was synthesized via SPPS in-house. Bacitracin, HEPES, and bovine serum albumin (BSA) were obtained from Serva (Heidelberg, Germany). Fetal bovine serum (FBS) was purchased from Pan-Biotech (Aidenbach, Germany). The radioligand [^{3}H]**1.7** (molar activity: 2.41 TBq/mmol) was prepared according to a described procedure.[24] Compound **6.7**[24] was synthesized according to a reported protocol. Millipore water was consistently used for the preparation of stock solutions, buffers, and aqueous eluents for HPLC. Polypropylene reaction vessels with screw cap (1.5 and 2 mL) from Sarstedt (Nümbrecht, Germany) were used for small-scale reactions (e.g., activation of Fmoc-protected amino acids) and to keep stock solutions.

Mass spectroscopy. High-resolution mass spectrometry (HRMS) was performed as described in Chapter 3.

Preparative HPLC. Preparative HPLC and lyophilization were performed using the same system as described under *Preparative HPLC* in Chapter 3.

Analytical HPLC. Analytical HPLC analysis was performed using the same system, column, flow rate, detection wavelength, eluents, and column temperature as described under *Analytical HPLC* in Chapter 3. The following gradient was applied: 0-14 min: acetonitrile/0.04% aqueous TFA 10:90-30:70, 14-15 min: 30:70-95:5, 15-18 min: 95:5 (isocratic). Retention (capacity) factors *k* were calculated as described in Chapter 3.

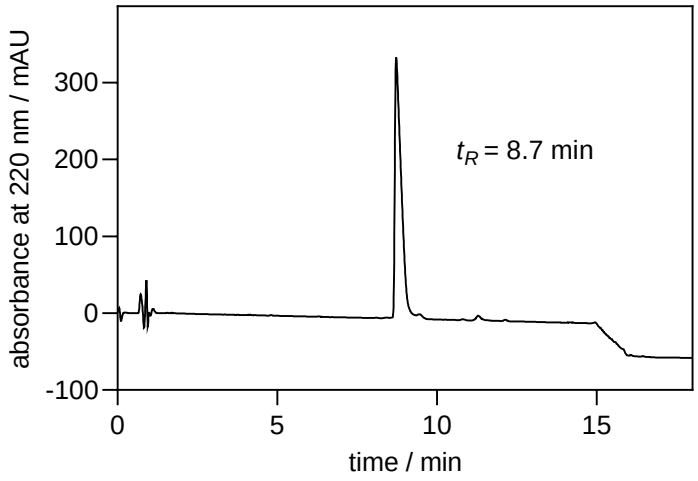
General procedure for solid phase peptide synthesis and on-resin cyclization. Peptides were synthesized manually by SPPS according to the Fmoc strategy. 5-mL NORM-JECT syringes (B. Braun-Melsungen, Melsungen, Germany), equipped with a 35-µm polypropylene frit (Roland Vetter Laborbedarf, Ammerbuch, Germany), were used as reaction vessels. The

first amino acid was attached to a HMBA-AM resin (loading: 0.6 mmol/g) by incubating the resin with the amino acid Fmoc-Leu-OH, MSNT and 1-methylimidazole (5/5/3.75 equiv.) in CH_2Cl_2 (about 3 mL/mmol amino acid) for 1 h at rt. This was carried out two times followed by washing with CH_2Cl_2 (5 ×) and DMF/NMP 4:1 v/v (in the following referred to as "solvent") (5 ×) and Fmoc deprotection with 20% piperidine in solvent (2 × 10 min at rt). Fmoc-amino acids (except for **6.7**), used in 5-fold excess, were preactivated with HOBt/HBTU/DIPEA (5/4.9/10 equiv.) in solvent (about 2.2 mL/mmol amino acid) for at least 5 min before addition to the resin. The Fmoc-protected unnatural amino acid **6.7** was used in 3-fold excess and was preactivated with HOBt/HBTU/DIPEA (3/3/6 equiv.) in anhydrous solvent (about 1.6 mL/mmol amino acid) for 5-10 min prior to addition to the resin. Amino acid coupling was carried out on a shaker (Heidolph Multi Reax; Heidolph Instruments, Schwabach, Germany) covered with a thermostat controlled (35 °C) box. In the case of standard amino acids, "double" coupling (2 × 45 min) was performed. **6.7** was attached by a single coupling procedure (35 °C, 16 h). After coupling of an Fmoc-amino acid, the resin was washed with solvent (4 ×) followed by Fmoc deprotection using 20% piperidine in solvent (2 × 10 min at rt) and subsequent washing of the resin with solvent (6 × ca. 1 mL). After coupling of the last amino acid and final Fmoc deprotection, the resin was treated with succinic anhydride and DIPEA (10/10 equiv.) for 30 min at 35 °C. The resin was washed with solvent (10 ×) followed by side-chain deprotection using 95% aqueous TFA (1 × 4 h at rt (**6.8**) or 2 × 2 h at rt (**6.9**)) and washing of the resin with solvent (10 ×). A solution of PyBOP, HOBt and DIPEA (5/5/10 equiv.) in solvent (2 mL) was added and the resin was shaken overnight at rt to cyclize the peptide on the resin. On the next day, the resin was washed with solvent (5 ×), CH_2Cl_2 (5 ×), 10% DIPEA in CH_2Cl_2 (5 ×) and CH_2Cl_2 (5 ×) followed by adding dioxane (3 mL) and shaking at rt for 30 min. After washing of the resin with dioxane (2 ×), peptides were cleaved off the resin with 0.1 M aqueous NaOH/dioxane 1:3 v/v (20 mL/g resin, 2 × 30 min at rt). After completed cleavage, the resin was washed with acetonitrile/H_2O 3:7 v/v supplemented with 1% TFA (2 ×). Liquid phases were combined and neutralized using 0.1 M HCl followed by dilution with H_2O and lyophilization. The obtained crude peptides were purified by preparative HPLC.

Compound characterization. Peptides **6.8** and **6.9** were characterized by HRMS and RP-HPLC, the latter giving purities of ≥ 96% (UV detection, 220 nm).

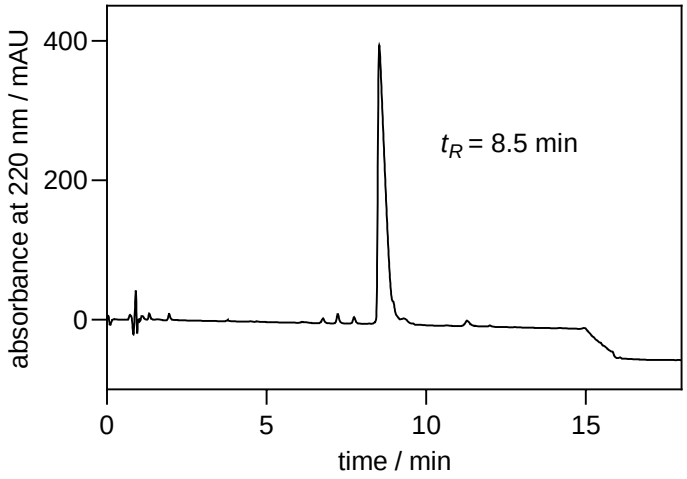
6.4.2 Experimental protocols and analytical data

((*S*)-2-((*S*)-2-((*S*)-1-((14*S*,17*S*,*Z*)-2-Amino-14-(3-guanidinopropyl)-4,9,12,15-tetraoxo-1,3,5,8,13,16-hexaazacycloicos-2-ene-17-carbonyl)pyrrolidine-2-carboxamido)-3-(4-hydroxyphenyl)propanamido)-3,3-dimethylbutanoyl)-L-leucine bis(hydrotrifluoroacetate) (6.8). Peptide **6.8** was synthesized on an HMBA-AM resin (150 mg, 0.96 mmol/g) according to the general procedure. Purification by preparative HPLC (gradient: 0-38 min: acetonitrile/0.1% aqueous TFA 15:85-35:65, t_R = 11 min) yielded **6.8** as a white fluffy solid (0.3 mg, < 1%). HRMS (ESI): *m/z* $[M+2H]^{2+}$ calcd. for $[C_{45}H_{74}N_{14}O_{11}]^{2+}$ 493.2825, found: 493.2833. RP-HPLC (220 nm): 96% (t_R = 8.7 min, k = 10.4). $C_{45}H_{72}N_{14}O_{11} \cdot C_4F_6O_4$ (985.16 + 228.05).



RP-HPLC analysis of compound **6.8**

((*S*)-2-((*S*)-3-(4-Hydroxyphenyl)-2-((*S*)-1-(((*S*)-2-imino-4,9,12-trioxo-1,3,5,8,13-pentaazacycloheptadecane-14-carbonyl)-L-arginyl)pyrrolidine-2-carboxamido)-propanamido)-3,3-dimethylbutanoyl)-L-leucine bis(hydrotrifluoroacetate) (6.9). Peptide **6.9** was synthesized on an HMBA-AM resin (100 mg, 0.96 mmol/g) according to the general procedure with one modification: pure DMF was used instead of DMF/NMP 4:1 v/v as solvent throughout the synthesis and for all washing steps. Purification by preparative HPLC (gradient: 0-38 min: acetonitrile/0.1% aqueous TFA 15:85-35:65, t_R = 12 min) yielded **6.9** as a white fluffy solid (0.4 mg, < 1%). HRMS (ESI): *m/z* $[M+2H]^{2+}$ calcd. for $[C_{45}H_{74}N_{14}O_{11}]^{2+}$ 493.2825, found: 493.2834. RP-HPLC (220 nm): 96% (t_R = 8.5 min, k = 10.2). $C_{45}H_{72}N_{14}O_{11} \cdot C_4F_6O_4$ (985.16 + 228.05).



RP-HPLC analysis of compound **6.9**

6.4.3 Cell culture

HT-29 colon carcinoma cells (DSMZ-no. ACC 299) were cultured in T75 culture flasks (Sarstedt). The cells were grown in antibiotic-free RPMI-1640 medium (Sigma) supplemented with 7.5% FBS (Sigma) in a humidified atmosphere (95% air and 5% CO_2) at 37 °C.

6.4.4 NTS_1R binding assay

NTS_1R radioligand competition binding experiments with [^{3}H]**1.7** (molar activity: 2.41 TBq/mmol) and the peptides **6.8** and **6.9** were performed with intact $hNTS_1R$-expressing human HT-29 colon carcinoma cells as described in Chapter 3. Data were analyzed as reported in Chapter 3.

6.5 References

1. Hanessian, S.; Auzzas, L. The practice of ring constraint in peptidomimetics using bicyclic and polycyclic amino acids. *Acc. Chem. Res.* **2008**, *41*, 1241-1251.
2. Kümmerle, A. E.; Vieira, M. M.; Schmitt, M.; Miranda, A. L. P.; Fraga, C. A. M.; Bourguignon, J. J.; Barreiro, E. J. Design, synthesis and analgesic properties of novel conformationally-restricted N-acylhydrazones (NAH). *Bioorg. Med. Chem. Lett.* **2009**, *19*, 4963-4966.
3. Graham, L. P. *An introduction to medicinal chemistry*; 5th Edition ed., Oxford University Press: United Kingdom, 2013.
4. Lawson, A. D. G.; MacCoss, M.; Heer, J. P. Importance of rigidity in designing small molecule drugs to tackle protein-protein interactions (PPIs) through stabilization of desired conformers. *J. Med. Chem.* **2018**, *61*, 4283-4289.
5. Ewles, M.; Goodwin, L. Bioanalytical approaches to analyzing peptides and proteins by LC--MS/MS. *Bioanalysis* **2011**, *3*, 1379-1397.
6. Van Eeckhaut, A.; Mangelings, D. Toward greener analytical techniques for the absolute quantification of peptides in pharmaceutical and biological samples. *J. Pharm. Biomed. Anal.* **2015**, *113*, 181-188.
7. Perez-Silva, J. G.; Espanol, Y.; Velasco, G.; Quesada, V. The Degradome database: expanding roles of mammalian proteases in life and disease. *Nucleic Acids Res.* **2016**, *44*, D351-355.
8. Schindler, L.; Bernhardt, G.; Keller, M. Modifications at Arg and Ile give neurotensin(8-13) derivatives with high stability and retained NTS(1) receptor affinity. *ACS Med. Chem. Lett.* **2019**, *10*, 960-965.
9. Nugrahadi, P. P.; Hinrichs, W. L. J.; Frijlink, H. W.; Schoneich, C.; Avanti, C. Designing formulation strategies for enhanced stability of therapeutic peptides in aqueous solutions: A review. *Pharmaceutics* **2023**, *15*.
10. Rozans, S. J.; Moghaddam, A. S.; Wu, Y.; Atanasoff, K.; Nino, L.; Dunne, K.; Pashuck, E. T. Quantifying and controlling the proteolytic degradation of cell adhesion peptides. *ACS Biomater. Sci. Eng.* **2024**, *10*, 4916-4926.
11. Marsault, E.; Peterson, M. L. Macrocycles are great cycles: Applications, opportunities, and challenges of synthetic macrocycles in drug discovery. *J. Med. Chem.* **2011**, *54*, 1961-2004.
12. Joo, S. H. Cyclic peptides as therapeutic agents and biochemical tools. *Biomol. Ther.* **2012**, *20*, 19-26.

13. Raghuwanshi, Y.; Etayash, H.; Soudy, R.; Paiva, I.; Lavasanifar, A.; Kaur, K. Proteolytically stable cyclic decapeptide for breast cancer cell targeting. *J. Med. Chem.* **2017**, *60*, 4893-4903.
14. Zorzi, A.; Deyle, K.; Heinis, C. Cyclic peptide therapeutics: past, present and future. *Curr. Opin. Chem. Biol.* **2017**, *38*, 24-29.
15. Abdalla, M. A.; McGaw, L. J. Natural cyclic peptides as an attractive modality for therapeutics: a mini review. *Molecules* **2018**, *23*.
16. Etayash, H.; Pletzer, D.; Kumar, P.; Straus, S. K.; Hancock, R. E. W. Cyclic derivative of host-defense peptide IDR-1018 improves proteolytic stability, suppresses inflammation, and enhances in vivo activity. *J. Med. Chem.* **2020**, *63*, 9228-9236.
17. Konieczny, A.; Conrad, M.; Ertl, F. J.; Gleixner, J.; Gattor, A. O.; Grätz, L.; Schmidt, M. F.; Neu, E.; Horn, A. H. C.; Wifling, D.; Gmeiner, P.; Clark, T.; Sticht, H.; Keller, M. N-Terminus to Arginine side-chain cyclization of linear peptidic neuropeptide Y Y receptor ligands results in picomolar binding constants. *J. Med. Chem.* **2021**, *64*, 16746-16769.
18. Muttenthaler, M.; King, G. E.; Adams, D. J.; Alewood, P. E. Trends in peptide drug discovery. *Nat. Rev. Drug Discovery* **2021**, *20*, 309-325.
19. Namsolleck, P.; Rodgers, K. E.; Franklin, R.; Moll, G. N. LP2, a stable lanthipeptide derived from cAng-(1-7), exerts myeloprotective action in mice. *Eur. J. Haematol.* **2023**, *110*, 534-539.
20. Muratspahic, E.; Deibler, K.; Han, J. M.; Tomasevic, N.; Jadhav, K. B.; Olivé-Marti, A. L.; Hochrainer, N.; Hellinger, R.; Koehbach, J.; Fay, J. F.; Rahman, M. H.; Hegazy, L.; Craven, T. W.; Varga, B. R.; Bhardwaj, G.; Appourchaux, K.; Majumdar, S.; Muttenthaler, M.; Hosseinzadeh, P.; Craik, D. J.; Spetea, M.; Che, T.; Baker, D.; Gruber, C. W. Design and structural validation of peptide-drug conjugate ligands of the kappa-opioid receptor. *Nat. Commun.* **2023**, *14*.
21. Desgagné, M.; Chartier, M.; Lagard, C.; Ferková, S.; Choquette, M.; Longprá, J. M.; Côté, J.; Boudreault, P. L.; Sarret, P. Development of macrocyclic neurotensin receptor type 2 (NTS2) opioid-free analgesics. *Angew. Chem. Int. Ed.* **2024**, *63*.
22. Ji, X. J.; Nielsen, A. L.; Heinis, C. Cyclic peptides for drug development. *Angew. Chem. Int. Ed.* **2024**, *63*.
23. Pei, Z. H.; Song, Q. X.; Xu, J. Q.; Yu, S.; Ma, H. X. The cyclic antimicrobial peptide C-LR18 has enhanced antibacterial activity, improved stability, and a longer half-life compared to the original peptide. *Antibiotics* **2025**, *14*.

24. Keller, M.; Kuhn, K. K.; Einsiedel, J.; Hübner, H.; Biselli, S.; Mollereau, C.; Wifling, D.; Svobodová, J.; Bernhardt, G.; Cabrele, C.; Vanderheyden, P. M. L.; Gmeiner, P.; Buschauer, A. Mimicking of arginine by functionalized N^{ω}-carbamoylated arginine as a new broadly applicable approach to labeled bioactive peptides: High affinity angiotensin, neuropeptide Y, neuropeptide FF, and neurotensin receptor ligands as examples. *J. Med. Chem.* **2016**, *59*, 1925-1945.
25. Gleixner, J.; Gattor, A. O.; Humphrys, L. J.; Brunner, T.; Keller, M. [(3)H]UR-JG102-A radiolabeled cyclic peptide with high affinity and excellent selectivity for the neuropeptide Y Y(4) receptor. *J. Med. Chem.* **2023**, *66*, 13788-13808.
26. Gleixner, J.; Kopanchuk, S.; Gratz, L.; Tahk, M. J.; Laasfeld, T.; Veiksina, S.; Horing, C.; Gattor, A. O.; Humphrys, L. J.; Muller, C.; Archipowa, N.; Kockenberger, J.; Heinrich, M. R.; Kutta, R. J.; Rinken, A.; Keller, M. Illuminating neuropeptide Y Y(4) receptor binding: Fluorescent cyclic peptides with subnanomolar binding affinity as novel molecular tools. *ACS Pharmacol. Transl. Sci.* **2024**, *7*, 1142-1168.
27. Carraway, R.; Leeman, S. E. The amino acid sequence of a hypothalamic peptide, neurotensin. *J. Biol. Chem.* **1975**, *250*, 1907-1911.
28. Sefler, A. M.; He, J. X.; Sawyer, T. K.; Holub, K. E.; Omecinsky, D. O.; Reily, M. D.; Thanabal, V.; Akunne, H. C.; Cody, W. L. Design and structure-activity relationships of C-terminal cyclic neurotensin fragment analogues. *J. Med. Chem.* **1995**, *38*, 249-257.
29. Akunne, H. C.; Darling, S.; Zoski, K.; Sefler, A. M.; He, J. X.; Sawyer, T. K.; Pugsley, T. A.; Cody, W. L. Functional activity of new C-terminal cyclic-neurotensin fragment analogs. *Neuropeptides* **1996**, *30*, 213-218.
30. Van Kemmel, F. M.; Dubuc, I.; Bourdel, E.; Fehrentz, J. A.; Martinez, J.; Costentin, J. A C-terminal cyclic 8-13 neurotensin fragment analog appears less exposed to neprilysin when it crosses the blood-brain barrier than the cerebrospinal fluid-brain barrier in mice. *Neurosci. Lett.* **1996**, *217*, 58-60.
31. de Zhang, L. A.; Liu, M.; Scott, D. J.; Chalmers, D. K. Re-evaluation of cyclic peptide binding to neurotensin receptor 1 by shifting the peptide register during synthesis. *ACS Med. Chem. Lett.* **2025**, *16*, 157-162.
32. Bredeloux, P.; Cavelier, F.; Dubuc, I.; Vivet, B.; Costentin, J.; Martinez, J. Synthesis and biological effects of c(Lys-Lys-Pro-Tyr-Ile-Leu-Lys-Lys-Pro-Tyr-Ile-Leu) (JMV2012), a new analogue of neurotensin that crosses the blood-brain barrier. *J. Med. Chem.* **2008**, *51*, 1610-1616.

33. White, J. F.; Noinaj, N.; Shibata, Y.; Love, J.; Kloss, B.; Xu, F.; Gvozdenovic-Jeremic, J.; Shah, P.; Shiloach, J.; Tate, C. G.; Grisshammer, R. Structure of the agonist-bound neurotensin receptor. *Nature* **2012**, *490*, 508-513.
34. Egloff, P.; Hillenbrand, M.; Klenk, C.; Batyuk, A.; Heine, P.; Balada, S.; Schlinkmann, K. M.; Scott, D. J.; Schutz, M.; Pluckthun, A. Structure of signaling-competent neurotensin receptor 1 obtained by directed evolution in Escherichia coli. *Proc. Natl. Acad. Sci. U. S. A.* **2014**, *111*, E655-662.
35. Krumm, B. E.; Lee, S.; Bhattacharya, S.; Botos, I.; White, C. F.; Du, H.; Vaidehi, N.; Grisshammer, R. Structure and dynamics of a constitutively active neurotensin receptor. *Sci. Rep.* **2016**, *6*, 38564.
36. Henry, J. A.; Horwell, D. C.; Meecham, K. G.; Rees, D. C. A structure-affinity study of the amino-acid side-chains in neurotensin - N and C-terminal deletions and Ala-scan. *Bioorg. Med. Chem. Lett.* **1993**, *3*, 949-952.
37. Hansen, J.; Diness, F.; Meldal, M. C-Terminally modified peptides via cleavage of the HMBA linker by O-, N- or S-nucleophiles. *Org. Biomol. Chem.* **2016**, *14*, 3238-3245.
38. Yu, R. X. R.; Mahto, S. K.; Justus, K.; Alexander, M. M.; Howard, C. J.; Ottesen, J. J. Hybrid phase ligation for efficient synthesis of histone proteins. *Org. Biomol. Chem.* **2016**, *14*, 2603-2607.
39. Usui, K.; Yokota, S.; Iwata, K.; Hamada, Y. Novel purification process for amyloid beta peptide(1-40). *Processes* **2020**, *8*.
40. Barredo-Vacchelli, G. R.; Rodríguez, J. A.; Eloy, J. A.; Camperi, S. A. A novel method for liraglutide synthesis and purification. *Pept. Sci.* **2024**, *116*.
41. Sigma-Aldrich. Novabiochem® Fmoc resin cleavage protocols. https://www.sigmaaldrich.com/DE/en/technical-documents/technical-article/chemistry-and-synthesis/peptide-synthesis/fmoc-cleavage-deprotection?srsltid=AfmBOorDMTpGioKVl4JxyFlQenXAeT34ZjSTo0mrslINt31iH4xafqr6 (2012).
42. Blankemeyer-Menge, B.; Nimtz, M.; Frank, R. An efficient method for anchoring Fmoc-amino acids to hydroxyl-functionalized solid supports. *Tetrahedron Lett.* **1990**, *31*, 1701-1704.
43. Maina, T.; Nikolopoulou, A.; Stathopoulou, E.; Galanis, A. S.; Cordopatis, P.; Nock, B. A. [99mTc]Demotensin 5 and 6 in the NTS1-R-targeted imaging of tumours: Synthesis and preclinical results. *Eur. J. Nucl. Med. Mol. Imaging* **2007**, *34*, 1804-1814.

44. Alshoukr, F.; Rosant, C.; Maes, V.; Abdelhak, J.; Raguin, O.; Burg, S.; Sarda, L.; Barbet, J.; Tourwe, D.; Pelaprat, D.; Gruaz-Guyon, A. Novel neurotensin analogues for radioisotope targeting to neurotensin receptor-positive tumors. *Bioconjugate Chem.* **2009**, *20*, 1602-1610.
45. Garcia-Garayoa, E.; Blauenstein, P.; Blanc, A.; Maes, V.; Tourwe, D.; Schubiger, P. A. A stable neurotensin-based radiopharmaceutical for targeted imaging and therapy of neurotensin receptor-positive tumours. *Eur. J. Nucl. Med. Mol. Imaging* **2009**, *36*, 37-47.
46. Mascarin, A.; Valverde, I. E.; Mindt, T. L. Structure-activity relationship studies of amino acid substitutions in radiolabeled neurotensin conjugates. *ChemMedChem* **2016**, *11*, 102-107.
47. Schindler, L.; Moosbauer, J.; Schmidt, D.; Spruss, T.; Gratz, L.; Ludeke, S.; Hofheinz, F.; Meister, S.; Echtenacher, B.; Bernhardt, G.; Pietzsch, J.; Hellwig, D.; Keller, M. Development of a neurotensin-derived (68)Ga-labeled PET ligand with high in vivo stability for imaging of NTS(1) receptor-expressing tumors. *Cancers (Basel)* **2022**, *14*.

Summary

The neurotensin receptor 1 (NTS_1R), belonging to the class A G-protein coupled receptors (GPCRs), represents a potential target concerning pain treatment, antipsychotic therapy, and, due to its (over)expression in certain tumor types, cancer diagnosis and therapy. The tridecapeptide neurotensin (**1.2**) is the endogenous ligand of the preferably $G_{q/11}$-coupled NTS_1R. Truncation studies demonstrated that the C-terminal hexapeptide NT(8-13) (**1.3**) represents the bioactive amino acid sequence of neurotensin. Therefore, NT(8-13) has been serving as a main lead compound in the development of peptidic NTS_1R ligands.

Radiochemical and fluorescence-based binding assays are the most common methods to determine binding affinities of newly synthesized compounds. Since the comparison of binding constants obtained from different types of binding assays is difficult, the main project of this thesis was the development of dually labeled NTS_1R ligands that bear a tritium and fluorescence label and, therefore, can be used in both kinds of assays. The reported bifunctional (SH, NH_2) NTS_1R ligand **2.5** (structure shown in Chapter 2) was considered a potential precursor since its conjugation to a fluorophore and a chelator led to an NTS_1R ligand with subnanomolar binding affinity. However, the (re)synthesized diastereomeric octapeptides **2.5a** and **2.5b**, one of them corresponding to the reported compound **2.5**, exhibited higher binding constants than reported (K_i values of 3.9 nM and 2.1 nM vs. an IC_{50} value of 0.43 nM). Moreover, the synthesis of the cyclic arginine derivative **2.8**, incorporated in **2.5**, was laborious. Therefore, compound **2.5** proved not to be the precursor of choice. Furthermore, the incorporation of the pyrrolidine-type β-amino acid **2.7** in NT(8-13) derivatives instead of Arg^8 or Arg^9 is presented in Chapter 2 (Collaboration with Prof. Reiser, Institute of Organic Chemistry, University of Regensburg). While the replacement of Arg^8 gave an NTS_1R binding affinity comparable to that of NT(8-13) (K_i = 0.12 nM), insertion of **2.7** in position 9 led to a marked decrease in binding affinity (K_i = 60 nM).

Pursuing a new strategy, different NT(6-13) analogs with two orthogonal functionalities (alkyne and amine group), allowing the attachment of a radio- and a fluorescence label, were synthesized (Chapter 3). Attachment of an azido-functionalized 5-TAMRA or Cy3B dye via the alkyne moiety and propionylation of the amine yielded five fluorescent NTS_1R ligands, of which **3.13** and **3.18** were chosen for radiolabeling. The resulting tritium-labeled analogs [^{3}H]**3.13** and [^{3}H]**3.18**, bearing a [^{3}H]propionyl group instead of the 'cold' propionyl moiety, were characterized in radiochemical binding experiments, whereas their cold congeners **3.13** and **3.18** were studied in three different fluorescence-based assays (high-content imaging, flow cytometry, fluorescence anisotropy). While saturation and competition binding studies gave

well comparable K_d and K_i values, kinetic studies revealed marked differences between the radiochemical and fluorescence-based assays, but also within the fluorescence-linked methods.

Another subproject of the thesis was the combination of three different reported achievements with respect to NTS_1R binding affinity, proteolytic stability (in vitro and in vivo), and conjugation of NT(8-13) derivatives (Chapter 4). This led to peptide **4.17a** which exhibits high NTS_1R binding affinity with a K_i value in the picomolar range (K_i = 0.055 nM). Conjugation of **4.17a** to a 5-TAMRA and sulfoCy5 fluorophore gave the fluorescent ligands **4.19** and **4.21** displaying similar NTS_1R binding affinities (K_i = 0.14 nM (**4.19**); K_i = 0.094 nM (**4.21**)) and high in vitro proteolytic stabilities. Compounds **4.19** and **4.21** proved to be valuable molecular tools for flow cytometric NTS_1R binding experiments and biomolecular imaging of NTS_1R expression in cells and tumor tissue.

Furthermore, **4.17a** was conjugated to three different chelators (DOTA (**5.6**), NOTA (**5.7**), (*R*)-NODA-GA (**5.8**)) followed by the incorporation of Ga^{3+} affording the potential PET ligands **5.9**-**5.11**, which displayed high NTS_1R binding affinities with subnanomolar K_i values of 0.13-0.31 nM and high in vitro stabilities in human plasma (Chapter 5). Insertion of the positron-emitting radionuclide $^{68}Ga^{3+}$ in **5.6** yielded the NTS_1R PET ligand [^{68}Ga]**5.9**, which also showed high in vitro stability in human plasma.

Finally, inspired by high-affinity cyclic peptidic neuropeptide Y Y_4 receptor ligands, two cyclic NT(8-13) derivatives (**6.8**, **6.9**) were synthesized via an on-resin cyclization approach (Chapter 6). However, the cyclic peptides **6.8** and **6.9** exhibited, compared to NT(8-13), markedly decreased NTS_1R binding affinities with K_i values of 112 nM and 11 nM, respectively.

Abbreviations

^{1}H-COSY	^{1}H-^{1}H correlation spectroscopy (NMR)
2-ClTrt	2-chlorotrityl
5-TAMRA	5'-carboxy-tetramethylrhodamine
AF	autofluorescence
AF®	Alexa Fluor® dyes
aq.	aqueous
Arg(carb)	*N*$^{\omega}$-carbamoylated arginine containing a tetramethylene spacer in the carbamoyl substituent (derived from the building block **3.1** in Chapter 3, 4, and 5) and *N*$^{\omega}$-carbamoylated arginine containing a dimethylene spacer in the carbamoyl substituent (derived from the building block **6.7** in Chapter 6)
BBV	budded baculovirus
Boc	*tert*-butyloxycarbonyl
BDP®	BODIPY® dyes
BRET	bioluminescence resonance energy transfer
BSA	bovine serum albumin
$CDCl_3$	deuterated chloroform
CD_3OD	deuterated methanol
CE	capillary electrophoresis
CEC	concentration-effect curve
CH_2Cl_2	dichloromethane
CHO cells	Chinese hamster ovary cells
compd.	Compound
Cy	cyanine

cycArg	cyclic arginine derivative derived from the building block **2.8** (Chapter 2)
D_2O	deuterated water
DPBS	Dulbecco´s phosphate buffered saline
DIPEA	*N*,*N*-diisopropylethylamine
DMF	*N*,*N*-dimethylformamide
DMSO	dimethylsulfoxide
DMSO-d_6	deuterated dimethylsulfoxide
DOTA	1,4,7,10-tetraazacyclododecane-1,4,7,10-tetraacetic acid
Dpaa	*N*,*N*-bis[(6-carboxypyridin-2-yl)methyl]glycine
DTPA	diethylenetriaminepentaacetic acid
E_{max}	efficacy (maximum effect) of a receptor agonist determined in a functional assay (Chapter 2, 3, 4, and 5) and efficacy of an allosteric modulator (Chapter 4)
EDT	ethane-1,2-dithiol
Et_3N	triethylamine
EtOH	ethanol
FA	fluorescence anisotropy
FBS	fetal bovine serum
FC	flow cytometry
FL	fluorescent ligand
Fmoc	fluorenylmethyloxycarbonyl
Fmoc-amino acid	N^{α}-Fmoc protected and side chain proteceted (if required) amino acid
GAB	γ-aminobutyryl
Gp-βAPCA	*cis*-4-aminopyrrolidine-3-carboxylic acid (βAPCA) with a 3-guanidinopropyl moiety (Gp)

GPCR	G-protein coupled receptor
GppNHp	guanosine-5'-[(β,γ)-imido]triphosphate
HBED	*N*,*N*'-bis(2-hydroxybenzyl)ethylenediamine-*N*,*N*'-diacetic acid
HBTU	3-[bis(dimethylamino)methyliumyl]-3H-benzotriazol-1-oxide hexafluorophosphate
HCI	high-content imaging
HEK293T	human embryonic kidney cells
HEPES	2-[4-(2-Hydroxyethyl)piperazin-1-yl]ethane-1-sulfonic acid
HMBA	4-(hydroxymethyl)benzamide
HMBC	heteronuclear multiple bond correlation experiment (NMR)
HOBt	hydroxybenzotriazole
(HR)MS	(high resolution) mass spectrometry
HT-29	human colorectal adenocarcinoma cell line
pIC_{50}	negative decadic logarithm of the half maximal inhibitory concentration (competition binding assays)
k	retention (or capacity) factor
K_d	dissociation constant from a saturation binding experiment
k_{obs}	observed association rate constant
k_{off}	dissociation rate constant
k_{on}	association rate constant
LDA	lithium diisopropylamide
$logD_{7.4}$	logarithm of the n-octanol/water distribution coefficient
Me	methyl
MeOH	methanol
MOI	multiplicity of infection
MSNT	1-(mesitylene-2-sulfonyl)-3-nitro-1,2,4-triazole

MTBD	7-methyl-1,5,7-triazabicyclo[4.4.0]dec-5-ene
n.a.	not applicable
n.d.	not determined
NEAA	non-essential amino acid solution
NHS	*N*-hydroxysuccinimide
NMP	1-methylpyrrolidin-2-one
NMR	nuclear magnetic resonance (spectroscopy)
NODA-GA	1,4,7-triazacyclononane-1-glutaric acid-4,7-acetic acid
NOPO	1,4,7-triazacyclononane-1,4-bis[methylene(hydroxymethyl)phosphinic acid]-7-[methylene(2-carboxyethyl)phosphinic acid]
NOTA	1,4,7-triazacyclononane-1,4,7-triacetic acid
NT	neurotensin
NTS_1R	neurotensin receptor type 1
NTS_2R	neurotensin receptor type 2
NTS_3R	neurotensin receptor type 3
Pbf	2,2,4,6,7-pentamethyl-dihydrobenzofuran-5-sulfonyl
PBS	phosphate-buffered saline
Pd/C	Palladium on activated charcoal (catalyst)
pEC_{50}	negative decadic logarithm of the half maximal effective concentration (functional assays)
PET	positron emission tomography
pipGly	piperidinylglycine
pK_d	negative decadic logarithm of the dissociation constant K_d (in M) obtained from a saturation binding experiment
pK_i	negative decadic logarithm of the dissociation constant K_i (in M) obtained from a competition binding experiment

PP	polypropylene
Pra	propargylglycine
PyBOP	benzotriazole-1-yl-oxytripyrrolidinophosphonium-hexafluorophosphate
ROI	region of interest
RP	reversed phase
(*R*,*R*)-Me-BPE-Rh	(-)-1,2-Bis((2*R*,5*R*)-2,5-dimethylphospholano)ethane(1,5-cyclooctadiene)rhodium(I) tetrafluoroborate
rt	room temperature
SEM	standard error of the mean
SPECT	single-photon emission computed tomography
SPPS	solid phase peptide synthesis
(*S*,*S*)-Me-BPE-Rh	(-)-1,2-Bis((2*S*,5*S*)-2,5-dimethylphospholano)ethane(1,5-cyclooctadiene)rhodium(I) tetrafluoroborate
$t_{1/2}$	half-life
*t*Bu	*tert* butyl
TFA	trifluoroacetic acid
THF	tetrahydrofuran
TIA	thioanisole
TIS	triisopropylsilane
Tle	α-*tert*-butylglycine, *tert*-leucine
TMSAla	(trimethylsilyl)alanine
τ_{fl}	fluorescence lifetime
t_r	retention time
TRIS	tris(hydroxymethyl)aminomethane
Trt	trityl, triphenylmethyl

Overview of bold compound numbers and corresponding laboratory codes

compound	lab code	compound	lab code	compound	lab code
Chapter 2		Chapter 3		Chapter 4	
2.5a	FE037-I	**3.6**	FE042	**4.10**	FE077
2.5b	FE037-II	**3.7**	FE043	**4.14**	FE080
2.8	FE027	**3.8**	FE044	**4.15**	FE081
2.11	FE006	**3.9**	FE045	**4.16a**	FE082-I
2.15	FE007	**3.10a**	FE055-I	**4.16b**	FE082-II
2.18	FE024	**3.10b**	FE055-II	**4.17a**	FE083-I
2.20	FE025	**3.13**	FE051	**4.17b**	FE083-II
2.21	FE026	**3.14**	FE050	**4.19**	FE093
2.22	FE022	**3.15**	FE052	**4.21**	FE094
2.25	FE012	**3.16**	FE053		
2.26	FE041	**3.17**	FE058		
2.27a	FE029-I	**3.18**	FE061		
2.27b	FE029-II	**3.19**	FE065		
2.28a	FE035-I	**3.20**	FE066		
2.28b	FE035-II				
2.29a	FE036-I				
2.29b	FE036-II				
2.30a	FE039-I				
2.30b	FE039-II				
2.31	FE040				
2.32	FE038				

Chapter 5		Chapter 6	
5.6	FE087	**6.8**	FE001
5.7	FE088	**6.9**	FE008
5.8	FE089		
5.9	FE090		
5.10	FE091		
5.11	FE092		

Eidesstaatliche Erklärung

Ich erkläre hiermit an Eides statt, dass ich die vorliegende Arbeit ohne unzulässige Hilfe Dritter und ohne Benutzung anderer als der angegebenen Hilfsmittel sowie ohne künstliche Intelligenz angefertigt habe; die aus anderen Quellen direkt oder indirekt übernommenen Daten und Konzepte sind unter Angabe des Literaturzitats gekennzeichnet.

Teile der experimentellen Arbeiten wurden in Zusammenarbeit mit anderen Institutionen und Personen durchgeführt. Entsprechende Vermerke zu den Beiträgen der betreffenden Personen finden sich jeweils zu Beginn des entsprechenden Kapitels und unter „Acknowledgments“.

Weitere Personen waren an der inhaltlich-materiellen Herstellung der vorliegenden Arbeit nicht beteiligt. Insbesondere habe ich hierfür nicht die entgeltliche Hilfe eines Promotionsberaters oder anderer Personen in Anspruch genommen. Niemand hat von mir weder unmittelbar noch mittelbar geldwerte Leistungen für Arbeiten erhalten, die im Zusammenhang mit dem Inhalt der vorgelegten Dissertation stehen.

Die vorliegende Arbeit wurde bisher weder im In- noch im Ausland in gleicher oder ähnlicher Form einer anderen Prüfungsbehörde vorgelegt.

Regensburg, den 13.08.2025

Fabian Ertl